ESPECTROFOTOMETRÍA DE BAJA FRECUENCIA APLICADA A SISTEMAS ALIMENTARIOS

Tesis doctoral
presentada por:

María Victoria Traffano Schiffo

Julio 2017

Directores:

Dr. Pedro J. Fito | Dra. Marta Castro Giráldez

UNIVERSITAT POLITÈCNICA DE VALÈNCIA

IIAD

Espectrofotometría de Baja Frecuencia aplicada a Sistemas Alimentarios

Instituto Universitario de Ingeniería de Alimentos para el Desarrollo

Universidad Politécnica de Valencia

TESIS DOCTORAL

Presentada por: María Victoria Traffano Schiffo

Dirigida por:

Dr. Pedro J. Fito

Dra. Marta Castro Giráldez

Julio 2017, Valencia, España

D. PEDRO J. FITO, PROFESOR TITULAR DE LA UNIVERSIDAD POLITÉCNICA DE VALENCIA, PERTENECIENTE AL INSTITUTO UNIVERSITARIO DE INGENIERÍA DE ALIMENTOS PARA EL DESARROLLO Y **Dª MARTA CASTRO GIRÁLDEZ** INVESTIGADORA DE LA UNIVERSIDAD POLITÉCNICA DE VALENCIA, PERTENECIENTE AL INSTITUTO UNIVERSITARIO DE INGENIERÍA DE ALIMENTOS PARA EL DESARROLLO

CONSIDERAN: Que la memoria titulada **ESPECTROFOTOMETRÍA DE BAJA FRECUENCIA APLICADA A SISTEMAS ALIMENTARIOS,** que presenta Dª **MARIA VICTORIA TRAFFANO SCHIFFO** para aspirar al grado de Doctora por la Universidad Politécnica de Valencia, reúne las condiciones adecuadas para constituir su tesis doctoral, por lo que **AUTORIZAN** a la interesada para su presentación.

Valencia, Julio 2017

Fdo: **Pedro J. Fito Suñer**
Director de tesis

Fdo: **Marta Castro Giraldez**
Directora de tesis

No te rindas, aún estás a tiempo
De alcanzar y comenzar de nuevo,
Aceptar tus sombras,
Enterrar tus miedos,
Liberar el lastre,
Retomar el vuelo.

No te rindas que la vida es eso,
Continuar el viaje,
Perseguir tus sueños,
Destrabar el tiempo,
Correr los escombros,
Y destapar el cielo.

Mario Benedetti

A la persona más importante de mi vida, a ***mamá***

A mis hermanas y sobrinos

A Toribio

A Facu

Agradecimientos

Qué difícil es cerrar esta etapa tan importante en mi vida, etapa que sin dudas cambió totalmente mi rumbo, así que no puedo dejar de agradecer a la gente que pasó a lo largo de ella y que estuvo a mi lado.

En primer lugar, tengo que agradecer a mis directores, ***Pedro*** *y* ***Marta****, no sólo por todo lo que me enseñaron a lo largo de estos años, si no más que nada por su amistad y por las innumerables risas, cafés y anécdotas inolvidables. Porque podría decir que son termodinámicamente increíbles y espectrofotométricamente incalculables, aunque no estoy segura en qué rango del espectro sería más alta su dispersión, si en* α*,* β *o* γ*, aunque creo que estaría entre 800 y 1900 MHz ;).*

A mi familia, por bancarme todos estos años lejos, pero a la vez nunca permitir que esa distancia sea tan grande. ***Mamá, Bel, Marce, Muma, Vicen, Manu*** *y* ***Toribio, son mi razón de ser****.*

A ***Facu****, por caminar juntos, por ser mi fortaleza y mi sostén. Te amo.*

A mis amigas de Argentina, por estar a mi lado cada día de estos 5 años, por sus buenos días de todos los días, por las pequeñas y las grandes cosas que nunca dejaron de hacer y así, hacerme sentir que cada domingo yo también estaba con ellas compartiendo unos mates. A ***DecoDreams (Fati y Magda)****, por conocer exactamente mis deseos y sin muchas palabras, plasmarlas de una manera increíble en la portada de esta tesis. Gracias chicas, son unas genias!*

A mis amigas/os de España (aunque muchos no sean de aquí), sin dudas si no fuera por uds. esta experiencia no hubiera sido lo que es. Pau, Magda, Ali, Nur, Encar, Maite, Lau, Sofi, Mariola, Lau y Jorge gracias por acompañarme en buenos y malos momentos.

A todos los que pasaron por la planta 1, por las comidas llenas de risas y anécdotas y también porqué no, por compartir las depresiones y angustias.

A los técnicos del IuIAD, por todo el apoyo y ayuda durante estos largos años.

A todos los que pasaron por el labo de Propiedades Dieléctricas, porque de cada uno de ellos me llevo una enseñanza y un recuerdo.

A la beca ERASMUS MUNDUS (programa EUROTANGO II) y a la Universidad Politécnica de Valencia, por hacer esto posible.

A Ricardo y todos los que forman parte del I3M, por materializar cada idea y transformarlas en sensores.

A mis directores de estancias, a ***Patricio*** *y* ***Ula****, un* ***gracias gigante****, gracias por ser unos grandes guías, pero por sobre todas las cosas por ser unos grandes amigos. Me enseñaron muchísimo y lo siguen haciendo día a día. Me hicieron ver la ciencia desde otra perspectiva y no saben cuánto enriquecieron mi camino.*

A todas las personas que acompañaron mis estancias, tanto en la ***Universidad de Buenos Aires*** *como en la* ***Universidad de Bologna****, gracias por hacer mi paso por allí tan especial.*

GRACIAS TOTALES!!!

RESUMEN

La industria agroalimentaria ha evolucionado notablemente durante las últimas décadas debido a la necesidad de tecnificar la producción con el objetivo de reducir los tiempos del proceso y aumentar las ganancias de las industrias, sin que ello suponga una disminución de la calidad del producto. En este contexto, la utilización de técnicas espectrofotométricas de monitorización y tratamiento para la optimización de procesos productivos pueden suponer un gran avance para la industria agroalimentaria.

La presente tesis doctoral aborda el estudio, diseño y desarrollo de sensores no destructivos basados en la espectrofotometría para la monitorización en línea de productos y procesos; así como el estudio de la aplicabilidad de técnicas espectrofotométricas de tratamiento para la mejora de procesos productivos alimentarios. Es por ello, que esta tesis doctoral se subdivide en tres grandes bloques abarcando los tres tipos de sistemas alimentarios: tejido animal, tejido vegetal y sistemas coloidales.

En el **bloque 1**, se realizaron estudios en ***tejidos animales***, buscando dar solución a problemáticas cada vez más frecuentes en la industria cárnica. En primer lugar, se analizó la utilización de sensores espectrofotométricos para el control del secado de la carne de cerdo como paso fundamental para la obtención del jamón serrano, producto de alto valor agregado. Para ello, se utilizaron dos técnicas, la termografía infrarroja y la monitorización por microondas. En el rango de los infrarrojos, el estudio se llevó a cabo utilizado una cámara termográfica Optris PI® para seguir la evolución de la emisividad en cada etapa del proceso de secado. Este estudio, acoplado a un modelo termodinámico y determinaciones fisicoquímicas han demostrado que la termografía infrarroja es una técnica capaz de monitorizar el proceso de secado, identificando cada etapa del mismo. Por otro lado, en el rango de las microondas se midió la permitividad desde 500 MHz a 20 GHz y ha sido posible demostrar que el factor de pérdidas en la dispersión-γ presenta una relación directa con el número de moléculas de agua en la superficie de la muestra de carne.

En segundo lugar y teniendo en cuenta que la congelación es una de las tecnologías más ampliamente utilizadas para prolongar la vida útil de la carne y productos cárnicos, se ha

desarrollado un sensor no destructivo y de fácil utilización en el rango de la radiofrecuencia, capaz de detectar si las muestras de carne de cerdo han sufrido ciclos de congelación/descongelación.

En tercer lugar, se realizó un exhaustivo estudio que solventa las problemáticas resultantes de una fuerte tecnificación e intensificación en la industria avícola, como son las carnes de baja calidad (PSE y DFD), la miopatía de las estrías blancas y del pectoral profundo, producidas principalmente como consecuencia de la utilización de estirpes hipertróficas. Para cada una de estas problemáticas, se realizaron estudios espectrofotométricos en los rangos de la radiofrecuencia y de las microondas y se relacionaron con parámetros fisicoquímicos y bioquímicos, obteniendo los parámetros de relajación para las dispersiones α, β y γ mediante un modelo logístico. Para cada una de las problemáticas, se desarrollaron sensores en el rango de la radiofrecuencia capaces de detectarlas, y además, para el estudio de las miopatías, los sensores desarrollados son capaces de medir inclusive a través de la piel en carcasas de pollo enteras.

En el **bloque 2** se abordan estudios en ***tejidos vegetales***. En primer lugar, se caracterizaron espectrofotométricamente los tejidos que componen la mandarina. Es por ello, que de forma conjunta a un estudio fisicoquímico y estructural se obtuvieron los valores de la permitividad en radiofrecuencia y microondas. Como uno de los resultados más importantes de esta investigación se obtuvo una herramienta basada en la constante dieléctrica de relajación en la dispersión-γ capaz de predecir la humedad de las muestras. Esto representa un primer paso en el desarrollo de sensores para distintas aplicaciones, como podría ser la detección de semillas en mandarinas enteras o enfermedades y/o contaminaciones en los frutos.

En segundo lugar, se abordó el estudio de la aplicación de campos eléctricos pulsados como pre-tratamiento a la deshidratación osmótica del kiwi. Esta técnica espectrofotométrica de tratamiento, acoplada a determinaciones fisicoquímicas y un estudio termodinámico han permitido demostrar que los campos eléctricos pulsados aceleran el proceso de deshidratación osmótica debido principalmente a la plasmolización de las células. Además, se llevó a cabo la monitorización del proceso mediante resonancia magnética nuclear, a partir del cual se pudieron analizar los transportes internos y las transformaciones que sufre el tejido en su interior. Por último, se ha podido concluir que la resonancia magnética nuclear es una técnica adecuada para

cuantificar las moléculas de agua de acuerdo a su situación dentro del tejido además de poder ser utilizada para obtener isotermas de sorción en todo el rango de actividades de agua.

Finalmente, el **bloque 3** de esta tesis se centra en el estudio del tercer tipo de sistema alimentario, los ***sistemas coloidales***. En este caso, se busca aumentar la estabilidad de compuestos bioactivos de alto valor (β-galactosidasa) mediante su encapsulación en hidrogeles de alginato-Ca(II) con y sin el agregado de excipientes secundarios. En este estudio se trató de evaluar el comportamiento de este sistema coloidal frente tratamientos térmicos y su cinética de transporte. Se llevaron a cabo estudios de caracterización, calorimétricos, de resonancia magnética nuclear y además un profundo análisis microestructural mediante dispersión de rayos-X de bajo ángulo y microscopia electrónica de barrido. Se ha demostrado que el agregado de excipientes secundarios mejora la estabilidad de la enzima frente a tratamientos térmicos (congelación, liofilización, secado a vacío, ciclos de congelación/descongelación y almacenamiento). Se ha estudiado la cinética cristalización durante la congelación de las cápsulas mediante resonancia magnética nuclear y finalmente se ha descrito el grado de compacidad de las varillas que conforman la estructura de caja de huevo, su interconexión y tamaño mediante la dispersión de rayos-X de bajo ángulo.

ABSTRACT

Food industry has evolved remarkably during the last decades due to the need to technify the production with the aim of reducing processing times and to increase industry profits, without this implying a decrease of the product quality. In this context, the use of spectrophotometric monitoring and treatment techniques for the optimization of production processes can represent a great progress for agri-food industry.

This doctoral thesis is focused on the study, design and development of non-destructive sensors based on spectrophotometry to monitor products and processes; as well as the application of treatment spectrophotometric techniques for the improvement of food production processes. This doctoral thesis is subdivided into three large blocks covering three types of food systems: animal tissue, plant tissue and colloidal systems.

In **block 1**, ***animal tissues*** were studied, in order to solve the increasingly frequent problems in meat industry. Firstly, the use of spectrophotometric sensors for the control of pork meat drying was analysed as a fundamental step to obtain cured ham, a product with high added-value. In this context, two techniques were used, infrared thermography and microwave monitoring. In the range of infrared, the study was carried out using a thermographic camera Optris PI® to follow the evolution of the emissivity at each stage of the drying process. This study, coupled to a thermodynamic model and some physicochemical determinations have shown that infrared thermography is a suitable technique able to monitor drying process, identifying each drying stage. On the other hand, in microwave range, permittivity was measured from 500 MHz to 20 GHz and it was demonstrated that the loss factor in γ-dispersion has a direct relation with the number of molecules on the meat sample surface.

Secondly, considering that freezing is one of the most widely used technologies to extend meat and meat products shelf life, a non-destructive and easy-to-use sensor in radiofrequency range able to detect if meat samples has been suffered freeze/thaw cycles has been developed.

Thirdly, an exhaustive study was carried out to solve the problems resulting from the strong technification and intensification in poultry industry, such as low-quality meats (PSE and DFD), the white striping and the deep pectoral myopathies, mainly produced because of the use of

hypertrophic strains. For each of these problems, spectrophotometric studies were performed in the radiofrequency and microwave ranges and they were related to physicochemical and biochemical parameters, obtaining the relaxation parameters for α, β and γ-dispersions by using a logistic model. For each problem, sensors were developed in radiofrequency range, and in addition, for the myopathy studies, the developed sensors were able even to measure through the skin in whole chicken carcasses.

In **Block 2** ***plant tissues*** were studied. Firstly, the tissues that compose the mandarin were characterized spectrophotometrically. Due to this, a physicochemical and structural study were coupled with the permittivity obtained in radiofrequency and microwave ranges. As one of the most important results of this research, a tool based on the dielectric relaxation constant in the γ-dispersion able to predict the moisture of the samples was obtained. This research represents a first step in the development of sensors with different applications such as the detection of seeds in whole mandarins, diseases and/or contaminations of the fruits.

Secondly, the study of the application of pulsed electric fields as a pre-treatment to the osmotic dehydration of kiwifruit was carried out. This spectrophotometric technique, coupled with physicochemical determinations and a thermodynamic study, has demonstrated that the pulsed electric fields accelerate the osmotic dehydration process, mainly due to the cells plasmolyzation. In addition, the monitoring of the process was carried out with nuclear magnetic resonance, where the internal transports and the transformations that the plant tissue suffers were analysed. Finally, it has been possible to conclude that nuclear magnetic resonance is a suitable technique to quantify the water molecules according to their location in the tissue and to obtain sorption isotherms throughout the complete range of water activities.

Finally, **block 3** of this thesis focuses on the study of the third type of food system, ***colloidal systems***. Particularly, the stability of high-value bioactive compounds (β-galactosidase) by its encapsulation in alginate-Ca(II) hydrogels with and without the addition of secondary excipients was studied. In this study, the behaviour of this colloidal system against thermal treatments and their transport kinetics were evaluated. Characterization, calorimetric and nuclear magnetic resonance studies were carried out as well as a deep microstructural analysis by small-

angle X-ray scattering and scanning electron microscopy. It has been demonstrated that the addition of secondary excipients has enhanced the stability of the enzyme against heat treatments (freezing, freeze drying, vacuum drying, freeze / thaw cycles and storage). It has been studied the kinetic crystallization during beads freezing by nuclear magnetic resonance and finally, the degree of compactness of the rods that form the egg-box structure, its interconnection and size by small-angle X-ray scattering has been described.

RESUM

La indústria agroalimentària ha evolucionat notablement durant les últimes dècades a causa de la necessitat de tecnificar la producció amb l'objectiu de reduir els temps del procés i augmentar els guanys de les indústries, sense que això suposi una disminució de la qualitat del producte. En aquest context, la utilització de tècniques espectrofotomètriques de monitorització i tractament per a l'optimització de processos productius poden suposar un gran avanç per a la indústria agroalimentària.

La present tesi doctoral aborda l'estudi, disseny i desenvolupament de sensors basats en l'espectrofotometria per al monitoratge no destructiu i en línia de productes i operacions de transformació; així com l'estudi de l'aplicabilitat de tècniques espectrofotomètriques de tractament per a la millora de processos productius alimentaris. És per això, que aquesta tesi doctoral es subdivideix en tres grans blocs abastant els tres tipus de sistemes alimentaris: teixit animal, teixit vegetal i sistemes col·loïdals.

Al bloc 1, es van realitzar estudis en teixits animals, buscant donar solució a problemàtiques cada vegada més freqüents en la indústria càrnia. En primer lloc, es va analitzar l'utilització de sensors espectrofotomètrics per al control de l'assecat de la carn de porc com a pas fonamental per a l'obtenció del pernil serrà, producte d'alt valor afegit. Per a això, es van utilitzar dues tècniques, la termografia infraroja i el monitoratge per microones. En el rang dels infrarojos, l'estudi es va dur a terme utilitzat una càmera termogràfica Optris PI®, per seguir l'evolució de l'emissivitat en cada etapa del procés d'assecatge. Aquest estudi, acoblat a un model termodinàmic i determinacions fisicoquímiques, han demostrat que la termografia infraroja és una tècnica capaç de monitoritzar el procés d'assecat, identificant cada etapa del mateix. D'altra banda, en el rang de les microones es va mesurar la permitivitat des de 500 MHz a 20 GHz i ha estat possible demostrar que el factor de pèrdues en la dispersió-γ presenta una relació directa amb el nombre de molècules d'aigua a la superfície de la mostra de carn.

En segon lloc i tenint en compte que la congelació és una de les tecnologies més àmpliament utilitzades per allargar la vida útil de la carn i productes carnis, s'ha desenvolupat un sensor no

destructiu i de fàcil utilització en el rang de la radiofreqüència, capaç de detectar si les mostres de carn de porc han patit cicles de congelació / descongelació.

En tercer lloc, es va realitzar un exhaustiu estudi que soluciona les problemàtiques resultants d'una forta tecnificació i intensificació en la indústria avícola, com són les carns de baixa qualitat (PSE i DFD), i les miopaties d'estries blanques i del pectoral profund, produïdes principalment com a conseqüència de la utilització d'estirps hipertròfiques. Per a cadascuna d'aquestes problemàtiques es van realitzar estudis espectrofotomètrics en els rangs de la radiofreqüència i de les microones i es van relacionar amb paràmetres fisicoquímics i bioquímics, obtenint els paràmetres de relaxació per a les dispersions α, β i γ mitjançant un model logístic. Per a cadascuna de les problemàtiques es van desenvolupar sensors en el rang de la radiofreqüència capaços de detectar-les, i a més, per a l'estudi de les miopaties, els sensors desenvolupats són capaços de mesurar inclusivament a través de la pell en carcasses de pollastre senceres.

En el bloc 2 s'aborden estudis en teixits vegetals. En primer lloc, es van caracteritzar espectrofotomètricament els teixits que componen la mandarina. És per això, que de manera conjunta a un estudi fisicoquímic i estructural es van obtenir els valors de la permitivitat en radiofreqüència i microones. Com un dels resultats més importants d'aquesta investigació es va obtenir una eina basada en la constant dielèctrica de relaxació a la dispersió-γ capaç de predir la humitat de les mostres. Això representa un primer pas en el desenvolupament de sensors per a diferents aplicacions, com podria ser la detecció de pinyols en mandarines senceres o malalties i/o contaminacions en els fruits.

En segon lloc, es va abordar l'estudi de l'aplicació de camps elèctrics polsats com pretractament a la deshidratació osmòtica del kiwi. Aquesta tècnica espectrofotomètrica de tractament, acoblada a determinacions fisicoquímiques i un estudi termodinàmic han permès demostrar que els camps elèctrics polsats acceleren el procés de deshidratació osmòtica degut principalment a la plasmolització de les cèl·lules. A més, es va dur a terme el monitoratge del procés mitjançant ressonància magnètica nuclear, a partir del qual es van poder analitzar els transports interns i les transformacions que pateix el teixit al seu interior. Finalment, s'ha pogut concloure que la ressonància magnètica nuclear és una tècnica adequada per quantificar les molècules d'aigua

d'acord a la seva situació dins el teixit a més de poder ser utilitzada per obtenir isotermes de sorció en tot el rang d'activitats d'aigua.

Finalment, el bloc 3 d'aquesta tesi se centra en l'estudi del tercer tipus de sistema alimentari, els sistemes col·loïdals. En aquest cas, es busca augmentar l'estabilitat de compostos bioactius d'alt valor (β-galactosidasa) mitjançant la seva encapsulació en hidrogels d'alginat-Ca (II) amb i sense l'agregat d'excipients secundaris. En aquest estudi es va tractar d'avaluar el comportament d'aquest sistema col·loïdal front tractaments tèrmics i la seva cinètica de transport. Es van dur a terme estudis de caracterització, calorimètrics, de ressonància magnètica nuclear i a més una profunda anàlisi microestructural mitjançant dispersió de raigs-x de baix angle i microscòpia electrònica de rastreig. S'ha demostrat que l'agregat de excipients secundaris millora l'estabilitat de l'enzim enfront de tractaments tèrmics (congelació, liofilització, assecat a buit, cicles de congelació / descongelació i emmagatzematge). S'ha estudiat la cinètica cristal·lització durant la congelació de les càpsules mitjançant ressonància magnètica nuclear i finalment s'ha descrit el grau de compacitat de les varetes que conformen l'estructura de caixa d'ou, la seva interconnexió i grandària mitjançant la dispersió de raigs-x de baix angle.

Índice de Contenidos

1. Introducción

1.1. Justificación

A lo largo de la última década y debido a las exigencias del mercado y de los consumidores, a la presión competitiva y a una economía cada vez más globalizada, las industrias agroalimentarias han sido objeto de continuos cambios con la finalidad de optimizar cada una de las etapas de sus procesos productivos, asegurando mayores rendimientos y productos seguros y de alta calidad. Sin embargo, a pesar de los esfuerzos realizados y de las mejoras que se han obtenido, los métodos utilizados para la monitorización de los procesos y de los productos terminados continúan siendo métodos tediosos, destructivos y que requieren largos tiempos de respuesta. Todo esto se traduce en una baja calidad de los productos, pudiendo verse comprometida también la seguridad alimentaria, lo que conllevaría importantes pérdidas, reduciendo la competitividad de la industria, afectando notablemente el consumo interno y el comercio exterior (Chico & Sánchez, 2012). En este contexto, la implementación de sensores basados en la espectrofotometría podría suponer un gran avance para la industria agroalimentaria.

La fotónica de señal o espectrofotometría se basa en la interacción entre un flujo de fotones y un sistema complejo, como un tejido o un sistema coloidal que conforma el sistema alimentario que se desea monitorizar y/o controlar. Esta técnica es capaz de proporcionar diferente información tanto química, física como estructural dependiendo de la región del espectro en el cual se trabaja (Scotter, 1997). La utilización y aplicación de la misma para la monitorización de procesos se ha incrementado notablemente en las últimas décadas (Nelson, 1999; Kremer, 2002) lográndose demostrar su efectividad en diversas áreas de estudio como la industria maderera (Torgovnikov, 1993; Ramasamy & Moghtaderi, 2010; Holmes *et al.*, 2013), la biotecnología (Markx & Davey 1999; Sabuncu *et al.*, 2012), la ciencias de los materiales (Lesmes & Morgan, 2001; Pötschke *et al.*, 2003) y la medicina entre otras (Pethig, 1984; Woodward *et al.*, 1996; Siegel, 2004; Grenier *et al.*, 2013; Ciurczak & Igne, 2014).

Particularmente en la industria alimentaria se han mostrado numerosas aplicaciones como por ejemplo su utilización para la identificación de fraudes y/o adulteraciones de los alimentos (Kent & Anderson, 1996; Kent *et al.*, 2002; Sadat *et al.*, 2006; Guo *et al.*, 2010; Lizhi *et*

al., 2010; Cataldo *et al.*, 2010; Guo *et al.*, 2011a; Balaguer *et al.*, 2013; Castro-Giráldez *et al.*, 2014), la monitorización del salado de carnes (Castro-Giráldez *et al.*, 2010a; 2011a; Liu *et al.*, 2013) y quesos (Fagan *et al.*, 2005; Smith *et al.*, 2011; Velázquez-Varela *et al.*, 2014) y el control de la maduración y de parámetros bioquímicos de frutas (Varlan & Sansen, 1996; László *et al.*, 1997; Sosa-Morales *et al.*, 2009; Castro-Giráldez *et al.*, 2010b; Soltani *et al.*, 2011; Guo *et al.*, 2011b; Castro-Giráldez *et al.*, 2013).

Además, la fotónica también es posible utilizarla con elevados niveles de densidad de flujo, denominándose fotónica de potencia. Esto permite inducir cambios controlados en el tejido biológico y orientar dichos cambios hacia una mejor conservación de los alimentos. En este sentido, se han demostrado novedosas aplicaciones industriales que involucran la aplicación de campos eléctricos pulsados como técnica espectrofotométrica de tratamiento. Su utilización como pre-tratamiento ha mostrado una gran utilidad para acelerar procesos de deshidratación osmótica de frutas (Tylewicz *et al.*, 2017; Dellarosa *et al.*, 2016; Dermesonlouoglou *et al.*, 2016; Amami *et al.*, 2006; Rastogi *et al.*, 1999) o la congelación (Ammar *et al.*, 2010; Jalté *et al.*, 2009; Phoon *et al.*, 2008), entre otros.

Dada la gran utilidad, fiabilidad de los resultados, sencillez, rapidez en la medida y la creciente aplicabilidad industrial que proporciona esta técnica, la presente tesis doctoral ha enfocado su estudio no sólo en demostrar nuevas aplicaciones sino, además, en lograr una transferencia tecnológica de los resultados obtenidos mediante el desarrollo y diseño de sensores de fácil implementación en líneas de producción o la adaptación de nuevas técnicas de transformación. Para ello, se ha utilizado un amplio rango del espectro electromagnético, abarcando desde la radiofrecuencia hasta el rango de los infrarrojos y utilizando diferentes técnicas, cada una de ellas adaptada al objetivo de cada trabajo en particular.

1.2. Sistemas Alimentarios

En cuanto a su organización, los sistemas alimentarios presentan diferentes niveles estructurales, los cuales se pueden clasificar en función de su nivel de complejidad. Desde los sistemas más simples, puros y homogéneos como son los cristales hasta los más complejos como

los sistemas celulares, que gracias a su complejidad permiten la vida en el universo (Velázquez Varela, 2014).

Es posible distinguir 4 niveles estructurales dentro de los sistemas alimentarios. En primer lugar, como sistema más simple, se encuentran los sistemas cristalinos como por ejemplo el NaCl. Estos sistemas forman una única fase la cual es homogénea, isótropa y estable. En un segundo nivel de complejidad estructural se encuentran las disoluciones, las cuales son mezclas homogéneas de dos o más sustancias, las cuales se encuentran en un mismo estado de agregación (fluido). En un tercer nivel de complejidad se encuentran los sistemas coloidales. Éstos, al menos presentan dos fases inmiscibles, de las cuales una de ellas mantiene la continuidad del sistema y se la define como fase continua, mientras que el resto, se encuentran repartidas en la fase continua y se denominan fases dispersas.

En el último nivel de complejidad estructural se encuentran los sistemas celulares. Éstos son sistemas multicompartimentados y multicomponentes, constituidos por distintas fases, separados mediante membranas y paredes celulares con un elevado nivel de organización y dotado de un sistema de regulación de transportes activos y pasivos que regulan el funcionamiento del sistema. Cabe destacar que los sistemas celulares se pueden dividir en tres: microorganismos, células animales y células vegetales.

Para comprender los sistemas alimentarios que serán objeto de estudio en la presente tesis doctoral, es de vital importancia conocer la composición y la estructura de los mismos.

1.2.1. Tejido Animal

1.2.1.1. Composición química

En cuanto a su composición química, el constituyente mayoritario del músculo esquelético es el agua, siendo su proporción en el tejido vivo un 75% (U.S. Department of Agriculture, 2008) del peso del músculo; sin embargo, este contenido puede variar particularmente durante el post-mortem (65-80%) (Traffano-Schiffo *et al.*, 2014b). El agua es el principal componente del líquido extracelular en el músculo, y con respecto a las células

musculares, también es considerado el constituyente mayoritario del fluido sarcoplasmático (citoplasmático). Su función es de vital importancia ya que in vivo, el agua es la encargada de la regulación térmica del organismo, actúa como medio para numerosos procesos celulares, además de transportar nutrientes dentro de las células, entre ellas y entre el músculo y el sistema vascular (Huff-Lonergan, 2010).

Las proteínas representan un 18,5% del peso del músculo esquelético (U.S. Department of Agriculture, 2008) aunque dicho valor puede variar entre un 16 y 22%. Cumplen diversas funciones, como la de mantener la estructura y la organización del músculo además de ser las responsables de los procesos de contracción y relajación (Huff-Lonergan, 2010).

El contenido de lípidos puede variar con respecto a varios factores como por ejemplo la edad del animal, el nivel nutricional y el tipo de músculo. Su contenido es de alrededor del 3% del peso del músculo, aunque se puede encontrar en un rango entre 1-13% (U.S. Department of Agriculture, 2008). Los lípidos cumplen un rol de almacenamiento de energía además de formar parte de la estructura de las membranas celulares, entre otras funciones.

En un porcentaje aproximado del 1% (aunque este valor puede variar entre un 0.5-1.5%) se encuentran los hidratos de carbono (Huff-Lonergan, 2010). Éstos cumplen una función muy importante en la obtención de energía mediante la transformación de la glucosa en acido pirúvico y adenosin tris fosfato (ATP) mediante el proceso fermentativo denominado Glucólisis.

Además, en la estructura del músculo esquelético existen compuestos nitrogenados no proteicos como creatina, creatina fosfato, nucleótidos (ATP, ADP), aminoácidos libres, péptidos (anserina, carnosina) y otras sustancias no nitrogenadas (Huff-Lonergan, 2010).

1.2.1.2. Estructura

Como se puede observar en la Figura 1.1., el músculo esquelético está integrado por fibras musculares, las cuales son células multinucleadas, rodeadas por una membrana plasmática eléctricamente excitable, llamada sarcolema, situada debajo de una capa de tejido conectivo denominada endomisio (Ponce-Alquicira, 2006).

Las fibras musculares pueden presentar una longitud que oscila de pocos a decenas de centímetros, mientras que su anchura varía entre 60-100 μm de diámetro, pudiendo ser incluso menor en animales de corta edad. Una característica única que presentan las fibras musculares es que están constituidas por un conjunto intracelular de miofibrillas embebidas en el sarcoplasma, altamente ordenadas y densamente empaquetadas, pudiendo haber en una sola fibra, entre mil y dos mil miofibrillas de aproximadamente 1 μm de diámetro cada una (Warris, 2003).

Las miofibrillas constituyen el aparato contráctil de la fibra. Su unidad básica es una estructura repetitiva denominada sarcómero. A su vez, cada uno de ellos está comprendido por haces adyacentes de actina y miosina y se encuentra delimitado en cada extremo por las llamadas líneas Z (Brandebourg, 2013).

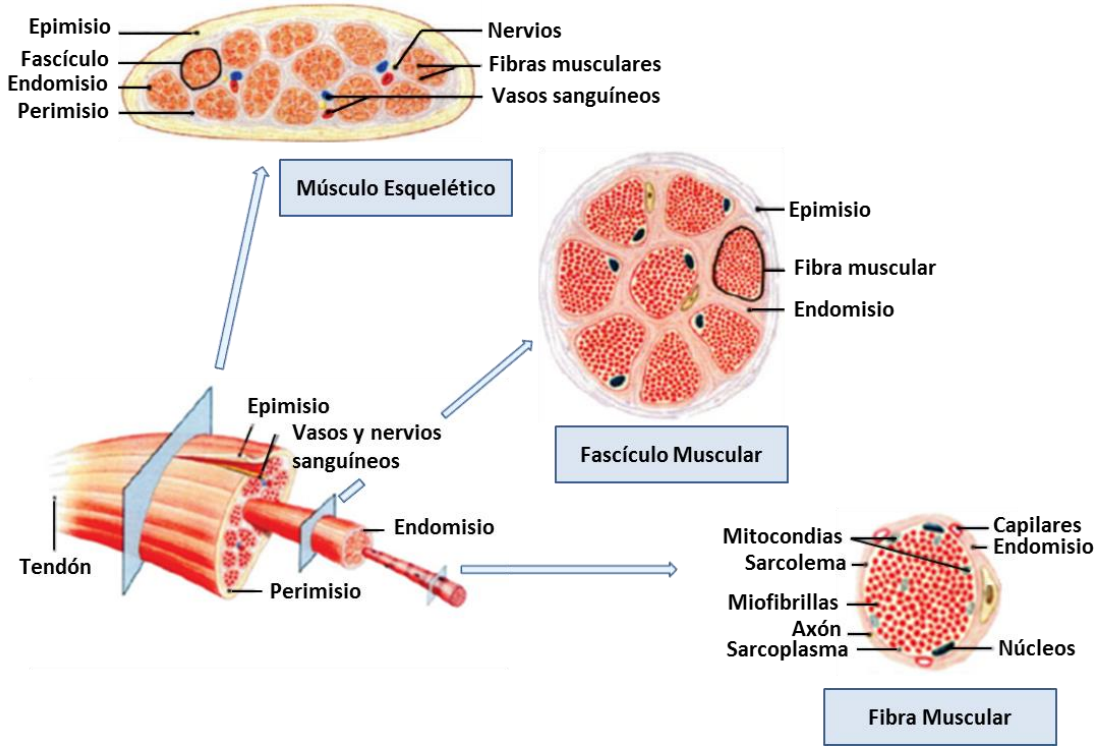

Figura 1.1. Organización del músculo esquelético (Adaptado de Brandebourg, 2013).

El carácter estriado del musculo esquelético es debido a la alternancia de zonas claras y oscuras (Figura 1.2.). Las bandas oscuras o bandas A, están constituidas por filamentos gruesos (miosina) conjuntamente con una parte de los filamentos delgados (actina) que se superponen,

mientras que la banda clara I está constituida principalmente por filamentos delgados (Warris, 2003).

En la región central de la banda A, entre las terminaciones de los filamentos opuestos de actina (de cada mitad del sarcómero), existe un área denominada zona H, la cual es algo menos densa que el resto ya que sólo posee filamentos de miosina. Además, una banda densa y estrecha, denominada línea M divide el centro de la banda A (Forrest *et al.*, 1979).

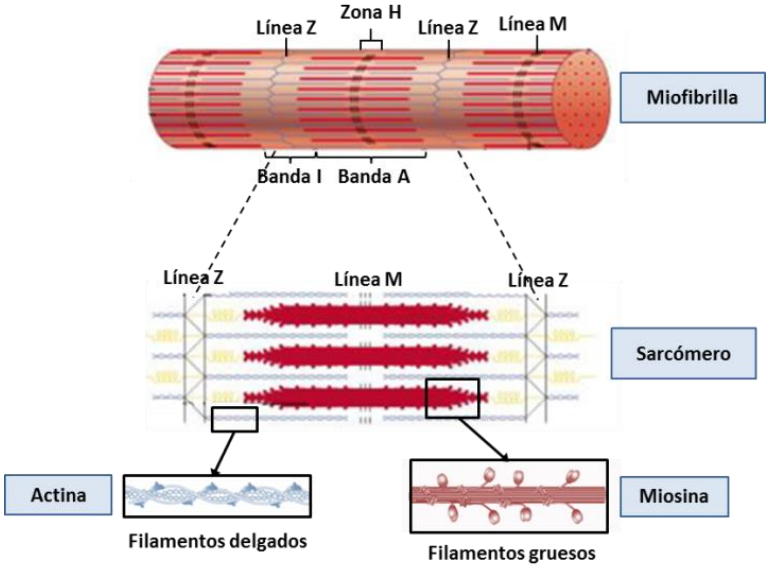

Figura 1.2. Organización estructural de las miofibrillas (Adaptado de Castro Giráldez, 2010).

1.2.1.3. Metabolismos implicados en la conversión de músculo a carne

Desde el punto de vista bioquímico, la carne es el resultado de una serie de reacciones y transformaciones bioquímicas que tienen lugar en el músculo esquelético tras la muerte del animal y que determinarán en gran medida la calidad de la misma (Lametsch *et al.*, 2002; Maltin *et al.*, 2003; Honikel, 2004; Ouali *et al.*, 2006; Paredi *et al.*, 2012).

In vivo, los animales al igual que los seres humanos, requieren energía para poder moverse, respirar y desempeñar las actividades físicas necesarias para vida. Esta energía se obtiene mediante la degradación del glucógeno muscular lo cual da como resultado 36 moléculas de ATP, las cuales se hidrolizan mediante la actividad de la enzima ATPasa (presente en la cabeza globular de la miosina), produciendo la formación del complejo actomiosina, responsable del acortamiento

del sarcómero (formación de enlaces entrecruzados entre filamentos gruesos y delgados) y, por ende, de la contracción muscular. Este complejo es capaz de separarse cuando otra molécula de ATP se une nuevamente a la cabeza globular de la miosina produciéndose la relajación muscular (Huff Lonergan *et al.*, 2010).

Tras el sacrificio del animal se desencadenan procesos metabólicos que se pueden dividir en dos fases separadas por el *rigor mortis*. En primer lugar, el ***prerigor*** se inicia con el sacrificio y el posterior cese del riego sanguíneo, lo que provoca una falta repentina de oxígeno en el músculo, parándose el proceso respiratorio celular e induciéndose los procesos anaerobios. Durante el proceso metabólico anaerobio, la producción de ATP tiene un rendimiento por mol de glucógeno 10 veces menor que la respiración, esto, unido a la reducción de disponibilidad de glucógeno, provoca una disminución de la concentración de ATP del medio, desencadenándose el proceso conocido como glucólisis o fermentación anaerobia (Maltin *et al.*, 2003).

Durante la fermentación anaerobia, la ruta metabólica que toma el ácido pirúvico es diferente y como consecuencia se produce una acumulación de iones hidrógeno a través de la formación de ácido láctico (McGeehin *et al.*, 2001), el cual se acumula disminuyendo el pH intracelular (Maltin *et al.*, 2003; Smith *et al.*, 1992). Dicho descenso continúa hasta que las enzimas que efectúan la degradación resulten inactivadas.

A nivel celular y debido a la falta de ATP, se ven afectados una serie de procesos como bombas de transporte (bomba Na^{+}/K^{+} y/o bomba Ca^{+2}) y el sistema de contracción/relajación muscular (Toldrá & Reig, 2006), lo cual produce una compactación de las fibras musculares acompañadas de rigidez. Fenómeno conocido como ***rigor mortis*** (Offer & Cousin, 1992). La instauración del rigor mortis depende principalmente de la temperatura, aunque también de la especie en cuestión, en el caso del pollo se produce a las 6 horas post mortem (McKee, 2002), mientras que en animales más grandes como cerdos o bovinos este período es mayor.

Como consecuencia del metabolismo anaerobio, se producen una serie de reacciones que inducen cambios en las propiedades eléctricas del tejido biológico. Se activan las enzimas endógenas y se inicia la degradación del ATP (Smulders, Hofbauer, & Geesink, 2014),

produciéndose ácido láctico y AMP, lo cual provoca la disminución del pH y como consecuencia, desnaturalización proteica.

Finalmente, en la fase ***postrigor*** de resolución o maduración, la extensibilidad de los músculos se recupera y la carne sufre un proceso de ablandamiento debido a la acción de las enzimas proteolíticas. Durante esta última etapa, la textura, la jugosidad y el sabor mejoran notablemente luego de un período de almacenamiento bajo condiciones controladas de temperatura (4 °C) (Ouali *et al.*, 2006). En esta etapa, las proteínas son fragmentadas por reacciones enzimáticas, produciéndose polipéptidos o fragmentos de la cadena proteica original (Lametsch *et al.*, 2002; Greaser, 1986). La degradación proteica más importante desde el punto de vista de la reducción de tamaño es la degradación de la miosina en un fragmento de la cabeza globular de la miosina (Lametsch *et al.*, 2002). En esta degradación, el tamaño original de la miosina de unos 250 kDa se reduce a nuevos fragmentos de 56 kDa (Li *et al.*, 2012). La actina (43 kDa) se degrada a fragmentos de 32 y 40 kDa (Lametsch *et al.*, 2002). La troponina-T, la cual forma parte de una estructura más compleja, la troponina (70 kDa) (Mudalal *et al.*, 2014; Huff-Lonergan, & Lonergan, 1999) se degrada a polipéptidos más pequeños, identificados como fragmentos de 28, 30, 32 y 34 kDa (Huang *et al.*, 2011). Finalmente, la desmina con un tamaño original de 53 kDa también es degradada a fragmentos de menor tamaño. Particularmente en la carne de pollo, la degradación de la desmina se lleva a cabo en las primeras 12 horas post-mortem para una carne normal (Li *et al.*, 2012).

1.2.2. Tejido Vegetal

1.2.2.1. Estructura

El tejido vegetal está constituido por células que se unen entre sí formando un tejido parenquimático, el cual presenta una estructura compleja formada por conexiones intercelulares con espacios intra y extracelulares (Castro-Giraldez *et al.*, 2011b; Fito *et al.*, 2007). Las células están constituidas por membranas celulares, pared celular, plasmalema, tonoplasto (membrana vacuolar) y orgánulos que se encuentran en el citoplasma. Además, dentro de las células parenquimáticas se encuentran las vacuolas (Figura 1.3.), las cuales son consideradas el

compartimento más grande, llegando a ocupar el 80% del volumen total de la misma (Martinoia *et al.*, 2000) y son las responsables del almacenamiento de compuestos que otorgan sabor y aroma a las frutas, como azúcares, ácidos orgánicos y metabolitos secundarios (compuestos fenólicos y/o terpenoides), los cuales pueden estar presentes incluso en concentraciones extremadamente altas (Shiratake & Martinoia, 2007).

Cabe destacar que a través del tejido parenquimático se llevan a cabo los distintos mecanismos de transporte celular, dentro de los cuales podemos nombrar al transporte pasivo, al transporte activo y al transporte transmembrana. El transporte pasivo, es promovido por los gradientes de potencial químico y se puede llevar a cabo dentro de las células a través de las vías simplásticas o fuera de ellas (espacio extracelular) a través de las vías apoplásticas (Steudle & Frensch, 1996). El transporte de agua entre el espacio extra e intracelular o dicho de otra manera entre el transporte apoplástico y el simplástico es el transporte transmembrana, el cual se lleva a cabo por canales proteicos conocidos como aquaporins (Agre *et al.*, 1998; Maurel & Chrispeels, 2001). Por otra parte, el transporte activo, requiere energía en forma de ATP e incluye a las bombas de Ca^{2+} para el transporte de agua (Moraga *et al.*, 2009), a las bombas de Na^{+} para el transporte de azúcares (Zeuthen, 2010) y por último a la bomba de Na^{+}/K^{+} para el transporte de electrolitos (Jaitovich & Bertorello, 2006).

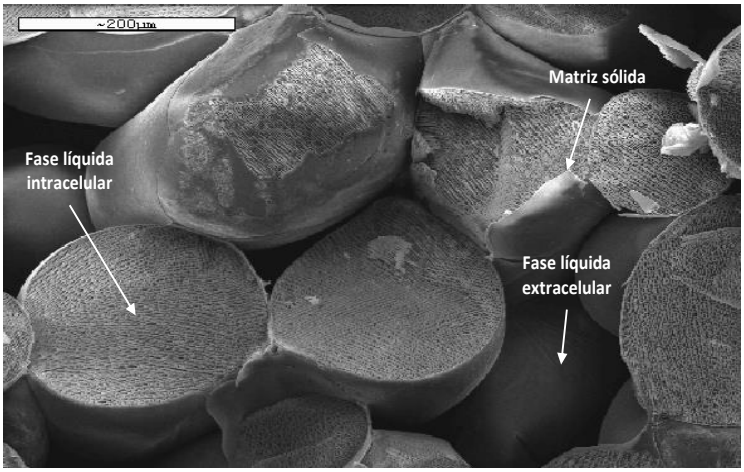

Figura 1.3. Micrografía del tejido parenquimático de manzana "*Granny Smith*" obtenida mediante Cryo-SEM (Adaptado de Fito *et al.*, 2007).

1.2.3. Sistemas Coloidales

Se denomina coloide a todo sistema compuesto por dos o más grupos de especies químicas inmiscibles, pudiéndose deber a insolubilidad o a estados de agregación distintos. Estas estructuras complejas presentan un grupo químico o fase que mantiene continuidad, estando el resto de forma dispersa. Se consideran hidrocoloides alimentarios a los biopolímeros hidrófilos de alto peso molecular utilizados como ingredientes funcionales en la industria alimentaria ya que otorgan características estructurales a los alimentos además de influir en su textura, sabor y mejorar su estabilidad o vida útil (Dickinson, 2003). Los sistemas coloidales se pueden clasificar en función del estado de agregación de la fase continua y de su inmiscibilidad con la fase dispersa, como se puede apreciar en la Tabla 1.1. (Trados, 2013).

Tabla 1.1. Clasificación de los sistemas coloidales

Fase continua	Fase dispersa	Estructura coloidal
Líquido	Líquido	Emulsión
	Sólido	Dispersión
	Gas	Dispersión Espuma
Sólido	Líquido	Emulsión sólida Gel
	Sólido	Suspensión
	Gas	Espumas sólidas
Gas	Líquido	Aerosol
	Sólido	Aerosol

Cabe destacar que las dispersiones coloidales son sistemas termodinámicamente inestables debido a su elevada energía libre superficial (Shaw, 1992). En la presente tesis doctoral

se abordará particularmente el estudio de geles con alta aplicabilidad industrial en la industria alimentaria mediante la encapsulación de compuestos bioactivos en matrices de biopolímeros.

1.3. Espectrofotometría

1.3.1. Principios básicos

Los fotones son partículas elementales con spin nulo que provoca una nula interacción con la malla de Higgs, es decir, sin masa, que por lo tanto no limita su velocidad, manteniéndose siempre a la velocidad de la luz. La falta de spin, de masa y por lo tanto de límite de velocidad provoca que la partícula solo pueda variar su movimiento o energía en su vibración. Dentro del modelo estándar de partícula, los fotones se engloban dentro del grupo de bosones o partículas con capacidad para transmitir alguna fuerza universal, en el caso del fotón las fuerzas electromagnéticas, que representan la vibración de la partícula sobre la malla de Higgs. Los fotones de baja frecuencia, de bajo nivel energético, inducen orientación e inducción en algunas especies químicas. Al generar interacciones de baja energía la penetración que se produce es muy elevada pudiéndose utilizar el efecto de la materia sobre la circulación de fotones para analizar tejidos complejos. Es decir, que mediante el análisis de las propiedades eléctricas y magnéticas de un flujo de fotones cuando atraviesa un sistema biológico (Velázquez Varela, 2014), es posible determinar la cantidad y el estado de las especies químicas que interaccionan con el citado flujo.

Un flujo de fotones genera interacciones eléctricas y magnéticas, pudiéndose cuantificar ambas interacciones mediante las relaciones de Maxwell.

$$\nabla\bar{E} = \frac{-\partial\bar{\mathrm{B}}}{\partial \mathrm{t}} - \bar{\mathrm{M}} \qquad \text{(Ec. 1.1a.)}$$

$$\nabla\bar{H} = \frac{\partial\bar{\mathrm{D}}}{\partial \mathrm{t}} + \bar{\mathrm{J}} \qquad \text{(Ec. 1.1b.)}$$

$$\nabla\bar{D} = \rho \qquad \text{(Ec. 1.1c.)}$$

$$\nabla\bar{B} = 0 \qquad \text{(Ec. 1.1d.)}$$

Donde E es el campo eléctrico, B es el desplazamiento del campo magnético, M es la densidad de corriente magnética, H es el campo magnético, D es el desplazamiento del campo eléctrico, J es la densidad del campo eléctrico y ρ es la densidad de carga eléctrica.

En el caso de la existencia de un medio dieléctrico, se produce una resistencia al flujo de fotones, lo cual provoca que parte se almacene y parte se transforme en otras energías, es por ello que se produce un desplazamiento en el campo eléctrico y/o magnético (Ecuaciones 1.2.) (Traffano-Schiffo *et al.*, 2014a), expresándose como:

$$\overline{D} = \varepsilon^* \cdot \varepsilon_0 \cdot E = (\varepsilon' - \varepsilon'' i)\varepsilon_0 \cdot E \qquad \text{(Ec. 1.2a.)}$$

$$\overline{\mathrm{B}} = \mu^* \cdot \mu_0 \cdot H = (\mu' - \mu'' i)\mu_0 \cdot \mathrm{H} \qquad \text{(Ec. 1.2b.)}$$

Donde D y B son desplazamientos, eléctrico y magnético respectivamente, E y H son los campos eléctricos y magnéticos respectivamente, ε^* se define a la permitividad vectorial del sistema (F/m) y representa a la propiedad física que describe la respuesta de un medio ante el efecto de un campo eléctrico. μ^* representa a la permeabilidad vectorial del sistema (H/m) y describe la respuesta de un medio ante el efecto de un campo magnético.

La cantidad y distribución de la energía eléctrica absorbida por el sistema analizado puede ser explicada mediante las ecuaciones de Maxwell (ecuaciones 1.1). Cuando un flujo de fotones circula a través de un sistema, parte se refleja, parte se transmite y parte se absorbe. La proporción de energía absorbida se define a través de las propiedades dieléctricas y magnéticas. La permitividad vectorial (ε^*) es la propiedad dieléctrica que describe la interacción entre un material y el campo eléctrico producido cuando un flujo de fotones circula a través de él (Castro-Giráldez *et al.*, 2012) y se la define mediante la siguiente ecuación:

$$\varepsilon^* = \varepsilon' - \varepsilon'' i \qquad \text{(Ec. 1.3.)}$$

Dónde: ε' corresponde a la constante dieléctrica y ε'' al factor de pérdidas.

La constante dieléctrica (ε') representa la proporción de energía eléctrica que es almacenada al orientarse el medio respecto a la dirección del campo, y el factor de pérdidas (ε'') representa el desplazamiento del campo inducido por las transformaciones de energía eléctrica en

otras energías. A bajas frecuencias, la interacción entre el medio y el campo genera un aumento en la movilidad molecular, desencadenando entre otros fenómenos colisiones y fricción entre moléculas, disipando la energía eléctrica en forma de energía mecánica y calorífica.

La permitividad vectorial se puede expresar como un número polar, el módulo representa la energía absorbida y el ángulo de pérdidas el desplazamiento del campo eléctrico producido por la interacción de molécula-fotón, induciendo la disipación de energía eléctrica en otras formas de energía como térmica o mecánica (Talens *et al.*, 2016a). La tangente del ángulo de pérdidas se representa mediante la siguiente ecuación:

$$tg\ \delta = \frac{\varepsilon\prime}{\varepsilon\prime\prime} = \frac{|\varepsilon| sen\ \delta}{|\varepsilon| cos\ \delta} \qquad \text{(Ec. 1.4.)}$$

Dentro del factor de pérdidas, las pérdidas de energía eléctrica debido a la vibración de especies químicas con mucha fuerza iónica se denomina conductividad iónica (σ), pudiéndose cuantificar, en el tramo de frecuencia de Hz a 1 GHz, con la siguiente ecuación (Nelson & Datta, 2001):

$$\sigma = \varepsilon_0 \varepsilon'' \omega \qquad \text{(Ec. 1.5.)}$$

Dónde σ presenta unidades de $S \cdot m^{-1}$, $\omega = 2\pi f$ y corresponde a la frecuencia angular en rad/s, la frecuencia f en Hz y ε_0 corresponde a la permitividad del vacío (ε_0=8.8542·10^{-12} $F \cdot m^{-1}$).

1.3.2. Interacciones entre los sistemas biológicos y un flujo de fotones

A lo largo del espectro eléctrico y magnético se producen distintas interacciones entre los fotones y los sistemas biológicos. En el caso del espectro de permitividad vectorial o interacciones eléctricas, es posible diferenciar dos tramos en función del nivel de energía de los fotones, siendo directamente proporcional el nivel de energía a la frecuencia. A bajas frecuencias, comprendidas entre los Hz y los GHz, se producen fenómenos de *orientación e inducción de moléculas iónicas o polares*, mientras que a alta frecuencia se producen fenómenos de *desplazamiento de otras partículas a nivel atómico.*

1.3.2.1. Fenómenos de relajación en el espectro de radiofrecuencia y microondas

La permitividad relativa de materiales biológicos, presentan diferentes dispersiones o interacciones sistema biológico/fotones dependiendo del rango de frecuencia de los fotones que circulan. Dentro de las dispersiones de orientación e inducción es posible distinguir tres dispersiones denominadas α, β y γ (Figura 1.4.), cada una de ellas en un tramo diferente del espectro de permitividades (Schwan, 1988).

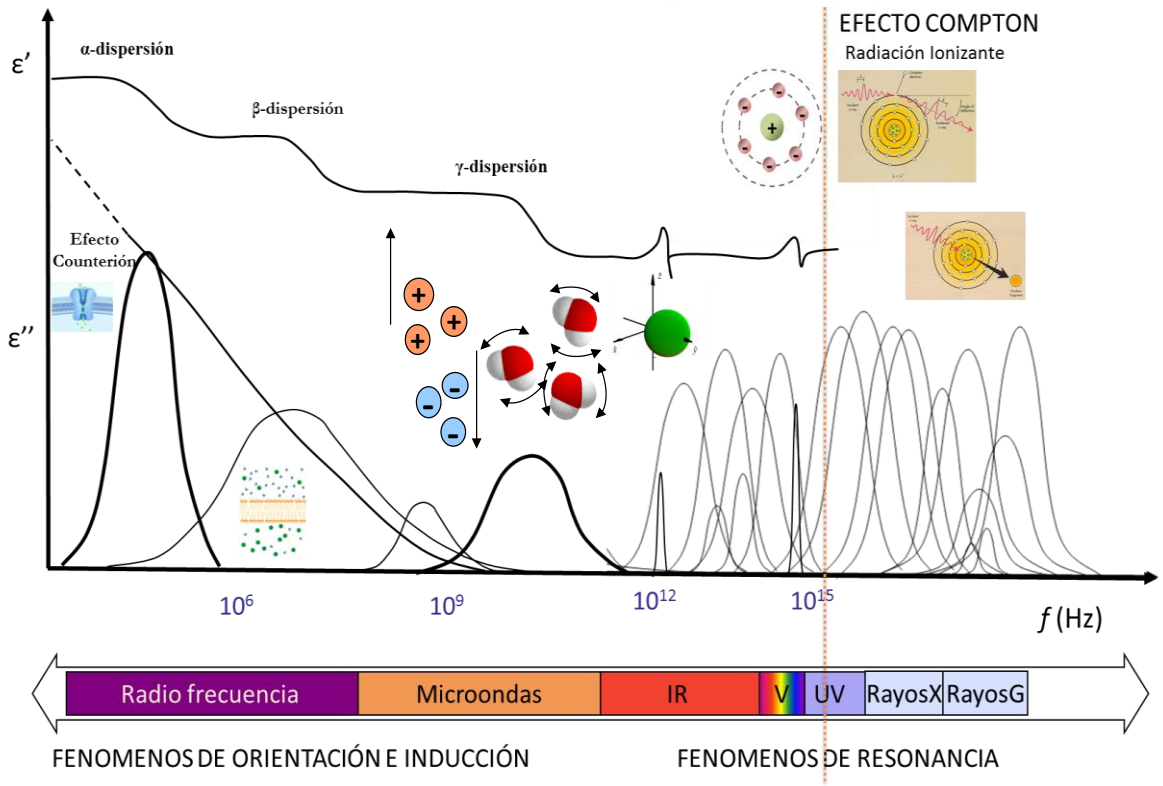

Figura 1.4. Representación de la constante dieléctrica y el factor de pérdidas en sistemas biológicos en función de la frecuencia (Adaptado de Castro-Giráldez *et al.*, 2010e).

La dispersión-α o también conocida como efecto counterion, es producida desde los Hz hasta unos pocos kHz y representa la orientación de las cargas móviles dentro del sistema biológico; en el cual un pequeño cambio en el movimiento de iones producirá un aumento de esta dispersión dieléctrica (Kuang & Nelson, 1997). En ocasiones, la orientación de los iones que poseen una carga determinada induce a una respuesta de movilidad contraria en iones que poseen cargas de signo opuesto, es por ello que esta dispersión también se denomina counterion "ion contra ion" (Foster & Schawn, 1989; Pethig, 1979; Kuang & Nelson, 1997).

La dispersión-β se produce en el rango del espectro de la radiofrecuencia (desde unos pocos KHz hasta los MHz) y describe las interacciones con cargas fijas o de baja movilidad que se encuentran en el sistema biológico. Esta dispersión se divide a su vez en dos tramos, las interacciones en el rango de kHz, en la que se engloban las interacciones con cargas pertenecientes a macromoléculas estructurales que conforman la fase sólida del sistema (cargas fijas), como por ejemplo las proteínas o los hidratos de carbono y el segundo tramo, de mayor energía (MHz) en donde se encuentran las interacciones de cargas asociadas a la tensión superficial o polarizaciones interfaciales de las superficies sólidas en contacto con el medio fluido, fenómeno conocido como efecto Maxwell-Wagner.

Por último, la dispersión-γ, se produce en la región del espectro comprendida entre 1 GHz-300 GHz y es debido a la inducción y orientación de las moléculas dipolares, siendo el agua la molécula más importante en cantidad y disponibilidad (Castro-Giráldez *et al.*, 2010b). Estas moléculas presentan un momento dipolar permanente, orientándose al azar en ausencia de un campo eléctrico. Al someter un sistema biológico a la influencia de un flujo de fotones en el rango espectral de microondas, se genera la orientación del spin de las moléculas dipolares (mayoritariamente moléculas de agua) en la dirección del flujo de fotones o campo eléctrico, así como una inducción o rotación de la molécula alrededor del spin.

Los fenómenos que ocurren en las dispersiones α, β y γ generan una acumulación de energía eléctrica, generada principalmente por la reorientación del spin. Sin embargo, parte de esta energía eléctrica se transforma en otras formas de energías como mecánicas y/o caloríficas, producidas por las colisiones y fricciones asociadas al incremento de la movilidad molecular.

En la Figura 1.5. se puede observar un resumen de todas las dispersiones descriptas anteriormente.

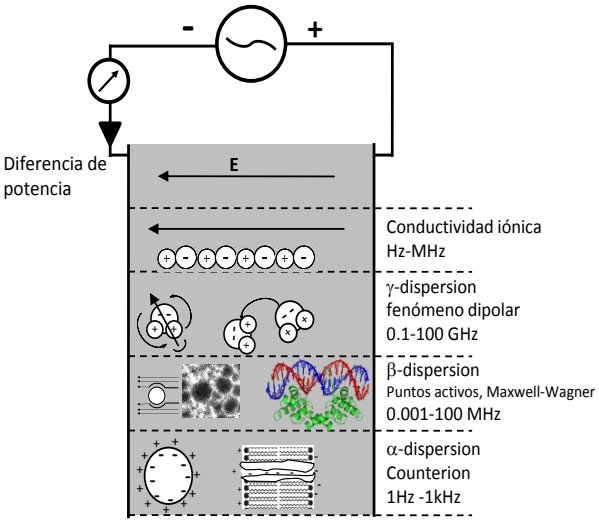

Figura 1.5. Mecanismos de polarización en una célula debido a la aplicación de un campo eléctrico (Adaptado de Castro-Giráldez *et al.*, 2010e).

1.3.2.2. Fenómenos de relajación en el espectro de infrarrojos

El espectro de infrarrojos se encuentra entre 1 a 400 THz, lo que corresponde con 0,78 a 300 μm de longitud de onda. En este tramo del espectro, los fenómenos de interacción de los fotones con la materia son de partícula, es decir, la colisión directa de los fotones con partículas elementales de los átomos. Específicamente en el espectro de infrarrojos (IR), las interacciones del flujo de fotones se producen con el electrón del orbital de valencia, este electrón acumula la mayor parte de energía del átomo, por esa razón cualquier excitación de dicho electrón provoca un aumento en la energía interna del átomo (Figura 1.6.). Hay una gran cantidad de relajaciones en este tramo del espectro, dividiéndose las mismas en tres tramos en función de la proximidad a la frecuencia de visible. Los tramos del espectro de infrarrojo son, FIR (Far Infrared) hasta 1THz, MIR (Middle Infrared) hasta 10 THz y NIR (Near Infrared) hasta 100 THz cruzando el límite del visible.

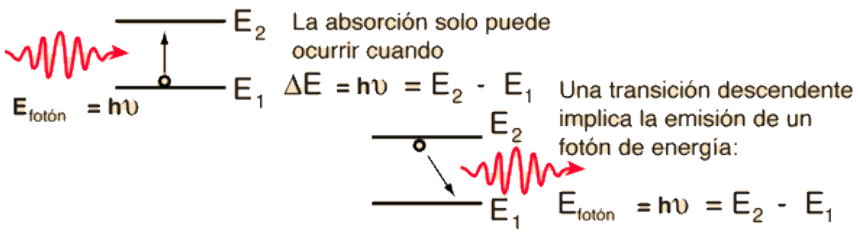

Figura 1.6. A la izquierda: Excitación de un electrón de valencia por colisión de un fotón en espectro de IR, VIS y NUV; A la derecha: Relajación de un electrón de valencia con liberación de un fotón a la energía del citado electrón (Adaptado de Hyperphysics ©C.R. Nave, 2010).

Toda excitación de los electrones de valencia provoca una posterior relajación que genera la emisión de un fotón al nivel de energía del electrón emisor. Este fenómeno se produce en todo el rango de IR, VIS y parte de ultravioleta de baja frecuencia o NUV (Near ultraviolet). De tal manera que, en el espectro IR, todo átomo que recibe un fotón que excite su orbital exterior sufrirá un proceso de relajación posterior asociado a la emisión de un fotón con una energía proporcional a la energía interna del átomo.

Basándose en este principio, a frecuencias de FIR, es posible desarrollar sistemas de recepción de fotones que permitan pronosticar la energía interna del cuerpo emisor.

La termografía infrarroja es una técnica de medición que permite predecir la temperatura de la superficie de un cuerpo mediante la medición del flujo de fotones emitidos por el mismo. Los fotones son absorbidos por los orbitales exteriores de carbonos depositados sobre un conductor denominado pirosensor o detector piroeléctrico cambiando su conductividad eléctrica, a una temperatura constante, la conductividad cambia en función al flujo de fotones que recibe, pudiendo convertir dicha variación en energía recibida.

Sin embargo, toda la energía recibida por el pirosensor, procedente de un cuerpo, no tiene porqué corresponder a la emitida por los orbitales de valencia, y, por ende, representar la energía interna del átomo, ya que además de absorber energía fotónica, la materia también sufre reflexión de parte de los fotones recibidos. Esta reflexión provoca una sobre estimación de la energía del cuerpo emisor. Si denominamos "cuerpo negro" a todo cuerpo que no sufre fenómenos de reflexión o de transmisión, es posible corregir la sobre estimación de energía interna desarrollando una propiedad que describa la relación entre la energía emitida por el cuerpo y la que emitiría si el citado cuerpo no sufriera fenómenos de reflexión o fuera un cuerpo negro, a esta propiedad se la denomina emisividad (ε). Por lo tanto, la cantidad de energía fotónica emitida por un cuerpo depende de su energía interna, cuya variable de estado dependiente es la temperatura y de su emisividad, esta energía fue explicada físicamente por primera vez por Planck en 1905, teniendo en cuenta distintas propiedades de los orbitales y de los fotones. Sin embargo, la ecuación de Stefan y Boltzmann (1884) fue desarrollada con anterioridad como una ecuación

empírica que permitía calcular las energías emitidas por un cuerpo. Hasta 1905, no pudo convertirse en ecuación física, desarrollándose posteriormente la ecuación final de Stefan Boltzmann incluyéndose la emisividad en la misma. Esto dio lugar a la siguiente ecuación:

$$E = \varepsilon \, \sigma \, T^4 \qquad (1.6.)$$

Dónde E, corresponde al flujo de energía recibido por el detector piroeléctrico de la cámara de infrarrojos (W/m^2); ε, a la emisividad (adimensional); σ, a la constante de Stefan-Boltzmann ($5{,}67 \cdot 10^{-8}$ W/m^2K^4) y T, a la temperatura (K).

1.3.2.3. Resonancia magnética nuclear

La Resonancia Magnética Nuclear (NMR) es una técnica espectroscópica que abarca un rango del espectro magnético desde 10 a 800 MHz (radiofrecuencia) (Keeler, 2011) y es considerada como una de las técnicas más importantes en la determinación y cuantificación de moléculas en los sistemas biológicos. Esta tecnología permite obtener información cuantitativa y estructural de cualquier molécula compuesta por átomos que posean permeabilidad vectorial ($\mu+\mu_i$). Los elementos principales de los sistemas biológicos, tales como H, O, P, C y N, presentan al menos un isótopo que puede ser detectable por la NMR, por lo tanto, la aplicabilidad de esta técnica puede considerarse prácticamente ilimitada (Laghi *et al.*, 2014).

En ausencia de un campo magnético impuesto, los spines atómicos se orientan en función de los microequilibrios magnéticos del átomo y de su entorno, teniendo todos niveles de energía similares. Sin embargo, cuando se aplica un campo magnético externo, los núcleos que presentan un spin positivo, se alinean en dirección al campo aplicado, en un estado de mínima energía que se denomina estado de espín α. Por otro lado, los núcleos que se orientan en dirección opuesta al campo magnético son aquellos que presentan un spin negativo o spin β, en un estado de mayor energía. Dependiendo de la intensidad del campo magnético, la diferencia entre los estados de los spines α y β será mayor, es decir, a mayor intensidad de campo magnético, mayor diferencia entre ambos (Moreno Pérez, 2016).

De tal manera que habrá una frecuencia de resonancia o relajación para cada grupo atómico en la cual el paso de un estado α a β u orientación del spin atómico. Al igual que en los fenómenos de relajación eléctricos, en el caso de los fenómenos magnéticos, cuanto mayor sea la intensidad de campo magnético aplicado, mayor será la diferencia de energía entre los dos niveles de spin (Fig. 1.7.).

Figura 1.7. Proceso de resonancia en el rango del espectro de la radiofrecuencia.

Una vez que cesa la aplicación del campo magnético, el spin de los átomos se relajan a su equilibrio nativo o estado de relajación, devolviendo la energía absorbida en la orientación. El proceso de orientación del spin atómico muestra dos tiempos: tiempo de orientación y el tiempo de relajación.

El **tiempo de orientación del spin** (T_1) corresponde al tiempo que transcurre en orientarse verticalmente, mientras que el **tiempo de relajación** (T_2) es el tiempo que tarda en relajarse, a su estado nativo, moviéndose en espiral.

A 20 MHz se encuentra la relajación atómica de los hidrógenos unidos con el oxígeno para formar agua. Es por esto que NMR provee información importante sobre la distribución del agua en el interior de las muestras, del grado de compartimentación de las células y de la dinámica del agua (Bianchi *et al.*, 2004).

1.4. Termodinámica irreversible en sistemas biológicos

El término termodinámica proviene de las palabras griegas *therme* (calor) y *dynamis* (potencia) y es considerada la ciencia de la energía en donde la temperatura (relacionada con el movimiento molecular) cumple un rol fundamental (Demirel, 2013). Los procesos físicos, químicos y biológicos involucrados en la mayoría de los procesos de transformación de la

industria alimentaria abarcan transportes de calor y de materia de forma simultánea (Demirel & Sandler, 2001).

La termodinámica irreversible no lineal es una herramienta que estudia los sistemas no-equilibrados, que involucran fenómenos de transferencia a través de los limites definidos del sistema, así como transformaciones internas, lo cual supone una eficaz herramienta para determinar la evolución de sistemas complejos compartimentados, con especies químicas en constante transformación, como lo son los sistemas alimentarios.

Cuando un sistema es sometido a transformaciones, se rige por los principios de la termodinámica, es por esto que, según el principio cero de la termodinámica, tienden a alcanzar espontáneamente un estado menor de energía, con un estado de mayor desorden molecular o mayor entropía (S). La inercia termodinámica se define como la variación de energía disponible dentro de un sistema para transformarse hacia un nuevo sistema con menor energía, es decir un sistema equilibrado. A la energía disponible dentro de un sistema para transformarse se denomina energía libre (G), pudiéndose cuantificar su evolución dentro de un sistema con la siguiente ecuación (Rao *et al.*, 2014):

$$G = H - TS \qquad \text{(Ec. 1.7.)}$$

Donde G es energía libre de Gibbs, H es entalpia, T temperatura y S entropía. En sistemas compartimentados, multicomponentes y con composición variable (como lo son los alimentos), la energía libre de Gibbs no sólo depende de las variables de estado (temperatura o presión), sino también de los componentes presentes en el sistema [$G = G(P, T, n_i)$]. Si sólo se tiene en cuenta las variables de estado; al derivar la energía libre respecto a las variables de estado, se obtiene la siguiente ecuación conocida como ecuación simplificada de Gibbs-Duhem (Demirel, 2013):

$$\Delta G = -S\Delta T + V\Delta P + \Sigma_i \left(\frac{\Delta G}{\Delta n_i}\right)_{P,T,n_{j\neq i}} \Delta n_i \qquad \text{(Ec. 1.8.)}$$

Sin embargo, otras variables del sistema aportan energía libre al medio, aportando fuerza impulsora al movimiento molecular. Demirel & Sandler (2001) analizaron distintos fenómenos que pueden producir energía libre para distintas especies químicas, desarrollando la siguiente ecuación:

$$\Delta G = -S\Delta T + V\Delta P + F\Delta l + \psi\Delta e + \Sigma_i \mu_i \Delta n_i \qquad \text{(Ec. 1.9.)}$$

Donde los términos $V\Delta P$ y $F\Delta l$ están asociados a los fenómenos mecánicos y estructurales del sistema, siendo F la capacidad de realizar un trabajo mecánico y l las elongaciones que sufre el sistema. Por otro lado, el término $\psi\Delta e$ representa el efecto del campo eléctrico inducido por los iones disueltos, siendo ψ el potencial eléctrico y e, el movimiento de dichas cargas (Talens *et al.*, 2016b; Castro-Giráldez *et al.*, 2010f).

El potencial químico del componente i (μ_i) representa la relación de energía libre por mol del componente i. El potencial químico puede calcularse en condiciones de T, P y número de moles de los componentes diferentes de i se mantienen constantes (Ec. 1.10.), en este caso el potencial químico se calcula con la siguiente ecuación:

$$\mu_i = \left(\frac{G}{n_i}\right)\Big|_{P,T,n_{j\neq i}} = RT \ln a_i \qquad \text{(Ec. 1.10.)}$$

Siendo R la constante de los gases ideales (0,08205746 atm L/mol K), T la temperatura (K) y a_i la actividad de la especie química estudiada, definida como la fugacidad de la especie i respecto a la fugacidad en condiciones de máxima movilidad.

Sin embargo, cuando las variables de estado dejan de ser constantes, el potencial químico de una especie debe contemplar las variaciones de energía libre del sistema (ecuación 1.9). Al tener en cuenta dichas variaciones se obtiene la siguiente ecuación también denominada ecuación de Gibbs-Duhem extendida, que permite calcular la verdadera fuerza impulsora del movimiento molecular.

$$\Delta\mu_i = \frac{\Delta G}{\Delta n_i} = -\bar{s}_i\Delta T + \bar{v}_i\Delta P + \bar{F}_i + \bar{\psi}_i\Delta e + \mu_i|_{P,T,n_{j\neq i}} + \Sigma\,\mu_j|_{P,T,n_{i\neq j}} \qquad \text{(Ec. 1.11.)}$$

En 1931, L. Onsager estableció una relación para los sistemas multicomponentes, en donde el flujo de la especie química i (J_i) se relaciona de manera lineal con todas las fuerzas impulsoras al movimiento molecular (X_i) mediante la siguiente expresión:

$$J_i = \sum_j L_{ij} X_j \qquad \text{(Ec. 1.12.)}$$

Donde L_{ij} corresponde a una constante cinética denominada coeficiente fenomenológico, que describe la relación entre el medio y la especie química para moverse a través del mismo.

Desde el punto de vista de la termodinámica irreversible no lineal, la primera relación de Onsager describe al flujo de una determinada especie química i como la relación entre el coeficiente fenomenológico de dicha especie a través de un medio determinado y el potencial químico de dicha especie química; obteniendo la siguiente expresión:

$$J_i = L_i \Delta \mu_i \qquad \text{(Ec. 1.13.)}$$

1.5. Operaciones de transformación

1.5.1. Isotermas de sorción

La relación de equilibrio entre el contenido de agua de un sistema y su a_w, a temperatura constante, se define como Isoterma de Sorción (Lewicki, 1997). Las isotermas de sorción son consideradas una herramienta eficaz capaz de predecir las reacciones que afectarían a la estabilidad de los alimentos a una determinada humedad (Bell & Labuza, 2000) y permiten relacionar el grado de interacción que existe entre el agua y la matriz.

Las isotermas de sorción son no lineales y generalmente poseen una forma de sigmoide, aunque esto puede variar de acuerdo a la composición química y al estado fisicoquímico de los constituyentes del alimento (Barbosa-Cánovas *et al.*, 2008). Es por ello, que varios modelos matemáticos basados en ecuaciones empíricas o semiempíricas han sido propuestos (Iglesias & Chirife, 1995), tales como el modelo de Guggenheim, Anderson and de Boer (GAB), el de Brunauer-Emmet-Teller (BET), de Oswin, de Smith, entre otros (Andrade, 2011).

El modelo de BET desarrollado en 1938 (Brunauer *et al.*, 1938), permite estimar el valor de la humedad adsorbida de la monocapa, y por lo tanto predecir la estabilidad física y química de los alimentos deshidratados mediante la siguiente ecuación:

$$X_w^{ADS} = \frac{X_{w0}\ C\ a_w}{(1-a_w)(1+(C-1)\ a_w)} \qquad \text{(Ec. 1.14.)}$$

Donde X_w^{ADS} corresponde a la humedad adsorbida ($kg_w/kg_{materia\ seca}$), X_{w0} a la humedad monomolecular ($kg_w/kg_{materia\ seca}$) y C es la constante de energía (adimensional).

El modelo de GAB, extensión del modelo de BET, ha sido ampliamente utilizado para el análisis de los alimentos y es considerado uno de los más versátiles debido a su simplicidad y significado físico (Lewicki, 1997) y se basa en un modelo de sorción semi-teórico, multimolecular, localizado y homogéneo (Al-Muhtaseb *et al.*, 2002). Este modelo posee muchas ventajas ya que es capaz de describir el comportamiento de sorción en un amplio rango de a_w (0 – 0.9) y ha sido demostrada su aplicabilidad en más del 75% de frutas, carnes y vegetales (Lomauro *et al.*, 1985), sus parámetros poseen un significado físico que permiten describir el efecto de la temperatura a través de las ecuaciones del modelo de Arrhenius (Andrade *et al.*, 2011).

La ecuación de GAB posee sólo tres parámetros en su ecuación y se describe como (Timmermann *et al.*, 2001):

$$X_w = \frac{X_{w0}\ C\ k\ a_w}{(1-k\ a_w)(1-k\ a_w+C\ k\ a_w)} \qquad \text{(Ec. 1.15.)}$$

Donde X_w corresponde al contenido de humedad ($kg_w/kg_{materia\ seca}$), X_{w0} al contenido de humedad de la monocapa ($kg_w/kg_{materia\ seca}$) y C y k son constantes de adsorción (adimensionales), las cuales se encuentran relacionadas con las energías de interacción entre la primera y las siguientes moléculas en los sitios de sorción individuales. De forma teórica dichas constantes se relacionan con entalpías de sorción.

1.5.2. Secado por aire caliente

El secado de alimentos es una de las operaciones unitarias más utilizadas para preservar los productos en el tiempo. Este proceso es promovido por la diferencia de potencial químico que

existe cuando el producto es expuesto a un fluido (aire caliente) con un potencial químico menor, por ende, el agua migra desde el interior del alimento hacia la superficie, donde se evapora y se transporta hacia el medio. Durante este proceso, se llevan a cabo cambios estructurales en el sistema, siendo que además se producen transferencias de calor y de masa de forma simultánea.

Según la teoría tradicional, el secado consta de tres etapas básicas: Período de inducción o de velocidad de secado creciente, período de velocidad de secado constante y período de velocidad de secado decreciente. Durante el *primer período* o *período de inducción*, se acoplan distintos mecanismos de transporte de agua promovido por la diferencia de potencial químico entre el alimento y el aire caliente, el producto se calienta y aumenta la temperatura de la interface, por lo tanto, el flujo de calor se emplea tanto para calentar el sólido como para evaporar agua. Durante la *segunda etapa*, la velocidad con que se elimina agua de la superficie del sólido es menor que la velocidad con que llega desde el interior del mismo, por lo tanto, la superficie del alimento se mantiene en la temperatura húmeda. Es decir, todo el calor que llega al sólido se emplea en evaporar el líquido, por ende, no existe transporte de calor en el seno del sólido y la velocidad a la cual el agua se evapora depende sólo de la velocidad con que llega al calor de cambio de estado.

A medida que transcurre el tiempo, el sólido se va secando hasta que llega un momento en que la velocidad con que el agua llega a la superficie se hace menor que la velocidad de evaporación. El contenido de humedad en dicho instante es lo que se conoce como HUMEDAD CRITICA (X_{wc}).

Por último, en la etapa de *velocidad de secado decreciente*, el proceso de transferencia de materia interno no es suficientemente rápido como para transportar toda el agua que se puede evaporar y por lo tanto el calor recibido del aire se emplea en el cambio de estado del agua y en el aumento de la temperatura de la superficie del sólido. La curva típica de secado se puede observar en la Figura 1.8. (Fito *et al.*, 2001).

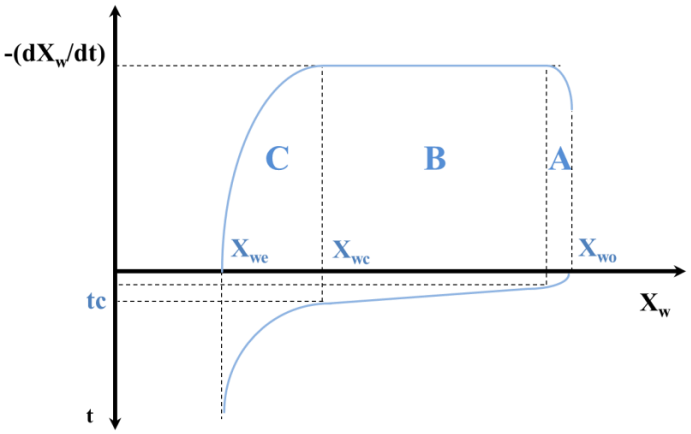

Figura 1.8. Curva típica de secado de materiales húmedos. A. Período de Inducción, B. Período de Velocidad Constante, C. Período de velocidad decreciente.

Se define a la velocidad de secado como la velocidad con que disminuye la humedad del producto, y está dada por la siguiente ecuación:

$$-(dX_w/dt) = f(X_w) = vs \qquad \text{(Ec. 1.16.)}$$

Desde el punto de vista termodinámico, en una operación de secado por aire caliente a una temperatura inferior a la del cambio de estado del agua (Traffano-Schiffo *et al.*, 2014b) y a partir de la ecuación 1.11. es posible calcular el gradiente de potencial químico del agua a través de la interfase aire caliente/alimento, como:

$$\Delta\mu_w = \frac{\Delta G}{\Delta n_i} = \bar{v}_w \Delta P - \bar{s}_w \Delta T + RT ln \frac{\varphi}{a_w} \qquad \text{(Ec. 1.17.)}$$

Donde φ es la humedad relativa del aire caliente expresada en tanto por uno.

Un gradiente de potencial químico del agua induce una inercia termodinámica que impulsa el transporte de agua (líquido) del alimento al aire caliente (gas) lo cual implica un cambio de estado, es decir requiere un aporte de energía tal que induzca el cambio de estado. Dicha energía generalmente se obtiene de la energía interna del aire (Talens, 2015).

El flujo de agua puede calcularse con la siguiente ecuación:

$$J_w = \frac{\Delta M_w M_0}{\Delta t\ A\ Mr_w} \qquad \text{(Ec. 1.18.)}$$

Dónde J_w corresponde al flujo de agua (mol/s m^2), ΔM_w representa la variación de masa de agua (adimensional), M_0 representa la masa inicial de la muestra (g), Δt es el tiempo de proceso (s), A es el área de la muestra (m^2) y, por último, Mr_w corresponde con la masa molecular del agua (18 g/mol).

Una vez calculado J_w, es posible obtener mediante la relación de Onsager, el coeficiente fenomenológico a partir del potencial químico del agua a través de la interfase aire/alimento (ecuación 1.17.).

1.5.3. Deshidratación Osmótica

La deshidratación osmótica (OD) es una técnica de conservación ampliamente utilizada que consiste en la reducción de la actividad de agua de los alimentos mediante su inmersión en soluciones hipertónicas (Castro-Giráldez *et al.*, 2011c). La diferencia del potencial químico del agua entre la fase líquida interna y la solución osmótica promueve el flujo de agua desde el interior del alimento hacia dicha solución y de forma simultánea un flujo de soluto desde el exterior al interior (Tylewicz *et al.*, 2011). La velocidad de transporte del agua del interior del tejido depende de varios factores como: el tamaño y la geometría del material, la temperatura y la concentración de la solución osmótica, el ratio entre la muestra y la solución y el nivel de agitación de esta última (Rastogi *et al.*, 2002).

La transferencia de materia durante el proceso de deshidratación en vegetales se lleva a cabo a través de diferentes vías en el tejido (Rastogi *et al.*, 2002); las vías apoplásticas o espacios extracelulares, por donde el transporte es rápido y normalmente asociado a gradientes químicos o de actividad, las vías simplásticas o vías a través de las células vegetales conectadas a través de canales denominados plasmodesmos, y por último los transportes transmembrana. Los transportes transmembrana se producen a través de los canales proteicos que pueden funcionar de manera pasiva a través de gradientes de potencial químico, como por ejemplo los *aquaporins*, proteínas transmembrana que permiten el paso libre de las moléculas de agua, o pueden funcionar a costa del consumo de ATP, como por ejemplo las bombas de Ca^{2+} para el transporte de agua, las

bombas Na^+, en el transporte de azucares C6 o las bombas Na^+/K^+ para el transporte de iones (ver Figura 1.9.).

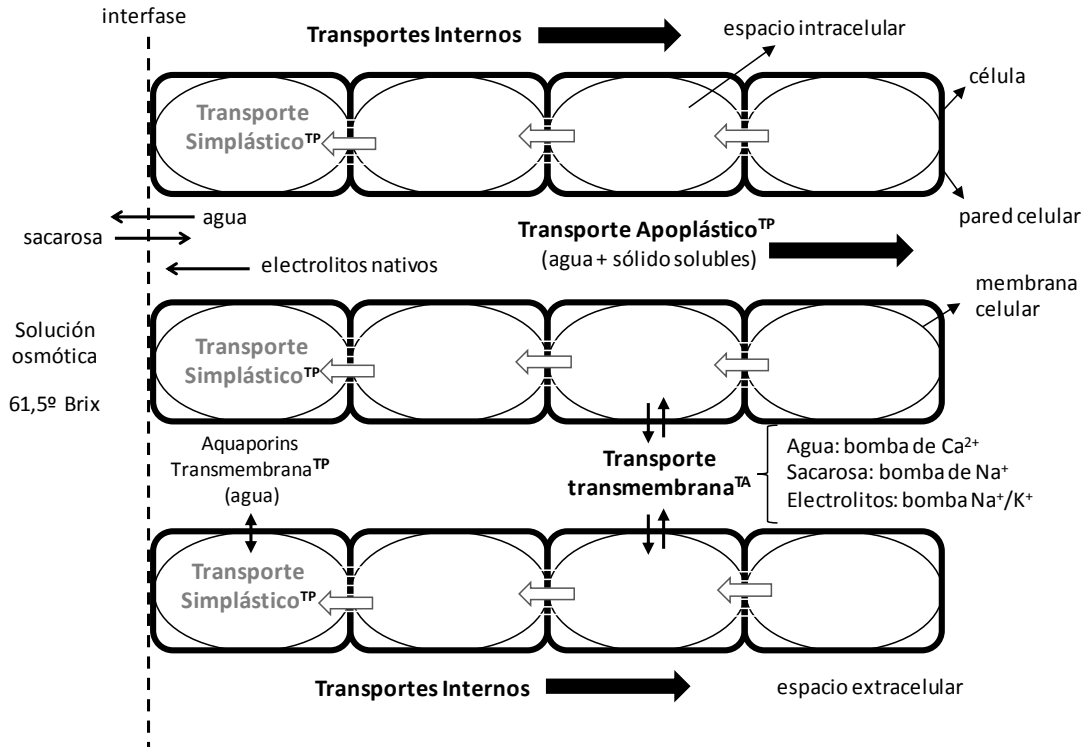

Figura 1.9. Representación esquemática de los transportes celulares durante la deshidratación osmótica. TP: transporte pasivo, TA: transporte activo (Adaptado de Traffano-Schiffo *et al.*, 2016, 2017).

En el caso de deshidratación osmótica con azúcares en tejido vegetal, el gradiente de potencial químico del agua a través de la interfase disolución osmótica/alimento se puede calcular con la siguiente ecuación:

$$\Delta\mu_w = \frac{\Delta G}{\Delta n_w} = -\bar{s}_w \Delta T + \bar{v}_w \Delta P + \bar{F}_w \Delta l + \mu_w|_{P,T,n_{j\neq i}} + \Sigma\, \mu_s|_{P,T,n_{i\neq j}} \quad \text{(Ec. 1.19.)}$$

Simplificándose de manera general a sistemas isotermos:

$$\Delta\mu_w = \bar{v}_w \Delta P + \bar{F}_w \Delta l + TR\frac{a_w^e}{a_w^i} + TR\frac{a_s^e}{a_s^i} \cdot \frac{dn_s}{dn_w} \quad \text{(Ec. 1.20.)}$$

La OD tiene como principal objetivo aumentar la vida útil de frutas y vegetales, aumentando la estabilidad y calidad del producto final. Sin embargo, esta técnica también ha sido utilizada como pre-tratamiento del secado por aire caliente (Fernandes *et al.*, 2006; Mandala *et al.*,

2005), secado combinado de aire caliente y microondas (Yousefi *et al.*, 2013; Torringa *et al.*, 2001) y congelación (Zhao *et al.*, 2014; Goula & Lazarides, 2012).

1.5.4. Campos Eléctricos Pulsantes

Los Campos Eléctricos Pulsantes o en inglés Pulsed Electric Fields (PEF) es una tecnología no térmica que consiste en someter a los alimentos a pulsos eléctricos cortos, generados entre dos electrodos (Dellarosa *et al.*, 2016) con una duración de micro a milisegundos (Puértolas *et al.*, 2012). El efecto del PEF se basa en los cambios estructurales que se producen a nivel celular al hacer pasar a través de ella un campo eléctrico de alta intensidad. En los sistemas biológicos, la membrana celular es una barrera semipermeable considerada como un capacitor natural de la célula presentando una diferencia de potencial de 10 mV cuando existe una acumulación de cargas opuestas a ambos lados de la misma (Singh & Heldman, 2001).

Cuando dicho sistema es sometido al efecto de un campo eléctrico, las líneas de fuerza provenientes de dicho campo generarán un cambio en la conformación eléctrica del sistema, lo cual romperá el equilibrio natural del mismo y provocará la ruptura de la membrana celular, conocida como electroporación.

La electroporación es un fenómeno físico que tiene efecto sobre la bicapa lipídica de la membrana celular. Esta bicapa es susceptible a la influencia de un campo eléctrico debido principalmente a las cargas o los dipolos dieléctricos de las moléculas lipídicas y a la permeabilidad de la misma a los iones. La aplicación de un campo eléctrico de alta intensidad provoca la debilitación de las cargas internas de los fosfolípidos en un punto determinado de la membrana y como consecuencia, los mismos tienden a reorientarse y acumularse entre sí a fin de aumentar la fuerza de su carga. Esto provoca la aparición de poros hidrofílicos afectando a la permeabilidad de la membrana (Tsong, 1991). Un esquema representativo de este fenómeno se puede observar en la siguiente figura:

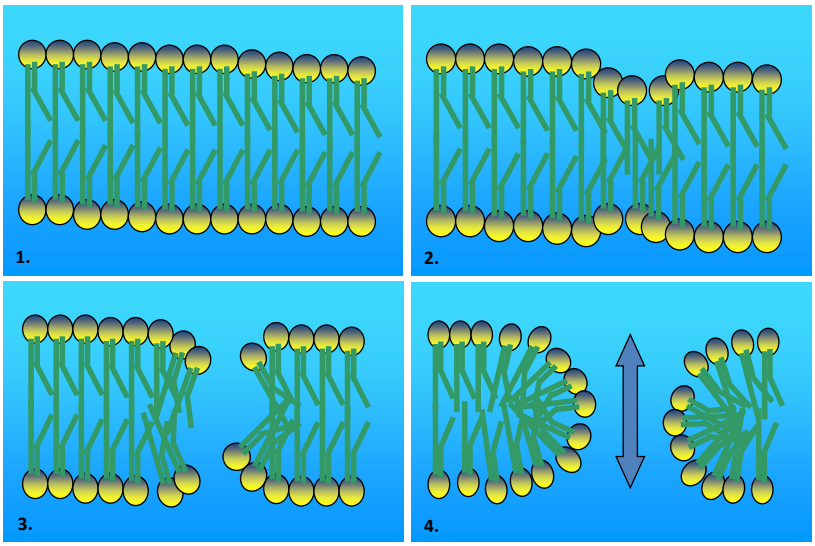

Figura 1.10. Fenómeno de electroporación de la bicapa lipídica (Adaptado de Traffano-Schiffo *et al.*, 2016).

Otra forma de electroporación de la membrana es la electrocompresión. Cuando el alimento es sometido a un campo eléctrico externo, las cargas eléctricas (electrolitos como Na^+ o K^+) a ambos lados de la membrana celular se incrementan generando una diferencia de potencial a través de ella. Dichas cargas se atraen entre sí, por lo que la membrana se comprime y su espesor original (4 nm) se reduce. Las fuerzas elásticas de la membrana se oponen a la compresión eléctrica, pero cuando la acumulación de cargas el tal que supera el punto límite de elasticidad, se generan poros en ella debido a la disrupción de la misma (Calderón-Miranda *et al.*, 1998).

Dependiendo de la intensidad del campo eléctrico aplicado y del número de pulsos, la electroporación puede ser reversible o irreversible (Knorr *et al.*, 2001). Si la intensidad del campo eléctrico (E) alcanza valores cercanos al valor crítico (E_c) y se aplican unos pocos pulsos, la ruptura de la membrana celular es reversible, permitiendo a la misma recuperar tanto su estructura como su funcionalidad cuando cesa la aplicación de dicho campo. Sin embargo, si el tratamiento aplicado es más intenso (E>>Ec), el proceso es irreversible produciéndose la desintegración de la membrana y, por ende, la pérdida de su funcionalidad (Mahnič-Kalamiza *et al.*, 2014; Donsì *et al.*, 2010; Singh & Heldman, 2001; Zimmermann, 1986).

Para calcular el campo eléctrico crítico capaz de producir la ruptura de la membrana, Zimmermann et al. (1996) utilizaron una membrana celular simulada, sobre la cual aplicaron

diferentes gradientes de voltaje, dando como resultado que la aplicación de diferencias de potencial eléctrico entre 5 mV a 1 V a 20 ºC y 1,2 V a 4 ºC son capaces de producir la desestructuración de la misma. Si el espesor medio de la bicapa fosfolipídica es de 4 nm (Briegel et al., 2009) y es considerada como un sistema de platos paralelos, el valor del campo eléctrico crítico se encuentra entre 12,5 kV/cm y 2,13 MV/cm a 2 ºC y 3 MV/cm a 4 ºC. Sin embargo, se ha demostrado la aplicación de PEF a bajas intensidades como pre-tratamiento de la deshidratación osmótica produce algunos efectos en el transporte químico. Rastogi et al. (1999) han demostrado que con la aplicación de campos eléctricos entre 0,22 y 1,6 kV/cm es posible acelerar la transferencia de agua en zanahorias. Taiwo et al. (2001) han conseguido aumentar la pérdida de agua, alterando mínimamente la estructura de las manzanas mediante la utilización de un campo eléctrico con una intensidad de 1,4 kV/cm a 40 ºC. Por último, Tedjo et al. (2002) han obtenido una reducción en la humedad sin alterar el sabor de los mangos mediante la aplicación de 1 a 3 kV/cm a 40 ºC.

La aplicación de PEF en el procesado de los alimentos ha obtenido gran popularidad a lo largo de los últimos años ya que al ser un tratamiento no térmico evita la degradación de productos termolábiles como vitaminas (Vega-Mercado *et al.*, 2007) y mantiene en gran medida el color, textura y sabor de los alimentos (Calderón-Miranda *et al.*, 1998).

En el caso de los alimentos líquidos las principales aplicaciones incluyen la inactivación microbiana total o parcial (Sharma *et al.*, 2014; Heinz *et al.*, 2003; Wouters & Smelt, 1997; Grahl & Märkl, 1996; Qin *et al.*, 1994; Zhang *et al.*, 1994), la inactivación enzimática total o parcial (Leong *et al.*, 2014; Yang *et al.*, 2004), el aumento del rendimiento en la producción de zumos y la mejora en la extracción de compuestos tales como antioxidantes y colorantes (Luengo *et al.*, 2015; Azmir *et al.*, 2013; Luengo *et al.*, 2013; Corrales *et al.*, 2008; López *et al.*, 2008). En el caso de alimentos sólidos se utiliza como pre-tratamiento para acelerar la transferencia de materia en procesos como secado (Shynkaryk *et al.*, 2008; Lebovka *et al.*, 2007; Arevalo *et al.*, 2004; Ade-Omowaye *et al.*, 2001), deshidratación osmótica (Dellarosa *et al.*, 2016; Amami *et al.*, 2006; Amami *et al.*, 2005; Rastogi *et al.*, 1999), congelación (Ammar *et al.*, 2010; Jalté *et al.*, 2009; Phoon *et al.*, 2008), etc. (Donsì *et al.*, 2010; Bouzrara & Vorobiev, 2003; Rastogi *et al.*, 2002; Knorr & Angersbach, 1998).

1.5.5. Encapsulación de compuestos bioactivos en matrices de biopolímeros

Existen diferentes métodos para llevar a cabo la encapsulación de compuestos bioactivos en matrices de biopolímeros, los cuales pueden generar micro o macrocápsulas. Para la obtención de microcápsulas se suelen utilizar técnicas como por el secado por atomización (Estevinho *et al.*, 2013; 2015), mientras que, para obtener cápsulas de mayor tamaño, el método más comúnmente utilizado debido a su sencillez, es el método por goteo (Austin *et al.*, 1996; Santagapita *et al.*, 2012). En este último, utilizando una aguja se realiza un goteo de la solución que contiene al polímero en presencia de la biomolécula de interés sobre una solución de $CaCl_2$ en agitación continua y termostatizada, para así obtener estructuras esféricas (Gombotz, & Wee, 2012). El diámetro de las cápsulas se puede regular ajustando parámetros como la viscosidad de la solución y el diámetro de la aguja (Santagapita, 2010). El alginato de sodio es uno de los hidrogeles más utilizados para la encapsulación debido a sus óptimas propiedades de gelación en presencia de cationes divalentes como el Ca^{2+}.

A nivel estructural, el alginato de sodio consiste en polímeros lineales que contienen monómeros de ácido β-D-manurónico (M) y ácido α-L-gulurónico (G) (Figura 1.11.) unidos covalentemente por enlaces α (1→4) en diferentes secuencias o bloques, compuestos por las mismas unidades (MMMMM o GGGGGGG) o de manera alternada (GMGMGM); la cantidad relativa de cada monómero y la distribución espacial de los mismos depende de la naturaleza del biopolímero (Sonego *et al.*, 2016; Aguirre Calvo, 2013).

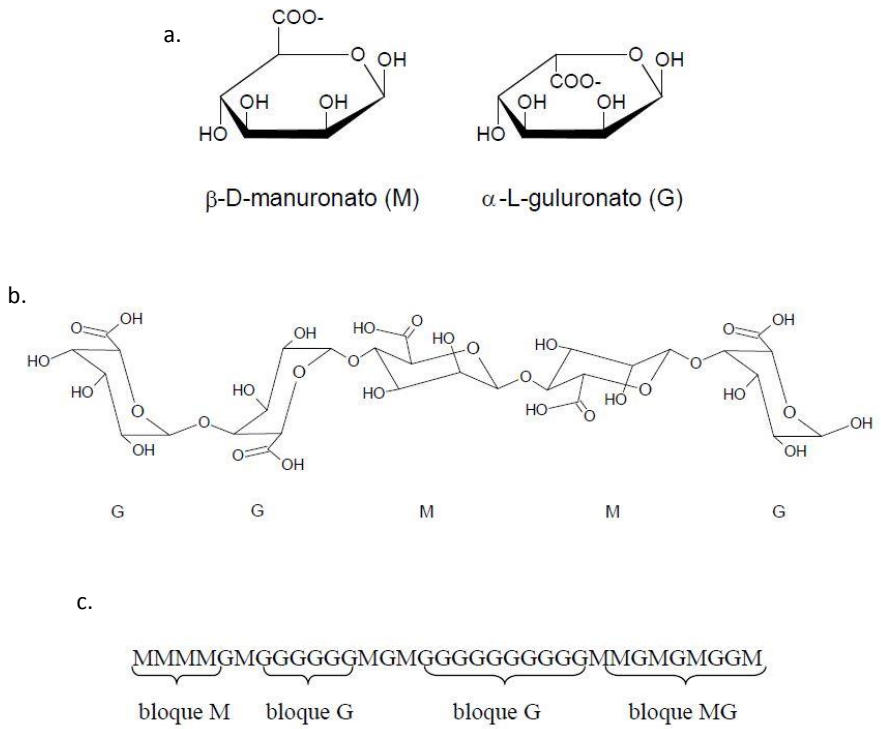

Figura 1.11. Estructura del alginato de sodio. a. monómeros: residuos manuronato y guluronato; b. posibles combinaciones entre los residuos en conformación silla; c. distribuciones de bloques posibles (Adaptado de Santagapita, 2010).

En presencia de iones Ca^{2+}, se produce un intercambio de iones Na^{+} que se encuentran atraídos a los ácidos carboxílicos de los bloques G, por iones Ca^{2+} de la solución de reticulación o entrecruzamiento (Zhang *et al.*, 2016). El bloque-G de una de las cadenas forma uniones con el bloque-G de una cadena polimérica adyacente, obteniendo de esta forma la estructura característica de "caja de huevo" (Zeeb *et al.*, 2015; Lee, & Mooney, 2012). Un esquema representativo del entrecruzamiento se puede observar en la Figura 1.12.

Un estudio reciente realizado mediante microscopia electrónica de tinción negativa ha revelado que también los residuos de los bloques-M interactúan en la estructura de caja de huevo, otorgándole una mayor flexibilidad y permitiendo de esta manera una mayor interacción de los bloques-G (He *et al.*, 2016).

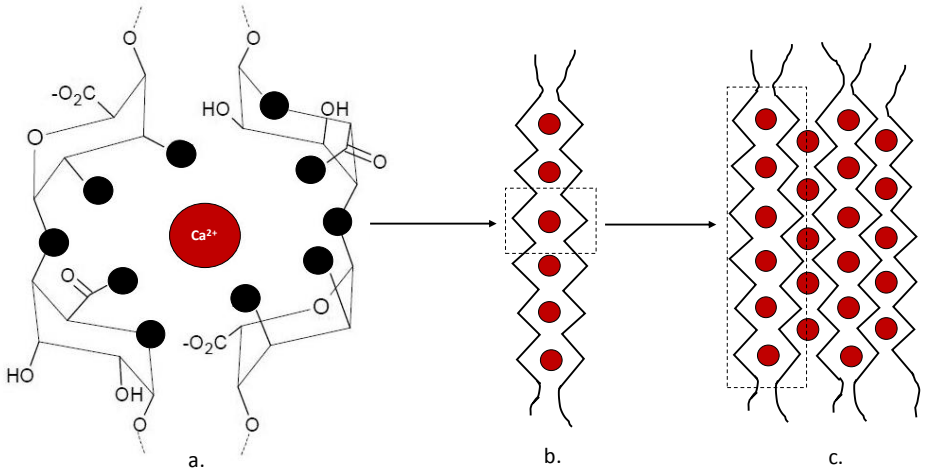

Figura 1.12. Esquema representativo del proceso de entrecruzamiento del alginato-Ca(II), a. coordinación del ion Ca^{2+} dentro de la cavidad creada por las cadenas de bloques guluronato (G); b. dímero con estructura "caja de huevo"; c. asociación lateral de más cadenas y gelificación. (●) representan a los átomos de oxígeno posiblemente involucrados en la coordinación con los iones (●) Ca^{2+} (Adaptado de Fang *et al.*, 2007).

1.6. Problemáticas Industriales

1.6.1. Problemáticas en la Industria Avícola

La producción de aves en España ha seguido su tendencia alcista en estos últimos años, hasta alcanzar las 1,418 Mt en 2014, de las cuales un 86% corresponde a la producción de carne de pollo o broiler, según datos del Ministerio de Agricultura, Alimentación y Medio Ambiente (2015). El sector avícola es uno de los principales motores económicos de la ganadería española, con un valor de producción aproximada de 2.500 millones de euros. La carne de pollo es considerada como un alimento básico y fuente económica y sana de proteína. Es la carne más consumida en fresco y la segunda en consumo total tras la carne de porcino. Este aumento en la producción del sector avícola ha sido posible mediante una fuerte tecnificación, profesionalización e intensificación del sector, así como una fuerte selección genética para alcanzar una alta velocidad de crecimiento y un buen rendimiento de la canal (Kijowski *et al.*, 2014). Esto ha dado lugar a un incremento en la incidencia de problemáticas de calidad como Carnes Pálidas, Suaves y Exudativas (PSE) y Oscuras, Firmes y Secas (DFD) y de la aparición de fisiopatías internas como la miopatía del pectoral profundo y estriado pectoral.

Por otro lado, la gran producción de carne fresca, y en algunos casos excesiva y/o la necesidad de conservación por largos períodos obliga a las empresas a utilizar metodologías de conservación con el fin de evitar su deterioro, siendo éste un producto altamente perecedero. Actualmente, el proceso de congelación es un método ampliamente utilizado en la industria cárnica con la finalidad de extender la vida útil, además de mantener en gran medida su valor nutricional y sus características organolépticas (Castro-Giráldez *et al.*, 2014). Sin embargo, muchas veces este proceso no está controlado o inclusive se abusa de él ya que, en algunos casos, carnes que se venden como frescas, han sido sometidas a uno o varios ciclos de congelación/descongelación.

La presente tesis doctoral busca solventar en cada una de las problemáticas mencionadas anteriormente. Se aborda en profundidad cada una de las temáticas de tal forma de comprender cambios estructurales, bioquímicos y físicos-químicos. Además, se plantea para cada uno de los casos, el desarrollo y la aplicación de sensores no destructivos basados en la espectrofotometría para poder detectar cada una de las problemáticas.

1.6.1.1. Carnes PSE, Normal y DFD

Una de las problemáticas más frecuentes a las que se debe enfrentar de forma diaria la industria cárnica es la determinación de carnes PSE y DFD, las cuales provocan problemas de calidad y de estabilidad en productos elaborados. Esta problemática ha sido estudiada por numerosos autores en el caso de la carne de cerdo (Castro-Giráldez *et al.*, 2010c; Castro-Giráldez, *et al.*, 2010d; Bendall & Swatland, 1988, Honikel & Fischer, 1977); sin embargo, existe muy poca bibliografía disponible con respecto a la carne de pollo.

La carne de pollo es considerada como "normal" cuando su pH se encuentra entre valores de 5.8 y 6.1 a 12 horas post-mortem (Zhang & Barbut, 2005a, b). La carne PSE se caracteriza por un pH significativamente menor, mayor valor del parámetro L* de color, textura suave y una baja capacidad de retención de agua (Barbut *et al.*, 2005). La principal causa de este defecto de la carne está asociada con la susceptibilidad hereditaria del estrés porcino, relacionado con el gen recesivo Halotano (asociado a la hipertrofia muscular) (Barbut *et al.*, 2008), más comúnmente observado

en animales mejorados genéticamente (Hernández Cázares, 2010). Otras causas que provocan carnes PSE están relacionadas con manejos inadecuados durante el transporte, manipulación y sacrificio de los animales, lo cual provoca una glucólisis post-mortem acelerada o ampliada (Barbut *et al.*, 2008). Estas características hacen que este tipo de carnes no sean aptas para la elaboración de productos (Castro-Giráldez *et al,* 2010c; Damez *et al.*, 2008). Existen informes científicos que demuestran que la incidencia de la carne de pollo PSE es superior que 37% (Woelfel *et al.*, 2002; Woelfel *et al.*, 1998).

En contraste, la carne DFD se caracteriza por un color oscuro y una vida útil más corta debido al alto valor de pH (Allen *et al.*, 1997), siendo susceptibles de contaminación. Esta problemática se debe principalmente a un estrés crónico prolongado, tales como períodos de transporte largos, que agotan el glucógeno muscular, y por lo tanto la caída en el pH está limitada por la cantidad de glucógeno disponible. Además de los problemas de contaminación, otro factor importante es el color oscuro debido principalmente al pH, el cual se encuentra alejado del punto isoeléctrico de las proteínas musculares y, por lo tanto, la mioglobina se desnaturaliza en menor medida (Hernández Cázares, 2010), afectando consecuentemente al color de los productos transformados y la aceptabilidad del consumidor (Chan *et al.*, 2011).

1.6.1.2. Miopatía del Pectoral Profundo

La miopatía pectoral profundo o en inglés Deep Pectoral Miopathy (DPM) es una necrosis isquémica que se desarrolla en el músculo pectoral profundo (*supracoracoideus* o *pectoralis minor*) principalmente porque está rodeado de una fascia inelástica y del esternón, los cuales no permiten que la masa muscular se hinche en respuesta a los cambios fisiológicos que ocurren cuando los músculos se ejercitan, por ejemplo, durante el aleteo. Se ha estimado que, en los pavos y pollos de engorde, los *pectoralis minor* aumentan alrededor de un 20% de su peso durante el aleteo debido al enorme flujo de sangre que se produce en el músculo (Petracci & Cavani, 2011). Las lesiones a menudo afectan a ambos solomillos y varían de color, evolucionando de una apariencia rosa hemorrágica a una coloración gris verdosa.

A nivel industrial, las miopatías son clasificadas en tres categorías (Figura 1.13.) en base a su apariencia visual (Bilgili & Hess, 2008). La primera categoría involucra muestras que presentan una lesión inflamatoria aguda en la que el músculo pectoral profundo aparece con coloración rojiza, inducida por una hemorragia interna. Las hemorragias también se aprecian en la envoltura fibrosa. Esto produce una supuración de fluido seroso en la zona dañada, lo que le da una apariencia húmeda a la lesión. En la segunda categoría, la lesión en el *Pectoralis minor* aparece bien definida y, en ocasiones, rodeada de un anillo hemorrágico y coágulos de sangre. En estas dos categorías, si el animal sigue vivo, el músculo puede recuperar su capacidad fisiológica y mecánica. La tercera categoría se caracteriza por la presencia de áreas con necrosis muscular, con una degradación progresiva y una coloración verde en el tejido muscular dañado. Esta zona verdosa y necrótica, persistirá y, con el tiempo, reducirá su tamaño gradualmente al irse reabsorbiendo. El color verde característico de esta lesión es producto de la ruptura de la hemoglobina y mioglobina, al descomponerse en sales biliares.

Figura 1.13. Categorías del *Pectoralis minor* afectado por la miopatía del pectoral.

En la industria avícola, los músculos afectados se desechan durante el deshuesado, lo cual produce pérdidas en el producto comercializable. Sin embargo, la cuestión fundamental de la DPM es que, si las aves se comercializan enteras el problema rara vez es detectado durante su procesado, ya que la pechuga queda en el interior de la canal y no se aprecia su baja calidad ni su mal aspecto, con las consiguientes quejas del consumidor, y la dificultad de identificar la causa del problema. Esta enfermedad no está relacionada con ningún agente infeccioso y, por consiguiente, no tiene mayor trascendencia para la salud pública, con la excepción de la apariencia antiestética y de baja calidad de la carne y la consiguiente mala imagen que ello otorga a los productores.

1.6.1.3. Fisiopatía de las Estrías blancas "White Striping"

La problemática de las estrías blancas es una condición que al igual que la miopatía del pectoral profundo descrita en el apartado anterior se presenta en pollos de engorde y que se caracteriza por la aparición de estrías blancas en dirección paralela a la de las fibras musculares. Se considera que la principal causa de aparición de esta problemática es el aumento del volumen de los músculos del pollo en la mitad del tiempo comparando con animales que no presentan dicha anomalía (Petracci *et al.*, 2013).

En función a una evaluación visual de la intensidad de las estrías blancas, las pechugas (*Pectoralis major*) se pueden clasificar en tres categorías: normal cuando el tejido no está afectado (Figura 1.14a.), moderado cuando los espesores de las estrías son menores a 1mm y severo cuando las estrías cubren la mayor parte de la superficie del tejido y su espesor es mayor a 1 mm (Figura 1.14b.) (Kuttappan *et al.*, 2013; Kuttappan *et al.*, 2012a).

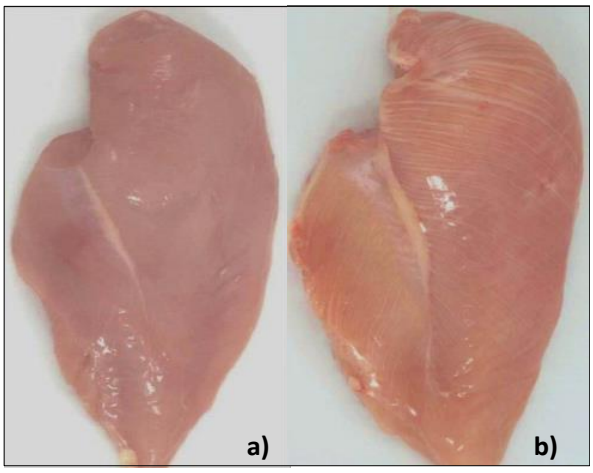

Figura 1.14. Fisiopatía de estrías blancas en pechugas de pollo, siendo a. pechuga normal y b. pechuga con estrías blancas (Adaptado de Kuttappan *et al.*, 2012b).

Kuttappan y colaboradores, (2012b) han demostrado que la decisión de los consumidores se ve significativamente influenciada por el aspecto del producto y que esto afecta en gran medida a su decisión de compra. Sin embargo, el impacto visual no es el principal problema; la problemática de las estrías blancas afecta a la composición química de la carne: el contenido de proteínas disminuye mientras existe una tendencia opuesta con respecto al contenido de grasa. Es

por ello, que la presencia de esta fisiopatía decrece el valor nutricional general de la carne (Petracci *et al.*, 2014).

1.6.2. Detección de semillas en mandarinas enteras

La industria citrícola se ve sometida a un mejoramiento tecnológico constante con el objetivo de hacer frente a un mercado cada vez más globalizado y exigente en cuanto a la calidad de los frutos. Un parámetro de calidad muy perseguido en la industria de los cítricos es la ausencia de semillas en las mandarinas tanto para el consumo interno como para las exportaciones. Por esta razón, se requiere variedades sin semillas, de naturaleza partenocárpica. Sin embargo, dicha condición se ve condicionada por la presencia de insectos polinizadores los cuales transportan el polen de unas plantaciones a otras, produciéndose la polinización y fecundación cruzada, lo cual conlleva a la formación de semillas en el fruto y donde su calidad se ve nuevamente reducida. Es por ello, que la detección en línea de los frutos que contienen semillas es de gran importancia.

1.6.3. Conservación de biomoléculas en hidrogeles mediante encapsulación

Actualmente, la utilización de geles para la conservación de biomoléculas lábiles como las enzimas está siendo ampliamente estudiada. Una enzima con gran aplicabilidad en la industria alimentaria y también farmacéutica es la β-galactosidasa o lactasa. Esta enzima es capaz de catalizar la bioconversión de lactosa en glucosa y galactosa. En los últimos años, se han reportado distintas aplicaciones de esta enzima como la revalorización del suero de la leche obtenido durante la producción de quesos mediante la utilización de β-galactosidasa, logrando reducir el impacto ambiental y otorgando un valor agregado a un subproducto industrial (Banaszewska *et al.*, 2014); se ha logrado mejorar la cremosidad en helados y el dulzor en productos lácteos debido a la hidrólisis de la lactosa (Rosenberg, 2006) y además se han mejorado la producción y formulación de productos lácteos frescos libres de lactosa de tal forma de satisfacer las necesidades de las personas intolerantes (Zhang *et al.*, 2017; Erich *et al.*, 2015; Zhang *et al.*, 2016). En este contexto, la encapsulación de lactasa en hidrogeles de tal forma de aumentar su estabilidad y vida útil es de gran importancia (Zhang *et al.*, 2016; Estevinho *et al.*, 2015; Santagapita, 2010).

Como ya se ha mencionado anteriormente, el alginato de sodio es uno de los biopolímeros ampliamente utilizados para la encapsulación de biopolímeros debido óptimas propiedades de gelación, su carácter no tóxico y su bajo coste (Aguirre Calvo *et al.*, 2017). Sin embargo, presenta desventajas, tales como baja resistencia a tratamientos térmicos de conservación como la liofilización, el secado a vacío o la congelación (Santagapita *et al.*, 2011; 2012). Es por ello, que la encapsulación de compuestos lábiles se suele llevar a cabo en presencia de disacáridos crioprotectores como la trehalosa (Giulio *et al.*, 2005). El efecto crioprotector de la trehalosa (β-D-glucopiranosil-(1,1)-β-D-glucopiranósido) puede ser atribuido a la formación de sistemas vítreos, evitando las reacciones deteriorativas (Mazzobre *et al.*, 2002). Por otra parte, se ha demostrado que la adición de otros biopolímeros a la formulación como goma arábiga (polisacárido del tipo arabinogalactano-proteína) o goma de guar (galactomanano) como ingredientes secundarios de la matriz aumenta la estabilidad de los sistemas encapsulados (Busch *et al.*, 2017; Aguirre Calvo, & Santagapita, 2016; Li *et al.*, 2008). Por ello, un estudio de la posibilidad de mejorar la aplicabilidad tecnológica de esta enzima mediante su inclusión en biopolímeros ha adquirido un gran interés para distintos sectores de la industria. En este contexto, la presente tesis no sólo aborda un análisis fundamental de la viabilidad de encapsulación y su microestructura mediante la utilización de técnicas como dispersión de rayos-X a bajo ángulo y microscopía electrónica de barrido, sino que además se estudia la aplicación de NMR como técnica espectrofotométrica de monitorización y análisis.

2. Objetivos y Plan de Trabajo

2.1. Objetivos

2.1.1. Objetivo General

El objetivo general de la presente tesis doctoral consiste en estudiar la viabilidad de la espectrofotometría de baja frecuencia como herramienta de monitorización no destructiva y en línea, y como sistema de tratamiento y transformación de sistemas alimentarios.

2.1.2. Objetivos Particulares

Para poder cumplimentar el objetivo general planteado, se propusieron los siguientes objetivos particulares subdivididos por tipo de sistema alimentario estudiado:

Tejido Animal

1. Desarrollo de un sistema de monitorización del ***secado por aire caliente*** de ***carne de cerdo*** mediante termografía infrarroja y espectrofotometría en el rango de microondas.

2. Desarrollo de un sensor no destructivo en el rango de la radiofrecuencia para la detección de ciclos de ***congelación/descongelación*** y el tiempo de almacenamiento en congelación de ***carne de cerdo.***

3. Estudio espectrofotométrico (en los rangos de radiofrecuencia y microondas) de ***carne fresca de pollo*** para clasificarla en función a su calidad: Normal; Pálida, Blanda y Exudativa (PSE); y Oscura, Firme y Seca (DFD).

4. Desarrollo de una metodología analítica capaz de clasificar en categorías las pechugas de pollo que han sufrido la ***Miopatía del pectoral profundo (DPM).*** Desarrollo de un sensor no destructivo en el rango de la radiofrecuencia capaz de detectar carcasas de pollo enteras (con piel) afectadas por DPM.

5. Análisis composicional y estructural de las pechugas de pollo que sufren de la fisiopatía de ***estrías blancas o "White Striping".*** Desarrollo de un sensor no destructivo en el rango de la radiofrecuencia capaz de detectar esta fisiopatía en carcasas de pollo enteras y con piel.

Tejido Vegetal

6. Caracterización ***espectrofotométrica*** los tejidos que componen la ***mandarina***. Análisis fisicoquímico y microestructural de cada tejido y su relación con la permitividad.

7. Análisis termodinámico del efecto de los ***campos eléctricos pulsados*** (PEF) en la transferencia de materia como pre-tratamiento de la deshidratación osmótica de ***kiwis orgánicos***. Análisis de la **redistribución del agua** en el tejido mediante **resonancia magnética nuclear**.

Sistema Coloidal

8. Estudio de la encapsulación de la enzima β-galactosidasa en ***hidrogeles de alginato-Ca(II)*** con y sin el agregado de excipientes secundarios (trehalosa, goma arábiga y goma guar). Análisis microestructural mediante ***dispersión de rayos-X de bajo ángulo (SAXS)***. Análisis de estabilidad enzimática frente a tratamientos térmicos. Análisis de los sistemas mediante **resonancia magnética nuclear (NMR).** Estudio de la cinética de transporte mediante ***SAXS***.

2.2. Plan de Trabajo

A continuación, se presenta una tabla a modo de resumen de la tesis doctoral con las distintas técnicas y tratamientos utilizados en función de los sistemas alimentarios estudiados.

Tabla 2.1. Resumen de tecnologías y tratamientos estudiados para cada sistema alimentario.

<table>
<tr><th></th><th></th><th colspan="5">Tecnología</th></tr>
<tr><th></th><th>Materia Prima</th><th>RF</th><th>MW</th><th>IR</th><th>NMR</th><th>SAXS</th></tr>
<tr><td rowspan="5">Tejido Animal</td><td rowspan="2">Cerdo (Longissimus dorsi)</td><td></td><td colspan="3">HAD: 40ºC; 1,5 m/s</td><td rowspan="5"></td></tr>
<tr><td colspan="3">Congelación: -40ºC, IQF</td></tr>
<tr><td rowspan="3">Pollo (Pectoralis)</td><td colspan="3">Calidades (Normal, PSE, DFD)</td></tr>
<tr><td colspan="3">Detección DPM</td></tr>
<tr><td colspan="3">Detección White Striping</td></tr>
<tr><td rowspan="2">Tejido Vegetal</td><td>Mandarina (Citrus Clementina)</td><td colspan="3">Caracterización de tejidos</td><td rowspan="2"></td></tr>
<tr><td>Kiwi Orgánico (Actinidia deliciosa)</td><td colspan="3" rowspan="2"></td><td>PEF (100, 250, 400 V/cm) OD (Sol: 61,5 ºBrix Sacarosa, 25ºC)</td></tr>
<tr><td>Sistema Coloidal</td><td>Hidrogeles de Alginato-Ca(II)</td><td colspan="2">Encapsulación: β-Galactosidasa</td></tr>
</table>

Para alcanzar los objetivos particulares propuestos para esta tesis, el plan de trabajo se subdividió en **8 planes experimentales** que se explican a continuación.

Tejido Animal

1. Estudio de la evolución del proceso de secado de carne de cerdo mediante termografía infrarroja y espectrofotometría.

A continuación, se presenta un diagrama de flujo del plan experimental llevado a cabo:

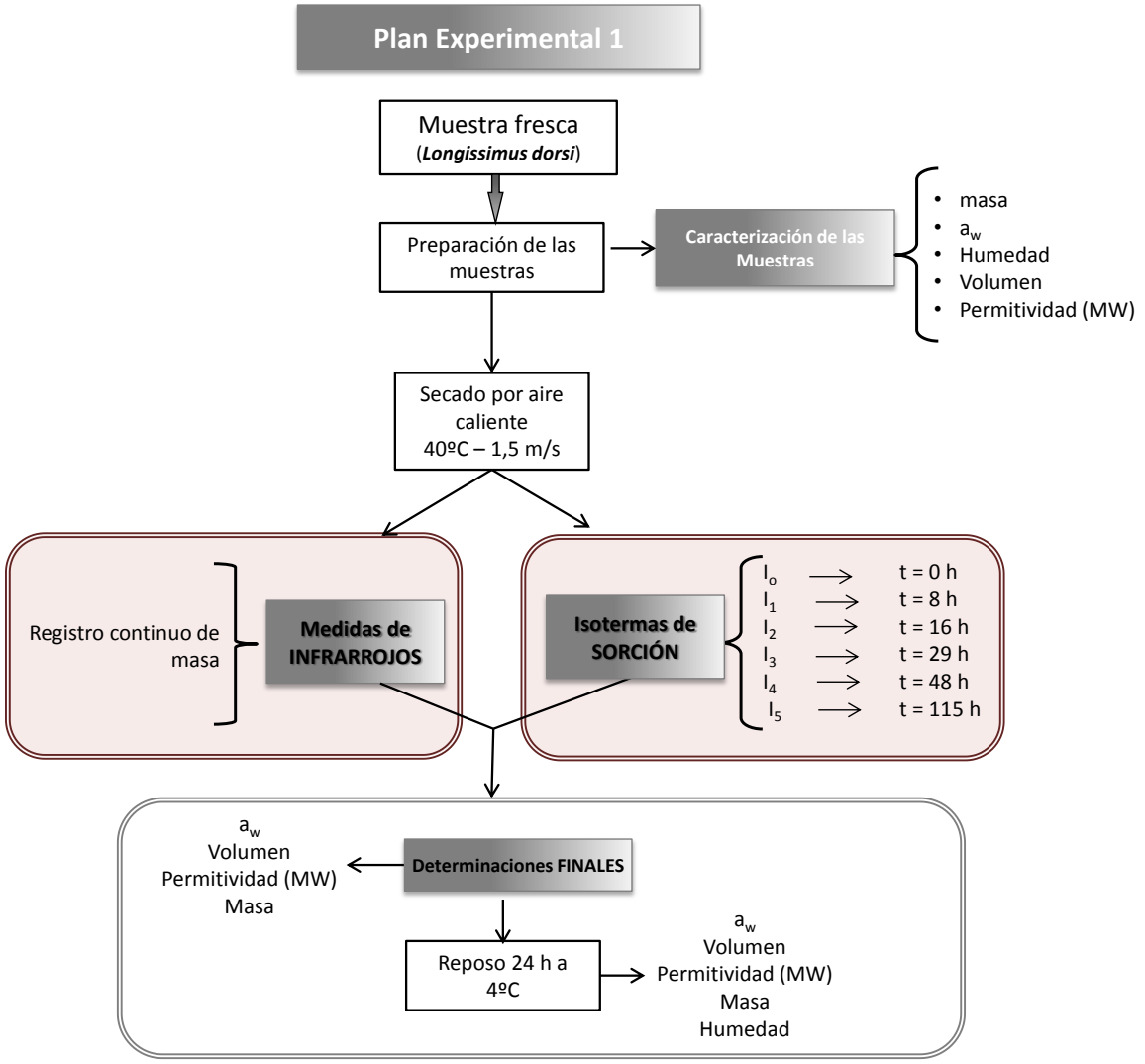

2. *Desarrollo de un sensor no destructivo en el rango de la radiofrecuencia para la detección de ciclos de congelación/descongelación en la carne de cerdo.*

A continuación, se presenta un diagrama de flujo con el plan experimental desarrollado:

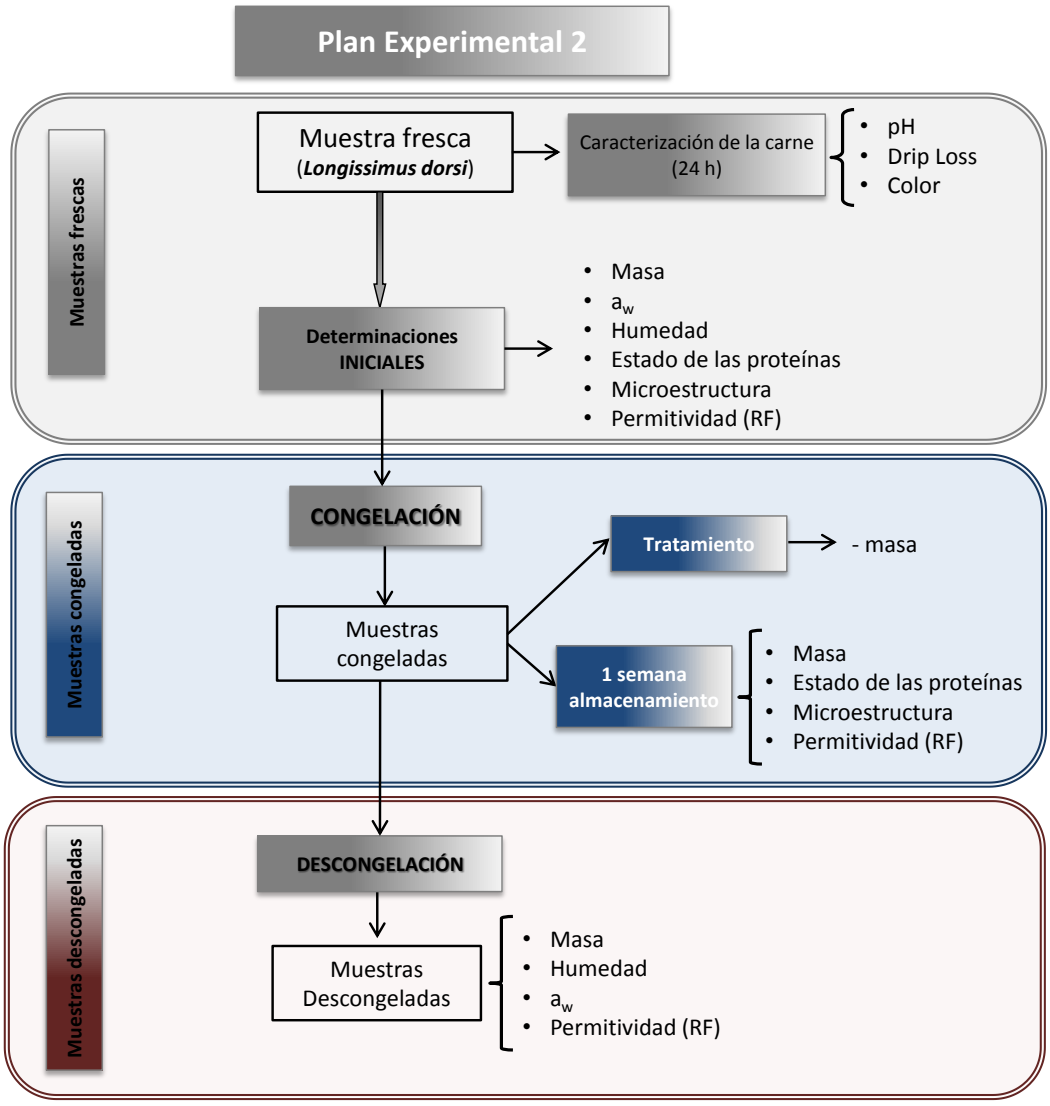

3. Estudio espectrofotométrico de carne fresca de pollo para clasificarla en función a su calidad: Normal; Pálida, Blanda y Exudativa (PSE); y Oscura, Firme y Seca (DFD).

El plan de trabajo llevado a cabo ha sido el siguiente:

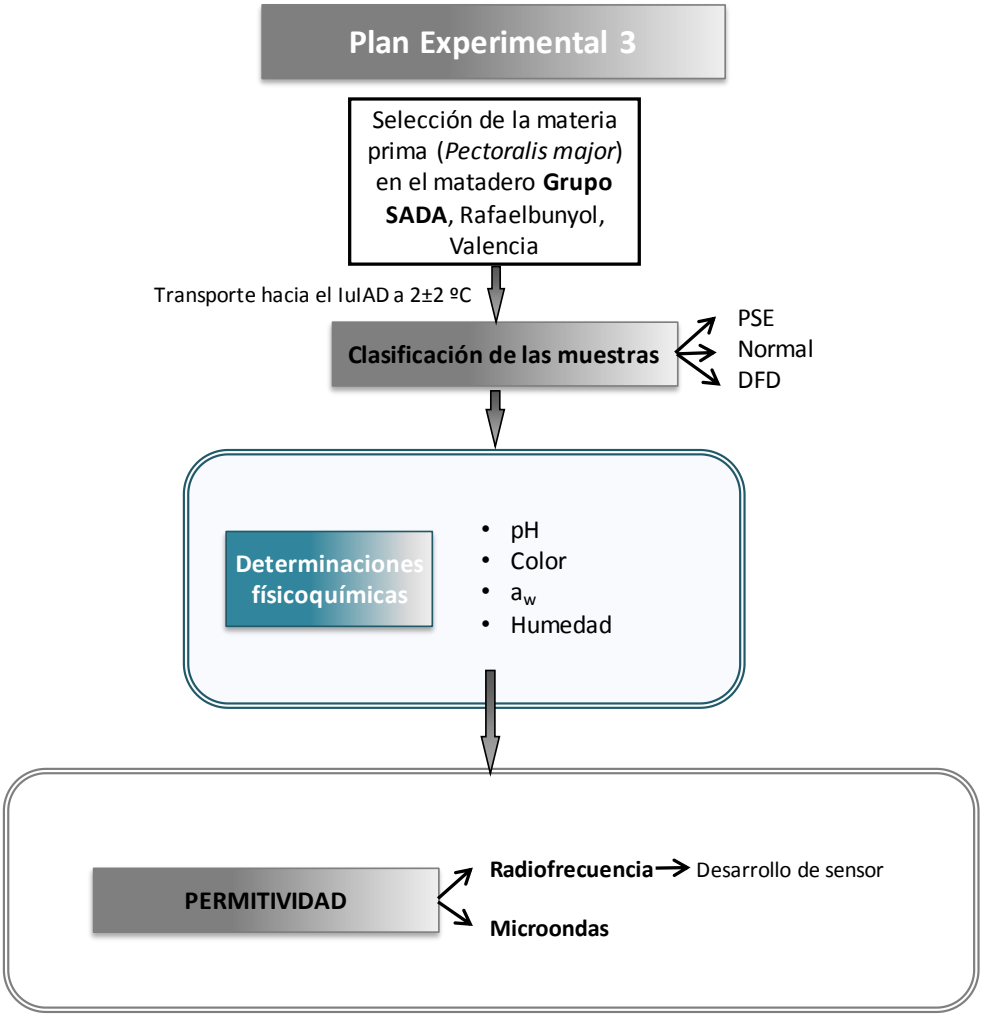

4. Desarrollo de una metodología analítica para clasificar las pechugas de pollo que han sufrido la Miopatía del Pectoral Profundo (DPM). Desarrollo de un sensor no destructivo capaz de detectar carcasas de pollo enteras (con piel) afectadas por DPM.

El plan de trabajo es el siguiente:

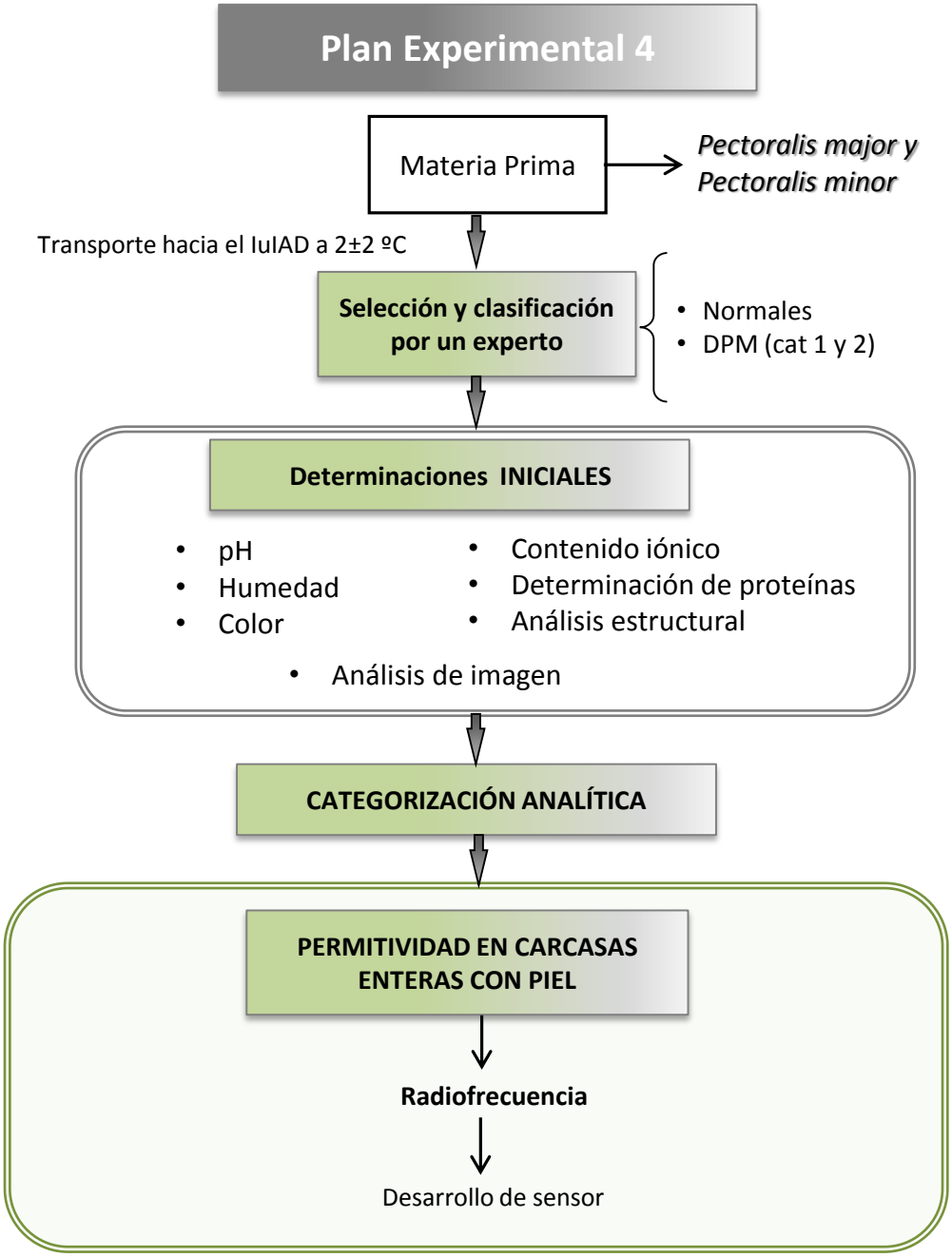

5. *Estudio de pechugas de pollo afectadas por las estrías blancas (White Striping). Desarrollo de un sensor no destructivo capaz de detectar WS en carcasas de pollo enteras (con piel).*

El plan experimental se explica a continuación:

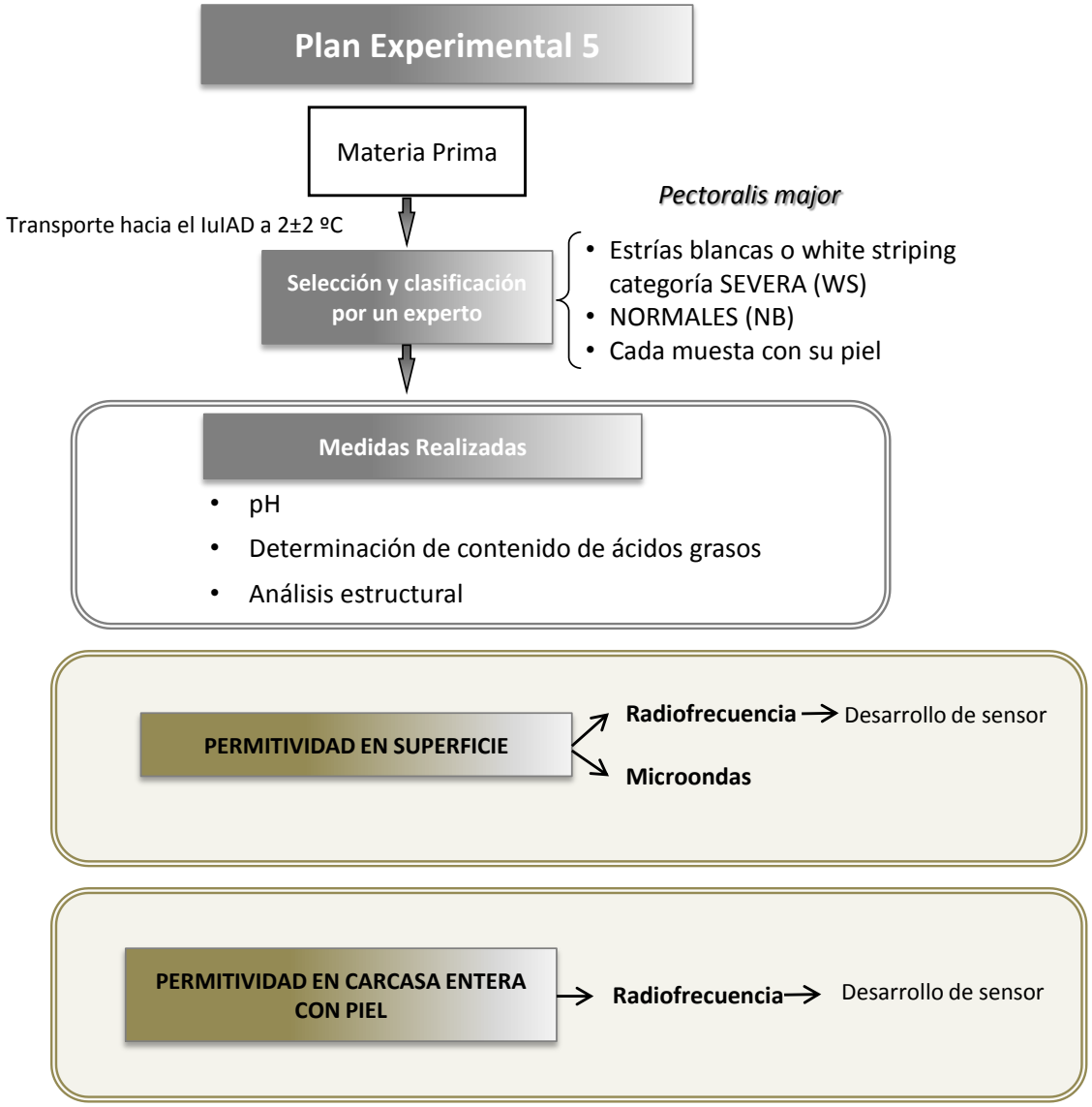

Tejido Vegetal

6. Caracterización dieléctrica de los tejidos que componen a la mandarina.

El plan experimental consiste en:

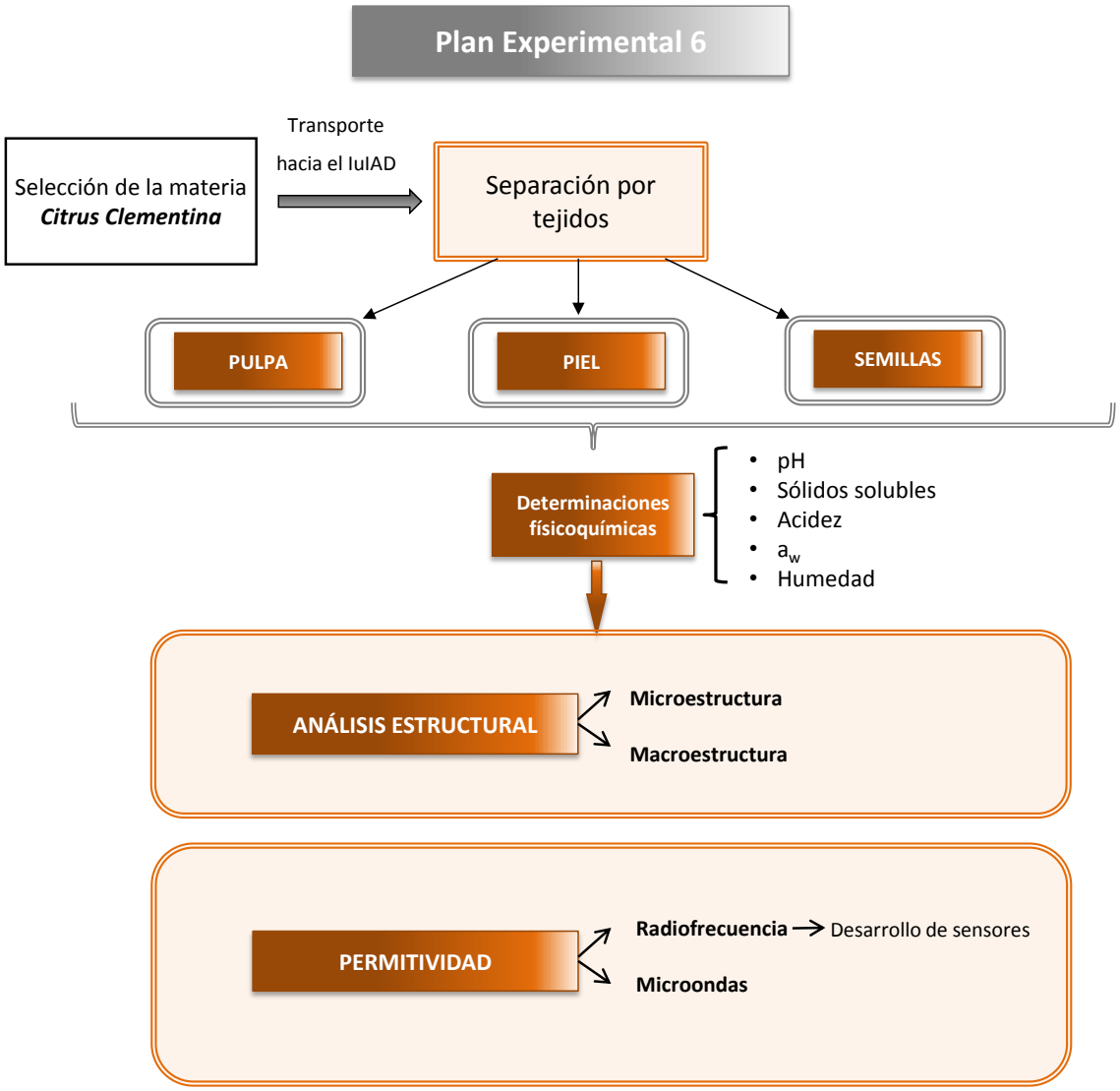

7. Estudio de los campos eléctricos pulsados (PEF) como pre-tratamiento de la deshidratación osmótica de kiwis orgánicos. Análisis termodinámico y monitorización por NMR. Análisis de la redistribución del agua.

El plan experimental 7 se explica a continuación en forma de diagrama de flujo:

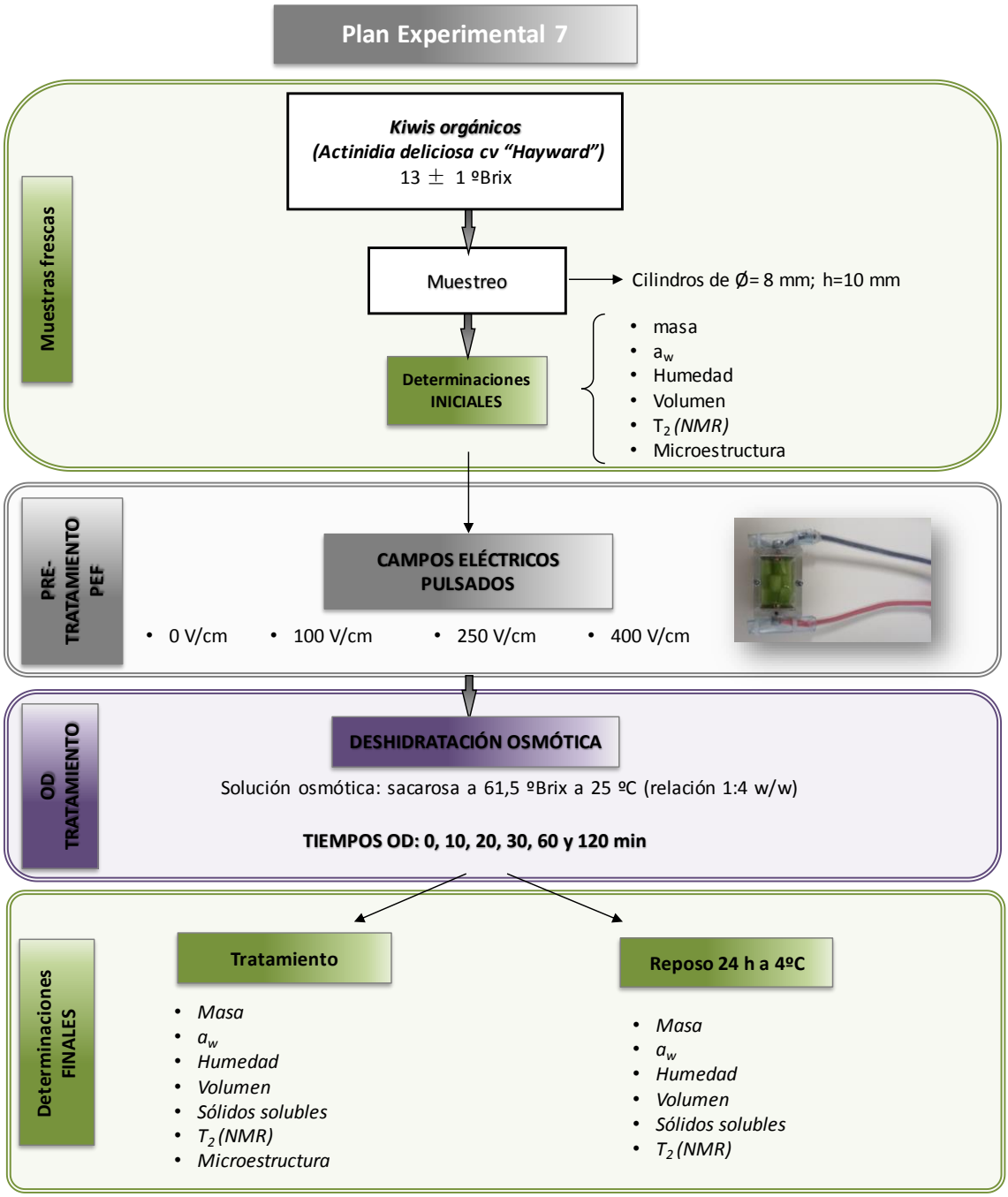

Sistema Coloidal

8. ***Estudio de la encapsulación de β-galactosidasa en hidrogeles de alginato-Ca(II) con y sin el agregado de trehalosa, goma arábiga y goma guar.***

El plan experimental llevado a cabo es el siguiente:

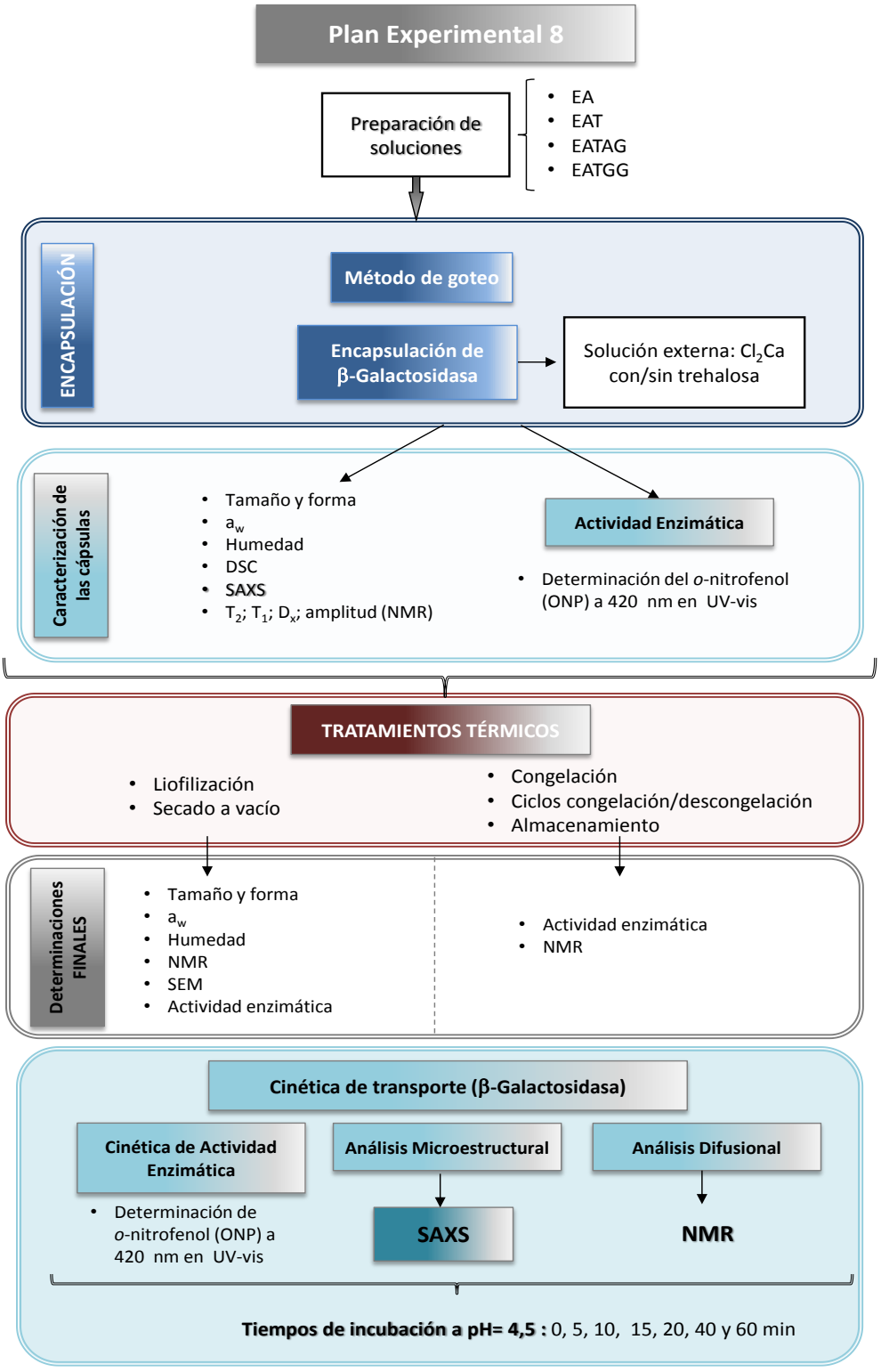

3. Materiales y Métodos

Tejido Animal

Para cada uno de los planes experimentales que forman parte de este apartado se han utilizado diferentes sensores y/o equipos adaptados a cada uno de los objetivos planteados. Un resumen de los sensores utilizados para los estudios llevados a cabo en tejido animal y para cada tramo de frecuencia se puede observar en la Figura 3.1.

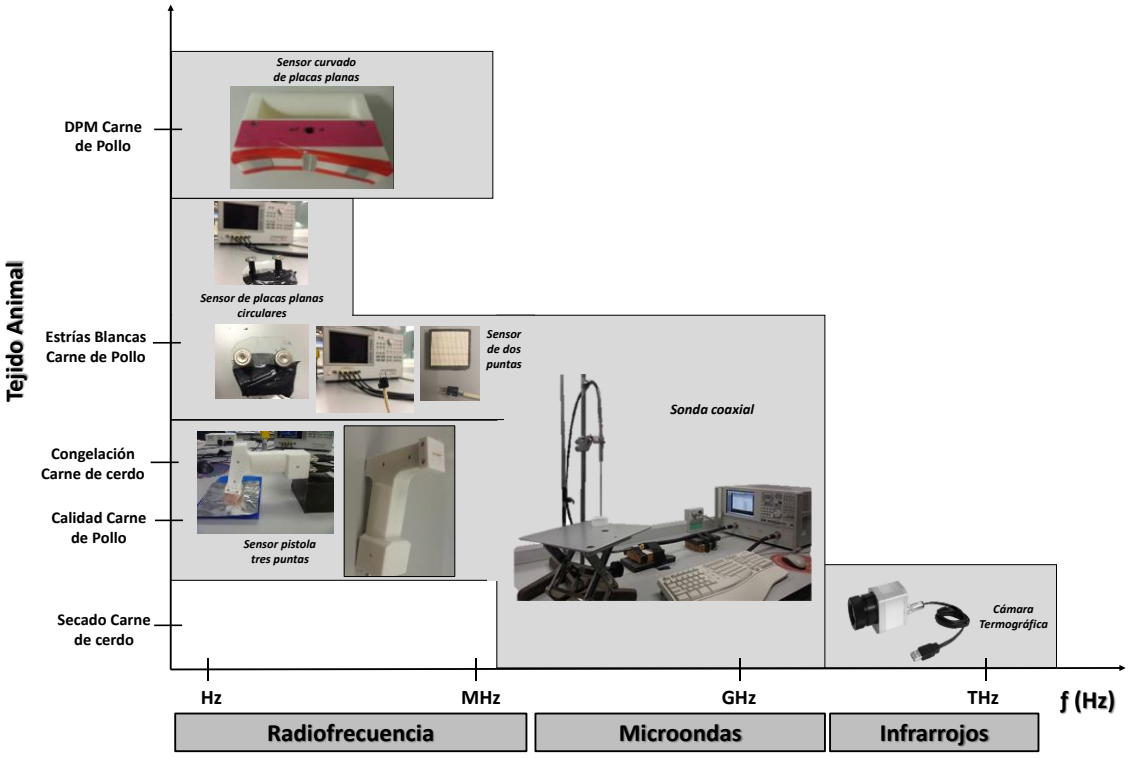

Figura 3.1. Resumen esquemático de los sensores utilizados para los planes experimentales llevados a cabo en tejido animal.

3.1. *Desarrollo de un sistema de monitorización de secado de carne de cerdo con aire caliente mediante termografía infrarroja y espectrofotometría en el rango de microondas.*

Materia prima

Las muestras de carne de cerdo fueron obtenidas de un matadero comercial localizado en Valencia, España. Se utilizaron 6 lomos (*Longissimus dorsi*) de cerdos del cruce Landrace x Duroc con un tiempo de post-mortem de 1,5 días con un peso vivo aproximado de 100-120 kg.

Muestreo y caracterización

56 muestras cilíndricas de lomo de cerdo fueron utilizadas para llevar a cabo este experimento. Los cilindros fueron obtenidos en dirección a las fibras musculares, utilizando un sacabocados con un diámetro de 3 cm y una altura de 1 cm.

Para la determinación de masa se utilizó balanza analítica Mettler Toledo® AB304-S con una precisión de ±0,001 g y para las medidas de actividad del agua (a_w), un higrómetro de punto de rocío Decagón de la marca Aqualab®, modelo serie 3 TE a 25 ºC con una precisión de ±0,003 (Decagon Devices, Inc., Washington, E.E.U.U.). Las medidas de a_w fueron obtenidas sin llevar a cabo una desestructuración previa de las muestras analizadas, es por ello, que los resultados obtenidos corresponden a la actividad de agua superficial. Las determinaciones de humedad se realizaron siguiendo la Norma ISO 1442 (1997), secando las muestras a una temperatura de 110 ºC, a presión atmosférica y hasta peso constante. La superficie y el volumen se obtuvieron mediante la técnica de análisis de imagen tanto del alzado como del perfil de las muestras (Figura 3.2.) utilizando el software Adobe® Photoshop® (Adobe Systems Inc., San José, CA, E.E.U.U.).

Figura 3.2. Montaje utilizado para la determinación de la superficie y volumen de las muestras de carne de cerdo.

Secado por aire caliente

Dos operaciones de secado por aire caliente fueron llevadas a cabo de forma simultánea en distintos secaderos (Figura 3.3.) y bajo las mismas condiciones operativas: velocidad del aire de 1,5 m/s, medido y controlado mediante un anemómetro digital TESTO 425 (precisión de ±0,03 m/s), una temperatura de 40 ºC y un tiempo total de secado de 115 h.

En uno de ellos, se registró la variación continua de masa con una balanza Mettler Toledo PG503-S (± 0,01 g de precisión). Se instaló una cámara de *infrarrojos* Optris PI® 160 (Optris GmbH, Berlín, Alemania) frente a la muestra, de tal forma de monitorizar todo el proceso de secado. Dicha cámara trabaja a longitudes de onda comprendidas entre 780 nm y 14 μm y utiliza un plano focal bidimensional con 160 x 120 píxeles, en un rango espectral de 7,5 a 13 cm, con una resolución de 0,05 °C y una precisión de ± 2%. La misma viene acompañada de un software Optris PI Connect (Optris GmbH, Berlín, Alemania) para el análisis de los resultados. Un material de referencia con emisividad conocida (ε = 0,95 - Optris GmbH, Berlín, Alemania) fue colocado al lado de la muestra en estudio a fin de corregir la emisividad de la muestra. Las temperaturas de la muestra, de una muestra de referencia, del material de referencia con emisividad conocida y del ambiente del secadero fueron monitorizadas mediante termocuplas tipo-*k* conectadas a un multiplexor Agilent 34901A (Agilent Technologies, Malasia) y registradas por sistema adquisición de datos Agilent 34972A (Agilent Technologies, Malasia).

El secadero continuo, se utilizó para realizar la isoterma de desorción secando muestras a diferentes tiempos: 8, 16, 29, 48 y 115 h.

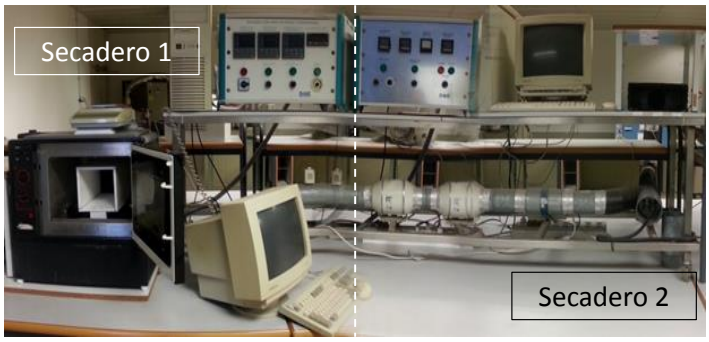

Figura 3.3. Imagen de los secaderos utilizados.

Permitividad

La permitividad tanto para las muestras frescas como para las muestras deshidratadas a cada tiempo de la isoterma se determinó en el rango de las microondas (500 MHz a 20 GHz) mediante una sonda coaxial Slim Form Probe *Agilent 85070E* (Agilent, Santa Clara, CA, E.E.U.U.) conectada a un analizador de redes *Agilent E8362B* (Agilent, Santa Clara, CA, E.E.U.U.). El montaje utilizado se puede observar en la siguiente figura:

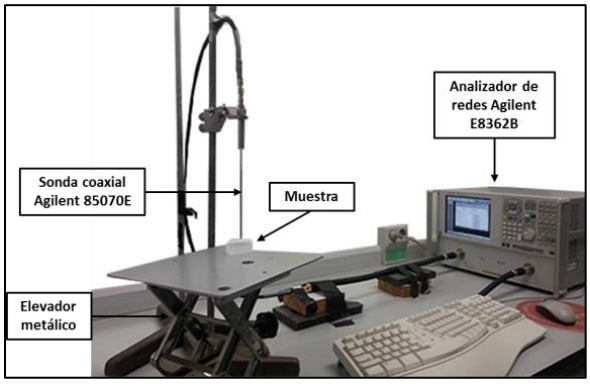

Figura 3.4. Representación del montaje utilizado para medir. Sonda coaxial *Agilent 85070E* conectada al analizador de redes *Agilent E8362B*.

La sonda posee un diámetro externo de 2,2 mm y una longitud de 200 mm. Para la calibración, en primer lugar, se debe medir aire, seguidamente se acopla un accesorio formado por un polímero conductor en la parte final de la sonda, el cual provoca un cortocircuito y para finalizar se procede a la calibración con agua Mili®-Q a la misma temperatura en la que se va a medir la muestra. Para la verificación de una correcta calibración se mide agua Mili®-Q y se compara la medida con una base de datos.

Determinaciones finales

Luego del tratamiento de secado, se realizaron las siguientes medidas: a_w, volumen, permitividad y masa. Posteriormente, se dejaron reposar las muestras 24 h a 4 °C y se midieron a_w, volumen, permitividad, masa y humedad.

3.2. Desarrollo de un sensor no destructivo en el rango de la radiofrecuencia para la detección de ciclos de congelación/descongelación en carne de cerdo.

Materia prima

Se utilizaron 5 lomos (*Longissimus dorsi*) de cerdos del cruce Landrace x Duroc con un tiempo de post-mortem de 6 h, obtenidos del matadero "La cope" (Torrente, Valencia).

Caracterización de las muestras

Los lomos de cerdo se caracterizaron a las 24 h de acuerdo al pH, a L* y a las pérdidas por goteo. El pH se midió utilizando un pH-metro SevenEasy™ de Mettler Toledo, conectado a un electrodo de punzón Inlab® Solids Pro, (Mettler Toledo, Barcelona, España). La coordenada L* de color se midió utilizando un espectrocolorímetro Minolta modelo CM-3600D (Minolta Co. Ltd., Tokio, Japón) con un observador 10º y un iluminante D65. Finalmente, para la determinación de las pérdidas por goteo, se pesaron 3 lonchas de aproximadamente 100 g y se introdujeron en bolsas de polietileno previamente pesadas y se mantuvieron suspendidas a 4 ºC durante 72 h. Finalmente, se pesaron por un lado la carne y por el otro la bolsa con el exudado.

Las muestras utilizadas para llevar a cabo la investigación fueron obtenidas con un sacabocados cilíndrico, de 6 cm de diámetro y 10 cm de altura y en dirección a las fibras musculares. Además, se midieron la masa, la humedad y la a_w.

Medidas realizadas

- *Microestructura mediante un microscopio electrónico de barrido a bajas temperaturas (Cryo-SEM)*

Las muestras se sumergen en nitrógeno líquido (N_2) a una temperatura de -210 ºC y luego transferirlas rápidamente a un Cryostage CT1-00C (Oxford Instruments Witney, Reino Unido), el cual se encuentra acoplado a un microscopio electrónico de barrido Jeol JSM-5410 (Jeol, Tokio, Japón), que con condiciones de congelación (T ≤ -130 ºC) a vacío (1 kPa). En el interior del Cryostage la muestra es fracturada a una temperatura ≤ -180 ºC, luego se la introduce en la cámara

del microscopio para posteriormente ser sublimada a -95 ºC, con el objetivo de eliminar el posible exceso de hielo superficial, el cual podría enmascarar la adecuada observación de la muestra. Por último, antes de proceder a la observación de la muestra, ésta es recubierta con oro (Au) en el mismo Cryostage a vacío (0,2 kPa) durante 3 minutos, aplicando una corriente ionizante de 2 mA. Las muestras fueron observadas a 20 kV y a una distancia de trabajo de 15 mm.

- *Estado de las proteínas por Calorimetría Diferencial de Barrido (DSC)* utilizando un calorímetro diferencial de barrido Mettler Toledo DSC 1 (Mettler Toledo, Barcelona, España) provisto un sensor de temperatura FRS5. La calibración del equipo se realizó mediante la función FlexCal de calibración automática suministrada por los fabricantes. Las muestras (30 mg) se colocaron en crisoles de aluminio de 40 μL de volumen interior sellados herméticamente (Mettler Toledo, ME-00026763). Como muestras de referencia y blanco se utilizaron crisoles de aluminio vacíos, cerrados herméticamente. El barrido utilizado ha sido el siguiente: calentamiento desde 15 ºC hasta 115 °C a una velocidad de calentamiento de 10 °C/min.

- *Permitividad en el rango de la radiofrecuencia*

Se ha diseñado un sensor no destructivo y de fácil implementación en líneas de producción industrial. Consiste en un modelo tipo pistola conformado por tres electrodos de punta roma retráctiles (Figura 3.5.) desarrollado por el Laboratorio de Propiedades Dieléctricas (Instituto Universitario de Ingeniería de Alimentos para el Desarrollo IuIAD) y el Instituto de Instrumentación para Imagen Molecular (I3M) ambos pertenecientes a la Universidad Politécnica de Valencia (UPV), Valencia, España. Patente Nº P201630956 (Castro-Giraldez *et al.*, 2016). Dicho sensor, conectado a un analizador de impedancias Agilent 4294A, es capaz de medir el espectro dieléctrico en el rango de 40 Hz hasta 1 MHz. La calibración del equipo se realiza en abierto y corto.

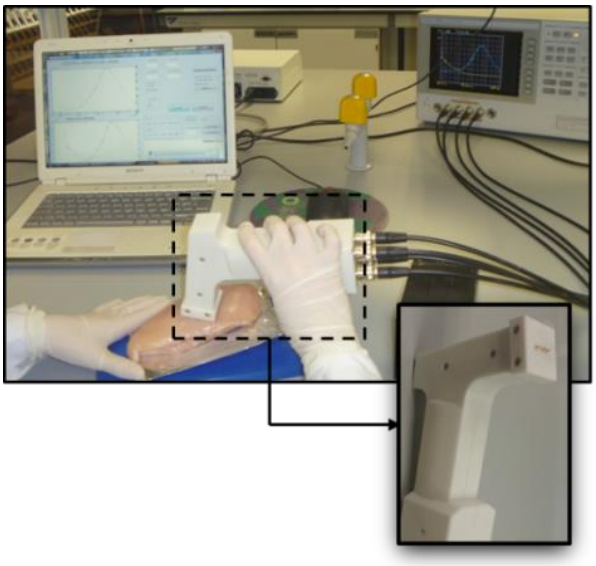

Figura 3.5. Sensor de tres electrodos de punta romas retráctiles conectado al analizador de impedancias *Agilent* 4294B. Patente Nº P201630956 (Castro-Giraldez *et al.*, 2016).

Congelación/descongelación

Congelamiento a -40 ºC en un congelador IQF (Modelo ACR-45/87, Dycometal, S.L., Barcelona, España), a una velocidad de 0,1 ºC/min durante un tiempo total de 245 min.

Las muestras se descongelaron manteniéndolas a 4 ºC durante 48 h.

Determinaciones finales

Una vez finalizados los procesos de congelación o descongelación, se registró la masa de los cilindros y, además, a las muestras descongeladas se midieron nuevamente la a_w, la humedad y la permitividad.

3.3. Estudio espectrofotométrico (en los rangos de radiofrecuencia y microondas) de carne fresca de pollo para clasificarla en función a su calidad: Normal; Pálida, Blanda y Exudativa (PSE); y Oscura, Firme y Seca (DFD).

Materia prima

Se utilizaron pechugas de pollo (*Pectoralis major*) con 12 horas post-mortem, suministrados por el matadero del Grupo Sada (Nutreco S.A.) localizado en Rafelbunyol, Valencia, España.

Caracterización de las muestras y medidas

A fin de clasificar las muestras como PSE, Normal o DFD se midió el pH y el L* teniendo en cuenta la clasificación propuesta por Zhang & Barbut (2005). La a_w y la humedad también fueron medidas para cada tipo de muestra.

Permitividad

La permitividad se midió tanto en el rango de la radiofrecuencia como de las microondas. En el rango de la radiofrecuencia, se utilizó el sistema descripto en el apartado 3.2., utilizando un sensor de tres electrodos de punta roma retráctiles Patente Nº P201630956 (Castro-Giraldez *et al.*, 2016), conectado a un analizador de impedancias Agilent 4294B. En el rango de las microondas, se utilizó una sonda coaxial conectada al analizador de redes Agilent E8362B (apartado 3.1.).

Análisis estadístico

El modelo logístico aplicado ha sido ajustado mediante el programa Statgraphics Centurion XVI (Statgraphic, Virginia, E.E.U.U.), utilizando la herramienta de regresión no lineal. El análisis estadístico se realizó mediante la herramienta One-way ANOVA con un post t-test mediante el programa Prism 6 (GraphPad Software Inc., California, E.E.U.U.).

3.4. Desarrollo de una metodología analítica para clasificar las pechugas de pollo que han sufrido la Miopatía del pectoral profundo (DPM). Desarrollo de un sensor no destructivo capaz de detectar carcasas de pollo enteras (con piel) afectadas por DPM.

Materia prima

Se utilizaron pechugas de pollo (*Pectoralis major y Pectoralis minor*) con 5 horas post-mortem, suministrados por el matadero del Grupo Sada (Nutreco S.A.) localizado en Rafelbunyol, Valencia, España. Las muestras fueron clasificadas por un experto del matadero de acuerdo a la apariencia visual en pechugas normales como CATEGORIA 0, pechugas con hemorragia y/o coágulos de sangre como CATEGORIA 1 y con necrosis como CATEGORIA 2. Se utilizaron un total de 76 muestras (36 categoría 0; 27 categoría 1 y 27 categoría 2).

Medidas realizadas

Las medidas realizadas durante este experimental han sido: pH, humedad, color, contenido de proteínas por DSC y microestructura por Cryo-SEM (tal y como se explicó en el apartado 3.2.). Además, se realizó un estudio del daño en el *Pectoralis minor* por análisis de imagen utilizando una cámara digital con una resolución de 16 píxeles/mm. Las imágenes fueron tomadas colocando las muestras dentro de una cámara de inspección con paredes interiores de color negro. Se utilizaron tres lámparas con luz fluorescente (PHILIPS TLD18W/965, 60 cm de longitud) para obtener una iluminación adecuada (iluminante D65), con una temperatura de color de 6500 K. Finalmente, la cámara se colocó en la parte superior, enfocando la muestra con 10º de pendiente. Para la calibración del sistema, se midieron los parámetros de color de 24 cartas (comprobador de color CLASSIC X-rite, 2010, E.E.U.U) con coordenadas CIE L*a*b* CIE. (1978) conocidas y se compararon las medidas con los parámetros proporcionados por el fabricante. El análisis de áreas dañadas (coágulos sanguíneos, áreas hemorrágicas y necróticas) fue realizado por el software Adobe® Photoshop® CS6 (Adobe Systems Inc., San José, CA, E.E.U.U.).

Además, se determinó el contenido catiónico y tal y como se explica a continuación:

Determinación del contenido iónico

El contenido iónico se analizó mediante cromatografía de intercambio iónico (Methrom Ion Analysis, Herisau, Suiza), utilizando una columna universal (Metrosep C2-250, 150 × 4,0 mm), equipada con detectores electrónicos y una fase móvil compuesta por ácido tartárico (4,0 mmol/L) y ácido dipicolítico (0,75 mmol/L). Las muestras se homogeneizaron previamente a 9000 rpm en un ultraturrax T25 durante 10 minutos y se centrifugaron a 10000 rpm durante 20 minutos (J.P. Selecta S.A., Medifriger BL-S, Barcelona, España). Luego, se tomó 1 mL del sobrenadante y se enrasó hasta 50 mL con agua Milli®-Q. Se filtraron utilizando filtros de jeringa de nylon de 0,45 μm para posteriormente tomar una alíquota de 15 mL a fin de realizar el análisis del contenido catiónico. Las determinaciones se llevaron a cabo por triplicado.

Permitividad

- El sensor utilizado fue desarrollado por el Laboratorio de Propiedades Dieléctricas (Instituto Universitario de Ingeniería de Alimentos para el Desarrollo IuIAD) y el Instituto de Instrumentación para Imagen Molecular (I3M) ambos pertenecientes a la Universidad Politécnica de Valencia (UPV), Valencia, España – Patente Nº P201630956 (Fito *et al.*, 2016). El mismo consiste en dos pares de electrodos de placas planas, donde cada par posee un tamaño y una distancia diferente entre ellos, de tal forma de obtener diferentes índices de penetración y así, que la señal llegue a los distintos músculos (*Pectoralis major* y *Pectoralis minor*), atravesando la piel. El sensor posee un diseño curvado realizado a medida con una impresora 3D, de tal forma de que se acople perfectamente a la curvatura del pectoral del pollo (Figura 3.6.). El sensor se conecta a un analizador de impedancias Agilent 4294A. El rango de frecuencia de medida es de 40 Hz a 1 MHz y la calibración se realiza en abierto y corto.

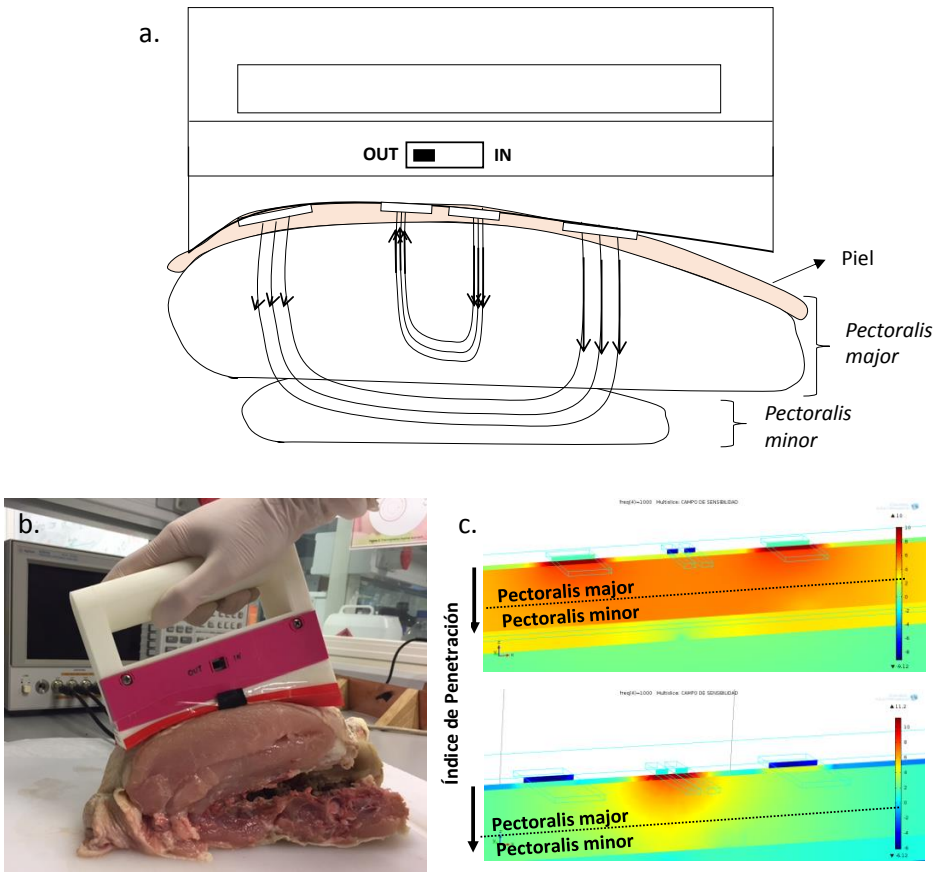

Figura 3.6. a. Esquema representativo del sensor curvado acoplado al *pectoralis* del pollo y la penetración de la señal, b. imagen del sensor acoplado a la carcasa de pollo y c. predicción de la penetración de la señal de las placas planas a distintas distancias: OUT (imagen superior)/ IN (imagen inferior). Patente española Nº P201630062 (Fito *et al.*, 2016).

Análisis estadístico

El análisis estadístico se llevó a cabo mediante el programa Statgraphics Centurion XVI (Statgraphic, Virginia, E.E.U.U.). Se utilizó la herramienta One-way ANOVA para determinar diferencias significativas entre los parámetros estudiados. Para el ajuste del modelo logístico se utilizó la herramienta de regresión no lineal.

3.5. Estudio de pechugas de pollo afectadas por las estrías blancas (White Striping). Desarrollo de un sensor no destructivo capaz de detectar WS en carcasas de pollo enteras (con piel).

Materia prima

Se utilizaron pechugas de pollo (*Pectoralis major y Pectoralis minor*) con 12 horas post-mortem, suministrados por el matadero del Grupo Sada (Nutreco S.A.) localizado en Rafelbunyol, Valencia, España. Las pechugas fueron clasificadas por un experto en la planta industrial como categoría SEVERA (WS) y normales. Para llevar a cabo la segunda parte de este experimental, junto a cada pechuga se utilizó la piel de cada una de ellas.

Medidas realizadas

Se analizó el pH, el contenido de ácidos grasos y además se llevó a cabo un análisis estructural. El *contenido de ácidos grasos* se analizó mediante DSC (descripto en el apartado 3.2.) pero utilizando un protocolo diferente. Las muestras (WS y normales) de entre 22-25 mg fueron colocadas en los crisoles de aluminio y liofilizadas durante 48 horas en un liofilizador Telstar Lyoalfa-6 (Telstar, Reino Unido), ya que el agua podría interferir en análisis calorimétrico. El barrido utilizado (Benedito *et al.*, 2001) consiste someter a las muestras (en crisoles cerrados herméticamente) a un mantenimiento de la temperatura a 60 ºC durante 5 minutos, un enfriamiento a -40 ºC a 10 ºC/min, un mantenimiento a dicha temperatura durante 5 min y finalmente un calentamiento desde -40 ºC hasta 50 ºC a una velocidad de 5 ºC/min.

Análisis estructural

El análisis estructural se llevó a cabo mediante Cryo-SEM (microestructura) (ver apartado 3.2.) y mediante una lupa binocular (macroestructura) modelo Leica MZ APO™ (Leica Microsystems, Wetzlar, Alemania) con baja magnificación (8x a 80x) utilizando una iluminación de luz incidente (luz reflejada de la superficie de la muestra). Dicho equipo utiliza dos trayectorias ópticas separadas con dos objetivos y dos oculares para proporcionar ángulos de visión ligeramente diferentes para los ojos izquierdo y derecho. De esta manera se permite una visualización tridimensional de la muestra.

Permitividad en la superficie del Pectoralis major

Para obtener la permitividad superficial en el rango de la radiofrecuencia, se utilizó un sensor de dos agujas con extremo romo (Figura 3.7.a). Este diseño presenta un bajo índice de penetración de la señal, de tal forma de que las señales obtenidas corresponden a tejidos específicos, ya sea a las estrías blancas de las pechugas afectadas, al tejido adiposo (tanto de las muestras normales como con estriación), al tejido muscular normal o al tejido muscular de las muestras afectadas por la fisiopatía WS. Además, en el rango de las microondas se utilizó una sonda coaxial conectada a un analizador de redes desde una frecuencia de 500 MHz a 20 GHz (ver apartado 3.1.)

Permitividad en carcasas enteras con piel

Para obtener un mayor índice de penetración de la señal, de tal forma de poder atravesar la piel y llegar al músculo pectoral, se diseñó un sensor con mayor superficie de contacto y mayor separación entre los electrodos de medida. Este sistema consiste en dos placas planas circulares (Figura 3.7.b.)

Ambos sensores utilizados para medir en radiofrecuencia fueron desarrollados por el Laboratorio de Propiedades Dieléctricas (Instituto Universitario de Ingeniería de Alimentos para el Desarrollo IuIAD) y el Instituto de Instrumentación para Imagen Molecular (I3M). Los mismos van conectados a un analizador de impedancias *Agilent* 4294A y son capaces de medir desde 40 Hz a 1 MHz.

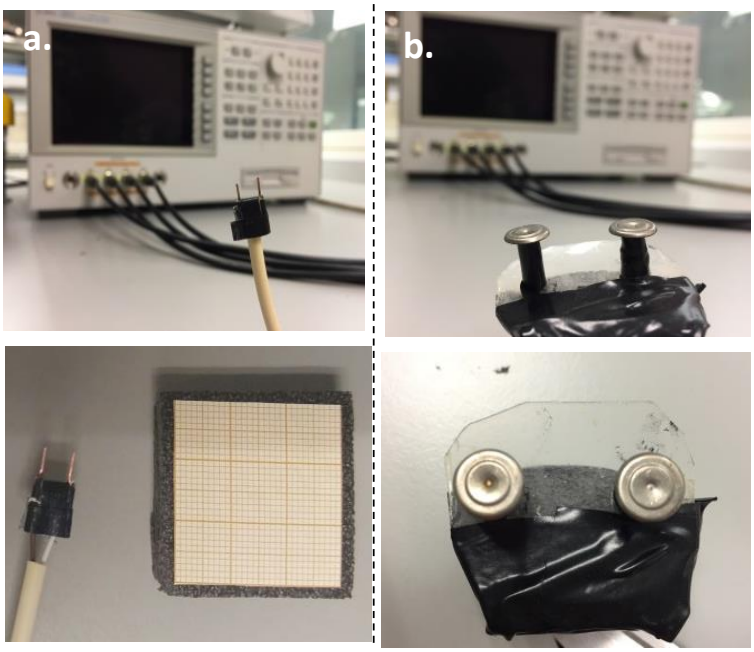

Figura 3.7. Sensores utilizados para medir en radiofrecuencia conectados al analizador de impedancias *Agilent* 4294A. a. sensor de dos agujas con extremo romo, b. sensor de dos placas planas circulares.

Análisis estadístico

El análisis estadístico se llevó a cabo mediante el programa Statgraphics Centurion XVI (Statgraphic, Virginia, E.E.U.U.). Se utilizó la herramienta One-way ANOVA para determinar diferencias significativas entre los parámetros estudiados. Para el ajuste del modelo logístico se utilizó la herramienta de regresión no lineal.

Tejido Vegetal

3.6. Caracterización dieléctrica de los tejidos que componen la mandarina

Materia prima

Se utilizaron 20 mandarinas de la variedad *Citrus Clementina*, de tamaño y color homogéneo, exentas de alteración fisiológica. Las mismas fueron obtenidas de una parcela situada en el municipio valenciano de Algimia de Alfara (Valencia, España). Las frutas se encontraban libres de recubrimientos de cera industrial. Para llevar a cabo las determinaciones, se separaron los distintos tejidos que componen la mandarina y se almacenaron en cápsulas Decagon® a fin de evitar su deshidratación.

Determinaciones fisicoquímicas

Se midió el pH y la a_w, tal y como fue previamente explicado en el apartado 3.2. Para la determinación de humedad se empleó el método AOAC 2000, secando en estufa de vacío a 60 ºC y hasta alcanzar peso constante.

La acidez de las mandarinas se determinó mediante una valoración con una solución de hidróxido sódico 0,1 N considerando que todo el ácido presente corresponde a ácido cítrico y utilizando un factor de conversión de 6,4 (AOAC 942.15, 2000) mediante la siguiente ecuación:

$$\text{Acidez total (g ácido cítrico /100 mL)} = \frac{6.4 \cdot V_1 \cdot N}{V_2} \qquad \text{(Ec. 3.1.)}$$

Dónde V_1 corresponde al volumen de NaOH utilizado, expresado en mL y V_2 el volumen de zumo pipeteado (5 mL).

Los sólidos solubles se determinaron a partir del índice de refracción de las muestras utilizando un refractómetro (ABBE, ATAGO, Modelo 3-T, Japón) termostatado a 20 ºC, previamente calibrado con agua destilada a 25 ºC. Finalmente, el Índice de Madurez (IM) se obtuvo a partir de la relación entre los sólidos solubles totales y la concentración de ácidos libres.

Análisis estructural

El análisis estructural se llevó a cabo mediante Cryo-SEM (microestructura) (ver apartado 3.2.) y mediante una lupa binocular (macroestructura), como se explicó en el apartado 3.5.

Medidas de Permitividad

La permitividad de cada uno de los tejidos se obtuvo en el rango de la radiofrecuencia (40 Hz a 1 MHz) y de las microondas (500 MHz a 20 GHz). En el rango de la radiofrecuencia se diseñaron dos sensores que consisten en dos electrodos de placas planas, con diferente tamaño de placas de tal forma de ejercer un buen contacto con cada una de las muestras. En la Figura 3.8. se puede observar un esquema representativo del diseño y construcción de los mismos. Ambos sensores fueron desarrollados por el Laboratorio de Propiedades Dieléctricas (Instituto Universitario de Ingeniería de Alimentos para el Desarrollo IuIAD) y el Instituto de Instrumentación para Imagen Molecular (I3M). Los mismos se conectan a un analizador de impedancias Agilent 4294A y miden desde 40 Hz a 1 MHz.

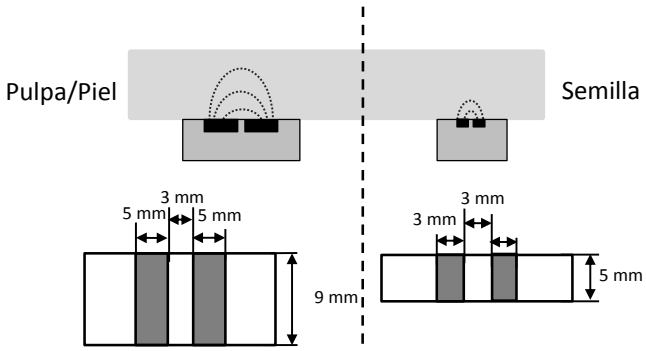

Figura 3.8. Esquema representativo de los sensores utilizados para medir los tejidos de las mandarinas en radiofrecuencia.

Análisis estadístico

El análisis estadístico se llevó a cabo mediante el programa Statgraphics Centurion XVI (Statgraphic, Virginia, E.E.U.U.). Se utilizó la herramienta One-way ANOVA para determinar diferencias significativas entre los parámetros estudiados. Para el ajuste del modelo logístico se utilizó la herramienta de regresión no lineal.

3.7. Estudio de los campos eléctricos pulsados (PEF) como pre-tratamiento de la deshidratación osmótica de kiwis orgánicos. Análisis termodinámico y monitorización por RMN. Análisis de la redistribución del agua.

Materia prima

Se utilizaron kiwis orgánicos (*Actinidia deliciosa cultivar ''Hayward''*), obtenidos de un productor local en la ciudad de Cesena, Italia. Los mismos fueron adquiridos a granel y mantenidos a 4±1 °C hasta su análisis. Al momento de la realización del trabajo de investigación, las frutas fueron seleccionadas en función a su contenido en sólidos solubles (13±1 °Brix) medidos utilizando un refractómetro digital (KRÜSS Optronic© GmbH, Alemania) previamente calibrado con agua destilada a 25 °C.

Muestreo y caracterización

La toma de muestra se realizó utilizando un sacabocados cilíndrico de 0,8 cm de diámetro y 1 cm de alto. Como determinaciones iniciales se midieron la masa, a_w, humedad y el volumen. Para la masa se utilizó una balanza analítica Kern ABS 320-4N (±0,001) (KERN & SOHN GmbH, Alemania); para la a_w un higrómetro de punto de rocío Decagón de la marca Aqualab®, modelo serie 3 TE a 25 °C con una precisión de ±0,003 (Decagon Devices, Inc., Washington, E.E.U.U.); la humedad se determinó siguiendo el método AOAC (2000) y el volumen se realizó por análisis de imagen (ver apartado 3.1.). Se utilizó un equipo de NMR para la determinación del T_2, utilizando un espectrómetro Bruker 'Minispec' mq20 (Bruker Biospin GmbH, Rheinstetten, Alemania) a 20 MHz. Además se realizó un estudio microestructural mediante Cryo-SEM (apartado 3.2.).

Aplicación de campos eléctricos pulsados como pre-tratamiento

El sistema de campos eléctricos pulsados consiste en un generador de pulsos basado en la tecnología MOSFET y capacitores que funcionan como fuentes de energía. El generador PEF proporciona pulsos monopolares de forma rectangular a diferentes voltajes, con un sistema ajustable de tiempos de repetición entre cada pulso. La cámara de tratamiento posee las siguientes medidas 30 x 20 x 20 mm (largo, ancho y alto) y está equipada con dos capacitores de acero inoxidable con un área de contacto de 20 x 20 mm^2 y una distancia entre ellos de 30 mm. Los

valores de corriente y de voltaje se registran por medio de un osciloscopio digital (PicoScope 2204A, Pico Technology, Reino Unido) conectado a un ordenador. Las intensidades aplicadas como pre-tratamientos fueron de 100, 250 y 400 V/cm y la cantidad de muestras colocadas en la cámara de tratamiento PEF eran de 12 cilindros (Figura 3.9.).

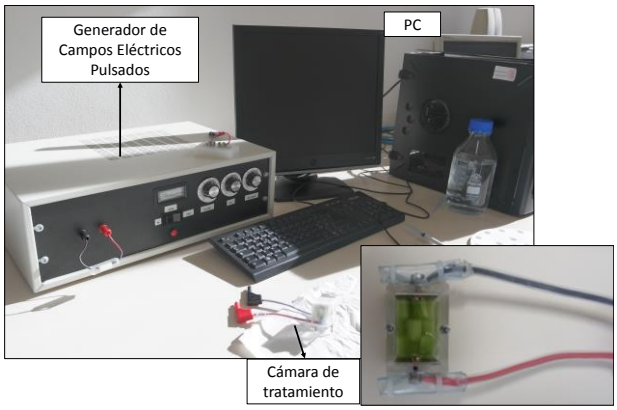

Figura 3.9. Equipo de campos eléctricos pulsados utilizado.

Deshidratación osmótica

La deshidratación osmótica se llevó a cabo utilizando una solución de sacarosa al 61,5% (p/p), preparada con sacarosa comercial y agua destilada a 25 ºC. Las muestras cilíndricas de kiwi fueron sumergidas en la solución osmótica manteniendo una relación de 1:4 (p/p) entre la fruta y la solución. Los tiempos de tratamiento seleccionados fueron: 10, 20, 30, 60 y 120 min. Se llevaron a cabo dos lotes de muestras (con y sin pre-tratamiento de PEF). A uno de los lotes se le realizaron las determinaciones finales inmediatamente después del tratamiento, mientras que al otro se lo dejó reposar por 24 h a 4 ºC de tal forma de conseguir un equilibrio interno en la muestra.

Determinaciones finales

Como determinaciones finales se realizaron las siguientes medidas tanto en las muestras tratadas como en las reposadas: masa, a_w, humedad, volumen, contenido de sólidos solubles y T_2. Además, se analizó la microestructura después del tratamiento por Cryo-SEM (ver apartado 3.2.).

Sistema Coloidal

3.8. Estudio de la encapsulación de β-galactosidasa en hidrogeles de alginato-Ca(II) con y sin el agregado de trehalosa, goma arábiga y goma guar.

Materias primas

Alginato de sodio (Algogel 5540) de la empresa Cargill S.A. (San Isidro, Buenos Aires, Argentina), con un peso molecular de $1{,}97 \cdot 10^5$ g/mol and un ratio mannuronato/guluronato de 0,6, D-trehalosa dihidratada (Hayashibara Co., Ltd., Shimoishii, Okayama, Japan/Cargill Inc., Minneapolis, Minnesota, USA) con un peso molecular de 378 g/mol; goma guar (Cordis S.A., Villa Luzuriaga, Buenos Aires, Argentina) con un peso molecular de 220,000 g/mol y un ratio de manosa/galactosa de 1,8; goma arábiga (Biopack, Zárate, Buenos Aires, Argentina) de peso molecular 250,000 g/mol y una pureza del 99%. El compuesto bioactivo a encapsular, la enzima β-galactosidasa (lactasa) obtenida a partir del alga *Aspergillus oryzae* (8,0 U/mg) (Sigma-Aldrich Co, Ltd, Saint Louis, E.E.U.U.). Una unidad enzimática se define como la cantidad de enzima capaz de hidrolizar 1,0 μmol de lactasa por minuto a pH 4,5 a 30 °C.

Preparación de las cápsulas

Para la obtención de las cápsulas se utilizaron cuatro formulaciones diferentes: EA, EAT, EATAG y EATGG, siendo E, enzima; A: alginato; T: trehalosa; AG: goma arábiga y GG: goma guar. Todas las soluciones fueron preparadas en buffer acetato 0,1 M a pH 3,8. Teniendo en cuenta que el punto isoeléctrico de la enzima es de 4,61 (Dashevsky, 1998) y los valores de p*K*a del alginato son de 3,38 y 3,65 (Santagapita *et al.*, 2011), el buffer acetato se utilizó a un pH de 3,8 a fin de generar interacción electrostática entre el alginato (cargado negativamente) y la enzima (cargada positivamente). La concentración final de lactasa fue de 0,775 mg/mL. La enzima diluída y las soluciones encapsulantes fueron cuidadosamente mezcladas y mantenidas a 4±1 °C para evitar pérdidas de actividad enzimática.

La encapsulación se llevó a cabo por el método del goteo, para la cual se utilizó una bomba peristáltica BT50-1J con cabezal JY10 (Boading Longer Precision Pump Co, Ltd, China), por la cual se hacía pasar 10 mL de las soluciones encapsulantes y se las dejaba caer en 100 mL de $CaCl_2$ de acuerdo al método propuesto por Austin *et al.*, 1996.

Para la preparación de las cápsulas EA, 1% (p/v) de la solución de alginato con la enzima se dejó caer en una solución 2,5% (p/v) de $CaCl_2$ (preparada en buffer acetato 0,1 M a pH 3,8). Para la preparación de las cápsulas de los sistemas EAT, EATGG y EATAG se utilizó alginato 1% (p/v) con 20% (p/v) de trehalosa con/sin 0,25% (p/v) de goma arábiga o guar. Esta solución que contenía la enzima se dejó caer por goteo en solución 2,5% (p/v) de $CaCl_2$ preparada con trehalosa al 20% (p/v).

Durante la formación de las cápsulas, la solución de $CaCl_2$ (con/sin trehalosa) se mantuvo en un baño frío con agitación constante. La aguja utilizada para el goteo tenía 0,25 mm de diámetro y 6 mm de largo (Novofine 32 G, Novo Nordisk A/S, Bagsvaerd, Dinamarca). La velocidad de la bomba era de 9,0 ± 0,1 rpm y la distancia entre la aguja y la solución de $CaCl_2$ fue de 6 cm. Luego de la generación de las cápsulas, las mismas fueron mantenidas durante 15 min en la solución de $CaCl_2$ (con agitación constante) y luego fueron lavadas 5 veces (5 s cada lavado) con agua fría bidestilada, para remover la enzima libre adherida en caso de que hubiera.

Tratamientos Térmicos

A fin de estudiar la estabilidad de la enzima frente a tratamientos de conservación, las mismas fueron sometidas a los siguientes tratamientos:

- Congelación: Las cápsulas húmedas fueron congeladas a -18 °C utilizando un congelador convencional durante 24 h.
- Ciclos de congelación/descongelación: Las cápsulas húmedas fueron sumergidas durante 1 min en nitrógeno líquido (a -196 °C) y descongeladas en una nevera convencional a 4 °C durante 30 min; este protocolo se repitió 4 veces para cada uno de los sistemas.
- Almacenamiento: Las cápsulas húmedas fueron mantenidas a 4 °C en nevera durante 48 h.

- Liofilización: Las cápsulas húmedas fueron congeladas a -18 °C durante 24 h. Posteriormente fueron liofilizadas durante 24 h utilizando un liofilizador (Heto Lab Equipment, Dinamarca), con trampa de enfriamiento modelo CT 110.
- Secado a vacío: Las cápsulas fueron secadas a vacío utilizando una estufa de vacío Fistreem (Fistreem International Ltd, Loughborough, Reino Unido) a 25 °C durante 24 h a una presión de 113 mbar.

Caracterización de las cápsulas

La a_w se determinó mediante un higrómetro de punto de rocío Decagón de la marca Aqualab®, modelo serie 3 TE a 25 °C con una precisión de ± 0,003 (Decagon Devices, Inc., Washington, E.E.U.U.). La humedad mediante secado en estufa a vacío a una temperatura de 96 ± 2 °C durante 48 h (Aguirre Calvo & Santagapita, 2016).

La forma y el tamaño se determinaron mediante análisis de imagen utilizando una cámara digital acoplada a un microscopio binocular y analizados mediante el software ImageJ (http://rsbweb.nih.gov/ij/), como fue descripto por Aguirre Calvo & Santagapita (2016). Se analizó el diámetro de Feret (distancia máxima entre los dos puntos más distantes que pasa por el centro), la circularidad (que se define como un valor entre 0 y 1 según cuanto se aproxime la forma a un círculo), el área y el perímetro. Al menos fueron analizadas unas 40 cápsulas. Para poder aumentar el contraste de las cápsulas húmedas, las mismas fueron teñidas con eritrosina 1% (p/v). El software se calibró mediante la adquisición de imágenes con la sección de un calibre para poder así transformar las medidas de píxeles a unidades de longitud (mm).

Actividad enzimática β-Galactosidasa

La actividad enzimática de las cápsulas ha sido evaluada en función a los valores de absorbancia a 420 nm utilizando un espectrofotómetro Jasco V-630 UV-VIS (JASCO Inc., Maryland, E.E.U.U) a temperatura ambiente y de acuerdo al método descripto por Park *et al.* (1979) con algunas modificaciones.

Para cada medida se utilizaron 9 cápsulas, las cuales fueron disueltas en 0,25 mL de buffer citrato 0,1 M a pH 4,5 durante 2 h a 4 °C y sin agitación para evitar pérdidas de actividad enzimática. Luego, se agregaron 0,25 mL de *o*-nitrofenil-β-D-galactopiranósido (ONPG) (Sigma Chemical Co.) preparado en buffer citrato 0,1 M a pH 4,5 y se incubaron durante 15 min a 33 °C. Posteriormente, se detuvo la reacción agregando 0,5 mL de carbonato de sodio al 10% (p/v) y 1,75 mL de agua destilada. Finalmente, se realizó la medida de la cantidad de *o*-nitrofenol (ONP) liberado, midiendo la absorbancia a 420 nm.

Análisis calorimétrico

Se utilizó el equipo Mettler Toledo 822 (Mettler Toledo AG, Urdorf, Suiza), utilizando de 14-23 mg de muestra (10 cápsulas) en crisoles de aluminio de 40 μL de volumen interior sellados herméticamente y utilizando el siguiente barrido: calentamiento desde -100 °C a 100 °C a 10 °C/min. Luego del primer barrido, las muestras fueron sometidas a un segundo barrido con el mismo protocolo para poder obtener Δcp del segundo barrido.

Análisis por resonancia magnética nuclear

Al igual que en el apartado 3.7. se utilizó espectrómetro Bruker 'Minispec' mq20 (Bruker Biospin GmbH, Rheinstetten, Alemania) a 20 MHz.

Microestructura

Microscopia electrónica de barrido (FEG-SEM)

Para las cápsulas de polielectrolitos, se tomaron imágenes con un microscopio electrónico de barrido con cañón de emisión de campo (FEG-SEM) marca ZEISS, modelo SUPRA 40 (Carl Zeiss SMT Inc., Peabody, MA, E.E.U.U.) con detector InLes, que permite obtener imágenes de muestras no conductoras sin la necesidad de realizar la cobertura metálica de las mismas. Las imágenes se tomaron a temperatura ambiente en un rango de 25000x and 200x a 1,00 kV.

Dispersión de rayos-X de bajo ángulo (SAXS)

Además, la microestructura de las cápsulas de hidrogeles fue analizada por dispersión de rayos-X de bajo ángulo en la línea LNLS SAXS2 en Campinas, Brasil trabajando a λ = 0,148 nm. El rango del vector de onda (q) se seleccionó en el intervalo de 0,096 nm^{-1} <q <2,856 nm^{-1}.

Estudio de la cinética de transporte

En esta parte del plan experimental se realizaron nuevas cápsulas con y sin enzima para poder entender los transportes internos. De forma paralela a la medida de actividad enzimática, se realizó un análisis microestructural por dispersión de rayos-X de bajo ángulo a distintos tiempos de incubación de las cápsulas en buffer acetato a pH 4.5 (t= 0, 5, 10, 15, 20, 40 y 60 min). La medida de la actividad enzimática se llevó a cabo siguiendo el protocolo explicado anteriormente pero con algunas modificaciones: para cada análisis se utilizaron 9 cápsulas a las cuales se le agregaron 0,25 mL de ONPG, preparada con 0,1 M de buffer acetato a pH 4,5 a los distintos tiempos mencionados anteriormente a una temperatura de 33 °C sin agitación. Posteriormente, se agregó 0,5 mL de carbonato de sodio al 10% (p/v) para detener la reacción y 0,25 mL de citrato de sodio al 10% (p/v) para disolver las cápsulas. Finalmente, se agregaron 1,75 mL de agua destilada y se midió el contenido de ONP a 420 nm por espectrofotometría.

Análisis estadístico

El análisis estadístico se realizó mediante el software Prism 6 (GraphPad Software Inc., California, E.E.U.U) utilizando la herramienta One-way ANOVA con Turkey´s post test, a fin de encontrar diferencias significativas entre los parámetros medidos.

4. Resultados

A continuación se describen los resultados obtenidos a lo largo de las investigaciones realizadas; los mismos se presentan en forma de publicaciones científicas y patentes de acuerdo a los objetivos particulares propuestos en el apartado 2.1.2.

4.1. Monitorización del secado de carne de cerdo mediante termografía infrarroja y espectrofotometría.

Traffano-Schiffo, M. V., Castro-Giráldez, M., Fito, P. J., & Balaguer, N. (2014). Thermodynamic model of meat drying by infrared thermography. ***Journal of Food Engineering***, 128, 103-110.

Traffano-Schiffo, M. V., Castro-Giráldez, M., Colom, R. J., & Fito, P. J. (2015). Study of the application of dielectric spectroscopy to predict the water activity of meat during drying process. ***Journal of Food Engineering***, 166, 285-290.

THERMODYNAMIC MODEL OF MEAT DRYING BY INFRARRED THERMOGRAPHY

Traffano-Schiffo, M.V., Castro-Giráldez, M., Fito, P.J.*, Balaguer, N.

Instituto Universitario de Ingeniería de Alimentos para el Desarrollo, Universidad Politécnica de Valencia, Camino de Vera s/n, 46022 Valencia, España.

*author for correspondence: pedfisu@tal.upv.es

ABSTRACT

Drying operation is one of the most important unit operations used to preserve meat products. Drying process involves a lot of mechanisms coupled together, and traditional kinetic theory of drying explains part of them, covering up the most important behaviours in the falling drying period. Therefore, it is necessary to determine the critical points of each transformation throughout the drying, and to analyse and quantify all of them. In this sense, an irreversible thermodynamic model has been developed, focusing on the falling drying period. In this work, infrared thermography has been used in order to obtain the evolution of meat surface temperature during drying operation. Infrared measurements were made with an Optris PI® 160 thermal imager (Optris GmbH, Berlin, Germany), with a spectral infrared range of wavelength from 7.5 to 13 μm. Surface water activity, volume, mass and moisture were obtained at different drying times. Drying analysis shows five stages, the traditional induction and the constant kinetic drying period (wet temperature of 22 ºC) and three more stages in the falling drying period, shared out by the evolution of the surface internal energy and the vitreous transition.

Keywords: meat drying model, thermodynamic model, infrared thermography.

NOTATION

E_j	flux energy emitted by a body surface (kg s^{-3})
F	geometric factor (-)
a_j	activity of the chemical specie j (-)
R	ideal gases universal constant (J mol^{-1} K^{-1})
T	temperature (K)
s	molar partial entropy (J $K^{-1}mol^{-1}$)
S	entropy (J K^{-1})
P	absolute pressure (Pa)
C_p	specific heat (kJ kg^{-1} K^{-1})
V	volume (L)
l	elongation (m)

L	Phenomenological coefficient ($mol^2\ J^{-1}\ s\text{-}1\ m^{-2}$)
n	number of moles (mol)
M	mass (kg)
A	surface (m^2)
J	molar flux ($mol\ s^{-1}\ m^{-2}$)
t	time (s)
G	free energy (J)
e	charge (C)

Greek Alphabet

ε_j	emissivity of a body (-)
σ	Stephan-Boltzmann constant ($W\ m^{-2}\ K^{-4}$)
Ψ	electric potential ($J\ mol^{-1}\ C^{-1}$)
μ_j	chemical potential of the specie j ($J\ mol^{-1}$)
ν_j	molar partial volume of the specie j ($L\ mol^{-1}$)
ϕ	relative humidity (-)

Subscripts and superscripts

T	total
obj	object
surr	surroundings
air	air
samp	sample
ref	reference
w	water
t	process time
0	initial time
surf	surface
cam	camera data
i	any chemical species

1. INTRODUCTION

Particularly, meat sector is one of the most important in European Union, being ham one of the highest added-value products. In the manufacturing process, drying is the most expensive stage because of the time and control required and the energy consumption associated (Clemente *et al.*, 2011). Moreover, it is one of the best unit operations to preserve the product in time, therefore it is very important to increase the knowledge about the critical points that occur during this treatment.

In relation to meat composition, water is the main constituent of muscle. In living tissue, the water content accounts for 75% of the muscle weight; nevertheless, it can vary in postmortem muscle (65-80%). The most part of this water content, about 85%, is located in the intra-myofibrillar space, and the other 15% is located outside the myofibrillar network (extra-myofibrillar space) (Pearce *et al.*, 2011). Also, it is the primary component of the extracellular fluid in the muscle. In relation to the muscle cells, it should be pointed out that is the principal constituent of sarcoplasmic (cytoplasmic) fluid (Huff-Lonergan, 2010).

Taking into account the water content, meat is considered as an ideal environment for the microorganism growth, therefore it is classified among the highly perishable foods. The conservation principle of the drying process is that the microorganisms that cause spoilage cannot grow and multiply in the absence of water.

According to the traditional kinetic theory, the different mechanisms involved in drying process are divided into three stages; the first stage corresponds to the induction period wherein different water flow mechanisms are coupled. The second stage represents the period in which the drying

velocity reaches its maximum value remaining this constant and the last one corresponds to the falling drying rate period. In this period, the water flux from the inside to the surface of the sample is smaller than the surface water evaporation rate. Due to this, many changes occur in the structure of the muscle fibres. Heat and mass transfer take place simultaneously (Clemente *et al.*, 2011; Akpinar *et al.*, 2006).

In the literature, different thermodynamic models of dehydration process have been developed in different foodstuff structures like pumpkin (Akpinar *et al.*, 2006), potatoes (McMinn and Magee, 2003), strawberry (Akpinar, 2007; Ferrando and Spiess, 2003), pineapple (Simal *et al.*, 2007), apple (Seguí *et al.*, 2012; Castro-Giráldez *et al.*, 2011; Seguí *et al.*, 2006), carrot (Ferrando and Spiess, 2002), and onion (Ferrando and Spiess, 2003). From a thermodynamic point of view, few data has been found in the literature about the structural changes of the meat which are produced as a consequence of the application of a drying process. Therefore, it is important to develop a thermodynamic study in order to describe the meat structural transformations and the phenomena that cause them. Currently, an innovative technique is being developed for the processing control. The Infrared thermography (IRT) is a good tool to carry out this challenge. Regarding the infrared spectrum, the IRT is an interesting tool which can provide important information about heat transfer in biological tissues (Workmaster *et al.*, 1999). It is a new technology that offers the possibility of determining meat drying kinetics through the measurement of temperature distribution on its surface in a short period of time (Vadivambal and Jayas, 2011). This technology is based on measuring infrared radiation emitted by a body surface to produce an image of its thermal distribution. This non-contact and non-destructive method can provide a temperature map of the whole body which is an important difference with other types of sensors that just provide information on one point.

IRT, as a control method, has a potential application in many operations in agriculture and food industry. Some of the developed studies had been focused on the fruits and vegetables quality evaluation during post-harvest operations, including maturity assessment (Offermann *et al.*, 1998), fruits processing (Fito *et al.*, 2004; Veraverbeke *et al.*, 2006; Cuccurullo *et al.*, 2012), fruit yields (Stajnko *et al.*, 2004; Bulanon *et al.*, 2008), meat classification (Nanni *et al.*, 2010; Gariepy *et al.*, 1989), food quality and safety assessment (Gowen *et al.*, 2010) and pathogen detection (Stoll *et al.*, 2008; Lahiri *et al.*, 2012).

The aim of this work is to determine the real critical points in the transformation of meat during the drying process, by means of an irreversible thermodynamic model which considers gradients of activity, temperature and mechanical energies.

2. MATERIALS AND METHODS

Experiments were made using 6 loins (*Longissimus dorsi*, from Landrace x Duroc carcasses). The pigs were slaughtered in a commercial slaughterhouse and were collected at 1.5 days post-mortem. At the time of the slaughtered, the animals had a live weight approximately of 100-120 kg. The muscles were removed and kept at 4 ºC until sampled. A diagram of the experimental procedure is shown in Fig. 1.

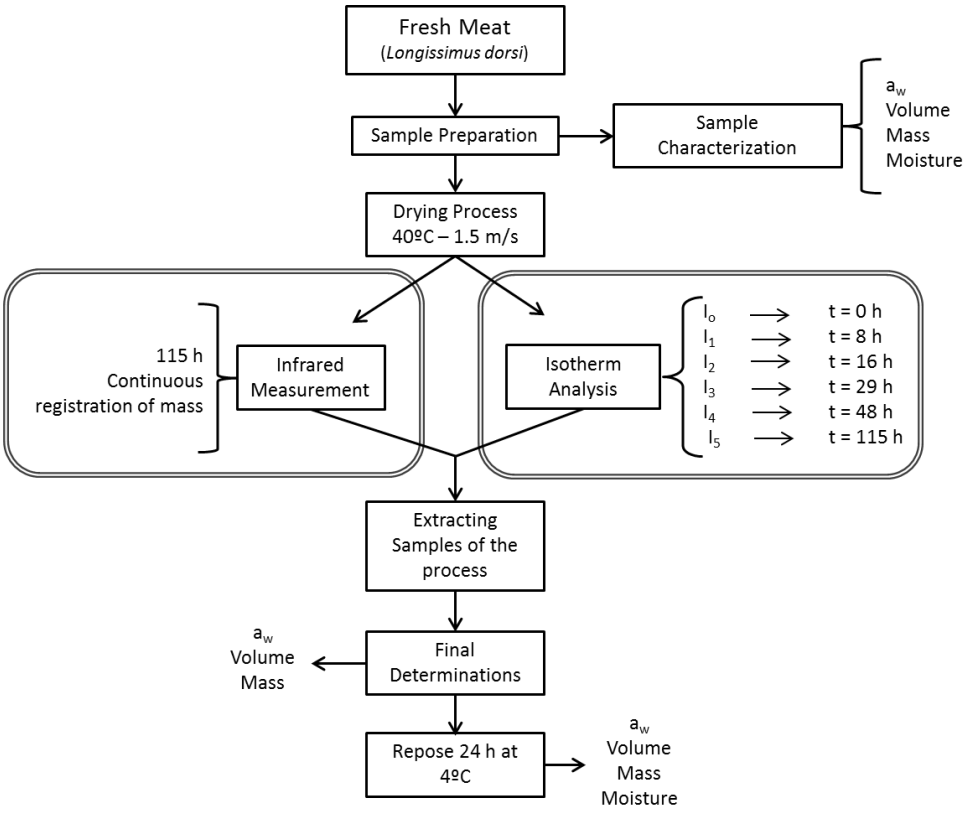

Fig. 1. Diagram of the experimental procedure.

2.1 Meat Sampling and characterization

72 cylinder samples were used for each analysis (diameter 30 mm, height ranging from 10 to 15 mm). The cylinders were cut in the direction of fibres. Mass samples were determined by a balance Mettler Toledo AB304-S with precision of ±0.001, and a dew point Hygrometer Decagon 143 (Aqualab®, series 3 TE) was used for measuring the surface water activity, with a precision ± 0.003. The analysis of the moisture was accomplished following the ISO 1442 (1997) for meat products, drying the samples at 110 ºC at atmospheric pressure during 48 hours until a constant weight was reached.

Volume was determined by an image analysis using Adobe© Photoshop© CS6 software to get the diameter and the thickness of the samples.

The experiments were made in triplicate.

2.2 Drying Operation

The meat sample was placed into the interior of a convective dryer, next to a meat reference sample. The mass difference of sample was registered continuously. An infrared camera was installed in front of the sample to observe and record the infrared emission from the sample surface during the process. The dryer air velocity was regulated, measured and controlled by a digital hot wire anemometer TESTO 425 (precision ± 0.03 m/s). Considering previous results, the temperature and the optimal air velocity values were determinated at 40 ºC and 1.5 m/s. A reference material of known emissivity (ε = 0.95 - Optris GmbH, Berlin, Germany) was placed

next to the sample and recorded with the infrared camera with the aim to correct the emissivity of the sample. The temperature of the drying air, meat reference sample, reference material and environment were measured with K-thermocouples connected to an Agilent multiplexer 34901A (Agilent Technologies, Malaysia) and registered by an Agilent Data Acquisition equipment 34972A (Agilent Technologies, Malaysia) with the aim to correct the emissivities registered by the camera. A schematic diagram of the dryer is illustrated in Fig. 2.

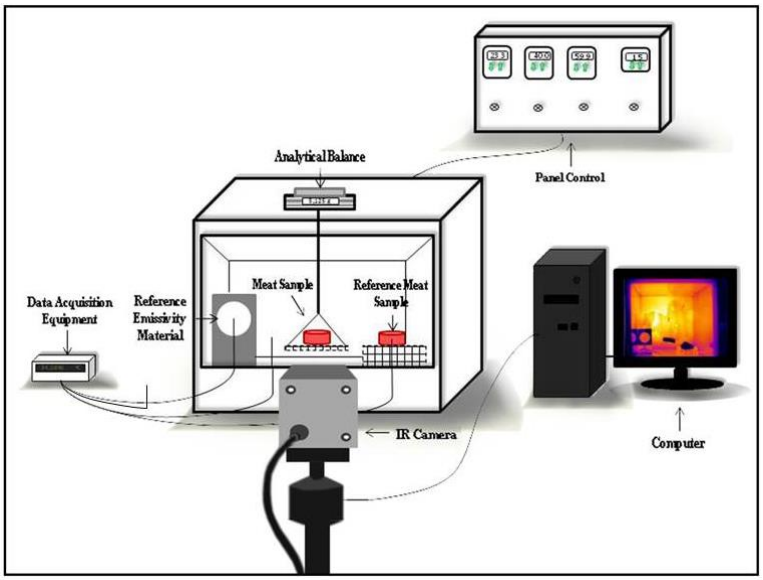

Fig. 2. Schematic diagram of the experimental dryer.

At the same time, a drying process to model the desorption isotherm was carried out with the aim to achieve the same atmosphere conditions in both drying processes. 15 samples were placed on a tray distributed in 3 columns and 5 lines. Each line corresponds to a different time of the isotherm curve, which had been previously determinate.

After the drying process, some measurements of every sample were made: mass, volume and water activity. Due to the fact that these determinations are non destructive, the samples were maintained for 24 h at 4 °C. After the repose time, the mass, volume, water activity and moisture were determined in the equilibrated samples.

2.3 Infrared Measurements

Thermal images were acquired using the Optris PI® 160 thermal imager (Optris GmbH, Berlin, Germany). It uses a two-dimensional Focal Plane array with 160x120 pixels, a spectral range of 7.5-13 μm, resolution of 0.05°C and an accuracy of ± 2%. The camera covers a temperature range of -20 to 100°C. It has a field of view of 23°x17° with a minimal focus distance of 0.02 m. The camera is supported by the software Optris PI Connect (Optris GmbH, Berlin, Germany).

3. RESULTS

3.1 Thermodynamic approach

Drying process involves complex structural phenomena which are hardly to explain in models that have already been published. The use of irreversible thermodynamics enables to involve the structure in water transport phenomena during drying.

It is important to highlight that the dried samples have a moisture and mechanical energy profile which induces a subsequent transport after the drying process. Due to this, the samples were measured immediately after drying and also after 24 hours of repose.

Mass variation of samples during the drying process can be obtained by the following Equation:

$$\Delta M = \frac{M^t - M^0}{M^0} \quad (1)$$

Where M represents the mass of the sample (kg) and the superscript t represents the process time, being 0 the initial time. The mass variation can be observed in the Fig. 3.

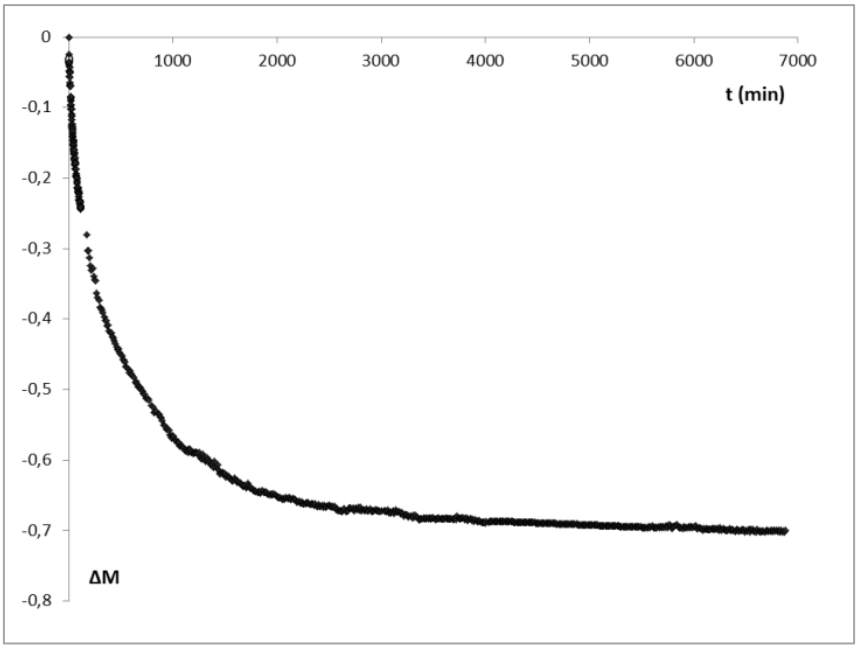

Fig. 3. Total mass variation of meat samples during the treatment.

In order to describe the different behaviours involved in the meat drying process, a thermodynamic approach has been developed. Gibbs free energy variation can be explained by the following equation (Castro-Giráldez *et al.*, 2010):

$$dG = -SdT + VdP + Fdl + \psi de + \sum_i \mu_i \, dn_i \quad (2)$$

Where: SdT corresponds to the thermic term and it is directly related to heat fluxes, VdP and Fdl are the mechanical energies related to the structural changes; where VdP corresponds to pressure variation and Fdl to the elongation force, finally ψde represents the effect of the electric field

induced by solved ions. The term $\sum_i \mu_i \, dn_i$ is the addition of the chemical potentials of all the compounds in the system considering P, T and the molar concentration of the rest of the compounds, constant.

This model fixes an interface between the sample and the air, and determines the free energy variation between them (Fig. 4).

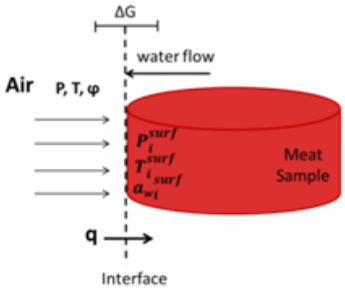

Fig. 4. Schematic diagram of the meat during the process.

If it is considered the free energy variation per mol of water, it is possible to define the extended water chemical potential according to the Equation 3:

$$\Delta\mu_w = \frac{\Delta G}{\Delta n_w} \tag{3}$$

From Equations 2 and 3 it is possible to obtain the Equation 4. The terms Fdl and ψde from equation 2 can be neglected because the muscular tissue is an elastic system and there is no ions effect since the sample only has the native ions of the meat, respectively.

$$\Delta\mu_w = -s_w(T_{air} - T_{surface}) + v_w(P_{air} - P_{surface}) + RT\ln\frac{\varphi^{air}}{a_w^{surface}} \tag{4}$$

Therefore, in order to obtain the extended water chemical potential, it is necessary to develop the partial molar entropy of water:

$$s_w = \frac{\Delta S}{n_w} = \frac{q}{n_w.T} = \frac{M\,.\,\Delta U}{n_w.T_{surf}} = \frac{c_p^{surf}.(T_{surf}-T_{ref})}{T_{surf}.x_w^{surf}}.Mr_W \tag{5}$$

Where c_p^{surf} corresponds to the specific heat of the sample surface (2.847 kJ/kgK), T_{surf} is the temperature of the sample surface (K), x_w^{surf} is the superficial moisture (g_w/g_{sample}) and Mr_W, the molar mass of water (18 g_w/mol_w). In order to estimate the internal energy, it has been used the reference system recommended by IuPAC for life systems (T_{ref}=273 K; P_{ref}=101325 Pa, liquid water) (IuPAC, 1997).

With the aim to estimate the moisture of the surface (x_w^{surf}), it was necessary to develop the desorption isotherm of the treated and equilibrated meat samples (Fig. 5). Water activity is a surface measurement and moisture is an average value of whole sample. In treated samples, a

moisture profile appears, but in equilibrated samples, moisture is homogeneous. Therefore, equilibrated isotherm represents the real relation between moisture and water activity. Thus, the equilibrated isotherm is an excellent tool to obtain, with the surface water activity of treated sample, the surface moisture of treated samples.

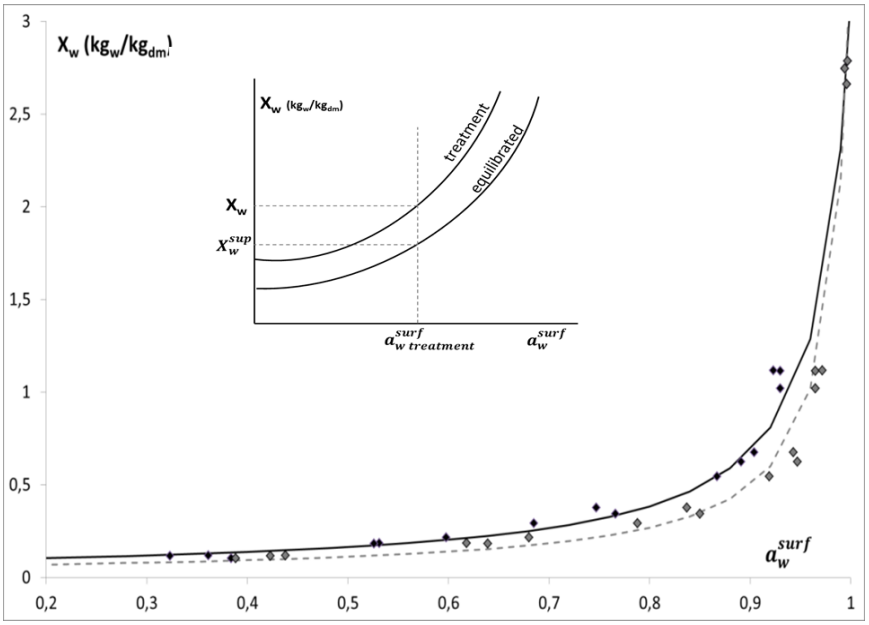

Fig 5. Desorption isotherm of treated (♦) and equilibrated (♦) samples. Where (—) correspond to the estimation of GAB model for the treatment samples and (- -) for equilibrated samples.

The sorption isotherms were fitted following the GAB model (Timmermann *et al.*, 2001), obtaining the parameters of table 1.

Table 1. GAB parameters of the treated and equilibrated meat samples.

Sample	X_{w0}	C	K
Treatment	0.085	250	0.972
Equilibrated	0.057	250	0.982

In order to obtain the surface temperature of the meat sample, an infrared model has been developed. For this purpose, it was obtained the energy flux received by IR the camera using the Equation 6.

$$E_T = \varepsilon_{cam}\sigma T_{cam}^4 \quad (6)$$

Where E_T is the energy flux received by the pyroelectrical detector of the IR camera (W/m2); ε, the emissivity (dimensionless); σ, the Stefan-Boltzmann constant ($5.67x10^{-8}$ W/m^2K^4) and T, the temperature (K), being the subscript "cam" the camera.

From equation 6, an energy flux balance of the pyroelectrical detector of the camera was developed, as it is shown in Equation 7.

$$E_T = F\,\varepsilon_{samp}\sigma T_{samp}^4 + (1 - \varepsilon_{sur})\sigma T_{sur}^4 - (1 - \tau_{air})F.\,\varepsilon_{samp}\sigma T_{samp}^4 \quad (7)$$

Where F is the geometric factor, being 1 because the meat surface was located in parallel with the camera, τ the transmissivity, being the subindexes: "samp" emitting object, "sur", emitting surroundings and "air", properties of air. The first term represents the energy flux emitted by the meat sample; the second term is the energy flux emitted by the surroundings and the third term represents the energy flux absorbed by the air. Latter was negligible due to the short distance between the sample and the camera (less than 20 cm) and because of the low air relative humidity.
To obtain the sample emissivity it was necessary to determine the energy emitted by the surroundings and it was estimated by the reference material energy (E_{ref}) with known emissivity (ε=0.95 - Optris GmbH, Berlin, Germany); it was estimated by following Equation:

$$E_T^{ref} = 0.95\,.\sigma\,.\,T_{ref}^4 + E_{sur} \quad (8)$$

Where, E_T^{ref} is the energy flux of the reference material (W/m^2) and T_{ref} is it temperature registered by the K-thermocouple (K). The energy flux emitted by the surroundings (E_{sur}) was calculated and subtracted from the energy flux emitted by the meat sample, which was registered by the IR camera.
The evolution of emissivity values with regard to the energy flux obtained for the meat sample can be observed in Fig. 6.

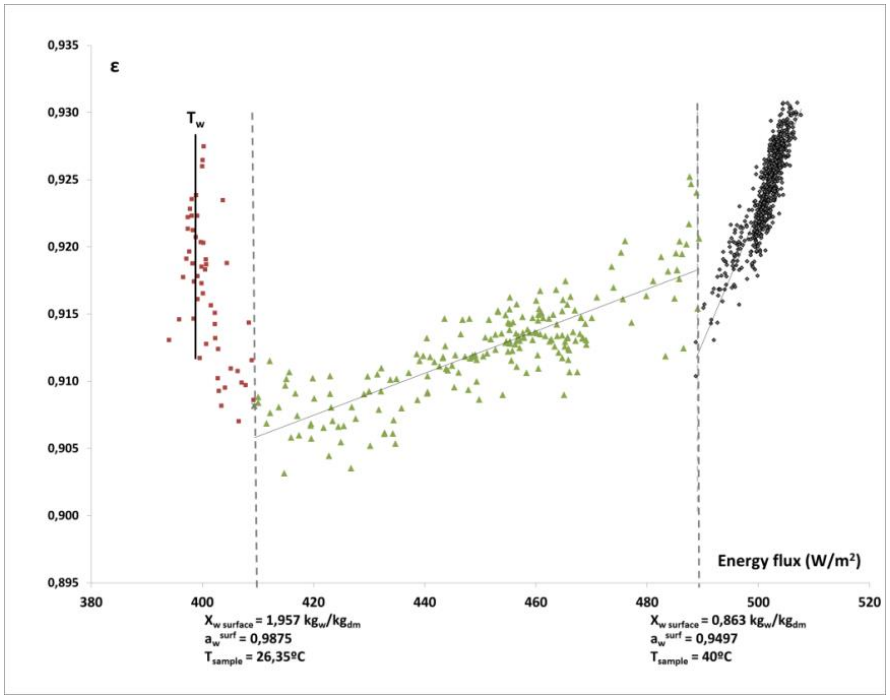

Fig. 6. Evolution of the meat emissivity in relation to the energy flux.

Emissivity shows the capability of meat sample to absorb radiant energy. Therefore, the evolution of the emissivity can describe the structural transformations of meat samples. Figure 6 shows three stages: the first at high moisture and low surface temperature, the second until the drying temperature and the last stage until the end of process. The traditional explanation of drying process divides the different mechanisms into three stages depending on the drying velocity. The first stage represents the coupling of mechanisms involved in the induction of water fluxes. The second stage represents the maximum and constant drying velocity. Through these stages the surface temperature decreases to the wet temperature of the air (induction period), and remains at the wet temperature (wet temperature increasing with the native solutes accumulation in surface) until the end of this period (constant drying velocity period). In Fig. 7, it is possible to observe the evolution of the surface temperature throughout the drying, where these two periods are shown.

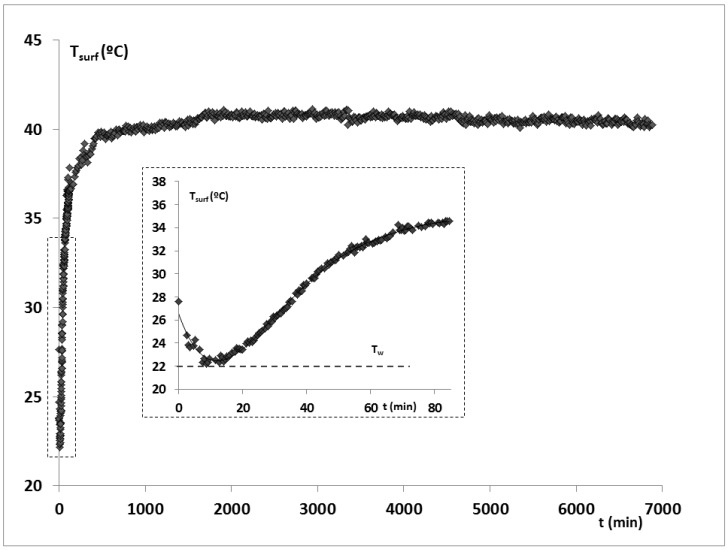

Fig. 7. Sample surface temperature with regard to the time.

In the traditional explanation, drying finishes with a period of falling drying rate, this period is driven by the low water internal transport, drying the surface and increasing the surface temperature till the air temperature. Fig. 7 shows two stages in the falling drying rate period: the first stage with surface temperature growing until air temperature (X_w^{surf} 1.957 kg_w/kg_{dm}, a_w^{surf} 0.9875 and T_{surf} 26.35 ºC) and the second with constant surface temperature (X_w^{surf} 0.863 kg_w/kg_{dm}, a_w^{surf} 0.9497 and T_{surf} 40 ºC). It is possible to appreciate that the response of the surface to absorb radiant energy (see Fig. 6) changes in the same critical points. The first critical point could be explained by the reduction of water mobility in the surface and the second critical point shows a structural transition in meat surface.

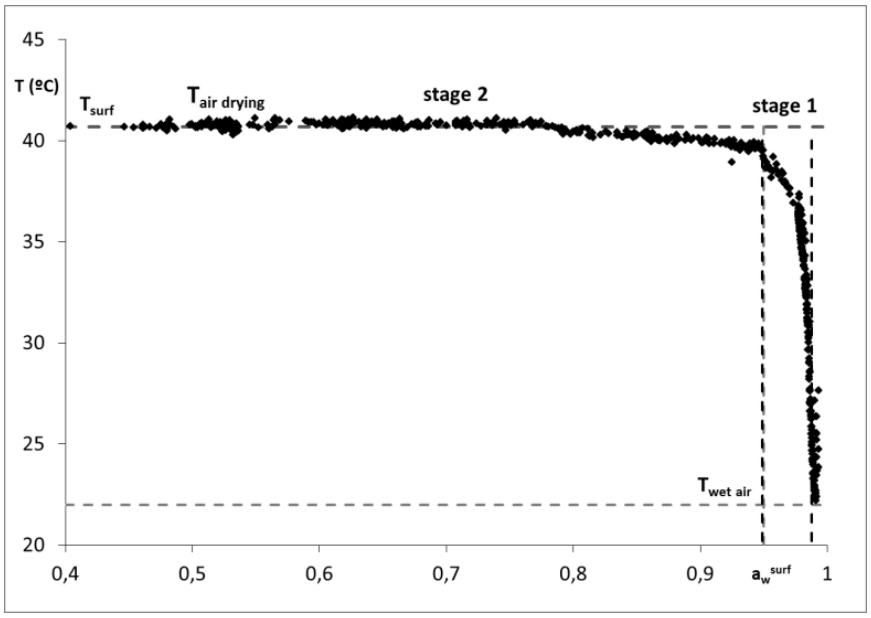

Fig. 8. Sample surface temperature with regard to the surface water activity of the sample.

In Fig. 8, it is represented the sample surface temperature versus the surface water activity. It can be distinguished the two stages, explained before, in the falling drying rate period. The figure shows, the first stage with high variation of the surface temperature and low variation of surface water activity, and the second stage with a high decrease of surface water activity with constant and maximum surface temperature (air drying temperature). As Fig. 6 shows, and it is repeated in Fig. 8, at 0.9497 of surface water activity, a critical point appears with a structural transformation of surface explained as a different response to the energy absorption and the water transport.
In order to understand how the water transports changes, it is necessary to estimate the water flux with next equation:

$$J_W = \frac{\Delta M_W . M_0}{\Delta t . A . Mr_W} \quad (9)$$

Where J_W is the water flux (mol/s m^2), ΔM_W represents the water mass variation (dimensionless), M_0 is the initial mass of the sample (g), Δt is the process time (s), A corresponds to the area of the sample during the treatment (m^2) and Mr_W is the molecular weight of water (18 g/mol). With parallel experiments (as explained in section 2.2.), the surface and volume variation has been obtained, and they are shown in Fig. 9.

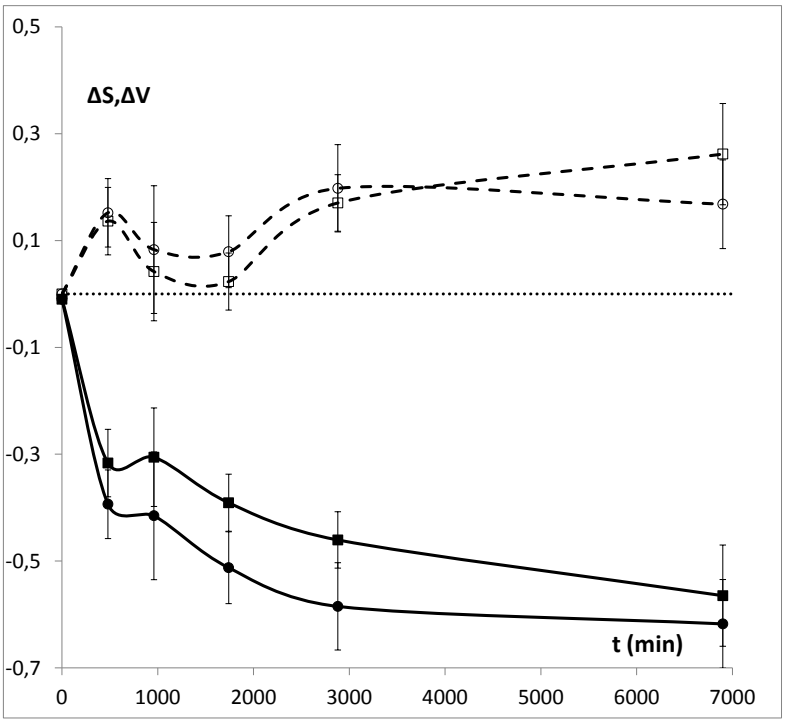

Fig. 9. Evolution of area (■;□) and volume (●;○) variation of the samples, where (—) corresponds to the treatment samples and (– –) equilibrated samples.

In Fig. 9, it is possible to observe the maximum volume and surface losses in the first 480 min, when the surface water activity is 0.9497. After this process time, the reduction is lower than before, and shows a different structural deformation after this critical point. The surface and volume variations show the liberation of mechanical energy through the equilibration time only in samples which have been dehydrated more than 2000 min; it could be shown a different mechanical response of the tissue.

With surface variation and Equation 9 it is possible to estimate the molar water flux (see Fig. 10).

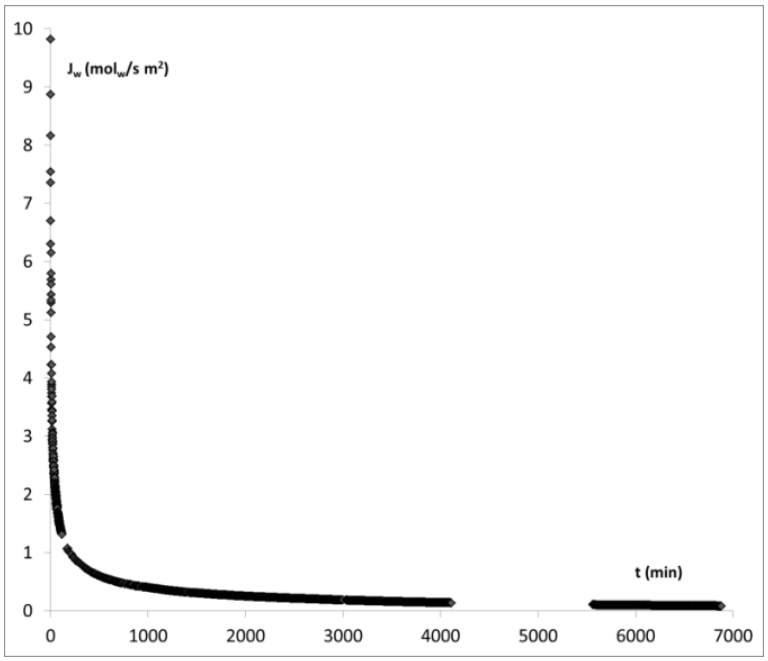

Fig. 10. Water fluxes of the treatment samples.

Applying the first relation of Onsager (Castro-Giráldez *et al.*, 2010), the water molar flux is related to the chemical potential, as a driving force of the water transport, by the phenomenological coefficient (Equation 10).

$$J_w = L_w \cdot \Delta\mu_w \tag{10}$$

In order to estimate the mechanical term of the chemical potential (see Equation 4), firstly it is necessary to determine the effect of the rest of terms (as Equation 11 shows):

$$\Delta\mu_w^* = -s_w \Delta T + RT\ln \frac{\varphi^{air}}{a_w^{surface}} \tag{11}$$

Where the superscript * represents the water chemical potential without considering the mechanical term.
Applying Equations 10 and 11, it is possible to obtain the phenomenological coefficient (Equation 12).

$$L_w^* = \frac{J_w}{\Delta\mu_w^*} \tag{12}$$

Where L_w^* represents the phenomenological coefficient without considering the mechanical term. In Fig. 11, it can be observed the L_w^* with regard to the water flux.

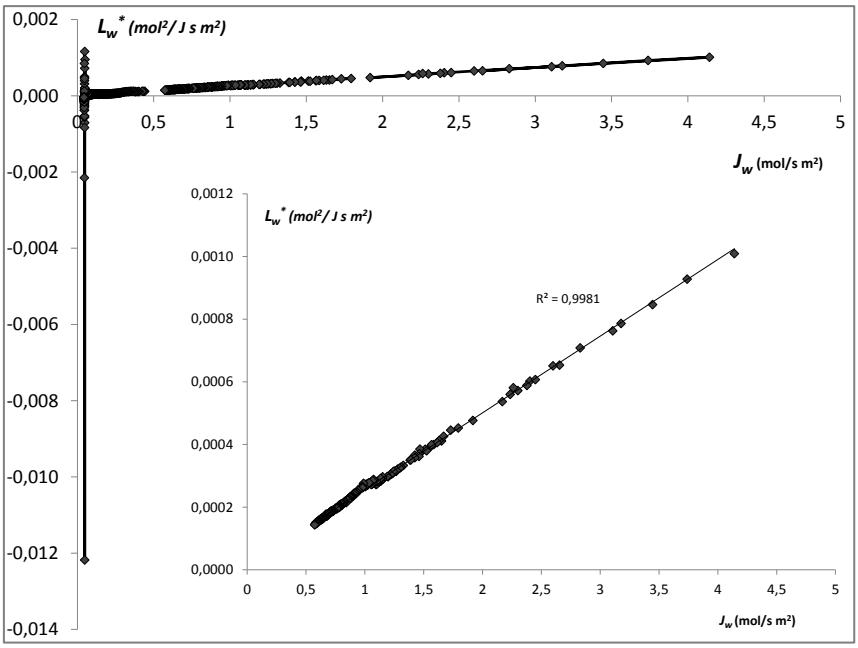

Fig. 11. Phenomenological coefficient (L_w^*) with regard to water flux (J_w).

Fig. 11 shows the relation between water flux and the phenomenological coefficient, being linear at the beginning of the dehydration, when the activity terms are bigger than the rest (amplification on Fig. 11 shows this range). Following the linear prediction of phenomenological coefficient, the real chemical potential could be estimated through the drying process. Therefore, mechanical term can be estimated as follows:

$$v_w \Delta P = \Delta\mu_w - \Delta\mu_w^* \quad (13)$$

Evolution of the mechanical energy, developed in the thermodynamic approach, is plotted in Fig. 12. Firstly, it can be appreciated small fluctuations of compression and relaxation, followed by a stage of high production of mechanical energy, which reduces the water flux. To liberate all the mechanical energy associated with the loss of water, as it is shown in Fig. 12, the tissue must be rigid (vitreous), unable to reduce its volume. This critical point is produced between a_w =0.481 and a_w =0.341, showing a new stage within the traditional falling rate period, called stage 3.

The mechanical energy compared with the deformation of treated samples is shown in Fig. 13, where it is possible to observe the different stages and periods of the drying process. Low level of mechanical energy production represents high deformation. When the deformation is finished, the mechanical energy grows, reducing the water flux and demonstrating the theory of a vitreous system.

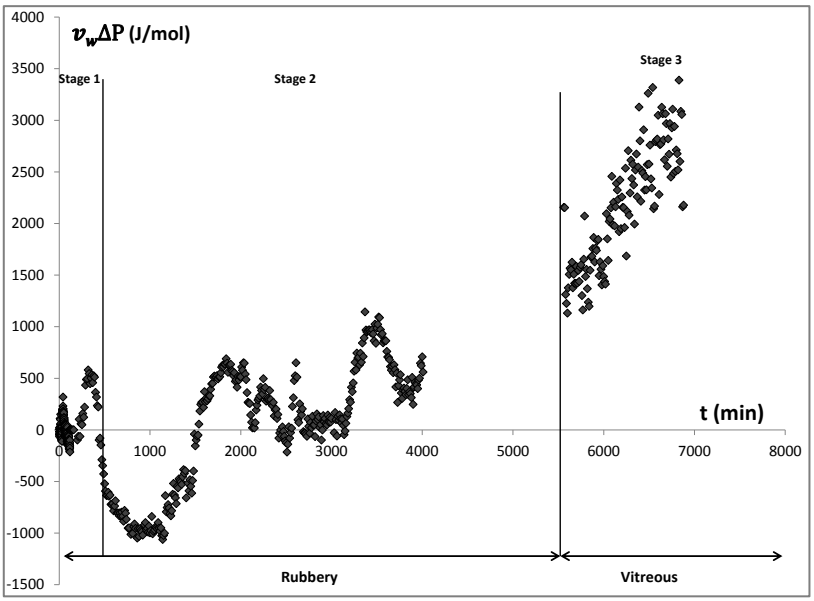

Fig.12. Evolution of the mechanical term through process.

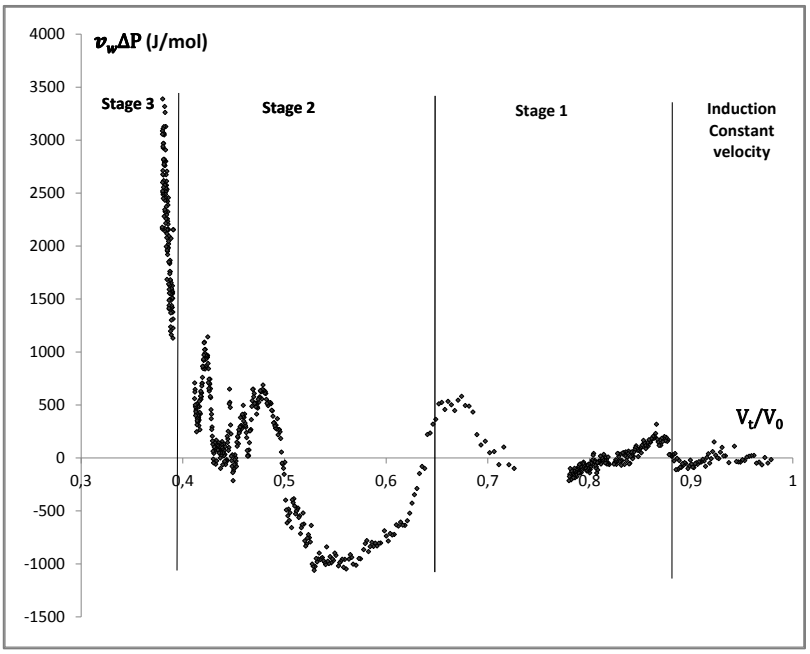

Fig. 13. Relationship between the mechanical term and deformation of samples.

4. CONCLUSIONS

It has been possible to demonstrate that the infrared thermography is a good tool for controlling the meat drying process, which provides information about the heat transfer in biological tissues, being possible to obtain the evolution of the meat emissivity and its clear relationship with the stages proposed for the falling rate period. So, with this technique, it is possible to identify the critical points and the surface temperature of the sample during the treatment.

The model allows us to predict the expansion/compression phenomena suffered by the sample throughout the drying process, predicting also the second order transition in the surface.

5. ACKNOWLEDGEMENTS

The authors acknowledge the financial support from the Spanish Ministerio de Ciencia e Innovación throughout the project AGL2011-30096 and also for the financial support from ERASMUS MUNDUS (Eurotango II Programme) for a scholarship to support María Victoria Traffano Schiffo´s PhD studies in Universidad Politécnica de Valencia, España.
Author Marta Castro-Giráldez thanks the Campus de Excelencia Internacional VLC/CAMPUS for their support.

6. REFERENCES

Akpinar, E. K. (2007). Thermodynamic analyses of strawberry drying process in a cyclone type dryer. *Journal of Scientific and Industrial Research*, 66(2), 152.

Akpinar, E. K., Midilli, A., & Bicer, Y. (2006). The first and second law analyses of thermodynamic of pumpkin drying process. *Journal of Food Engineering*, 72(4), 320-331.

Bulanon, D. M., Burks, T. F., & Alchanatis, V. (2008). Study on temporal variation in citrus canopy using thermal imaging for citrus fruit detection. *Biosystems Engineering*, 101(2), 161-171.

Castro-Giráldez, M., Fito, P. J., & Fito, P. (2011). Nonlinear thermodynamic approach to analyze long time osmotic dehydration of parenchymatic apple tissue. *Journal of Food Engineering*, 102(1), 34-42.

Castro-Giráldez, M., Fito, P.J., & Fito P., (2010). Non-equilibrium thermodynamic approach to analyze the pork meat (Longissimus dorsi) salting process. *Journal of Food Engineering*. 99 (1), 24-30.

Clemente, G., Bon, J., Sanjuán, N., & Mulet, A. (2011). Drying modelling of defrosted pork meat under forced convection conditions. *Meat science*, 88(3), 374-378.

Cuccurullo, G., Giordano, L., Albanese, D., Cinquanta, L., & Di Matteo, M. (2012). Infrared thermography assisted control for apples microwave drying. *Journal of Food Engineering*, 112(4), 319-325.

Ferrando, M., & Spiess, W. E. L. (2002). Transmembrane mass transfer in carrot protoplasts during osmotic treatment. *Journal of food science*, 67(7), 2673-2680.

Ferrando, M., & Spiess, W. E. L. (2003). Effect of osmotic stress on microstructure and mass transfer in onion and strawberry tissue. *Journal of the Science of Food and Agriculture*, 83(9), 951-959.

Fito, P. J., Ortolá, M. D., De los Reyes, R., Fito, P., & De los Reyes, E. (2004). Control of citrus surface drying by image analysis of infrared thermography. *Journal of Food Engineering*, 61(3), 287-290.

Gariepy, C., Amiot, J., & Nadai, S. (1989). Ante-mortem detection of PSE and DFD by infrared thermography of pigs before stunning. *Meat Science*, 25(1), 37-41.

Gowen, A. A., Tiwari, B. K., Cullen, P. J., McDonnell, K., & O'Donnell, C. P. (2010). Applications of thermal imaging in food quality and safety assessment. *Trends in Food Science & Technology*, 21(4), 190-200.

Huff-Lonergan, E. (2010). Chemistry and biochemistry of meat. In F. Toldrá (Eds.), Handbook of meat processing (pp. 5-24). Wiley-Blackwell, Iowa.

ISO 1442:1997. (1997). Methods of test for meat and meat products. Determination of moisture content. BS 4401-3:1997.

IUPAC (1997). Compendium of Chemical Terminology, 2nd ed. (the "Gold Book").

Lahiri, B. B., Dicya, M. P., Bagavathiappan, S., Thomas S., & Philip, J., (2012). Detection of pathogenic gram negative bacteria using infrared thermography. *Infrared Physics & Technology*, 55, 485-490.

McMinn, W. A. M., & Magee, T. R. A. (2003). Thermodynamic properties of moisture sorption of potato. *Journal of Food Engineering*, 60(2), 157-165.

Nanni Costa, L., Stelletta, C., Cannizzo, C., Gianesella, M., Lo Fiego, D. P., & Morgante, M. (2010). The use of thermography on the slaughter-line for the assessment of pork and raw ham quality. *Italian Journal of Animal Science*, 6(1s), 704-706.

Offermann, S., Bicanic, D., Krapez, J. C., Balageas, D., Gerkema, E., Chirtoc, M., et al. (1998). Infrared transient thermography for noncontact, non-destructive inspection of whole and dissected apples and of cherry tomatoes at different maturity stages. *Instrumentation Science and Technology*, 26(2&3), 145–155.

Pearce, K. L., Rosenvold, K., Andersen, H. J., & Hopkins, D. L. (2011). Water distribution and mobility in meat during the conversion of muscle to meat and ageing and the impacts on fresh meat quality attributes—A review. *Meat science*, 89(2), 111-124.

Seguí, L., Fito, P. J., & Fito, P. (2012). Understanding osmotic dehydration of tissue structured foods by means of a cellular approach. *Journal of Food Engineering*, 110(2), 240-247.

Seguí, L., Fito, P. J., Albors, A., & Fito, P. (2006). Mass transfer phenomena during the osmotic dehydration of apple isolated protoplasts (*Malus domestica* var. *Fuji*). *Journal of Food Engineering*, 77(1), 179-187.

Simal, S., Femenia, A., Castell-Palou, Á., & Rosselló, C. (2007). Water desorption thermodynamic properties of pineapple. *Journal of Food Engineering*, 80(4), 1293-1301.

Stajnko, D., Lakota, M., & Hočevar, M. (2004). Estimation of number and diameter of apple fruits in an orchard during the growing season by thermal imaging. *Computers and Electronics in Agriculture*, 42(1), 31-42.

Stoll, M., Schultz, H. R., & Berkelmann-Loehnertz, B. (2008). Exploring the sensitivity of thermal imaging for Plasmopara viticola pathogen detection in grapevines under different water status. *Functional plant biology*, 35(4), 281-288.

Timmermann, E.O., Chirife, J., Iglesias, H.A. (2001). Water sorption isotherms of foods and foodstuffs: BET or GAB parameters?. *Journal of Food Engineering*, 48, 19-31.

Vadivambal, R., & Jayas, D. S. (2011). Applications of thermal imaging in agriculture and food industry-a review. *Food and Bioprocess Technology*, 4(2), 186-199.

Veraverbeke, E. A., Verboven, P., Lammertyn, J., Cronje, P., De Baerdemaeker, J., & Nicolai, B. M. (2006). Thermographic surface quality evaluation of apple. *Journal of food engineering*, 77(1), 162-168.

Workmaster B. A., Palta, J. P., & Wisniewski, M., (1999). Ice nucleation and propagation in cranberry uprights and fruit using infrared video thermography. *Journal of the American Society for Horticultural Science*, USA, 124, 619.

STUDY OF THE APPLICATION OF DIELECTRIC SPECTROSCOPY TO PREDICT THE WATER ACTIVITY OF MEAT DURING DRYING PROCESS

Traffano-Schiffo, M.V., Castro-Giráldez, M., Colom, R.J., Fito, P.J.*

Instituto Universitario de Ingeniería de Alimentos para el Desarrollo, Universidad Politécnica de Valencia, Camino de Vera s/n, 46022 Valencia, España.

*author for correspondence: pedfisu@tal.upv.es

ABSTRACT

Drying is considered the most expensive operation because of the time and control required; therefore, it is necessary to optimize this stage of the production process. The measurement of dielectric properties appears to be a promising method for on-line monitoring of the drying process in the meat industry. Dielectric properties were measured for raw and dried Longissimus dorsi pork samples. The dielectric spectra were measured with an Agilent 85070E open-ended coaxial probe connected to an Agilent E8362B Vector Network Analyser in the frequency range of 500 MHz to 20 GHz. With this technique it was possible to conclude that there is a direct relationship between the dielectric loss factor at 20 GHz, considering the number of water molecules on the surface of samples. It was possible to determine the point of water activity at which the surface temperature reaches the air drying temperature, by using the loss angle at 20 GHz. At this point of water activity, the liquid phase disappears and internal transport controls the drying process. As a result, it was possible to develop a useful tool to predict the surface water activity by using the loss angle at 20 GHz.

Keywords: dielectric properties, sensor, microwave, drying, pork meat.

Nomenclature

a_j	activity of the chemical specie j (dimensionless)
M	mass (kg)
S	surface (m^2)
J	molar flux (mol s^{-1} m^{-2})
t	time (s)
M_r	Molecular weight (mol g^{-1})
x	fraction (gi g_T^{-1})
X	ratio (g_i g_{1-i}^{-1})

N	water molecules (water molecules g_{dm}^{-1})	Subscripts and superscripts	
N_A	Avogadro's number	w	water
		t	time point
		0	initial time
Greek Alphabet			
ε'	dielectric constant (dimensionless)	S	surface
		i	any chemical species
ε''	loss factor (dimensionless)	T	Total
δ	loss angle (rad)	ADS	adsorbed
		LP	Liquid Phase

1. INTRODUCTION

In recent years, the meat industry has been the object of numerous changes in order to optimize each operation of the production process. Despite the efforts and improvements made, the industry continues to use destructive methods with long response times to monitor the different process operations. With this in mind, non-invasive control methods and equipment based in dielectric spectroscopy have been developed and applied as useful tools.

Permittivity, expressed as complex or polar coordinates, defined by Maxwell's equations (Pozar, 1998), is the physical property that defines the interaction between any material and an electric field produced by a photon flux passing through it. Expressed as a complex number, the real part of permittivity is called the dielectric constant (ε'), which is related to the material's ability to store electric energy, and the dielectric loss factor (ε'') which is related to the absorption and dissipation of the electric energy. Expressed as a polar number, the modulus represents all the permittivity and electric energy absorbed, and loss angle represents the displacement of the electric field produced by the photon-molecule interaction, inducing electric energy dissipation.

In the microwave range, the interaction of the electric field with biological tissue produces two effects, γ-dispersion and ionic conductivity. The first can be observed at GHz frequencies (Gabriel *et al.*, 1996; Mohiri *et al.*, 2011; Venkatesh & Raghavan, 2004) and is due to the orientation and induction of the dipolar molecules. γ-dispersion produces electric storage (dielectric constant) and dissipation of the electric energy as other energy such as work or heat (loss factor). The main dipolar molecule of the muscle tissue is water; therefore, the dielectric measurements are a good tool to follow any mechanism driven by water molecules (Castro-Giraldez *et al.*, 2010b). The other important effect in the microwave range is ionic conductivity; this phenomenon covers a wider

range than the microwave range also including the range of radiofrequencies (Hz to 1GHz). The application of an electric field to biological tissue causes the vibration of ions, increasing the internal energy of the molecules; therefore, ionic conductivity only affects the loss factor.

Dielectric spectroscopy, in the range of radiofrequency and microwaves, has been used to monitor some products and processes, for example, salting level, composition of added compounds or quality determination in meat products (Castro-Giráldez *et al.*, 2010a; Castro-Giráldez *et al.*, 2010b; Kent *et al.*, 2002; Lyng *et al.*, 2005), ripening indexes, sugar content or moisture in fruits and cereals (Castro-Giráldez *et al.*, 2013; Nelson, 2005; Nelson, 2008; Nelson & Trabelsi 2006), degree of alcohol and sugar content throughout the beer fermentation process (Velázquez-Varela *et al.*, 2013).

In a previous work on meat drying (Traffano-Schiffo *et al.*, 2014), a thermodynamic model was proposed using average measures in samples (such as moisture, volume and weight), surface measures (such as surface water activity, surface thermal properties by infrared techniques and surface deformation) and thermodynamic air properties. This approach explained the internal behaviour throughout the surface phenomena, as the two mechanisms are coupled. During the meat drying process, critical transformations in the tissue produce different driving forces. This process has several different stages, the first stage corresponds to the induction period wherein different water flow mechanisms are coupled. The second stage represents the period in which the drying velocity reaches its maximum value, remaining constant and three more stages in the falling drying rate period, divided into the evolution of the surface internal energy and a vitreous transition at the end of the process.

Dielectric spectroscopy presents some advantages with regard to the traditional methods used for determining meat composition. In fact, it can be considered a relatively low cost, rapid method for monitoring the meat drying process, which gives us valuable information about water content, moisture and water activity during treatment. Therefore, describing its evolution and determining the final time of the process is feasible. Thus, the objective of the present research is to develop a non-invasive technique to predict the surface water activity throughout the meat drying process in real time by analysing the permittivity in the microwave range.

2. MATERIALS AND METHODS

Experiments were carried out using 6 loins (Longissimus dorsi, from Landrace x Duroc carcasses). The pigs were slaughtered in a commercial slaughterhouse and were collected at 1.5 days post-mortem. At the time of slaughter, the animals had a live weight of approximately 100-120 kg. The muscles were removed and kept at 4 ºC until sampled. A diagram of the experimental procedure is shown in Figure 1.

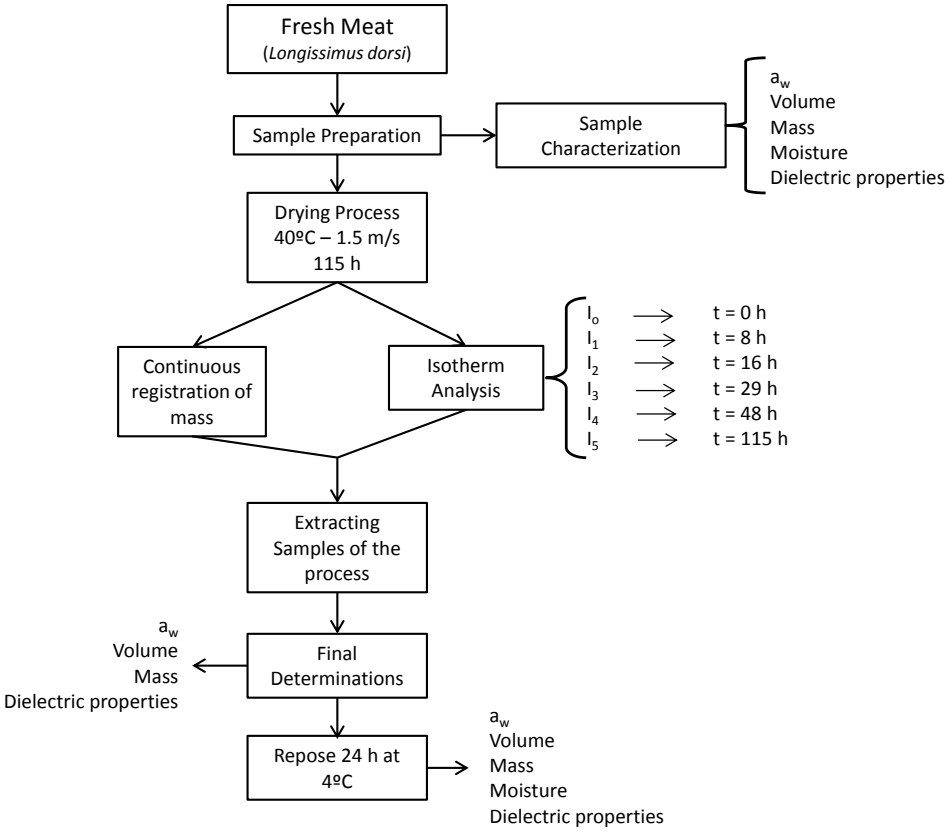

Figure 1. Diagram of the experimental procedure.

2.1 Meat Sampling and Characterization

56 cylindrical samples were used for each analysis (30 mm in diameter, height ranging from 10 to 15 mm). The cylinders were cut in the direction of the fibres. The mass of the samples were determined by a balance Mettler Toledo AB304-S (precision of ±0.001 g), and a dew point Hygrometer Decagon (Aqualab®, series 3 TE) was used to measure the surface water activity (precision of ±0.003, dimensionless). Water activity was obtained without mincing the sample, by inducing equilibrium between the sample's surface and the air, in order to measure the surface water activity.

Analysis of meat moisture was carried out following ISO 1442 (1997), i.e. drying the samples at 110 ºC at atmospheric pressure for 48 hours until a constant weight was reached.

Volume was determined by Image analysis using Adobe© Photoshop© CS6 software to obtain the diameter and the thickness of the samples.

The experiments were carried out in triplicate.

2.2. Drying Operation

Two drying operations were realized concurrently in different hot air dryers. In one of them, the sample was hung from a Mettler Toledo PG503-S balance (precision of ± 0.01 g) in order to register the mass throughout the drying process. However, in the second hot air dryer, 15 samples were placed in a tray distributed in 3 columns and 5 lines to model the desorption isotherm. Each line corresponds to a different time of the isotherm curve (8, 16, 29, 48 and 115 hours), which had been determined previously.

The dryer air velocity was regulated, measured and controlled by a digital hot wire anemometer TESTO 425 (precision of ±0.03 m/s).

The drying temperature and air velocity were chosen to reduce the mass and heat fluxes and to facilitate the coupling of transport phenomena (internal and external), and to avoid the crusting phenomenon on the surface of the meat. The chosen values were: 40 ºC and 1.5 m/s (Traffano-Schiffo *et al.*, 2014).

After the drying treatment (non-equilibrated samples), the following measurements were made for every sample: mass, volume, water activity and dielectric properties. Samples are without internal equilibrium, as mechanical profiles (gradients of internal pressure induced by the shrinkage-swelling phenomenon) and chemical profiles (internal gradients of water concentration) induced during the drying, maintain internal transport after treatment. Therefore, some properties change after treatment, until internal equilibrium is reached. In order to measure the properties in equilibrium, samples were packed in aqualab® disposable sample cups, sealed with parafilm®, for 24 hours at 4 ºC (equilibrated samples). After, permittivity, mass, volume, surface water activity and moisture were measured.

2.3 Permittivity measurement

Permittivity was measured with an Agilent 85070E open-ended coaxial probe connected to an Agilent E8362B Vector Network Analyser.

The system was calibrated using three different types of loads: air, short-circuit and 25 ºC Milli®-Q water. Once the calibration was carried out, 25 ºC Milli®-Q water was measured again to check calibration suitability.

Permittivity was measured by placing the probe on the surface of the samples perpendicular to the fibres. All determinations were carried out from 500 MHz to 20 GHz. The measurements were realized in triplicate.

3. RESULTS AND DISCUSSION

In order to understand the surface phenomena that occur throughout the drying process in meat, desorption isotherms of non-equilibrated and equilibrated samples, expressed in surface water activity were obtained (Figure 2). Water activity was obtained without mincing the sample, in order to measure the surface water activity. Moisture is an average measurement of the whole sample and was measured after the repose time. Moisture just after the treatment was estimated using mass balances. In non-equilibrated samples, a water concentration profile appears (induced by the drying process) but in equilibrated samples, moisture is homogeneous (internal equilibrium in samples is reached). Therefore, the equilibrated isotherm represents the real relationship between moisture and water activity. This is a good tool to obtain, with this isotherm and the surface water activity of non-equilibrated samples, the surface moisture of non-equilibrated samples. The sorption isotherms were fitted following the GAB model (Traffano-Schiffo *et al.*, 2014).

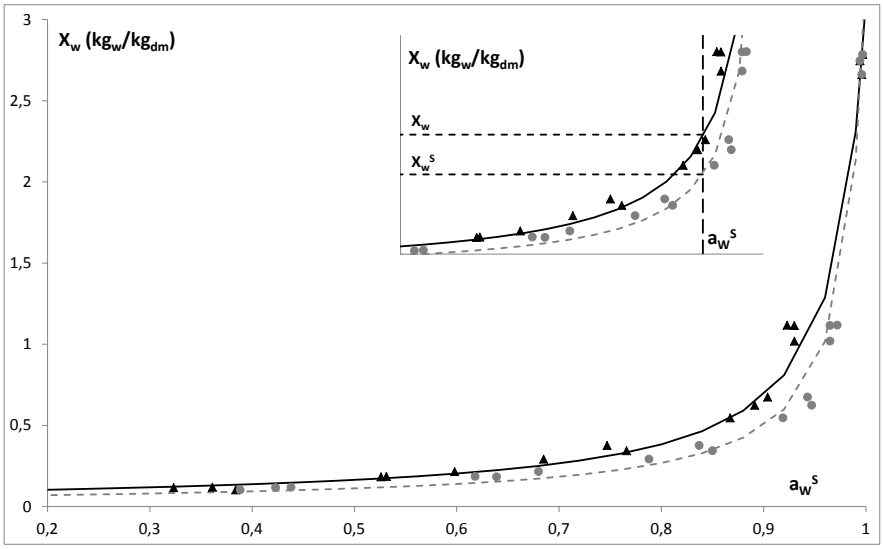

Figure 2. Representation of the desorption isotherm of (▲) non-equilibrated and (●) equilibrated samples. Where, (−) corresponds to the estimation of GAB model for the non-equilibrated samples and (- -) for equilibrated samples.

In Figure 3, the loss factor spectra of meat (from 500 MHz to 20 GHz) throughout the drying process can be observed. In this range, the spectrum shows two electric mechanics: γ-dispersion and ionic conductivity. In this figure, the initial frequency of γ-dispersion is observed at 2 GHz, below this frequency, the ionic conductivity effect can be observed. As was explained before, the main dipolar molecule in biological systems is water; therefore, any direct property related to water can be predicted with γ-dispersion. During the drying process, much of the behaviour related to water molecules appear, such as water fluxes, internal transitions related to moisture or surface water evaporation; all these mechanisms have the reduction of the quantity and the

mobility of the water molecules in common. The continuous reduction of sample spectra throughout the drying process is caused for this reason (Figure 3). The maximum effect of γ-dispersion (relaxation frequency) occurs around 20 GHz and decreases with process time. On the other hand, below 2 GHz, the main electric mechanism is ionic conductivity. Throughout the meat drying process, ion concentration increases with water loss, but ion mobility (ionic strength) decreases as its mobility depends on the quantity of water present. Consequently, the loss factor in this frequency range decreases with treatment as ionic conductivity is more dependent on ion mobility than ion concentration.

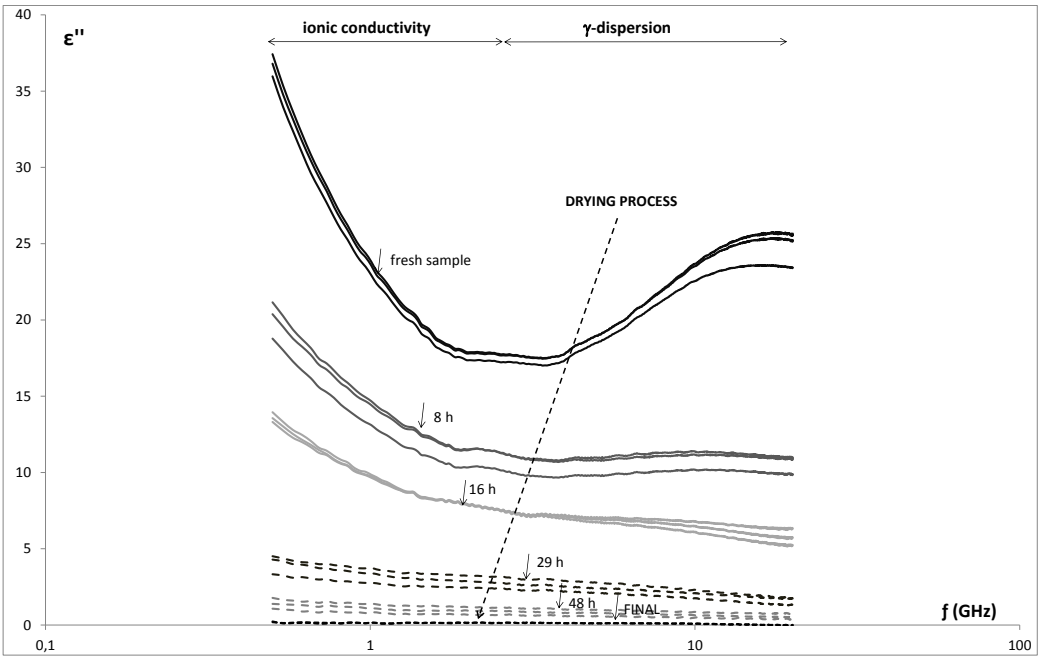

Figure 3. Dielectric loss factor spectra, where (—) corresponds to the fresh sample and the others lines correspond to different drying times: (—) 8, (—)16, (——) 29, (——) 48 and (- -) 115 hours.

Therefore, it is possible to relate the permittivity at frequencies of γ-dispersion with the quantity of water molecules on the surface of the sample. In order to estimate the quantity of water molecules, it is necessary to obtain the mass of these molecules. For this purpose, it is possible to consider the dry matter as a constant throughout the meat drying process, as the volatile compounds in meat are negligible in comparison with the quantity of water. Therefore, the evolution of the surface water mass can be expressed as surface moisture in dry basis. From this point of view, the water molecules can be calculated with the following equation (Eq. 1):

$$N = \frac{X_w^s \, N_A}{Mr_w} \qquad (1)$$

Where N represents the water molecules (water molecules/g_{dm}), X_w^s the surface moisture (g_w/gd_m), N_A the Avogadro constant ($6.022 \cdot 10^{23}$ mol^{-1}) and Mr_W the molar mass of water (18 g_w/mol_w).

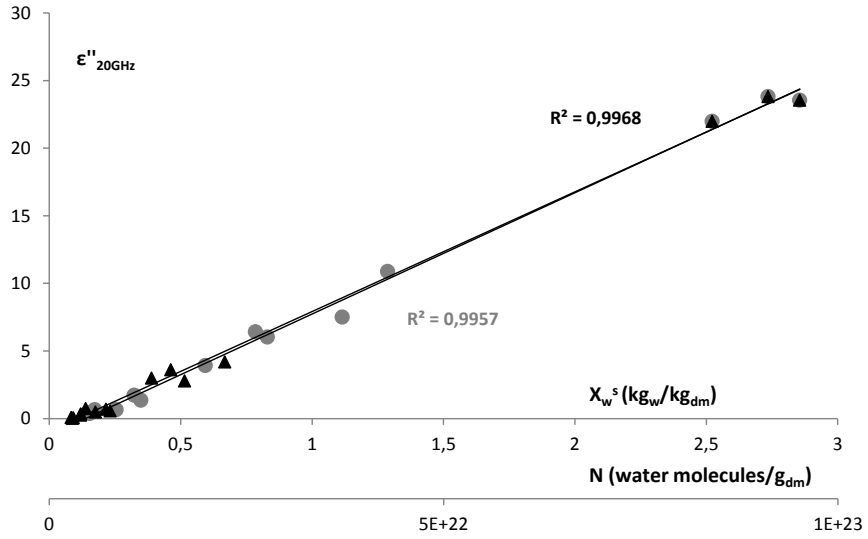

Figure 4. Dielectric loss factor at 20 GHz with regard to surface moisture in dry bases and number of water molecules, where (▲) non-equilibrated samples and (●) equilibrated samples.

Figure 4 shows the linear relationship between the surface moisture in dry basis and the number of water molecules on the surface with the loss factor at 20 GHz. This frequency is close to the γ-dispersion relaxation (as figure 3 shows).

If the surface moisture in dry basis explains the loss factor, it is possible to develop an isotherm based on dielectric properties to predict the surface water activity in non-equilibrated and equilibrated samples (Figure 5). Applying an adapted GAB model, developed for dielectric properties (eq. 2), some parameters were obtained: ε_0''=0.254, C = 250 and K = 0.999.

$$\varepsilon''(t) = \frac{\varepsilon_0'' C\, a_w}{(1-K\, a_w)(1+(C-1)a_w)} \qquad (2)$$

Where: $\varepsilon''(t)$ corresponds to the loss factor at 20 GHz and at a determined time point, ε_0'' corresponds to the minimum value of loss factor, C and K are empirical constants (dimensionless).

As figure 3 shows, a strong reduction of γ-dispersion appears after 16 hours of treatment, the bell shape of the dispersion disappears. This behaviour can be explained by the reduction of water mobility, as the liquid phase of samples disappears and only absorbed or retained water remains in the sample. The dielectric isotherm, shown in figure 5, is not accurate enough for water activities

below 0.82. At values of aw below 0.82, the loss factor in the γ-dispersion does not explain the water activity of the sample's surface well, as the reduction in water activity does not produce a reduction in the loss factor at 20 GHz. Therefore, an alternative model is necessary to describe the behaviour of the water in the whole water activity range, as is a useful tool to predict it.

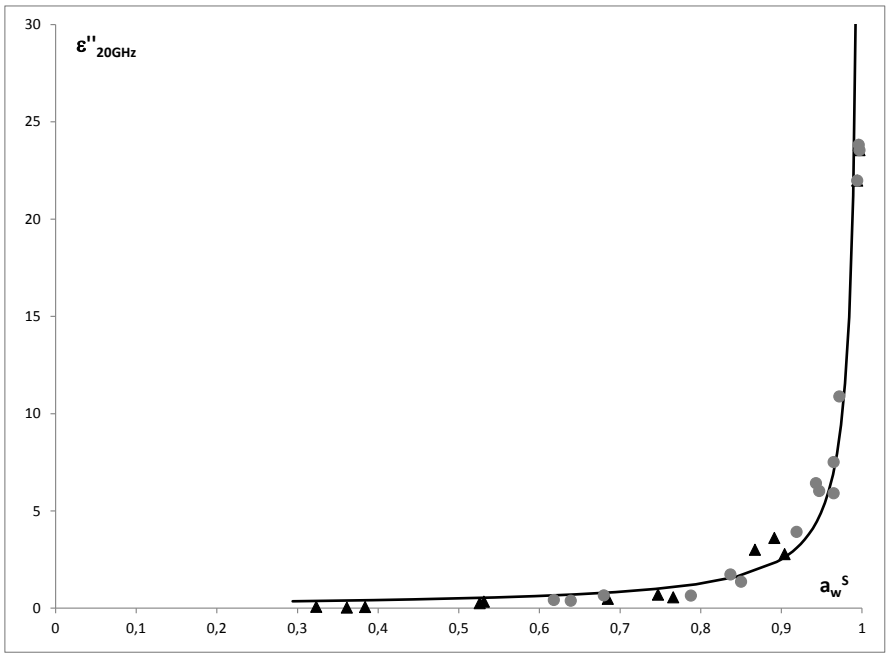

Figure 5. Relationship between the loss factor at 20 GHz and surface water activity, where (▲) non-equilibrated samples and (●) equilibrated samples and (—) represents the prediction of loss factor values versus surface water activity by the adapted GAB model.

In order to better comprehend how the water molecules are distributed in the tissue during the drying process, and to better predict the water activity, permittivity was transformed from a complex to a polar number. Polar permittivity is expressed by the modulus and phase (loss angle). Loss angle represents the displacement of the electric field produced by the quantity and mobility of water molecules. Figure 6a shows the loss angle with regard to the water activity, where it is possible to observe two tendencies of the data, with two different slopes and with the intersection value of water activity at 0.815. Figure 6b, adapted from Traffano-Schiffo *et al.*, 2014, shows a parallel experiment of this work, in the same drying conditions, where it is possible to observe the critical point of water activity at the same value (a_w^S = 0.815); at this point, the surface temperature reaches the air drying temperature. This means that the liquid water on the surface (liquid phase) disappears, and internal transport takes control of the process (internal water transport is the slowest because there is only adsorbed or retained water). This same critical water activity was reported by several authors, such as Labuza *et al.*, (1970), and Roos and Karel (1991), where they describe this critical point of water mobility as the main phenomenon responsible for the inhibition of microbiological reactions and food deterioration.

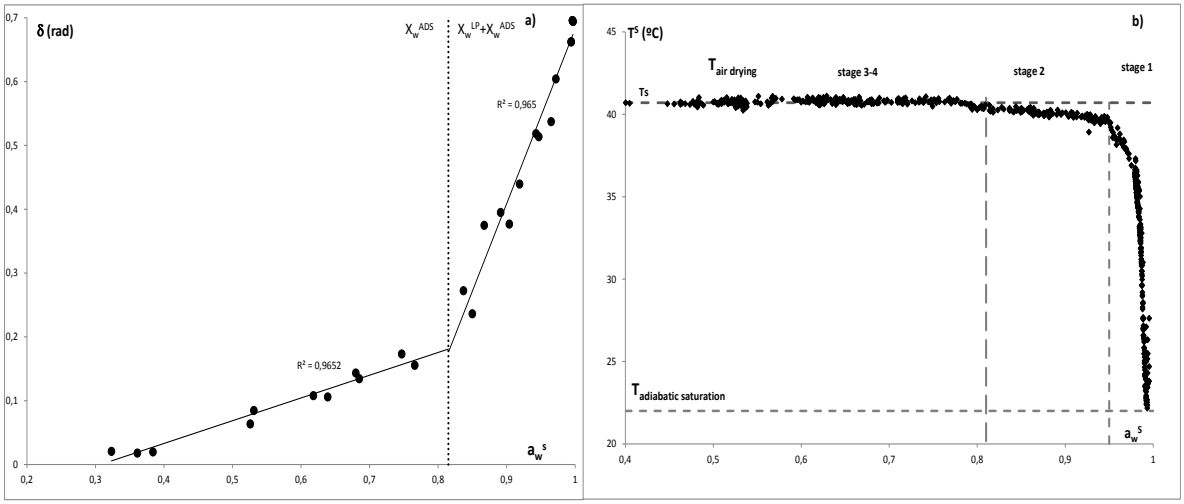

Figure 6. a) Loss angle at 20 GHz versus surface water activity, b) Sample surface temperature with regard to the surface water activity (Adapted from Traffano-Schiffo *et al.*, 2014).

Figure 6a also shows an exponential shape, common in coupled behaviour, as was explained before; therefore it is possible to develop a useful tool to predict the surface water activity by using the loss angle at 20 GHz, as this parameter has an exponential relationship with the aw (Eq.3) (Figure 7).

$$\log_{10}\delta = \log_{10}\delta_0 + k \cdot a_w^S \qquad (3)$$

Where: δ is the loss angle at 20 GHz, δ_0 corresponds to the loss angle at the minimum a_w^S, being the value: 0.0038 ± 0.0009. k is an empirical parameter that explains the exponential relation between the loss angle and water activity, with a value of 2.26±0.11.

Figure 7 has a correlation coefficient of R^2 = 0.9841, which shows that this model is a good tool to describe food systems during drying.

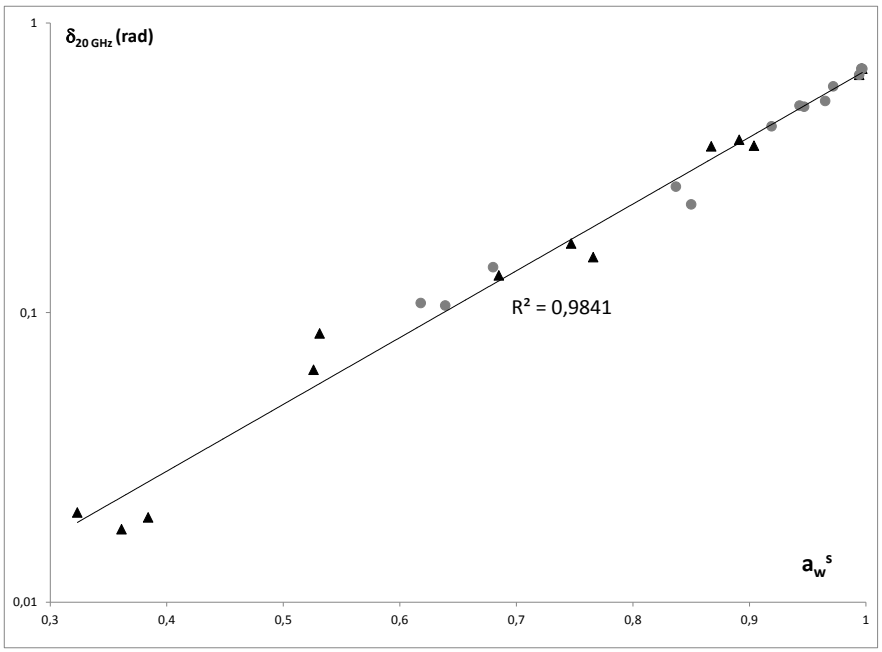

Figure 7. Semi-logarithmic plot of loss angle at 20 GHz versus surface water activity, where (▲) non-equilibrated samples and (●) equilibrated samples.

4. CONCLUSIONS

It was possible to demonstrate that the loss factor in γ-dispersion presents a direct relationship with the number of water molecules on the sample's surface. It was possible to determine the point of water activity at which the surface temperature reaches the air drying temperature, using the loss angle at 20 GHz. At this point of water activity, the liquid phase disappears and internal transport controls the drying process. As a result, it was possible to develop a useful tool to predict the surface water activity using the loss angle at 20 GHz.

5. ACKNOWLEDGEMENTS

The authors acknowledge the financial support of the Spanish Ministerio de Ciencia e Innovación through the project AGL2011-30096 and also for the financial support from ERASMUS MUNDUS (Eurotango II Programme) for a scholarship to support María Victoria Traffano Schiffo's PhD studies at Universidad Politécnica de Valencia, España. The author Marta Castro-Giráldez wishes to thank the UPV Postdoctoral Program (PAID-10-14) of Universidad Politécnica de Valencia for their support.

6. REFERENCES

Castro-Giráldez, M., Aristoy, M., Toldrá, F., & Fito, P., 2010a. Microwave dielectric spectroscopy for the determination of pork meat quality. *Food Research International*, 43, 2369-2377.

Castro-Giráldez, M., Fito, P.J. & Fito, P., 2010b. Application of microwaves dielectric spectroscopy for controlling pork meat (*Longissimus dorsi*) salting process. *Journal of Food Engineering*, 97 (4), 484-490.

Castro-Giráldez, M., Fito, P. J., Ortolá, M. D., & Balaguer, N., 2013. Study of pomegranate ripening by dielectric spectroscopy. *Postharvest Biology and Technology*, 86, 346-353.

Gabriel, C., Gabriel, S., & Corthout, E.,1996. The dielectric properties of biological tissues: I. Literature survey. *Physics in medicine and biology*, 41, 2231-2249.

ISO 1442:1997. 1997. Methods of test for meat and meat products. Determination of moisture content. BS 4401-3:1997.

Kent, M., Peymann, A., Gabriel, C., & Knight, A., 2002. Determination of added water in pork products using microwave dielectric spectroscopy. *Food Control*, 13, 143-149.

Labuza, T.P., Tannenbaum, S.R., and Karel, M., 1970. Water content and stability of low moisture and intermediate moisture foods. *Food Technology* 24:543–550.

Lyng, J. G., Zhang, L., & Brunton, N. P., 2005. A survey of the dielectric properties of meats and ingredients used in meat product manufacture. *Meat Science*, 69, 589-602.

Mohiri, A., Burhanudin, Z. A., & Ismail, I., 2011. Dielectric properties of slaughtered and non-slaughtered goat meat. In RF and Microwave Conference (RFM), 2011 IEEE International (pp. 393-397). IEEE.

Nelson, S. O., 2005. Dielectric spectroscopy in agriculture. *Journal of non-crystalline solids*, 351, 2940-2944.

Nelson, S. O., 2008. Dielectric properties of agricultural products and some applications. *Research in Agricultural Engineering*, 54, 104-112.

Nelson, S. O., & Trabelsi, S., 2006. Dielectric spectroscopy of wheat from 10 MHz to 1.8 GHz. *Measurement Science and Technology*, 17, 2294-2298.

Pozar, D.M., 1998. Electromagnetic Theory. In Microwave Engineering (2nd ed., pp.5-9), John Wiley & Sons, Inc., U.S.A.

Roos, Y., and Karel, M., 1991. Applying state diagrams to food processing and development. *Food Technology,* 45(12):66–71.

Traffano-Schiffo, M.V., Castro-Giráldez, M., Fito, P.J. & Balaguer, N., 2014. Thermodynamic model of meat drying by infrarred thermography. *Journal of Food Engineering*, 128, 103-110.

Velázquez-Varela, J., Castro-Giráldez, M., & Fito, P. J., 2013. Control of the brewing process by using microwaves dielectric spectroscopy. *Journal of Food Engineering*, 119, 633-639.

Venkatesh, M. S., & Raghavan, G. S. V., 2004. An overview of microwave processing and dielectric properties of agri-food materials. *Biosystems Engineering*, 88, 1-18.

4.2. Desarrollo de un sensor en radiofrecuencia para la detección de ciclos de congelación/descongelación en carne de cerdo.

Castro-Giraldez, M., Colom, R.J., Fito, P.J., Herrero, V., Lidón, J.V., Monzó, J.M., Tébar, A., **Traffano-Schiffo, M.V.** (2016). Aparato y método no invasivo de detección de roturas de la cadena de frío en carne congelada. **Patente Española P201630956.**

PATENTE P201630956: APARATO Y MÉTODO NO INVASIVO DE DETECCIÓN DE ROTURAS DE LA CADENA DE FRÍO EN CARNE CONGELADA

OBJETO DE LA INVENCIÓN

La presente invención permite el análisis de aspectos clave relacionados con la calidad y la seguridad alimentaria de carne congelada mediante la aplicación de espectros dieléctricos en la carne congelada.

Concretamente, el objeto de la presente invención se refiere a un aparato y método no invasivo de detección de roturas de la cadena de frío en carne congelada. Asimismo, la presente invención es capaz determinar los ciclos de congelación/descongelación a los que la carne congelada ha sido expuesta, así como cuantificar su tiempo de almacenamiento en estado de congelación.

MODALIDAD: **PATENTE DE INVENCIÓN**

SOLICITANTE: **UNIVERSITAT POLITÈCNICA DE VALÈNCIA**

INVENTORES:

Inventor 1: Marta Castro Giráldez (España)

Inventor 2: Ricardo José Colom Palero (España)

Inventor 3: Pedro José Fito Suñer (España)

Inventor 4: Vicente Herrero Bosch (España)

Inventor 5: José Vicente Lidón Roger

Inventor 6: José María Monzó Ferrer (España)

Inventor 7: Ángel Tébar Ruiz (España)

Inventor 8: María Victoria Traffano Schiffo (Argentina)

RESUMEN

La presente invención se refiere a un aparato no invasivo de detección de roturas de la cadena de frío en carne congelada, que comprende un sensor, un dispositivo de acondicionamiento vinculado con dicho sensor y una unidad de control vinculada con el dispositivo de acondicionamiento, donde el sensor comprende:

- Un electrodo de inyección, contactable con la superficie de la carne congelada de manera no invasiva para aplicar sobre dicha carne congelada una señal de inyección generada en el dispositivo de acondicionamiento, y,

- Un primer y un segundo electrodo de medición, contactables con la superficie de la misma carne congelada de manera no invasiva para recibir desde dicha carne congelada la señal de medición; y para enviar esta señal de medición a la unidad de control, a través del dispositivo de acondicionamiento, además de al método que hace uso de dicho aparato.

4.3. Estudio espectrofotométrico en carne de pollo y su relación con los parámetros de calidad de la carne fresca (PSE, Normal y DFD).

Traffano-Schiffo, M. V., Castro-Giráldez, Colom, R., J., M., & Fito, P. J., (2017). Innovative spectrophotometric system to determine chicken meat quality. ***Innovative Food Science and Emerging Technologies***. Artículo enviado.

INNOVATIVE SPECTROPHOTOMETRIC SYSTEM TO DETERMINE CHICKEN MEAT QUALITY

Maria Victoria Traffano-Schiffo[a], Marta Castro-Giraldez[a], Ricardo J. Colom[b] & Pedro J. Fito[a]*
[a] Instituto Universitario de Ingeniería de Alimentos para el Desarrollo, Universidad Politécnica de Valencia, Camino de Vera s/n, 46022 Valencia, España.
[b] Instituto de Instrumentación para Imagen Molecular, Universitat Politecnica de Valencia, Camino de Vera s/n, 46022 Valencia, Spain.

*author for correspondence: pedfisu@tal.upv.es

ABSTRACT

Nowadays, one of the most important challenges of poultry industry is to determine individually the meat quality class (PSE, normal and DFD) by non invasive, accurate and fast technique. For this purpose, dielectric spectra in radiofrequency and microwave ranges were studied. In radiofrequency range, the permittivity was measured by a non-destructive sensor conformed by three points with blunt-ended electrodes connected to an Agilent 4294A impedance analyser, and in microwave range an Agilent 85070E open-ended coaxial probe connected to an Agilent E8362B Vector Network Analyser were used. This work demonstrates the direct relation between the pH evolution and the dielectric constant at α-dispersion, and also, that the main structural proteins degradation has direct relation with the dielectric constant at β-dispersion, being possible to segregate meat depending on the level of protein degradation. Finally, this paper ends with a classification model for quality poultry meat based on a spectrophotometric analysis at radiofrequency range by using the Traffano-Schiffo model.

Keywords: poultry meat, quality, permittivity, radiofrequency, microwave, dispersion.

Industrial relevance

In recent decades, poultry slaughterhouses and the entire fresh poultry meat and poultry products industry have suffered from the difficulty to detect low quality meat such as PSE and DFD. Nowadays, the techniques used are tedious and require destroying the sample, therefore, any classification system that allows the segregation of poultry meats according to their quality would greatly improve the productivity of the industry.

This paper presents a classification model for quality poultry meat based on spectrophotometric techniques in radiofrequency range, and represents a good and non-destructive tool able to determine poultry meat quality.

1. Introduction

Meat sector is one of the most important in Europe (Traffano-Schiffo, Castro-Giráldez, Fito, & Balaguer, 2014), being poultry meat which shows one of the highest consumption increases all over the world (Barbin *et al.*, 2016) since it is considered one of the healthiest meats of the diet (Barbin *et al.*, 2015). Normal poultry meat is considered when the pH range is between 5.8 to 6.0 at 12 hours post-mortem time (pmt), due to the right post mortem pathways (Zhang, & Barbut, 2005). However, one of the most frequent defects of poultry meat is the Pale, Soft and Exudative (PSE) and Dark, Firm and Dry (DFD) meats, which causes quality and stability problems in processed products (Adzitey, & Nurul, 2011; Castro-Giráldez, Aristoy, Toldrá, & Fito, 2010a; Langer *et al.*, 2010; Swatland, 2008; Damez, Clerjon, Abouelkaram, & Lepetit, 2008).
PSE meat is characterized by a significantly lower pH, higher L* colour value, soft texture and low water retention (Barbut, Zhang, & Marcone, 2005). The main cause of these meat defects is an accelerated post-mortem glycolysis rate, causing sarcoplasmic and myofibrillar protein denaturation (Sosnicki, Greaser, Pietrzak, Pospiech, & Sante, 1998). Some reports have linked the PSE meat with two genetic mutations in pigs: Ryanodine receptor or Halothane gene mutation, causing Porcine Stress Syndrome or Malignant Hyperthermia; however, these gene mutations have not been demonstrated in poultry (Barbut *et al.*, 2008). It has been reported that the incidence in PSE chicken meat is higher than 37% (Woelfel, Owens, Hirschler, Martinez-Dawson, & Sams, 2002; Woelfel, Owens, Hirschler, & Sams, 1998), which represents high economic losses.

In contrast, DFD meat is characterized by a dark colour and a short shelf life due to the high pH value (Allen, Russell, & Fletcher, 1997), being susceptible to contamination. This quality issue is mainly caused by a prolonged chronic stress, such as long transportation periods, which depletes muscle glycogen, and therefore the drop in the pH is limited by the amount of the glycogen available. Besides the contamination problems, another important factor is the dark appearance, which affects the colour of processed products and consumer acceptability (Chan, Omana, & Betti, 2011).
Despite efforts in a rapid detection system of PSE and DFD meats, nowadays this problem remains being one of the major challenges for the food industry. Therefore, sensors based on spectrophotometry at radiofrequency (RF) and microwave (MW) ranges can provide a huge improvement on the monitoring system.
Spectrophotometry expressed as permittivity and defined by Maxwell´s equations (Pozar, 1998) must be explained as a vector, polar or complex number. As a complex number, the real term or dielectric constant (ε') is related to the tissue´s ability to store electric energy and the imaginary term or dielectric loss factor (ε'') is related to the absorption and dissipation of the electric energy (Traffano-Schiffo, Castro-Giraldez, Colom, & Fito, 2017; Castro-Giráldez, Fito, Chenoll, & Fito,

2010b). In RF and MW ranges, it is possible to distinguish different dispersions along the electric spectra, being α, β, and γ the most relevant (Schwan, 1957).

α-dispersion, appears from few Hz to few kHz, is related with the phenomenon of the orientation of charges with mobility, soluble or suspended (electrolytes, charges with low molecular weight and high charge) in liquid phase.

β-dispersion usually occurs in the frequency region from tens of kHz to tens of MHz. This dispersion covers all the mechanisms involved in the orientation of fixed charges in solid surfaces in macromolecules such as proteins. These charges may belong to the chemical structure of the food or can be produced by the surface tension of the structure matrix. At higher frequency range of β-dispersion the main interactions are the surface tension charges; this interaction is called Maxwell-Wagner effect (Wolf, Gulich, Lunkenheimer, & Loidl, 2012).

In the range of microwaves, the interaction of the electric field with biological tissue produces two effects, γ-dispersion and ionic conductivity (Traffano-Schiffo, Castro-Giraldez, Colom, & Fito, 2015). The first one can be observed at GHz frequencies (Mohiri, Burhanudin, & Ismail, 2011; Venkatesh & Raghavan, 2004) and it is due to the dipolar molecules orientation and induction, being the water the main dipolar molecule of the muscle tissue. Other important effect in microwave range is ionic conductivity at frequencies from Hz to MHz. The application of an electric field to biological tissue causes vibration of ions increasing the internal energy of the molecules, therefore, the ionic conductivity only affects to the loss factor (Talens, Castro-Giraldez, & Fito, 2016).

The aim of this research was to analyse the viability of using the dielectric spectroscopy (in RF and MW ranges) to identify PSE, normal and DFD quality classes in chicken breast meat.

2. Materials and methods

The experiments were carried out using chicken breasts (Pectoralis major) with 12 hours of pmt, obtained from SADA Group slaughterhouse located in Rafelbunyol, Valencia, Spain. In the slaughterhouse, carcasses were cooled at 4 hours of pmt in the cooling tunnel and after that, the breasts were collected boneless and skinless at 5 hours of pmt, which were transported to the laboratory using isothermal bags with ice in order to maintain the samples at 2 ºC. Once arrived at the laboratory, the samples were maintained at 4 ºC until 12 hours of pmt till its analysis.

The pH of samples was measured with a punch pH-meter S-20 SevenEasy™ (Mettler Toledo, Barcelona, Spain). The colour was measured by the surface reflectance spectra in a spectrocolorimeter Minolta CM-3600D (Minolta Co. Ltd., Tokio, Japan). The colour coordinates CIE L*a*b* (CIE, 1978) were instrumentally calculated based on D65 illuminant and 10º observer. The water activity was determined by a dew point Hygrometer Decagon (Aqualab®, series 3 TE) with a precision of ± 0.003. The analysis of moisture was accomplished following the ISO 1442 (1997) by drying the samples at 110 ºC at atmospheric pressure during 48 hours until a constant weight was reached.

All measurements were made in triplicate.

2.1. Dielectric Spectroscopy Measurements

2.1.1. Radiofrequency range

The system used consists on a non-destructive sensor conformed by three points with blunt-ended electrodes, developed by The Institute of Food Engineering for Development (IuIAD) and The Institute for Molecular Imaging Technologies (I3M), patented by the authors, P201630956 (Castro-Giraldez *et al.*, 2016), connected to an impedance analyser *Agilent* 4294A (Fig. 1). The frequency range measured was from 40 Hz to 1 MHz. Calibration of the equipment was performed in open (air) and short-circuit.

The signal obtained by the Agilent analyser is the impedance $\boldsymbol{Z}$, and taking into account that the impedance is a vector and can be expressed as a complex number as $\overline{\boldsymbol{Z}} = \boldsymbol{R} + \boldsymbol{jX}$, where the real part of the impedance is the resistance R and the imaginary part is the reactance X. It is possible to estimate ε', ε'' by using R and X parameters as follows:

$$\varepsilon' = \frac{-X}{(R^2 + X^2)} \frac{1}{2\pi C_0} \quad (1)$$

$$\varepsilon'' = \frac{R}{R^2 + X^2} \frac{1}{2\pi f C_0} \quad (2)$$

$$C_0 = \frac{\varepsilon_0 S}{d} \quad (3)$$

Where f is the frequency (Hz), $\boldsymbol{C_0}$ is the capacitance in the vacuum (F), S is the surface of the electrodes (m2), $\boldsymbol{\varepsilon_0}$ is the vacuum permittivity (F/m) and $\boldsymbol{d}$ is the separation between the electrodes with differential tension (V_H-V_L) (m).

2.1.2. Microwave range

The system used consists on an *Agilent* 85070E open-ended coaxial probe connected to an *Agilent* E8362B Vector Network Analyser. Calibration was performed by using three different types of loads: air, short-circuit and 4 °C Mili®-Q water. Once the calibration was made, 4 °C Milli®-Q water was measured again to check calibration suitability. All determinations were made from 500 MHz to 20 GHz.

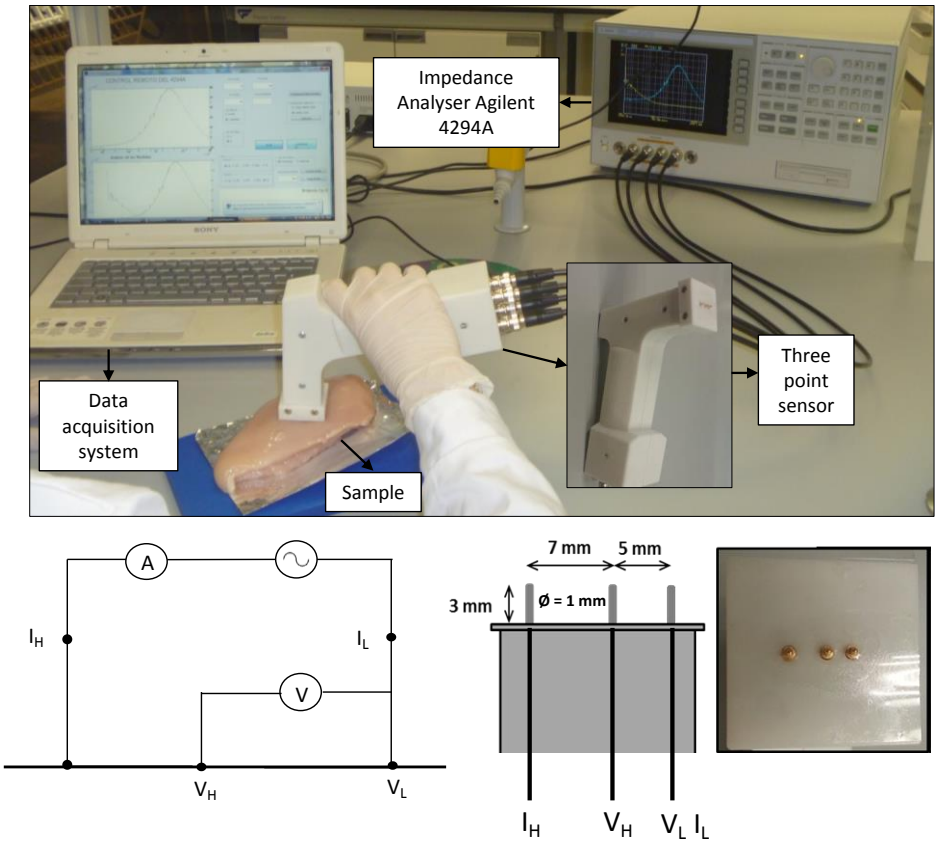

Figure 1. Experimental set-up for measuring meat dielectric properties in radiofrequency range. A: ampere meter; V: voltmeter; IL: low current; IH: high current; VL: low voltage and VH: high voltage. * Three points sensor: Spanish patent P201630956 (Castro-Giraldez *et al.*, 2016).

2.2. Statistical analyses

The dielectric constant spectra were fitted by the Traffano-Schiffo and co-workers model (Traffano-Schiffo *et al.*, 2017) by using a nonlinear regression with Statgraphics Centurion XVI Software (Statgraphics, Virgina, U.S.A.).

The statistical analyses were performed by one-way ANOVA with Tukey`s post test by using Prism 6 (GraphPad Software Inc., San Diego, CA, USA) in order to determine significant differences between the mean values on the parameters. When the analysis of variance indicates differences among means, a t test was used to differentiate means with 95 % of confidence ($p < 0.05$).

3. Results and discussion

Based on pH and L* value 8 breasts were classified as PSE, 8 as DFD and 30 as normal (Zhang & Barbut, 2005).

During the conversion of muscle to meat, complex biochemical reactions are produced in normal meat and partially in low quality meat. After the animal slaughter, the oxygen content in blood decreases, causing anoxia and resulting in an anaerobic metabolism, which is necessary to produce ATP in order to maintain the energy production inside the cell (Sams, 1999).

As a consequence of an anaerobic metabolism, many reactions that change the electrical properties of the biological tissue are produced. The endogenous enzymes and the ATP breakdown are activated (Smulders, Hofbauer, & Geesink, 2014) and produce lactic acid and adenosine monophosphate, causing the drop of the pH and as a consequence, the structural proteins denaturalization (reaching the normal breast a pH value of 5.87 ± 0.12 at 12 h pmt). As products of the proteolytic enzymatic actions, lower molecular weight peptides are produced. Under controlled conditions, meat ageing affects positively to meat tenderness, colour and flavour; however, PSE and DFD meats exhibits different behaviours due to the uncontrolled glycolysis, which affect the final quality of the product.

PSE meat is characterized by a fast drop of pH, reaching values of 5.63 ± 0.06 at 12 h pmt. The higher reduction of the pH, comparing with the rest of the meat qualities, is mainly due to the faster anaerobic degradation of glycogen and higher production of lactate and phosphate. This phenomenon causes the greater degradation and the collapse of the myofibrillar structure and the increase of the liquid phase in sarcoplasmic and intercellular compartments. The sarcoplasm (intracellular liquid phase) is governed by ions with high mobility such as Ca^{2+}, Cl^{-}, K^{+} and Na^{+} and the extracellular liquid phase by Cl^{-} and Na^{+} (Pliquett, Altmann, Pliquett, & Schöberlein, 2003; Damez *et al.*, 2008; Damez, Clerjon, Abouelkaram, & Lepetit, 2007). Damez *et al.* (2008), also include the effect of the phosphate group ($\boldsymbol{PO_4^-}$) in the intracellular liquid phase.

In contrast, DFD meats show high ultimate pH values (6.20 ± 0.07), mainly due to the limited availability of glycogen and ATP to obtain lactic acid by the anaerobic pathway and therefore the free $\boldsymbol{PO_4^-}$ groups content is also restricted. As a consequence, the degradation of the muscle structure is also restricted, thus, proteins remain contracted, retaining ions within its structure.

Consequently, these biochemical and structural transformations change the electrical equilibriums between the protein structure and the chemical compounds with charge flowing in the liquid phase; therefore, the permittivity of the muscle tissue is changing through the conversion from muscle to meat. With this point of view, any disruption in the muscle transformation can be detected analysing the permittivity spectrum (Castro-Giráldez, Botella, Toldrá, & Fito, 2010c).

As was aforementioned in the introduction along the permittivity spectra in RF and MW ranges, α, β and γ dispersions can be distinguished. However, one of the main problems of working with such a wide range of spectrum (40 Hz to 20 GHz) is to fit and to relate the dispersions with sigmoidal shape. In this context, the Gompertz sigmoidal model (Gompertz, 1825), has gained wide acceptance for applications in biological systems (Li, 2012; El-Gohary, Alshamrani, & Al-Otaibi, 2013) and it could be a useful tool to describe the dispersions.

The Debye model (1929) is a physic model that explains the electric dispersions induced by orientation phenomenon, and allows fitting the permittivity tensor; however, it is difficult to adjust this model in the whole range of orientation phenomenon. In this sense, a sigmoidal math model can be used to fit the dielectric constant spectrum. In order to obtain the relaxation dielectric constant, which describes the three relaxations phenomena involved in RF and MW dispersions (frequency, dielectric constant of relaxation), Traffano-Schiffo model (Traffano-Schiffo *et al.*, 2017) was used (Equation 4):

$$l\varepsilon'(\omega) = l\varepsilon'_{\infty} + \sum_{n=1}^{3} \frac{\Delta l\,\varepsilon'_n}{1+e^{\left(\left(l\omega^2 - l\omega_t^2\right)*\alpha_n\right)}} \quad (4)$$

Where, $l\varepsilon'$ represents the decimal logarithm of the dielectric constant, $l\varepsilon'_{\infty}$ the logarithm of the dielectric constant at high frequencies, $l\omega$ represents the decimal logarithm of the angular velocity (rad/s), $\Delta l\varepsilon'_n$ ($\Delta l\varepsilon'_n = log\,\varepsilon'_n - log\,\varepsilon'_{n-1}$) the magnitude of the dispersion, $l\omega_t$ the logarithm of the angular velocity at relaxation time for each dispersion n, and α_n are the dispersion slopes. Figure 2 shows the data of dielectric constant and the adjusted model obtained for normal chicken breast meat), where data are plotted as dots and model as lines, where α, β and γ dispersion can be appreciated. All the parameters of the model can be observed in the figure.

According to the parameters of equation 4 and using equations 5 to 8, the relaxation frequencies and the dielectric constant of each relaxation can be calculated.

$$\varepsilon'_{\alpha} = 10^{\left(l\varepsilon'_{\infty} + \Delta l\varepsilon'_{\gamma} + \Delta l\varepsilon'_{\beta} + \frac{\Delta l\varepsilon'_{\alpha}}{2}\right)} \quad (5)$$

$$\varepsilon'_{\beta} = 10^{\left(l\varepsilon'_{\infty} + \Delta l\varepsilon'_{\gamma} + \frac{\Delta l\varepsilon'_{\beta}}{2}\right)} \quad (6)$$

$$\varepsilon'_{\gamma} = 10^{\left(l\varepsilon'_{\infty} + \frac{\Delta l\varepsilon'_{\gamma}}{2}\right)} \quad (7)$$

$$f_i = 10^{\frac{l\varpi_i}{2\cdot\pi}} \quad (8)$$

Being i for equation 8 each dispersion (α, β and γ).

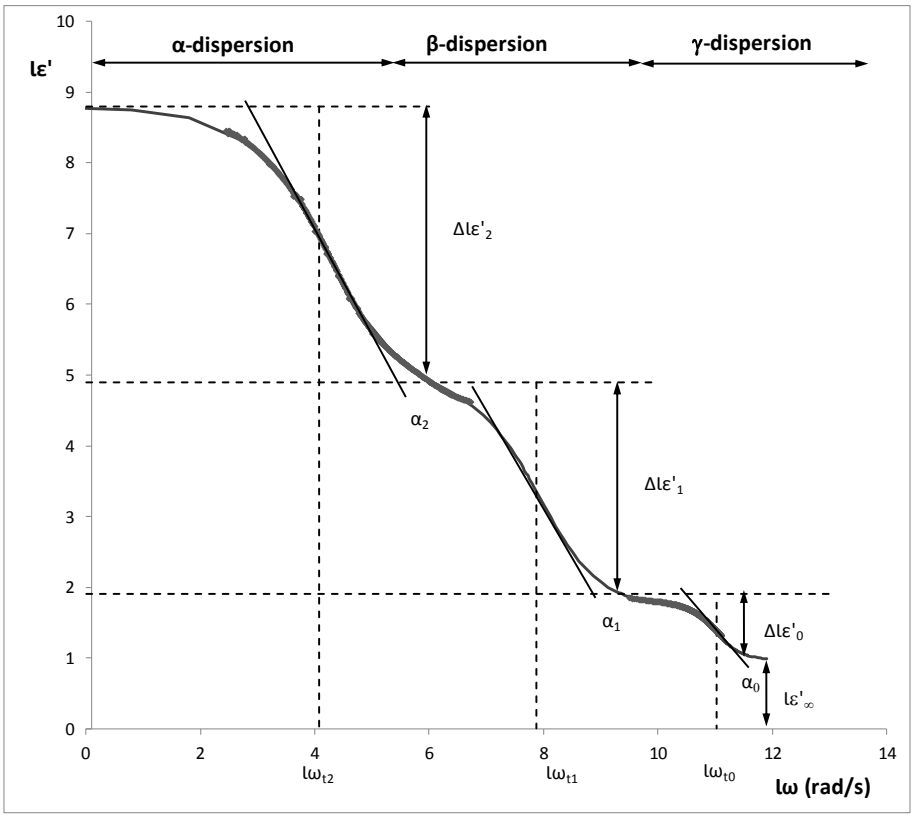

Figure 2. Representation of the dielectric constant of normal chicken breast meat according to the angular velocity. Where (—) corresponds to the values of mathematical model and (♦) the experimental data.

The dielectric constant and frequency, of each relaxation, obtained from equations 5 to 8, can be appreciated in Table 1.

Table 1. Relaxation dielectric constant of PSE, normal and DFD chicken breast meat at each dispersion (α, β and γ). Relaxation frequency of PSE, normal and DFD chicken breast meat at each dispersion (α, β and γ).

	ε'								
	α ($\cdot 10^6$)			β ($\cdot 10^2$)			γ		
PSE	12	±	1[a]	35	±	3[a]	36.0	±	1.4[a]
Normal	7	±	2[b]	20	±	4[b]	34.00	±	0.90[a]
DFD	3.8	±	0.2[c]	13.5	±	0.5[c]	33.7	±	0.5[a]
	f								
	α (kHz)			β (MHz)			γ (GHz)		
PSE	1.23	±	0.06[c]	7.1	±	0.3[c]	8.5	±	0.5[a]
Normal	2.5	±	0.7[b]	12.8	±	1.3[b]	10.0	±	0.7[a]
DFD	3.7	±	0.2[a]	58	±	18[a]	10.54	±	0.14[a]

a-c Different letters on the columns indicate significant differences between means for each parameter ($p < 0.05$).

In the permittivity spectrum the three dispersions are affected by different chemical groups; in the alpha dispersion the orientation of chemical species with charge in liquid medium can be

observed, in beta dispersion the orientation of structural macromolecules with charges are observed and finally in gamma dispersion, the effect corresponds to the dipolar chemical species (Traffano-Schiffo *et al.*, 2017). In the case of normal chicken breast meat during in postmortem time, the chemical species with charges in liquid medium are the electrolytes and the lactate (Castro-Giráldez *et al.*, 2010c), the macromolecules with fixed charges are the structural proteins (actin, myosin and collagen) (Gabriel, Gabriel, & Corthout, 1996) and the main dipolar molecule is the water (Traffano-Schiffo *et al.*, 2015). Table 1 shows the dielectric constant and frequency of normal, PSE and DFD poultry meat, where α and β dispersions show significant differences among the three quality groups.

In case of α-dispersion, the maximum value of dielectric constant corresponds to PSE, where the anaerobic pathway was the highest of the three quality levels, and therefore the production of ion phosphate and lactate were also the highest. However, the lowest value corresponds to DFD, where the anaerobic pathway is limited by the low availability of glycogen and ATP, and thus this quality meat has the lowest quantity of lactate and ion phosphate. In order to understand the effect of lactate during the transformation of muscle to meat, some authors relate the pH with the lactate generation (England, Matarneh, Scheffler, Wachet, & Gerrard, 2014; Zhu, Ruusunen, Gusella, Zhou, & Puolanne, 2011). It is possible to relate lactate content with pH values for poultry breast meat from 1 to 24 hours of pmt (Huang *et al.*, 2014). Therefore, lactate content for each quality meat was obtained using the following equation:

$$x_{lactate} = -29.566\, pH + 233.98 \quad (9)$$

Being $\boldsymbol{x_{lactate}}$ the lactate content expressed in μmol/g.

Figure 3a shows the relationship of lactate content with regard to the dielectric constant in α-dispersion, where the dielectric constant increases when the lactate content in the muscle increases. Thus, PSE quality meat showed the highest dielectric constant values, and in contrast, DFD, the lowest, because PSE samples produces more lactate than the rest of quality levels as was explained before. In addition, Figure 3b shows the relationship of the lactate content of each meat quality with regard to the relaxation frequency in α-dispersion, where big differences among each quality can be appreciated, being PSE meat, which showed the lowest values of relaxation frequency and DFD, the highest. The relaxation frequency depends on the molecular weight of the orientated molecule. It should be taking into account that high content of lactate and ion phosphate (90-95 g/mol) is the main contribution in the signal in α-dispersion, however, other chemical species with ionic force, presented in meat liquid phase, also affect to the orientation phenomena (Ca^{2+}, Cl^{-}, K^{+}, Na^{+}, Mg^{2+} from 23-40 g/mol). The effect of these molecules is higher as lower is the production of lactate and ion phosphate. Thus, PSE meat shows a relaxation frequency in α-dispersion mainly affected by lactate and ion phosphate. In contrast, DFD meats showed the lowest lactate content being the relaxation frequency also affected by the electrolytes of the liquid phase.

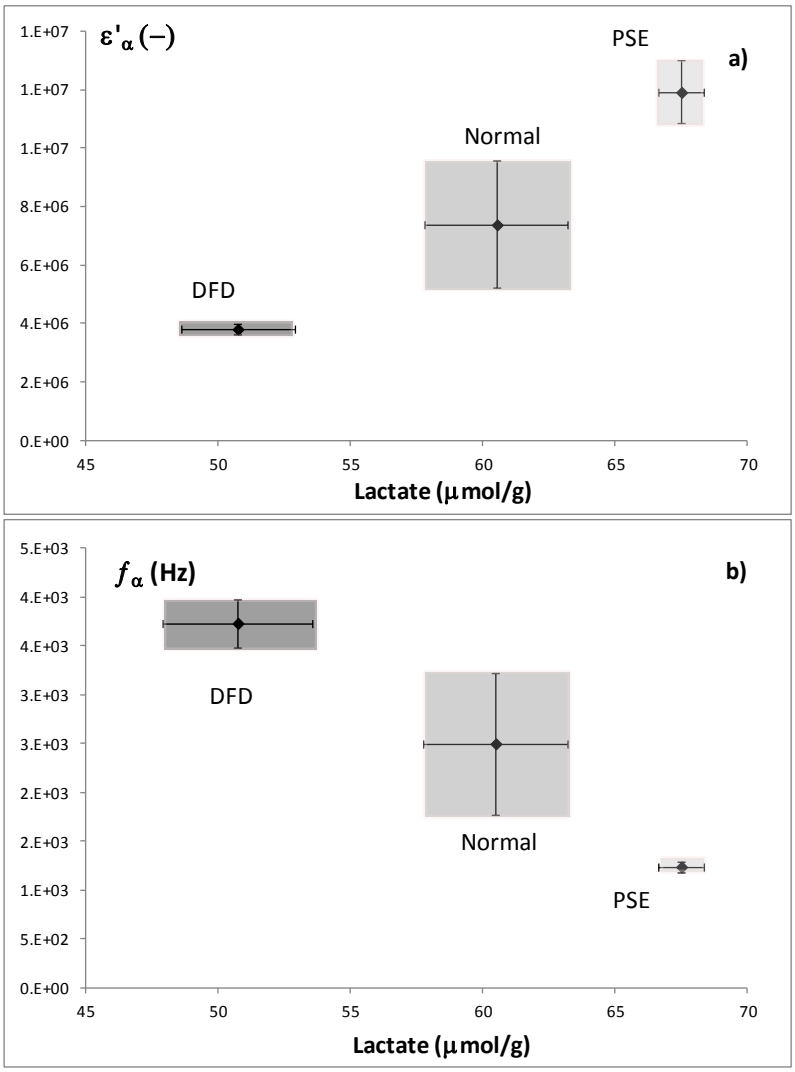

Figure 3. Relationship between the lactate content and a) relaxation dielectric constant and b) relaxations frequencies in α-dispersions for each meat quality. Where: (□) corresponds to PSE, (■) normal, and (■) DFD.

As Table 1 shows, the dielectric constant in β-dispersion for normal quality is 20 ± 4 and the relaxation frequency is 12.8 ± 1.3 MHz; in this dispersion, the main chemical group with fixed charges are the structural proteins. Throughout the maturation pathways, some proteins are fragmented by enzymatic reactions, producing polypeptides or fragments of the original protein chain (Lametsch, Roepstorff, & Bendixen, 2002; Greaser, 1986). The most important degradation from the size reduction point of view, is the degradation of myosin into a globular myosin head fragment (Lametsch *et al.*, 2002), in this degradation the original size of myosin was 250 kDa, producing a new fragment of 56 kDa (Li, Xu, & Zhou, 2012). The degradation of actin (43 kDa) derived in new fragments of 32 kDa and 40 kDa (Lametsch *et al.*, 2002). Troponin-T, which is a portion of troponin (70 kDa) (Mudalal, Babini, Cavani, & Petracci, 2014; Huff-Lonergan, & Lonergan, 1999), is degraded to others smaller polypeptides identified as fragments of 28, 30, 32 and 34 kDa (Huang, Huang, Xue, Xu, & Zhou, 2011). Desmin (53 kDa) in normal breast is also degraded during the first 12 hours of pmt (Li *et al.*, 2012).

As was explained above, the ultimate pH in chicken is negatively correlated with the amount of glycogen stored in the muscle at slaughter. PSE meats present higher amount of glycogen stored than the DFD meats. This kind of quality follows glycolytic pathway to produce energy after the slaughter. It is important to highlight that the glycogen content for DFD meat quality is limited, therefore, this chicken quality takes alternative sources of energy production such as ketogenic amino acid degradation and lipid β-oxidation (Beauclercq et al., 2016).

The dielectric constant in β-dispersion for PSE quality is 35 ± 3 and the relaxation frequency is 7.1 ± 0.3 MHz (Table 1). PSE meat quality follows the same protein metabolic pathways as normal meat but faster, which means that this quality meat presents higher protein degradation than normal (Offer, 1991). Therefore, more fragments of proteins are generated, producing new active sites with orientation capacity (Li et al., 2014). Due to this, PSE quality meat shows higher value of dielectric constant than normal meat. Moreover, the protein degradation produces polypeptides with small molecular weight, and therefore, in an accelerated glycolysis pathway (PSE quality meat) this effect provokes the reduction of the relaxation frequency.

On the other hand, the dielectric constant of DFD meat quality in β-dispersion is 13.5 ± 0.5 and the relaxation frequency is 58 ± 18 MHz. Due to the less availability of glucose and glycogen storage in the muscle of DFD meat quality, the glycolysis pathway is limited. As a consequence, DFD meats take alternative metabolic routes as the ketogenic metabolic degradation which produces amino acids, mainly alanine and glycine to obtain energy (Beauclercq et al., 2016). This metabolism reduces the size of the structural proteins, producing amino acids without interactions in β-dispersion. This protein degradation provokes a reduction of charges with orientation capacity and therefore lower dielectric constant than the rest of meat qualities. Moreover, the remaining structural protein are the unique molecules with capacity to orientate, thus the molecular weight of remaining structural proteins are bigger than the rest of the quality meats, it can be appreciated in the higher relaxation frequency of β-dispersion.

Finally, γ-dispersion is produced by the orientation of dipolar molecules, being the water the main dipolar molecule in muscle tissue. The moisture and the water activity were measured obtaining non-significant differences among the three quality classes, being the average moisture 0.756 ± 0.006 kg_w/kg_T, and the average water activity 0.989 ± 0.003. The quantity and the activity of water are not the only variables that can affect the water mobility, the state variables, such as pressure, can also affect (Traffano-Schiffo *et al.*, 2014). Comparing the three quality classes, PSE meat is characterized by a soft tissue and in contrast, DFD meat quality by a firm tissue, which means that the soft tissue corresponds to an expanded fibre structure and the firm tissue to a contracted fibre structure, both compared to normal meat. Contracted fibre structure has mainly capillarity effect because fibres present lower gaps between them, reducing the internal pressure and therefore reducing the mobility of water. In contrast, the expanded structure of PSE meats have higher gaps and thus higher water mobility. As a result, the maximum dielectric constant in γ-dispersion corresponds to PSE quality meat and the minimum to DFD (Table 1), nevertheless, no significant differences were observed among the three quality meats.

4. Conclusion

This paper presents a classification model for quality poultry meat based on a spectrophotometric analysis at radiofrequency and microwave ranges by using the Traffano-Schiffo model. It has been demonstrated the direct relation between the pH evolution and the dielectric constant at α-dispersion, extending this relation to the generation of lactic acid, at 12 h pmt. It has been demonstrated that the main structural proteins degradation has direct relation with the dielectric constant at β-dispersion, being possible to segregate meat depending on the level of protein degradation.

Finally, it has been possible to join the dielectric constants at α and β-dispersions in order to classify poultry meat in PSE, normal and DFD meat qualities. It can be concluded that the spectrophotometry at radiofrequency and microwave ranges represents a good and non-destructive tool able to determine poultry meat quality.

5. Acknowledgements

The authors acknowledge the financial support from: the Spanish Ministerio de Economía, Industria y Competitividad, Programa Estatal de I+D+i orientada a los Retos de la Sociedad AGL2016-80643-R, Agencia Estatal de Investigación (AEI) and Fondo Europeo de Desarrollo Regional (FEDER). The author Maria Victoria Traffano Schiffo wants to thank the FPI Predoctoral Program of the Universidad Politécnica de Valencia for its support.

6. References

Adzitey, F., & Nurul, H. (2011). Pale soft exudative (PSE) and dark firm dry (DFD) meats: Causes and measures to reduce these incidences-a mini review. *International Food Research Journal*, 18, 11-20.

Allen, C. D., Russell, S. M. & Fletcher, D. L. (1997). The relationship of broiler breast meat color and pH to shelf-life and odor development. *Poultry Science*, 76, 1042-1046.

Barbin, D. F., Kaminishikawahara, C. M., Soares, A. L., Mizubuti, I. Y., Grespan, M., Shimokomaki, M., & Hirooka, E. Y. (2015). Prediction of chicken quality attributes by near infrared spectroscopy. *Food Chemistry*, 168, 554-560.

Barbin, D. F., Mastelini, S. M., Barbon, S., Campos, G. F., Barbon, A. P. A., & Shimokomaki, M. (2016). Digital image analyses as an alternative tool for chicken quality assessment. Biosystems Engineering, 144, 85-93.

Barbut, S., Sosnicki, A. A., Lonergan, S. M., Knapp, T., Ciobanu, D. C., Gatcliffe, L. J., Huff-Lonergan, E. & Wilson, E. W. (2008). Progress in reducing the pale, soft and exudative (PSE) problem in pork and poultry meat. *Meat Science*, 79, 46-63.

Barbut, S., Zhang, L. & Marcone, M. (2005). Effects of pale, normal, and dark chicken breast meat on microstructure, extractable proteins, and cooking of marinated fillets. *Poultry Science*, 84, 797-802.

Beauclercq, S., Nadal-Desbarats, L., Hennequet-Antier, C., Collin, A., Tesseraud, S., Bourin, M., Le Bihan-Duval, E., & Berri, C. (2016). Serum and muscle metabolomics for the prediction of ultimate pH, a key factor for chicken-meat quality. *Journal of Proteome Research*, 15(4), 1168-1178.

Castro-Giráldez, M., Aristoy, M., Toldrá, F. & Fito, P. (2010a). Microwave dielectric spectroscopy for the determination of pork meat quality. *Food Research International*, 43, 2369-2377.

Castro-Giráldez, M., Botella, P., Toldrá, F., & Fito, P. (2010c). Low-frequency dielectric spectrum to determine pork meat quality. *Innovative Food Science & Emerging Technologies*, 11, 376-386.

Castro-Giraldez, M., Colom, R.J., Fito, P.J., Herrero, V., Lidón, J.V., Monzó, J.M., Tébar, A., Traffano-Schiffo, M.V. (2016). Aparato y método no invasivo de detección de roturas de la cadena de frío en carne congelada. Spanish Patent P201630956.

Castro-Giráldez, M., Fito, P. J., Chenoll, C., & Fito, P. (2010b). Development of a dielectric spectroscopy technique for the determination of apple (Granny Smith) maturity. *Innovative Food Science & Emerging Technologies*, 11(4), 749-754.

Chan, J. T., Omana, D. A. & Betti, M. (2011). Effect of ultimate pH and freezing on the biochemical properties of proteins in turkey breast meat. *Food Chemistry*, 127, 109-117.

CIE (1978). International Commission on Illumination, recommendations on uniform color spaces, color, difference equations, psychometric colour terms. CIE publication No. 15 (Suppl.2), (E-1.31) 1971/(TC-1.3). Paris, France: Bureau Central de la CIE.

Damez, J. L., Clerjon, S., Abouelkaram, S. & Lepetit, J. (2007). Dielectric behavior of beef meat in the 1–1500 kHz range: Simulation with the Fricke/Cole–Cole model. *Meat Science*, 77, 512-519.

Damez, J. L., Clerjon, S., Abouelkaram, S. & Lepetit, J. (2008). Beef meat electrical impedance spectroscopy and anisotropy sensing for non-invasive early assessment of meat ageing. *Journal of Food Engineering*, 85, 116–122.

Debye P. (1929). Polar molecules. Chemical Cataloge Company. New York: Dover Publications.

El-Gohary, A., Alshamrani, A. & Al-Otaibi, A. N. (2013). The generalized Gompertz distribution. *Applied Mathematical Modelling*, 37, 13-24.

England, E. M., Matarneh, S. K., Scheffler, T. L., Wachet, C., & Gerrard, D. E. (2014). pH inactivation of phosphofructokinase arrests postmortem glycolysis. *Meat Science*, 98(4), 850-857.

Gabriel, C., Gabriel, S., & Corthout, E. (1996). The dielectric properties of biological tissues: I. Literature survey. *Physics in Medicine and Biology*, 41(11), 2231.

Gompertz, B. (1825). On the nature of the function expressive of the law of human mortality, and on a new mode of determining the value of life contingencies. *Philosophical Transactions of the Royal Society of London*, 115, 513-583.

Greaser, M. L. (1986) *Conversion of muscle to meat.* In P. J. Bechtel (Ed.), Muscle as Food (pp. 37-87). London: Academic Press.

Huang, J. C., Huang, M., Wang, P., Zhao, L., Xu, X. L., Zhou, G. H., & Sun, J. X. (2014). Effects of physical restraint and electrical stunning on plasma corticosterone, postmortem metabolism, and quality of broiler breast muscle. Journal of Animal Science, 92(12), 5749-5756.

Huang, M., Huang, F., Xue, M., Xu, X., & Zhou, G. (2011). The effect of active caspase-3 on degradation of chicken myofibrillar proteins and structure of myofibrils. *Food Chemistry*, 128(1), 22-27.

Huff-Lonergan, E., & Lonergan, S. M. (1999). Postmortem mechanisms of meat tenderization: the roles of the structural proteins and the calpain system. In Y. L. Xiong, C. T. Ho, & F. Shahidi, (Eds.), *Quality attributes of muscle foods* (pp 229-254). New York: Springer Science & Business Media, LLC.

ISO 1442:1997 (1997). *Methods of test for meat and meat products.* Determination of moisture content. BS 4401-3:1997.

Lametsch, R., Roepstorff, P., & Bendixen, E. (2002). Identification of protein degradation during post-mortem storage of pig meat. *Journal of Agricultural and Food Chemistry*, 50(20), 5508-5512.

Langer, R. O. D. S., Simões, G. S., Soares, A. L., Oba, A., Rossa, A., Shimokomaki, M., & Ida, E. I. (2010). Broiler transportation conditions in a Brazilian commercial line and the occurrence of breast PSE (Pale, Soft, Exudative) meat and DFD-like (Dark, Firm, Dry) meat. *Brazilian Archives of Biology and Technology*, 53, 1161-1167.

Li, G. (2012). Optimal and efficient designs for Gompertz regression models. *Annals of the Institute of Statistical Mathematics*, 64, 945-957.

Li, S., Xu, X., & Zhou, G. (2012). The roles of the actin-myosin interaction and proteolysis in tenderization during the aging of chicken muscle. *Poultry Science*, 91(1), 150-160.

Mohiri, A., Burhanudin, Z. A. & Ismail, I. (2011). Dielectric properties of slaughtered and non-slaughtered goat meat. In RF and Microwave Conference (RFM). *IEEE International*, 393-397

Mudalal, S., Babini, E., Cavani, C., & Petracci, M. (2014). Quantity and functionality of protein fractions in chicken breast fillets affected by white striping. *Poultry Science*, 93(8), 2108-2116.

Offer, G. (1991). Modelling of the formation of pale, soft and exudative meat: Effects of chilling regime and rate and extent of glycolysis. *Meat Science*, 30(2), 157-184.

Pliquett, U., Altmann, M., Pliquett, F. & Schöberlein, L. (2003). Py—a parameter for meat quality. *Meat Science*, 65, 1429-1437.

Pozar, D.M. (1998). Microwave Engineering. (2nd ed.). New York: John Wiley & Sons Inc, (Chapter 1).

Sams, A. R. (1999). Meat quality during processing. *Poultry Science*, 78, 798-803.

Schwan, H. P. (1957). Electrical properties of tissues and cell suspensions. *Advances in Biological and Medical Physics*, 5, 147–209.

Smulders, F., Hofbauer, P. & Geesink, G. H. (2014). The Conversion of Muscle to Meat. In T. Ninios, J. Lundén, H. Korkeala, & M. Fredriksson-Ahomaa (Eds.), *Meat Inspection and Control in the Slaughterhouse* (pp. 399-421). Oxford: John Wiley & Sons, Ltd.

Sosnicki, A. A., Greaser, M. L., Pietrzak, M., Pospiech, E. & Sante, V. (1998). PSE-like syndrome in breast muscle of domestic turkeys: A review. *Journal of Muscle Foods*, 9, 13–23.

Swatland, H. J. (2008). How pH causes paleness or darkness in chicken breast meat. Meat Science, 80, 396-400.

Talens, C., Castro-Giraldez, M., & Fito, P. J. (2016). Study of the effect of microwave power coupled with hot air drying on orange peel by dielectric spectroscopy. *LWT-Food Science and Technology*, 66, 622-628.

Traffano-Schiffo, M. V., Castro-Giraldez, M., Colom, R. J., & Fito, P. J. (2017). Development of a spectrophotometric system to detect white striping physiopathy in the whole chicken carcase. *Sensors*.

Traffano-Schiffo, M. V., Castro-Giraldez, M., Colom, R. J., & Fito, P. J. (2015). Study of the application of dielectric spectroscopy to predict the water activity of meat during drying process. *Journal of Food Engineering*, 166, 285-290.

Traffano-Schiffo, M. V., Castro-Giráldez, M., Fito, P. J., & Balaguer, N. (2014). Thermodynamic model of meat drying by infrarred thermography. *Journal of Food Engineering*, 128, 103-110.

Venkatesh, M. S., & Raghavan, G. S. V. (2004). An overview of microwave processing and dielectric properties of agri-food materials. *Biosystems Engineering*, 88, 1-18.

Woelfel, R. L., Owens, C. M., Hirschler, E. M. & Sams, A. R. (1998). The incidence and characterization of pale, soft and exudative chicken meat in a commercial plant. *Poultry Science*, 77, 62.

Woelfel, R. L., Owens, C. M., Hirschler, E. M., Martinez-Dawson, R. & Sams, A. R. (2002). The characterization and incidence of pale, soft, and exudative broiler meat in a commercial processing plant. *Poultry Science*, 81, 579-584.

Wolf, M., Gulich, R., Lunkenheimer, P., & Loidl, A. (2012). Relaxation dynamics of a protein solution investigated by dielectric spectroscopy. *Biochimica et Biophysica Acta (BBA)-Proteins and Proteomics*, 1824, 723-730.

Zhang, L. & Barbut, S. (2005). Rheological characteristics of fresh and frozen PSE, normal and DFD chicken breast meat. *British Poultry Science*, 46, 687-693.

Zhu, X., Ruusunen, M., Gusella, M., Zhou, G., & Puolanne, E. (2011). High post-mortem temperature combined with rapid glycolysis induces phosphorylase denaturation and produces pale and exudative characteristics in broiler Pectoralis major muscles. *Meat Science*, 89(2), 181-188.

4.4. Estudio de la Miopatía del Pectoral Profundo (DPM) en carne de pollo. Categorización y desarrollo de sensor.

Traffano-Schiffo, M. V., Castro-Giráldez, Herrero, V., Colom, R. J., & Fito, P. J., (2017). Development of a methodology to categorize chicken meat affected by Deep Pectoral Myopathy. ***Meat Science***. Artículo enviado.

Fito, P. J., Colom, R. J., Castro-Giraldez, M., Herrero, V., Monzó, J. M., **Traffano-Schiffo, M. V.**, Tébar, A., (2016). Aparato y método de detección de daño producido por la miopatía del pectoral profundo en aves. **Patente Española P201630062**.

DEVELOPMENT OF A METHODOLOGY TO CATEGORIZE CHICKEN MEAT AFFECTED BY DEEP PECTORAL MYOPATHY

Maria Victoria Traffano-Schiffo, Marta Castro-Giraldez, Pedro J. Fito*

Instituto Universitario de Ingeniería de Alimentos para el Desarrollo, Universitat Politecnica de Valencia, Camino de Vera s/n, 46022 Valencia, España.

Corresponding author: pedfisu@tal.upv.es

ABSTRACT

The intensification of chicken meat production has led to an increase in the incidence of internal malformations in chicken and turkey broilers, as Deep Pectoral Myopathy. Currently, the visual appearance is the only parameter used to categorize the damage level. The aim of this research was to develop an analytical methodology to determine the level of damage in chicken breasts affected by this myopathy. For this purpose, the microstructure, pH, proteins and ions content and color were studied for non-damaged and affected breasts. The results of this research allowed identifying three damage levels: Non-damaged, hemorrhagic samples with hematomas and blood clots, and necrotic tissues, based on significant variables (p<0.05) measured in *Pectoralis minor* (pH, L* and a*).

Keywords: Deep Pectoral Myopathy, chicken meat, poultry quality, DPM categorization, meat quality.

1. Introduction

According to the estimation of the Food and Agriculture Organization of the United Nations (FAO), global meat production would have reached 308.3 million tons in 2013, implying an increase of 1.4% over 2012 production. In this context, the production of poultry would be the second largest (after pork meat) (Traffano-Schiffo, Castro-Giraldez, Colom, & Fito, 2017a) and represents 34.6% of the total, reaching 106.8 million tons (OECD-FAO, 2013). This production increase of the poultry sector has been made possible by a strong technification, professionalization and strengthening of the sector as well as a strong genetic screening to achieve high growth rate and good carcass yield (Kijowski, Kupinska, Stangierski, Tomaszewska-Gras, & Szablewski, 2014). However, this intensification has led to an increase in the incidence of internal malformations in chicken and turkey broilers (Traffano-Schiffo, Castro-Giraldez, Colom, & Fito, 2017b; Hafez, & Hauck, 2005). Within these internal malformations, this research aims to deal with a common problem in broilers, especially those which have been genetically selected for the development of the breast, the Deep Pectoral Myopathy (DPM).

Other common names by which the DPM is designated are The Green Muscle Disease or Oregon Disease. The DPM is produced by different reasons, being common in chickens with hypertrophic musculature, and consists on a breakup of muscle tissue accompanied by internal hemorrhage that can lead necrosis or muscle infarction in their most critical levels (Petracci, & Cavani, 2012). The DPM disease occurs through an interaction between the heart and the muscle adjacent, therefore the main affected muscle is the *supracoracoideus* or *Pectoralis minor*. This muscle is very susceptible to this type of injury because it is surrounded by an elastic membrane (fascia) and located between the sternum and the *Pectoralis major* or *Pectoralis superficialis* muscle, limiting the expansion during the animal wing beat (Martindale, Siller, & Wight, 1979). Although this disease affects largely to the Pectoralis minor muscles, in some cases the *Pectoralis major* can also be affected.

In industry, the myopathies in poultry are commonly divided in different categories based on visual appearance (Bilgili, & Hess, 2008); First category presents samples with inflammatory injury in which the deep pectoral muscle shows red coloration, induced by an internal bleeding. The hemorrhages also can be seen in the fibrous surface. It produces an exudation of serous fluid in the damaged area, which gives it a moist and sticky appearance to the lesion. In the Second category, the injury to the *minor* muscle appears well defined, and sometimes surrounded by a hemorrhagic ring. The affected areas are pale pink color and blood clots are observed. In these two categories, after ischemic episode and being the animal still alive, muscle maintains its capacity to recover the physiological and mechanical activity. In these cases, the muscle necrosis does not appear. The third category is characterized by the presence of muscular necrotic areas, with a progressive degeneration and consequently a greening of muscle tissue produced by the oxidation of blood.

Ischemia can be defined as the lack of blood flow to supply the tissue with oxygen and nutrients and to transport metabolic end products out of the tissue (Schäfer, Schlegel, Kirlum, Gersing, & Gebhard, 1998). On the other hand, necrosis can be understood as a cellular death. Cells swell up to the point where the lysis of their plasmic membrane occurs. It can be considered as a cellular explosion which leads to release of the cytoplasmic contents in the surrounding medium which affects other cells by the action of the released intracellular enzymes (Ouali *et al.*, 2006).

The aim of this research was to develop a scientific methodology to categorize the damage level in chicken meat affected by DPM.

2. Materials and methods

2.1. Raw material

The experiments were performed using non-damaged and affected by DPM chicken breasts (*Pectoralis major* and *Pectoralis minor*) with 5 hours post-mortem. The samples were provided by a slaughterhouse of Grupo Sada (Nutreco S.A. Company) located in Rafelbunyol, Valencia (Spain) and kept at 4 °C until analysis. An industrial trained expert classified the samples by the visual appearance in damaged samples (samples with hemorrhages, blood clots, and necrosis) and non-damaged samples. Within the damaged samples, samples were classified in necrotic samples or category 2 (samples with any necrotic area) and hemorrhagic samples with hematomas and blood

clots or category 1 (in this category were the remaining damaged samples that were not classified in the category 2).

2.2. Experimental Procedure

Pectoralis minor and *major* of the same animal were used to carry out the experiment. A total of 76 samples were analyzed: 22 correspond to non-damaged tissues, 27 to category 1 and 27 to category 2. Chicken breasts were transported to the laboratory of the Institute of Food Engineering for Development (IuIAD) at the Polytechnic University of Valencia (UPV) using isothermal bags with ice in order to maintain the samples at 2 ± 2 ºC. Once arrived to the laboratory, the microstructural analyses of damaged and non-damaged samples with 5 h post-mortem were carried out. At 12 h post-mortem, photos of the samples were taken in order to perform the image analyses. Moreover, the pH, protein content and the color coordinates measures were performed. Finally, the ion content was determined in pectoralis minor and major of the different categories.

The pH analysis was carried out by triplicate with a punch pH-metre S-20 SevenEasy^{TM} (Mettler Toledo, Barcelona, Spain).

The colour was measured by the surface reflectance spectra in a spectrocolorimeter Minolta CM-3600D (Minolta Co. Ltd., Tokio, Japan). The colour coordinates CIE L*a*b* (CIE, 1978) were instrumentally calculated based on D65 illuminant and 10° observer.

2.3. Image Analysis

The image analysis was performed obtaining the images of non-damaged and damaged *Pectoralis minor* chicken meat by a digital camera (Canon EOS 550D, with a size of 2592 x 1728 pixels and a resolution of 16 pixel/mm).

The images were taken placing the samples inside an inspection wooden chamber where the interior walls were painted black in order to minimize the background light, and where the camera and the lighting system were contained. For a correct illumination three lamps with a fluorescent tube (PHILIPS TLD18W/965, 60 cm in length) natural daylight were used in order to obtain the appropriate lighting condition (illuminant D65), with a color temperature of 6500 K. Finally, the camera lens was installed on the top, focusing the sample with 10º slope.

In order to calibrate the digital color system, the color values of 24 color charts (color checker CLASSIC X-rite, 2010, USA) with a known CIE L*a*b*(CIE , 1978) coordinates were measured and compared with the parameters provided by the manufacturer. The analysis of damaged areas (blood clots, hemorrhagic and necrotic areas) was performed by Adobe® Photoshop® CS6 software (Adobe Systems Inc., San Jose, CA, USA).

2.4. Differential Scanning Calorimetry (DSC)

The energy of proteins phase transitions were calculated using a differential scanning calorimeter Mettler Toledo DSC 1 (Mettler Toledo, Barcelona, Spain) provided with the full range temperature sensor FRS5. The calibration of the equipment was performed by the automatic calibration function FlexCal supplied by the manufacturers. Samples of around 30 mg were

enclosed in hermetically sealed aluminum pans (Mettler Toledo, ME-00026763) and then loaded onto the equipment at room temperature. An empty hermetically sealed pan was used as the reference sample. In the experiments, samples were heated from 15 to 115 °C at a heating rate of 10 °C/min in order to evaluate the protein state within meat. All determinations were performed in triplicate.

Once the scans were finished, analyses of the samples were carried out by the STARe software fitted with the DSC equipment. Mass fraction of each protein was calculated from free energy of phase transition for each protein (Ross, 2006) and the energy of proteins phase transitions obtained from endotherm area. The following initial denaturalization temperatures were considered: myosin 55 ºC, collagen and sarcoplasmic proteins between 63 to 76 ºC and actin 79-80 ºC (Ross, 2006; Fernández-Martín, Fernández, Carballo, & Jiménez-Colmenero, 2000).

2.5. Analyses of microstructural changes: Low-temperature scanning electron microscopy (Cryo-SEM)

Microstructure of non-damaged and DPM samples were analyzed by Cryo-SEM. A Cryostage CT-1500C unit (Oxford Instruments, Witney, UK), coupled to a Jeol JSM-5410 scanning electron microscope (Jeol, Tokyo, Japan), was used. The sample was immersed in slush N_2 (-210 ºC) and then quickly transferred to the Cryostage at 1 kPa where sample fracture took place. The sublimation (etching) was carried out at -95 ºC. The final point was determined by direct observation in the microscope, working at 5 kV. Then, once again in the Cryostage unit, the sample was coated with gold in vacuum (0.2 kPa), applied for 3 min, with an ionization current of 2 mA. The observation in the scanning electron microscope was carried out at 20 kV, at a working distance of 15 mm and a temperature ≤ -130 ºC.

2.6. Determination of ions by ion exchange chromatography

Ion quantification was carried out by means of an ion chromatograph (Methrom Ion Analysis, Herisau, Switzerland), using a universal standard column (Metrosep C2-150, 4.0 × 150 mm) along with an eluent composed of tartaric acid (4.0 mmol/L) and dipicolinic acid (0.75 mmol/L), equipped with electronic detectors. In every case, the chicken meat samples were previously homogenized at 9000 rpm in an ultraturrax T25 for 10 min and centrifuged (J.P. Selecta S.A., Medifriger-BL, Barcelona, Spain) at 10000 rpm for 20 min. Afterwards, 1 mL of supernatant was diluted with Milli®-Q water in a 50 mL volumetric flask. The clarified extract was filtered through a 0.45 μm Millipore filter. Finally, 15 mL was used to analyze the cation content. Measurements were taken in triplicate.

2.7. Statistical analysis

The statistical analysis was carried out with the Statgraphics Centurion XVI Software (Statgraphics, Warrenton, VA, USA). One-Way ANOVA analyses were made in order to find statistically significant differences between the studied parameters with 95 % of confidence (p<0.05).

3. Results and discussion

After an ischemic episode, the muscle tissue can recover its structure if the blood flow is restored in an interval of 15 – 20 minutes and if there was not suffered any structural lesion (Martín-García, 2009). Above this time, all the glycogen has been consumed, appearing major structural alterations (see Figure 1): myofibrils suffer an excessive elongation and the sarcolemma develops separation areas. Some studies reported that after the infarct, collagen content is reduced significantly (Takahashi, Barry, & Factor, 1990). Also, the presence of lesions in the cell membrane is evident.

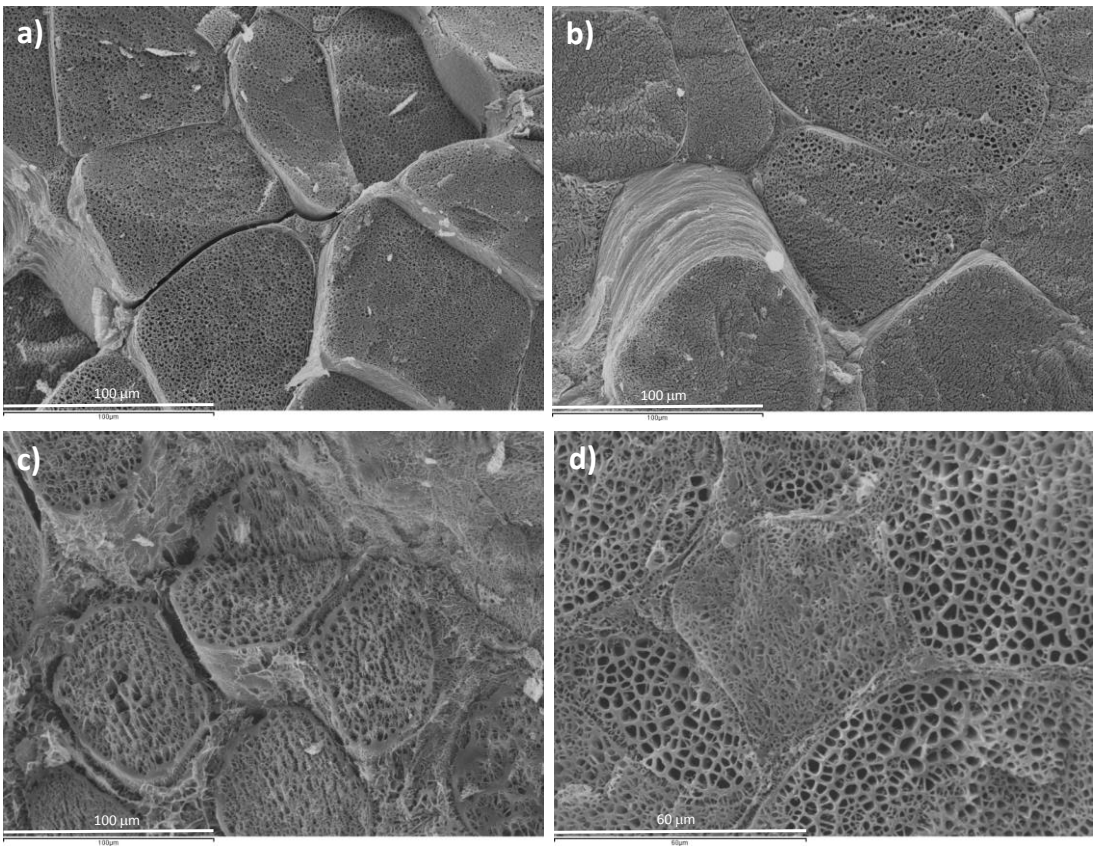

Figure 1. a) non-damaged *Pectoralis minor* with 5 hpm 500x; b) non-damaged *Pectoralis major* with 5 hpm 500x; c) necrotic *Pectoralis min*or with 5 hpm 500x; and d) necrotic *Pectoralis major* with 5 hpm 1000x.

In the Figure 1a and 1b, micrographies of non-damaged breast chicken after 5 hours of post-mortem time are shown, where it is possible to appreciate the correct packaging of the fibrillar cells formed by the structural proteins, myosin and actin, which are responsible of the muscular contraction and relaxation, and packaged by the collagen protein which confers capacity to maintain the tension. However, in Figure 1c and 1d, it is possible to observe micrographies of muscle tissue after an infarct episode where the strong myopathy shows a high level of collagen degradation (endomysium), induced by the accumulation of electrolytes in this area, generating strong repulsions between the adjacent collagen covers, and a high degradation level of structural proteins (actin and myosin).

Figure 2 shows three samples of *Pectoralis minor* with different DPM damages. Figure 2a shows a non-damaged tissue, 2b hemorrhagic sample with hematomas and a blood clots, and 2c a necrotic sample. Moreover, Figure 2d shows a micrograph of hemorrhagic tissue, where it is possible to observe the presence of blood clots (detailed by arrows) and the muscular breakdown. However, Figure 2e shows a micrograph of a necrotic Pectoralis minor, where the loss of the cellular structure and the endomysial inflammation can be appreciated (indicated by arrows).

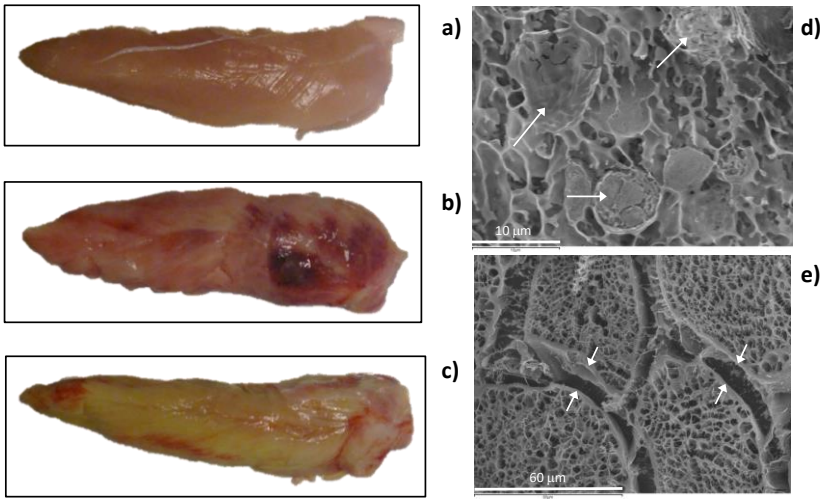

Figure 2. *Pectoralis minor*, where: a) non-damaged tissue, b) hemorrhagic sample with hematomas and blood clots, c) necrotic, d) Micrograph (1500x) of hemorrhagic tissue, and e) Micrograph (500x) of necrotic sample.

This classification is named in other fields as: angina for hemorrhagic with hematomas and blood clots muscle tissue (category 1) and infarct for necrotic muscle tissue (category 2).

Table 1. Electrolytes content of non-damaged and damaged tissues.

	NORMAL	Category 1	Category 2
Na^+	130 ± 8	1580 ± 28	868 ± 63
K^+	353 ± 27	1646 ± 86	556 ± 81
Ca^{2+}	190 ± 43	342 ± 69	213 ± 69
Mg^{2+}	80 ± 12	78 ± 6	87 ± 12

Muscle rupture processes reach the breakdown of some organs such as mitochondria, K^+_{ATP} channels stores in the mitochondrial intermediate space a high concentration of potassium ions, which, when broken, increase the concentration of free potassium ions (Horimoto, Gaudette, Saltman, & Krukenkamp, 2000; Gürke *et al.*, 2000). The same happens with other ions as sodium, which are found in other organelles where the Na^+_{ATP} channels stores high quantity of sodium ions (Immke & McCleskey, 2001) and induced by the lactic generation, which are release to the muscle. In degenerative processes with loss of blood supply, pH decrease after the ischemic phenomenon (lactic and phosphate formation). And time after the ischemic phenomenon the pH

is equilibrated, increasing again, favoring the formation of salts from the cationic and anionic species causing a decrease of free ions (Zweier, Wang, Samouilov, & Kuppusamy, 1995). Therefore, the haemorrhagic category presents high levels of potassium and sodium ions, which are reduced if the system becomes infarcted and necrotic tissue (Horimoto *et al.*, 2000). However, no significant differences among the Mg^{+2} were found. The K^{+}_{ATP} channels imbalance effect and lactate and phosphate production cause a change in the electric disequilibrium inside the muscle tissue. This causes an imbalance in the protein transmembrane transports (Ca^{2+} protein channel and Na^{+}/K^{+} protein channel) inducing a release of calcium and sodium ions to the medium. This effect is observed slightly in the increase of calcium of the Table 1 (Miyoshi *et al.*, 1992).

The structural proteins degradation was estimated by DSC. Ageing process and myopathies produce degradation in the structural proteins, and it is possible to determine the effect of the myopathy comparing non-damaged with damaged tissue at the same post-mortem time. Figure 3 shows the mass fraction of each structural protein (myosin, actin, collagen and sarcoplasmic proteins) in non-damaged (code samples 0), hemorrhagic with hematomas and/or blood clots samples (code samples 1), and necrotic samples (code samples 2), where it is possible to observe how the quantity of myosin decreases in *Pectoralis minor* depending on the level of damage (Fig. 3a). On the other hand, necrotic samples show a higher decrease of the collagen and sarcoplasmic proteins contents comparing with non-damaged tissue in Pectoralis minor (Fig. 3b). This result can be related with the high level of degradation in the collagen observed in the micrographies showed in Figure 1c and 1d. Also, similar results were obtained in the research developed in 1990 by Takahashi et al. (1990) With regard to *Pectoralis major*, a significant decrease in myosin content is appreciated in necrotic tissue comparing with the others two categories (Fig 3d). Collagen and sarcoplasmic proteins also show a significant decrease comparing to hemorrhagic samples (Fig. 3e). Finally, actin degradation of damaged categories is significant higher with regard to the non-damaged samples both in *Pectoralis minor* and in *major* (Fig. 3c and f).

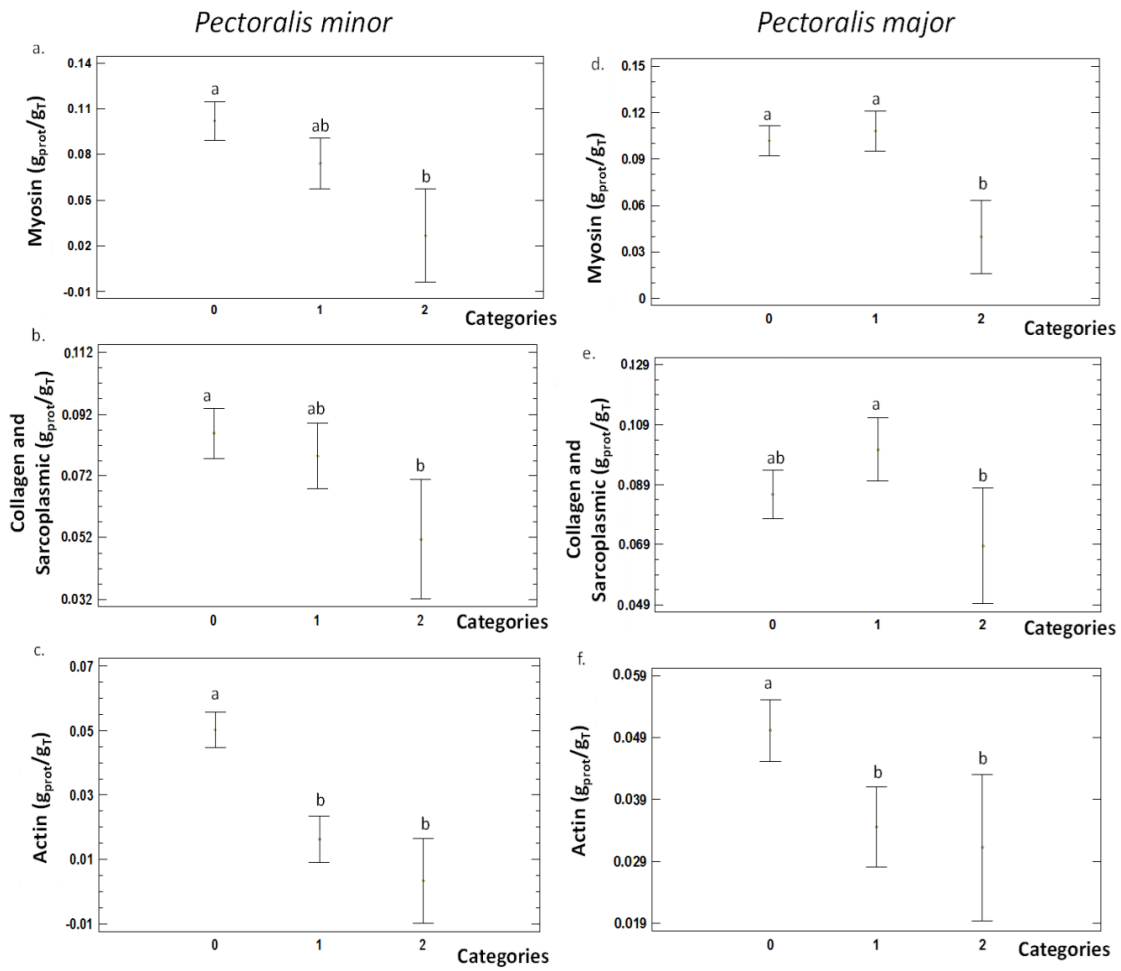

Figure 3. Mass fraction of myosin ($g_{protein}/g_{Total}$), collagen and sarcoplasmic proteins, and actin of *Pectoralis minor* and *major*, where: 0 corresponds to non-damaged tissues, 1 to hemorrhagic samples with hematomas and blood clots, and 2 to necrotic samples. Different letters in the same graphic (a-b) indicate significant differences (p<0.05).

The process of necrosis is progressive and the damage produced in muscle tissue is not uniform. An image analysis was performed in order to estimate the damaged areas (blood clots, hemorrhagic and necrotic areas) by category. The criterion used to select the damages in the muscle can be observed in Figure 4 and the results obtained are shown in Tables 2 and 3.

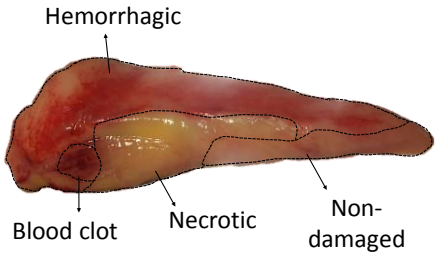

Figure 4. Schematic representation of the area selection according to the DPM damage in *Pectoralis minor*.

Table 2. Hemorrhagic, hematoma/blood clots and necrotic areas of DPM samples.

	Average area per category (%)	
	Category 1	Category 2
Hemorrhagic	41 ± 17	9 ± 8
Blood clots	5 ± 3	3 ± 3
Necrotic	0 ± 0	31 ± 22

Table 2 shows the distribution of hemorrhagic areas, blood clots and necrotic, where it is possible to observe how category 1 does not present necrotic areas but accumulates large hemorrhagic areas, however, category 2 shows large necrotic areas with very few hemorrhages, not showing significant differences in the presence of blood clots between the two categories.

Table 3. Percentage of samples with low incidence (less than 30% of affected area), medium incidence (between 30 and 60% of affected area) and high incidence (more than 60% of affected area) of categories 1 and 2.

		Percentage of samples	
		Category 1	Category 2
Hemorrhagic area	1-30 %	24	84.6
	30-60%	60	0
	60-100%	16	0
Blood clots	1-30 %	16	53.8
	30-60%	4	7.7
	60-100%	0	0
Necrotic	1-30 %	0	53.8
	30-60%	0	23.1
	60-100%	0	23.1

Table 3 shows the percentage of samples with low incidence (less than 30% of affected area), medium incidence (between 30 and 60% of affected area) and high incidence (more than 60% of affected area). For the three incidences mentioned above, hemorrhagic area, coagulated area and necrotic area.

In Table 3 it is possible to observe how category 1 shows a low incidence of samples with blood clots while category 2 incidence reaches more than 50% of samples. In addition, category 1 shows a homogeneous distribution of the incidence of hemorrhagic areas, the majority being in a medium incidence, however, in category 2 the hemorrhagic areas have a slight incidence. Finally, in Table 3, it can be observed that category 2 presents half of the necrotic samples with slight incidence.

Figure 5 shows the L*, a*, b* coordinates and the ΔE* obtained for the three categories studied. The least significance difference (LSD) intervals (95% confidence) are also shown. In the CIE L* a* b* space, L* coordinate represents lightness, where L*= 0 is completely black, and L* = 100 is

completely white, a* represents the red-green color and b* the yellow-blue color of the sample. Significant differences ($p < 0.05$) in L* coordinate between non-damaged and damaged samples can be observed. Samples with damaged tissue by DPM show a decrease in the L* coordinate (Fig. 5a). Hemorrhagic samples with hematomas and blood clots show significant ($p < 0.05$) higher a* values (redder color) (Fig.5b) than non-damaged and necrotic samples, as a consequence of the blood clots formation. On the other hand, b* coordinate (Fig. 5c) is higher in non-damaged samples than in DPM samples, showing a higher yellow color in non-damaged samples. ΔE* parameter show that the color differences among non-damaged samples and DPM samples are significant.

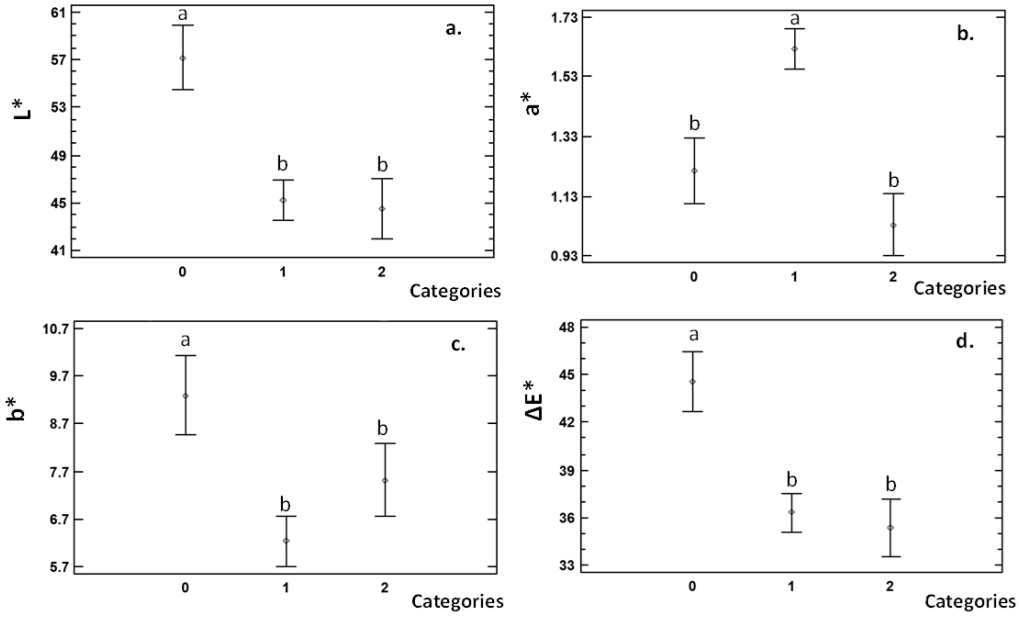

Figure 5. CIELab coordinates, where: (a) L*, (b) a*, (c) b* and (d) ΔE* color variation, where: 0 non-damaged tissues, 1 hemorrhagic samples with hematomas and blood clots, and 2 necrotic samples. Different letters on the columns (a-b) indicate significant differences ($p<0.05$).

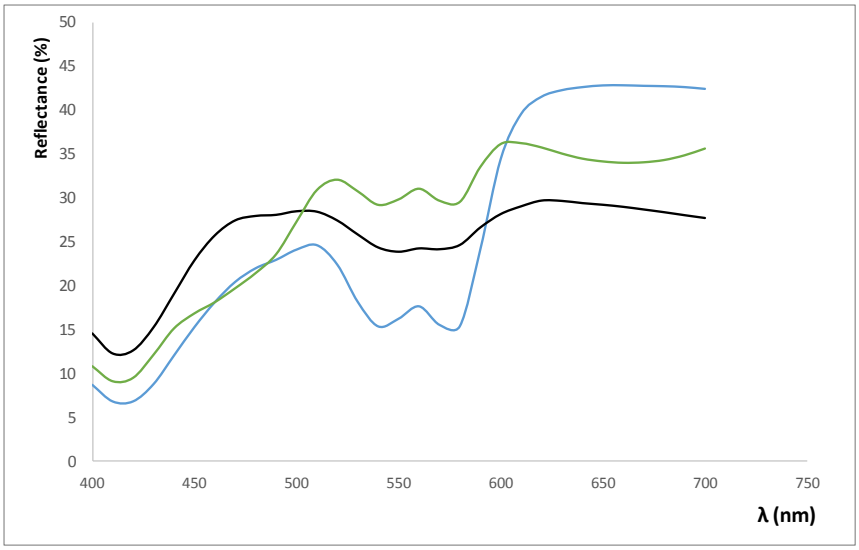

Figure 6. Average reflectance spectra for the non-damaged tissue (grey color), category 1 tissue (blue color) and category 2 tissue (green color).

Haemorrhages are considered as a release of blood into the tissues and follow the haemoglobin metabolism, where the haemoglobin is degraded to biliverdin, carbon monoxide and free iron due to an oxidative reaction catalysed by heme oxygenase. This oxidation involves the consumption of three molecules of O_2 (Fondevila, Busuttil, & Kupiec-Weglinski., 2003). It is known that this metabolism is related with bruises formations in muscle tissues (Jeney, Eaton, Balla, & Balla, 2013; Biswas, Singh, & Sharma, 2012; Hughes, Ellis, Burt, & Langlois, 2004) and it also explains the green colour of the necrotic tissues (Brooks, 2016; Hill, & Miller, 2013). In this context, a colorimetric analysis of the muscle tissue according to the deep pectoral myopathy category can let to understand the involved metabolites in the muscle damage. Lindahl (2005) identified different peaks in the reflectance spectrum at 473, 572 and 610 nm, which correspond to myoglobin, metamyoglobin and oximyoglobin, respectively. On the other hand, Thavarajah, Vanezis, & Perrett. (2012) identified a peak at 530 nm for biliverdin. Figure 6 shows the average reflectance spectra for damaged and non-damaged tissues, where it is possible to observe that the hemorrhagic samples with hematomas and blood clots present higher reflectance values in the range from 600 nm to 700 nm which can be related with the higher haemoglobin content of this category. In contrast, category 2 or necrotic samples showed a peak near 530 nm, which can be related with the higher biliverdin content of this category. Finally, non-damaged samples present similar reflectance values along the spectra, resulting in the normal white colour of chicken breast.

Figure 7 shows that the pH (at 12 hours post-mortem) of *Pectoralis minor* allow us to discriminate the non-damaged tissues from hemorrhagic samples with hematomas and blood clots and necrotic samples. Also, it can be observed that the damaged tissues present higher pH values than the non-damaged tissue. In the same figure, the pH of *Pectoralis major* is shown, but in this case, there were no significant differences among categories.

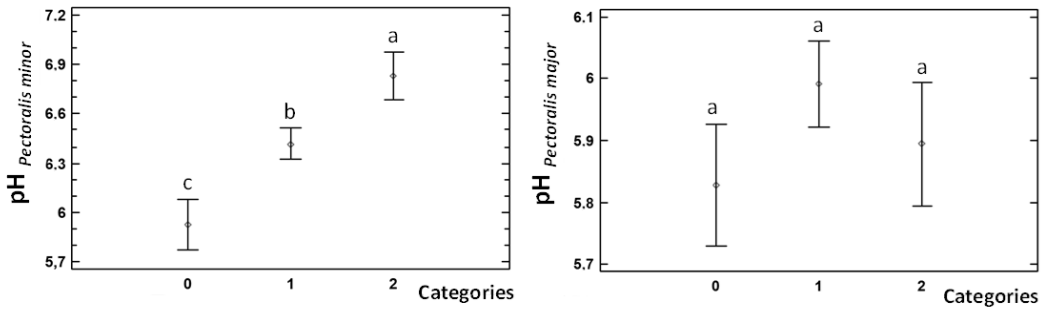

Figure 7. a) pH of the *Pectoralis minor* at 12 h post-mortem, b) pH of the *Pectoralis major*, where: 0 non-damaged tissues, 1 hemorrhagic samples with hematomas and blood clots and 2 necrotic samples.

As it was explained in the introduction section, there exists an industrial categorization of DPM (Martindale *et al.*, 1979). This categorization consists in an inaccurate and unquantifiable parameter (visual), so it is necessary to categorize the damage in poultry objectively. For this purpose, the authors propose a classification based on significant (p<0.05) variables, measured in *Pectoralis minor* (pH, L* and a* coordinates) (Table 4).

Table 4. Categorization of the poultry *Pectoralis minor* muscle according to the deep pectoral myopathy.

	Category 0	**Category 1**	**Category 2**
L*	>53	<47	<47
a*	<1.33	>1.53	<1.13
pH	<6.05	<6.05	>6.5

In order to demonstrate the reliability of the classification proposed by the authors, a multifactorial algorithm using the parameters shown in Table 4 was developed. Figure 8 shows the predicted categories based on the algorithm proposed by the authors with regard to the industrial trained expert categorization, where it is possible to observe the effectiveness of the previously classification proposed.

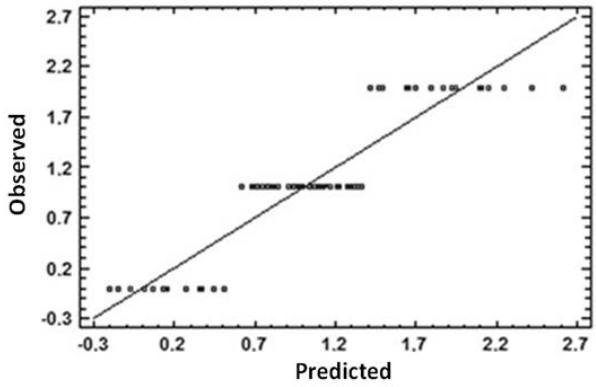

Figure 8. Predicted categories based on the developed algorithm versus the industrial categories.

4. Conclusions

By means of a microstructural and physicochemical analysis of *pectoralis minor* and *major*, which include the analysis of cations, proteins, pH, microstructural changes, or color variations by areas, it has been possible to describe the transformations that occur during an ischemia with a hemorrhagic or necrotic process, namely an angina or an infarct disease.

Finally, it has been developed an objective and scientific methodology to categorize the level of the DPM in poultry. This categorization is able to differentiate three categories: non-damaged, hemorrhagic samples (angina) and necrotic samples (infarct).

Acknowledgements

The authors acknowledge the financial support from: the Spanish Ministerio de Economía, Industria y Competitividad, Programa Estatal de I+D+i orientada a los Retos de la Sociedad AGL2016-80643-R, Agencia Estatal de Investigación (AEI) and Fondo Europeo de Desarrollo

Regional (FEDER). The author Maria Victoria Traffano Schiffo wants to thank the FPI Predoctoral Program of the Universidad Politécnica de Valencia for its support. The authors would like to thanks the Electronic Microscopy Service of the Universidad Politécnica de Valencia for its assistance in the use of Cryo-SEM.

References

Bilgili, S. F., & Hess, J. (2008). Green muscle disease. Reducing the incidence in broiler flock. *Ross Technology*, 8(48), 3.

Biswas, G., Singh, V. P., & Sharma, J. (2012). Ageing of Bruise: Review of Histo-Chemical Changes with Time. *Indian Internet Journal of Forensic Medicine & Toxicology*, 10(1), 15-17.

Brooks, J. W. (2016). Postmortem changes in animal carcasses and estimation of the postmortem interval. *Veterinary Pathology*, 53(5) 1-12.

CIE (1978). International Commission on Illumination, recommendations on uniform color spaces, color, difference equations, psychometric color terms. CIE publication No. 15 (Suppl.2), (E-1.31) 1971/(TC-1.3). Paris, France: Bureau Central de la CIE.

Fernández-Martín, F., Fernández, P., Carballo, J., & Jiménez-Colmenero, F. (2000). DSC study on the influence of meat source, salt and fat levels, and processing parameters on batters pressurisation. *European Food Research and Technology*, 211(6), 387-392.

Fondevila, C., Busuttil, R. W., & Kupiec-Weglinski, J. W. (2003). Hepatic ischemia/reperfusion injury-a fresh look. *Experimental and Molecular Pathology*, 74(2), 86-93.

Gürke, L., Mattei, A., Chaloupka, K., Marx, A., Sutter, P. M., Stierli, P., Harder, F., & Heberer, M. (2000). Mechanisms of ischemic preconditioning in skeletal muscle. *Journal of Surgical Research*, 94(1), 18-27.

Hafez, H. M., & Hauck, R. (2005). Genetic selection in turkeys and broilers and their impact on health conditions. *World's Poultry Science Association, 4th European Poultry Genetics Symposium*. (1-10).

Hill, A. G., & Miller, R. (2013). Exercise-induced deep pectoral necrosis in white-headed pigeons (Columba leucomela). *Journal of Zoo and Wildlife Medicine*, 44(4), 990-995.

Horimoto, H., Gaudette, G. R., Saltman, A. E., & Krukenkamp, I. B. (2000). The role of nitric oxide, K+ ATP channels, and cGMP in the preconditioning response of the rabbit. *Journal of Surgical Research*, 92(1), 56-63.

Hughes, V. K., Ellis, P. S., Burt, T., & Langlois, N. E. I. (2004). The practical application of reflectance spectrophotometry for the demonstration of haemoglobin and its degradation in bruises. *Journal of Clinical Pathology*, 57(4), 355-359.

Immke, D. C., & McCleskey, E. W. (2001). Lactate enhances the acid-sensing Na^+ channel on ischemia-sensing neurons. *Nature Neuroscience*, 4(9), 869-870.

Jeney, V., Eaton, J. W., Balla, G., & Balla, J. (2013). Natural history of the bruise: formation, elimination, and biological effects of oxidized hemoglobin. *Oxidative Medicine and Cellular Longevity*, 2013, 1-9.

Kijowski, J., Kupińska, E., Stangierski, J., Tomaszewska-Gras, J., & Szablewski, T. (2014). Paradigm of deep pectoral myopathy in broiler chickens. *World's Poultry Science Journal*, 70(01), 125-138.

Lindahl, G. (2005). Colour characteristics of fresh pork. Doctoral Thesis. Uppsala (Sweden). Swedish University of Agricultural Sciences.

Martindale, L., Siller, W. G., & Wight, P. A. L. (1979). Effects of subfascial pressure in experimental deep pectoral myopathy of the fowl: an angiographic study. *Avian Pathology*, 8(4), 425-436.

Martín-García, A (2009). Estudio de marcadores bioquímicos de interés en el diagnóstico y pronóstico del síndrome coronario agudo. Doctoral Thesis. Madrid (Spain). Universidad Complutense de Madrid.

Miyoshi, Y., Nakaya, Y., Wakatsuki, T., Nakaya, S., Fujino, K., Saito, K., & Inoue, I. (1992). Endothelin blocks ATP-sensitive K^+ channels and depolarizes smooth muscle cells of porcine coronary artery. *Circulation Research*, 70(3), 612-616.

OECD/Food and Agriculture Organization of the United Nations (2013), OECD-FAO Agricultural Outlook 2013, OECD Publishing. http://dx.doi.org/10.1787/agr_outlook-2013-en.

Ouali, A., Herrera-Mendez, C. H., Coulis, G., Becila, S., Boudjellal, A., Aubry, L., & Sentandreu, M. A. (2006). Revisiting the conversion of muscle into meat and the underlying mechanisms. *Meat Science*, 74(1), 44-58.

Petracci, M., & Cavani, C. (2012). Muscle growth and poultry meat quality issues. *Nutrients*, 4(1), 1-12.

Ross, Y. H (2006). Phase transitions and transformations in food systems. In D. R. Heldman, D. B. Lund (Eds.), *Handbook of Food Engineering* (pp. 287-352). Florida: CRC Press.

Schäfer, M., Schlegel, C., Kirlum, H. J., Gersing, E., & Gebhard, M. M. (1998). Monitoring of damage to skeletal muscle tissues caused by ischemia. *Bioelectrochemistry and Bioenergetics*, 45(2), 151-155.

Takahashi, S., Barry, A. C., & Factor, S. M. (1990). Collagen degradation in ischaemic rat hearts. *Biochemical Journal*, 265(1), 233-241.

Thavarajah, D., Vanezis, P., & Perrett, D. (2012). Assessment of bruise age on dark-skinned individuals using tristimulus colorimetry. *Medicine, Science and the Law*, 52(1), 6-11.

Traffano-Schiffo, M. V., Castro-Giraldez, M., Colom, R. J., & Fito, P. J. (2017a) Innovative spectrophotometric system to determine chicken meat quality. *Innovative Food Science and Emerging Technologies*.

Traffano-Schiffo, M. V., Castro-Giraldez, M., Colom, R. J., & Fito, P. J. (2017b). Development of a Spectrophotometric System to Detect White Striping Physiopathy in Whole Chicken Carcasses. *Sensors*, 17(5), 1024.

Zweier, J. L., Wang, P., Samouilov, A., & Kuppusamy, P. (1995). Enzyme-independent formation of nitric oxide in biological tissues. *Nature Medicin*e, 1(8), 804-809.

PATENTE P201630062: APARATO Y MÉTODO DE DETECCIÓN DE DAÑO PRODUCIDO POR LA MIOPATÍA DEL PECTORAL PROFUNDO EN AVES

OBJETO DE LA INVENCIÓN

La presente invención pretende abordar un problema que se produce frecuentemente en aves para consumo humano, especialmente en aquellas criadas en granjas, concretamente el problema de la miopatía del pectoral profundo (DPM).

El objeto de la presente invención se refiere a un aparato y método de detección del daño producido por miopatías en el pectoral, o comúnmente llamado pechuga, de aves sacrificadas para el consumo humano.

MODALIDAD: **PATENTE DE INVENCIÓN**

SOLICITANTE: **UNIVERSITAT POLITÈCNICA DE VALÈNCIA**

INVENTORES:

Inventor 1: Pedro José Fito Suñer (España)

Inventor 2: Ricardo José Colom Palero (España)

Inventor 3: Marta Castro Giráldez (España)

Inventor 4: Vicente Herrero Bosch (España)

Inventor 5: José María Monzó Ferrer (España)

Inventor 6: María Victoria Traffano Schiffo (Argentina)

Inventor 7: Ángel Tébar Ruiz (España)

RESUMEN

La presente invención se refiere a un aparato y método de detección del daño producido por miopatías en el pectoral de aves sacrificadas para el consumo humano. Este aparato, comprende un sensor de transductores múltiples que aplica una señal eléctrica sobre el pectoral de un ave; y que recibe una señal de respuesta de dicho pectoral. El sensor de transductores múltiples está vinculado con un dispositivo de acondicionamiento, que genera la señal eléctrica y que recibe y acondiciona la señal de respuesta, para transferirla a una unidad de control. Esta unidad de control calcula la permitividad en función de la frecuencia, detecta las dispersiones alfa y beta mediante algoritmos logísticos y mediante la predicción de algunas especies químicas y el tiempo postmortem detecta y cuantifica los daños producidos por miopatías.

4.5. Detección de rayas blancas en pechugas de pollo mediante espectrofotometría.

Traffano-Schiffo, M. V., Castro-Giraldez, M., Colom, R. J., & Fito, P. J. (2017). Development of a spectrophotometric system to detect white striping physiopathy in the whole chicken carcass. ***Sensors***, 17(5), 1024.

DEVELOPMENT OF A SPECTROPHOTOMETRIC SYSTEM TO DETECT WHITE STRIPING PHYSIOPATHY IN WHOLE CHICKEN CARCASSES

Maria Victoria Traffano-Schiffo[1], Marta Castro-Giraldez[1], Ricardo J. Colom[2], Pedro J. Fito[1]*

[1]Instituto Universitario de Ingeniería de Alimentos para el Desarrollo, Universitat Politecnica de Valencia, Camino de Vera s/n, 46022 Valencia, España.

[2]Instituto de Instrumentación para Imagen Molecular, Universitat Politecnica de Valencia, Valencia, España.

Corresponding author information:

Phone: +34 636998785; fax: +34 963879832.

e-mail: pedfisu@tal.upv.es

Abstract: White striping in chicken breast is one of the most frequent myopathies in poultry due to the high intensification in production in recent years. The aim of this research was to develop a sensor based in spectrophotometry to detect white striping physiopathy in chicken breast meat in whole chicken carcass with skin. Experiments were carried out using normal and white striping breasts. In order to understand the mechanism involved in this physiopathy, the different tissues that conform each breast were analyzed. Permittivity in radiofrequency (40 Hz to 1 MHz) was measured using two different sensors; a sensor of two flat plates to analyze the whole breast with skin (NB or WSB), and a two needles with blunt-ended sensor to analyze the different surface tissues of the skinless breast. In microwave range (500 MHz to 20 GHz), permittivity was measured as just was described for the two needles with blunt-ended sensor. Moreover, fatty acids composition was determined by calorimetry techniques from -40ºC to 50ºC at 5 ºC/min with previous freeze-drying of sample, and pH, microstructure by Cryo-SEM and binocular loupe were also analyzed. The results showed that white striping physiopathy consists of the partial breakdown of the pectoral muscle causing an increase in fatty acids, reducing the quality of the meat. It was possible to detect white striping physiopathy in chicken carcasses with skin using spectrophotometry in radiofrequency spectra.

Keywords: White striping, poultry, dielectric spectroscopy, fatty acids, radiofrequency, microwave, spectrophotometry, dispersion, microstructure.

1. Introduction

In recent decades, the overall consumption of chicken and turkey meat has increased considerably and it is expected that in the coming years, chicken will become the most produced type of meat in the world. It has been estimated that in 2020, global chicken meat production will be around 122.5 million tons [1]. The two main reasons that are driving the success of poultry meat are the low price and the healthy nutritional profile compared to pork and beef.

As a result of increasing demand, there has been an intensification in poultry production, where modern hybrid broilers show a pectoral development greater than 20% of the body weight [2]. This production intensification has increased the incidence of abnormalities in the Pectoralis muscle [3-5]. The most common malformations are Deep Pectoral Myopathy [6,7] and White Striping [8,9].

White Striping disease is a serious, emerging issue characterized by the appearance of white stripes (WS) parallel to muscle fiber on the surface of the Pectoralis major muscle [10]. Some authors classified the incidence into three categories according to the intensity and thickness of the WS: NORMAL when the breast is not affected, MODERATE when the thickness of the WS is less than 1 mm and SEVERE when the WS cover most of the surface and the thickness is greater than 1 mm [11,12].

The presence of WS on the surface of chicken breasts affects the visual appearance of the product and decreases the degree of consumer acceptance [11]. However, the negative visual impact is not the only problem; white striping also affects the chemical composition: protein content decreases as the degree of affection increases, while there is an opposite trend in fat content, thus the presence of this hypertrophy decreases the nutritional value of the meat [13].

For this reason, white striping breasts (WSB) should not be commercialized as normal breast (NB), they should be used in the formulation of meat products such as sausages and nuggets, however, when the chicken is sold whole, the presence of the skin means that it is not possible to see the effects of this disorder. Considering this issue, it is necessary to find a reliable, efficient industrial system to detect the presence of white striping; for this reason, non-invasive sensors based on spectrophotometry at range of radiofrequency and microwaves could be a good tool to meet this challenge.

Dielectric properties expressed as permittivity can be explained as vector, polar or complex numbers. As a complex number, permittivity (ε) is composed of two terms, the dielectric constant ε' and the loss factor ε'', which are the real and imaginary terms of permittivity, respectively. The dielectric constant is related to the tissue's ability to absorb and store electric energy, and the loss

factor is related to the dissipation of the electric energy into other energies such as thermal or mechanical energies.

In the range of radiofrequency and microwaves, the interaction of the photon flux with biological tissue produces three main dispersions: α, β, and γ [14]. In particular, α-dispersion (from a few Hz to a few kHz), also called the counterion effect, is induced by the orientation of mobile charges in a dielectric medium [15]. β-dispersion (from kHz to tens of MHz) is related to the orientation of fixed charges in macromolecules such as proteins [16]. At higher frequencies of the radiofrequency range, β-dispersion results due to the surface tension charges, this phenomenon is called the Maxwell-Wagner effect. Finally, in the microwave range, γ-dispersion occurs at GHz frequencies and is due to the orientation and induction of dipolar molecules such as water [17-19].

Another important effect in the microwave range is ionic conductivity. It only affects the loss factor, as it produces a repulsion of charged molecules, transforming electric energy into other types [20].

The usefulness of spectrophotometry at low frequencies in the food industry has been demonstrated as a monitoring technique in a wide range of the permittivity spectra: radiofrequency, microwave and infrared (from Hz to THz). Talens *et al.* (2016) [20] developed a dielectric isotherm technique able to predict the water activity in dried orange peel using the ε' at 20 GHz (microwave range); Shang, Guo, and Nelson (2015) [21] identified the variety of apples in the radiofrequency range. Castro-Giráldez *et al.* (2010) [22] demonstrated the usefulness of two dielectric ageing indexes at different frequencies (140 Hz, 500 Hz and 300 kHz) to determine pork meat ageing. Also, Trabelsi and Roelvink (2014) [23] and Damez *et al.* (2008) [24] demonstrated that dielectric spectroscopy is able to predict chicken and beef ageing using microwave and radiofrequency ranges, respectively. Finally, Cuibus *et al.* (2014) [25] and Traffano-Schiffo *et al.* (2014) [26] demonstrated that infrared is a good non-destructive technique to monitor freezing and drying processes.

The aim of this research was to develop a sensor based in spectrophotometry to detect white striping physiopathy in chicken breast meat in whole chicken carcass with skin.

2. Experimental

2.1. Raw material

The experiments were carried out using boneless broiler breasts (Pectoralis major) obtained from SADA Group slaughterhouse located in Rafelbunyol, Valencia. After slaughter, male broilers of 42 d were bleeding, plucked, tempered in a cooling tunnel at 4 ºC during 3 h and finally

dismembered. Breasts were classified by the quality experts of the slaughterhouse plant, according to the appearance of severe WS (WSB) or NB. The selected breasts (including its skin) were transported using an isothermal bag with ice blocks to the laboratory of Institute of Food Engineering for Development (IuIAD) at the Polytechnic University of Valencia (UPV). The samples were measured at 12 h post-mortem and maintained at 2 ºC during the experimental procedure.

2.2. Experimental procedure

Experiments were carried out using 40 chicken breasts: 20 were classified as NB and 20 as WSB. Prior to the dielectric measures, pH analyses of the samples were carried out using a punch pH-meter S-20 SevenEasy™ (Mettler Toledo, Barcelona, Spain) to characterize the samples according to their quality. Permittivity of the samples was measured in the surface of the breasts (ventral side) in radiofrequency and microwave ranges (non-destructive measurements). In radiofrequency range, firstly, a sensor of two flat plates with circular surfaces was used to measure the permittivity of whole breast with skin (NB or WSB). After that, a two needles with blunt-ended sensor was used to measure the permittivity of each tissue of the skinless breast (muscle and adipose tissues of NB and WSB, and white stripes of WSB). In microwave range, permittivity was measured as was described above for the two needles with blunt-ended sensor.

Subsequently, with the aim of analyzing the state of the fatty acids, a differential scanning calorimetry (DSC) study was performed by triplicate for samples of the ventral portion of NB and WSB.

Finally, a macro and microstructural study of NB and WSB was performed using a binocular loupe and a low-temperature Scanning Electron Microscope, respectively.

2.3. Structural analysis

2.3.1. Low-temperature Scanning Electron Microscopy (Cryo-SEM)

The microstructure of NB and WSB was analyzed by Cryo-SEM. A Cryostage CT-1500C unit (Oxford Instruments, Witney, UK), coupled to a Jeol JSM-5410 scanning electron microscope (Jeol, Tokyo, Japan), was used. The sample was immersed in N_2 slush (-210 ºC) and then quickly transferred to the Cryostage at 1 kPa where sample fracture took place. Sublimation (etching) was carried out at -95 ºC. The final point was determined by direct observation under the microscope, working at 5 kV. Then, once again in the Cryostage unit, the sample was coated with gold in vacuum (0.2 kPa) applied for 3 min, with an ionization current of 2 mA. The observation in the scanning electron microscope was carried out at 20 kV, at a working distance of 15 mm and temperature ≤ -130 ºC.

2.3.2. Optical measurements

Optical measurements were made with a binocular loupe Leica MZ APO™ (Leica Microsystems, Wetzlar, Germany) with low magnification (8x to 80x) using incident light illumination (light reflected off the surface of the sample). It uses two separate optical paths with two objectives and two eyepieces to provide slightly different viewing angles for the left and right eyes. In this way, it permits a three-dimensional visualization of the sample.

2.4. Permittivity measurements

2.4.1. Radiofrequency range

As was explained above, two different sensors were used to carry out this experimental work (see Figure 1). One of them consists of two flat plates with circular surfaces sensor (Figure 1a) and it was used to measure the whole breast with skin (NB or WSB) (this configuration has high penetration depth). The other sensor consists of two needles with blunt-ended (Figure 1b) and it was used to measure the different tissues of surface breast (this configuration has low penetration depth): muscle and adipose tissues in NB and WSB, and WS in WSB. In case of two needles sensor, its size was small enough to touch the specific tissue, and its penetration depth was low enough just to include the specific tissue. In WS and in adipose tissue, the globular conformation of the fat adipocytes, similar in the three axes, does not affect to the displacement of photon flux. However, in case of muscle, the mobility of liquid phase in the direction of the fibers changes the displacement of photon flux if it is compared with the perpendicular direction. Therefore, it was measured in perpendicular direction of fibers. It is important to highlight that the muscle tissue of WSB is referred to the muscle between the WS.

Both sensors were developed by The Institute of Food Engineering for Development (IuIAD) and The Institute for Molecular Imaging Technologies (I3M), both at the Polytechnic University of Valencia. The sensors were connected to an impedance analyzer Agilent 4694A. Permittivity were estimated using equations 1, 2 and 3. The frequency range measured was from 40 Hz to 1 MHz. Calibration of the equipment was performed in open (air) and short-circuit.

The signal obtained by the Agilent analyser is the impedance Z, and taking into account that the impedance as a complex number is $\bar{Z} = R + jX$, where the real part of the impedance is the resistance R and the imaginary part is the reactance X. The parameters R and X were transformed in ε', ε'' as follows:

$$\varepsilon' = \frac{-X}{(R^2 + X^2)} \frac{1}{2\pi C_0} \quad (1)$$

$$\varepsilon'' = \frac{R}{R^2 + X^2} \frac{1}{2\pi f C_0} \quad (2)$$

$$C_0 = \frac{\varepsilon_0 S}{d} \quad (3)$$

Where f is the frequency (Hz), C_0 is the capacitance in the vacuum (F), S is the surface of the electrodes (m^2), ε_0 is the vacuum permittivity (F/m) and d is the separation between the electrodes with differential tension (V_H-V_L) (m).

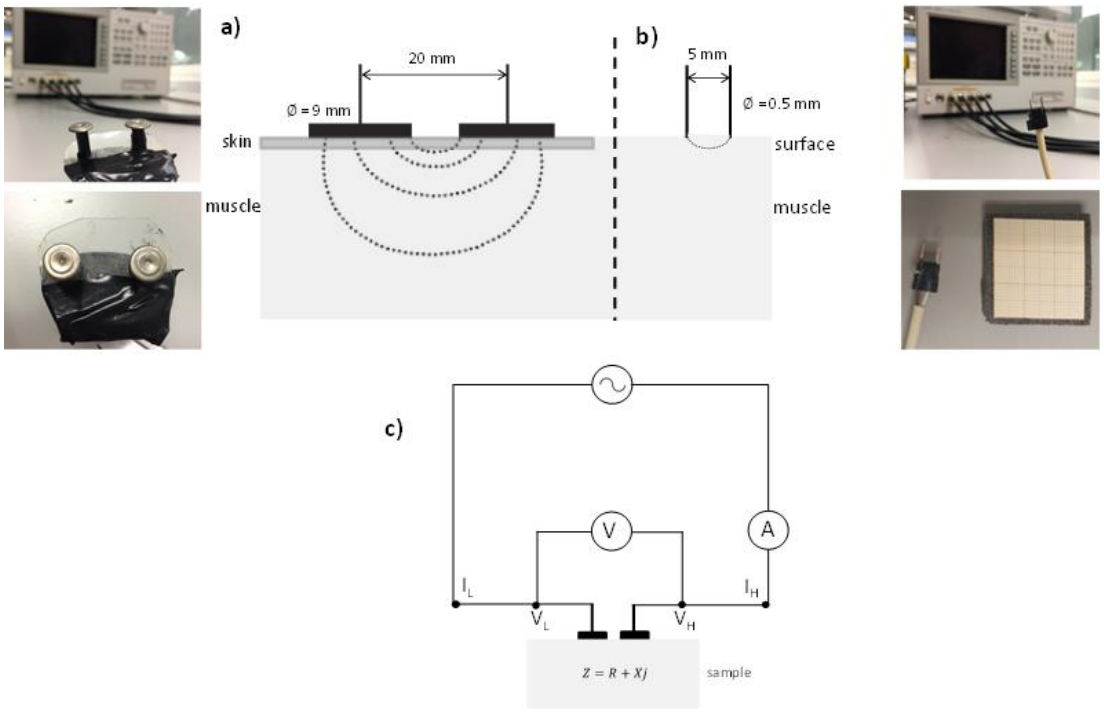

Figure 1. Permittivity measurement in radiofrequency, detail of each sensor: a) two flat plates sensor to measure the whole breast with skin, b) two needles with blunt-ended sensor to determine the permittivity in surface of the breast and c) electric circuit of both sensors.

2.4.2. Microwave range

Permittivity of the samples in the microwave range was measured with an Agilent 85070E open-ended coaxial probe connected to an Agilent E8362B Vector Network Analyzer.

The system was calibrated using three different types of loads: open (air), short-circuit and 4 ºC Milli®-Q water. Once the calibration was carried out, 4 ºC Milli®-Q water was measured again to check calibration suitability. All determinations were made from 500 MHz to 20 GHz.

All permittivity measurements were performed by triplicate.

2.5. Differential Scanning Calorimetry (DSC)

The thermal transitions of the fatty acids was performed according to the method proposed by Benedito *et al.* (2001) [27] using a differential scanning calorimeter Mettler Toledo DSC 1 (Mettler Toledo, Barcelona, Spain) provided with a full range temperature sensor FRS5. The

calibration of the equipment was performed with the automatic calibration function FlexCal supplied by the manufacturers. Samples taken from the surface of tissue (around 22-25 mg) were introduced into aluminium pans (Mettler Toledo, ME-00026763). Water was removed by lyophilisation for 48 hours using a lyophiliser Telstar Lyoalfa-6 (Telstar, Dewsbury, U.K.) as it can interfere with the fat melting in the DSC curve. The pans were hermetically sealed and an empty one was used as the reference sample. Before obtaining the DSC curves, the samples were tempered at 60 ºC for 5 minutes, cooled to -40 ºC at 10 ºC/min and held at -40 ºC for 5 minutes. The DSC curves were obtained by heating the sample from -40 ºC to 50 ºC at a rate of 5 ºC/min.

2.6. Statistical Analysis

The statistical analysis was carried out with the Statgraphics Centurion XVI software (Statgraphics, Virgina, U.S.A.). One-Way ANOVA analyses were made in order to find statistically significant differences between the parameters studied for the different samples. The logistic model of modified Gompertz was fitted by using nonlinear regression.

3. Results and discussion

All the samples presented a pH value between 5.7 and 6.1, which were classified as NORMAL according by Zhang and Barbut (2005) [28] classification.

In Figure 2, a microstructural analysis of NB and WSB samples is shown. Figures 2a and 2b correspond to NB, where muscle tissue with correct packaging of the myofibrils is observed. However, in Figures 2c and 2d, it is possible to observe the deposition of adipocytes, conforming a new adipose tissue surrounded by muscle tissue, named white stripe (WS). This deposition of adipocytes is produced in areas which have suffered muscle breakdown. Other authors suggested that there is also an accumulation of collagen in the WS [13, 29].

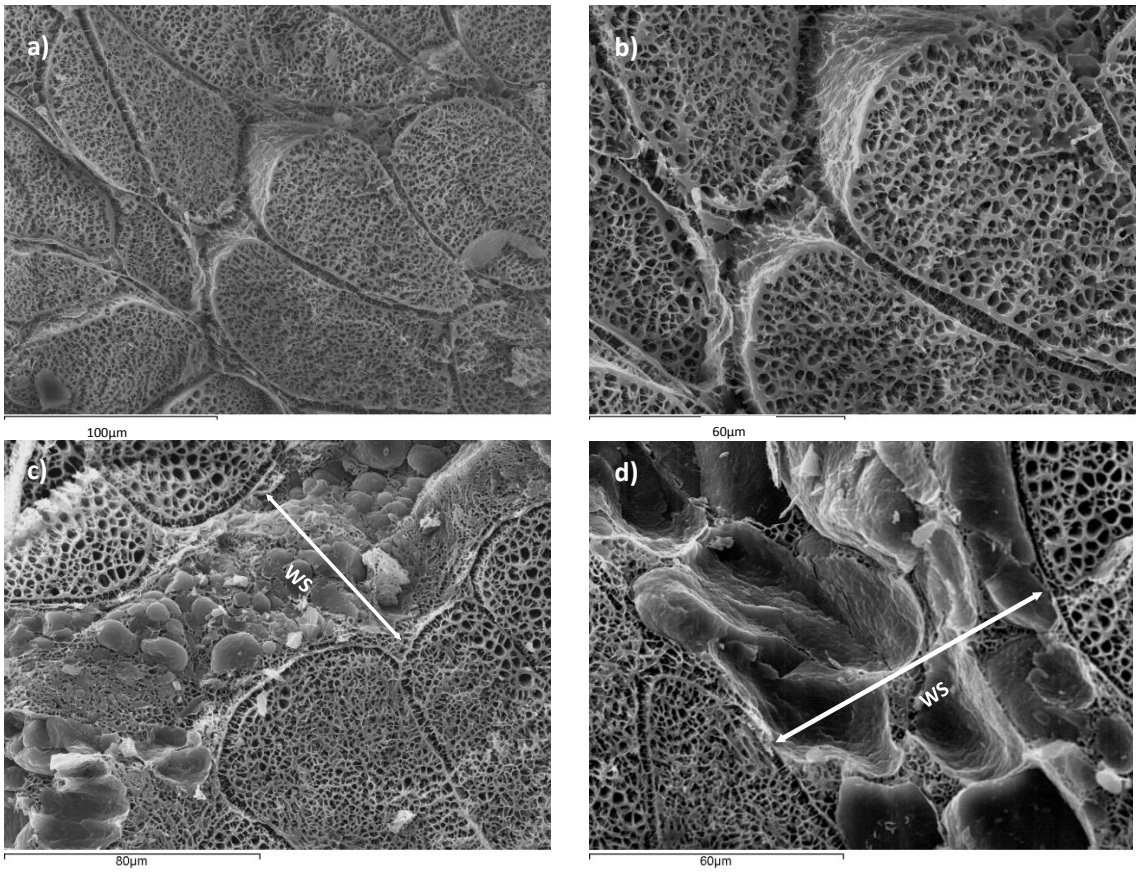

Figure 2. Micrographs of normal breast (NB) a) 500x, b) 1000x and breast affected by white striping (WSB), with the detail of the white stripe (WS) c) 750x and d) 1000x at 12 h post-mortem.

Figure 3 shows a detail of WS in chicken breast, where it can be appreciated a muscular rupture, from the surface breast to the internal muscle, induced by perpendicular forces to the fissure, and filled with fat tissue, in order to maintain the integrity of breast. Thus, the accelerated muscular growth induced by pectoral hypertrophy has caused partial muscular rupture and the deposition of adipose tissue in this area. Adipose tissue maintains the cohesion between muscle fibers and the elasticity of muscle tissue and therefore its activity of contraction-relaxation, conferring to the muscle the ability to transmit mechanical tension.

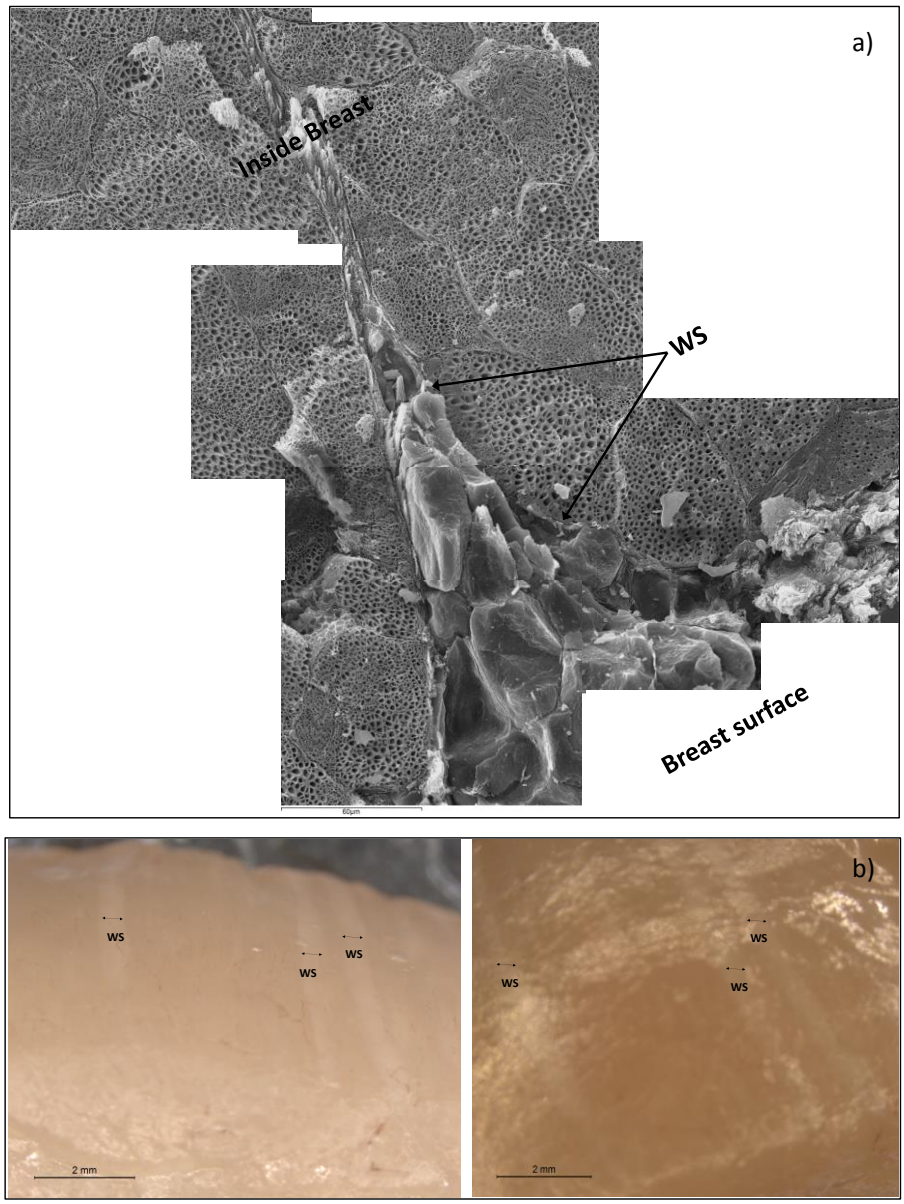

Figure 3. a) Micrographs showing the detail of a white stripe (WS) (1000x), b) binocular microscope images of WS in surface breast samples (8x).

In addition, it is possible to appreciate that tissue breakdown is generated from the outside to the inside, so the quantity of adipose tissue is higher at the surface of the breast than the interior. Major muscle breakdown is in the external surface because the maximum tension is caused by the pectoral activity of poultry during flapping. This phenomenon produces a *pectoralis major* expansion, being maximum in the surface (reaching in this area the breakdown tension level).

Compared to NB, the WSB contains higher quantities of fatty acids, which cause the diminution of the protein content [30]. In particular, collagen increases due to hypertrophy as it is necessary to maintain the muscle structure, however, sarcoplasmic and myofibrillar proteins decrease [13].

The fatty acids of WSB and NB, in the surface, were measured by differential scanning calorimetry. The thermograms obtained show four transitions for the WSB (Figure 4a). According

to the melting temperatures, it was possible to relate each transition to the different groups of fatty acids [31,32], where polyunsaturated fatty acids (PUFA) show a melting point in the range between -17 °C and -5 °C; monounsaturated fatty acids (MUFA) between -5 °C and 27 °C and saturated fatty acids (SFA) between 27 °C and 40 °C.

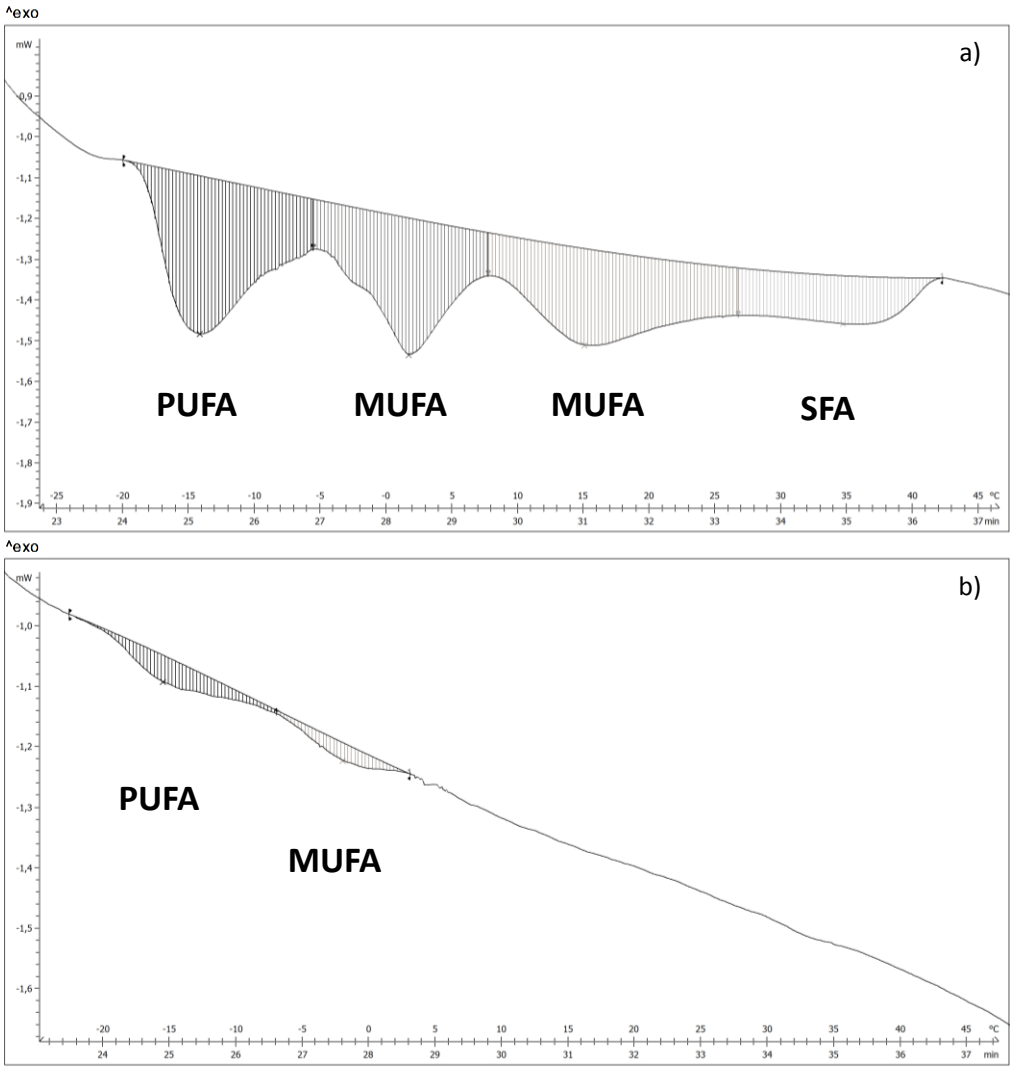

Figure 4. DSC thermogram of a) white striping breast and b) normal breast.

Figure 4b shows a thermogram corresponding to a NB, where it is possible to appreciate that there are only two transition peaks associated with PUFA and MUFA, which suggests that there is a big difference in fatty acids content between NB and WSB. Energy values and the temperature of the different transitions for both groups of samples are shown in Tables 1 and 2, respectively.

Table 1. Energy (J/g) and temperatures (°C) values of the fatty acids transitions of the white striping samples. Where: T_0 corresponds to the initial transition temperature, T_p peak transition temperature and T_f the final transition temperature.

	1st transition	2nd transition	3th transition	4th transition
E (J/g)	3.3 ± 1.3	2.9 ± 1.3	3.8 ± 1.9	1.3 ± 0.5
T_0 (°C)	17 ± 2	4.6 ± 1.7	5 ± 3	27 ± 6
T_P (°C)	12.6 ± 1.6	0.9 ± 1.8	13.68 ± 0.96	35.0 ± 1.9
T_f (°C)	5 ± 2	4 ± 3	27 ± 5	39.9 ± 1.4

Table 2. Energy (J/g) and temperatures (°C) values of the fatty acids transitions of the normal samples. Where: T_0 corresponds to the initial transition temperature, T_p peak transition temperature and T_f the final transition temperature.

	1st transition	2nd transition	3th transition	4th transition
E (J/g)	0.57 ± 0.04	0.24 ± 0.06	-	-
T_0 (°C)	20 ± 2	7.3 ± 0.2	-	-
T_P (°C)	15.1 ± 0.4	1.5 ± 0.6	-	-
T_f (°C)	8.1 ± 1.5	3.5 ± 0.6	-	-

According to Kuttappan *et al.* (2012) [31] and Knothe and Dunn (2009) [32], the majority of fatty acids per groups are PUFA: linoleic acid (18: 2n-6), MUFA: palmitoleic (16:1c) and oleic acids (18:1c), and finally SFA: palmitic acid (16:0). The transition temperatures of these fatty acids correspond to the temperatures 1st, 2nd, 3th and 4th, respectively, from Tables 1 and 2.

Mass fraction of fatty acids of NB and WSB (Table 3) were obtained from the transition energies and the latent heat of fusion of the major fatty acids in each transition [32] according to equation 4:

$$x_{fa} = \frac{E}{\Delta H^f} \tag{4}$$

Being x_{fa} the mass fraction of fatty acids (kg/kg), E the transition energy of specific fatty acids group (J/g) and the ΔH^f the latent heat of fusion of specific fatty acid (J/g).

As can be appreciated in the table, WSB show a much higher total fatty acid content than NB.

Table 3. Mass fractions of fatty acids performed by DSC in normal (NB) and white striping (WSB) samples.

	Chain	ΔH^{f*} (J/g)	NB x_{fa} (kg/kg)	WSB x_{fa} (kg/kg)
SFA Palmitic Acid	16:0	208.2	0	0.0050 ± 0.0013
MUFA Oleic acid Palmitoleic acid	18:1 c9 16:1c	75.5 189.6	0 0.0013 ± 0.0003	0.059 ± 0.019 0.013± 0.005
PUFA Linoleic acid	18:2 n-6	139	0.0041 ± 0.0003	0.0235 ± 0.0091
TOTAL Fatty Acids			0.005367 ± 0.000007	0.101 ± 0.013

*Datta obtained from [33,34].

The fatty acid profile also differs between NB and WSB. WSB show approximately 5% SFA, 23% PUFA and a 72% MUFA (expressed in relation to total fatty acids); while samples NB showed 76% PUFA, 24% MUFA and no presence of SFA (expressed in relation to total fatty acids). The change in the fatty acid profile of WSB is very important, mainly due to the presence of saturated fatty acids, principally palmitic acid. Numerous studies have shown that the consumption of saturated fat increases blood cholesterol levels, especially the LDL fraction [35-37]. Furthermore, the presence of WS produces, in tissue surface, an increase in total fatty acid content from 0.54% to 10.1%, so the chicken breast can no longer be considered a totally lean meat.

Permittivity was measured with different sensors. A small sensor with two needles with blunt-ended was used at radiofrequency and a coaxial probe was used in the microwave range in order to characterize the dielectric properties of the different parts of breast: muscle and adipose tissues, in NB and WSB, and WS in WSB.

One of the main problems to fit the full spectrum of radiofrequency and microwave is the appearance of three dispersions on a very large frequency range with sigmoidal shape. The Debye model is a physic model that explains the electric behaviors in this specific frequency range. This model uses different parameters to define each relaxation [38], but it is tedious to handle and difficult to fit with statistic tools. Others authors have used different math models trying to approach the Debye model [39,40]. A powerful sigmoidal model used in biological systems is the Gompertz model [41].

The dispersions shown in the dielectric constant spectra, α, β and γ, are similar to the sigmoidal models aforementioned. Therefore, dielectric constant (ε') was modelled adjusting the experimental data using an own adaptation of the modified Gompertz model (equation 5) in order to obtain information on each of the dispersions.

$$l\varepsilon'(\omega) = l\varepsilon'_{\infty} + \sum_{n=1}^{3} \frac{\Delta l'\varepsilon_n}{1 + e^{((l\omega^2 - l\varpi_\tau{}^2)*\alpha_n)}} \qquad (5)$$

Where, $l\varepsilon'$ represents the decimal logarithm of the dielectric constant, $l\varepsilon'_{\infty}$ the logarithm of the dielectric constant at high frequencies, lω represents the decimal logarithm of the angular velocity (obtained from the frequency), $\Delta l\varepsilon'_n$ $(\Delta l\varepsilon'_n = \log \varepsilon'_n - \log \varepsilon'_{n-1})$ the magnitude of the dispersion, $l\omega_t$ the logarithm of the angular velocity at relaxation time for each dispersion n, and α_n are the dispersion slopes.

Figure 5 shows an example of the different dispersions that have been modelled. In the figure the parameters of the Gompertz model are also represented.

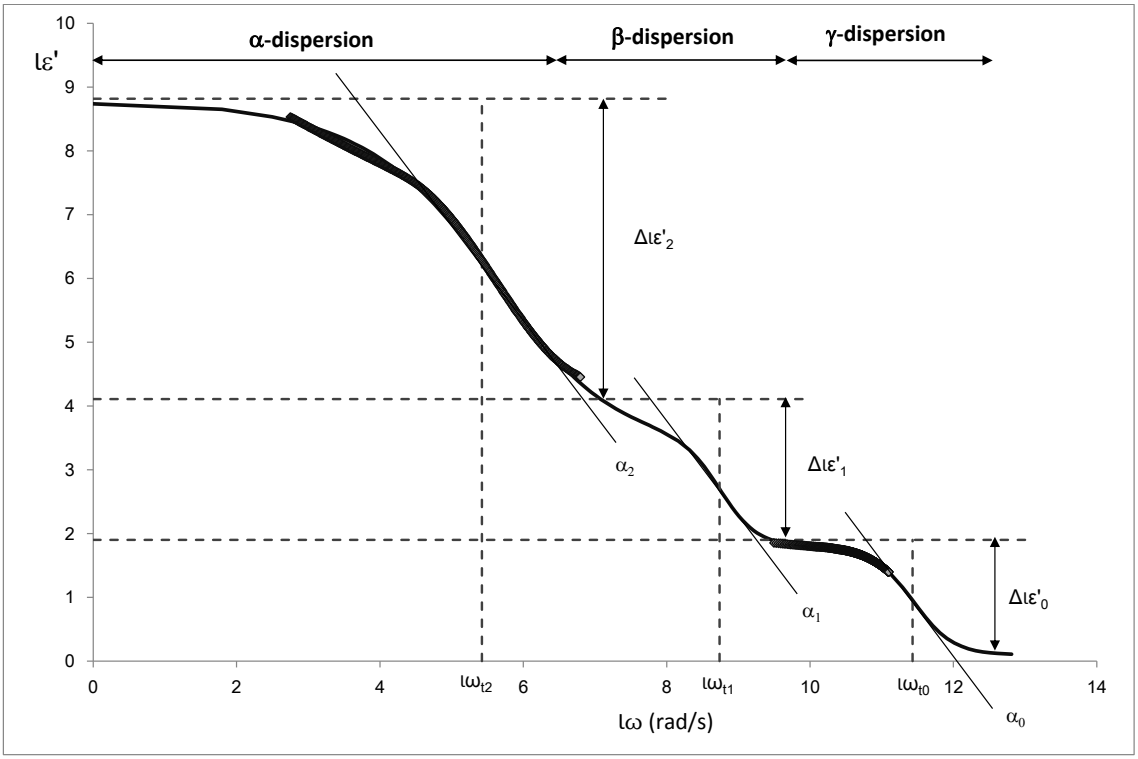

Figure 5. The adapted modified Gompertz model application, where the black line corresponds to the values of the mathematical model and the black diamonds are the measured data of normal breast.

From the Gompertz parameters, it is possible to determine the relaxation frequencies and dielectric constants of each relaxation (equations 6 to 9).

$$\varepsilon'_{\alpha} = 10^{\left(l\varepsilon'_{\infty} + \Delta l\varepsilon'_{\gamma} + \Delta l\varepsilon'_{\beta} + \frac{\Delta l\varepsilon'_{\alpha}}{2}\right)} \quad (6)$$

$$\varepsilon'_{\beta} = 10^{\left(l\varepsilon'_{\infty} + \Delta l\varepsilon'_{\gamma} + \frac{\Delta l\varepsilon'_{\beta}}{2}\right)} \quad (7)$$

$$\varepsilon'_{\gamma} = 10^{\left(l\varepsilon'_{\infty} + \frac{\Delta l\varepsilon'_{\gamma}}{2}\right)} \quad (8)$$

$$f_i = 10^{\frac{l\varpi_{ri}}{2\cdot\pi}} \quad (9)$$

Being i for equation 9 each dispersion (α, β and γ).

Figure 5 shows an example of radiofrequency and microwave spectra for each tissue.

From the Gompertz adjustment and using equations 6 to 9, it was possible to obtain the relaxation dielectric constants and the relaxation frequencies for each dispersion (Table 4 and 5).

Table 4. Relaxation dielectric constant at each dispersion (α, β and γ) of the different tissues of normal breast (NB) and white striping breast (WSB). Data obtained by the two needles with blunt-ended sensor.

	ε'								
	α ($\cdot 10^6$)			β ($\cdot 10^2$)			γ		
muscle tissue WSB	22	±	6^a	25	±	3^a	17.3	±	0.2^a
white stripe WSB	13	±	6^b	11	±	5^b	15.5	±	0.9^b
adipose tissue WSB,NB	6	±	2^c	4	±	1^c	15.0	±	0.9^b
muscle tissue NB	18	±	4^a	21	±	5^a	17.15	±	0.14^a

Different letters (a-c) indicate significant difference between values in each column with $p< 0.05$.

Table 5. Relaxation frequency at each dispersion (α, β and γ) of the different tissues of normal breast (NB) and white striping breast (WSB), obtained by the two needles with blunt-ended sensor.

	f								
	α (kHz)			β (MHz)			γ (GHz)		
muscle tissue WSB	6	±	1^b	8	±	4^b	45	±	3^a
white stripe WSB	7	±	4^b	10	±	1^b	38	±	1^b
adipose tissue WSB,NB	6	±	4^b	110	±	7^a	34	±	2^c
muscle tissue NB	18	±	4^a	13	±	5^b	43	±	1^a

Different letters (a-c) indicate significant difference between values in each column with $p< 0.05$.

As Figure 6 shows, three relaxations per tissue can be appreciated. In α-dispersion, the relaxation dielectric constant of muscles tissues (WSB and NB) shows a significant higher value ($p < 0.05$) than the fatty tissues (WS and adipose). The main mobile charges in muscle tissue are Ca^{2+}, K^{+}, Na^{+} and Mg^{2+}, which have different functions, for example as the second messenger of ATP signaling; these electrolytes are solved in liquid phase, and their mobility is high. However, in fatty tissues, the electrolytes suffer the high attraction of surface tension of fatty globules, thus electrolytes maintain their orientation ability although this ability is reduced. Moreover, the white stripe shows a significant higher value ($p < 0.05$) than the adipose tissue because white stripe has an accumulation of electrolytes in the interface between the partially breakdown muscle tissue and the fat globules deposited in this fissure (Table 4), where the MUFA predominance increases the adsorption of electrolytes. In order to understand the nature and interaction of the electrolytes responsible of α dispersion, the relaxation frequencies were analyzed (Table 5). The fatty tissues show the electrolytes in the same state (spin orientation); nevertheless, in case of muscle tissues, the muscle in WSB shows a similar state of electrolytes as fatty tissues. It could be due to the effect of the partially breakdown muscle of WSB, where the electrolytes nature associated with the interface between fat globules and muscle tissue is different from the electrolytes in liquid phase. This is shown clearly in the very significant difference ($p < 0.001$) of the relaxation frequency (state of electrolytes) between the muscle tissue in NB (muscle fibers without fat interactions) and the muscle in WSB.

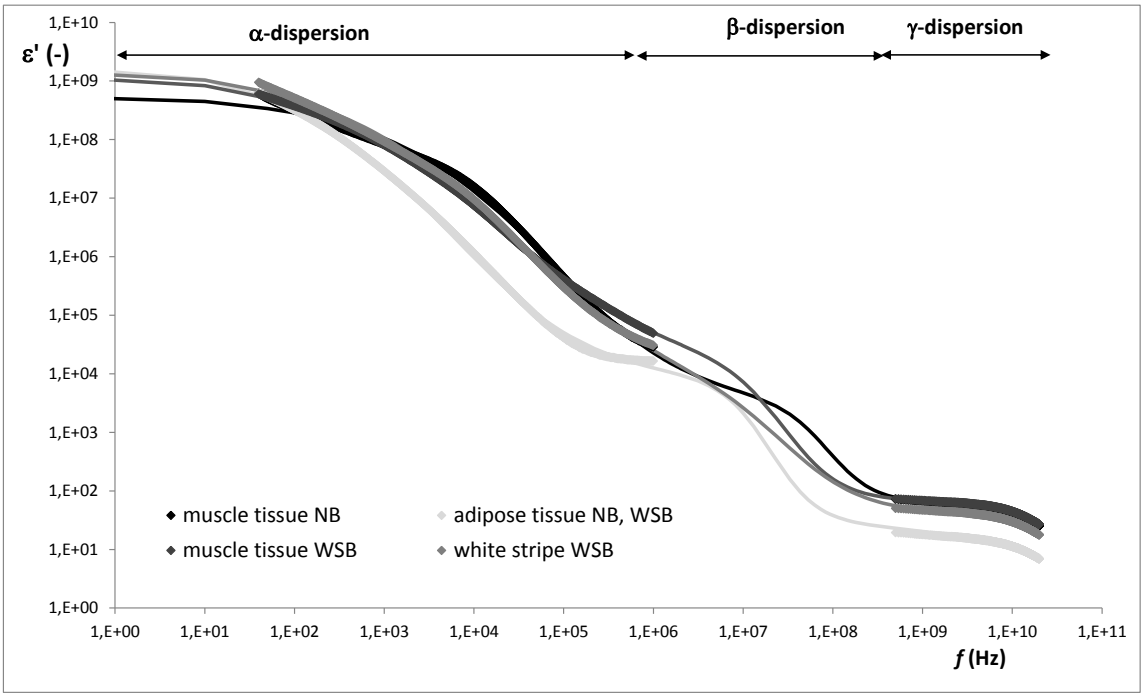

Figure 6. Dielectric constant spectra in radiofrequency and microwave ranges of the different tissues of white striping breast (WSB) and normal breast (NB). Where, the lines correspond to Gompertz model and the diamonds to the experimental data for each tissue.

With regard to β-relaxation, the dielectric constant of muscles tissues (WSB and NB) shows a significant higher value ($p < 0.05$) than the fatty tissues (WS and adipose), being also significant ($p < 0.05$) the difference between WS and adipose tissue.

The β-relaxation phenomena are explained by the by the orientation of fixed charges of the dielectric media. In muscle tissue, the structural proteins have active sites, fixed charges with orientation capacity; moreover, the main of these charges with orientation capacity are the charges involved in the actin-myosin complex [42]. This phenomenon is produced in the low MHz range as Table 5 shows, where muscles tissues have 8 ± 4 and 13 ± 5 MHz, for WSB and NB respectively, without significant differences. Nevertheless, in the high MHz range other phenomenon occurs which is associated to the surface tension, this phenomenon is called Maxwell-Wagner [15,43], and produces less absorption of energy than the effect of the active sites of proteins. In case of adipose tissue, as the relaxation frequency shows (110 ± 7 MHz), the high surface tension of the fat globules is the main contribution to β-relaxation, being the relaxation dielectric constant the lowest. In case of WS, the breakdown of the muscle tissue and the formation of the white stripes by fat globules deposition produce both effects: the breakdown of the structural proteins of muscle tissue produces a partial degradation of myosin-actin complex and new active sites with orientation capacity, and the effect of the orientation of surface charges of fat globules. Comparing the dielectric constant of muscle tissue and adipose tissue (Table 4), it is possible to observe that the orientation capacity of active sites of protein produces more absorption of energy than the capacity of orientation of surface charges of the fat globules. Taking into account that the WS is composed by broken muscle tissue and fat globules, then the β-relaxation of WS should be affected by the stronger effect, which is the orientation of active sites of proteins. This theory is strengthened by observing the β-relaxation frequency in range of the effect of protein charges (10 ± 1 MHz) and an intermediate dielectric constant value between muscles tissues and adipose tissue. The partial denaturalization of myosin-actin complex, the protein breakdown and the reduction of the electric field space occupied by proteins (Figure 3) produces a reduction of the absorption energy capacity in the WS with regard to the muscles tissues, as Table 4 shows.

Finally, regarding the γ-dispersion, the dielectric constant of the muscle tissues is higher than that of the adipose tissues (Table 4). Orientation of the dipolar molecules occurs at these frequencies, the main dipolar molecule in animal tissue is water; the adipose tissue shows less interaction with water molecules than muscle tissue due to its hydrophobic character. Water molecules in adipose tissue interact with adsorbed electrolytes of the fat, while in muscle tissue the water can be in liquid phase and also adsorbed to the tissue. Therefore, the relaxation frequency is larger in muscle tissue with regard to the fat tissue since water has a higher mobility in liquid phase than adsorbed in the solid matrix (Table 5).

The permittivity of NB and WSB samples were also measured using a sensor with two flat circular plates. This kind of sensor with a raised surface was used in order to increase the penetration and to measure the permittivity at radiofrequency through the chicken skin.

Table 6 shows the average values of the dielectric constant of α and β dispersions after adjusting the data with the adapted modified Gompertz model (equation 5). The ANOVA performed on the WS samples compared to the normal samples reveals that the differences in the dielectric constant are significant (p <0.05). As was explained in the analysis of the different tissues, in α and β dispersion, the muscle tissue produces the major effect in the dielectric constant. The measurements made in the whole breast (including the skin) follows the same behaviors, where the NB (Table 6) behaves as the muscle of the NB (Table 4) and the WSB (Table 6) behaves as a mixture between muscle of the WSB and WS (Table 4). Therefore, using sensors in the radio frequency range, it is possible to segregate chickens with white striping physiopathy before dismembering, carrying out the measurements on whole chickens.

Table 6. Values of dielectric constant in α and β dispersions of White Striping Breast (WSB) and Normal Breast (NB), obtained by the sensor with two flat plates with circular surfaces.

	ε'	
	α ($\cdot 10^6$)	β ($\cdot 10^2$)
WSB	3.1 ± 0.8^b	21 ± 5^b
NB	4.2 ± 0.3^a	31 ± 3^a

Different letters (a-b) indicate significant difference between values in each line with p< 0.05.

4. Conclusions

It was possible to conclude that white striping physiopathy consists of the partial rupture of the pectoral muscle, possibly associated with the overgrowth process of hypertrophic breeds; the organism solves this rupture of the tissue by depositing fat globules in the break area in order to maintain the functionality of contraction-relaxation of the muscular system. The fat content and the relationship between types of fatty acids vary when white striping occurs. The change in fat content is remarkable, rising from 0.5 to 10.1%, exhibiting a higher content of MUFA and SFA fatty acids; thus, WSB cannot be considered to be a healthy food with low saturated fats.

Finally, it was possible to detect white striping physiopathy in chicken carcasses with skin using sensors with flat circular surfaces in radiofrequency spectra.

Acknowledgements

The authors acknowledge the financial support from: the Spanish Ministerio de Economía, Industria y Competitividad, Programa Estatal de I+D+i orientada a los Retos de la Sociedad AGL2016-80643-R, Agencia Estatal de Investigación (AEI) and Fondo Europeo de Desarrollo Regional (FEDER). The author Maria Victoria Traffano Schiffo wants to thank the FPI Predoctoral Program of the Universidad Politécnica de Valencia for its support. The authors would like to thank the Electronic Microscopy Service of the Universidad Politécnica de Valencia for its assistance in the use of Cryo-SEM.

Conflicts of Interest

The authors declare no conflict of interest.

References

1. Best, P. *Worldwide poultry meat production, consumption forecasts*. Watt: Rockford, IL, USA. 2011.
2. Havenstein, G. B., Ferket, P. R., & Qureshi, M. A. Growth, livability, and feed conversion of 1957 versus 2001 broilers when fed representative 1957 and 2001 broiler diets. *Poult. Sci.* 2003, 82(10), 1500-1508.
3. Soglia, F., Laghi, L., Canonico, L., Cavani, C., & Petracci, M. Functional property issues in broiler breast meat related to emerging muscle abnormalities. *Food Res. Int.* 2016, 89, 1071-1076.
4. Petracci, M., Mudalal, S., Soglia, F., & Cavani, C. Meat quality in fast-growing broiler chickens. *World Poultry Sci J.* 2015, 71(02), 363-374.
5. Dransfield, E., & Sosnicki, A. A. Relationship between muscle growth and poultry meat quality. *Poult. Sci.* 1999, 78(5), 743-746.
6. Kijowski, J., & Konstańczak, M. Deep pectoral myopathy in broiler chickens. *Bull Vet Inst Pulawy.* 2009, 53, 487-491.
7. Lien, R. J., Bilgili, S. F., Hess, J. B., & Joiner, K. S.. Induction of deep pectoral myopathy in broiler chickens via encouraged wing flapping. *J. Appl Poultry Res.* 2012, 21(3), 556-562.
8. Bailey, R. A., Watson, K. A., Bilgili, S. F., & Avendano, S. The genetic basis of pectoralis major myopathies in modern broiler chicken lines. *Poult. Sci.* 2015, 94, 2870-2879.
9. Russo, E., Drigo, M., Longoni, C., Pezzotti, R., Fasoli, P., & Recordati, C. Evaluation of White Striping prevalence and predisposing factors in broilers at slaughter. *Poult. Sci.* 2015, 94, 1843-1848.
10. Petracci, M., Mudalal, S., Bonfiglio, A., & Cavani, C. Occurrence of white striping under commercial conditions and its impact on breast meat quality in broiler chickens. *Poult. Sci.* 2013, 92(6), 1670-1675.
11. Kuttappan, V. A., Lee, Y. S., Erf, G. F., Meullenet, J. F., McKee, S. R., & Owens, C. M. Consumer acceptance of visual appearance of broiler breast meat with varying degrees of white striping. *Poult. Sci.* 2012, 91(5), 1240-1247.
12. Lorenzi, M., Mudalal, S., Cavani, C., & Petracci, M. Incidence of white striping under commercial conditions in medium and heavy broiler chickens in Italy. *The J. Appl Poultry Res.* 2014, 23(4), 754-758.
13. Petracci, M., Mudalal, S., Babini, E., & Cavani, C. Effect of white striping on chemical composition and nutritional value of chicken breast meat. *Ital. J. Anim. Sci.* 2014, 13, 179-183.

14. Schwan, H. P. Electrical properties of tissues and cell suspensions. *Adv. Biol. Med. Phys.* 1957, 5, 147–209.
15. Kuang, W., & Nelson, S. O. Low-frequency dielectric properties of biological tissues: a review with some new insights. *T. ASAE.* 1998, 41(1), 173-184.
16. Wolf, M., Gulich, R., Lunkenheimer, P., & Loidl, A. Relaxation dynamics of a protein solution investigated by dielectric spectroscopy. *BBA-Proteins Proteom.* 2012, 1824(5), 723-730.
17. Metaxas, A. C., & Meredith, R. J. *Industrial Microwave Heating.* IEE Power Engineering Series 4, Institution of Electrical Engineers. Peter Peregrinus Ltd., London, United Kingdom, 1983.
18. Castro-Giráldez, M., Fito, P. J., Dalla Rosa, M., & Fito, P. Application of microwaves dielectric spectroscopy for controlling osmotic dehydration of kiwifruit (*Actinidia deliciosa cv Hayward). Innov. Food Sci. Emerg Technol.* 2011, 12(4), 623-627.
19. Traffano-Schiffo, M. V., Castro-Giraldez, M., Colom, R. J., & Fito, P. J. Study of the application of dielectric spectroscopy to predict the water activity of meat during drying process. *J. Food Eng.* 2015, 166, 285-290.
20. Talens, C., Castro-Giraldez, M., & Fito, P. J. Study of the effect of microwave power coupled with hot air drying on orange peel by dielectric spectroscopy. *LWT-Food Sci. Technol.* 2016, 66, 622-628.
21. Shang, L., Guo, W., & Nelson, S. O. Apple variety identification based on dielectric spectra and chemometric methods. *Food Anal Method.* 2015, 8(4), 1042-1052.
22. Castro-Giráldez, M., Botella, P., Toldrá, F., & Fito, P. Low-frequency dielectric spectrum to determine pork meat quality. *Innov. Food Sci. Emerg Technol.* 2010, 11(2), 376-386.
23. Trabelsi, S., & Roelvink, J. Investigating the influence of aging on radiofrequency dielectric properties of chicken meat. *J Microwave Power EE.* 2014, 48(4), 215-220.
24. Damez, J. L., Clerjon, S., Abouelkaram, S., & Lepetit, J. Beef meat electrical impedance spectroscopy and anisotropy sensing for non-invasive early assessment of meat ageing. *J. Food Eng. 2008*, 85(1), 116-122.
25. Cuibus, L., Castro-Giráldez, M., Fito, P. J., & Fabbri, A. Application of infrared thermography and dielectric spectroscopy for controlling freezing process of raw potato. *Innov. Food Sci. Emerg Technol.* 2014, 24, 80-87.
26. Traffano-Schiffo, M. V., Castro-Giráldez, M., Fito, P. J., & Balaguer, N. Thermodynamic model of meat drying by infrarred thermography. *J. Food Eng.* 2014, 128, 103-110.
27. Benedito, J., Carcel, J. A., Rossello, C., & Mulet, A. Composition assessment of raw meat mixtures using ultrasonics. *Meat Sci.* 2001, 57(4), 365-370.
28. Zhang, L., & Barbut, S. Rheological characteristics of fresh and frozen PSE, normal and DFD chicken breast meat. *British Poult. Sci.* 2005, 46(6), 687-693.
29. Kuttappan, V. A., Shivaprasad, H. L., Shaw, D. P., Valentine, B. A., Hargis, B. M., Clark, F. D., ... & Owens, C. M. Pathological changes associated with white striping in broiler breast muscles. *Poult. Sci.* 2013, 92(2), 331-338.
30. Mudalal, S., Babini, E., Cavani, C., & Petracci, M. Quantity and functionality of protein fractions in chicken breast fillets affected by white striping. *Poult. Sci.* 2014, 93, 2108-2116.
31. Knothe, G., & Dunn, R. O. A comprehensive evaluation of the melting points of fatty acids and esters determined by differential scanning calorimetry. *J. Am. Oil Chem. Soc.* 2009, 86(9), 843-856.
32. Kuttappan, V. A., Brewer, V. B., Apple, J. K., Waldroup, P. W., & Owens, C. M. Influence of growth rate on the occurrence of white striping in broiler breast fillets. *Poult. Sci.* 2012, 91(10), 2677-2685.
33. Uehara, H., Suganuma, T., Negishi, S., Uda, Y., Furukawa, Y., Ueno, S., & Sato, K. Physical properties of two isomers of conjugated linoleic acid. *J. Am. Oil Chem. Soc.* 2008, 85(1), 29-36.
34. Cedeño, F. O., Prieto, M. M., Espina, A., & García, J. R. Measurements of temperature and melting heat of some pure fatty acids and their binary and ternary mixtures by differential scanning calorimetry. *Thermochim Acta.* 2001, 369(1), 39-50.

35. Lichtenstein, A. H., Ausman, L. M., Jalbert, S. M., & Schaefer, E. J. Effects of different forms of dietary hydrogenated fats on serum lipoprotein cholesterol levels. *N Engl J Med.* 1999, 340(25), 1933-1940.

36. Mauger, J. F., Lichtenstein, A. H., Ausman, L. M., Jalbert, S. M., Jauhiainen, M., Ehnholm, C., & Lamarche, B. Effect of different forms of dietary hydrogenated fats on LDL particle size. *Am. J. Clin. Nutr.* 2003, 78(3), 370-375.

37. Socarrás Suárez, M. M. & Bolet Astoviza, M. Alimentación saludable y nutrición en las enfermedades cardiovasculares. *Revista Cubana de Investigaciones Biomédicas.* 2010, 29(3), 353-363.

38. Kuang, W., & Nelson, S. O. Low-frequency dielectric dispersion from ion permeability of membranes. *J Colloid Interface Sci.* 1997, 193(2), 242-249.

39. Hurt, W. D. Multiterm Debye dispersion relations for permittivity of muscle. *IEEE T Bio-Med. Eng.* 1985, 32, 60-64.

40. Gabriel, S., Lau, R. W., & Gabriel, C. The dielectric properties of biological tissues: III. Parametric models for the dielectric spectrum of tissues. *Phys. Med. Biol.* 1996, 41(11), 2271.

41. El-Gohary, A., Alshamrani, A., & Al-Otaibi, A. N. The generalized Gompertz distribution. *Appl Math Model.* 2013, 37(1), 13-24.

42. Rayment, I., Holden, H. M., Whittaker, M., Yohn, C. B., Lorenz, M., Holmes, K. C., & Milligan, R. A. Structure of the actin-myosin complex and its implications for muscle contraction. *Science.* 1993, 261, 58-65.

43. Traffano-Schiffo, M. V., N. Balaguer, M. Castro-Giráldez, & Fito, P. J. Emerging technologies in juice processing. In A. Ibartz, V. Falguera, (Eds.), *Juice processing: Quality, safety and value-added opportunities.* CRC Press Taylor & Francis Group: Boca Raton, FL., USA. 2014, pp. 197-212.

4.6. Caracterización dieléctrica de los tejidos de la mandarina.

Traffano-Schiffo, M. V., Castro-Giraldez, M., Colom, R., & Fito, P. J. (2017). New spectrophotometric system to segregate tissues in mandarin fruit. ***Food and Bioprocess Technology.*** Artículo enviado.

NEW SPECTROPHOTOMETRIC SYSTEM TO SEGREGATE TISSUES IN MANDARIN FRUIT

Maria Victoria Traffano-Schiffo[a], Marta Castro-Giraldez[a*], Ricardo J. Colom[b], Pedro J. Fito[a]

[a] Instituto Universitario de Ingeniería de Alimentos para el Desarrollo, Universidad Politécnica de Valencia, Camino de Vera s/n, 46022 Valencia, España.
[b] Instituto de Instrumentación para Imagen Molecular, Universitat Politecnica de Valencia, Camino de Vera s/n, 46022 Valencia, Spain.

*author for correspondence: marcasgi@upv.es

ABSTRACT

The knowledge of the electrical properties of the fruits tissues and their relation with the structural and compositional properties opens an endless number of opportunities in the development and design of industrial equipment. Therefore, a deep study of the dielectric properties of mandarin tissues, coupled with a_w, X_w, pH, maturity index, Cryo-SEM and optical measurements were performed. Dielectric properties were studied in radiofrequency and microwave ranges. α, β and γ-dispersions and its relaxation parameters were obtained. Also, a tool based on the relaxation dielectric constant in γ-dispersion able to determine the moisture content of the samples, has been developed.

Keywords: mandarin, spectrophotometry, radiofrequency, microwave, dispersions, microstructure.

INTRODUCTION

During the last decade, there has been a continuous increase in the consumption and demand of citrus fruits in the international market, being the mandarin fruit the one that shows the greater growth.[1] The consumption habits promoted by a healthy diet and the nutritional qualities are some of the elements that explain this behaviour.[2]

Histologically, mandarin fruit, as all citrus fruits, consists in three parts: peel, pulp and seeds. The outer part of the peel is made up of an epidermis commonly called exocarp or flavedo and the inner part is the mesocarp or albedo. The albedo consists in vascular bundles, which are distributed along the pulp.[1] The endocarp is the innermost part of the fruit and it is composed by carpels or locules (pulp) covered by slightly thick layer of vascular bundles,[3] which have a large number of juice vesicles. It is important to highlight that each tissue has different functionality, structure and composition.

Regarding to the composition, mandarin tissues show big differences in the content of ions, essential oils, sugars, fiber content and principally, water. It should be taking into account that each of the components aforementioned show different electric properties, which provide valuable information such as physical, chemical and compositional. Due to this, a spectrophotometric analysis able to describe the electric behavior of each tissue represents a first step in the development and design of industrial equipment with different applications.

Permittivity (ε) is the physical property which describes the interaction between the materials such as foodstuffs and a photon flux.[4] Expressed as a complex number, the real part of the ε is called dielectric constant (ε') and it is related to the material´s ability to store energy, and the imaginary part, called dielectric loss factor (ε'') represents the energy fraction which is absorbed or dissipated.[5] Along the electric spectrum between radiofrequency (RF) and microwaves (MW), three main dispersions can be observed: α and β dispersion in radiofrequency range and γ in microwave range.[6]

α-dispersion (from a few Hz to a few kHz) is induced by the orientation of mobile charges in a dielectric medium.[7] β-dispersion (from kHz to tens of MHz) is related to the orientation of fixed charges in macromolecules such as proteins and carbohydrates, and it could explain complex conformations of these molecules. At higher frequencies of β-dispersion the main effect is the surface tension; this phenomenon is called Maxwell-Wagner effect.[7,8] In MW range, the interaction of the electric field with biological tissue produces the γ-dispersion. It is observed at GHz frequencies and it is due to the dipolar molecules (mainly water) orientation and induction.[9,10] Other important effect in microwave range is ionic conductivity at frequencies from Hz to MHz.[11] The application of a photon flux to biological tissue causes vibration of ions increasing the internal energy of the molecules, therefore, the ionic conductivity only affects to the loss factor.[12,13]

The aim of this research is to determine the electric properties of mandarin fruit tissues in order to characterize them. This study represents a first step in the development of a method for detecting seeds inside mandarin fruit with a non-destructive method.

MATERIAL AND METHODS

Raw material

Fresh mandarins (*Citrus clementina*) obtained from a plantation located in Algimia de Alfara, Valencia, Spain were used in this experiment. Mandarins were selected according to its homogeneity in size and color and stored at 8 ºC until sampled.

Experimental Procedure

20 samples were used for the experiments. Fruits were tempered at 25 ºC and the tissues (pulp, peel and seeds) were separated and maintained in aqualab® disposable sample cups, sealed with parafilm® in order to avoid water losses. The tegument of the seeds was removed in order to avoid

measurement errors due to adsorbed water to the tegument that comes from the pulp. After that, physicochemical, structural and permittivity determinations were performed. Permittivity was measured in RF range by using two sensors which consist on two plates electrodes (developed by the authors). In MW range a coaxial probe (Agilent) was used.

Physicochemical determinations

The pH of the pulp was measured by using a punch pH-meter S-20 SevenEasy™ (Mettler Toledo, Barcelona, Spain). A dew point Hygrometer Decagon (Aqualab®, series 3 TE) with a precision of ± 0.003 was used to determine the water activity (a_w) of each mandarin tissue. Moisture of each tissue was determined by drying in a vacuum oven at 60 ºC until constant weight was reached.[14] Soluble solids content of the pulp liquid phase was determined by measuring the refractometric index (ºBrix) with a refractometer (ABBE, ATAGO Model 3-T, Japan) calibrated with distilled water at 25 ºC. Titratable acidity, expressed a citric acid in 100 mL of juice, was analyzed following AOAC Method 934.06[14] titrating an aliquot of juice with 0.1 N NaOH.
Analytical determinations described above were obtained by triplicate.
Finally, maturity index (MI) was calculated by dividing the soluble solids content of the extractable juice by its acid content.[15]

Structural analysis

Low-temperature scanning electron microscopy (Cryo-SEM).

The microstructure of each fruit tissue was analyzed by Cryo-SEM. A Cryostage CT-1500C unit (Oxford Instruments, Witney, UK), coupled to a Jeol JSM-5410 scanning electron microscope (Jeol, Tokyo, Japan), was used. The sample was immersed in slush N_2 (-210 ºC) and then quickly transferred to the Cryostage at 1 kPa where sample fracture took place. The sublimation (etching) was carried out at –95 ºC. The final point was determined by direct observation in the microscope, working at 5 kV. Then, once again in the Cryostage unit, the sample was coated with gold in vacuum (0.2 kPa), applied for 3 min, with an ionization current of 2 mA. The observation in the scanning electron microscope was carried out at 20 kV, at a working distance of 15 mm and a temperature ≤ -130 ºC.

Optical measurements

Optical measurements of each fruit tissue were made by a binocular loupe Leica MZ APO™ (Leica Microsystems, Wetzlar, Germany) with low magnification (8x to 80x) using incident light illumination (light reflected off the surface of the sample). It uses two separate optical paths with two objectives and two eyepieces to provide slightly different viewing angles to the left and right eyes. In this way it allows a three-dimensional visualization of the sample.

Permittivity Measurements

Radiofrequency range

Two different non-destructive sensors developed by The Institute of Food Engineering for Development (IuIAD) and The Institute for Molecular Imaging Technologies (I3M), both at the Polytechnic University of Valencia (Spain) were used to measure the permittivity in radiofrequency range. Sensors consist of two flat plates electrodes with different dimensions of the plates (Figure 1a), which were connected to an impedance analyzer Agilent 4294A (Agilent, Santa Clara, CA, USA). The measured frequency range was from 40 Hz to 1 MHz. Calibration of the equipment was performed in open (air) and short-circuit.
The signal obtained by the Agilent analyzer is the impedance Z, which was transformed to permittivity as was described by Traffano-Schiffo et al.[7]

Microwave range

Permittivity in microwave range was measured from 500 MHz to 20 GHz with an Agilent 85070E open-ended coaxial probe (Agilent, Santa Clara, CA, USA) (Figure 1b) connected to an Agilent E8362B Vector Network Analyzer (Agilent, Santa Clara, CA, USA). The system was calibrated using three different types of loads: open (air), short-circuit and 25 ºC Milli®-Q water. Once the calibration was carried out, 25 ºC Milli®-Q water was measured again to check calibration suitability.
Permittivity measurements were performed in triplicate.

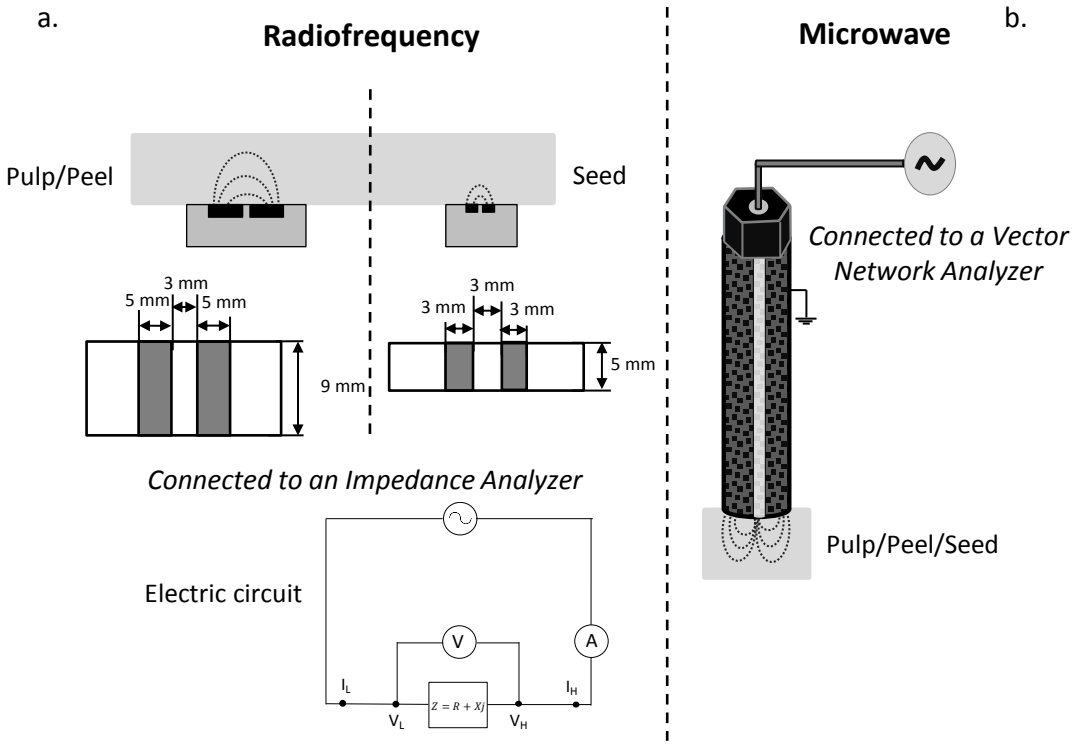

Figure 1. Schematic representation of the sensors used at different frequency ranges. a. radiofrequency and b. microwave.

Statistical analysis

The statistical analysis was carried out with the Statgraphics Centurion XVI Software (Statgraphics, Warrenton, VA, USA). One-Way ANOVA analyses were made in order to find statistically significant differences between the parameters studied for the different samples. The logistic model developed by Traffano-Schiffo and co-workers was fitted by using nonlinear regression.[7]

RESULTS AND DISCUSSION

The macro and microstructural analysis of mandarin fruit can be observed in Figure 2, where big differences among the different types of tissues can be appreciated. Firstly, the peel is composed by the flavedo, which is the outer part of the peel and the albedo, the inner part. The flavedo is constituted by the epidermis which is covered by a cuticle, while inward parenchymatic cells can be appreciated. The parenchymatic cells are isodiametric and have spherical or oval shapes with very compacted structure, where practically does not exist intercellular spaces and thus the liquid phase inside is very low. These cells are found below the epidermis and surrounding oil glands cavities (trichomes). Furthermore, the importance of flavedo is that they contain the stomas, which are cellular complex responsible for the gas exchange between the interior and exterior of the fruit. Therefore, the flavedo shows various functions, first the outer part or cuticle reduces the water exchange with the outside maintaining high internal water activity, and on the other hand, the stomas (indicated by an arrow) are surrounded by two cells defined as guard or occlusive cells, which regulate the opening of the stoma by integrating different signals (endogenous or exogenous). Proper stoma regulation provides an efficient use of water and optimum CO_2 exchange rate.

The albedo is the inner and white part of the peel and it consists in meristematic cells, with irregular shape and size and with large air gaps. The cells have tubular geometry, which are interconnected with large intercellular spaces. Macroscopically, tubular geometry can be correlated with a spongy structure, free of turgidity and compartmentalization. With regard to the pulp, it is composed by lengthened cells called vesicles, where most of its space is occupied by vacuoles, which contain the majority of the liquid phase of the system (juice reservoir) and where the sugars and the organic acids, such as citric acid produced during the ripening, are stored. Finally, seed cells show a very tightly packed structure with very low liquid phase.

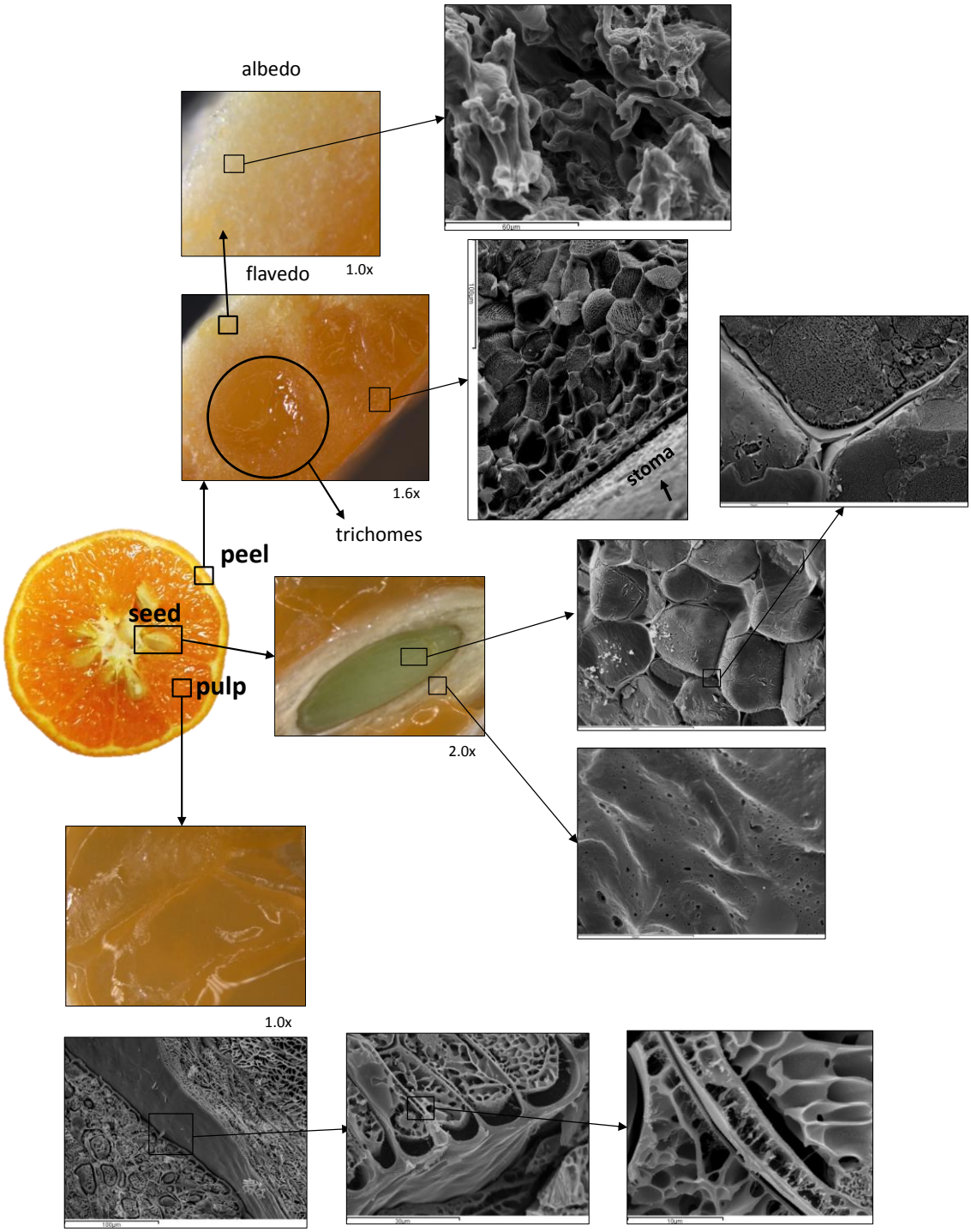

Figure 2. Overview of the macro and microstructure of mandarin.

It should be taking into account that the physicochemical parameters greatly affect the electrical properties, so, in Table 1 these parameters, segregated according to the MI of the fruits, can be observed. Both the moisture and the water activity show significant differences ($p< 0.05$) between the tissues.

Table 1. Physicochemical parameters of each mandarin tissue according to its maturity index.

MI	Tissue	pH	X_w (kg_w/kg_{dm})	a_w
10-15	Pulp	3.9 ± 0.3	5.490 ± 0.003^c	0.981 ± 0.003^c
	Peel		2.157 ± 0.008^b	0.976 ± 0.008^b
	Seed		0.722 ± 0.005^a	0.958 ± 0.005^a
15-20	Pulp	3.9 ± 0.2	4.8 ± 0.5^c	0.980 ± 0.005^c
	Peel		1.8 ± 0.4^b	0.9659 ± 0.0098^b
	Seed		0.7 ± 0.2^a	0.955 ± 0.005^a
20-25	Pulp	3.5 ± 1.4	5.1 ± 0.6^c	0.981 ± 0.003^c
	Peel		1.9 ± 0.4^b	0.967 ± 0.006^b
	Seed		0.67 ± 0.19^a	0.9526 ± 0.0096^a

Different letters (a-c) indicate significant difference among values of each tissue according to each MI with $p< 0.05$.

The dielectric properties of a biological tissue result from the interaction between its constituents at cellular and molecular level and the photon flux.[16] Permittivity was measured in RF and MW ranges, however, one of the main problems to fit the full spectrum is the appearance of three dispersions (α, β and γ) on a very large frequency range with sigmoidal shape. Traffano-Schiffo et al. developed a modified Gompertz model to describe the dielectric constant spectra.[7] This model allows determining the dielectric constants and the relaxation frequencies of each dispersion (Tables 2 and 3, respectively). Relaxation parameters are important because they allow us to characterize the dielectric behavior of biological tissues.[8] Figure 3 shows the average data obtained for the three characteristics dispersions of the different types of mandarin tissues.

As Figure 3 and Table 2 show, the dielectric constant of the pulp is higher than those of the peel and the seed along the spectrum. Particularly, in α-dispersion the dielectric constant of relaxation of the pulp shows a significant higher value ($p< 0.05$) than the other tissues due to the fact that the pulp is rich in electrolytes such as Ca^{2+}, Mg^{2+}, K^+, Na^+, Fe^{3+}, Cu^{2+}, Mn^{2+} and Zn^{2+} [17] (with high mobility) and highly electronegative organic acids (citric and ascorbic acids);[18-20] all solved in liquid phase, which increase the dielectric constant of relaxation. In contrast, in both peel and seeds, the ion content with mobility is low, thus the signal decreases considerably and not significant differences between both samples can be appreciated (Table 2). However, the relaxation frequency in this spectrum range (Table 3) show significant differences among all the tissues ($p< 0.05$), which means that the use of the relaxation frequency in α-dispersion could represent a useful tool of tissue differentiation.

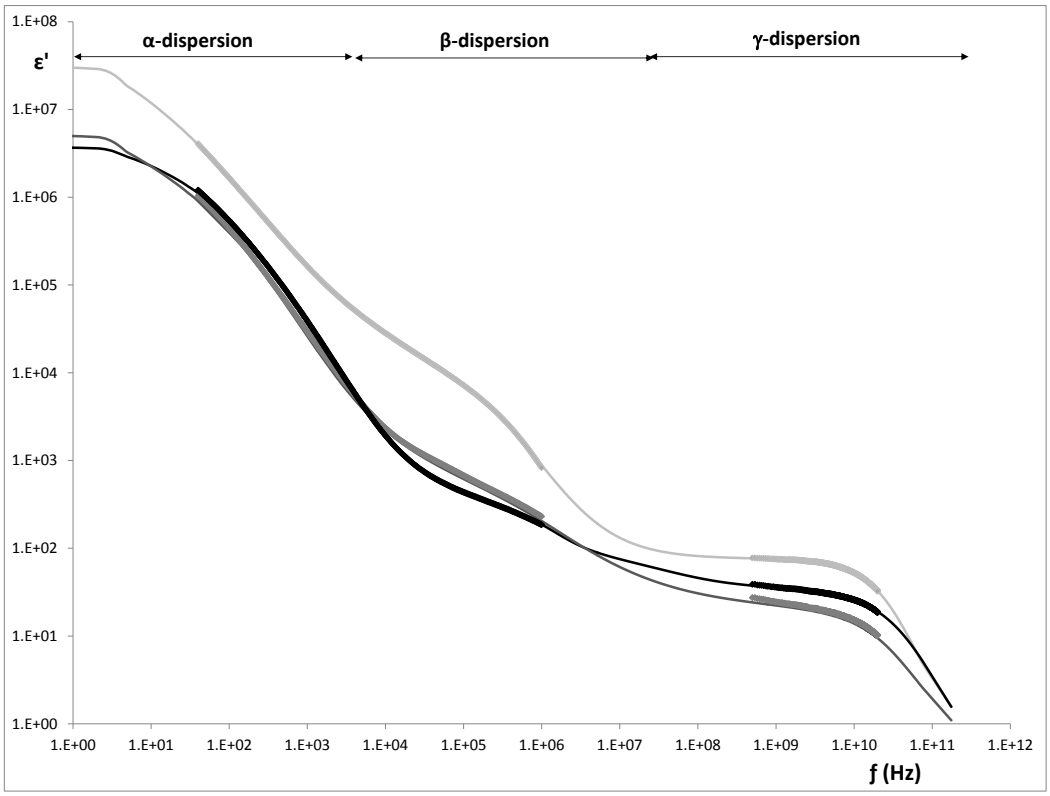

Figure 3. Gompertz model adjusted to the three different mandarin tissues. Where: the lines correspond to the values of the mathematical model and the points to the average of the experimental data. (—) corresponds to the pulp, (—) the peel and (—) the seed.

Table 2. Relaxation dielectric constant at each specific dispersion (α, β and γ).

		ε'								
MI	Tissue	α ($\cdot 10^4$)			β ($\cdot 10^2$)			γ		
10-15	Pulp	345	±	50^a	11	±	2^a	34.6	±	0.92^a
	Peel	5	±	0.4^b	1.8	±	0.15^b	16	±	4^b
	Seed	18	±	6^b	3	±	1^b	11	±	3^c
15-20	Pulp	304	±	56^a	13	±	4^a	34.2	±	0.8^a
	Peel	17	±	13^b	2.1	±	0.5^b	15	±	4^b
	Seed	20	±	8^b	2	±	1^b	10	±	3^c
20-25	Pulp	356	±	158^a	12	±	3^a	34	±	1^a
	Peel	6	±	2^b	1.6	±	0.3^b	15	±	2^b
	Seed	13	±	10^b	2	±	1^b	10	±	3^c

Different letters (a-c) indicate difference among values of each tissue according to each MI with $p< 0.05$.

With regard to β-dispersion, there are not significant differences ($p< 0.05$) between seeds and peel in terms of the dielectric constant of relaxation (Table 2). β-dispersion can be understood by the orientation of the fixed charges of proteins or carbohydrates which have active sites and orientation capacity. The seeds are composed by proteins (in low proportions) and the peel presents high carbohydrates content, however it seems that they do not present orientation capacity, thus the signal in both cases is low. In addition, the only samples that show significant differences ($p< 0.05$) in β-relaxation frequency are peel and pulp (Table 3).

Table 3. Relaxation frequency at each specific dispersion (α, β and γ).

		f								
MI	Tissue	α (kHz)			β (MHz)			γ (GHz)		
10-15	Pulp	0.4	±	0.3^{c}	0.9	±	0.1^{b}	20	±	3^{a}
	Peel	6.2	±	0.7^{a}	2.2	±	0.5^{a}	22	±	4^{a}
	Seed	3	±	1^{b}	1.2	±	0.4^{ab}	18	±	4^{a}
15-20	Pulp	0.4	±	0.2^{c}	0.597	±	0.093^{b}	18	±	3^{a}
	Peel	5	±	2^{a}	2	±	0.7^{a}	24	±	4^{a}
	Seed	4	±	2^{b}	1.90	±	0.5^{ab}	19	±	2^{a}
20-25	Pulp	0.5	±	0.3^{c}	0.63	±	0.11^{b}	18	±	2^{a}
	Peel	8	±	1^{a}	2	±	0.3^{a}	25	±	5^{a}
	Seed	4.2	±	0.9^{b}	2	±	0.2^{ab}	19	±	2^{a}

Different letters (a-c) indicate significant difference among values of each tissue according to each MI with $p< 0.05$.

Finally, in the spectrum range of the γ-dispersion, significant differences ($p< 0.05$) in the dielectric relaxation constant between the three types of tissues can be observed (Table 2). As was explained in the introduction, γ-dispersion is related with the orientation and induction of dipolar molecules (water) and as Table 1 shows there are significant differences in moisture and water activity for all samples ($p< 0.05$), being the pulp which presents the highest values and the seed, the lowest. In addition, also the micrographies (Figure 2) show differences in water content among tissues. Thus, microwave range can be considered as the optimum range to differentiate mandarin tissues and therefore, a deep analysis is needed.

Taking into account the imaginary part of the permittivity, the dielectric loss factors of the different mandarin tissues are shown in Figure 4. At low frequencies of the microwave range, the effect of the ionic conductivity can be appreciated. Ionic conductivity produces vibration of charged molecules; therefore, it only produces electrical energy losses.[5,21] It should be noted that the pulp presents the highest ionic effect due to the high ions concentration [17] which generate vibrations when the tissue is subjected to an external electric field.[11]

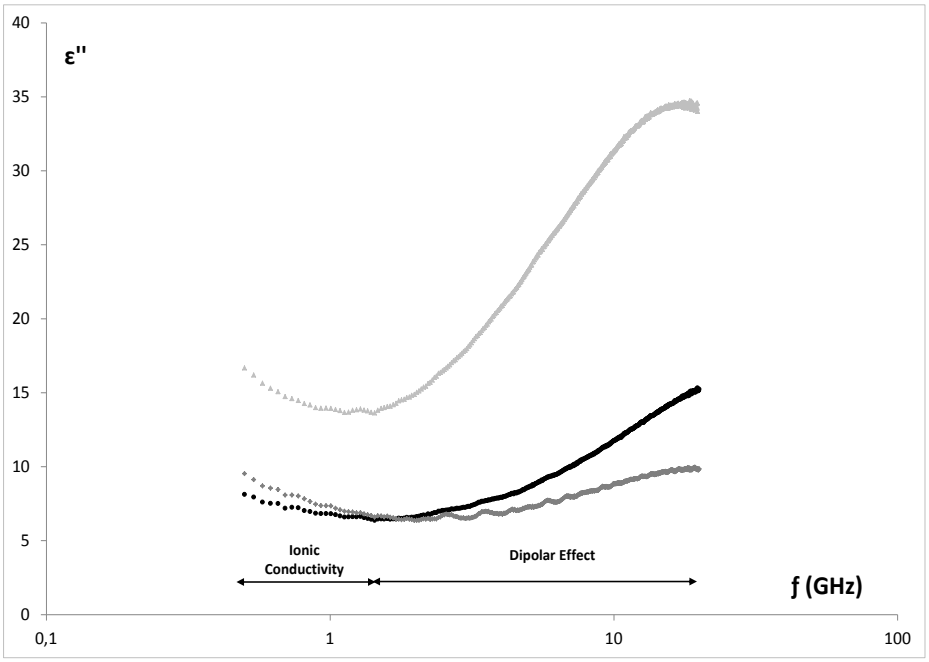

Figure 4. Dielectric loss factor in MW ranges. Where: (♦) corresponds to the pulp, (♦) the peel and (♦) the seed.

Figure 5 shows the relations between the logarithm of the moisture in dry basis and the dielectric constant in γ-relaxation, where it is possible to observe a linear relation between both parameters (R^2 = 0.948). Therefore, the relaxation dielectric constant in γ-dispersion is a useful tool to predict the moisture in dry basis by using dielectric spectroscopy.

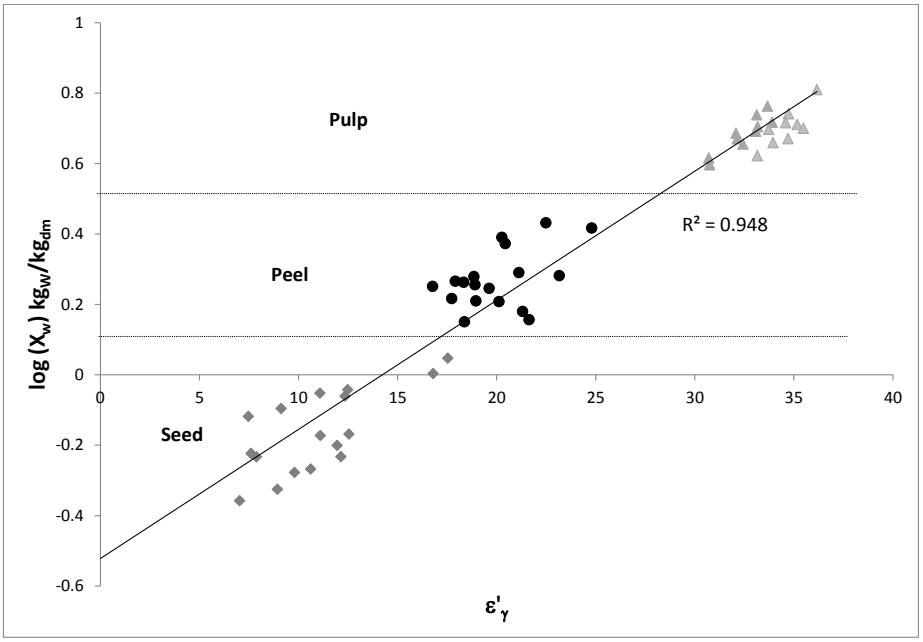

Figure 5. Evolution of the relaxation dielectric constant in γ-dispersion with regard to the moisture for the different tissues. Where: (▲) corresponds to the pulp, (●) the peel and (♦) the seed.

CONCLUSIONS

It was possible to study deeply all mandarin tissues at macroscopic and microscopic level, to understand and to relate the structure with physicochemical and electric properties. The relaxations parameters (dielectric constant and frequency) of each tissue in α, β and γ-dispersions were obtained. Finally, a tool based on the relaxation dielectric constant in γ-dispersion, able to determine the moisture of the samples in dry basis, has been developed.

ACKNOWLEDGEMENTS

The authors acknowledge the financial support from: the Spanish Ministerio de Economía, Industria y Competitividad, Programa Estatal de I+D+i orientada a los Retos de la Sociedad AGL2016-80643-R, Agencia Estatal de Investigación (AEI) and Fondo Europeo de Desarrollo Regional (FEDER). Maria Victoria Traffano Schiffo wants to thank the FPI Predoctoral Program of the Universidad Politécnica de Valencia for its support. The authors would like to thank the Electronic Microscopy Service of the Universidad Politécnica de Valencia for its assistance in the use of Cryo-SEM and also Multiscan Technologies S.L. for their support.

Conflict of Interest

The authors report there are no conflicts of interest.

REFERENCES

1. Liu, Y., Heying, E., & Tanumihardjo, S. A. "History, global distribution, and nutritional importance of citrus fruits". Compr. Rev. Food Sci. F. 2012. 11, 530-545.
2. Mateus-Cagua, D., & Orduz-Rodríguez, J. O. "Mandarina Dancy: una nueva alternativa para la citricultura del piedemonte llanero de Colombia". Corpoica Ciencia y Tecnología Agropecuaria. 2015. 16, 105-112.
3. Goldschmidt, E. E. "Regulatory aspects of chloro-chromoplast interconversions in senescing Citrus fruit peel". Israel J. Bot. 1988. 37, 123-130.
4. M. V. Traffano-Schiffo; N. Balaguer; M. Castro-Giráldez; P. J. Fito-Suñer. "Emerging technologies in juice processing". In A. Ibartz, V. Falguera, editors. Juice processing: Quality, safety and value-added opportunities. CRC Press USA: Taylor & Francis Group, 2014. Pp. 197-212.
5. Talens, C., Castro-Giraldez, M., & Fito, P. J. "Study of the effect of microwave power coupled with hot air drying on orange peel by dielectric spectroscopy". LWT-Food Sci. Technol. 2016. 66, 622-628.
6. Schwan, H. P. "Electrical properties of tissue and cell suspensions". Adv. Biol. and Med. Phys. 1957. 5, 147.
7. Traffano-Schiffo, M. V., Castro-Giraldez, M., Colom, R. J., & Fito, P. J. "Development of a Spectrophotometric System to Detect White Striping Physiopathy in Whole Chicken Carcasses". Sensors. 2017. 17(5), 1024.
8. Traffano-Schiffo, M. V., Castro-Giraldez, M., Colom, R. J., & Fito, P. J. "Innovative spectrophotometric system to determine chicken meat quality". Innov. Food Sci. Emerg. 2017.
9. Castro-Giráldez, M., Fito, P. J., & Fito, P. "Application of microwaves dielectric spectroscopy for controlling long time osmotic dehydration of parenchymatic apple tissue". J. Food Eng. 2011, 104(2), 227-233.

10. Gabriel, S.; Lau, R. W.; Gabriel, C. "The dielectric properties of biological tissues: III. Parametric models for the dielectric spectrum of tissues". Phys. Med. Biol. 1996, 41, 2271.

11. Traffano-Schiffo, M. V., Castro-Giraldez, M., Colom, R. J., & Fito, P. J. "Study of the application of dielectric spectroscopy to predict the water activity of meat during drying process". J. Food Eng. 2015, 166, 285-290.

12. Castro-Giráldez, M., Fito, P. J., Ortolá, M. D., & Balaguer, N. "Study of pomegranate ripening by dielectric spectroscopy". Postharvest Biol. Tec. 2013, 86, 346-353.

13. Castro-Giráldez, M., Fito, P. J., Chenoll, C., & Fito, P. "Development of a dielectric spectroscopy technique for determining key chemical components of apple maturity". J. Agr. Food Chem. 2010, 58, 3761-3766.

14. AOAC. (2000). AOAC, Association of Official Analytical Chemist Official Methods of Analysis. Washington, D.C.

15. Alférez, F., Sala, J. M., Sanchez-Ballesta, M. T., Mulas, M., Lafuente, M. T., & Zacarias, L. "A comparative study of the postharvest performance of an ABA-deficient mutant of oranges: I. Physiological and quality aspects". Postharvest Biol. Tec. 2005, 37(3), 222-231.

16. Kuang, W., & Nelson, S. O. "Low-frequency dielectric properties of biological tissues: a review with some new insights". Trans ASAE (Am Soc Agric Eng). 1998, 41, 173-184.

17. Pérez-López, A. J., López-Nicolás, J. M., & Carbonell-Barrachina, A. A. "Effects of organic farming on minerals contents and aroma composition of Clemenules mandarin juice". Eur. Food Res. Technol. 2007, 225, 255-260.

18. Traffano-Schiffo, M. V., Laghi, L., Castro-Giraldez, M., Tylewicz, U., Rocculi, P., Ragni, L., Dalla Rosa, M. & Fito, P. J. "Osmotic dehydration of organic kiwifruit pre-treated by pulsed electric fields and monitored by NMR". Food Chem. 2017. https://doi.org/10.1016/j.foodchem.2017.02.046

19. Traffano-Schiffo, M. V., Laghi, L., Castro-Giraldez, M., Tylewicz, U., Romani, S., Ragni, L., Dalla Rosa, M. & Fito, P. J. "Osmotic dehydration of organic kiwifruit pre-treated by pulsed electric fields: Internal transport and transformations analyzed by NMR". Innov. Food Sci. Emerg. 2017, 41, 259-266.

20. Traffano-Schiffo, M. V., Tylewicz, U., Castro-Giraldez, M., Fito, P. J., Ragni, L., & Dalla Rosa, M. "Effect of pulsed electric fields pre-treatment on mass transport during the osmotic dehydration of organic kiwifruit". Innov. Food Sci. Emerg. 2016, 38, 243-251.

21. Castro-Giráldez, M., Fito, P. J., & Fito, P. "Application of microwaves dielectric spectroscopy for controlling pork meat (*Longissimus dorsi*) salting process". J. Food Eng. 2010, 97, 484-490.

4.7. Aplicación de Pulsos Eléctricos de Alta Intensidad como pretratamiento de la deshidratación osmótica del kiwi.

Los resultados obtenidos en el presente apartado corresponden a la estancia realizada en la

Università di Bologna, Italia.

Traffano-Schiffo, M. V., Tylewicz, U., Castro-Giraldez, M., Fito, P. J., Ragni, L., & Dalla Rosa, M. (2016). Effect of pulsed electric fields pre-treatment on mass transport during the osmotic dehydration of organic kiwifruit. ***Innovative Food Science & Emerging Technologies***, 38, 243-251.

Traffano-Schiffo, M. V., Laghi, L., Castro-Giraldez, M., Tylewicz, U., Rocculi, P., Ragni, L., Dalla Rosa, M., & Fito, P. J. (2017). Osmotic dehydration of organic kiwifruit pre-treated by pulsed electric fields and monitored by NMR. ***Food Chemistry,*** 236, 87-93.

Traffano-Schiffo, M. V., Laghi, L., Castro-Giraldez, M., Tylewicz, U., Romani, S., Ragni, L., Dalla Rosa, M., & Fito, P. J. (2017). Osmotic dehydration of organic kiwifruit pre-treated by pulsed electric fields: Internal transport and transformations analyzed by NMR. ***Innovative Food Science & Emerging Technologies***, 41, 259-266.

Artículo 7

Traffano-Schiffo, M. V., Tylewicz, U., Castro-Giraldez, M., Fito, P. J., Ragni, L., & Dalla Rosa, M. (2016). Effect of pulsed electric fields pre-treatment on mass transport during the osmotic dehydration of organic kiwifruit. *Innovative Food Science & Emerging Technologies*, 38, 243-251.

EFFECT OF PULSED ELECTRIC FIELDS PRE-TREATMENT ON MASS TRANSPORT DURING THE OSMOTIC DEHYDRATION OF ORGANIC KIWIFRUIT

Traffano-Schiffo, M. V.[a], Tylewicz, U.[b]*, Castro-Giraldez, M.[a], Fito, P. J.[a], Ragni, L.[b,c] and Dalla Rosa, M.[b,c]

[a] Instituto Universitario de Ingeniería de Alimentos para el Desarrollo, Universidad Politécnica de Valencia, Camino de Vera s/n, 46022 Valencia, España.

[b] Department of Agricultural and Food Sciences, University of Bologna, Cesena, Italy.

[c] Interdepartmental Centre for Agri-Food Industrial Research, University of Bologna, Cesena, Italy.

*author for correspondence: urszula.tylewicz@unibo.it

ABSTRACT

Recently, some authors have applied pulsed electric fields (PEF) as a pre-treatment of osmotic dehydration, showing a faster kinetics of dehydration. Osmotic dehydration of fruit tissue shows complex mass transfer mechanism associated with active and passive transports of the vegetal matrix, usually driven by electrolytes. The aim of this work was to analyze the effect of different PEF values (100, 250, 400 V/cm) as a pre-treatment of the osmotic dehydration (61.5 °Brix, up to 120 min) on mass transport mechanism of organic kiwifruit.

A thermodynamic model able to describe the mass transfer and tissue deformation in kiwifruit was developed. It was possible to conclude that pulsed electric field as a pre-treatment, remove a part of the native electrolytes, reducing the activity of protein active pumps, leaving alone the passive protein channels as a main mass transmembrane transport and therefore affecting to the regular functionality of cell homeostasis system.

Keywords: kiwifruit, Pulsed Electric Fields, osmotic dehydration, mass transfer, thermodynamics, phenomenological coefficients.

Industrial relevance

This research develops a thermodynamic model able to describe mass transfer and kiwifruit deformation during OD and using PEF as a pre-treatment. Moreover, a deep analysis of active and passive mechanisms transports affected by PEF was done. The results of this research have demonstrated that PEF used as a pre-treatment of OD accelerated water mass transfer and removes part of the fruit natives electrolytes, affecting the functionality of the cell homeostasis system. Therefore, the present work represents an opportunity in the design of new candying products (less calories and sweetness).

NOTATION

a_j	activity of the chemical specie j (-)
R	ideal gases universal constant (J mol $^{-1}$ K^{-1})
T	temperature (K)
S	entropy (J K^{-1})
P	absolute pressure (Pa)
F	Force (N)
F	Faraday Constant (C mol^{-1})
V	volume (m^3)
l	elongation (m)
L	Phenomenological coefficient (mol^2 J^{-1} s^{-1} m^{-2})
n	number of moles (mol)
M	mass (g)
Mr	molecular weight (g mol^{-1})
x	mass fraction (g g^{-1})
S	surface (m^2)
J	molar flux (mol s^{-1} m^{-2})
t	time (min)
G	Gibbs free energy (J)
e	charge (C)
s	molar partial entropy (J K^{-1} mol^{-1})
z	Valence of each electrolyte (-)

Greek Alphabet

ψ	electric potential (J mol^{-1} C^{-1})
μ	chemical potential (J mol^{-1})
ν	molar partial volume of the specie j (L mol^{-1})

Subscripts

w	water
t	treatment time
0	initial time
s	sucrose
i	principal chemical species
j	any chemical species

Superscripts

s	surface
OD	osmotic dehydration solution
PT	passive transport
AT	active transport

1. Introduction

Osmotic dehydration (OD) is a widely used preservation technique which consists in the reduction of food water activity by immersing a biological tissue in hypertonic solutions (Castro-Giráldez, Fito, Dalla Rosa, & Fito, 2011a). The difference in water chemical potential between the internal liquid phase and external solution promotes the release of water from the food into the osmotic medium with the simultaneous incorporation of the solute into the product (Panarese *et al.*, 2012).

Cellular systems evolve by free energy gradients known as passive transports (Tyerman, Bohnert, Maurel, Steudle, & Smith, 1999); however, occasionally biological systems require that the

chemical species move in the opposite direction to these energy gradients; therefore, biological systems have developed transport mechanisms based on protein channels (Agre, Bonhivers, & Borgnia, 1998), which work with energy consumption as ATP (Ferrari, Sarantopoulos, Carmello-Guerreiro, & Hubinger, 2013). When a biological tissue is subjected to a dehydration process, the cells suffer water losses which produce cell stress. The mechanisms of the tissue to survive to this level of water stress are multifold. While cell is losing water by passive transport, driven by the water chemical potential gradient, multiple mechanisms to preserve the intracellular water content are developed, such as active water pump transport or the vesicles process formation (Tylewicz, Romani, Widell, & Galindo, 2013), maintaining cell homeostasis and protecting the function of the structure (Bohnert & Jensen, 1996).

Kiwifruit has a complex organized cellular structure where the cells are interconnected by plasmodesmatas, which allow them to generate solute and solvent fluxes by symplastic ways. The mass transfer throughout the extracellular space is named apoplastic way. Finally, the transport between intra and extra cellular space is the transmembrane transport where the passive water transport is given by protein channels named aquaporins (Maurel & Chrispeels, 2001). The main active transports pumps are: Ca^{2+}, Na^{+} and Na^{+}/K^{+}, which are the responsible of the transport of water, sucrose and electrolytes, respectively.

It should be taking into account that OD treatment removes the water from materials (fruits and vegetables) only partially (Rastogi, Eshtiaghi, & Knorr, 1999). Therefore, the combined use of OD treatment with other techniques such as Pulsed Electric Fields (PEF) represents a promising tool to improve mass transfer, increasing yields and reducing processing times (Rastogi & Niranjan, 1998).

PEF is a non-thermal promising technology which consists on applying electric fields pulsed through a material placed between two electrodes for very short periods of time (microseconds to milliseconds) (Dellarosa *et al.*, 2016; Parniakov, Lebovka, Bals, & Vorobiev, 2015; Puértolas, Luengo, Álvarez, & Raso, 2012), increasing the osmotic yield (Baier, Bußler, & Knorr, 2015).

Cell membrane is a semipermeable barrier conformed by phospholipid bilayer with native electric field, and is considered as a natural capacitor of the cell (Singh & Heldman, 2001). However, when the system is subjected to an external electric field bigger than the native one, changes in the electric conformation and also reorganization of phospholipidic bilayer are produced. This phenomenon could be cause of the cell membrane breakdown, and it is known as electroporation (Baier *et al.*, 2015), a representative diagram can be seen in Figure 1. Another way of membrane breakdown is the electrocompression; when food is subjected to an external electric field the electric charges (particularly electrolytes, such as Ca^{2+}, Na^{+} or K^{+}) accumulate at both sides of the cell membrane generating a potential difference through it. These charges attract each other, therefore the membrane suffers a compression, and as a consequence its original thickness is reduced. The elastic forces of the membrane oppose to the electric compression, but when the charge accumulation exceed the limit point of elasticity, pores are generated due to the disruption of it (Calderón-Miranda, Fernanda, Martín, Barbosa-Cánovas, & Swanson, 1998).

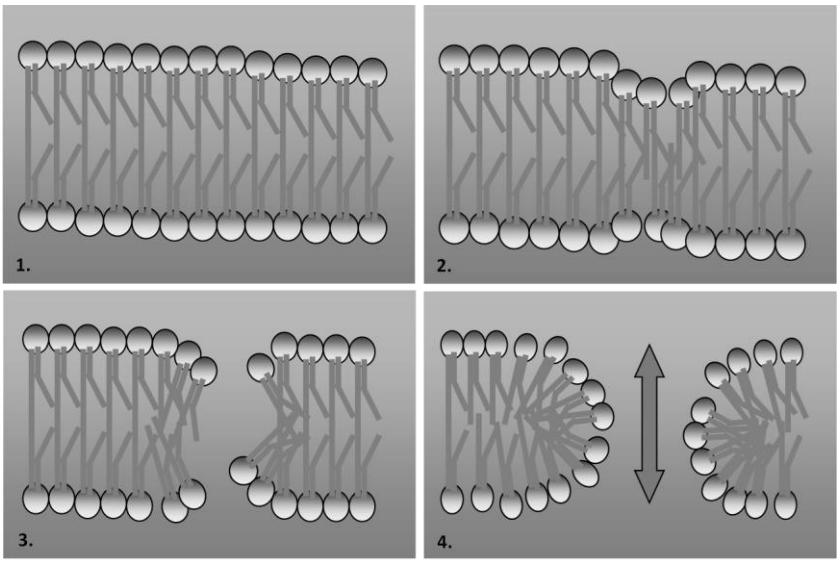

Figure 1. Electroporation phenomenon of the lipid bilayer.

According to the intensity of the applied electric field, the numbers of pulses, and the temperature, the electroporation could be reversible or irreversible (Knorr, Angersbach, Eshtiaghi, Heinz, & Lee, 2001). In order to estimate the critical electric field of membrane breakdown, Zimmermann, Pilwat, Beckers, & Riemann (1976) applied voltage gradients in a simulated cell membrane. They reported values between 5 mV to 1 V at 20 °C and 1.2 V at 4 °C as an electric potential difference to cell membrane breakdown. If the average thickness of the phospholipidic bilayer is 4 nm (Briegel *et al.*, 2009) and it is considered as a parallel plates system, the critical electric field obtained are 12.5 kV/cm to 2.13 MV/cm at 20 °C and 3 MV/cm at 4 °C. However, some effects in chemical transport by using PEF at lower electric fields intensities used as pre-treatment of OD have been reported. Rastogi, Eshtiaghi, & Knorr, (1999) have been able to accelerate the water mass transfer of carrots by applying electric fields between 0.22 to 1.6 kV/cm at 40 °C; Taiwo, Angersbach, Ade-Omowaye, & Knorr, (2001) have increased the water loss with a minimal alteration of apples using an intensity electric field of 1.4 kV/cm at 40 °C. Finally, Tedjo, Taiwo, Eshtiaghi, & Knorr, (2002), have obtained a moisture reduction without altering the taste of mangos by applying 1 to 3 kV/cm at 40 °C.

Moreover, PEF application in food processing maintains the activity of vitamins (Vega-mercado, Gongora-Nieto, Barbosa-Cánovas, & Swanson, 2007) and preserves some physical properties, such as color, texture or fresh taste (Calderón-Miranda, Fernanda, Martín, Barbosa-Cánovas, & Swanson, 1998).

The aim of this work was to analyze the effect of pulsed electric fields as a pre-treatment of the osmotic dehydration of kiwifruit, and determine the transport mechanism affected by the pre-treatment.

2. Material and methods

2.1. Raw material

Organic kiwifruits (*Actinidia deliciosa* cultivar ''*Hayward*'') were bought on a local market located in Cesena (Italia) and stored at 4±1 ºC until their processing. The fruits were tempered at 25 ºC, hand peeled and cut with a manual cork borer from the outer pericarp in order to obtain cylinders with homogeneous size of 8 mm diameter and a length of 10 mm (the core and the inner pericarp were removed). The refractometric indexes of the fruits used for the experiment were 13±1 ºBrix.

2.2. Experimental procedure

The fresh samples were characterized according the following parameters: mass, volume, refractometric index (ºBrix), water activity and moisture by quadruplicate. 12 sample cylinders were used for each treatment (576 samples). They were placed inside the Pulsed electric field (PEF) chamber and subjected to different electric fields strengths. Immediately after, the samples were weighed and introduced to the osmotic dehydration solution. Considering previous results, the OD treatment times were 0, 10, 20, 30, 60 and 120 minutes. Due to the fact that the samples after treatments show concentration profiles, another batch of samples were reposed after the treatments at 4 ºC during 24 hours in decagon containers closed with parafilm® in order avoid the sample dehydration. Finally, mass, volume, ºBrix, water activity and moisture were measured as final determinations for fresh, treated and reposed samples.

2.3. Pulsed electric field (PEF) treatment

Pulsed electric field treatments were applied to the cylinders using a pulse generator equipment based on MOSFET technology and capacitors as energy tanks. The samples (12 cylinders per experiment) were placed in a rectangular treatment chamber equipped with two electrodes (20 x 20 mm^2) with a separation between them of 30 mm and filled with 5 mL of tap water with known conductivity at 25 ºC.

PEF pre-treatments were done by applying three different pulsed electric field (100, 250 and 400 V/cm at 100 Hz) with near-rectangular shape pulses, a train of 60 pulses, a fixed pulse width of 100 ± 2 μs and a repetition time of 10.0 ± 0.1 ms.

2.4. Osmotic dehydration treatment

The OD was carried out by immersing the samples in 61.5 ºBrix sucrose solution prepared with commercial sugar and distilled water at 25 ºC and maintaining a relationship 1:4 (w/w) between the fruit and the OD solution in order to avoid changes in the solution concentration during the treatment time of 0, 10, 20, 30, 60 and 120 min.

2.5. Analytical determinations

Mass was determined by using a Kern balance ABS 320-4N (±0.0001) (KERN & SOHN GmbH, Germany), and a dew point Hygrometer Decagon (Aqualab®, series 3 TE) was used for measuring the water activity, with a precision ±0.003.
Volume was determined by an image analysis using Adobe© Photoshop© CS6 software (Adobe Systems Inc., San Jose, CA, USA) in order to get the diameter and the thickness of the samples.
The analysis of the moisture was accomplished following the AOAC Method 934.06, 2000. Sugar content was determined by measuring the refractometric index with a digital refractometer (KRÜSS Optronic© GmbH, Germany) calibrated with distilled water at 25 ºC. Refractometric index was measured in both kiwifruit samples and agent solution after the treatment.
Analytical determinations described above were obtained by quadruplicate.

3. Results and discussion

During the osmotic treatments, kiwifruit suffers mass variations which involve the total mass, the water mass losses and the sucrose mass gain and they can be calculated using the following equations:

$$\Delta M = \frac{M_t - M_0}{M_0} \quad (1)$$

$$\Delta M_w = \frac{M_t x_{wt} - M_0 x_{w0}}{M_0} \quad (2)$$

$$\Delta M_s = \frac{M_t x_{st} - x_{s0} \cdot M_0}{M_0} \quad (3)$$

Where M represents the mass (g), x the mass fraction (g/g), the subscripts w represents the water, s the sucrose, t the treatment time and 0 the initial value.

Figure 2 shows the water and sucrose mass variation during the osmotic dehydration of the kiwifruit PEF pre-treated at different electric fields (0, 100, 250 and 400 V/cm). In the figure, water mass decreases due to high water losses for all the treatments, however, the water losses for samples that have not been pre-treated are considerably less than the PEF pre-treated samples. In addition, no differences in water losses between the samples pre-treated with 250 V/cm and 400 V/cm can be appreciated. Nevertheless, the sucrose mass gain is ordered in inverse sense of water losses; samples without PEF pre-treatment present the maximum sucrose mass gain.

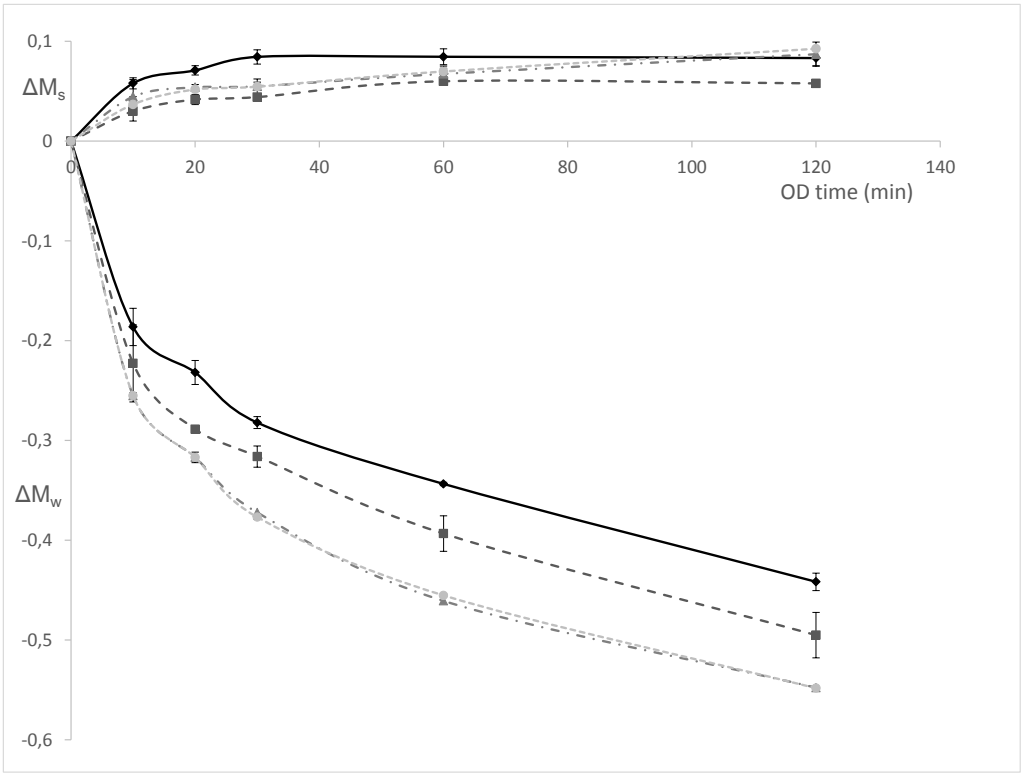

Figure 2. Water (ΔM_w) and sucrose (ΔM_s) mass variation through osmotic dehydration treatment pre-treated with PEF at different electric field intensities. (♦) corresponds to no PEF (0 V/cm), (■) 100 V/cm, (▲) 250 V/cm and (●) 400 V/cm.

Figure 3 shows the relationship between the overall mass variation and the water and sucrose mass variation. The line with a slope equal to 1 represents the mass balance $\Delta M = \Delta M_w + \Delta M_s$. No PEF samples are not fitted to the line which means that other flux is present in the process and it is not considered, probably a flux of other native solutes (sugar and electrolytes). However, the data of the samples pre-treated with PEF (all electric fields intensities) are located on the line, confirming that the kiwi mass variation is only due to the variation of water and sucrose (Castro-Giraldez, Fito, & Fito, 2010).

It is important to highlight that besides the water and sucrose mass variation, the native soluble solids present in the vegetal tissue should be considered, which can be estimated as follows:

$$\Delta M_i = \Delta M - (\Delta M_w + \Delta M_s) \quad (4)$$

Where ΔM_i represents the mass variation of native soluble solids leaving the fruit matrix to the osmotic solution.

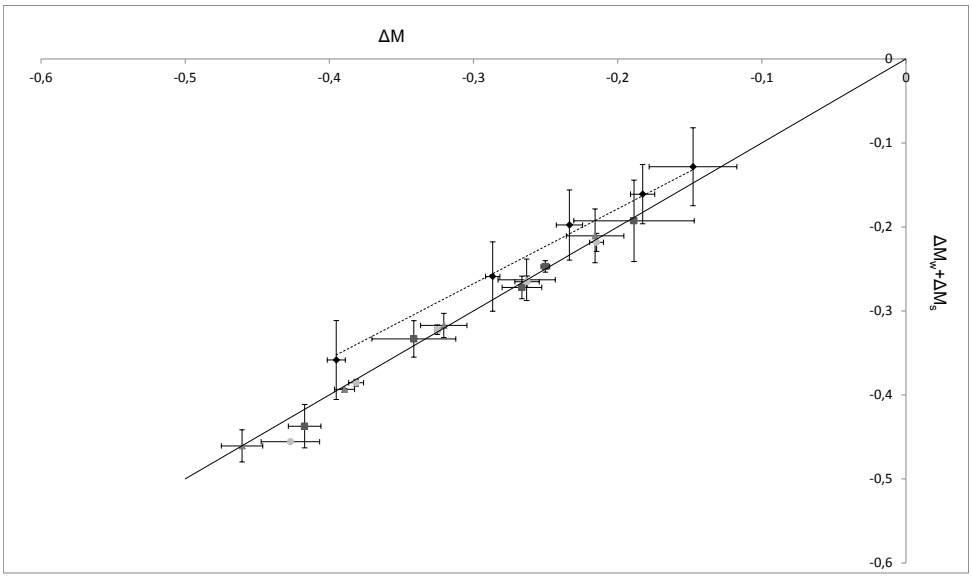

Figure 3. Relation between the overall mass variation and the water and sucrose mass variation, where (♦) corresponds to no PEF (0 V/cm), (■) 100 V/cm, (▲) 250 V/cm and (●) 400 V/cm.

Sugars present driving forces for mass gain as reported in Figure 2. However, as can be seen in Figure 4, samples without PEF pre-treatment lost up to 4% of native soluble solids thus the nature of them has two characteristics: they are affected by the applied electric field and they play an important role in the transport of water and sugars. Therefore, these native compounds could be electrolytes. Throughout the traditional osmotic treatment, fruit tissue losses part of the native electrolytes (Peiró, Dias, Camacho, & Martínez-Navarrete, 2006), reducing the active transmembrane transport; however the samples pre-treated with PEF start the osmotic treatment with low amount of electrolytes.

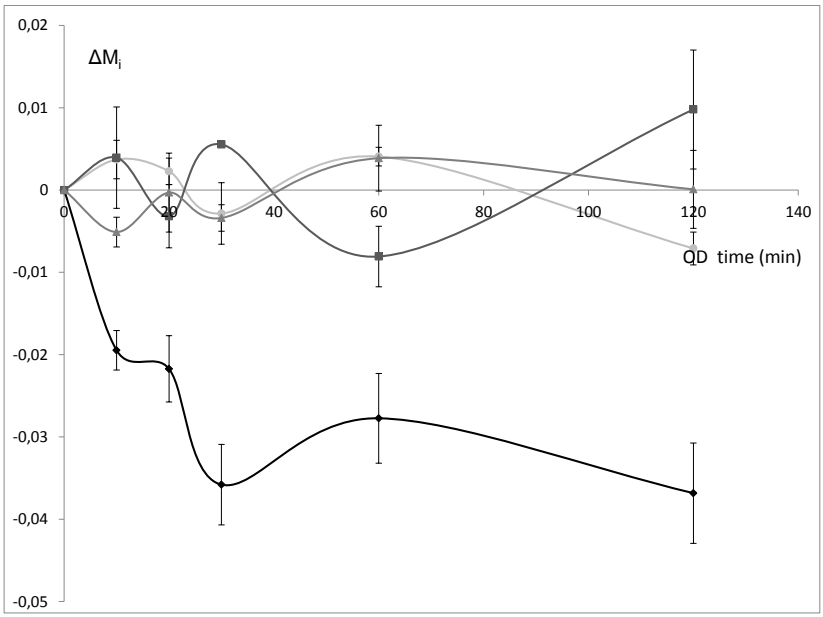

Figure 4. Native soluble solids variation during OD time, where (♦) corresponds to no PEF (0 V/cm), (■) 100 V/cm, (▲) 250 V/cm and (●) 400 V/cm.

In order to understand the different behaviors involved in the mass transfer, Figure 5 shows a scheme of a cellular system with the active and passive transports. Interface sucrose solution/surface fruit is defined in order to develop the transport models.

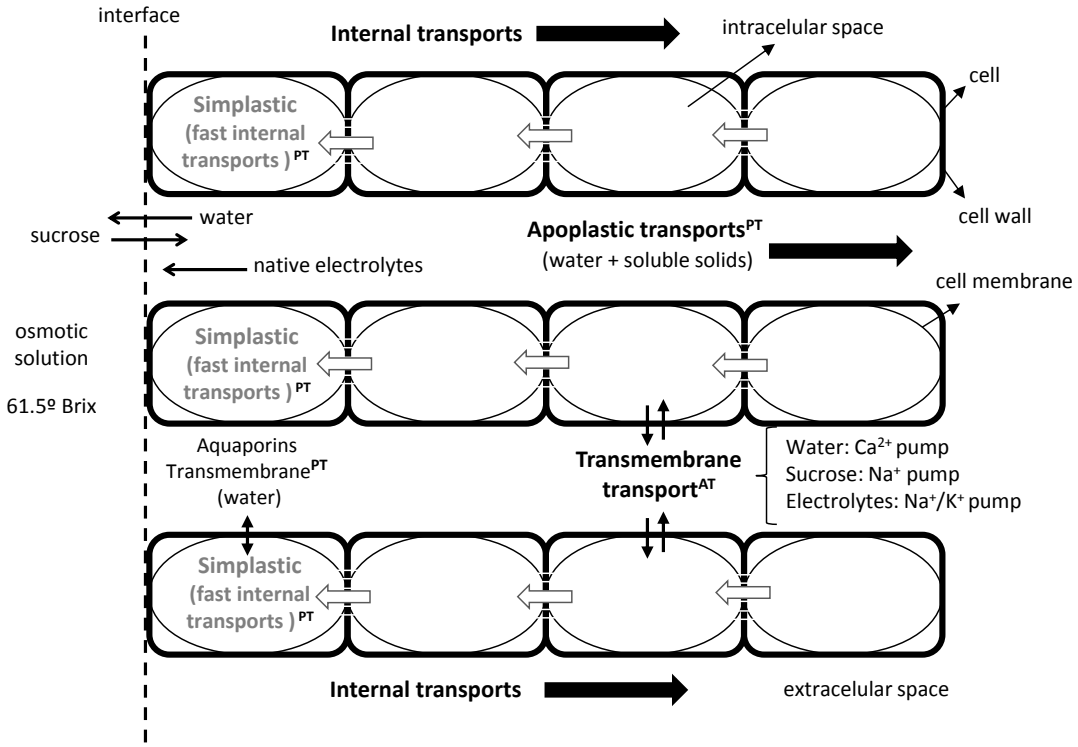

Figure 5. Schematic representation of the cellular transports during osmotic dehydration treatment, where **PT:** passive transport and **AT:** active transport.

Each chemical specie involved in the osmotic dehydration treatment has different driving forces to move into the cell system. Particularly, water fluxes can be generated by passive and active transports. Passive transport is driven by water chemical potential gradients and it could be produced outside the cells by the apoplastic pathways (Steudle & Frensch, 1996) and through transmembrane protein channels by the aquaporins (Agre *et al.*, 1998; Shiratake & Martinoia, 2007). On the other hand, active transmembrane transport requires energy as ATP and is driven by Ca^{2+} pump. In case of high water stress, the homeostatic cell system counteracts the water losses by the aquaporins introducing water in cell by calcium pump (Moraga, Moraga, Fito, & Martínez-Navarrete, 2009). Regarding the sucrose fluxes, they are driven by passive transport in the apoplastic ways and by active transport throughout the membrane, by the sodium pump (Zeuthen, 2010).

Electrolytes transmembrane transport is produced by the sodium/potassium pump (Jaitovich & Bertorello, 2006); however, the rest of active transports depend on the pass of some electrolytes such as Ca^{2+}, Na^{+}, K^{+} or Mg^{2+} throughout this pump.

In order to understand and quantify the passive transport, a non-equilibrium thermodynamic model based in Gibbs free energy has been developed (Talens, Castro-Giraldez, & Fito, 2016):

$$dG = -SdT + VdP + Fdl + \psi de + \sum_i \mu_i dn_i|_{P,T,n_i} \quad (5)$$

Where SdT corresponds to the thermic term, VdP and Fdl are the mechanical energies, ψde the electric term and finally $\sum_i \mu_i dn_i$ is the activity term and represents the addition of the chemical potentials of all the compounds in the system considering pressure and temperature constants, and without molecular interactions. Developing the chemical potential for i compound affected by j compounds, by using the equation 5, next equation is obtained:

$$d\mu_i = \frac{dG}{dn_i} = -s_i dT + v_i dP + F_i dl + \psi_i de + RTln\, a_i + \sum_j RTln\, a_j \frac{dn_j}{dn_i} \quad (6)$$

During the PEF treatment, cellular tissue was immersed in a water bath with two poles, inducing an electric field throughout the samples. Taking into account the interface tap water/fruit surface, the chemical fluxes were defined. In case of water and sugars only the activity terms induce chemical potential gradients to produce transports, because internal pressure and temperature are constant (no deformations appear and the system is tempered). Nevertheless, electrolytes (chemical species with high charge) are also affected by the external electric field, producing high gradients of chemical potential and therefore ion fluxes leaving the tissue. Taking into account only the PEF pre-treatment, the ion chemical potential throughout the interface water/tissue can be defined as follows (Velázquez-Varela, Fito, & Castro-Giráldez, 2014):

$$\Delta\mu_i = \sum_i z_i FE\, \Delta n_i + \sum_j RT\, ln \frac{a_j^{ext}}{a_j^{int}}\, \Delta n_j \quad (7)$$

Where z is the valence of each electrolyte (with sign), F is the Faraday constant (96485.3415 C/mol), E is the Electric field applied (V/m), Δn_i is the variation of each ion and the subscripts i and j represent the electrolytic and chemical species, respectively. The first term of the equation represents the electric term and the second one is the activity term. Considering that the electric fields applied are moderately high (100 to 400 V/cm) and the electrolytes concentrations are low (low activity of each chemical specie) the driving force that governs the ion transport is the electric term. Therefore, during the PEF pre-treatment electrolyte fluxes are induced, leaving the tissue. Final quantity of electrolytes that will remain in the tissue depends on the electric field strength. Depending on the amount of electrolytes with physiological activity in the tissue, the water and sucrose transmembrane active transport, during the osmotic treatment, will be affected.

In order to quantify the effect of the reduction of the amount of electrolytes, the driving forces during the osmotic dehydration treatment must be defined by using equation 6, fixing the interface between osmotic solution and fruit surface.

In the osmotic dehydration treatment, equation 6 could be transformed according to the research developed by Castro-Giráldez, Fito, & Fito, (2011b) and Tylewicz, Fito, Castro-Giráldez, Fito, & Dalla Rosa (2011). For this treatment, the thermal (SdT) and electric (ψde) terms can be neglected because it is an isothermal process and the amount of native ions is low. Therefore, it is possible to obtain the water chemical potential as follows:

$$\Delta\mu_w = \frac{\Delta G}{\Delta n_w} = v_w \Delta P + F_w \Delta l + RTln \frac{a_w^S}{a_w^{OD}} + RTln \frac{a_s^S}{a_s^{OD}} \frac{J_s}{J_w} \quad (8)$$

Where the superscript OD represents the osmotic dehydration solution (sucrose solution), and superscript S represents the properties of fruit surface.
In order to understand the transports, it is necessary to calculate the water molar flux with the following equation:

$$J_w = \frac{\Delta M_w \,.M_0}{\Delta t \,.S \,.Mr_w} \tag{9}$$

Where J_w is the water flux (mol/s m^2), ΔM_w represents the water mass variation (dimensionless), M_0 is the initial mass of the sample (g), Δt is the process time (s), S corresponds to the surface of the sample during the treatment (m^2) and Mr_w is the molecular weight of water (18 g/mol).

Figure 6 shows the maximum water flux ordered by the PEF pre-treatment intensity. The electric field applied before the osmotic treatment increases the water flux because the pre-treatment removes a part of the basic electrolytes, reducing the homeostatic cell system based on the Ca^{2+} pump.

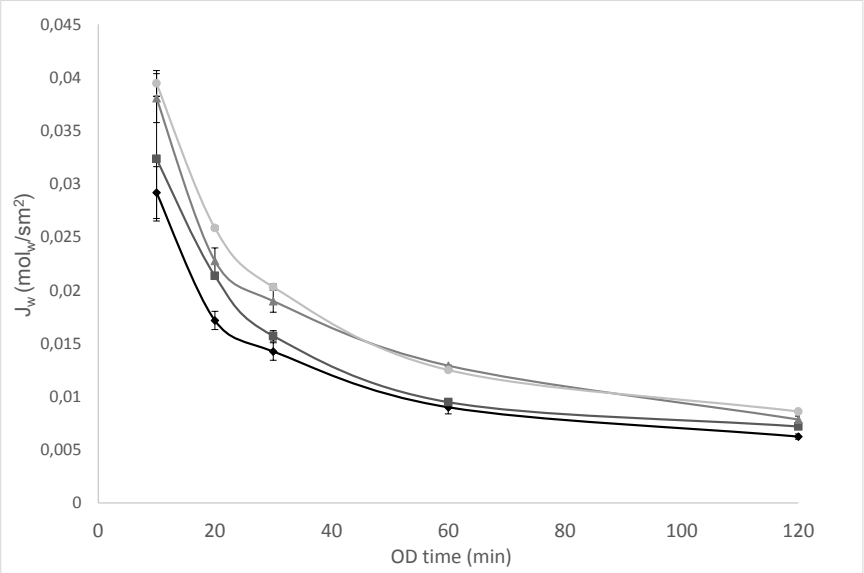

Figure 6. Water fluxes during OD treatment with PEF pre-treatment at different voltages, where (♦) corresponds to no PEF (0 V/cm), (■) 100 V/cm, (▲) 250 V/cm and (●) 400 V/cm.

Applying the first relation of Onsager (Traffano-Schiffo, Castro-Giráldez, Fito, & Balaguer, 2014), the molar fluxes are related to the chemical potential, as a driving force of the transport of the component i, by the phenomenological coefficient (L_i) (equation 10).

$$J_i = L_i \,.\Delta\mu_i \tag{10}$$

Where the component *i* represents the water or the sucrose. The phenomenological coefficient is the physical property than explains the overall transport of each chemical specie. Nevertheless, the chemical potential is needed in its estimation where mechanical forces induced by the tissue deformations increase the complexity in the calculation. Tissue deformation is produced by the plasmolysis cell process, thus, this effect is punctual and it affects in determined periods of the

osmotic treatment. Therefore, it is necessary to analyze the tissue deformation in order to determine the periods without mechanical effects, in order to estimate the phenomenological coefficient.

In order to analyze the tissue deformation, volume and surface variation were calculated by using the following equations:

$$\Delta V = \frac{V_t - V_0}{V_0} \tag{11}$$

$$\Delta S = \frac{S_t - S_0}{S_0} \tag{12}$$

Where V corresponds to the volume (m^3), S is the surface (m^2) and the subscripts t and 0 correspond to the treatment time and the initial value (0 minutes), respectively.

In Figure 7, it is possible to observe the volume deformation during the osmotic treatment, where a shrinkage/swelling process occurs in two phases divided by the plasmolysis process of the different tissues as was explained by (Castro-Giráldez, Tylewicz, Fito, Dalla Rosa, & Fito, 2011c) where activity terms are predominant in the shrinkage periods and mechanical terms are predominant in swelling periods (equation 8). The samples pre-treated by PEF show the critical point of plasmolysis before than the no pre-treated samples. This phenomenon could be accelerated, in the pre-treated samples, by higher water fluxes, and therefore higher intracellular shrinkage. The initial shrinkage is ordered according to the pre-treatment intensity.

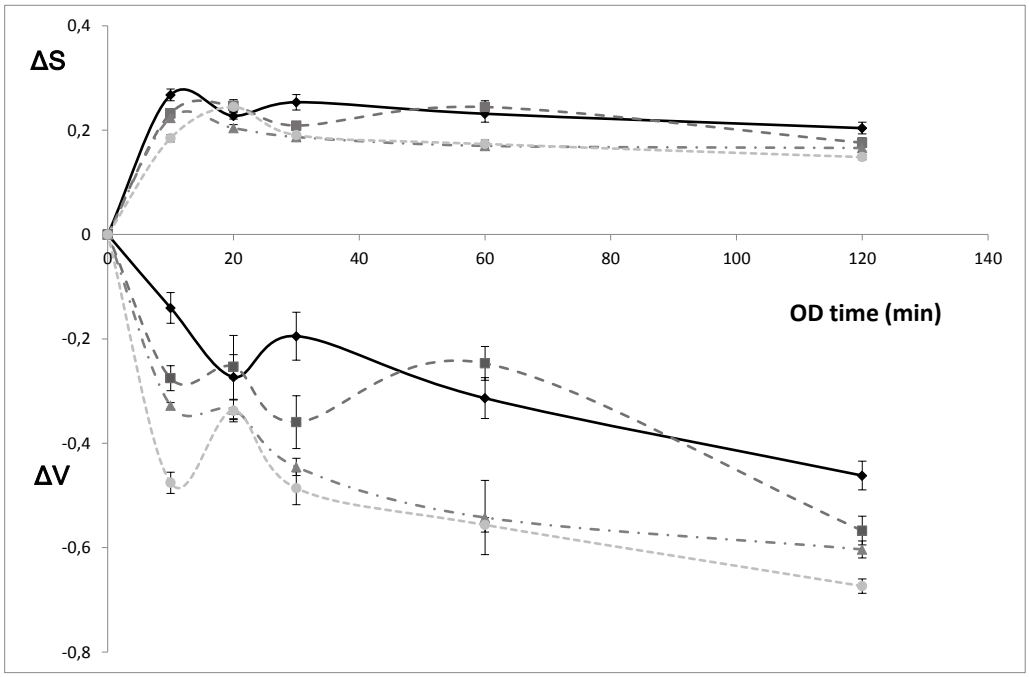

Figure 7. Evolution of area (ΔS) and volume (ΔV) variation of the samples during OD treatment pre-treated with PEF at different voltages, where (♦) corresponds to no PEF (0 V/cm), (■) 100 V/cm, (▲) 250 V/cm and (●) 400 V/cm.

Consequently, at the initial shrinkage (10 min of OD), mechanical term could be considered neglected, therefore, the chemical potential could be estimated as follows:

$$\Delta\mu_w = RTln\frac{a_w^S}{a_w^{OD}} + RTln\frac{a_s^S}{a_s^{OD}}\frac{J_s}{J_w} \quad (13)$$

And for sucrose chemical potential:

$$\Delta\mu_S = RTln\frac{a_w^S}{a_w^{OD}}\frac{J_w}{J_S} + RTln\frac{a_s^S}{a_s^{OD}} \quad (14)$$

Applying equations 13 and 14, the phenomenological coefficients of water and sucrose were obtained (Table 1). The phenomenological coefficient has a physical meaning which describes the contribution of driving forces of the compounds according to the fluxes (Ferrando & Spiess, 2003). From literature, similar phenomenological coefficients values were reported for water transport; Castro-Giráldez *et al.*, (2011c) obtained a value of $2.46{\cdot}10^{-5}$ mol^2/J s m^2 for OD of kiwifruit at 30 ºC and using a 65% w/w sucrose solution; Segui, Fito, & Fito, (2012) obtained L_w = $0.9 \pm 0.3 \cdot 10^{-4}$ mol^2/J s m^2 for apple isolated cells during OD at 30 ºC using a 45% (w/w) sucrose solution, also Segui, Fito & Fito, (2013) obtained $L_w = 1.3 \pm 0.3 \cdot 10^{-4}$ mol^2/J s m^2 for apple isolated cells during rehydration. In contrast, few data are available for sucrose phenomenological coefficients (L_s).

In Table 1, it is possible to observe the increase of water phenomenological coefficient according to the electric field intensity applied as pre-treatment. Water transmembrane transport works with active and passive transport. The homeostatic cellular system, in case of water stress, induces the activity of Ca^{2+} pump in opposite way of aquaporins (passive transport). However, before the osmotic treatment, the PEF pre-treatment removes the electrolytes, reducing the activity of Ca^{2+} pump, affecting to the osmotic treatment and increasing the kinetics of the dehydration, as the values of Table 1 show. The case of sucrose is the opposite; sucrose transmembrane transport works by the Na^+ pump, therefore any reduction of the overall quantity of the electrolytes reduces the sucrose transmembrane transport maintaining the sucrose transport in the apoplastic ways.

Table 1. Phenomenological coefficient of water (L_w) and sucrose (L_s) for the first 10 minutes of the kiwifruit osmotic dehydration treatment.

PEF (V/cm)	L_w (10^{-4}) (mol^2/J s m^2)	L_S (10^{-8}) (mol^2/J s m^2)
0	1.7 ± 0.4	8.5 ± 3.8
100	1.83 ± 0.15	1.5 ± 0.5
250	2.04 ± 0.7	2.9 ± 1.7
400	2.4 ± 0.5	1.75 ± 0.5

Sorption isotherms describe the relationship between the surface water activity of the samples and its moisture (in dry basis) (Traffano-Schiffo, Castro-Giraldez, Colom, & Fito, 2015). Figure 8 shows the sorption isotherms after treatment (Fig. 8a) and after reposed 24 h (Fig. 8b) at 4 ºC for all the dehydrated samples at each PEF treatment condition. Moreover, data of a pure solution of water and sucrose is shown (Starzak & Mathlouthi, 2006). Surface water activity is a punctual value and moisture is an average value, thus the distance between surface data and line of pure sucrose solution explains the concentration profile inside sample (Castro-Giráldez *et al.*, 2011b). Samples fitted in pure sucrose solution line represent equilibrated samples (no concentration profile), thus it is possible to rename this line to "equilibrated sample line". The relations between both isotherms permit to predict the internal transport, strongly driven by the symplastic ways (Fisher & Oparka, 1996).

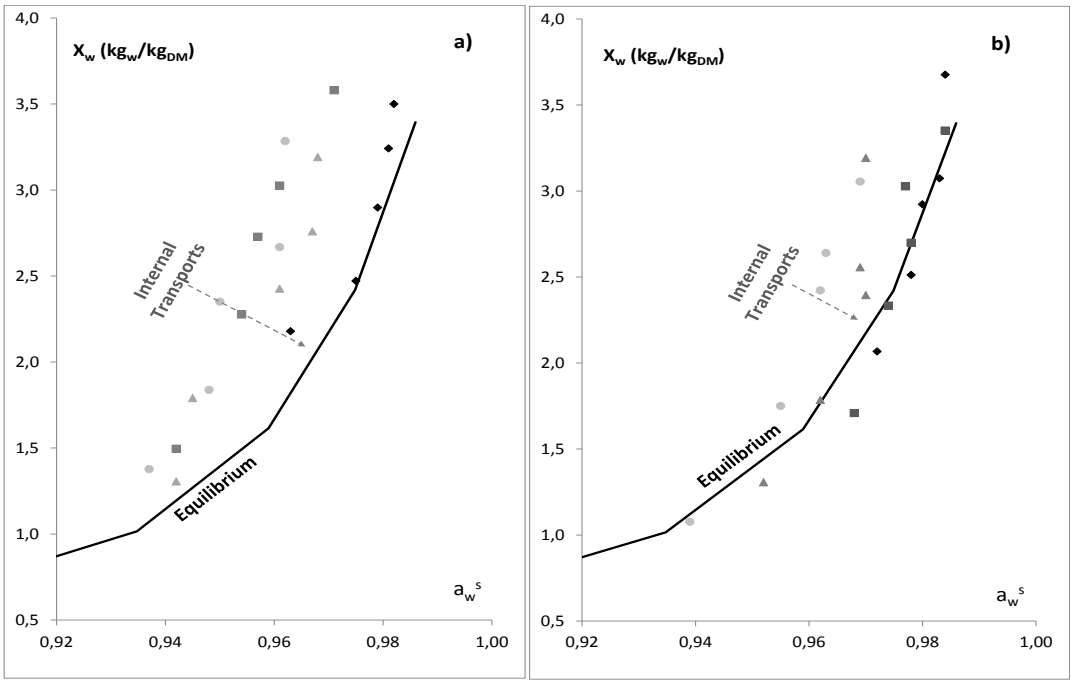

Figure 8. Sorption isotherm a) after osmotic dehydration treatment and b) after reposed 24 h, where (♦) corresponds to no PEF (0 V/cm), (■) 100 V/cm, (▲) 250 V/cm and (●) 400 V/cm and (—) sucrose solutions (obtained from Starzak & Mathlouthi, 2006).

After osmotic treatment, samples are close the equilibrium line depending on the pre-treatment intensity (see figure 8a). However, in Figure 8b it is possible to observe that the no pre-treated samples and samples pre-treated at low electric field intensity reach the equilibrium line at 24h, nevertheless the samples pre-treated with PEF are far from the equilibrated sample line. It could be explained because sucrose molecules, in samples without Na^+ pump working (affected by PEF pre-treatment), equilibrate the sucrose content by the apoplastic ways. The symplastic transport of sucrose, without active transport, does not work because symplastic transport needs first a transmembrane transport. Therefore, samples pre-treated by PEF, increase the water transport but reduce the sucrose transport.

Therefore, PEF pre-treatment opens an opportunity in osmotic dehydration treatments in fruits, accelerating the water losses, but reducing the sugar gained in fruit (less calories and sweetness).

4. Conclusions

The application of pulsed electric fields as a pre-treatment of the osmotic dehydration in kiwifruit increase the water mass transfer and reduces the final sugar concentration comparing with samples that have not been pre-treated. The water phenomenological coefficient, in osmotic treatment, increases according to the electric fields applied in the pre-treatment. Thus because, the application of electric field prior to the osmotic treatment removes the electrolytes, reducing the activity of Ca^{2+} pump, and leaving alone the aquaporins as a main protein channel of water transmembrane transport and therefore affecting to the regular functionality of cell homeostasis system. However, the sucrose phenomenological coefficient, in osmotic treatment, decrease according to the electric field applied, because the sucrose transmembrane transport is made by the Na^{+} pump, therefore, any reduction of the overall quantity of the electrolytes reduces the sucrose content.
PEF pre-treatment opens an amazing opportunity in the design of new products of candying fruits with high dehydration and less sugar content.

5. Acknowledgements

The authors Urszula Tylewicz and Marco Dalla Rosa want to thank for the financial support provided by funding bodies within the FP7 ERA-Net CORE Organic Plus, and with cofounds from the European Commission. The author Marta Castro-Giráldez wants to thank the UPV Postdoctoral Program (PAID-10-14) of the Universidad Politécnica de Valencia for its support. The author Maria Victoria Traffano Schiffo wants to thank the FPI Predoctoral Program of the Universidad Politécnica de Valencia for support her PhD studies, ERASMUS PRÁCTICAS program to finance her mobility to Italy and also Silvia Tappi and Wei Luo for their cooperation during the experiment.

6. References

Agre, P., Bonhivers, M., & Borgnia, M. J. (1998). The aquaporins, blueprints for cellular plumbing systems. *Journal of Biological Chemistry*, *273*(24), 14659–14662.

Baier, A. K., Bußler, S., & Knorr, D. (2015). Potential of high isostatic pressure and pulsed electric fields to improve mass transport in pea tissue. *Food Research International*, *76*, 66–73.

Bohnert, H. J., & Jensen, R. G. (1996). Strategies for engineering water-stress tolerance in plants. *Trends in Biotechnology*, *14*(3), 89–97.

Briegel, A., Ortega, D. R., Tocheva, E. I., Wuichet, K., Li, Z., Chen, S., … Dobro, M. J. (2009). Universal architecture of bacterial chemoreceptor arrays. *Proceedings of the National Academy of Sciences*, *106*(40), 17181–17186.

Calderón-Miranda, M. L., Fernanda, M., Martín, S., Barbosa-Cánovas, G. V, & Swanson, B. G. (1998). MÉTODOS NO TÉRMICOS PARA PROCESAMIENTO DE ALIMENTOS: VARIABLES E INACTIVACIÓN MICROBIANAl, *1*, 3–11.

Castro-Giráldez, M., Fito, P. J., Dalla Rosa, M., & Fito, P. (2011a). Application of microwaves dielectric spectroscopy for controlling osmotic dehydration of kiwifruit (Actinidia deliciosa cv Hayward). *Innovative Food Science & Emerging Technologies*, *12*(4), 623–627.

Castro-Giraldez, M., Fito, P. J., & Fito, P. (2010). Non-equilibrium thermodynamic approach to analyze the pork

meat (Longissimus dorsi) salting process. *Journal of Food Engineering*, *99*(1), 24–30.

Castro-Giráldez, M., Fito, P. J., & Fito, P. (2011b). Nonlinear thermodynamic approach to analyze long time osmotic dehydration of parenchymatic apple tissue. *Journal of Food Engineering*, *102*(1), 34–42.

Castro-Giráldez, M., Tylewicz, U., Fito, P. J., Dalla Rosa, M., & Fito, P. (2011c). Analysis of chemical and structural changes in kiwifruit (Actinidia deliciosa cv Hayward) through the osmotic dehydration. *Journal of Food Engineering*, *105*(4), 599–608.

Dellarosa, N., Ragni, L., Laghi, L., Tylewicz, U., Rocculi, P., & Dalla, M. (2016). Time domain nuclear magnetic resonance to monitor mass transfer mechanisms in apple tissue promoted by osmotic dehydration combined with pulsed electric fi elds. *Innovative Food Science and Emerging Technologies*. http://doi.org/10.1016/j.ifset.2016.01.009

Ferrando, M., & Spiess, W. E. L. (2003). Effect of osmotic stress on microstructure and mass transfer in onion and strawberry tissue. *Journal of the Science of Food and Agriculture*, *83*(9), 951–959.

Fisher, D. B., & Oparka, K. J. (1996). Post-phloem transport: principles and problems. *Journal of Experimental Botany*, *47*(Special Issue), 1141–1154.

Jaitovich, A. A., & Bertorello, A. M. (2006). Na+, K+-ATPase: an indispensable ion pumping-signaling mechanism across mammalian cell membranes. In *Seminars in nephrology* (Vol. 26, pp. 386–392). Elsevier.

Knorr, D., Angersbach, A., Eshtiaghi, M. N., Heinz, V., & Lee, D. U. (2001). Processing concepts based on high intensity electric field pulses. *Trends in Food Science and Technology*, *12*(3-4), 129–135. http://doi.org/10.1016/S0924-2244(01)00069-3

Maurel, C., & Chrispeels, M. J. (2001). Aquaporins. A molecular entry into plant water relations. *Plant Physiology*, *125*(1), 135–138.

Moraga, M. J., Moraga, G., Fito, P. J., & Martínez-Navarrete, N. (2009). Effect of vacuum impregnation with calcium lactate on the osmotic dehydration kinetics and quality of osmodehydrated grapefruit. *Journal of Food Engineering*, *90*(3), 372–379.

Panarese, V., Laghi, L., Pisi, A., Tylewicz, U., Dalla, M., & Rocculi, P. (2012). Effect of osmotic dehydration on Actinidia deliciosa kiwifruit : A combined NMR and ultrastructural study. *Food Chemistry*, *132*(4), 1706–1712. http://doi.org/10.1016/j.foodchem.2011.06.038

Parniakov, O., Lebovka, N. I., Bals, O., & Vorobiev, E. (2015). Effect of electric field and osmotic pre-treatments on quality of apples after freezing-thawing. *Innovative Food Science and Emerging Technologies*, *29*, 23–30. http://doi.org/10.1016/j.ifset.2015.03.011

Peiró, R., Dias, V. M. C., Camacho, M. M., & Martínez-Navarrete, N. (2006). Micronutrient flow to the osmotic solution during grapefruit osmotic dehydration. *Journal of Food Engineering*, *74*(3), 299–307.

Puértolas, E., Luengo, E., Álvarez, I., & Raso, J. (2012). Improving Mass Transfer to Soften Tissues by Pulsed Electric Fields: Fundamentals and Applications. *Annual Review of Food Science and Technology*, *3*(1), 263–282. http://doi.org/10.1146/annurev-food-022811-101208

Rastogi, & Niranjan. (1998). Enhanced mass transfer during osmotic dehydration of high pressure treated pineapple. *Journal of Food Science*, *63*(3), 508–511.

Rastogi, N. K., Eshtiaghi, M. N., & Knorr, D. (1999). Accelerated mass transfer during osmotic dehydration of high intensity electrical field pulse pretreated carrots. *Journal of Food Science*, *64*(6), 1020–1023.

Segui, L., Fito, P. J., & Fito, P. (2012). Understanding osmotic dehydration of tissue structured foods by means of a cellular approach. *Journal of Food Engineering*, *110*(2), 240–247.

Seguí, L., Fito, P. J., & Fito, P. (2013). A study on the rehydration ability of isolated apple cells after osmotic dehydration treatments. *Journal of Food Engineering*, 115(2), 145-153.

Shiratake, K., & Martinoia, E. (2007). Transporters in fruit vacuoles. *Plant Biotechnology*, *24*(1), 127–133.

Singh, R. P., & Heldman, D. R. (2001). *Introduction to food engineering*. Gulf Professional Publishing.

Starzak, M., & Mathlouthi, M. (2006). Temperature dependence of water activity in aqueous solutions of sucrose. *Food Chemistry*, *96*(3), 346–370.

Steudle, E., & Frensch, J. (1996). Water transport in plants: role of the apoplast. *Plant and Soil*, *187*(1), 67–79.

Taiwo, K. A., Angersbach, A., Ade-Omowaye, B. I. O., & Knorr, D. (2001). Effects of pretreatments on the diffusion kinetics and some quality parameters of osmotically dehydrated apple slices. *Journal of Agricultural and Food Chemistry*, *49*(6), 2804–2811.

Talens, C., Castro-Giraldez, M., & Fito, P. J. (2016). A thermodynamic model for hot air microwave drying of orange peel. *Journal of Food Engineering*, *175*, 33–42.

Tedjo, W., Taiwo, K. A., Eshtiaghi, M. N., & Knorr, D. (2002). Comparison of pretreatment methods on water and solid diffusion kinetics of osmotically dehydrated mangos. *Journal of Food Engineering*, *53*(2), 133–142.

Traffano-Schiffo, M. V., Castro-Giráldez, M., Fito, P. J., & Balaguer, N. (2014). Thermodynamic model of meat drying by infrarred thermography. *Journal of Food Engineering*, *128*, 103–110. http://doi.org/10.1016/j.jfoodeng.2013.12.024

Traffano-Schiffo, M. V, Castro-Giraldez, M., Colom, R. J., & Fito, P. J. (2015). Study of the application of dielectric spectroscopy to predict the water activity of meat during drying process. *Journal of Food Engineering*, *166*, 285–290.

Tyerman, S. D., Bohnert, H. J., Maurel, C., Steudle, E., & Smith, J. A. C. (1999). Plant aquaporins: their molecular biology, biophysics and significance for plant water relations. *Journal of Experimental Botany*, 50(Special Issue), 1055–1071.

Tylewicz, U., Fito, P. J., Castro-Giráldez, M., Fito, P., & Dalla Rosa, M. (2011). Analysis of kiwifruit osmodehydration process by systematic approach systems. *Journal of Food Engineering*, *104*(3), 438–444.

Tylewicz, U., Romani, S., Widell, S., & Galindo, F. G. (2013). Induction of vesicle formation by exposing apple tissue to vacuum impregnation. *Food and Bioprocess Technology*, *6*(4), 1099–1104.

Vega-mercado, H., Gongora-Nieto, M. M., Barbosa-Cánovas, G. V, & Swanson, B. G. (2007). Pulse electric fields in food preservation. *Handbook of Food Preservation*, 783–814.

Velázquez-Varela, J., Fito, P. J., & Castro-Giráldez, M. (2014). Thermodynamic analysis of salting cheese process. *Journal of Food Engineering*, *130*, 36–44.

Zeuthen, T. (2010). Water-transporting proteins. *Journal of Membrane Biology*, *234*(2), 57–73.

Zimmermann, U., Pilwat, G., Beckers, F., & Riemann, F. (1976). Effects of external electrical fields on cell membranes. *Bioelectrochemistry and Bioenergetics*, *3*(1), 58–83.

Artículo 8

Traffano-Schiffo, M. V., Laghi, L., Castro-Giraldez, M., Tylewicz, U., Rocculi, P., Ragni, L., Dalla Rosa, M., & Fito, P. J. (2017). Osmotic dehydration of organic kiwifruit pre-treated by pulsed electric fields and monitored by NMR. *Food Chemistry*, 236, 87-93.

OSMOTIC DEHYDRATION OF ORGANIC KIWIFRUIT PRE-TREATED BY PULSED ELECTRIC FIELDS AND MONITORED BY NMR

Maria Victoria Traffano-Schiffo[a], Luca Laghi[b,c], Marta Castro-Giraldez[a]*, Urszula Tylewicz[b], Pietro Rocculi[b,c], Luigi Ragni[b,c], Marco Dalla Rosa[b, c], Pedro J. Fito[a]

[a] Instituto Universitario de Ingeniería de Alimentos para el Desarrollo, Universidad Politécnica de Valencia, Camino de Vera s/n, 46022 Valencia, Spain

[b] Department of Agricultural and Food Sciences, University of Bologna, P.zza Goidanich 60, 47521 Cesena, Italy

[c] Interdepartmental Centre for Agri-Food Industrial Research, University of Bologna, Via Quinto Bucci 336, 47521 Cesena, Italy

*author for correspondence: marcasgi@upv.es

ABSTRACT

Osmotic dehydration (OD) is a widely used preservation technique that consists in the reduction in food water activity by the immersion of the biological tissue in hypertonic solutions. The aim of this work was to analyze the effect of Pulsed Electric Fields (PEF) in mass transfer as a pre-treatment of the OD using NMR. In this sense, PEF pre-treatments were done using three different voltages (100, 250 and 400 V/cm) and 60 number of pulse. The OD of kiwifruit was carried out in 61.5% of sucrose solution at 25 ºC, for a contact period from 0 to 120 min. The water distribution into the cellular tissue was studied by NMR relaxometry. In conclusion, NMR is an excellent technique for quantifying water molecules according to their interactions in the fruit tissue, obtaining the adsorbed water and opening the possibility to apply the BET model to fit the adsorbed isotherm over the whole range of water activity.

Keywords: Kiwifruit, Pulsed Electric Fields, Osmotic dehydration, TD-NMR, Water distribution.

1. Introduction

Kiwifruit is well known as a source of vitamin C besides its high levels of fiber, minerals, antioxidants and other bioactive substances that present beneficial effects on health (Diamante, Savage, & Vanhanen, 2012). It is constituted by three distinct types of tissues: outer pericarp, inner pericarp and core, which have structural and compositional differences (Castro-Giráldez, Tylewicz, Fito, Dalla Rosa, & Fito, 2011a).

Osmotic dehydration (OD) is a conservation process commonly used to increase the shelf-life of fruits. It consists in the immersion of the biological tissue in a hypertonic solution, which generates fluxes of water and solutes and, as a consequence, the water activity of the product is reduced (Moraga, Moraga, Fito, & Martínez-Navarrete, 2009). From a thermodynamic point of view, the difference in the chemical potentials (water and sucrose) between the sample and the dipping solution promotes the water release from the fruit to the osmotic solution and the simultaneous solutes inflow from the external solution to the fruit (Castro-Giráldez, Fito, & Fito, 2011b). In order to increase yields and to reduce processing times, different techniques coupled to OD treatment have been studied, such as ultrasound (Ahmed, Qazi, & Jamal, 2016; Nowacka, Tylewicz, Laghi, Dalla Rosa, & Witrowa-Rajchert, 2014; Li, Zhao, Guo, An, Ding, & Wang, 2012), pulsed-vacuum (Corrêa, Pereira, Vieira, & Hubinger, 2010; Rastogi, Raghavarao, Niranjan, & Knorr, 2002) and pulsed electric fields (Wiktor, Śledź, Nowacka, Chudoba, & Witrowa-Rajchert, 2014; Amami, Vorobiev, & Kechaou, 2006).

Pulsed electric fields (PEF) is a non-thermal and preservation technology which consists in applying electric pulses through a biological tissue placed between two electrodes for very short periods of time (micro- to milli-seconds) (Dellarosa, Ragni, Laghi, Tylewicz, Rocculi, & Dalla Rosa, 2016; Faridnia, Burritt, Bremer, & Oey, 2015; Toepfl, Heinz, & Knorr, 2005), causing structural changes in the cell membrane (Angersbach, Heinz, & Knorr, 2000). This phenomenon could be classified as electroporation or electrocompression and according to the electric field strength they could be reversible or irreversible. Electroporation is produced when the external electric field induces conformational changes and the reorganization of the phospholipidic bilayer, generating pores (Liu, Han, Zeng, Sun, & Aadil, 2016; Baier, Bußler, & Knorr, 2015). On the other hand, the electrocompression is produced due to the charges (electrolytes) accumulation at both sides of the cell membrane, which attracts each other, compressing it. When this compression exceeds the elastic restoration force, the disruption of the membrane is produced generating pores (Traffano-Schiffo, Tylewicz, Castro-Giraldez, Fito, Ragni, & Dalla Rosa, 2016; Saulis, 2010; Calderón-Miranda, González, Barbosa-Cánovas, & Swanson, 1998).

In a previous work about the use of a coupled treatment (PEF/OD) in organic kiwifruit (Traffano-Schiffo el at., 2016) it has been demonstrated that water losses have increased and accelerated compared to samples which had not been pretreated with PEF. In addition, it has been

demonstrated that the pulse electric field produces electrolytes mass losses, affecting the active transmembrane transports, inducing changes on the overall transport. However, this study could not explain the water distribution inside the cell and the internal transports. Due to this, Time Domain Nuclear Magnetic Resonance (TD-NMR) represents a valuable tool able to study the redistribution of the water during sample processing (Santagapita, Laghi, Panarese, Tylewicz, Rocculi, & Dalla Rosa, 2013), the state of the cell membranes disruption, protoplast and tonoplast (Aguiló-Aguayo, Downey, Keenan, Lyng, Brunton, & Rai, 2014) and the block of water and sucrose active pumps due to the electric pulses (Traffano-Schiffo el at., 2016).

TD-NMR is a fast, non-destructive and non-invasive technique able to determine the relaxation times parameters, such as the spin-lattice or longitudinal relaxation (T_1) and the spin-spin or transverse relaxation (T_2) of protons differentiating vacuoles, cytoplasm/extracellular spaces and cell wall (Santagapita, Tylewicz, Panarese, Rocculi, & Dalla Rosa, 2016; Tylewicz *et al.*, 2011). Panarese, Laghi, Pisi, Tylewicz, Dalla Rosa, & Rocculi, (2012) were able to separately observe, in the pericarp of kiwifruit, water located in extracellular spaces and cytoplasm, water located in vacuole and protons ascribable to water tightly bound to the most rigid biopolymers.

The aim of this work was to analyze the effect of PEF used as a pre-treatment of the OD of organic kiwifruit (Actinidia deliciosa cv Hayward) in water redistribution by NMR.

2. Material and methods

Organic kiwifruits (*Actinidia deliciosa cv Hayward*) with the same ripeness and similar size were bought on a supermarket located in Cesena (Italy) and kept refrigerated at 4 ± 1 °C until use. The fruits were tempered at 25 °C, peeled and cylinders (8 mm diameter and 10 mm length) were obtained from the parenchymatic part of the tissue. The initial refractometric indexes (° Brix) of the fruits used were 13 ± 1 °Brix.

Fresh kiwifruits were characterized by mass, volume, soluble solids content (°Brix), water activity (a_w), moisture (kg_w/kg_T) and TD-NMR by quadruplicate. 12 sample cylinders were used for each treatment (considering all OD times and the triplications for each measurement, the total number of treated samples was 576). They were placed inside the PEF chamber avoiding free spaces between them and subjected to different electric fields strengths (12 extra samples were used as control, without PEF-treatment). After, the samples were weighed and introduced into the osmotic dehydration solution. According to previous results, the selected OD treatment times were 0, 10, 20, 30, 60 and 120 minutes (Traffano-Schiffo *et al.*, 2016).

Due to the fact that the samples after treatments show concentration profiles (non-equilibrated samples), another batch of samples were treated and reposed at 4 °C during 24 hours in decagon containers closed with parafilm® (equilibrated samples). Finally, mass, volume, soluble solids, aw, soluble solids content and TD-NMR were measured as final determinations for non-equilibrated

and equilibrated samples. In addition, at each osmotic time, an aliquot of sucrose solution was taken to measure aw and soluble solids content.

2.1. Pulsed electric field (PEF) treatment

Pulsed electric field treatments were applied to the samples using monopolar pulse generator equipment based on MOSFET technology and capacitors as energy tanks (Dellarosa et al., 2016). The cylinders of organic kiwifruit were placed in a rectangular treatment chamber equipped with two stainless steel electrodes (20 x 20 mm^2) with a separation between them of 30 mm and filled with 5 mL of tap water with known conductivity at 25 °C.
PEF pre-treatments were done by applying three different pulsed electric fields (100, 250 and 400 V/cm at 50 Hz) with near-rectangular shape pulses, a train of 60 pulses, a fixed pulse width of 100 ± 2 μs and a repetition time of 10.0 ± 0.1 ms.

2.2. Osmotic dehydration treatment

The osmotic solution at 61.5% (w/w) was prepared with commercial sucrose (Eridana SpA, Bologna, Italia) and distilled water at 25 °C. Samples were immersed into the sucrose solution maintaining a relationship of 1:4 (w/w) between the fruit and the solution.

2.3. Analytical determinations

A dew point Hygrometer Decagon (Aqualab™, series 3 TE) was used for measuring the water activity (aw), with a precision ± 0.003. Mass was determined by using a Kern balance ABS 320-4N (±0.0001) (KERN & SOHN GmbH, Germany).
Volume was determined by image analysis using Adobe® Photoshop® CS6 software (Adobe Systems Inc., San Jose, CA, USA). Moisture was determined following the AOAC Method 934.06, 2000.
Soluble solid content was determined by measuring the refractometric index with a digital refractometer (KRÜSS Optronic© GmbH, Germany) calibrated with distilled water at 25 °C. Refractometric index was measured in both kiwifruit samples and agent solution after the treatment.
Analytical determinations described above were obtained by quadruplicate.

2.4. TD-NMR measurements

Proton transverse relaxation time (T_2) decay was measured for each sample by applying the CPMG pulse sequence (Meiboom & Gill, 1958), using a Bruker 'The Minispec' spectrometer (Bruker Corporation, Germany) operating at 20 MHz, as described by Dellarosa *et al.* (2016). Each measurement comprised 32000 echoes, with an interpulse spacing of 0.08 ms and a recycle delay of 10 s, which allowed the measurement of proton decays included between 1 and 3000 ms and avoided sample overheat. Each acquisition was performed over 8 scans giving rise to a total time of analysis around 90 s. The registered spectra were normalized to unitary area and analyzed by UpenWin software (Borgia, Brown, & Fantazzini, 1998) to give quasi-continuous distributions of relaxation time. The number of output relaxation times, sampled logarithmically in the 1–3000 ms range, was set to 100. To obtain quantitative information from the T_2-weighted decay curves, signals were fitted using a discrete multi-exponential curve. The fitting was run using the 'Levenberg–Marquardt nonlinear least squares' algorithm implemented in 'R' software (R Foundation for Statistical Computing, Austria). Unlike Santagapita *et al.* (2013), the optimum number of exponential curves for each tested treatment was found to be three, without removing any initial T_2 weighted point.

2.5. Desorption isotherm

The desorption isotherm of the adsorbed water was fitted following the BET model using equation 1 (Brunauer, Emmett, & Teller, 1938).

$$X_w^{ADS} = \frac{X_{w0}\, C\, a_w}{(1-a_w)(1+(C-1)\, a_w)} \quad (1)$$

Where: X_w^{ADS} corresponds to the kiwifruit adsorbed moisture (kgw/kgdm), X_{w0} is the monomolecular moisture layer (kgw/kgdm) and C is the energy constant (dimensionless). BET model was fitted by using a non-linear regression with the Statgraphics Centurion XVI software (Statgraphics, Virgina, U.S.A.).

3. Results and discussion

During the osmotic treatments, kiwifruit suffers mass variations which involve the water losses and the sucrose gain. Each chemical specie involved in the osmotic dehydration treatment has different driving forces and ways to move into the cell system. Particularly, water fluxes can be generated by passive and active transports. Passive transport is driven by water chemical potential

gradients and it could be produced outside the cells by the apoplastic pathways (Steudle, & Frensch, 1996), through transmembrane protein channels by the aquaporins (Agre, Bonhivers, & Borgnia, 1998) and across the plasmodesmata channels between cells by the symplastic pathways. On the other hand, active transmembrane transport is produced by Ca^{2+} pump and requires energy as ATP. In case of high water stress, the homeostatic cell system counteracts the water losses by the aquaporins introducing water in cell by calcium pump (Moraga *et al.*, 2009). Transmembrane transports (active or passive) are affected by the quantity of water molecules adsorbed in the membrane, especially in treatments with high water liquid phase (Fito, Fito, Betoret, Argüelles & Chenoll, 2011).

In Figure 1 it is possible to observe the relation between moisture expressed in dry matter and the surface water activity, for equilibrated and non-equilibrated samples pre-treated at different intensities of pulsed electric field. Taking into account that moisture is an average value of the whole sample and the water activity is a surface value, the non-equilibrated samples are far from the sucrose pure solution curve because they have concentration profiles, however, the equilibrated samples will approximate to the pure sucrose solution curve as a function of the amount of water that they have in liquid phase.

The equilibrated samples seem to be ordered as a function of the intensity of the pretreatment, observing that the higher the pre-treatment the less quantity of water in the liquid phase the samples present.

In order to know the water distribution and to quantify the amount of water molecules that are not in liquid phase, NMR measurements have been performed.

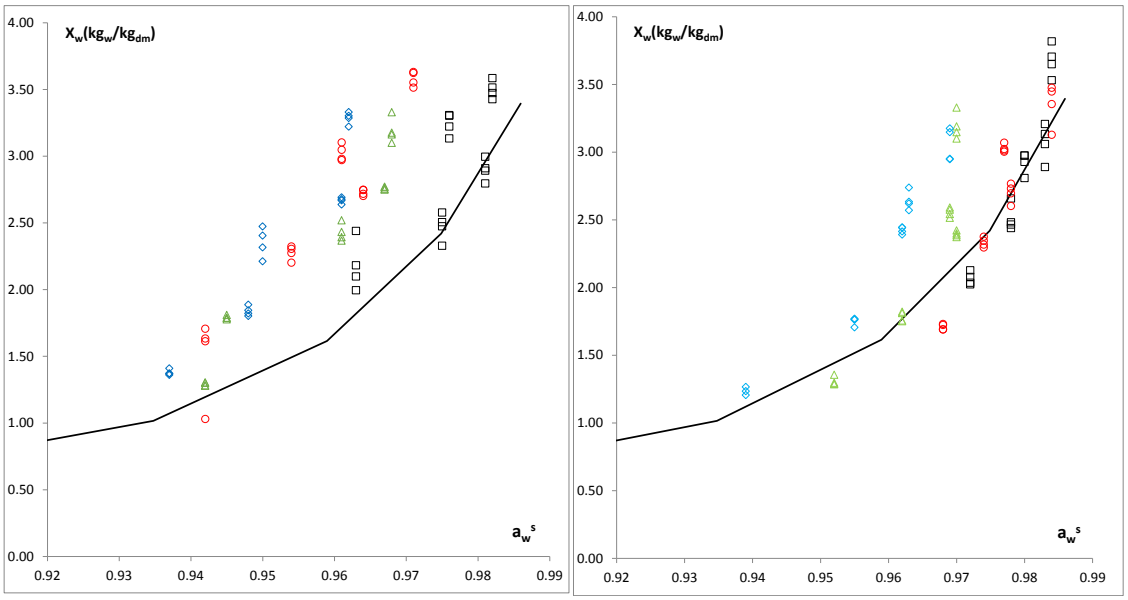

Figure 1. Relation of moisture in dry basis vs. surface water activity of treated samples; left plot: non-equilibrated samples; right plot: equilibrated samples, where: (□) corresponds to no PEF (0 V/cm), (○) 100 V/cm, (△) 250 V/cm, (◇) 400 V/cm and (solid black line) pure sucrose solution.

Figure 2a shows an example of the distribution of T_2-weighted signals obtained by TD-NMR in parenchyma tissue of fresh and pre-treated with PEF at 250 V/cm kiwifruit. Three protons population observed in the non pre-treated samples presented T_2 of 1170, 425, and 53 ms. Moreover, Figure 2b shows the intensity (area of distribution T_2-weight) by the T_2 for each molecular water group and pre-treatment. The smaller the T_2, the lower the mobility of the water molecule, for this reason it is possible to determine the origin of each group of molecules in function of the different motion capacity that the water molecules have in the tissue.
The lower value of T_2 corresponds to water molecules with less mobility, in this group most of water molecules in parenchyma tissue are the molecules subjected to electrical adsorption forces. This group is adsorbed on the cell wall and on the cell membrane (protoplast and tonoplast). The remaining groups might correspond to the different liquid phases that make up the parenchyma, from the interior of the cell mostly occupied by the vacuole (higher T_2 and higher intensity), to the cytoplasm and external liquid phase or intra liquid phase produced in the plasmolization process (intermediate T_2).

PEF treatment caused, for each of the intensities applied, a decrease of average T_2 of vacuole and cytoplasm protons populations. Chemical exchange between water (with a T_2 around 2s) and exchangeable sites of the biopolymers of the structures (with a T_2 of milliseconds) dominates T_2 of these protons populations, as demonstrated for kiwifruit (Panarese *et al.*, 2012) and other fruits (Mauro *et al.*, 2016). The simultaneous shortening of the T_2 of both compartments suggests therefore that in both cases exchangeable protons of carbohydrates induced increase their contribution to the overall protons populations upon PEF treatment, but in minimum sense considering negligible. It is worth noticing that the T_2 decrease was not proportional to the voltage applied, with 100 V/cm giving rise to marginal modifications, and the stronger treatments giving rise to similar and much higher T_2 decreases. The T_2 of each group does not converge to the same value, this suggests that the liquid phase of samples are not mixed, remaining in each compartment.

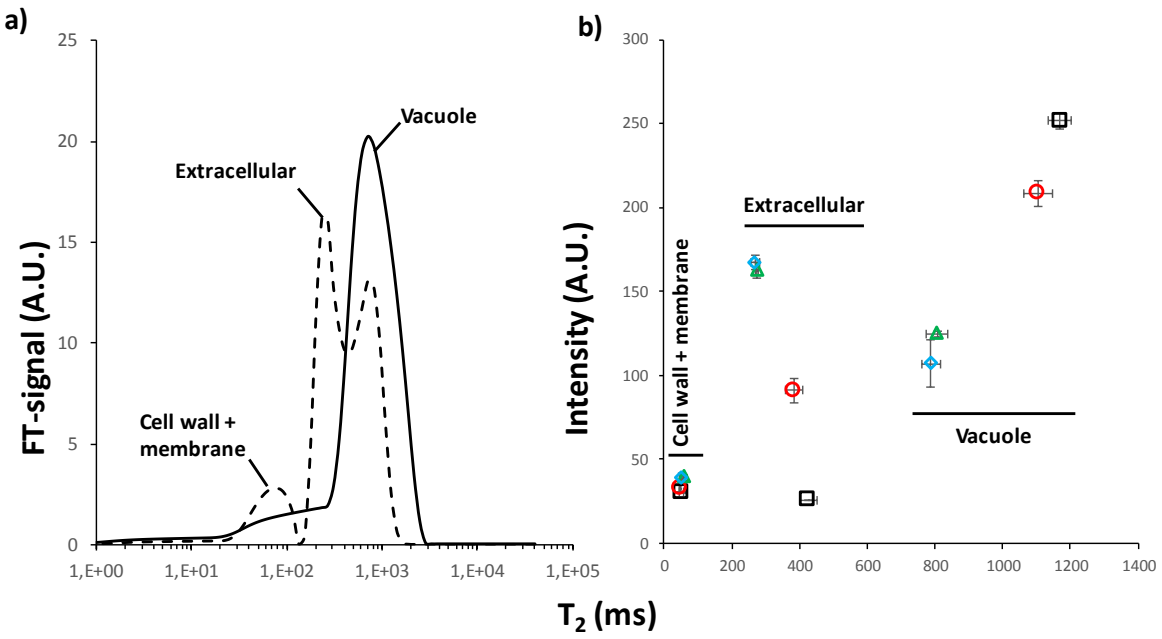

Figure 2. a) T_2-weighted signal distribution, normalized to unitary area, registered on fresh samples treated by PEF at 0 (solid line) and 250 V/cm (dashed line). b) T_2 and intensity of the signals from vacuole, cytoplasm + extracellular space and cell wall + membrane protons at 0 (□), 100 (○), 250 (Δ) and 400 (◊) V/cm for samples before OD treatment. For both T_2 and intensity, bars highlight standard deviation around mean.

It is possible to define a proportionality variable to describe the relation between the intensity of each group of water molecules and overall measured intensity; this relation follows the next equation:

$$r_I^j = \frac{I_j}{I_T} \qquad (2)$$

Where r_I^j is the relative intensity of water group j (1: water adsorbed; 2: external liquid phase, 3: vacuole liquid phase), I_j is the intensity of water group, and I_T is the overall measured intensity.

Figure 3 shows the relative intensity along osmotic treatment for the samples treated with increasing PEF voltage (non-equilibrated and equilibrated samples). Non-equilibrated samples show the state of the three populations of water just after the osmotic dehydration process when the samples present internal profiles; the equilibrated samples show the distribution of water populations when the transports have finished. On the other hand, samples skipping PEF treatment allow observing the fate of the three populations upon osmosis only, while Santagapita *et al.* (2013) showed that the cell wall population was poorly affected by osmotic treatment. In the present work it reached a relative intensity around 20-25% and, consequently, confirming the contribution from extracellular protons suggested by the data obtained with no osmosis applied.

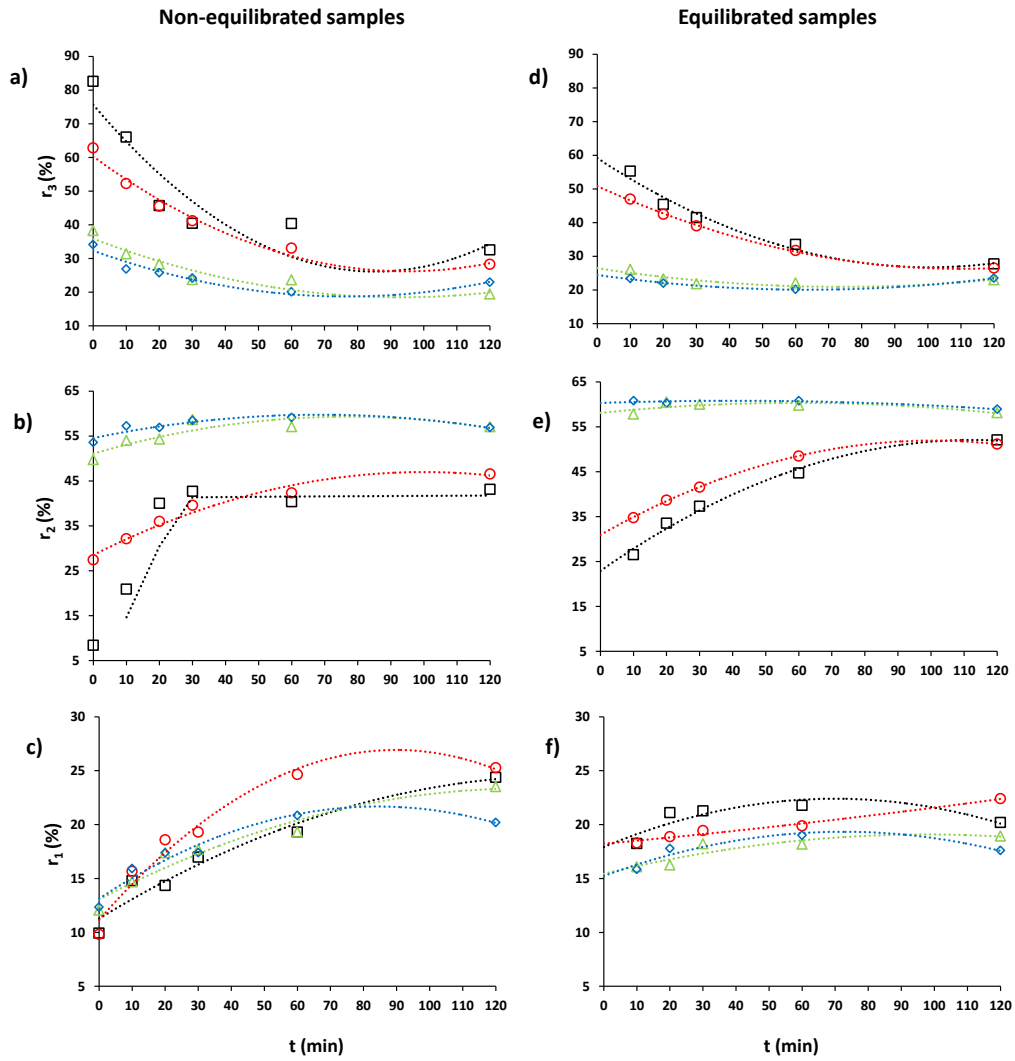

Figure 3. Relative intensity of the three proton populations identified by TD-NMR for non-equilibrated and equilibrated samples, where: (□) corresponds to no PEF (0 V/cm), (○) 100 V/cm, (Δ) 250 V/cm and (◊) 400 V/cm, being a) and d) vacuole, b) and e) cytoplasm and extracellular liquid phase, c) and f) cell wall and membrane.

As it is described by some authors (Lauffer, 1987; Otting & Wuethrich, 1989; Tsukahara, Hibara, Ikeda, & Kitamori, 2007), the intensity is proportional to the induced protons. When induction occurs at a fixed frequency that only affects the protons of a specific molecule, in this case water, the intensity is proportional to the overall number of water molecules present in the tissue. Therefore, the relative intensity will be a parameter of proportionality of the water mass distribution, and the distribution of water will follow the next equation:

$$x_w^j = x_w \cdot r_I^j \qquad (3)$$

Where x_w^j is the water mass fraction of water group j (kg_w in j/kg_T) and x_w is the water mass fraction (kg_w/kg_T). Thus, it is possible to segregate the low mobility water molecules, adsorbed to the surface of the cell matrix, from the rest of water molecules, as follows:

$$X_w^{ADS} = X_w \cdot r_I^1 \quad (4)$$

Where X_w^{ADS} is the adsorbed moisture expressed in dry matter (kg_w/kg_{dm}) and X_w is the moisture expressed in dry matter (kg_w/kg_{dm}).

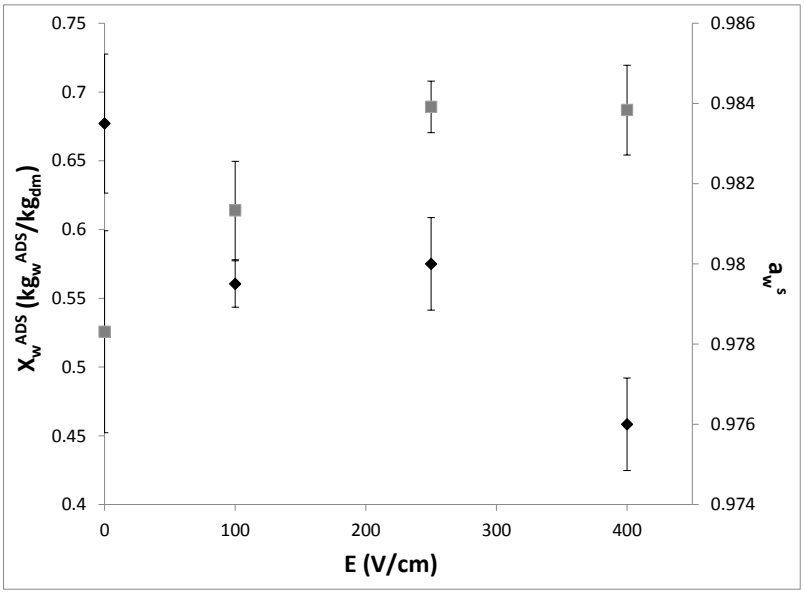

Figure 4. Pre-treated fresh samples (without OD): where adsorbed moisture (■) and surface water activity (♦) at different PEF (V/cm) pre-treatments.

Figure 4 shows the adsorbed moisture of kiwifruit samples at different PEF pre-treatment with regard to the surface water activity. It is possible to observe that PEF pre-treatment produces an increase of adsorbed moisture and a reduction of the water activity. This is because the electric field increases the surface electrical energy of the cell membrane (protoplast and tonoplast) and the cell wall, increasing the surface free energy available for molecular adsorption. This means that the number of layers of adsorbed water molecules increased, reducing the number of water molecules in the liquid phase. For this reason, increasing adsorbed moisture reduces water activity.

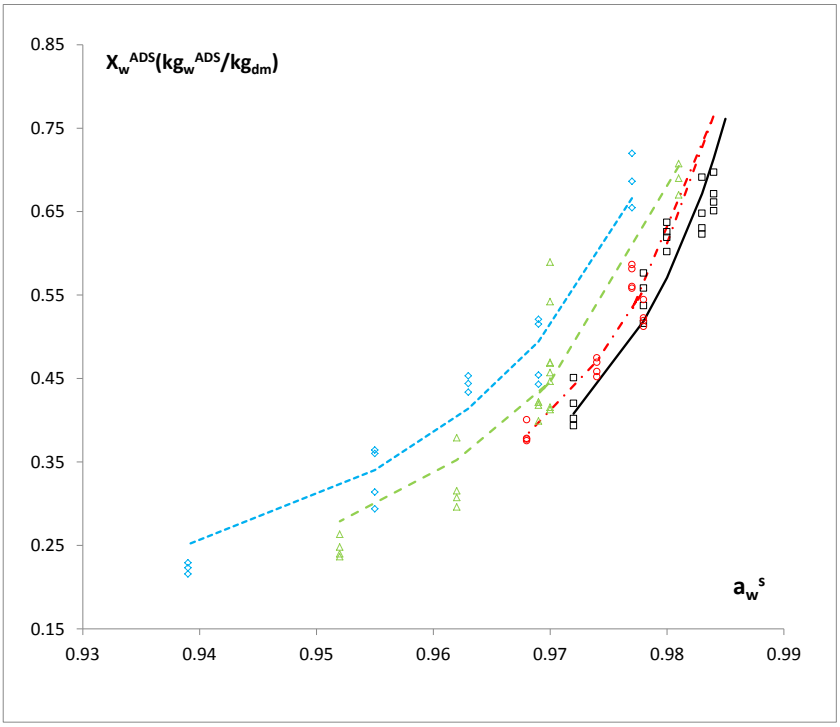

Figure 5. Adsorbed water content of equilibrated samples with regard to the surface water activity at different PEF pre-treatments, where experimental points (□) 0 V/cm, (○) 100 V/cm, (Δ) 250 V/cm and (◊) 400 V/cm and calculated BET model (—) 0 V/cm, (— · —) 100 V/cm, (– –) 250 V/cm and (- -) 400 V/cm.

The moisture and relative intensity were measured after the treatment (non-equilibrated samples) and in equilibrium, thus, the adsorbed moisture of the non-equilibrated samples may undergo variations due to the internal water chemical potential gradients. Nevertheless, the adsorbed moisture of the equilibrated samples may be valid to obtain the sorption isotherm fitted by BET model in the whole range of water activity.

Figure 5 shows the adsorbed moisture with regard to the surface water activity for equilibrated samples fitted by BET model. The correlation coefficients (R^2) obtained adjusting the BET model for each PEF treatment (0, 100, 200 and 400 V/cm) were 0.90, 0.96, 0.92, 0.91 respectively. Moreover, it is possible to observe how the samples are sorted in function of the pre-treatment.

From the adsorbed moisture fitting by BET model, it is possible to obtain two parameters with physic sense: the moisture monomolecular layer (X_{w0}) related with the minimum water adsorbed in the surface of matrix and the C parameter related with the isosteric heat by next equation (Labuza & Altunakar, 2007):

$$Q_c = RT \ln C \tag{5}$$

Where Q_c is the isosteric heat of sorption (kJ/mol), R is ideal gas constant (J/mol K) and T is absolute temperature (K).

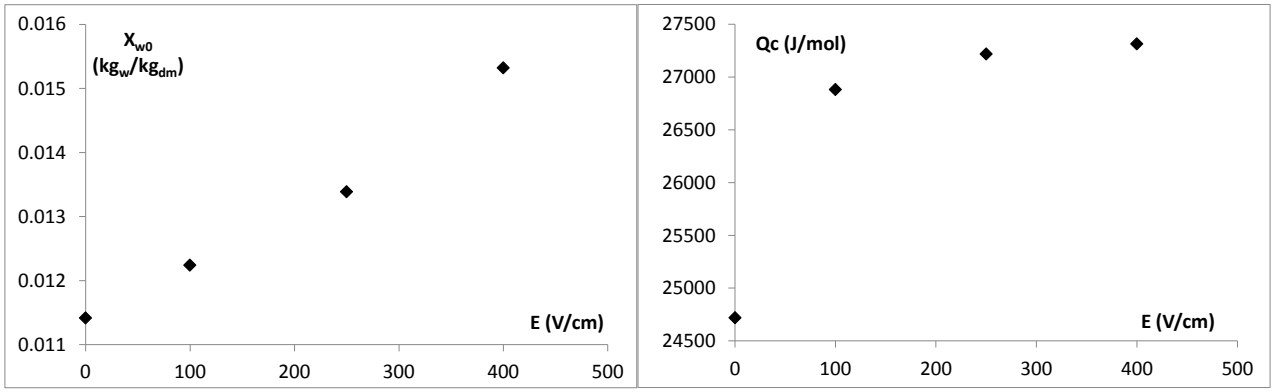

Figure 6. Relationship between the moisture monomolecular layer (X_{w0}) and the Isosteric heat (Q_c) with the PEF pre-treatment.

Figure 6 shows the moisture monomolecular layer and the isosteric heat with regard the electric field applied throughout the tissue. As the figure shows, the electric field charges the surface of the tissue increasing its energy of adsorption or isosteric heat. This fact produces an addition amount of water adsorbed and, therefore, a hydration of the tissue. This induces a reduction of water in the liquid phase and changes in the transmembrane transport mechanisms that are shown in an increase of the water fluxes during the osmotic treatment.

Therefore, the use of NMR to quantify the water distribution in the tissue allows estimating the sorption isotherms of the absorbed moisture in the whole range of water activities; this allows quantifying the electrical energy stored in the tissue in form of energy of adsorption.

4. Conclusions

NMR is a suitable technique for quantifying water molecules according to their situation in the fruit tissue. This technique allows us to obtain the adsorbed water and open the possibility to apply the BET model over the whole range of water activity. It has been demonstrated that the application of electric fields across the plant tissue causes a storage of electrical energy that is converted into free energy to attract and retain water molecules on the surface of membranes and cell walls.

5. Acknowledgements

The authors Urszula Tylewicz and Marco Dalla Rosa want to thank for the financial support provided by funding bodies within the FP7 ERA-Net CORE Organic Plus, and with cofounds from the European Commission. The author Maria Victoria Traffano Schiffo wants to thank the FPI Predoctoral Program of the Universidad Politécnica de Valencia for support her PhD studies,

ERASMUS PRÁCTICAS program to finance her mobility to Italy. The authors Pedro J. Fito, Marta Castro-Giraldez and M. Victoria Traffano-Schiffo acknowledge the financial support from the Spanish Ministerio de Economía, Industria y Competitividad, Programa Estatal de I+D+i orientada a los Retos de la Sociedad AGL2016-80643-R.

6. References

Agre, P., Bonhivers, M., & Borgnia, M. J. (1998). The aquaporins, blueprints for cellular plumbing systems. *Journal of Biological Chemistry*, 273(24), 14659-14662.

Aguiló-Aguayo, I., Downey, G., Keenan, D. F., Lyng, J. G., Brunton, N., & Rai, D. K. (2014). Observations on the water distribution and extractable sugar content in carrot slices after pulsed electric field treatment. *Food Research International*, 64, 18-24.

Ahmed, I., Qazi, I. M., & Jamal, S. (2016). Developments in osmotic dehydration technique for the preservation of fruits and vegetables. *Innovative Food Science & Emerging Technologies*, 34, 29-43.

Amami, E., Vorobiev, E., & Kechaou, N. (2006). Modelling of mass transfer during osmotic dehydration of apple tissue pre-treated by pulsed electric field. *LWT-Food Science and Technology*, 39(9), 1014-1021.

Angersbach, A., Heinz, V., & Knorr, D. (2000). Effects of pulsed electric fields on cell membranes in real food systems. *Innovative Food Science & Emerging Technologies*, 1(2), 135-149.

AOAC. (2000). AOAC, Association of Official Analytical Chemist Official Methods of Analysis. Washington, D.C.

Baier, A. K., Bußler, S., & Knorr, D. (2015). Potential of high isostatic pressure and pulsed electric fields to improve mass transport in pea tissue. *Food Research International*, 76, 66-73.

Borgia, G. C., Brown, R. J. S., & Fantazzini, P. (1998). Uniform-penalty inversion of multiexponential decay data. *Journal of Magnetic Resonance*, 132(1), 65-77.

Brunauer, S., Emmett, P. H., & Teller, E. (1938). Adsorption of gases in multimolecular layers. *Journal of the American Chemical Society*, 60(2), 309-319.

Calderón-Miranda, M. L., González, M. F. S. M., Barbosa-Cánovas, G. V., & Swanson, B. G. (1998). Métodos no térmicos para procesamiento de alimentos: Variables e inactivación microbiana. *Brazilian Journal of Food Technology*, 1, 3-11.

Castro-Giráldez, M., Fito, P. J., & Fito, P. (2011b). Application of microwaves dielectric spectroscopy for controlling long time osmotic dehydration of parenchymatic apple tissue. *Journal of Food Engineering*, 104(2), 227-233.

Castro-Giráldez, M., Tylewicz, U., Fito, P. J., Dalla Rosa, M., & Fito, P. (2011a). Analysis of chemical and structural changes in kiwifruit (Actinidia deliciosa cv Hayward) through the osmotic dehydration. *Journal of Food Engineering*, 105(4), 599-608.

Corrêa, J. L., Pereira, L. M., Vieira, G. S., & Hubinger, M. D. (2010). Mass transfer kinetics of pulsed vacuum osmotic dehydration of guavas. *Journal of Food Engineering*, 96(4), 498-504.

Dellarosa, N., Ragni, L., Laghi, L., Tylewicz, U., Rocculi, P., & Dalla Rosa, M. (2016). Time domain nuclear magnetic resonance to monitor mass transfer mechanisms in apple tissue promoted by osmotic dehydration combined with pulsed electric fields. *Innovative Food Science & Emerging Technologies*, 37, 345-351.

Diamante, L. M., Savage, G. P., & Vanhanen, L. (2012). Optimisation of vacuum frying of gold kiwifruit slices: application of response surface methodology. *International Journal of Food Science & Technology*, 47(3), 518-524.

Faridnia, F., Burritt, D. J., Bremer, P. J., & Oey, I. (2015). Innovative approach to determine the effect of pulsed electric fields on the microstructure of whole potato tubers: Use of cell viability, microscopic images and ionic leakage measurements. *Food Research International*, 77, 556-564.

Fito, P., Fito, P. J., Betoret, N., Argüelles, A. & Chenoll, C. (2011).Thermodynamic approach to equilibrium isotherms in salted structured food. *Journal of Food Process Engineering*, 34, 623–638.

Labuza, T. P., Altunakar, B. (2007). *Water Activity Prediction and Moisture Sorption Isotherms.* In G. V. Barbosa-Cánovas, A. J. Fontana, S. J. Schmidt, & T. P. Labuza (Eds.), Water Activity in Foods: Fundamentals and Applications (Vol. 109-154). Iowa, USA: IFT Press and Blackwell Publishing.

Lauffer, R. B. (1987). Paramagnetic metal complexes as water proton relaxation agents for NMR imaging: theory and design. *Chemical Reviews*, 87(5), 901-927.

Li, H., Zhao, C., Guo, Y., An, K., Ding, S., & Wang, Z. (2012). Mass transfer evaluation of ultrasonic osmotic dehydration of cherry tomatoes in sucrose and salt solutions. *International Journal of Food Science & Technology*, 47(5), 954-960.

Liu, Z. W., Han, Z., Zeng, X. A., Sun, D. W., & Aadil, R. M. (2016). Effects of vesicle components on the electro-permeability of lipid bilayers of vesicles induced by pulsed electric fields (PEF) treatment. *Journal of Food Engineering*, 179, 88-97.

Mauro, M. A., Dellarosa, N., Tylewicz, U., Tappi, S., Laghi, L., Rocculi, P., & Dalla Rosa, M. (2016). Calcium and ascorbic acid affect cellular structure and water mobility in apple tissue during osmotic dehydration in sucrose solutions. *Food Chemistry*, 195, 19-28.

Meiboom, S., & Gill, D. (1958). Modified spin-echo method for measuring nuclear relaxation times. *Review of Scientific Instruments*, 29(8), 688-691.

Moraga, M. J., Moraga, G., Fito, P. J., & Martínez-Navarrete, N. (2009). Effect of vacuum impregnation with calcium lactate on the osmotic dehydration kinetics and quality of osmodehydrated grapefruit. *Journal of Food Engineering*, 90(3), 372-379.

Nowacka, M., Tylewicz, U., Laghi, L., Dalla Rosa, M., & Witrowa-Rajchert, D. (2014). Effect of ultrasound treatment on the water state in kiwifruit during osmotic dehydration. *Food Chemistry*, 144, 18-25.

Otting, G., & Wuethrich, K. (1989). Studies of protein hydration in aqueous solution by direct NMR observation of individual protein-bound water molecules. *Journal of the American Chemical Society*, 111(5), 1871-1875.

Panarese, V., Laghi, L., Pisi, A., Tylewicz, U., Dalla Rosa, M., & Rocculi, P. (2012). Effect of osmotic dehydration on Actinidia deliciosa kiwifruit: A combined NMR and ultrastructural study. *Food Chemistry*, 132(4), 1706-1712.

Rastogi, N. K., Raghavarao, K. S. M. S., Niranjan, K., & Knorr, D. (2002). Recent developments in osmotic dehydration: methods to enhance mass transfer. *Trends in Food Science & Technology*, 13(2), 48-59.

Santagapita, P. R., Tylewicz, U., Panarese, V., Rocculi, P., & Dalla Rosa, M. (2016). Non-destructive assessment of kiwifruit physico-chemical parameters to optimise the osmotic dehydration process: A study on FT-NIR spectroscopy. *Biosystems Engineering*, 142, 101-109.

Santagapita, P., Laghi, L., Panarese, V., Tylewicz, U., Rocculi, P., & Dalla Rosa, M. (2013). Modification of transverse NMR relaxation times and water diffusion coefficients of kiwifruit pericarp tissue subjected to osmotic dehydration. *Food and Bioprocess Technology*, 6(6), 1434-1443.

Saulis, G. (2010). Electroporation of cell membranes: the fundamental effects of pulsed electric fields in food processing. *Food Engineering Reviews*, 2(2), 52-73.

Steudle, E., & Frensch, J. (1996). Water transport in plants: role of the apoplast. *Plant and Soil*, 187(1), 67-79.

Toepfl, S., Heinz, V., & Knorr, D. (2005). *Overview of pulsed electric field processing for food.* In D. W. Sun (Ed.), Emerging technologies for food processing (pp. 69–99). Oxford, UK: Elsevier.

Traffano-Schiffo, M. V., Tylewicz, U., Castro-Giraldez, M., Fito, P. J., Ragni, L., & Dalla Rosa, M. (2016). Effect of pulsed electric fields pre-treatment on mass transport during the osmotic dehydration of organic kiwifruit. *Innovative Food Science & Emerging Technologies*, 38, 243-251.

Tsukahara, T., Hibara, A., Ikeda, Y., & Kitamori, T. (2007). NMR study of water molecules confined in extended nanospaces. *Angewandte Chemie International Edition*, 46(7), 1180-1183.

Tylewicz, U., Panarese, V., Laghi, L., Rocculi, P., Nowacka, M., Placucci, G., & Dalla Rosa, M. (2011). NMR and DSC water study during osmotic dehydration of Actinidia deliciosa and Actinidia chinensis kiwifruit. *Food Biophysics*, 6(2), 327-333.

Wiktor, A., Śledź, M., Nowacka, M., Chudoba, T., & Witrowa-Rajchert, D. (2014). Pulsed electric field pretreatment for osmotic dehydration of apple tissue: Experimental and mathematical modeling studies. *Drying Technology*, 32(4), 408-417.

Artículo 9

Traffano-Schiffo, M. V., Laghi, L., Castro-Giraldez, M., Tylewicz, U., Romani, S., Ragni, L., Dalla Rosa, M., & Fito, P. J. (2017). Osmotic dehydration of organic kiwifruit pre-treated by pulsed electric fields: Internal transport and transformations analyzed by NMR. *Innovative Food Science and Emerging Technologies,* 41, 259-266.

OSMOTIC DEHYDRATION OF ORGANIC KIWIFRUIT PRE-TREATED BY PULSED ELECTRIC FIELDS: INTERNAL TRANSPORT AND TRANSFORMATIONS ANALYZED BY NMR

Maria Victoria Traffano-Schiffo[a], Luca Laghi[b,c], Marta Castro-Giraldez[a], Urszula Tylewicz[b], Santina Romani[b,c], Luigi Ragni[b,c], Marco Dalla Rosa[b,c], Pedro J. Fito[a]*

[a] Instituto Universitario de Ingeniería de Alimentos para el Desarrollo, Universitat Politecnica de Valencia, Camino de Vera s/n, 46022 Valencia, Spain

[b] Department of Agricultural and Food Sciences, University of Bologna, Piazza Goidanich 60, 47521 Cesena, Italy

[c] Interdepartmental Centre for Agri-Food Industrial Research, University of Bologna, Via Quinto Bucci 336, 47521 Cesena, Italy

*author for correspondence: pedfisu@tal.upv.es

ABSTRACT

This work analyzes the effect of Pulsed Electric Fields (PEF) as a pre-treatment of the osmotic dehydration (OD) of kiwifruit (*Actinidia deliciosa cv Hayward*) in the internal structure and in the internal water transport. PEF pre-treatments were done using three PEF intensities (100, 250 and 400 V/cm) and analyzed by TD-NMR. The OD was carried out by immersing the samples in 61.5% sucrose solution at 25 ºC. The application of a PEF pre-treatment before the OD produces a process of plasmolysis proportional to the electric field applied. It is because the PEF removes the mobile charges of the medium, such as electrolytes, organic acids, aminoacids; Ca^{+2} is the major culprit of the plasmolysis because it fixes some of the junctions of the microtubules between the cell wall and the membrane. Therefore, a previous plasmolysis produces an increase in the apoplastic transport increasing the rate of dehydration.

Keywords: Kiwifruit, Pulsed Electric Fields, Osmotic dehydration, TD-NMR, Water distribution, Plasmolysis.

Industrial relevance

This research describes the effect of the PEF pre-treatment of osmotic dehydration in the microstructure and in the internal water liquid phases transports of the kiwifruit tissue by using TD-NMR. The results of this research have demonstrated that the application of an electric field prior to the osmotic dehydration produces a process of plasmolysis more the

greater the electric field applied, due to the elimination of the mobile charges of the medium and mainly affecting the internal transports. Therefore, PEF pre-treatment accelerate the OD treatment preserving the structure and consequently remaining the life cycles, necessaries to obtain a long shelf life of the product. It has been demonstrated the useful of the TD-NMR as a technique able to analyzed the effect of PEF at a microstructural degree.

NOTATION

x_i	mass fraction of i chemical specie (kg_i kg_T^{-1})
T_2	spin-spin or proton transverse relaxation time
r_I	relative intensities
M	mass (kg)
S	surface of samples (m^2)
r	radius (m)
X_{w0}^{ADS}	monomolecular moisture layer (kg_w kg_{dm}^{-1})
N_A	avogadro number ($6.022 \cdot 10^{23}$ molecules mol^{-1})
M_w	molecular weight of water (18 g mol^{-1})
t	treatment time
I	Intensity
E	electric field (V cm^{-1})

Subscripts

w	water
T	total
0	raw sample
1	sample after the pre-treatment by PEF
i	internal
j	any chemical species

Superscripts

j	specific group of water molecules j
t	treatment time (s)
0	initial time
ELP	extracellular liquid phase
ILP	intracellular liquid phase
ADS	adsorbed water

1. Introduction

Cellular structure is considered as a complex organized system where flows are carried out by different solutes or solvents transports systems. Based on the free energy gradients, commonly known as passive transports, symplastic, aplopastic and aquaporins transmembrane transports are involved. Firstly, cells are interconnected by plasmodesmatas which led to generate symplastic transports across them. In the extracellular space, the fluxes are produced by apoplastic pathways (Marcotte, Toupin, & Le Maguer, 1991) and finally, the transmembrane transport is characterized by the exchange between intra and extracellular spaces by protein channels, called aquaporins (Agre *et al.*, 2002; Maurel & Chrispeels, 2001). In contrast, when the flows occur in the opposite direction of the free energy gradients, they are produced by protein channels and they require energy consumption as adenosine triphosphate (ATP) (Moraga, Moraga, Fito, & Martínez-Navarrete, 2009). The main active pumps are Ca^{2+}, Na^+ and Na^+/K^+, which are the responsible of the transport of water, sucrose and electrolytes (Traffano-Schiffo *et al.*, 2016).

Taking into account the water content, Tylewicz, Fito, Castro-Giráldez, Fito, & Dalla Rosa (2011) explain that the water distribution in fresh kiwifruit can be segregated in adsorbed water (solid matrix) and liquid water. In turn, for parenchymatic tissue, the liquid water can be divided into intra and extracellular liquid phases. During osmotic dehydration (OD) treatment, the water distribution of the cellular structure changes due to mass transfer phenomena, which are

generated as a consequence of the water and sucrose chemical differences between the tissue and the osmotic solution (Traffano-Schiffo et al., 2016; Khin, Zhou, & Perera, 2006, Castro-Giráldez, Tylewicz, Fito, Dalla Rosa, & Fito, 2011; Castro-Giráldez, Fito, Dalla Rosa, & Fito, 2011). From the contact of the fruit tissue with the osmotic solution, the semipermeable membranes, plasma membrane and the tonoplast are forced to separate, due to the water losses from the vacuoles, starting the process known as plasmolysis, characterized by the loss of the turgor pressure (Lang, Sassmann, Schmidt, & Komis, 2014; Lang, Barton, & Overall, 2004). Plasmolysis occurs in two stages: partial and the complete plasmolysis. Partial plasmolysis is produced when the plasma membrane starts to detach from the cell wall and the complete plasmolysis occurs when the complete separation of the protoplast is produced (Seguí, Fito, & Fito, 2012).

For many years, OD has been extensively studied around the world for the partial dehydration of fruits and vegetables; however, it presents some limitations such as the low dehydration rate and the high solute content in the final product. Therefore, the use of pre-treatment such as Pulsed Electric Fields (PEF) has been reported to facilitate water removal and to improve the quality of the dried products (Dermesonlouoglou, Zachariou, Andreou, & Taoukis, 2016; Dellarosa et al., 2016; Barba et al., 2015).

PEF is a non-thermal technology which involves the application of short and repeated voltage pulses to a biological tissue placed between two electrodes (Gürsul, Gueven, Grohmann, & Knorr, 2016); it induces changes and reorganization in the electric conformation of the cell membrane (Baier, Bußler, & Knorr, 2015), modifying the normal fluxes during drying process when it is used as a pre-treatment.

Time Domain Nuclear Magnetic Resonance (TD-NMR) is a non-destructive technique able to determine the spin-spin or transverse relaxation (T_2) of protons and the intensity of the signal, differentiating extracellular space, vacuoles and solid matrix (Santagapita *et al.*, 2013). TD-NMR is considered as one of the most powerful techniques able to follow the water distribution in cellular tissues, thus, it is necessary for describe the driving forces that promote the water fluxes.

The aim of this research was to determine the effect of PEF pre-treatment in the microstructure and in the internal water transport throughout an osmotic treatment of kiwifruit in hypertonic sucrose solution.

2. Material and methods

Organic kiwifruits (*Actinidia deliciosa* cv ‘‘*Hayward*’’) with the same ripeness and similar size were bought on a supermarket located in Cesena (Italy) and kept refrigerated at 4 ± 1 ºC until use. The fruits were tempered at 25 ºC, peeled and cylinders (8 mm diameter and 10 mm length) were obtained from the outer pericarp, avoiding the core, the inner pericarp and the seeds. The initial solute content of the fruits used were 13 ± 1 ºBrix.

Fresh kiwifruits were characterized by mass, volume, solutes (ºBrix), water activity (a_w), moisture (x_w) and TD-NMR by quadruplicate. 12 sample cylinders were used for each treatment (total number of treated samples of 576). They were placed inside the PEF chamber avoiding free spaces between them and subjected to different electric fields strengths. Immediately after, the samples were weighed and introduced into the osmotic dehydration solution. According to previous

results, the selected OD treatment times were 0, 10, 20, 30, 60 and 120 min (Traffano-Schiffo *et al.*, 2016).
Due to the fact that the samples after treatments show concentration profiles, another batch of samples were treated and equilibrated at 4 °C during 24 hours in decagon containers closed with parafilm®. Finally, mass, volume, solute content (°Brix), a_w, x_w and TD-NMR were measured as final determinations for treated and equilibrated samples. In addition, at each osmotic time, an aliquot of sucrose solution was taken to measure a_w and solute content.

2.1. PEF treatment

Pulsed electric field treatments were applied to the samples using monopolar pulse generator equipment based on MOSFET technology and capacitors as energy tanks (Dellarosa *et al.*, 2016). The cylinders of organic kiwifruit were placed in a rectangular treatment chamber avoiding free spaces between them. The chamber was equipped with two stainless steel electrodes (20 x 20 mm^2) with a separation between them of 30 mm and filled with 5 mL of tap water with an electrical conductivity of 328 ± 4 µS/cm at 25 °C.
PEF pre-treatments were done by applying three different pulsed electric fields (100, 250 and 400 V/cm at 50 Hz) with near-rectangular shape pulses, a train of 60 pulses, a fixed pulse width of 100 ± 2 µs and a repetition time of 10.0 ± 0.1 ms.

2.2. Osmotic dehydration treatment

The osmotic solution at 61.5% (w/w) was prepared with commercial sucrose and distilled water at 25 °C. Samples were immersed into the sucrose solution maintaining a relationship of 1:4 (w/w) between the fruit and the solution.

2.3. Analytical determinations

A dew point Hygrometer Decagon (Aqualab™, series 3 TE) was used for measuring the water activity, with a precision ± 0.003. Mass was determined by using a Kern balance ABS 320-4N (± 0.0001) (KERN & SOHN GmbH, Germany).
The analysis of the moisture was accomplished following the AOAC Method 934.06, 2000.
Sugar content was determined by measuring the refractometric index with a digital refractometer (KRÜSS Optronic© GmbH, Germany) calibrated with distilled water at 25 °C. The sample was pressed in order to extract the external liquid phase. Solute content was measured by refractometry of both kiwifruit samples and osmotic solution after the treatments.
Analytical determinations described above were obtained by quadruplicate.

2.4. TD-NMR measurements

Proton transverse relaxation time (T_2) decay was measured for each sample by applying the CPMG pulse sequence (Meiboom & Gill, 1958), using a Bruker 'The Minispec' spectrometer

(Bruker Corporation, Germany) operating at 20 MHz, as described by Dellarosa *et al.* (2016). Each measurement comprised 32000 echoes, with an interpulse spacing of 0.08 ms and a recycle delay of 10 s, which allowed the measurement of proton decays included between 1 and 3000 ms and avoided sample overheat. Each acquisition was performed over 8 scans giving rise to a total time of analysis around 90 s. The registered spectra were normalized to unitary area and analyzed by UpenWin software (Borgia, Brown, & Fantazzini, 1998) to give quasi-continuous distributions of relaxation time. The number of output relaxation times, sampled logarithmically in the 1–3000 ms range, was set to 100. To obtain quantitative information from the T_2-weighted decay curves, signals were fitted using a discrete multi-exponential curve. The fitting was run using the 'Levenberg–Marquardt nonlinear least squares' algorithm implemented in 'R' software (R Foundation for Statistical Computing, Austria). Unlike Santagapita *et al.* (2013), the optimum number of exponential curves for each tested treatment was found to be three, without removing any initial T_2 weighted point.

2.5. Low-temperature scanning electron microscopy (Cryo-SEM)

Microstructure was analyzed by Cryo-SEM. A Cryostage CT-1500C unit (Oxford Instruments, Witney, UK), coupled to a Jeol JSM-5410 scanning electron microscope (Jeol, Tokyo, Japan). The sample was immersed in N_2 slush (-210 °C) and then quickly transferred to the Cryostage at 1 kPa where sample fracture took place. Sublimation (etching) was carried out at -95 °C. The final point was determined by direct observation under the microscope, working at 5 kV. Then, once again in the Cryostage unit, the sample was coated with gold in vacuum (0.2 kPa) applied for 3 min, with an ionization current of 2 mA. The observation in the scanning electron microscope was carried out at 20 kV, at a working distance of 15 mm and temperature ≤ -130 °C.

4. Results and discussion

Fruit tissue, such as kiwifruit, is composed by parenchymatic and vascular tissues, where cells with big vacuoles coexist with vascular cells. This system is full of chemical species charged, with capacity to orientate and move with an external electric field. Moreover, these compounds, with high electric activity, are responsible of part of the cell pathways and metabolisms. Therefore, any electric disturb in the fruit tissue produces high disorder in the cell functionality. Moreover, biological cells are delimited by a phospholipid bilayer membrane (protoplast and tonoplast), which separates the internal liquid phase from a completely different external medium. Despite there is an electric equilibrium at both sides of the bilayer, the concentration and nature of the charged compounds are different (Bezanilla, 2008). When a biological tissue is subjected to an external electric field, it induces changes in the electric conformation of the bilayer and in the involved chemical species (Traffano-Schiffo *et al.*, 2016). Therefore, the different liquid mediums and the solid matrix suffer transformations with the application of external electric fields.

Table 1 shows the main chemical species of kiwifruit with capability to orientate and migrate when an external electric field at low frequency is applied. These species are: electrolytes with

biological activity, responsible of the active transport pumps and bonds of the middle lamella; aminoacids, part of proteins channels or passive transport pumps; chlorophylls, carotenoids and anthocyanins, greatly charged antioxidant compounds with functional activity and organic acids, which regulate de pH of the fruit and play an important role in the respiration pathway. These quantities of different chemical species, with different electric nature, shows the complexity in the explanation of the effects in the kiwifruit tissue affected by an external electric field.

In order to understand the correct functionality of the biological tissue under the effect of an external electric field, it is necessary to know the involved metabolic transports. Figure 1a shows a schematic representation of the cellular transports. Inside the cellular tissue, fluxes occur by different pathways: apoplastic, symplastic and transmembrane (aquaporins) transports or passive transports, produced by free energy gradients and the transmembrane transport or active transport, which is based on proteins channels and with ATP consumption (Johansson, Karlsson, Johanson, Larsson, & Kjellbom, 2000). Previously, it has been demonstrated that the application of an external electric field through the vegetal tissue induces compositional changes (removing part of the native electrolytes such as Ca^{2+} and Na^{+}) and, as a consequence, the transmembrane active transports are affected. The main affected transmembrane active transports are: Ca^{2+} pump which is the responsible to maintain the homeostatic cellular system (water transport) and Na^{+} pump, responsible of sucrose transmembrane transport (Traffano-Schiffo *et al.*, 2016).

Table 1. Main chemical species of fruit tissue that can be affected by the PEF.

Chemical group	Specie	Biological activity	Position	Macroscopic changes	Reference
Electrolytes	K^{+}	Secondary signal, active transmembrane pump	Intracellular, Extracellular liquid phase and membrane	Nutritional Textural and nutritional Functional activity	Traffano-Schiffo *et al.*, 2016 Sivakumaran, Huffman, Sivakumaran, & Drummond, 2016
	Na^{+}				
	Mg^{2+}	Part of the chlorophyll complex			Park *et al.*, 2011 Bohn, Walczyk, Leisibach & Hurrell, 2004
	Ca^{2+}	Calcium bridges in the middle lamella Bridges in microtubules (actin microfilaments)			Tarchevsky & Marchenko, 1991 Lang *et al.*, 2014
Aminoacids	Arg Asp Glu	Protein channel Products of the metabolic γ-aminobutyrate conversion Microtubules in cell structure	Free, cell membrane and tonoplast	Maillard browning, nutritional value and taste	Ma *et al.*, 2017; Snowden, Thomas, Baxter, Smith, & Sweetlove, 2015; Keutgen, & Pawelzik, 2008; Castaldo *et al.*, 1992
Chlorophylls	Chlorophyll	O_2 transporter, main	Liquid phase	Color, functional	Park *et al.*, 2013; Park et a.,

	a Chlorophyll b	role in photosynthesis	and Chloroplast	activity	2016; Montefiori McGhie, Costa, & Ferguson, 2005; Cano & Marin, 1992
Carotenoids	Neolutein β-carotene	Secondary role in photosynthesis	Chloroplast and chromoplast	Color, chloroplast membrane stabilizer, source of vitamin A, antioxidant capacity	Park *et al.*, 2013; Havaux, 1998; Ampomah-Dwamena *et al.*, 2009; Cano & Marin, 1992; Dorai, Papadopoulos, & Gosselin, 2001
Organic acids	Citric acid Malic acid Quinic acid Ascorbic acid	Krebs cycle intermediate; part of cytosolic pyruvate metabolism Fruit maturity Antioxidant, enzyme Cofactor, electron transport, chloroplast activity	Extra and Intracellular liquid phases	Antioxidant Acidity, flavor Sugar/acid balance, flavor Bioactive compound	Sivakumaran *et al.*, 2016; Famiani, Battistelli, Moscatello, Cruz-Castillo, & Walker, 2015 Khan *et al.*, 2013; Nishiyama, Fukuda, Shimohashi, & Oota, 2008 Marsh, Boldingh, Shilton, & Laing, 2009 Barboni, Cannac, & Chiaramonti, 2010; Cassano, Donato, Conidi, & Drioli, 2008

Figure 1a shows the schematic diagram of a plant cell tissue where it is possible to observe the different active and passive transports that can be produced. These transports are classified by the extracellular transport (apoplastic), the transport between cells or intracellular (symplastic) and the transmembrane that communicates both phases. These spaces are described by their corresponding liquid phases, extracellular (ELP) and intracellular (ILP). Figure 1b shows two micrographs obtained by Cryo-SEM, the upper picture shows raw parenchyma tissue of kiwifruit and the lower one shows partially dehydrated parenchymal tissue with symptoms of plasmolysis.
Figure 1c shows examples of the distribution of T_2-weighted signals obtained by TD-NMR in parenchyma tissue of kiwifruit in the present research. The three protons populations that were observed in the non pre-treated samples had T_2 or relaxation times of 1170, 425 and 53. The smaller the T_2, the lower the mobility of the molecule with the induced proton is, so that it is possible to determine the origin of each group of molecules in function of the different motion capacity of water molecules in the tissue. The lower value of T_2 corresponds to water molecules with less mobility, water molecules subjected to electrical adsorption forces. This group is adsorbed on the cell wall and on the cell membrane (protoplast and tonoplast), thus it can be considered the entire adsorbed water of tissue. The remaining groups might correspond to the different liquid phases that make up the parenchyma, from the interior of the cell mostly occupied by the vacuole (higher T_2 and higher intensity), named ILP, and external liquid phase

(intermediate T_2), named ELP. Therefore, the intensities measured in NMR, can be divided in three groups of water molecules; Adsorbed, ELP and ILP. They are shown in Table 2.

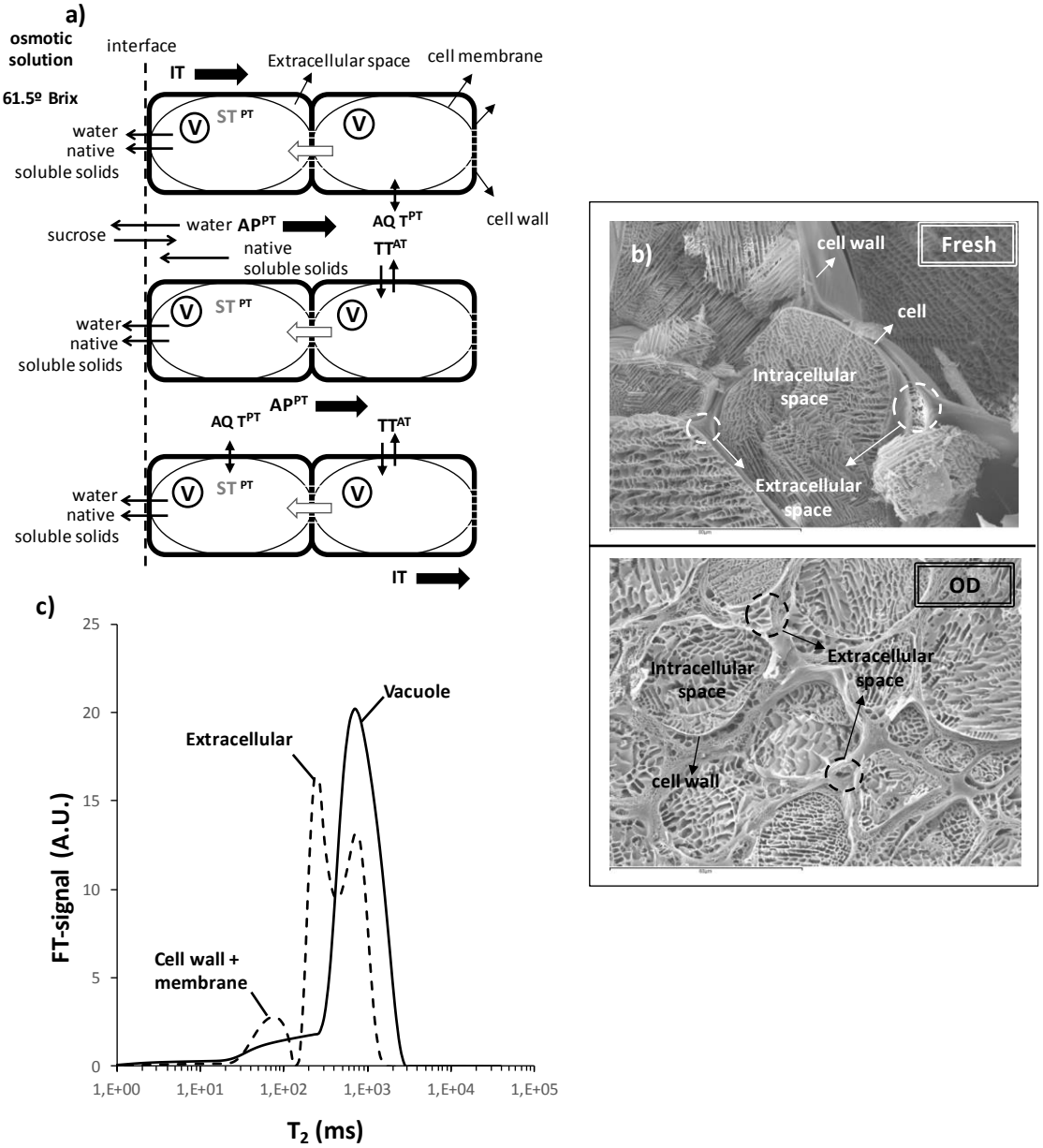

Figure 1. a) Schematic representation of system and the cellular transports during osmotic dehydration treatment (adapted from Traffano-Schiffo *et al.*, 2016), b) Cryo-SEM observation of fresh (750x) and 30 min osmodehydrated kiwifruit tissue (1000x), c) T2-weighted signal distribution, normalized to unitary area, registered on fresh samples treated by PEF at 0 (black solid line) and 250 V/cm (black dashed line) samples before OD treatment (adapted from Traffano-Schiffo *et al.*, 2017). PT: Passive transport, AT: Active transport, V: Vacuole, IT: Internal transport, ST: Symplastic transport, AP: Apoplastic transport, AQ T: Aquaporins transmembrane transport (water) and TT: Transmembrane transport.

As previously described by different authors (Nakashima, 2001; Muller, Scrivener, Gajewicz, & McDonald, 2013; Traffano-Schiffo *et al.*, 2017), it is possible to divide the water molecules into

groups according to their situation in the tissue using a value of proportionality to the intensity measured by NMR as it is shown in Table 2. The relative intensities (r_I^j) of a specific group of water molecules (j) along OD treatment can be defined as the relationship between the intensity of each group of water molecules and the overall measured intensity. This parameter let to obtain the water distribution (x_w^j) of a specific group of water molecules (j) as follows:

$$x_w^j = x_w \cdot r_I^j \tag{1}$$

Where x_w^j is the water mass fraction of water group j ($kg_{w\ in\ j}/kg_T$) and x_w is the water mass fraction (kg_w/kg_T).

Table 2. Intensity values of the samples obtained by TD-NMR during OD treatment (I^{ADS}: intensity of water adsorbed; I^{ELP}: intensity of extracellular liquid phase; I^{ILP}: intensity of internal liquid phase).

E (V/cm)		OD time (min)					
		0	10	20	30	60	120
0	I^{ADS}	31 ± 4	41.78 ± 0.91	45 ± 2	50 ± 8	59 ± 2	74 ± 2
	I^{ELP}	25 ± 8	58 ± 5	103 ± 6	132 ± 5	120 ± 9	131 ± 11
	I^{ILP}	251 ± 4	183 ± 12	165 ± 9	125 ± 11	124 ± 12	107 ± 7
100	I^{ADS}	33 ± 2	49 ± 3	59 ± 1	61 ± 3	73 ± 5	77 ± 5
	I^{ELP}	91 ± 7	101 ± 12	115 ± 8	126 ± 11	126 ± 14	123 ± 6
	I^{ILP}	208 ± 7	172 ± 13	146 ± 7	131 ± 13	96 ± 8	104 ± 8
250	I^{ADS}	39 ± 2	48 ± 2	56 ± 3	54 ± 6	57 ± 4	70 ± 12
	I^{ELP}	163 ± 5	175 ± 9	174 ± 9	184 ± 5	165 ± 10	169 ± 6
	I^{ILP}	125 ± 2	101 ± 7	91 ± 10	71 ± 8	70 ± 2	57 ± 8
400	I^{ADS}	39 ± 3	50.8 ± 0.4	53 ± 6	54 ± 5	64 ± 2	60 ± 6
	I^{ELP}	167 ± 4	183 ± 9	174 ± 9	183 ± 6	181 ± 2	170 ± 5
	I^{ILP}	107 ± 14	86 ± 5	79 ± 8	75 ± 7	61 ± 6	68 ± 7

In order to understand the structural transformations induced by the PEF pre-treatment it is possible to estimate the water mass variation of each liquid phase, considering the initial state as non PEF pre-treated samples and the state after the PEF pre-treatment. In this sense, the next equation estimates the water mass variation after the PEF:

$$\Delta M_w^j = \frac{M_1 x_{w1}^j - M_0 x_{w0}^j}{M_0} \tag{2}$$

Where M represents the mass (g), x the mass fraction (kg/kg), the subscripts w represents the water, 0 and 1 represent the samples before and after the pre-treatment by PEF (V/cm) respectively, and the superscript j corresponds to a specific group of molecules (ELP, ILP, ADS or overall).

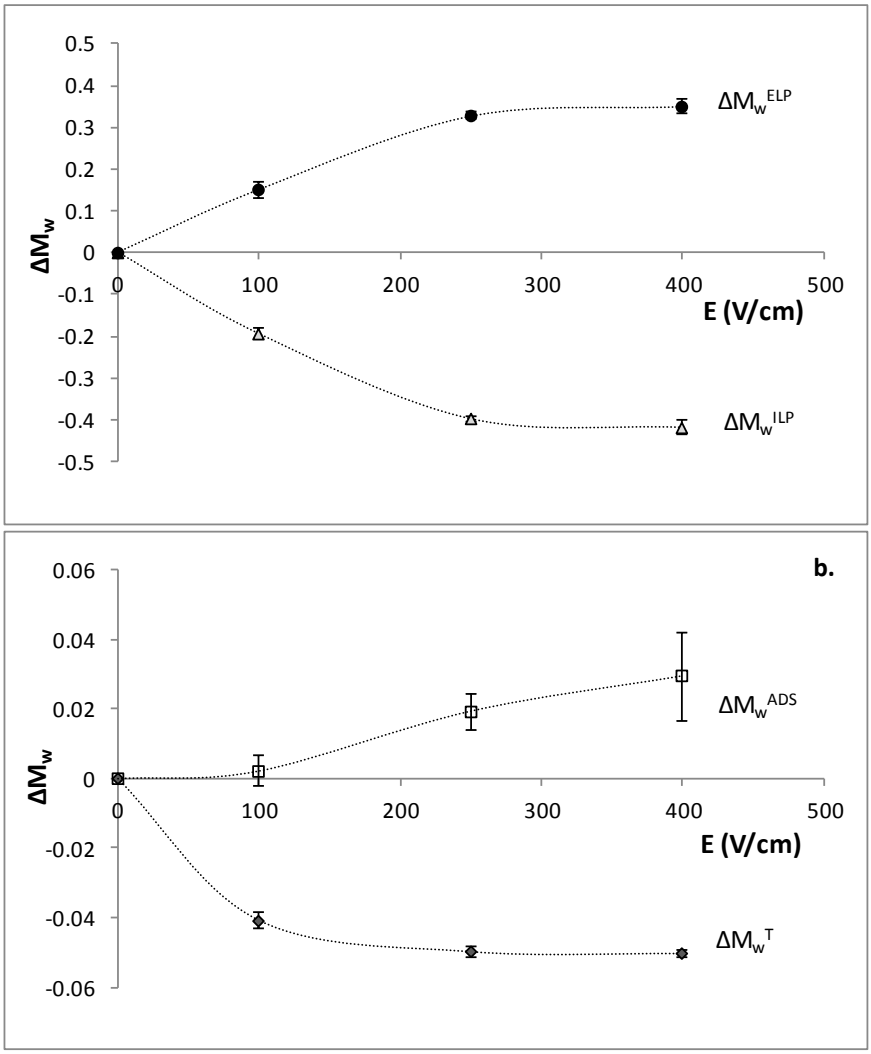

Figure 2. Water mass variation a. (●) extracellular liquid phase (ELP), (▲) intracellular liquid phase (ILP) and b. (□) adsorbed water (ADS) and (♦) total mass (T) variation at different PEF treatments (V/cm).

Figure 2a shows the water mass variation in the intracellular space and in the extracellular space after the PEF treatment, where it is possible to observe how the water mass variation of intracellular space decreases proportionally to the increase of the water mass variation of extracellular space when the electric field grows. Considering that the composition of both phases is different, since the relaxation times are different, the only possible explanation for this liquid phase exchange is that the electric field induces a process of plasmolysis. In interphase cells, plasmolysis (which is the disruption of the cell wall—plasma membrane—cortical cytoskeleton continuum) is expected to exert the strongest impact on cortical microtubules since they are closely linked to the plasma membrane (Ambrose, Allard, Cytrynbaum & Wasteneys, 2011). These microtubules are formed by different microfilaments, and one of the most important

microfilament is the actin (Wen & Janmey, 2011). Actin microfilament links the microtubules with the membrane by using Ca^{2+}, maintaining the membrane mechanical integrity (Lang *et al.*, 2014). Therefore, any perturbation in the calcium bonding between microtubules and membrane can initiate a plasmolysis process.
Figure 2b shows how the overall water mass variation, induced by the electric field applied (Traffano-Schiffo *et al.*, 2016) is smaller (external transport) than the water mass variation of internal and external liquid phase (internal transport). Moreover, Figure 2b shows the water adsorbed mass variation, where the greater the electric field applied the greater the amount of adsorbed water.

In order to understand the behaviors involved in the increasing of water adsorption, the internal surface of samples (m^2) where estimated as follows (Farroni, 2011; Condon, 2006):

$$S_i = \frac{\pi\, r_w^2\, M\, (1-x_w)\, X_{w0}^{ADS} N_A}{M_w} \quad (3)$$

Where r_w is the radius of the water molecule based in Lewis model ($1.375 \cdot 10^{-10}$ m) (Pierotti, 1965), M corresponds to the mass of the sample (g), x_w is the moisture of the sample (g_w/g_T), X_{w0}^{ADS} represents the moisture of the monomolecular layer obtained by BET model (g_w/g_{dm}), N_A corresponds to the Avogadro constant ($6.022 \cdot 10^{23}$ molecules/mol) and M_w is the molecular weight of water (18 g/mol).

Figure 3a shows the internal surface variation of the samples according to the intensity of the applied PEF pre-treatment, where at higher intensities of the electric pulses, the internal surface of the sample increases. The internal surface, calculated from the moisture of the monomolecular layer (equation 3), covers the entire surface with capacity to adsorb water. In this sense, any process of surface release or surface availability will cause an increase in the amount of adsorbed water, previously observed by Traffano-Schiffo *et al.*, 2017. As described above, the electric field applied on the tissue produces a partial plasmolysis associated with the displacement of calcium ions in the fixations of the actin microfilaments (cell wall-plasma membrane bond). It induces a water transport from inside to the outside of the cells and increases the availability of surface, as Figure 3a shows, and as was corroborated in Figure 3b in which the mass of adsorbed water increases proportionally to the internal surface.

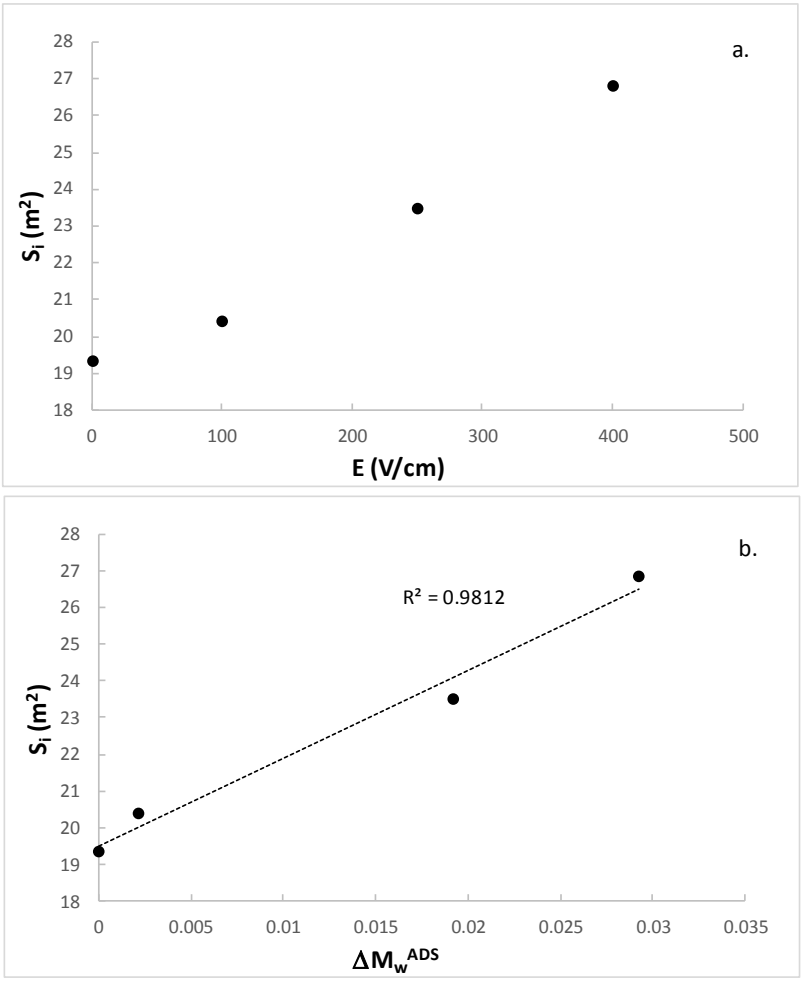

Figure 3. a. Internal Surface of the solid matrix; b. relationship between the water mass variation of the adsorbed water and the internal surface of the solid matrix.

In order to understand the movement of water across the kiwifruit tissue affected by the PEF pre-treatment throughout OD treatment, the water mass flow was estimated as follows:

$$m_w^j = \frac{M^t x_{wi}^t - M^0 x_{wi}^0}{t} \quad (4)$$

Where m_w^j represents the water mass flow (g_w/s), M represents the mass sample (g), x_w the water mass fraction of specific phase (g_w/g_T), t is treatment time (s), the superscript j corresponds to a specific water phase (ELP, ILP or total), t to the treatment time and 0 to the initial time.

Figure 4 shows schematically the directions that water flows can take inside the fruit tissue. The water mass flow produced in the ILP can only leave, and it can be produced towards the external liquid phase or towards the osmotic solution through the symplastic pathways, whereas the water mass flow in the ELP can be coming in from the ILP or can be leaving to the osmotic solution. Finally, total water mass flow represents the water molecules that cross the interface sample/osmotic solution.

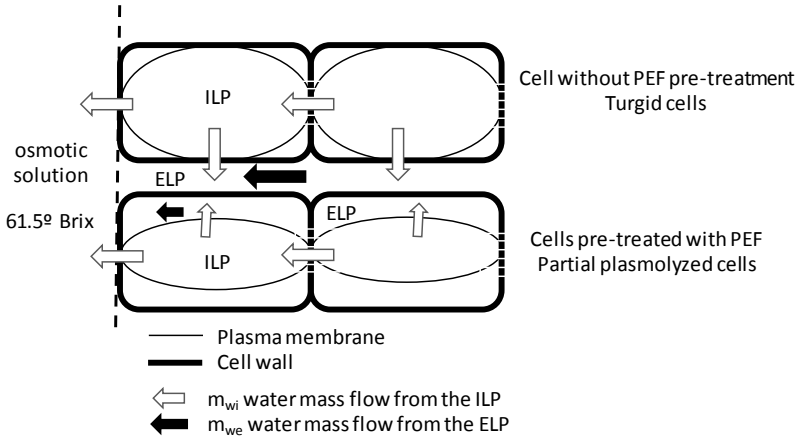

Figure 4. Schematic representation of cell structure with and without PEF pre-treatment.

Water mass flow from ILP, ELP and whole tissue (total) was estimated by using equation 4, where positive value of water mass flow represents a water flux coming in the phase and negative value represents a water flux leaving the phase. Samples pre-treated with PEF show an increment of ELP as Figure 4 shows, induced by a plasmolysis process.

Figure 5 shows the evolution of each water mass flow (ILP, ELP and total) throughout the OD treatment per PEF pre-treatment. As it can be appreciated, the water mass flow in ELP shows positive values in non pre-treated samples (Figure 5a). Taking into account that the water activity in the osmotic solution is lower than in the ELP, the mass of water has to come from the ILP (as Figure 4 shows). However, negative values of water mass flow in samples pre-treated (Figure 5 b, c and d) indicate that the water leaves from ELP to the osmotic solution. With regard to ILP, the water mass flow decreases the higher the applied PEF. Nevertheless, the overall water mass flow increases the higher the applied PEF, because water from the ELP is joined with the water from the ILP. Finally, the water mass flow of the ELP increases with PEF pre-treatment with negative values (negative values mean that the water mass flow is leaving the liquid phase), therefore only the non-pretreated samples show the effect of plasmolysis. In conclusion, PEF treatment produces a partial plasmolysis in parenchymatic kiwifruit tissue, and this plasmolysis process depends on the intensity of PEF pre-treatment (as was observed in Figure 2).

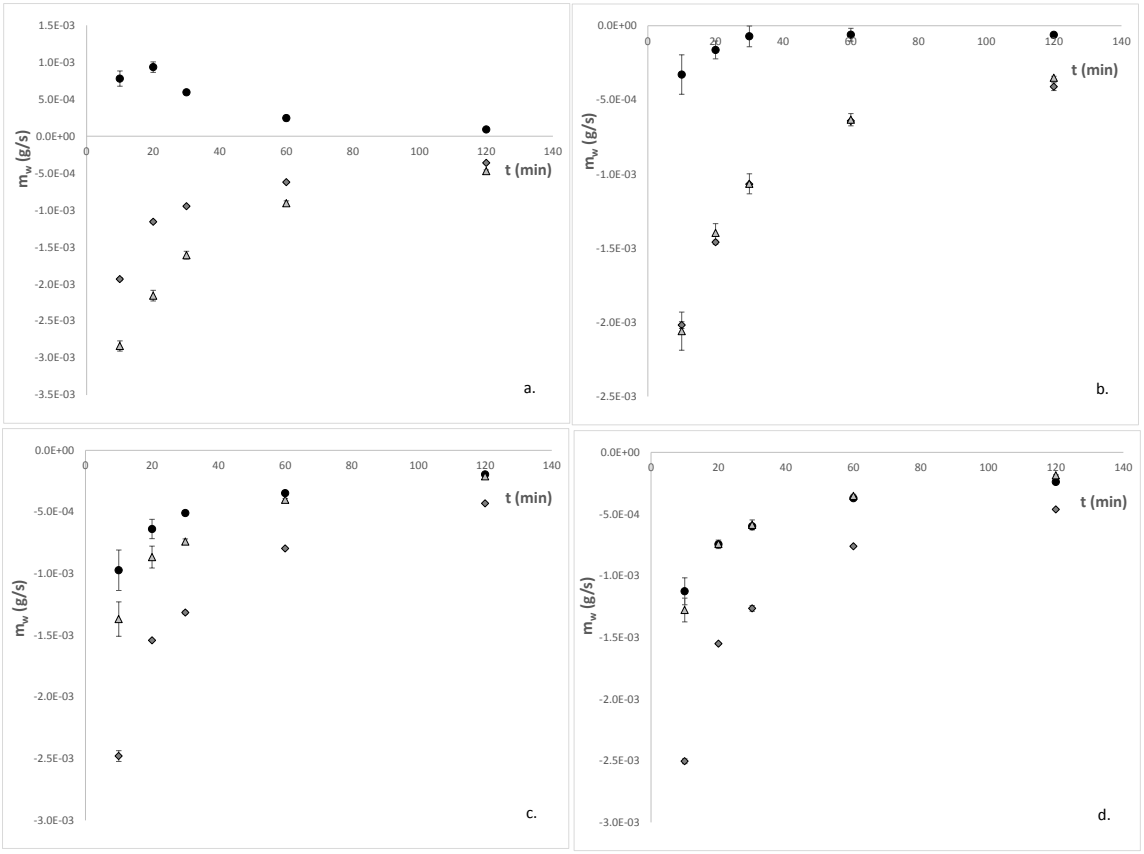

Figure 5. Water mass flow during osmotic dehydration treatment of the samples pre-treated with PEF. a. 0 V/cm, b. 100 V/cm, c. 250 V/cm and d. 400 V/cm, where: (●) extracellular liquid phase (ELP), (▲) intracellular liquid phase (ILP) and (♦) total water mass flow.

4. Conclusions

It has been proven that the application of an electric field prior to the osmotic dehydration produces a process of plasmolysis proportional to the applied electric field. The induction of the plasmolysis process is caused by the elimination of mobile charges of the medium, such as electrolytes, organic acids, etc.; among them Ca^{+2} is the major culprit because it is not available to fix some of the junctions of the microtubules between the cell wall and the membrane.

In addition, the process of plasmolysis induced by the electric field changes the behavior of kiwifruit tissue during the OD process. In a normal OD, the main transport is the symplastic, whereas if previously treated with PEF, the apoplastic transport is as important as the symplastic, considerably increasing the rate of dehydration.

5. Acknowledgements

The authors Urszula Tylewicz and Marco Dalla Rosa want to thank for the financial support provided by funding bodies within the FP7 ERA-Net CORE Organic Plus, and with cofounds from the European Commission. The author Maria Victoria Traffano Schiffo wants to thank the FPI Predoctoral Program of the Universidad Politécnica de Valencia for support her PhD studies,

ERASMUS PRÁCTICAS program to finance her mobility to Italy. The authors Pedro J. Fito, Marta Castro-Giraldez and M. Victoria Traffano-Schiffo acknowledge the financial support from the Spanish Ministerio de Economía, Industria y Competitividad, Programa Estatal de I+D+i orientada a los Retos de la Sociedad AGL2016-80643-R, Agencia Estatal de Investigación (AEI) and Fondo Europeo de Desarrollo Regional (FEDER).

6. References

Agre, P., King, L. S., Yasui, M., Guggino, W. B., Ottersen, O. P., Fujiyoshi, Y., ... & Nielsen, S. (2002). Aquaporin water channels–from atomic structure to clinical medicine. *The Journal of Physiology*, 542(1), 3-16.

Ambrose, C., Allard, J. F., Cytrynbaum, E. N., & Wasteneys, G. O. (2011). A CLASP-modulated cell edge barrier mechanism drives cell-wide cortical microtubule organization in Arabidopsis. *Nature Communications*, 2, 430.

Ampomah-Dwamena, C., McGhie, T., Wibisono, R., Montefiori, M., Hellens, R. P., & Allan, A. C. (2009). The kiwifruit lycopene beta-cyclase plays a significant role in carotenoid accumulation in fruit. *Journal of Experimental Botany*, 60(13), 3765-3779.

AOAC. (2000). AOAC, Association of Official Analytical Chemist Official Methods of Analysis. Washington, D.C.

Baier, A. K., Bußler, S., & Knorr, D. (2015). Potential of high isostatic pressure and pulsed electric fields to improve mass transport in pea tissue. *Food Research International*, 76, 66-73.

Barba, F. J., Parniakov, O., Pereira, S. A., Wiktor, A., Grimi, N., Boussetta, N., Saraiva, J. A., Raso, J., Martin-Belloso, O., Witrowa-Rajchert, D., Lebovka, N., & Lebovka, N. (2015). Current applications and new opportunities for the use of pulsed electric fields in food science and industry. *Food Research International*, 77, 773-798.

Barboni, T., Cannac, M., & Chiaramonti, N. (2010). Effect of cold storage and ozone treatment on physicochemical parameters, soluble sugars and organic acids in Actinidia deliciosa. *Food Chemistry*, 121(4), 946-951.

Bezanilla, F. (2008). How membrane proteins sense voltage. *Nature Reviews Molecular Cell Biology*, 9(4), 323-332.

Bohn, T., Walczyk, T., Leisibach, S., & Hurrell, R. F. (2004). Chlorophyll-bound Magnesium in Commonly Consumed Vegetables and Fruits: Relevance to Magnesium Nutrition. *Journal of Food Science*, 69(9), S347-S350.

Borgia, G. C., Brown, R. J. S., & Fantazzini, P. (1998). Uniform-penalty inversion of multiexponential decay data. *Journal of Magnetic Resonance*, 132(1), 65-77.

Cano, M. P., & Marin, M. A. (1992). Pigment composition and color of frozen and canned kiwi fruit slices. *Journal of Agricultural and Food Chemistry*, 40(11), 2141-2146.

Cassano, A., Donato, L., Conidi, C., & Drioli, E. (2008). Recovery of bioactive compounds in kiwifruit juice by ultrafiltration. *Innovative Food Science & Emerging Technologies*, 9(4), 556-562.

Castaldo, D., Lo Voi, A., Trifiro, A., & Gherardi, S. (1992). Composition of Italian kiwi (Actinidia chinensis) puree. *Journal of Agricultural and Food Chemistry*, 40(4), 594-598.

Castro-Giráldez, M., Fito, P. J., Dalla Rosa, M., & Fito, P. (2011). Application of microwaves dielectric spectroscopy for controlling osmotic dehydration of kiwifruit (*Actinidia deliciosa cv Hayward*). *Innovative Food Science & Emerging Technologies*, 12(4), 623-627.

Castro-Giráldez, M., Tylewicz, U., Fito, P. J., Dalla Rosa, M., & Fito, P. (2011). Analysis of chemical and structural changes in kiwifruit (*Actinidia deliciosa cv Hayward*) through the osmotic dehydration. *Journal of Food Engineering*, 105(4), 599-608.

Condon, J. B. (2006). *Surface area and porosity determinations by physisorption: measurements and theory*. (1st ed.) Amsterdam, The Netherlands: Elsevier.

Dellarosa, N., Ragni, L., Laghi, L., Tylewicz, U., Rocculi, P., & Dalla Rosa, M. (2016). Time domain nuclear magnetic resonance to monitor mass transfer mechanisms in apple tissue promoted by osmotic dehydration combined with pulsed electric fields. *Innovative Food Science & Emerging Technologies*, 37, 345-351.

Dermesonlouoglou, E., Zachariou, I., Andreou, V., & Taoukis, P. S. (2016). Effect of pulsed electric fields on mass transfer and quality of osmotically dehydrated kiwifruit. *Food and Bioproducts Processing*, 100, 535-544.

Dorai, M., Papadopoulos, A., & Gosselin, A. (2001). Influence of electric conductivity management on greenhouse tomato yield and fruit quality. *Agronomie*, 21(4), 367-383.

Famiani, F., Battistelli, A., Moscatello, S., Cruz-Castillo, J. G., & Walker, R. P. (2015). The organic acids that are accumulated in the flesh of fruits: occurrence, metabolism and factors affecting their contents–a review. *Revista Chapingo Serie Horticultura*, 21(2).

Farroni, A. E. (2011). Transformaciones estructurales y físico-químicas de maíces argentinos en la producción de alimentos obtenidos por procesos de gelatinización-laminación (Doctoral dissertation, Facultad de Ciencias Exactas y Naturales. Universidad de Buenos Aires).

Gürsul, I., Gueven, A., Grohmann, A., & Knorr, D. (2016). Pulsed electric fields on phenylalanine ammonia lyase activity of tomato cell culture. *Journal of Food Engineering*, 188, 66-76.

Havaux, M. (1998). Carotenoids as membrane stabilizers in chloroplasts. *Trends in Plant Science*, 3(4), 147-151.

Johansson, I., Karlsson, M., Johanson, U., Larsson, C., & Kjellbom, P. (2000). The role of aquaporins in cellular and whole plant water balance. *Biochimica et Biophysica Acta (BBA)-Biomembranes*, 1465(1), 324-342.

Keutgen, A. J., & Pawelzik, E. (2008). Contribution of amino acids to strawberry fruit quality and their relevance as stress indicators under NaCl salinity. *Food Chemistry*, 111(3), 642-647.

Khan, S. A., Beekwilder, J., Schaart, J. G., Mumm, R., Soriano, J. M., Jacobsen, E., & Schouten, H. J. (2013). Differences in acidity of apples are probably mainly caused by a malic acid transporter gene on LG16. *Tree Genetics & Genomes*, 9(2), 475-487.

Khin, M. M., Zhou, W., & Perera, C. O. (2006). A study of the mass transfer in osmotic dehydration of coated potato cubes. *Journal of Food Engineering*, 77(1), 84-95.

Lang, I., Barton, D. A., & Overall, R. L. (2004). Membrane–wall attachments in plasmolysed plant cells. *Protoplasma*, 224(3-4), 231-243.

Lang, I., Sassmann, S., Schmidt, B., & Komis, G. (2014). Plasmolysis: Loss of Turgor and Beyond. *Plants*, 3(4), 583-593.

Ma, T., Sun, X., Zhao, J., You, Y., Lei, Y., Gao, G., & Zhan, J. (2017). Nutrient compositions and antioxidant capacity of kiwifruit (Actinidia) and their relationship with flesh color and commercial value. *Food Chemistry*, 218, 294-304.

Marcotte, M., Toupin, C. J., & Le Maguer, M. (1991). Mass transfer in cellular tissues. Part I: The mathematical model. *Journal of Food Engineering*, 13(3), 199-220.

Marsh, K. B., Boldingh, H. L., Shilton, R. S., & Laing, W. A. (2009). Changes in quinic acid metabolism during fruit development in three kiwifruit species. *Functional Plant Biology*, 36(5), 463-470.

Maurel, C., & Chrispeels, M. J. (2001). Aquaporins. A molecular entry into plant water relations. *Plant Physiology*, 125(1), 135-138.

Meiboom, S., & Gill, D. (1958). Modified spin-echo method for measuring nuclear relaxation times. *Review of Scientific Instruments*, 29(8), 688-691.

Montefiori, M., McGhie, T. K., Costa, G., & Ferguson, A. R. (2005). Pigments in the fruit of red-fleshed kiwifruit (Actinidia chinensis and Actinidia deliciosa). *Journal of Agricultural and Food Chemistry*, 53(24), 9526-9530.

Moraga, M. J., Moraga, G., Fito, P. J., & Martínez-Navarrete, N. (2009). Effect of vacuum impregnation with calcium lactate on the osmotic dehydration kinetics and quality of osmodehydrated grapefruit. *Journal of Food Engineering*, 90(3), 372-379.

Muller, A. C. A., Scrivener, K. L., Gajewicz, A. M., & McDonald, P. J. (2013). Use of bench-top NMR to measure the density, composition and desorption isotherm of C–S–H in cement paste. *Microporous and Mesoporous Materials*, 178, 99-103.

Nakashima Y. (2001) Pulsed field gradient proton NMR study of the self-diffusion of H_2O in montmorillonite gel: Effects of temperature and water fraction. *American Mineralogist*, 86, 132–138.

Nishiyama, I., Fukuda, T., Shimohashi, A., & Oota, T. (2008). Sugar and organic acid composition in the fruit juice of different Actinidia varieties. *Food Science and Technology Research*, 14(1), 67-73.

Park, Y. S., Ham, K. S., Park, Y. K., Leontowicz, H., Leontowicz, M., Namieśnik, J., Katrich, E., & Gorinstein, S. (2016). The effects of treatment on quality parameters of smoothie-type 'Hayward' kiwi fruit beverages. *Food Control*, 70, 221-228.

Park, Y. S., Im, M. H., Ham, K. S., Kang, S. G., Park, Y. K., Namiesnik, J., Leontowicz, H., Leontowicz, M., Katrich, E., & Gorinstein, S. (2013). Nutritional and pharmaceutical properties of bioactive compounds in organic and conventional growing kiwifruit. *Plant Foods for Human Nutrition*, 68(1), 57-64.

Park, Y. S., Leontowicz, H., Leontowicz, M., Namiesnik, J., Suhaj, M., Cvikrová, M., Martincová, O., Weisz, M., & Gorinstein, S. (2011). Comparison of the contents of bioactive compounds and the level of antioxidant activity in different kiwifruit cultivars. *Journal of Food Composition and Analysis*, 24(7), 963-970.

Pierotti, R. A. (1965). Aqueous Solutions of Nonpolar Gases1. *The Journal of Physical Chemistry*, 69(1), 281-288.

Santagapita, P., Laghi, L., Panarese, V., Tylewicz, U., Rocculi, P., & Dalla Rosa, M. (2013). Modification of transverse NMR relaxation times and water diffusion coefficients of kiwifruit pericarp tissue subjected to osmotic dehydration. *Food and Bioprocess Technology*, 6(6), 1434-1443.

Seguí, L., Fito, P. J., & Fito, P. (2012). Understanding osmotic dehydration of tissue structured foods by means of a cellular approach. *Journal of Food Engineering*, 110(2), 240-247.

Sivakumaran, S., Huffman, L., Sivakumaran, S., & Drummond, L. (2016). The nutritional composition of Zespri® SunGold Kiwifruit and Zespri® Sweet Green Kiwifruit. *Food Chemistry*. http://dx.doi.org/10.1016/j.foodchem.2016.08.118

Snowden, C. J., Thomas, B., Baxter, C. J., Smith, J. A. C., & Sweetlove, L. J. (2015). A tonoplast Glu/Asp/GABA exchanger that affects tomato fruit amino acid composition. *The Plant Journal*, 81(5), 651-660.

Tarchevsky I.A., Marchenko G.N. (1991). *Cellulose: Biosynthesis and Structure*. Berlin, Germany: Springer-Verlag, Berlin Heidelberg, (Chapters 1 & 8).

Traffano-Schiffo, M. V., Laghi, L., Castro-Giraldez, M., Tylewicz, U., Roculi, P., Ragni, L., Dalla Rosa, M., & Fito, P. J. (2017). Osmotic dehydration of organic kiwifruit pre-treated by pulsed electric fields and monitored by NMR. *Food Chemistry*. http://dx.doi.org/10.1016/j.foodchem.2017.02.046

Traffano-Schiffo, M. V., Tylewicz, U., Castro-Giraldez, M., Fito, P. J., Ragni, L., & Dalla Rosa, M. (2016). Effect of pulsed electric fields pre-treatment on mass transport during the osmotic dehydration of organic kiwifruit. *Innovative Food Science & Emerging Technologies*, 38, 243-251.

Tylewicz, U., Fito, P. J., Castro-Giráldez, M., Fito, P., & Dalla Rosa, M. (2011). Analysis of kiwifruit osmodehydration process by systematic approach systems. *Journal of Food Engineering*, 104(3), 438-444.

Wen, Q., & Janmey, P. A. (2011). Polymer physics of the cytoskeleton. *Current Opinion in Solid State and Materials Science*, 15(5), 177-182.

4.8. Encapsulación enzimática en sistemas de biopolímeros y su estudio mediante NMR y SAXS.

Los resultados obtenidos en el presente apartado corresponden a la estancia realizada en la

Universidad de Buenos Aires, Argentina.

Reimpreso con permiso de "**Traffano-Schiffo, M. V.**, Aguirre Calvo, T., R., Castro-Giráldez, M., Fito, P. J., & Santagapita, P., R. (2017). Alginate beads containing lactase: stability and microstructure. ***Biomacromolecules***, 18, 1785-1792. Copyright 2017 American Chemical Society.

http://pubs.acs.org/doi/abs/10.1021/acs.biomac.7b00202

Traffano-Schiffo, M. V., Castro-Giráldez, M., Fito, P. J., & Santagapita, P., R. (2017). Encapsulation of lactase in alginate-Ca(II) beads: effect of trehalose and gums inclusion and of drying methods. ***Food Research International.*** *Artículo enviado.*

Traffano-Schiffo, M. V., Castro-Giráldez, M., Fito, P. J., Perullini, M., & Santagapita, P., R. (2017). Gums induced microstructure stability in Ca(II)-alginate beads containing lactase analysed by SAXS. ***Carbohydrate Polymers.*** *Artículo enviado.*

ALGINATE BEADS CONTAINING LACTASE: STABILITY AND MICROSTRUCTURE

Maria Victoria Traffano-Schiffo,[†] *Tatiana R. Aguirre Calvo,*[§]

Marta Castro-Giraldez,[†] *Pedro J. Fito,*[†] *and Patricio R. Santagapita*[§,‡⋆]

[†] Instituto Universitario de Ingeniería de Alimentos para el Desarrollo, Universidad Politécnica de Valencia, Camino de Vera s/n, 46022 Valencia, Spain.

[§] Universidad de Buenos Aires, Facultad de Ciencias Exactas y Naturales, Departamentos de Industrias y Química Orgánica (FCEN-UBA), Buenos Aires, Argentina.

[‡] Consejo Nacional de Investigaciones Científicas y Técnicas (CONICET), Buenos Aires, Argentina.

Corresponding Author:

* Phone/ Fax: 54 11 4576 3366; e-mail: prs@di.fcen.uba.ar

ABSTRACT

β-galactosidase (lactase) is a widely used enzyme in food industry; however, it has low stability against thermal and mechanical treatments. Due to this, the purpose of present research was to analyze the encapsulation of lactase in alginate-Ca(II) beads in order to maintain its enzymatic activity towards freezing, freezing/thawing and storage. Also, the effect of the addition of trehalose, arabic and guar gums and its influence in the microstructure as well as in thermal properties and molecular mobility were studied. Lactase was successfully encapsulated in alginate-Ca(II) beads and the inclusion of trehalose was critical for activity preservation towards treatments, being improved in guar gum-containing systems. The gums increased the T_m' values which represents a valuable technological improvement. Finally, the presence of secondary excipients affected the microstructure, showing rods with smaller outer diameter and with lower compactness than alginate-Ca(II) beads. Also, beads composition greatly affects the size, shape and relaxations times.

Keywords: alginate beads, encapsulation, enzyme stability, β-galactosidase, microstructure, Small-Angle X-ray scattering.

Table of Contents graphic

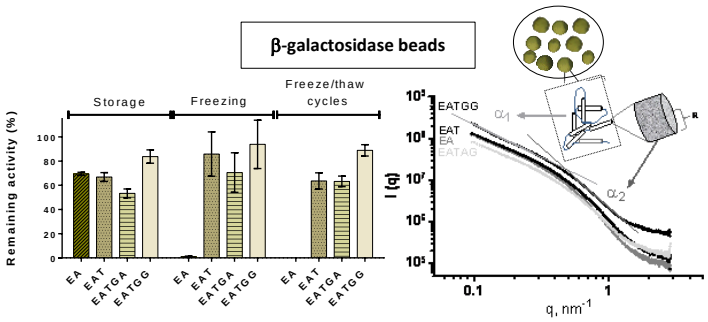

INTRODUCTION

β-galactosidase or commonly known lactase is a widely used enzyme in the food industry because is able to catalyze the bioconversion of lactose into glucose and galactose.[1,2] Several applications of β-galactosidase have been reported in recent years, such as the valorization of cheese whey which reduce the environmental impact,[3] the improvement of ice creams creaminess and the sweetness of dairy products due to the lactose hydrolysis[4] and the production of lactose-free fresh dairy products in order to satisfy the needs of lactose intolerance people.[5-7] However, enzyme stability upon treatment and dosification can be improved.

In recent years, some researchers have been demonstrated feasibility of lactase encapsulation in different biopolymers matrices and by different methods. Zhang *et al.* (2017) successfully encapsulated lactase within potassium carrageenan-based hydrogel beads loaded with $Mg(OH)_2$ buffer using the injection-gelation method, obtaining good results on encapsulation and protection for simulated gastric condition.[8] Sen *et al.* (2014) encapsulated lactase in calcium alginate using micro-encapsulation technique to produce galactooligosaccharides in a packed bed bioreactor, obtaining good enzyme retention and activity, even though the enzyme was partially blocked.[9] In this context, the encapsulation of β-galactosidase in hydrogels represents a promising tool. Particularly, alginate consists of α-L-guluronic acid and β-D-mannuronic acid residues and is one of the most used anionic polyelectrolyte due to its gelation properties in presence of divalent cations (usually Ca^{2+} for food science applications), which interact ionically, crosslinking a pair of α-L-guluronic acids blocks within the alginate chains.[10,11] Alginate-Ca(II) shows important advantages because its biocompatibility, easy availability, low cost, resistance to contamination, simplicity and its applicability in food industry due to its non-toxic nature.[12,13] Nevertheless, it shows disadvantages associated to its low mechanical strength, the presence of macropores and especially some technological problems i.e. the enzymatic activity losses during beads formation and the low resistance to physical treatments such as freezing and dehydration.[13] Freitas and co-workers optimized the lactase immobilization by a combined approach using alginate, gelatin, and crosslinking the enzyme with glutaraldehyde, obtaining beads by the

dropping method to overcome enzyme leakage.[14] Other researchers have demonstrated that the combined use of alginate with sugars and/or other biopolymers allow to increase the resistance of the beads or microparticles.[15-17] Particularly, trehalose (1-α-glucopyranosyl-1-α-glucopyranoside) is a non-reducing disaccharide which acts as a protecting agent of bioactive compounds against stress conditions such as heat treatments, dehydration or freezing.[18,19] On the other hand, it has been demonstrated that the addition of biopolymers such as arabic gum (arabinogalactan-protein type polysaccharide) and guar gum (galactomannan) as second matrix ingredients increases the stability of encapsulated systems.[17,20,21]

One of the most precise and powerful technique to evaluate the microstructure of alginate hydrogels is the Small-Angle X-ray scattering (SAXS). SAXS method is able to analyze differences in electron density in hydrogels crosslinked networks from wavelengths of sub-nanometers up to 100 nm, providing information of the biopolymers morphology.[22] The main parameters of SAXS analysis are the rod cross-sectional radius (R), the fractal dimension at distances higher than R (α_1), which describes the junction zone, and the fractal dimension at distances lower than R (α_2) describing the nanostructure within the rods.[23,24]

The purpose of present research was to analyze the encapsulation of lactase in alginate-Ca(II) beads in order to maintain its enzymatic activity towards freezing, freezing/thawing and storage. Also, the effect of the addition of trehalose, arabic and guar gums and its influence in the microstructure as well as in thermal properties and molecular mobility were studied.

MATERIALS AND METHODS

Materials

The used materials were listed below: sodium alginate (Algogel 5540) from Cargill S.A. (San Isidro, Buenos Aires, Argentina), molecular weight of $1.97 \cdot 10^5$ g/mol and mannuronate/guluronate ratio of 0.6; D-trehalose dihydrate (Hayashibara Co., Ltd., Shimoishii, Okayama, Japan/Cargill Inc., Minneapolis, Minnesota, USA) molecular weight of 378 g/mol; guar gum (Cordis S.A., Villa Luzuriaga, Buenos Aires, Argentina) molecular weight of 220.000 g/mol and a mannose/galactose ratio of 1.8; arabic gum (Biopack, Zárate, Buenos Aires, Argentina) molecular weight of 250.000 g/mol and a purity of 99%; β-galactosidase (lactase) from Aspergillus oryzae (8.0 U/mg) (Sigma-Aldrich Co, Ltd, Saint Louis, USA). One enzymatic unit was defined as the amount of enzyme able to hydrolyze 1.0 μmol of lactose per minute at pH 4.5 at 30 °C.

Gel beads preparation

Four different formulations containing enzyme (E) were prepared, with the following composition: alginate (EA); alginate-trehalose (EAT); alginate-trehalose-guar gum (EATGG);

alginate-trehalose-arabic gum (EATAG). All the solutions were prepared in 0.1 M acetate buffer pH 3.8. Taking into account that the isoelectric point of the enzyme was 4.61[25,26] and the pKa values of alginate are 3.38 and 3.65,[16] the acetate buffer at pH 3.8 was used in order to obtain an electrostatic interaction between the alginate (negatively charged) and the enzyme (positively charged). The final concentration of lactase was 0.775 mg/mL. The enzyme and the initial solutions were carefully mixed and maintained at 4 ± 1 °C in order to avoid enzyme activity losses. A peristaltic pump was used to drop 10 mL of the alginate-enzyme mixture into 100 mL of the gelling solution, according to the drop method described by Austin, Bower, & Muldoon[27] with some modifications. For EA beads preparation, 1% (w/v) alginate solution containing the enzyme was dropped into 2.5% (w/v) $CaCl_2$ solution (prepared in 0.1 M acetate buffer pH 3.8). For EAT, EATGG and EATAG beads preparation, a 1% (w/v) alginate with 20% (w/v) trehalose and/or with 0.25% (w/v) of guar or arabic gums solutions containing the enzyme were dropped into the 2.5% (w/v) $CaCl_2$ solution supplemented with 20% (w/v) trehalose.

$CaCl_2$ solution (with or without trehalose) was maintained in a cold bath with constant stirring. A needle of 0.25 mm diameter and 6 mm length (Novofine 32 G, Novo Nordisk A/S, Bagsvaerd, Denmark) was used for the dropping. The pump speed was 9.0 ± 0.1 rpm. The distance between the needle and the $CaCl_2$ solution was 6 cm. After beads generation, they were maintained 15 min in $CaCl_2$ solution (with constant stirring) and after that, there were washed 5 times (for 5 s each wash) with bidistilled cold water, in order to remove adhered free enzyme (if any).

Thermal Treatments

Freezing

Wet beads were frozen at -18 °C by using a conventional freezer during 24 h.

Freeze/thaw cycles

The Freeze/thaw treatment was performed freezing the beads during 1 min using liquid nitrogen (at -196 °C) and thawing in a conventional fridge at 4 °C during 30 min; this procedure was repeated 4 times for each system.

Storage

In order to analyze the stability of the enzyme during the storage, beads were maintained at 4 °C in a conventional fridge during 48 h.

Beads characterization

Digital image analysis

The size and shape of the wet beads was analyzed through digital images captured by a digital camera coupled to a binocular microscope and analyzed by the free license software ImageJ (http://rsbweb.nih.gov/ij/), as described by Aguirre Calvo & Santagapita[28]. The Feret's diameter (size) corresponds to the longest distance between any two points along the bead boundary. The circularity indicates how similar the bead is to a circle. At least 40 beads were analyzed by applying the "analyze particle" command of the software. In order to increase the contrast of the images, the beads have been stained with erythrosine 1% (w/v). The ImageJ software was calibrated to transform the measured pixels in length units (mm) by taking pictures of a caliper section.

Water content and water activity

Water content of the beads was obtained gravimetrically by the difference in weight before and after drying in vacuum oven for 48 h at 96 ± 2 °C.[28] Water activity (a_w) was determined by a dew point Hygrometer Decagon (Aqualab®, series 3 TE, Decagon Devices, Pullman, WA, USA). A special sample holder was used to reduce the quantity of beads needed. A calibration curve was performed with salts with known aw (between 0.25 and 1). All determinations were made in triplicate.

Microstructure characterization

The microstructure characterization was performed by small angle X-ray scattering (SAXS) at the LNLS SAXS2 beamline in Campinas, Brazil, working at λ =0.1488 nm. The wave vector (q) range was selected in the range 0.096 $nm^{-1} < q < 2.856\ nm^{-1}$. All the alginate-Ca(II) beads analyzed showed isotropic scattering and were modeled as a fractal system composed of rod-like structures, although the rigorous interpretation of experimental results as indicating "fractality" requires many orders of magnitude of power-law scaling.[23] Three parameters were analyzed: i) α_1, the fractal dimension at distances higher than R, which describes the multiplicity of the junction zone, at $q < 0.28$; ii) α_2, the fractal dimension at distances lower than R, at $q > 0.55$, describing the degree of compactness within the rods. Parameters α_1 and α_2 were evaluated from the slope of the scattering intensity averaged along azimuthal angles versus the scattering vector q in the log–log scale; iii) R, the outer radius of the rods, which is given by $R = R_g\sqrt{2}$, R_g being the mean gyration radius in the cross-section of the rods, which is obtained from the maximum exhibit by the Kratky plot at $q \approx 1/R_g$. The Kratky plot: scattering intensity multiplied by the square modulus of the scattering vector, $I(q)\cdot q^2$, as a function of the modulus of the scattering vector, q, gives a

maximum value at the intersection of power law regions and allows the calculation of parameter R. All measurements were made in triplicate.

β-Galactosidase activity

The enzyme activity was evaluated based on the absorbance values at 420 nm by using a Jasco V-630 UV-VIS spectrophotometer (JASCO Inc., Maryland, USA) at room temperature and following the method described by Park, Santi, & Pastore,[29] with some modifications.

Firstly, each analysis was performed using 9 beads which were dissolved into 0.25 mL of 0.1 M citrate buffer pH 4.5 during 2 h at 4 °C and without stirring in order to avoid enzymatic activity losses. Subsequently, 0.25 mL of o-nitrophenyl-β-D-galactopyranoside (ONPG) (Sigma Chemical Co.) prepared with 0.1 M acetate buffer pH 3.8 was added and incubated during 15 min at 33 °C. Finally, the reaction was stopped adding 0.5 mL of sodium carbonate 10% (w/v) and 1.75 mL of distilled water for subsequent measurement of o-nitrophenol (ONP) at 420 nm. Measurements were made in triplicate.

The effect of the composition of the beads on enzyme stability immediately after beads generation was evaluated through an activity index calculated with the following equation:

$$Activity\ Index\ (\%) = \frac{Activity_i}{Activity_{EA}} \times 100 \quad (1)$$

Where $Activity_i$ corresponds to the activity of any the studied systems (EA, EAT, EATAG or EATGG) and $Activity_{EA}$ is the activity of the EA system.

On the other hand, in order to analyze the activity of the beads after thermal treatments, the remaining activity was calculated as follows:

$$Remaining\ Activity\ (\%) = \frac{Activity_t}{Activity_0} \times 100 \quad (2)$$

Where $Activity_t$ is the activity value of each system obtained after a given treatment and $Activity_0$ is related to the activity of the same system before the treatment.

The loading efficiency of the enzyme in the beads was calculated as the amount of enzyme loaded in the beads after generation (L) related to the initial amount of enzyme in the alginate solution (L_0), as defined in eq 3.

$$Loading\ efficiency\ (\%) = \frac{L}{L_0} \times 100 \quad (3)$$

Differential scanning calorimetry (DSC)

Glass transition temperature (T_g), the variations in heat capacity at T_g (Δcp), the onset temperatures of ice melting (T_m') and the endothermal melting peak were determined by differential scanning calorimetry (DSC) by means of a Mettler Toledo 822 equipment (Mettler Toledo AG, Urdorf, Switzerland) and STARe Thermal Analysis System version 3.1 software (Mettler Toledo AG). The instrument was calibrated using standard compounds (indium and zinc) of defined melting point and heat of melting.

All measurements were made in duplicate with 14-23 mg sample mass (10 beads), using hermetically sealed aluminum pans of 40 µl inner volume (Mettler), heated from -100 °C to 50 °C at 10 °C/min; an empty crucible was used as a reference. Measurements were made in duplicate.

The unfreezable water (dimensionless) was calculated as follows:[30]

$$x_{nfw} = 1 - \frac{\Delta H}{\Delta H_{ice}} \quad (4)$$

Where ΔH (J/gw) corresponds to the difference of crystallization and melting heats of water per gram of sample obtained by the integration of crystallization and melting peaks, respectively and ΔH_{ice} is the latent heat of melting of pure water at 0 °C (-333 J/g).

Low Field Nuclear Magnetic Resonance (LF-NMR)

Transversal or spin–spin relaxation times (T_2) and longitudinal relaxation or spin-lattice (T_1) were measured by time resolved low field proton nuclear magnetic resonance (^{1}H-LF-NMR) in a Bruker Minispec mq20 (Bruker Biospin Gmbh, Rheinstetten, Germany) with a 0.47 T magnetic field operating at a resonance frequency of 20 MHz. All samples were previously equilibrated at 25.00 ± 0.01 °C in a thermal bath (Haake, model Phoenix II C35P, Thermo Electron Corporation Gmbh, Karlsruhe, Germany). All determinations were made in duplicate.
T_1 was obtained by inversion recovery sequence.[31] The following settings were used: first and final pulse separation of 2 ms and 10 s, scans = 4, number of points = 20, recycled delay = 5, gain = 81-84 dB; phase cycling was used. A monoexponential equation was used for fitting curves. T_2 was obtained by using Carr–Purcell–Meiboom–Gill (CPMG) sequence,[32,33] with the following setting: τ = 2 ms, scans = 4, number points = 500, dummy shots = 0, gain = 83 dB; phase cycling was used. A biexponential decay was used to fitting curves, as previously reported.[34]

Statistical analyses

The statistical analyses were performed by one-way ANOVA with Tukey`s post test by using Prism 6 (GraphPad Software Inc., San Diego, CA, USA) in order to determine significant differences between the mean values of beads of different composition on the measured

parameters. When the analysis of variance indicates differences among means, a t test was used to differentiate means with 95 % of confidence ($p < 0.05$).

RESULTS AND DISCUSSION

Beads characterization

Spherical alginate beads were obtained by the dropping method. The size and shape of the beads were analyzed by measuring Feret´s diameter and circularity by optical microscopy and a digital image processing technique. Figure 1 shows Feret´s diameter (Figure 1a) and the circularity (Figure 1b) obtained for the beads of different composition. All the beads showed a Feret´s diameter close to 1.5 mm, similar to the one reported in other works.[13,16] However, the addition of gums resulted in a significant increment of the size, reaching 1.63 ± 0.07 mm for guar gum containing beads. The increase in viscosity produced by the addition of guar gum35 and the well-known interfacial properties of arabic gum (due to its protein-polysaccharide combined structure[36]) directly affects the surface tension of the drops prior to gelation, which could be responsible for the higher size observed. All beads showed high circularity values (near 0.7), very similar among all the systems. The inclusion of gums showed opposite behavior: arabic gum containing beads showed the highest circularity, and the guar gum containing ones the lowest. This is consistent with the previous discussion: an increment in viscosity will impact on bead size and shape (having a drop-like form, accounting for it higher deformation); instead, a reduction of the interfacial properties[36] will reduce the deformation, even increasing the circularity.

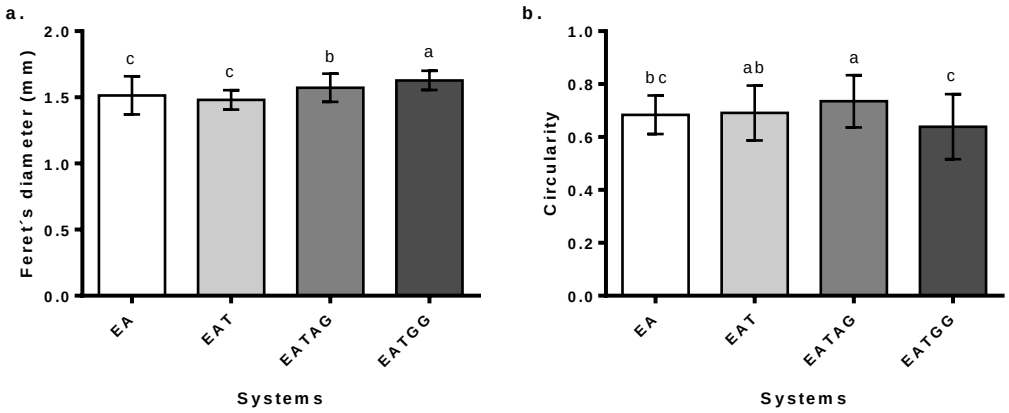

Figure 1. a) Feret´s diameter and b) circularity of beads of different composition. E: enzyme; A: alginate; T: trehalose; AG: arabic gum; GG: guar gum. Standard deviation values are included. Different letters on the columns (a-c) indicate significant differences ($p < 0.05$).

Taking into account the high influence of the water in the structure and the stability of the systems, water content and a_w of beads were determined. As Table 1 shows, the a_w values obtained were between 0.939 and 0.949, without significant differences between beads of different composition. However, the beads containing trehalose showed significantly lower values of moisture with regard to alginate beads, as previously reported by Santagapita *et al.*[16] This difference could be due to the fact that the trehalose is a polyol, able to make multiple hydrogen

bonds, replacing water molecules. On the other hand, the addition of biopolymers (guar and arabic gums) to alginate/trehalose system produced higher moisture values ($p< 0.05$) due to its capability to interact with water molecules.

Table 1. Water activity and moisture content (kg_w/kg_T) obtained for wet beads. E: enzyme; A: alginate; T: trehalose; AG: arabic gum; GG: guar gum. Standard deviation values are included.

Systems	a_w	x_w (kg_w/kg_T)
EA	0.939 ± 0.006[a]	0.9683 ± 0.0088[a]
EAT	0.944 ± 0.008[a]	0.852 ± 0.005[c]
EATAG	0.949 ± 0.003[a]	0.871 ± 0.002[b]
EATGG	0.949 ± 0.001[a]	0.872 ± 0.003[b]

[a-c] Different letters on the columns indicate significant differences between means ($p < 0.05$).

Microstructure analysis

The microstructure of the hydrogel beads was investigated by SAXS where R, α_1 and α_2 parameters were obtained. Figure 2 shows the SAXS scattering profile, indicating the power law regimes at a low and high q value. Also, the characteristic size of the rods composing the structure is deduced from the maxima observed on Kratky plots, which is included as an inset.

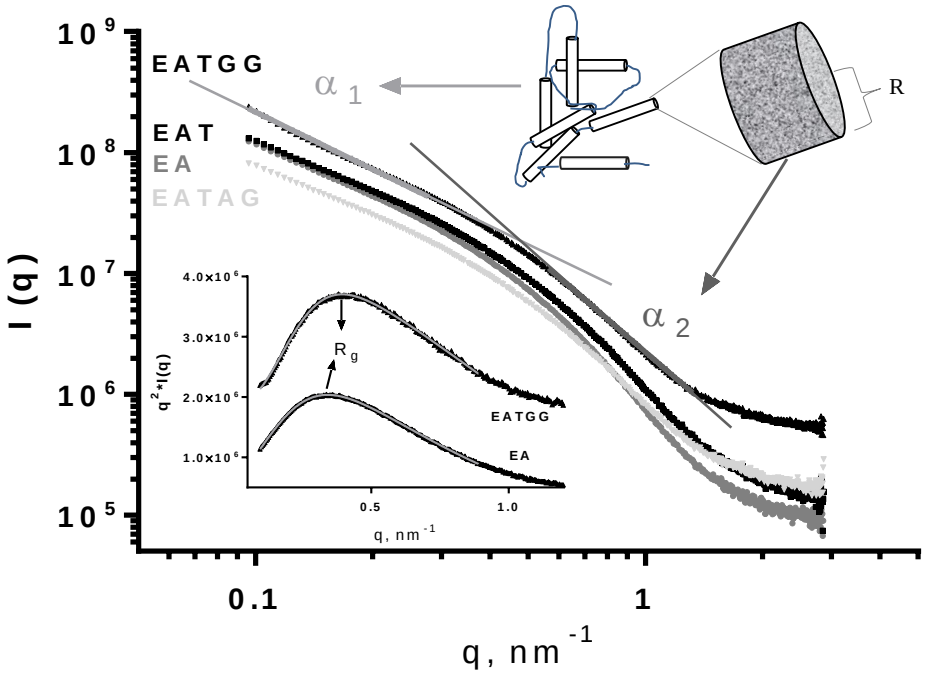

Figure 2. log-log SAXS profile plots of representative samples of alginate-Ca(II) hydrogels containing lactase with the addition of trehalose and biopolymers. Parameters α_1 and α_2 were evaluated from the slope of the scattering intensity at low and high values of q, respectively, and the radius of gyration of the rods (parameter R) was obtained from the Kratky plot (inset). A representative scheme of the parameters is also included. E: enzyme; A: alginate; T: trehalose; AG: arabic gum; GG: guar gum.

α_1 reflects the degree of interconnection of the rods which depends on the composition of the beads. α_1 can take values between 1 and 2. A representative scheme of the parameter can be observed in Figure 2. When $\alpha_1 = 1$, it can be related to randomly oriented rods and when $\alpha_1 = 2$ means that the rods are interconnected.[23] Figure 3 a shows the α_1 parameter for all the systems, where no significant differences can be appreciated, with mean values around 1.45. This suggests that the addition of any excipients did not affect the interconnection of the structure via the coordination of carboxylic groups belonging to alginate chains, as the egg-box model predicts.[37] Figure 3 b shows the R parameter deduced from Kratky plot which indicates the size of the rods. The values obtained for alginate-Ca(II) gels were in agreement to previous observation.[23,24] However, significant differences between enzyme/alginate and the rest of the samples can be appreciated, being much smaller for trehalose containing beads. These differences could be due to a different compactness of the nanostructures of the hydrogels on the rods. Then, α_2 was analyzed and, as shown in Figure 3 c, there were significant differences between the beads containing trehalose with regard to alginate beads, being also smaller for trehalose containing beads. Then, the addition of trehalose and/or gums affected the extent of the rod formation, reducing the outer radius of the fibrils as well as their compactness. On the other hand, the compactness was further

reduced by the addition of gums, which could be explained by the produced steric hindrance along alginate chains. The changes at microstructural level could impact the enzyme stability, by affecting the extent of interaction between the excipients (being involved inside the rods, or outside of them) and the enzyme. This issue will be analyzed in the next section.

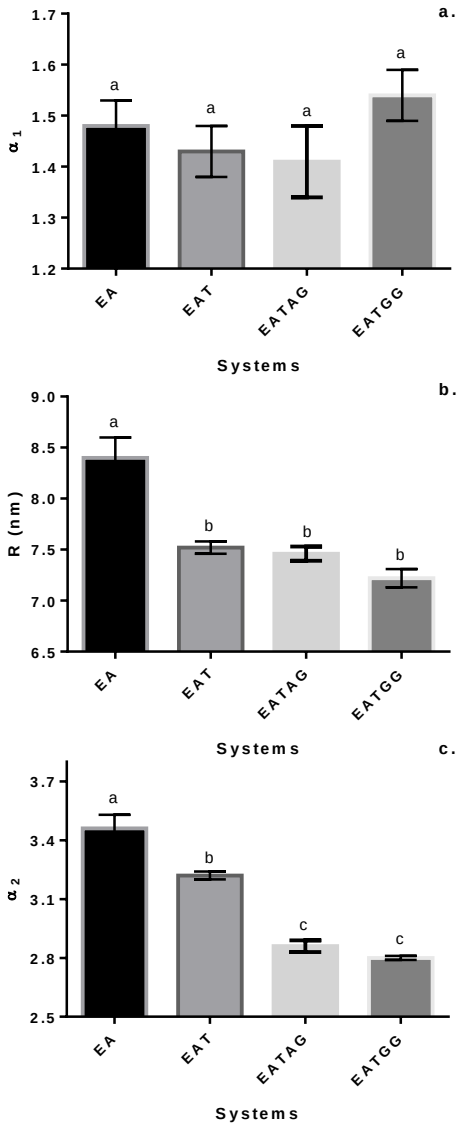

Figure 3. Parameter α_1 (a) and α_2 (c) of the microstructure derived from log-log SAXS profiles and R (outer radius of the rods) (b), deduced from the maxima obtained on Kratky plots. Standard deviations values are included. Different letters on the columns (a-c) indicate significant differences between values with $p < 0.05$. E: enzyme; A: alginate; T: trehalose; AG: arabic gum; GG: guar gum.

Effects of beads composition and thermal treatments on lactase activity preservation

High loading efficiencies (L.E.) were obtained, as expected, similar to those reported in literature to the same enzyme[9] or different (invertase),[16] but using the same procedure. Alginate trehalose

containing beads showed 92 ± 4 % of L.E., and the incorporation of guar or arabic gums lead to similar results (88 ± 8 %).

β-galactosidase activity after beads generation was evaluated as an activity index (%), which was determined as the amount of active enzyme in the beads with different composition related to the enzyme/alginate system (equation 1). Besides, the enzyme activity of the beads subjected to thermal treatments was studied as remaining activity (%), which relates the activity of the beads after the treatment with regard to the enzyme activity of the same composition before it (equation 2). Figure 4 shows the activity index and the remaining activity of lactase.

Immediately after beads generation, the beads that only contain alginate showed the highest activity index comparing with the rests of compositions. However, the changes in beads formulation had showed major effects on the conservation of lactase activity subjected to different treatments. Thus, the enzymatic activity of the alginate systems decreases significantly at 24 h of storage at 4 ºC and with more intensive treatments such as freezing, the activity is practically zero. In contrast, the beads containing trehalose showed significant higher remaining activity values after subjecting the beads to freezing or freezing/thawing cycles. As was previously reported by Santagapita *et al.*[16], trehalose greatly improves the enzymes stability during thermal treatments, but do not show any protective effect during beads generation.

After four cycles of freezing/thawing, the beads with guar gum showed significant highest remaining enzymatic activity, close to 90%, than any of the other systems. Thus, the addition of guar gum as excipient improves the stability of the protein probably due to the improvement in characteristics of the beads. Since changes in molecular mobility and thermal properties of the systems such glass transition temperature and freezable/unfreezable water fractions could explain the present results, NMR and DSC analysis were conducted.

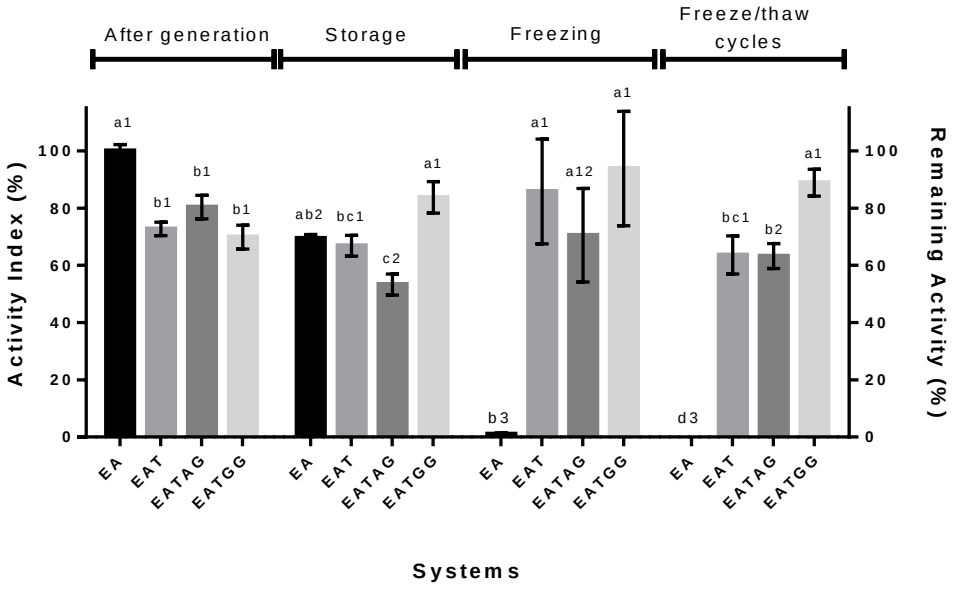

Figure 4. Activity index of lactase (%) in beads after generation and remaining activity of lactase (%) after different treatments: storage (48 h at 4 ºC), frozen (24 h at -18 ºC) and four freeze/thaw cycles (-196 / 4 ºC). E: enzyme; A: alginate; T: trehalose; AG: arabic gum; GG: guar gum. For a certain treatment bars with the same letter (a-d) indicate no significant differences ($p < 0.05$); for beads of same composition bars with the same number (1-3) have no significant differences between treatments ($p < 0.05$).

It is already known that the thermal properties of the glassy matrix produced during freezing of the beads could have a direct impact on enzyme stability. Table 2 shows the glass transition temperature (T_g), the specific heat capacities variation associated to T_g (Δcp), the crystallization and melting enthalpies (ΔH), the onset temperatures of ice melting (T_m') and the mass fraction of unfreezable water (x_{nfw}). The beads containing trehalose had a T_g value near -65 ºC and no significant differences were found between the different compositions. On the other hand, it was not possible to obtain a T_g value for EA beads, probably due to the T_g of polymers (alginate, in this case) is much harder to be observed, since is wider (it is develop in a longer range of temperatures) and of lower Δcp than the transition observed for smaller carbohydrates like trehalose.[38] This fact was already reported by Santagapita *et al.*[13] for dehydrated beads containing invertase. It is interesting to observe than the T_g values obtained for trehalose containing beads is lower than the T_g' value of -41 ºC reported by Roos & Pehkonen,[39] for trehalose. This is due to the fact that the determined T_g is not the T_g` of the systems (there is still water associated to the matrix, as revealed by the small crystallization event observed post T_g), and also that the glassy matrix formed includes both trehalose and alginate (plus water). Regarding enzyme stability, the outstanding bioprotective properties of trehalose are not only explained by the capacity of the sugar to form glassy structures, in which biomolecules are kinetically stabilized, but also by the specific hydrogen bond interactions established between the sugar and the biomolecule during freezing or drying.[40] Also, no significant differences among the specific heat capacities variations between the systems can be appreciated, which implies that the glassy matrix formed in each bead along freezing is similar in all cases.[19] Then, it seems that the differences observed in EATGG

beads respect to the other systems are not due to changes on T_g or in the glassy matrix formed. However T_m' values showed significative differences among the beads. This parameter has strong technological implications, since is the lowest temperature at which the frozen material could be stored without melting. For the beads containing trehalose, the obtained values are quite higher than the T_m` of trehalose,[39] due to the alginate and/or biopolymers presence. In fact, the presence of hydrocolloids reduced the $T_m$` value. This is consistent with the calculation of the unfrozen water associated to the bead matrix (x_{nfw}): in the absence of trehalose, the EA beads showed much higher water content associated to the matrix. The presence of gums, however, significantly reduced the x_{nfw}, due to gums ability to associate water.

Table 2. Glass transition temperature (T_g), change in heat capacity at T_g (Δcp), crystallization and melting enthalpies, and onset melting temperature (T_m') obtained by DSC. The mass fraction corresponding to unfreezable water (x_{nfw}) was calculated according to equation 4. E: enzyme; A: alginate; T: trehalose; AG: arabic gum; GG: guar gum. Standard deviation values are included.

	Glass transition		Crystallization	Melting		
Systems	T_g (°C)	Δcp (J/gK)	ΔH (J/g)	ΔH (J/g)	T_m' (°C)	x_{nfw}
EA	-	-	-	-278.8 ± 0.6^{a}	-1.82 ± 0.06^{d}	0.135 ± 0.002^{c}
EAT	-64 ± 2^{a}	0.12 ± 0.05^{a}	1.3 ± 0.2^{ab}	-232 ± 1^{b}	-7.53 ± 0.02^{a}	0.187 ± 0.002^{a}
EATAG	-65 ± 2^{a}	0.12 ± 0.05^{a}	0.765 ± 0.007^{b}	-245 ± 5^{bc}	-6.7 ± 0.1^{b}	0.157 ± 0.005^{b}
EATGG	-65 ± 1^{a}	0.12 ± 0.05^{a}	1.595 ± 0.007^{a}	-246.01 ± 0.06^{c}	-5.50 ± 0.05^{c}	0.158 ± 0.001^{b}

a-d Different letters on the columns indicate significant differences between means ($p < 0.05$).

Longitudinal and transverse relaxation times obtained at 25 °C were measured by LF-NMR and are shown in Table 3.

T_1 (or spin-lattice) and T_2 (or spin-spin) relaxations represent the efficiency of the protons to relax in the z and x-y directions, respectively. In both cases, the principal mechanism involved in the relaxation is magnetic field fluctuations. The main source of these fluctuations arises from molecular motion. For larger molecules like biopolymers, $T_1 >> T_2$, since the correlation time (the time it takes an average molecule to rotate one radian) is between 10^{-8}-10^{-5}.[41] This behavior was observed for our systems. The presence of trehalose reduced T_1, which is probably related to the lower correlation time of this molecule respect to alginate, even though the amount of protons contributed by trehalose is small respect to those contributed by water (as manifested by amplitude values). The presence of gums increases the T_1 respect to EAT beads. The CMPG sequence for T_2 allows the analysis of systems with high proton mobility (> 1 ms). The beads showed two T_2 times, in the range 54-66 ms and 379-710 ms, respectively. These two relaxation times were consistent to the ones determined by Aguirre Calvo at al.[34] and Rayment *et al.*[42] As expected, the obtained T_2 values were lower than the correspondent to pure water due to the reduced flexibility of the biopolymers chains.[43] Among the amplitudes, it is possible to observe

that more than 85% of protons contributed to the first population (lower T_2). There were no significant differences between amplitudes among the beads of different composition, as previously observed,[34] with the only exception of EAT and EA for A_{22}. However, the T_2 times were affected by composition, being especially high for EA beads for T_{22} and low for T_{21}.

It is important to highlight that the magnitude of T_2 reduction depends on the aggregation state and if the system is gelled or not. The NMR water proton response in gels or diluted polysaccharides systems is modulated by the exchange between water and biopolymers protons.[44,45] As a consequence, there are small differences among the systems in terms of populations (two for all the beads) and in terms of relative amplitudes. The second proton population corresponds to the water with high mobility, corresponding to the less associated water to biopolymers/sugar/gelled structure. Instead, the first proton population corresponds to the associated water (first hindrance layers), and even the absorbed water (to the solid matrix) and the solids itself (even though in a low proportion). The presence of trehalose strongly influenced the T_{22}, due to the fact that trehalose can be found in the entire bead, interacting with all the components. Only guar gum provokes a significant increment in T_{21} with respect to trehalose-containing beads. T_{22} shows also a higher mean value, even though this increment was not significant. This increment is translated in a slightly higher mobility in the EATGG beads than in the other systems, which could account for a higher degree of rearrangement of the protons excipients inside the beads, allowing a higher degree of interaction with the enzyme.

Table 3. Longitudinal (T_1), transversal (T_{21} and T_{22}) relaxation times and their correspondent amplitudes of beads containing lactase. E: enzyme; A: alginate; T: trehalose; AG: arabic gum; GG: guar gum. Standard deviation values are included.

Systems	$Amplitude_1$ (%)	T_1 (ms)	$Amplitude_{21}$ (%)	T_{21} (ms)	$Amplitude_{22}$ (%)	T_{22} (ms)
EA	-181 ± 1^{a}	1550 ± 10^{a}	85.5 ± 0.3^{a}	53.9 ± 0.3^{c}	14.5 ± 0.3^{a}	710 ± 20^{a}
EAT	-182 ± 9^{a}	1292 ± 12^{d}	87.1 ± 0.2^{a}	57 ± 1^{bc}	12.9 ± 0.2^{b}	403 ± 47^{b}
EATAG	-193 ± 1^{a}	1338 ± 6^{c}	86.6 ± 0.9^{a}	58.1 ± 0.3^{b}	13.3 ± 0.9^{ab}	379 ± 62^{b}
EATGG	-194 ± 2^{a}	1395 ± 15^{b}	86 ± 1^{a}	66 ± 1^{a}	14 ± 1^{ab}	495 ± 69^{ab}

a-d Different letters on the columns indicate significant differences between means ($p < 0.05$).

CONCLUSIONS

Alginate-Ca(II) beads containing lactase were successfully produced by the dropping method. Even though the inclusion of secondary excipients negatively influences the enzyme recovery with 20-30% losses, trehalose additions was critical for enzyme conservation during freezing and freeze/thawing treatments. Besides, the presences of guar gum improved the enzyme stability in a

better way than in other trehalose containing beads during storage at 4 °C and freeze/thawing. This effect was probably related to a slighter higher molecular mobility on EATGG beads, which could account for a higher degree of rearrangement of the protons excipients inside the beads, allowing a higher degree of interaction with the enzyme.

The establishment of glassy matrix during freezing was critical to assure the maintenance of the lactase activity. The obtained glassy matrices showed similar T_g and Δcp values in all trehalose containing systems, but the inclusion of gums slightly increased the T_m' values, representing a valuable technological improvement.

The microstructure of the alginate-Ca(II) beads showed interesting results: the presence of secondary excipients affected the microstructure, showing rods with smaller cross-sectional radius R and with lower compactness within the rods (α_2) than alginate-Ca(II) beads. However, there were no significant changes in rods interconnection (α_1). This lower compactness of the rods in the presence of trehalose could also explain the higher enzyme activity recovered, having the enzyme great possibilities of being located within the rods, increasing the possibility of establish more effective interactions.

The addition of both gums resulted in a significant increment of the bead size. However, arabic gum containing beads showed the highest circularity, and the guar gum containing ones the lowest. In this case, the increment in viscosity produced by the addition of guar gum accounts for a higher deformation during dropping. Further analysis should be conducted by changing the guar gum concentration, in order to optimize all the analyzed parameters.

ACKNOWLEDGEMENTS

The author María Victoria Traffano Schiffo wants to thank "Programa para la Formación de Personal Investigador (FPI)" Pre-doctoral Program of the Universitat Politècnica de València (UPV) for support her PhD studies and also her mobility to Argentina. This work was supported by the Brazilian Synchrotron Light Laboratory (LNLS, Brazil, proposal SAXS1-20160278), Universidad de Buenos Aires (UBACyT 20020130100610BA), Agencia Nacional de Promoción Científica y Tecnológica (ANPCyT PICT 2013 0434 and 2013 1331), CIN-CONICET (PDTS 2015 n° 196), and Consejo Nacional de Investigaciones Científicas y Técnicas. The authors acknowledge Dr. Pombero of R.D.C. for the useful discussions. PRS is a member of CONICET (Argentina).

REFERENCES

(1) Geiger, B.; Nguyen, H. M.; Wenig, S.; Nguyen, H. A.; Lorenz, C.; Kittl, R.; ... Nguyen, T. H. *Biochem. Eng. J.* **2016**, 116, 45-53.

(2) Pereira-Rodríguez, Á.; Fernández-Leiro, R.; González-Siso, M. I.; Cerdán, M. E., Becerra, M.; Sanz-Aparicio, J. *J. Struct. Biol.* **2012**, 177, 392-401.

(3) Banaszewska, A., Cruijssen, F., Claassen, G. D. H.; van der Vorst, J. G. A. J. *J. Dairy Sci.* **2014**, 97, 1893-1908.

(4) Mlichová, Z.; Rosenberg, M. *J. Food Nutr. Res.* **2006**, 45, 47-54.

(5) Erich, S.; Kuschel, B.; Schwarz, T.; Ewert, J.; Böhmer, N.; Niehaus, F.; ... Fischer, L. *J. Biotechnol.* **2015**, 210, 27-37.

(6) Harju, M.; Kallioinen, H.; Tossavainen, O. *Int. Dairy J.* **2012**, 22, 104-109.
(7) Husain, Q. *Crit. Rev. Biotechnol.* **2010**, 30, 41-62.
(8) Josef, E.; Zilberman, M.; Bianco-Peled, H. *Acta Biomater.* **2010**, 6, 4642-4649.
(9) Khattak, S. F.; Chin, K. S.; Bhatia, S. R.; Roberts, S. C. *Biotechnol. Bioeng.* **2007**, 96, 156-166.
(10) Rehman, H. U.; Aman, A.; Silipo, A.; Qader, S. A. U.; Molinaro, A.; Ansari, A. *Food Chem.* **2013**, 139, 1081-1086.
(11) Santagapita, P. R.; Mazzobre, M. F.; Buera, M. P. *Food Res. Int.* **2012**, 47, 321-330.
(12) Córdoba, A. L.; Deladino, L.; Martino, M. *Carbohyd. Polym.* **2013**, 95, 315-323.
(13) Santagapita, P. R.; Mazzobre, M. F.; Buera, M. P. *Biomacromolecules* **2011**, 12, 3147-3155.
(14) Li, X. Y.; Chen, X. G.; Liu, C. S.; Peng, H. N.; Cha, D. S. *Dry. Technol.* **2008**, 26, 895-901.
(15) Santagapita, P. R.; Buera, M. P. *J. Non-Cryst. Solids* **2008**, 354, 1760-1767.
(16) Busch, V. M.; Pereyra-Gonzalez, A.; Šegatin, N.; Santagapita, P. R.; Ulrih, N. P.; Buera, M. P. *LWT-Food Sci. Technol.* **2017**, 75, 227-235.
(17) Estevinho, B. N.; Damas, A. M.; Martins, P.; Rocha, F. *Food Res. Int.* **2014**, 64, 134-140.
(18) George, M.; Abraham, T. E. *Int. J. Pharm.* **2007**, 335, 123-129.
(19) Waters, D. J.; Engberg, K.; Parke-Houben, R.; Hartmann, L.; Ta, C. N.; Toney, M. F.; Frank, C. W. *Macromolecules* **2010**, 43, 6861-6870.
(20) Sonego, J. M.; Santagapita, P. R.; Perullini, M.; Jobbágy, M. *Dalton Trans.* **2016**, 45, 10050-10057.
(21) Agulhon, P.; Robitzer, M.; David, L.; Quignard, F. *Biomacromolecules* **2012**, 13, 215-220.
(22) Dashevsky, A. *Int. J. Pharm.* **1998**, 161, 1-5.
(23) Ullmann's Encyclopaedia of Industrial Chemistry, 5th ed.; Elvers, B., Ed.; VCH. 1995.
(24) Austin, L.; Bower, J. J.; Muldoon, C. *P. Int. Sym. Contr. Release Bioact. Mater.* **1996**, 23, 739-740.
(25) Aguirre Calvo, T.; Santagapita, P. *J. Qual. Reliab. Eng.* **2016**, 2016, 1-7.
(26) Park, Y. K.; Santi, M. S. S.; Pastore, G. M. *J. Food Sci.* **1979**, 44, 100-103.
(27) Tylewicz, U.; Panarese, V.; Laghi, L.; Rocculi, P.; Nowacka, M.; Placucci, G.; Dalla Rosa, M. *Food Biophys.* **2011**, 6, 327-333.
(28) Belotti, M.; Martinelli, A.; Gianferri, R.; Brosio, E. *Phys. Chem. Chem. Phys.* **2010**, 12, 516-522.
(29) Carr, H. Y.; Purcell, E. M. *Phys. Rev.* **1954**, 94, 630.
(30) Meiboom, S.; Gill, D. *Rev. Sci. Instrum.* **1958**, 29, 688-691.
(31) Aguirre Calvo, T. R; Busch, V. M.; Santagapita, P. R. *LWT-Food Sci. Technol.* **2017**, 77, 406-412.
(32) Busch, V. M.; Kolender, A. A.; Santagapita, P. R.; Buera, M. P. *Food Hydrocolloid.* **2015**, 51, 495-502.
(33) Vasile, F. E.; Martinez, M. J.; Ruiz-Henestrosa, V. M. P.; Judis, M. A.; Mazzobre, M. F. *Food Hydrocolloid.* **2016**, 56, 245-253.
(34) Fang, Y.; Al-Assaf, S.; Phillips, G. O.; Nishinari, K.; Funami, T.; Williams, P. A.; Li, L. *J. Phys. Chem. B* **2007**, 111, 2456-2462.
(35) Katayama, D. S.; Carpenter, J. F.; Manning, M. C.; Randolph, T. W.; Setlow, P.; Menard, K. P. *J. Pharm. Sci.* **2008**, 97, 1013–1024.
(36) Roos, Y. H.; Pehkonen, K. S. In *Water Properties in Food, Health, Pharmaceutical and Biological Systems: ISOPOW 10.* Reid, D. S., Sajjaanantakul, T., Lillford, P.J.,Charoenrein, S., Eds.; Wiley-Blackwell, a John Wiley & Sons, Inc.: Ames, Iowa, USA. 2010; pp 285-290.
(37) Schebor, C.; Mazzobre, M. F.; Buera, M. P. *Carbohyd. Res.* **2010**, 345, 303-308.
(38) Bloembergen, N.; Purcell, E.M.; Pound R.V. *Phys. Rev.* **1948**, 73, 679.
(39) Rayment, P.; Wright, P.; Hoad, C.; Ciampi, E.; Haydock, D.; Gowland, P.; Butler, M. F. *Food Hydrocolloid.* **2009**, 23, 816-822.
(40) Ablett, S.; Lillford, P. J.; Baghdadi, S. M. A.; Derbyshire, W. Am. *Chem. Soc. Symp. Series* **1976**, 34, 344-359.
(41) Hills, B. P.; Cano, C.; Belton, P. S. *Macromolecules* **1991**, 24, 2944-2950.
(42) Kimberlee, P.; Adrian, C. T.; Laurence, H. *Carbohyd. Res.***1993**, 246, 43-49.

Artículo 11

Traffano-Schiffo, M. V., Castro-Giraldez, M., Fito, P. J., & Santagapita P. R. (2017). Encapsulation of lactase in alginate-Ca(II) beads: effect of trehalose and gums inclusion and of drying methods. *Food Research International.* Artículo enviado.

ENCAPSULATION OF LACTASE IN ALGINATE-Ca(II) BEADS: EFFECT OF TREHALOSE AND GUMS INCLUSION AND OF DRYING METHODS

Maria Victoria Traffano-Schiffo[a], Marta Castro-Giraldez[a], Pedro J. Fito[a], Patricio R. Santagapita[b,c,*]

[a]Instituto Universitario de Ingeniería de Alimentos para el Desarrollo, Universidad Politécnica de Valencia, Camino de Vera s/n, 46022 Valencia, Spain.

[b]Universidad de Buenos Aires. Facultad de Ciencias Exactas y Naturales. Departamentos de Industrias y Química Orgánica. Buenos Aires, Argentina.

[c]CONICET-Universidad de Buenos Aires. Instituto de Tecnología de Alimentos y Procesos Químicos (ITAPROQ). Buenos Aires, Argentina.

*Corresponding author: prs@di.fcen.uba.ar

ABSTRACT

The purpose of the present work was to analyze the effect of trehalose, arabic and guar gums on the preservation of β–galactosidase activity in freeze-dried and vacuum dried alginate-Ca(II) beads. Freezing process was also studied as a first step of freeze-drying. Trehalose was critical for β-galactosidase conservation, and guar gum as a second excipient showed the highest conservation effect. Systems with T_g values ~ 40 °C which were stables at ambient temperature were obtained, being trehalose the main responsible of the formation of an amorphous matrix. Vacuum dried beads showed smaller size, higher circularity and large cracks in their surface than freeze-dried beads, which were more spongy and voluminous. Ice crystallization of the beads revealed that the crystallization of alginate-Ca(II) system follows the Avrami kinetics of nucleation and growth. These results open an opportunity in the development of new lactic products able to be consumed by lactose intolerance people.

Keywords: hydrogels, β-galactosidase, stability, freeze-drying, vacuum drying, microstructure.

Graphical Abstract

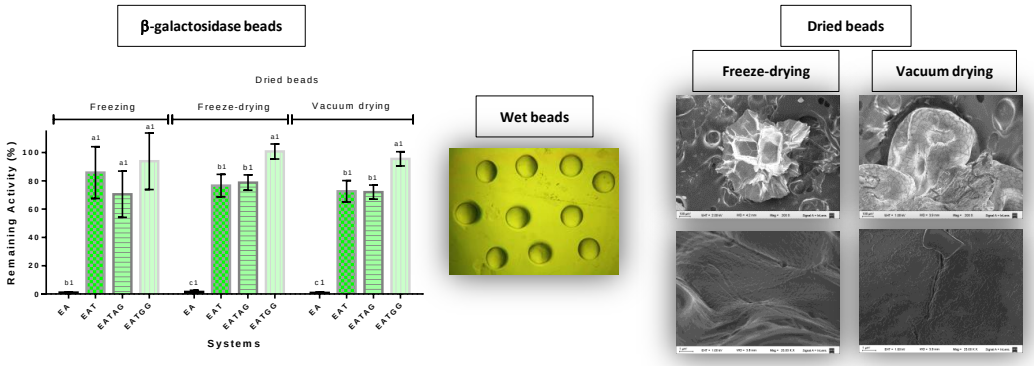

1. Introduction

Lactose is a disaccharide sugar that is found in milk, composed of galactose and glucose covalently bound by a β-galactoside linkage. Most of adult western Europeans can consume milk, however nowadays more and more people are suffering lactose intolerance condition. Lactose intolerance is a condition in which people's ability to digest lactose is decreased, due to insufficiency or lack of the enzyme called β-galactosidase (lactase) in the small intestines, which is crucial to break lactose down into its monosaccharides, suffering several digestive syndromes (Heaney, 2013; Misselwitz *et al.*, 2013). People who suffer this alteration should consume lactose free products or include the enzyme as a supplement (Zhang, Zhang, & McClements, 2017). However, lactase cannot be consumed in its free form due to its instability against to thermal, chemical and mechanical effects, so it, the encapsulation of the enzyme in biopolymers matrices could not only maintain its catalytic activity but also opens the possibility of its incorporation and consumption inside different foods.

Sodium alginate is a biopolymer widely used in encapsulation due to its gelation properties in presence of cations such as Ca^{2+}. The gelation occurs due to the exchange of Na^{+} ions from the carboxylic acids of the guluronate (G) blocks with Ca^{2+} ions from the crosslinking solution (Zhang, Zhang, Zou, & McClements, 2016). The G-block of one chain then form junctions with the G-block of the adjacent polymer chain, obtaining the characteristic egg-box structure forming rod-type structures (Zeeb, Saberi, Weiss, & McClements, 2015; Lee, & Mooney, 2012). A recently study performed by negative-staining electron microscopy has revealed that mannunorate (M) residues also interact in the structure giving flexibility and allowing a greater interaction of G-blocks (He, Liu, Li, & Li, 2016).

Although alginate-Ca(II) beads are easy to perform by the dropping method, are non-toxic, low cost and eco-friendly (Aguirre Calvo, Busch, & Santagapita, 2017), it shows disadvantages, such as low mechanical strength and low resistance to conservation treatments such as freeze-drying and vacuum-drying (Santagapita, Mazzobre, & Buera, 2012). Therefore, the encapsulation of labile structures in dehydrated or frozen systems is generally carried out in presence disaccharides such as trehalose (Santagapita *et al.*, 2012).

Trehalose is a non-reducing disaccharide with protectants properties against dehydration treatments, and lactase was successfully immobilized in trehalose matrix (Santagapita & Buera, 2008b). As was described by Mazzobre, Longinotti, Corti, and Buera (2002), the cryoprotectant effect of the trehalose can be attributed to promote the formation of glassy systems, avoiding deteriorative reactions. It should be taking into account that trehalose interacts with OH-rich biomolecules by hydrogen bonds, stabilizing the structure during thermal and drying treatments. Finally, the addition of others excipients (as natural occurring gums) can improve the stabilizing character of the system (Vasile, Romero, Judis, & Mazzobre, 2016), due to the changes in viscosity and/or interfacial properties, especially relevants for emulsions and suspensions.

In a previous work of the encapsulation of lactase in alginate-Ca(II) (Traffano-Schiffo, Aguirre Calvo, Castro-Giraldez, Fito, & Santagapita, 2017) it has been demonstrated that the presence of secondary excipients affected the microstructure of the alginate-Ca(II) network, showing rods with smaller cross-sectional radius and with lower compactness within the rods. Besides, trehalose was critical for activity preservation towards freezing and thawing treatments, being improved in guar gum-containing systems. The gums increased the onset temperatures of ice melting (T_m') determined by DSC in alginate-Ca(II) beads containing trehalose. However, this parameter nor the T_g were adequate predictors of the enzyme recovery in beads.

The aim of this research was to improve the stability of lactase against freeze-drying and vacuum drying by its encapsulation in alginate-Ca(II) beads and using trehalose, arabic and guar gums as excipients. Freezing was also studied as a first step of freeze-drying, including isothermal LF-NMR analysis.

2. Material and methods

2.1. Materials

The materials used for beads preparation were: sodium alginate (Algogel 5540) from Cargill S.A. (San Isidro, Buenos Aires, Argentina) with a molecular weight of $1.97 \cdot 10^5$ g/mol and mannuronate/guluronate ratio of 0.6; D-trehalose dihydrate (Hayashibara Co., Ltd., Shimoishii, Okayama, Japan/Cargill Inc., Mineapolis, Minnesota, USA) molecular weight of 378 g/mol; arabic gum (Biopack, Zárate, Buenos Aires, Argentina) molecular weight of 250.000 g/mol and a purity of 99%;guar gum (Cordis S.A., Villa Luzuriaga, Buenos Aires, Argentina) molecular weight of 220.000 g/mol and a mannose/galactose ratio of 1.8 and β-galactosidase from *Aspergillus Oryzae* (8.0 U/mg) (Sigma-Aldrich Co, Ltd, Saint Louis, USA). One enzymatic unit was defined as the amount of enzyme able to hydrolyze 1.0 μmol of lactose per minute at pH 4.5 at 30°C.

2.2. Gel beads preparation

Four different formulations were prepared, with the following composition: alginate (EA); alginate-trehalose (EAT); alginate-trehalose-guar gum (EATGG); alginate-trehalose-arabic gum (EATAG). All the solutions were prepared in 0.1 M acetate buffer pH 3.8. The final concentration of lactase solution was 0.775 mg/mL. The enzyme and the initial solutions were carefully mixed

and maintained at 4 ± 1 ºC in order to avoid enzyme activity losses. Taking into account that the isoelectric point of the enzyme was 4.61 (Dashevsky, 1998) and the pk_a values of alginate are 3.38 and 3.65 (Santagapita, Mazzobre, & Buera, 2011), the buffer acetate at pH 3.8 was used in order to obtain an electrostatic interaction between the alginate (negatively charged) and the enzyme (positively charged). A peristaltic pump was used to drop 10 mL of the alginate-enzyme mixture into 100 mL of the gelling solution, according to the drop method described by Austin, Bower and Muldoon (1996) with some modifications. For EA beads preparation, 1% (w/v) alginate solution containing enzyme was dropped into 2.5% (w/v) $CaCl_2$ solution (prepared in 0.1 M acetate buffer pH 3.8). For EAT, EATGG and EATAG preparation, a 1% (w/v) alginate with 20% (w/v) trehalose and/or with 0.25% (w/v) of guar or arabic gums solutions containing the enzyme were dropped into the 2.5% (w/v) $CaCl_2$ solution supplemented with 20% (w/v) trehalose using the same procedure described previously.

$CaCl_2$ solution (with or without trehalose) was maintained in a cold bath with constant stirring (9.0 ± 0.1 rpm) and a needle with 0.25 mm diameter and 6 mm length (Novofine 32 G, Novo Nordisk A/S, Bagsvaerd, Denmark) was used for the dropping. The distance between the needle and the $CaCl_2$solution was 6 cm. After beads generation, they were maintained 15 min in $CaCl_2$ solution (with constant stirring) and after that, there were washed 5 times with bidestilled cold water.

2.3. Thermal Treatments

2.3.3. Freezing

Wet beads were frozen at -18ºC by using a conventional freezer during 24 h.

2.3.4. Freeze-drying

The beads were frozen at -18ºC in a conventional freezer during 24 h. Freeze-drying (FD) was performed during 24 h in a Heto Holten A/S, cooling trap model CT 110 freeze-dryer (Heto Lab Equipment, Allerød, Denmark) operating at a condenser plate temperature of −110 °C and a minimum chamber pressure of $4{\cdot}10^{-4}$ mbar. The secondary drying was performed at 25 °C without shelf-control temperature.

2.3.5. Vacuum drying (VD)

VD was carried out in a vacuum Oven (Fistreem International Ltd, Loughborough, United Kingdom) at 25ºC and a pressure of 113 mbar during 24 h. Silica gel was used as desiccant agent.

After dehydration (by VD or FD), the beads were kept in vacuum desiccators until its determination.

2.4. β-Galactosidase activity

The enzyme activity was evaluated following the method described by Park, Santi, and Pastore (1979) with some modifications. 9 wet or dried beads were dissolved into 0.25 mL of 0.1 M citrate buffer pH 4.5 during 2 h at 4 ºC (without stirring, in order to avoid enzymatic activity losses). Subsequently, 0.25 mL of o-nitrophenyl-β-D-galactopyranoside (ONPG) (Sigma Chemical Co.)

prepared in 0.1 M acetate buffer pH 3.8 was added and incubated during 15 min at 33 °C. Finally, the reaction was stopped adding 0.5 mL of sodium carbonate 10% (w/v) and 1.75 mL of distilled water was added for subsequent measurement of o-nitrophenol (ONP) at 420 nm by using a Jasco V-630 UV-VIS spectrophotometer (JASCO Inc., Maryland, USA) at room temperature. Measurements were made in triplicate.
The remaining activity of the beads after thermal treatments was calculated as follows:

$$Remaining\ Activity\ (\%) = \frac{Activity_t}{Activity_0} \times 100 \quad (1)$$

Where $Activity_t$ is the activity value of each system obtained after a given treatment and $Activity_0$ is related to the activity of the same system before the treatment.

2.5. Beads characterization

2.5.1. Digital image analysis

The size and shape of the beads were analysed through digital images captured by a digital camera coupled to a binocular microscope and analysed by the free license software ImageJ (http://rsbweb.nih.gov/ij/), as was described by Aguirre Calvo & Santagapita, (2016). The Feret's diameter (size) corresponds to the longest distance between any two points along the bead boundary. The circularity indicates how similar the bead is to a circle. At least 40 wet or dried beads of each system were analysed by applying the "analyse particle" command of the software. The ImageJ software was calibrated to transform the measured pixels in length units (mm) by taking pictures of a caliper section.

2.5.2. Water activity and water content

Water activity (a_w) of dried beads was determined by a dew point Hygrometer Decagon (Aqualab®, series 3 TE, Decagon Devices, Pullman, WA, USA). A special sample holder was used to reduce the quantity of beads needed. A calibration curve was performed with salts with known a_w (between 0.25 and 1). Measurements were made in triplicate.
Water content of the dried beads was obtained gravimetrically by the difference in weight before and after drying in vacuum oven for 48 h at 96 ± 2 °C (Aguirre Calvo, & Santagapita, 2016). Water content determination was performed in duplicate.

2.6. Microstructure analysis by Scanning Electron Microscopy (SEM-FEG)

The morphology of dried beads was observed by a scanning electron microscopy with field emission gun (SEM-FEG) model supra 40 (Carl Zeiss SMT Inc., Peabody, MA, USA) with InLes detector. The sensitivity of the detector allowed to observed details in the beads structure without applying a metal cover to the samples. The magnifications used were 25000x and 200x at 1.00 kV.

2.7. Differential scanning calorimetry (DSC)

Glass transition temperature (T_g), the variations in heat capacity at T_g (Δcp) and the enthalpy relaxation of freeze-dried and vacuum dried beads were determined by differential scanning calorimetry (DSC) by means of a Mettler Toledo 822 equipment (Mettler Toledo AG, Urdorf, Switzerland) and STARe Thermal Analysis System version 8 software (Mettler Toledo AG). The instrument was calibrated using standard compounds (indium and zinc) of defined melting point and heat of melting.

All measurements were made in duplicate with 14-23 mg sample mass, using hermetically sealed aluminum pans of 40 µl inner volume (Mettler), heated from -100 ºC to 100 ºC at 10 ºC/min; an empty crucible was used as a reference. The reported data are the average of two determinations. After the first scan, the same sample was scanned in the same conditions in order to obtain the Δcp of the rescan.

In order to analyze the enthalpy relaxation, the dried beads were aged at 25 ºC during 37 days into hermetically sealed micro-centrifuge tubes. At the ageing temperature the samples were about 10-15 ºC below T_g for trehalose-containing samples (Santagapita & Buera, 2008a). Glass transitions were recorded as the onset temperature of the discontinuities in the curves of heat-flow versus temperature (change in heat capacity).

2.8. Low Field Nuclear Magnetic Resonance (LF-NMR): isothermal studies

A Bruker Minispec mq20 (Bruker BiospinGmbh, Rheinstetten, Germany) with a 0.47 T magnetic field operating at a resonance frequency of 20 MHz was used to study the transversal or spin–spin relaxation decay. The FID (free induction decay) sequence was used with the following setting: scans = 8, dummy shots = 0, recycle delay = 5 ms, gain = 81-83 dB. Wet beads equilibrated at 25.00 ± 0.01 ºC in a thermal bath (Haake, model Phoenix II C35P, Thermo Electron Corporation Gmbh, Karlsruhe, Germany) were measured at -20.05 ºC ± 0.05, controlled by a BVT3000 unit (Bruker Biospin GmbH). Measurements were taken any 10 s during 10 min. The obtained signal (% solid component) is defined as the ratio of the signal from the solid component divided by the total NMR signal. This is based on the fact that the signal from the solid component decays very quickly, whereas the signal from the liquid component is preserved significantly longer. To account for the receiver dead time, the signal is extrapolated to t = 0 by multiplying with a correction factor called f-factor.

The Johnson–Mehl–Avrami–Komogorov (JMAK) equation (eq. 2) was used to fit the experimental data (Avrami, 1939; Johnson, & Mehl, 1939; Kolmogorov, 1937).

$$\alpha = 1 - \exp(-K_c t)^n \qquad (2)$$

Where α is the solid crystal fraction obtained over time t; n is known as Avrami index, related to nucleation and dimension of crystal growing; and K_c [$(\text{time})^{-n}$], related to the isothermal crystallization rate (which mainly depends of temperature).

Data was normalized by the freezable water content, which was obtained by multiplying the fraction of the freezable water (x_{fw}, which were 0.86 for EA, 0.813 for EAT and 0.842 for EATAG and EATGG) with the water content (Traffano-Schiffo *et al.*, 2017).

2.9. Statistical analysis

The statistical analyses were performed by one-way ANOVA with Tukey`s post test by using Prism 6 (GraphPad Software Inc., San Diego, CA, USA) in order to determine significant differences between the mean values of beads of different composition on the measured parameters for the same treatment. A*t* test was used to differentiate means of different treatments for the same system with 95 % of confidence between (p< 0.05).

3. Results and discussion

3.1. Effects of beads composition and drying on β-galactosidase activity preservation

Figure 1 shows the remaining activity of lactase after freezing, freeze-drying and vacuum drying, where EA systems shows a remaining activity practically null after thermal treatments. The inclusion of trehalose was critical in order to stabilize the enzyme for all the applied treatments. According to the "water replacement theory", the conformation of the protein is maintained by the hydrogen bonds with the water. Upon freezing or drying, trehalose replaces the water establishing hydrogen bonds with the protein and therefore, stabilizing it. Also, the capacity of the sugar to generate a glassy matrix allows to immobilize the protein inside its matrix, reducing molecular movements and hereby avoiding protein denaturation (Grasmeijer, Stankovic, de Waard, Frijlink, & Hinrichs, 2013).

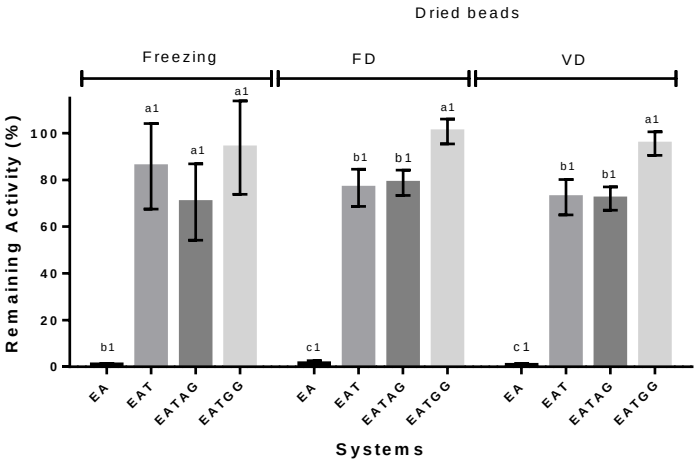

Figure 1. Remaining activity of lactase (%) after thermal treatments: freezing (24 h at -18 ºC); freeze-drying (FD) and vacuum drying (VD). E: enzyme; A: alginate; T: trehalose; AG: arabic gum; GG: guar gum. For a certain treatment bars with the same letter (a-c) indicate no significant differences (p < 0.05); for beads of same composition bars with the same number have no significant differences between treatments (p < 0.05).

The addition of guar gum as a second excipient showed the highest remaining activity values for FD and VD (close to 95%) comparing with the other formulations. Similar results were obtained by Traffano-Schiffo *et al.* (2017) which showed that the presence of this gum also increases the remaining activity after 24 h of storage at 4 °C and after four freeze/thaw cycles using liquid nitrogen. The conservative effect of guar gum in wet beads could be due to its high molecular mobility measured by LF-NMR, showing a high degree of rearrangement of the protons excipients inside the beads (Traffano-Schiffo *et al.*, 2017), allowing a greater degree of interaction with the enzyme. In light of present results, it could be proposed that these interactions (mainly hydrogen bonds and van der Waals forces) were maintained during dehydration.

3.2. Effect of drying on physicochemical characteristics of beads

Water activity was determined for FD and VD beads. EA systems showed the higher a_w values, being 0.412 ± 0.004 and 0.386 ± 0.003 for FD and VD beads, respectively. a_w values obtained for trehalose-containing beads were between 0.365 and 0.392, where the lower values correspond to VD samples.

Table 1 shows the water content, the glass transition temperatures, the change in heat capacity at T_g (during the scan and rescan), and enthalpy relaxation (E.R.) for freeze-dried and vacuum dried beads.

Table 1. Water content (X_w, on dry basis), glass transition temperature (T_g), change in heat capacity at T_g (Δcp), enthalpy relaxation (E.R.) and the change in heat capacity (Δcp) during the rescan were obtained for freeze-dried (FD) and vacuum dried (VD) beads by DSC. E: enzyme; A: alginate; T: trehalose; AG: arabic gum; GG: guar gum. Standard deviation values are included.

Treatment	Systems	Glass Transition		E. R. (J/g)	Δcp^{rescan}(J/gK)	X_w (kg_w/kg_{db})
		T_g (°C)	Δcp (J/gK)			
FD	EA	-24±2^{b}	0.11 ± 0.08^{b}	-	-	0.1810 ± 0.0006^{a}
	EAT	40±2^{a}	0.63 ± 0.04^{a}	-2.3 ± 0.7^{a}	0.2 ± 0.2^{a}	0.079 ± 0.009^{b}
	EATAG	37±5^{a}	0.37 ± 0.04^{a*}	-3.3 ± 0.3^{a}	0.147 ± 0.007^{a*}	0.069 ± 0.002^{b}
	EATGG	40.4±0.1^{a}	0.6 ± 0.1^{a}	-2 ± 1^{a}	0.27 ± 0.01^{a}	0.07 ± 0.01^{b}
VD	EA	-	-	-	-	0.19 ± 0.01^{a}
	EAT	35.7 ± 0.1^{b}	0.71 ± 0.05^{a}	-0.3 ± 0.2^{b}	0.46 ± 0.08^{a}	0.088 ± 0.003^{b}
	EATAG	37.60 ± 0.08^{ab}	0.65 ± 0.02^{a*}	-1.17 ± 0.07^{b}	0.45 ± 0.03^{a*}	0.082 ± 0.003^{b}
	EATGG	38.1 ± 0.9^{a}	0.5 ± 0.1^{a}	-2.3 ± 0.4^{a}	0.40 ± 0.08^{a}	0.083 ± 0.004^{b}

$^{a-b}$ Different letters on the columns indicate significant differences between means of the same treatment; * indicate significant differences between means of the same system ($p < 0.05$).

The T_g value obtained for freeze-dried EA system was -24 ± 2 °C, however, the T_g value of EA vacuum-dried beads could not be observed. Santagapita *et al.* (2012) were not able to obtain a T_g value for alginate-Ca(II) beads containing invertase. In contrast, the glass transitions temperatures for beads containing trehalose were significantly higher than EA, reaching values between 35 and 40 °C for all the studied treatments. These high T_g values indicate that the trehalose-containing beads were in the glassy state at ambient temperature, stabilizing the enzyme as observed in Figure 1, and assuring stability as long as temperature or humidity did not increase. Similar T_g values for

trehalose containing beads were previously reported (Santagapita *et al.*, 2012; Santagapita & Buera, 2008a).

The significant higher Δcp values associated to T_g obtained for trehalose containing beads than for EA beads is consistent with fact that sugars depict transitions with higher Δcp values than polymers, which also developed the transition in a longer range of temperatures, being more difficult to be observed (Santagapita *et al.*, 2012; Katayama *et al.*, 2008). Among the trehalose-containing beads, no significant differences were observed by the addition of guar or arabic gums, revealing that trehalose is the main contributor to the generation of the amorphous matrix.

Being the T_g a reversible transition, the Δcp values after the rescan can be interpreted as the capacity of the matrix to regenerate the glassy state from the supercooled state after the first scan. According to the data of Table 1, no significant differences were obtained among the drying treatments, showing similar capacity of recovery.

Enthalpy relaxation is an important characteristic of the amorphous materials, and is often observed as an endothermic event within the T_g region during heating (Santagapita, & Buera, 2008a). Since glassy materials are thermodynamically unstable, their structure could relax towards the equilibrium state during storage above T_g, being it extent also a function of temperature and time (Santagapita, & Buera, 2008a). Beads containing trehalose were aged during 37 days between 10 and 15 °C below their T_g value prior DSC analysis. No significant differences were obtained between VD and FD treatments for each type of beads. Besides, FD beads showed similar stability among the different systems. Among the VD beads, the presence of guar gum produced glassy matrices of higher enthalpy values than the others trehalose-containing beads, indicating a key role in the matrix formation, which in turn could favor the enzyme activity conservation. Higher relaxation enthalpy values were linked to higher remaining activity conservation in lactase-trehalose model systems (Santagapita & Buera, 2008a). A higher relaxation enthalpy value corresponds to a more perfect glass, represented by an extended glassy region formed during ageing.

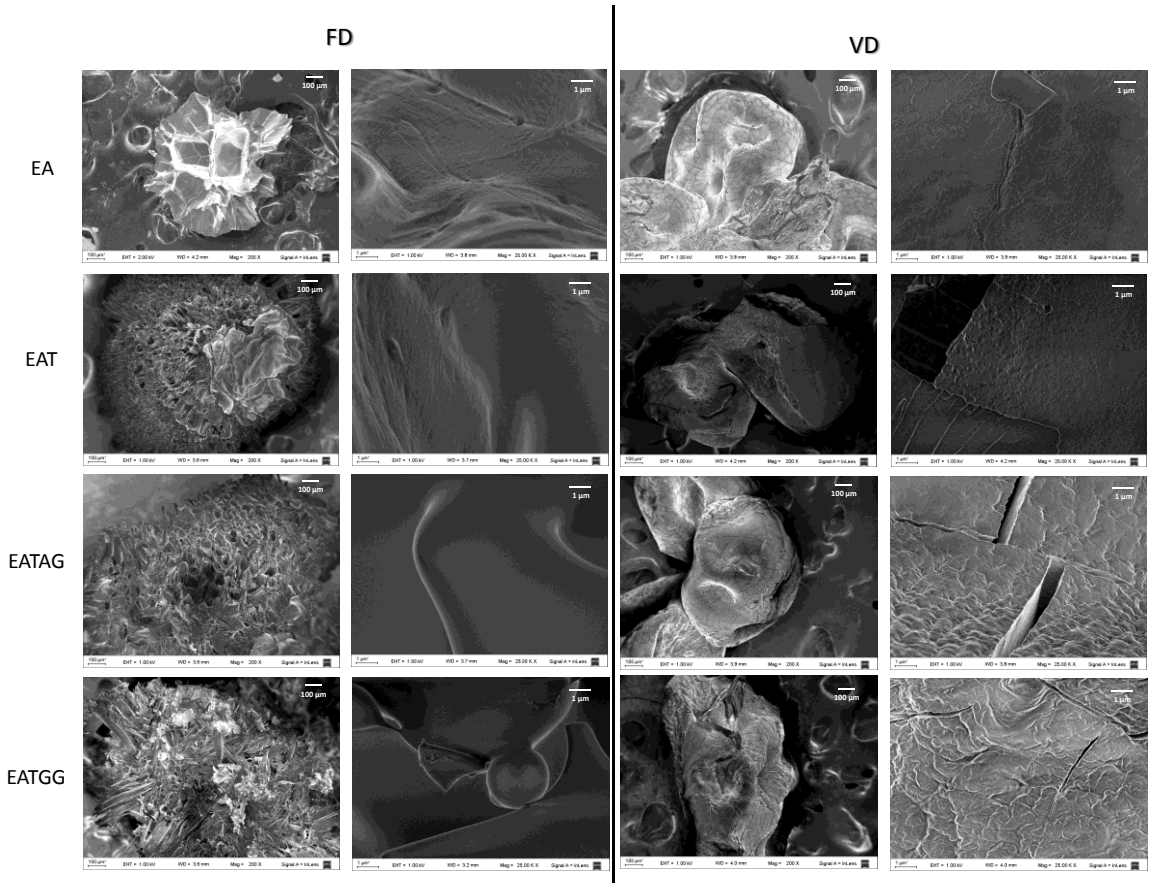

Figure 2. Images obtained in a scanning electron microscope (SEM) of freeze-drying (FD) and vacuum-drying (VD) beads at two different magnifications. E: enzyme; A: alginate; T: trehalose; AG: arabic gum; GG: guar gum.

Figure 2 shows the images obtained by SEM for freeze and vacuum dried beads. As can be seen in the images on the left side of each treatment (200x), freeze-dried beads had more spongy and voluminous surface, while the vacuum dried beads were more compact and showed less exposed surface area compared with FD samples. At higher magnifications (25000x) big differences in the surface of the beads can be appreciated: the beads subjected to VD showed large cracks, as a result of its breakable surface, and also consistent with the high size reduction of the beads. However, this structural characteristic did not affect the enzyme remaining activity (Figure 1). All trehalose-containing beads showed the typical glassy structure, which is supported by the DSC analysis showed in Table 1.Instead, EA beads showed the typical structure of supercooled liquid, showing a less smooth surface, as result of the lower viscosity of the supercooled liquid respect to the glassy state.

In order to characterize the beads according to its size and shape, Feret´s diameter and circularity were obtained (Figure 3). Figure 3a shows the Feret´s diameter of wet (after generation) and dried beads (FD and VD) with different composition. VD beads showed significant smaller Feret´s diameter comparing with FD and wet beads, reaching values close to 1 mm. It is important to highlight that the addition of trehalose significantly incremented the beads size respect to alginate beads for each drying treatment. In addition, the presence of gums further increased the size respect to trehalose-containing beads, especially in FD beads. These facts are linked to the raise in viscosity produced by the addition of guar gum and to the modification in the interfacial

properties (protein-polysaccharide structure) caused by arabic gum (Busch *et al.*, 2017). Guar gum inclusion even avoided the size reduction in FD beads, which could have interesting technological implications.

Figure 3b shows the circularity of the beads, where trehalose containing beads subjected to VD treatment showed a significant higher circularity value close to 0.8 and FD beads showed much lower circularity values (between 0.5 and 0.6). These results are consistent with the FEG-SEM images previously discussed (Figure 2) and it could be explained from the physic point of view of the applied drying treatments. During VD, the beads contract due to the evaporation of the water molecules, reducing its volume. In contrast, during the sublimation step, large pores are formed on the FD beads. These pores correspond to the spaces previously occupied by ice crystals, showing as a consequence a spongy surface of higher volume. In addition, the contraction of the VD beads could also explain the presence of the cracks observed in FEG-SEM images.

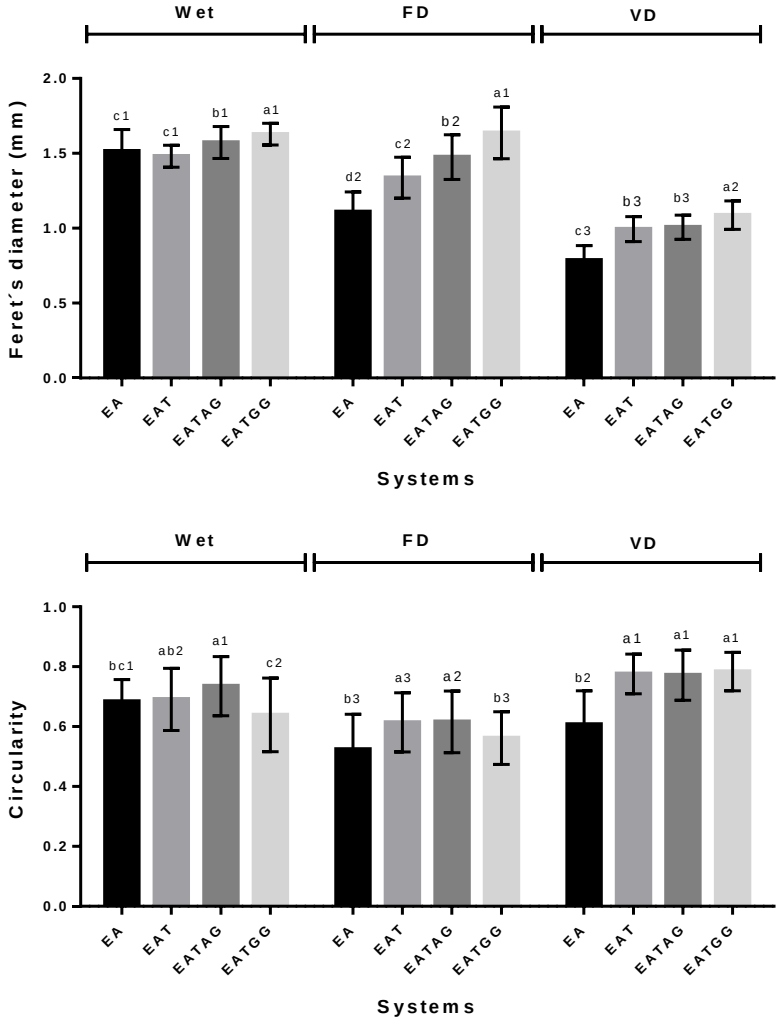

Figure 3. a) Feret´s diameter and b) circularity of wet, freeze-dried (FD) and vacuum dried (VD) beads with different composition. E: enzyme; A: alginate; T: trehalose; AG: arabic gum; GG: guar gum. For a certain treatment bars with the same letter (a-d) indicate no significant differences ($p < 0.05$); for beads of

same composition bars with the same number (1-3) have no significant differences between treatments ($p < 0.05$).

3.3. Isothermal crystallization by LF-NMR

In a previous work, Traffano-Schiffo and co-workers (2017) observed that the presence of gums increased the onset temperatures of ice melting (T_m') determined by DSC in alginate-Ca(II) beads containing trehalose. Besides, these beads depicted T_g values around-65 °C. However, neither of these parameters were adequate predictors of the remaining activity of the enzyme in beads. In order to deeply understand the results obtained by freezing alginate-Ca(II) beads, LF-NMR studies were conducted.

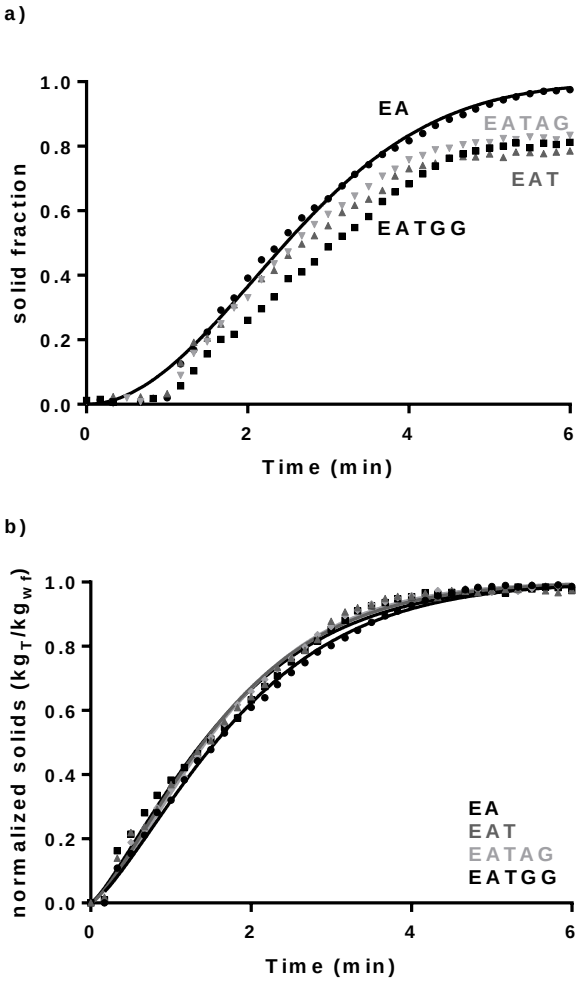

Figure 4. Isothermal LF-NMR: solid fraction vs time at -20 °C. a) raw data (solid fraction) and b) normalized solids by freezable water content. Experimental data (symbols) were fitted using Avrami equation (lines).

Figure 4 shows the increment of the solid fraction on wet beads isothermally treated at -20 °C. The measurement relays on the different relaxation times between the protons belonging to liquid and

solid phases. Typically, wet beads depicted two mobile protons populations between 54-66 ms and 379-710 ms, respectively (Traffano-Schiffo *et al.*, 2017). When a solid fraction is generated, a much shorter T_2 is observed. By relating the T_2 from both solid and total (solid plus liquid) contributions, it is possible to study the increment of the solid fraction at subzero temperatures from wet beads due to ice crystallization.

Considering that T_m' of the beads systems lies between -8 and -2 °C and T_g around -64/65 °C (for trehalose containing beads) (Traffano-Schiffo *et al.*, 2017), ice crystallization will be the main phenomenon produced at -20 °C. Figure 4a shows the unprocessed data of the solid fraction on wet beads. It is clearly observed that EA samples achieved complete ice crystallization. Instead, in trehalose containing samples only 80% of the solid fraction was achieved. The final solid percentage at which each sample finally stabilizes at -20 °C follows the same trend of unfreezable water present in each system obtained by DSC data (Traffano-Schiffo *et al.*, 2017).

JMAK equation (Avrami, 1939; Johnson, & Mehl, 1939; Kolmogorov, 1937) was used to fit the experimental data. Two parameters are derived: n, which gives information about nucleation and dimension of crystal growing; and K_c, related to the isothermal crystallization rate. The model implies that the crystallization starts randomly at different points and it propagates from each nucleation point (Gedde, 1995). Avrami equation only adequately fitted EA samples in Figure 4a, following sigmoidal crystallization kinetics, with an n value of 2.03 ± 0.07. This implies that the dimension of crystal growing is bidimensional. Xu and co-workers (2016) obtained a n~1 by studying amorphous solid water films, even though they experiments involved grow from a well-defined interface, while the model assumes randomly nucleation points. However, they observed a sigmoideal crystallization kinetics, typical from a nucleation and growth process, such as the one observed here. It is already known that alginate can retard the rate of ice-crystal growth in ice creams (Nussinovitch, 1997) by increasing viscosity or by quelating Ca(II). Besides, Gryshkov, Pogozhykh, Hofmann, Mueller and Glasmacher (2014) employed alginate-Ca(II) beads for cryopreservation purposes, thinking that gel-like structures and mild environment inside alginate beads could resist the reorganization of ice crystals during thawing, minimizing cell damage. However, to the best of our knowledge, for the first time ice crystallization kinetics inside alginate-Ca(II) beads were obtained through LF-NMR.

Figure 4b shows the normalized solid fraction for comparison of the crystal growing of the four beads systems. It is clearly see that ice crystallization in alginate-Ca(II) beads followed the so called Avrami kinetics of nucleation and growth. Figure 4b shows that the inclusion of trehalose or gums did not affect the dimension of the ice growing (= n) nor its rate (= K_c). Then, it is possible to conclude that the main effect on enzyme stability is the generation of glassy matrix during freezing, with the concomitant reduction of crystallized water. There was not effect of trehalose or gums on ice crystallization inside beads, leaving unaffected kinetics rate, nucleation and growing. It was proved that the addition of a second excipient to sugar or polyol matrices designed for protecting biomolecules (in pharmaceutical or food-ingredient formulations) can be beneficial. Buera, Schebor and Elizalde, (2005) showed that the presence of proteins retarded sugar crystallization, and in parallel, sugars retarded protein denaturation. There is also evidence that the presence of polymers or salts produced inhibition of trehalose crystallization (Mazzobre,

Santagapita, Gutiérrez, Buera, 2008, Santagapita, & Buera, 2008a). However, this effects were not observed for ice crystallization in alginate-Ca(II) beads.

4. Conclusions

Trehalose was critical for β-galactosidase conservation in alginate-Ca(II)beads after drying treatments. Guar gum as a second excipient showed the higher conservation effect for both treatments.

Trehalose was the main responsible of the formation of an amorphous matrix in the beads, showing T_g values close to 40 °C, assuring very stable systems at ambient temperature. The presence of guar gum produced glassy matrices of high enthalpy values for both types of drying, indicating a key role in the matrix formation and, in turn, in enzyme activity conservation.

According to the size and morphology, VD beads showed smaller size and higher circularity comparing with FD and wet beads. The presence of trehalose significantly incremented the size respect alginate beads for both drying treatments. Besides, gums further increased the size, especially in FD beads. FEG-SEM images have revealed that FD beads had more spongy and voluminous surface, while VD beads showed large cracks (breakable surface). All trehalose-containing beads showed the typical glassy structure, which was supported by the DSC analysis.

For the first time, an isothermal crystallization analysis of alginate-Ca(II) beads containing β-galactosidase was carried out by LF-NMR. It revealed that the ice crystallization inside the beads follows the Avrami kinetics of nucleation and growth. The final ice fraction obtained was in agreement with the freezable water obtained by DSC.

The results of this research open an opportunity in the design and development of new lactose-containing foods able to be consumed by lactose intolerance people.

5. Acknowledgements

This work was supported by Universidad de Buenos Aires (UBACyT 20020130100610BA), Agencia Nacional de Promoción Científica y Tecnológica (ANPCyT PICT 2013 0434 and 2013 1331), CIN-CONICET (PDTS 2015 n° 196), and Consejo Nacional de Investigaciones Científicas y Técnicas.

The author María Victoria Traffano Schiffo wants to thank "Programa para la Formación de Personal Investigador (FPI)" Pre-doctoral Program of the Universitat Politècnica de València (UPV) for support her PhD studies and also her mobility to Argentina.

6. References

Aguirre Calvo, T. R., Busch, V. M., & Santagapita, P. R. (2017). Stability and release of an encapsulated solvent-free lycopene extract in alginate-based beads. *LWT-Food Science and Technology*, 77, 406-412.

Aguirre Calvo, T., & Santagapita, P. (2016). Physicochemical characterization of alginate beads containing sugars and biopolymers. *Journal of Quality and Reliability Engineering*, 2016.

Austin, L., Bower, J. J., & Muldoon, C. (1996). The controlled release of leukaemia inhibitory factor (LIF) from gels. *Proceeding of the International Symposium on Controlled Release of Bioactive Materials*, 23, 739-740.

Avrami, M. (1939). Kinetics of phase change. I General theory. *The Journal of Chemical Physics*, 7(12), 1103-1112.

Buera, M. P., Schebor, C., & Elizalde, B. (2005). Effects of carbohydrate crystallization on stability of dehydrated foods and ingredient formulations. *Journal of Food Engineering*, 67(1), 157-165.

Busch, V. M., Pereyra-Gonzalez, A., Šegatin, N., Santagapita, P. R., Ulrih, N. P., & Buera, M. P. (2017). Propolis encapsulation by spray drying: characterization and stability. *LWT-Food Science and Technology*, 75, 227-235.

Dashevsky, A. (1998). Protein loss by the microencapsulation of an enzyme (lactase) in alginate beads. *International Journal of Pharmaceutics*, 161(1), 1-5.

Gedde, W.U. (1995). Crystallization kinetics. In U.W. Gedde (Ed.), *Polymer Physics* (pp. 169-198). London: Springer.

Grasmeijer, N., Stankovic, M., de Waard, H., Frijlink, H. W., & Hinrichs, W. L. (2013). Unraveling protein stabilization mechanisms: vitrification and water replacement in a glass transition temperature controlled system. *Biochimica et Biophysica Acta (BBA)-Proteins and Proteomics*, 1834(4), 763-769.

Gryshkov, O., Pogozhykh, D., Hofmann, N., Mueller, T., & Glasmacher, B. (2014). C-1009: Cryopreservation of monkey mesenchymal stem cells inside alginate 3D micro-spheres after a high voltage encapsulation. *Cryobiology*, 69(3), 514.

He, X., Liu, Y., Li, H., & Li, H. (2016). Single-stranded structure of alginate and its conformation evolvement after an interaction with calcium ions as revealed by electron microscopy. *RSC Advances*, 6(115), 114779-114782.

Heaney, R. P. (2013). Dairy intake, dietary adequacy, and lactose intolerance. *Advances in Nutrition: An International Review Journal*, 4(2), 151-156.

Johnson, W. A., & Mehl, R. F. (1939). Reaction kinetics in processes of nucleation and growth. *Trans. Aime*, 135(8), 396-415.

Katayama, D. S., Carpenter, J. F., Manning, M. C., Randolph, T. W., Setlow, P., & Menard, K. P. (2008). Characterization of amorphous solids with weak glass transitions using high ramp rate differential scanning calorimetry. *Journal of Pharmaceutical Sciences*, 97(2), 1013-1024.

Kolmogorov, A. N. (1937). On the statistical theory of the crystallization of metals. *Bulletin of the Russian Academy of Science*.1, 355-359.

Lee, K. Y., & Mooney, D. J. (2012). Alginate: properties and biomedical applications. *Progress in Polymer Science*, 37(1), 106-126.

Mazzobre, M. F., Longinotti, M. P., Corti, H. R., & Buera, M. P. (2002). Effect of salts on the properties of aqueous sugar systems, in relation to biomaterial stabilization. 1. Water sorption behavior and ice crystallization/melting. *Cryobiology*, 43(3), 199-210.

Mazzobre, M. F., Santagapita, P. R., Gutiérrez, N., & Buera, M. P. (2008). Consequences of matrix structural changes on functional stability of enzymes as affected by electrolytes. In G. Gutiérrez-López, G. Barbosa-Cánovas, J. Welti-Chanes, & E. Parada-Arias (Eds.), *Food Engineering: Integrated Approaches* (pp. 73–87). New York: Springer.

Misselwitz, B., Pohl, D., Frühauf, H., Fried, M., Vavricka, S. R., & Fox, M. (2013). Lactose malabsorption and intolerance: pathogenesis, diagnosis and treatment. *United European Gastroenterology Journal*, 1(3), 151-159.

Nussinovitch, A. (1997). Hydrocolloid applications: gum technology in the food and other industries. In A. Nussinovitch (Ed.), *Alginates* (pp. 19-39). London: Chapman & Hall.

Park, Y. K., Santi, M. S. S., & Pastore, G. M. (1979). Production and characterization of β-galactosidase from *Aspergillus oryzae*. *Journal of Food Science*, 44(1), 100-103.

Santagapita, P. R., & Buera, M. P. (2008a). Electrolyte effects on amorphous and supercooled sugar systems. *Journal of Non-Crystalline Solids*, 354(15), 1760-1767.

Santagapita, P. R., & Buera, M. P. (2008b). Trehalose–water–salt interactions related to the stability of β-galactosidase in supercooled media. *Food Biophysics*, 3(1), 87-93.

Santagapita, P. R., Mazzobre, M. F., & Buera, M. P. (2011). Formulation and drying of alginate beads for controlled release and stabilization of invertase. *Biomacromolecules*, 12(9), 3147-3155.

Santagapita, P. R., Mazzobre, M. F., & Buera, M. P. (2012). Invertase stability in alginate beads: effect of trehalose and chitosan inclusion and of drying methods. *Food Research International*, 47(2), 321-330.

Traffano-Schiffo, M. V., Aguirre Calvo, T. R., Castro-Giraldez, M., Fito, P. J. & Santagapita, P. R. (2017). Alginate beads containing lactase: stability and microstructure. *Biomacromolecules.*

Vasile, F. E., Romero, A. M., Judis, M. A., & Mazzobre, M. F. (2016). *Prosopis alba* exudate gum as excipient for improving fish oil stability in alginate–chitosan beads. *Food Chemistry*, 190, 1093-1101.

Xu, Y., Petrik, N. G., Smith, R. S., Kay, B. D., & Kimmel, G. A. (2016). Growth rate of crystalline ice and the diffusivity of supercooled water from 126 to 262 K. *Proceedings of the National Academy of Sciences*, 113(52), 14921-14925.

Zeeb, B., Saberi, A. H., Weiss, J., & McClements, D. J. (2015). Formation and characterization of filled hydrogel beads based on calcium alginate: factors influencing nanoemulsion retention and release. *Food Hydrocolloids*, 50, 27-36.

Zhang, Z., Zhang, R., & McClements, D. J. (2017). Lactase (β-galactosidase) encapsulation in hydrogel beads with controlled internal pH microenvironments: Impact of bead characteristics on enzyme activity. *Food Hydrocolloids*, 67, 85-93.

Zhang, Z., Zhang, R., Zou, L., & McClements, D. J. (2016). Protein encapsulation in alginate hydrogel beads: Effect of pH on microgel stability, protein retention and protein release. *Food Hydrocolloids*, 58, 308-315.

Traffano-Schiffo, M. V., Aguirre Calvo, T. R., Castro-Giraldez, M., Fito, P. J., Perullini, M. & Santagapita P. R. (2017). Gums induced microstructure stability in Ca(II)-alginate beads containing lactase analysed by SAXS. *Carbohydrate Polymers*. **Artículo enviado.**

GUMS INDUCED MICROSTRUCTURE STABILITY IN Ca(II)-ALGINATE BEADS CONTAINING LACTASE ANALYSED BY SAXS

Maria Victoria Traffano-Schiffo,[†] Marta Castro-Giraldez,[†] Pedro J. Fito,[†] Mercedes Perullini, [§,‡,*]

and Patricio R. Santagapita, [ℸ,#,*]

[†]Instituto Universitario de Ingeniería de Alimentos para el Desarrollo, Universidad Politécnica de Valencia, Camino de Vera s/n, 46022 Valencia, Spain.

[§]Universidad de Buenos Aires. Facultad de Ciencias Exactas y Naturales. Departamento de Química Inorgánica, Analítica y Química Física. C1428AOE, Buenos Aires, Argentina.

[‡]CONICET-Universidad de Buenos Aires. Instituto de Química Física de los Materiales, Medio Ambiente y Energía (INQUIMAE). C1428AOE, Buenos Aires, Argentina.

[ℸ]Universidad de Buenos Aires. Facultad de Ciencias Exactas y Naturales. Departamentos de Industrias y Química Orgánica. C1428AOE, Buenos Aires, Argentina.

[#]CONICET-Universidad de Buenos Aires. Instituto de Tecnología de Alimentos y Procesos Químicos (ITAPROQ). C1428AOE, Buenos Aires, Argentina.

*Corresponding authors: prs@di.fcen.uba.ar; mercedesp@qi.fcen.uba.ar

ABSTRACT

Previous works show that the addition of trehalose and gums in β-galactosidase (lactase) Ca(II)-alginate encapsulation systems improved its stability against freezing and dehydration processes. However, there is no available information on how the microstructure is affected due to the constraints imposed by the operation conditions. The aim of this research is to study the microstructural changes of Ca(II)-alginate matrices driven by the presence of trehalose, arabic and guar gums as excipients and to correlate these changes with the enzymatic activity of the encapsulated lactase.

The structural modifications at different scales were assessed by SAXS. The incorporation of gums as second excipients induces a significant stabilization in the microstructure not only at the rod scale, but also in the characteristic size and density of alginate dimers (basic units of construction of rods) and the degree of interconnection of rods at a large scale, improving the performance in terms of lactase activity.

Keywords: alginate beads, hydrocolloids, encapsulation, β-galactosidase, microstructure, Small-Angle X-ray scattering (SAXS).

Table of Contents graphic

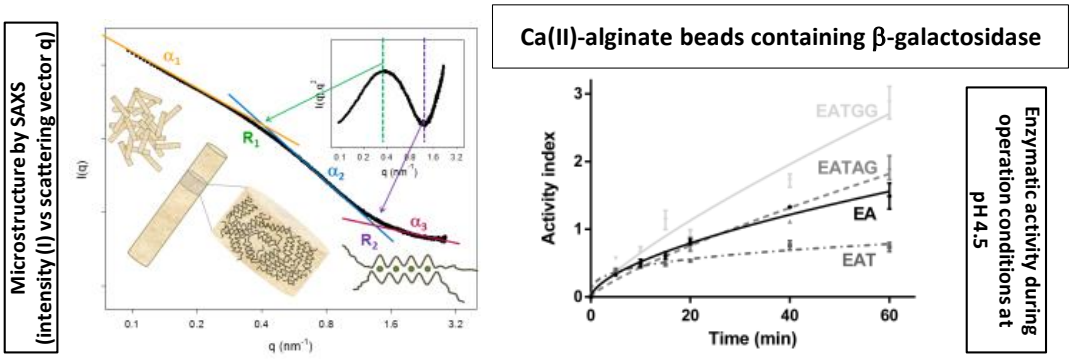

R_1: rods cross-sectional radius; **α_1:** interconnection of the rods; **α_2:** compactness of the rods; **α_3:** connectivity of the basic units (alginate dimers); **R_2:** basic unit radius

E: enzyme; **A:** alginate; **T:** trehalose; **AG:** arabic gum; **GG:** guar gum

INTRODUCTION

In recent years, the encapsulation of β-galactosidase (lactase) in order to control its release and improve its stability against thermal and mechanical effects has been widely investigated.[1-4]

Alginate is one of the most used anionic polyelectrolytes for the encapsulation of bioactive compounds.[5] It consists of (1→4)-linked residues of β-D-mannuronate (M) and α-L-guluronate (G), and in solution it generates a hydrogel matrix through the complexation of G-blocks with di- or trivalent cations such as Ca^{2+}, Mn^{2+}, Zn^{2+}, Al^{3+}, Cr^{3+}, and Ce^{3+},[6] embodying them into the cavities formed by a cooperative pairing of contiguous G-blocks[7] forming the structure commonly known as "egg-box".[8] Additionally, the sodium alginate solution can be gelled at acidic pH. Once a critical fraction of carboxylate residues are protonated, the decrease in the polymer charge density allows for chain-chain interactions leading to gelation. The inherent pH for the consolidation of H–alginate hydrogel is around 3.5, depending on the mannuronic (p*K*a = 3.38) to guluronic acid (p*K*a = 3.65) relative content of the employed alginate. Moreover, the Ca(II)–alginate structure can be obtained by cation exchange from a parent H–alginate hydrogel,[9] indicating a higher affinity of alginate polymer for Ca^{2+}. It has been demonstrated that the combined use of alginate with sugars and/or other biopolymers such as arabic and guar gums allows to improve the stability of enzymes within the hydrogel.[1]

The alginate microstructure depends on several factors such as the alginate's concentration, average molecular weight and monomer composition (M/G ratio), as well as the presence of secondary excipients and the synthesis conditions (mainly the Ca^{2+} concentration and pH). On the other hand, the alginate bead constitutes an intrinsically inhomogeneous system, determined by the dropping method followed in conventional synthesis procedures. This method generates a Ca^{2+} gradient established from the surface to the core of the forming bead.[10] All these parameters are related to the capacity of the hydrogel network to interact with the encapsulated biomolecule and the surrounding medium.[6,11]

One of the most precise and powerful techniques to evaluate the microstructure of hydrogels is the small-angle X-ray scattering (SAXS). The SAXS method is able to reveal subtle differences in electron density within hydrogels cross-linked networks in the range 1-100 nm, providing information on the supramolecular structure formed by biopolymers.[12] SAXS patterns are indicative of rod like objects formed as the accumulation of cross-linked alginate chain dimers randomly orientated, establishing junction zones of different multiplicity.[13] Previous works of lactase encapsulation in Ca(II)-alginate beads[1,14] revealed that the remaining lactase activity after storage, freezing and freeze/thaw cycles, and dehydration, preserved by trehalose, was even improved by the presence of gums. The microstructure of the beads generated at pH 3.8 showed rods with smaller cross-sectional radius and with lower compactness when gums were used as additives. However, there is no available information on how the microstructure is affected due to the constraints imposed by the operation conditions. Thus, the aim of this research is to study the microstructural changes of Ca(II)-alginate matrices driven by the presence of trehalose, arabic and guar gums as excipients and to correlate these changes with the enzymatic activity of the encapsulated lactase in operation conditions.

MATERIALS AND METHODS

Materials

The employed materials are listed below: sodium alginate (Algogel 5540) from Cargill S.A. (San Isidro, Buenos Aires, Argentina), molecular weight of $1.97 \cdot 10^5$ g/mol and mannuronate/guluronate ratio of 0.6; D-trehalosedihydrate (Hayashibara Co., Ltd., Shimoishii, Okayama, Japan/Cargill Inc., Minneapolis, Minnesota, USA), molecular weight of 378 g/mol; guar gum (Cordis S.A., Villa Luzuriaga, Buenos Aires, Argentina), molecular weight of 220.000 g/mol and a mannose/galactose ratio of 1.8; arabic gum (Biopack, Zárate, Buenos Aires, Argentina), molecular weight of 250.000 g/mol and a purity of 99%; β-galactosidase (lactase) from Aspergillus Oryzae (8.0 U/mg) (Sigma-Aldrich Co., Ltd., Saint Louis, USA). One enzymatic unit was defined as the amount of enzyme able to hydrolyze 1.0 μmol of lactose per minute at pH 4.5 at 30 °C.

Gel beads preparation

Four different formulations for the encapsulation of the enzyme (E) were prepared, with the following composition: alginate (EA); alginate-trehalose (EAT); alginate-trehalose-guar gum (EATGG); alginate-trehalose-arabic gum (EATAG). All the solutions were prepared in 0.1 M acetate buffer pH 3.8. The final concentration of lactase was 0.775 mg/mL. The enzyme and the precursor solutions were carefully mixed and maintained at 4 ± 1 °C in order to avoid enzyme activity losses. Taking into account that the isoelectric point of the enzyme is 4.61[15] and the p*K*a values of alginate are 3.38 and 3.65,[16] the buffer acetate at pH 3.8 was used in order to generate favorable electrostatic interactions between the negatively charged alginate and the positively charged enzyme. A peristaltic pump was used to drop 10 mL of the alginate-enzyme mixture into

100 mL of the gelling solution, according to the drop method described by Austin, Bower and Muldoon with some modifications.[17] For EA beads preparation, 1% (w/v) alginate solution containing lactase was dropped into 2.5% (w/v) $CaCl_2$ solution prepared in 0.1 M acetate buffer pH 3.8. For EAT, EATGG, and EATAG preparation, a 1% (w/v) alginate with 20% (w/v) trehalose with or without 0.25% (w/v) of guar or arabic gums containing the enzyme was dropped into the 2.5% (w/v) $CaCl_2$ solution supplemented with 20% (w/v) trehalose using the same procedure previously described.

The $CaCl_2$ solution (with or without trehalose) was maintained in a cold bath with constant stirring. A needle with 0.25 mm diameter and 6 mm length (Novofine 32 G, Novo Nordisk A/S, Bagsvaerd, Denmark) was used for the dropping. The pump speed was 9.0 ± 0 rpm. The distance between the needle and the $CaCl_2$ solution was 6.0 cm. After beads generation, they were maintained for 15 min in $CaCl_2$ solution (with constant stirring), and then they were washed 5 times with bidistilled cold water (5±1 °C) in order to remove free Ca^{2+}. Previous to SAXS measurements, beads were maintained at (5±1 °C) for 96 h.

Control beads without enzyme were also prepared using the same methodology.

Microstructure Analyses

Beads synthesized at pH 3.8 were incubated in 0.1 M acetate buffer pH 4.5 for different times (5, 10, 15, 20, 40, and 60 min). The microstructure characterization was performed by SAXS at the LNLS SAXS2 beamline in Campinas, Brazil, working at λ =0.1488 nm. The wave vector range was selected in the range 0.096 $nm^{-1} < q < 2.856\ nm^{-1}$. All the Ca(II)-alginate beads analyzed showed isotropic scattering and were modeled as a fractal system composed of rodlike structures, although the rigorous interpretation of experimental results as indicating "fractality" requires many orders of magnitude of power-law scaling.[9] Five parameters were analyzed: i) α_1, the fractal dimension at distances higher than the characteristic size of the rods composing the structure (R_1), which describes the multiplicity of the junction zone, at $q < 0.28$; ii) α_2, the fractal dimension at distances lower than R_1, at $q > 0.55$, describing the degree of compactness within the rods; iii) R_1, the outer radius of the fibrils, which is given by $R_1 = Rg\sqrt{2}$, R_g being the mean gyration radius in the cross-section of the rods, which is obtained from the maximum exhibit by the Kratky plot at $q \approx 1/R_g$; iv) α_3, related to the connectivity between associated polymer chains forming dimers (basic units composing the rods) at $q > 1.5$ and v) R_2, related to the outer radius of these aforementioned units.

The Kratky plot: scattering intensity multiplied by the square modulus of the scattering vector, $I(q)\cdot q^2$, as a function of the modulus of the scattering vector, q, gives a maximum value at the intersection of the α_1 and α_2 power law regions and a minimum value at the intersection of the α_2 and α_3 power law regions, allowing the calculation of parameters R_1 and R_2, respectively. All

measurements were made in triplicate. Parameters α_1, α_2 and α_3 were evaluated from the slope of the scattering intensity averaged along azimuthal angles versus the scattering vector q in the log–log scale.

β-Galactosidase Activity

The enzyme activity was evaluated based on the absorbance values at 420 nm by using a Jasco V-630 UV-vis spectrophotometer (JASCO Inc., Maryland, USA) at room temperature and following the method described by Park, Santi, and Pastore, with some modifications.[18]

Each analysis was performed using a pool of 9 beads which were mixed with 0.25 mL of 0.25% (w/v) o-nitrophenyl-β-D-galactopyranoside (ONPG) (Sigma Chemical Co.) prepared with 0.1 M acetate buffer pH 4.5 and incubated during 5, 10, 15, 20, 40, and 60 min at 33 °C, without stirring in order to avoid possible enzymatic activity losses. The reaction was stopped adding 0.5 mL of sodium carbonate 10% (w/v) and 0.25 mL of sodium citrate 10% (w/v) was added to dissolve the beads and finally, 1.75 mL of distilled water was added for subsequent measurement of o-nitrophenol (ONP) at 420 nm. Measurements were made in triplicate.

The effect of the composition of the beads on the enzyme stability was evaluated through an activity index calculated with the following equation:

$$Activity\ Index\ (dimensionless) = \frac{Activity_t}{Activity_0} \quad (1)$$

where $Activity_t$ corresponds to the activity of any of the studied systems (EA, EAT, EATAG or EATGG) at time t (5, 10, 15, 20, 40, or 60 min) and $Activity_0$ is the activity of the same system determined as described by Traffano-Schiffo et al.[14]

Low Field Nuclear Magnetic Resonance (LF-NMR)

Diffusion coefficient of water (D_w) was measured by time resolved low field proton nuclear magnetic resonance (^{1}H-LF-NMR) in a Bruker Minispec mq20 (Bruker Biospin Gmbh, Rheinstetten, Germany) with a 0.47 T magnetic field operating at a resonance frequency of 20 MHz. Two samples of each bead system were previously equilibrated at 25.00 ± 0.01 °C in a thermal bath (Haake, model Phoenix II C35P, Thermo Electron Corporation Gmbh, Karlsruhe, Germany).

Measurements were performed though the pulsed magnetic field gradient-spin echo sequence.[19] The applied magnetic field gradient intensity was calibrated in the range between 1.4 and 2.4 T/m by employing 1.25 g/L $CuSO_4 \cdot 5H2O$ water solution, characterized by a known Dw value ($2.3 \cdot 10^{-9}$ m^2/s at 25 °C).[20] The bead samples were analyzed by setting the magnetic field gradient amplitude to 1.4 T/m, t (the time between 90 and 180 pulses) to 7.5 ms, δ to 0.5 ms, and Δ to 7.5 ms. The

number of scans, the recycle delay and gain were 16, 2 s and 69 dB, respectively. D_w was calculated following the procedure reported by Santagapita et al. (2013).[21]

Statistical Analyses

The statistical analyses were performed by one-way ANOVA with Tukey`s post test by using Prism 6 (GraphPad Software Inc., San Diego, CA, USA) in order to determine significant differences between the mean values of beads of different compositions on the measured parameters.

Results and Discussion

Figure 1 shows the scattering intensity as a function of the scattering vector for a representative sample of Ca(II)-alginate hydrogel containing lactase (EA), incubated in 0.1 M acetate buffer pH 4.5 for 20 minutes. A schematic representation of the scale of different structural parameters derived from SAXS scattering experiments is included. SAXS scattering curves can be divided in three regions: at low, intermediate and high q values. From the slope of the log-log plot at low q, α_1 parameter is indicative of the interconnectivity of the rods composing the alginate network. At intermediate q values, α_2 parameter represents the compactness within the rods, and at high q values α_3 parameter characterizes the connectivity between associated polymer chains forming dimers. Besides, two characteristic radii of gyration can be derived: R_1, related to the multiplicity of the junction zone domains in the alginate rod, and R_2 denoting the size of the polymer dimers basic units. Kratky plots ($q_2 \cdot I(q)$ vs q) were used to evaluate R_1 as already reported.[9,13] Characteristic SAXS profiles and Kratky plots from all the systems analyzed are presented in Supplementary File (Figures S1 and S2, respectively).

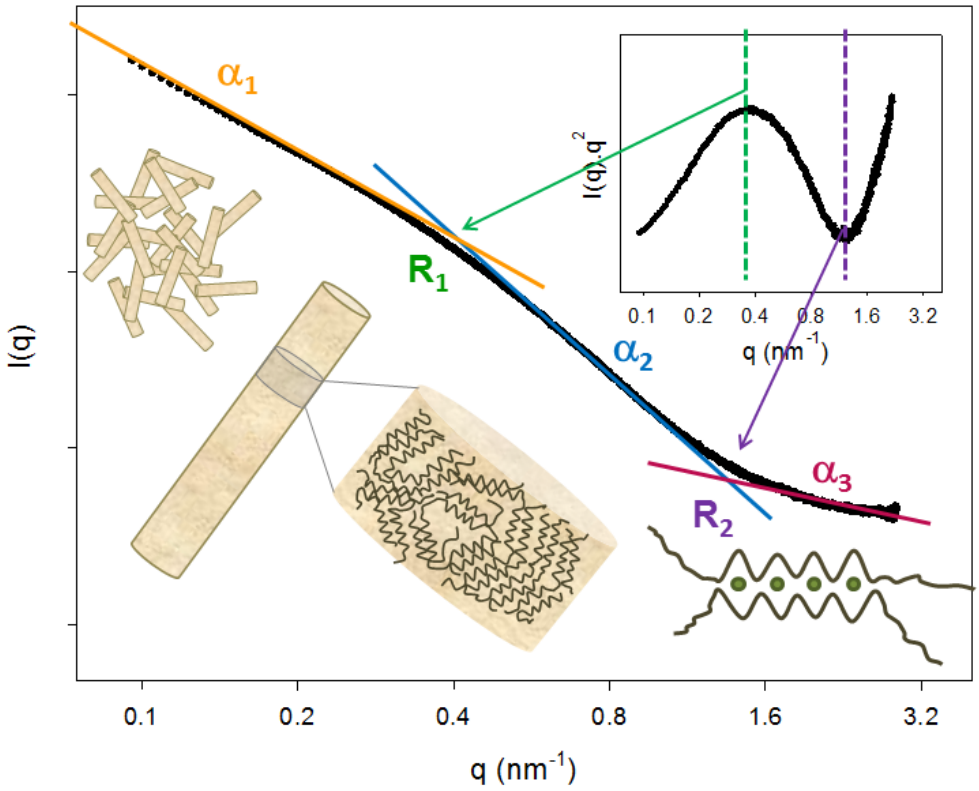

Figure 1. log–log SAXS profile plot of a representative sample of Ca(II)-alginate hydrogel containing lactase (EA), incubated in 0.1 M acetate buffer pH 4.5 for 20 minutes. Parameters α_1, α_2 and α_3 were evaluated from the slope of the scattering intensity at low, intermediate and high q values, respectively. The radius of gyration of the rods (parameter R_1) and the characteristic size of the Ca(II)-alginate dimers (parameter R_2) was obtained from the Kratky plot (inset).

Control systems without the enzyme were also conducted in order to analyze the influence of the presence of lactase in the microstructure of the alginate gel. Except for subtle changes, the microstructure remains the same for all the systems under study and thus it can be concluded that the enzyme is not directly involved in the formation of the alginate rods. A complete description of these results is included in Supplementary File (Figure S3).

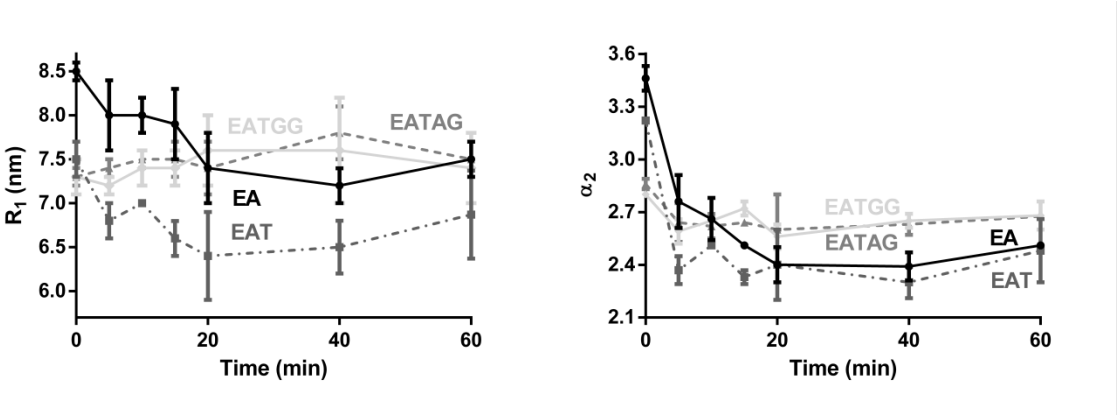

Figure 2. Microstructure parameters of Ca(II)-alginate beads synthesized at pH 3.8 vs. time of incubation in 0.1 M acetate buffer pH 4.5. a. Rod cross-sectional radius (R_1) deduced from the maxima obtained on Kratky plots. b. Fractal dimension at distances lower than R_1 or parameter α_2 of the microstructure derived from log-log SAXS profiles. Standard deviations values are included. E, enzyme; A, alginate; T, trehalose; AG, arabic gum; GG, guar gum.

Figure 2 shows the evolution of the microstructure parameters related to the size and compactness of the rods (R_1 and α_2, respectively). For the non-incubated beads (synthesized at pH 3.8), the addition of trehalose with or without gums affected the extent of the rod formation, reducing the outer radius of the fibrils (Figure 2a, time = 0) as well as their compactness (Figure 2b, time = 0), as previously discussed Traffano-Schiffo et al.[14]

As a general trend, the increase in pH (from 3.8 to 4.5) generates a decrease both in size and compactness of the rods for the systems in the absence of gums. However, the presence of guar or arabic gums generates a much stable structure, maintaining a constant rod size and significantly reducing the initial drop in α_2, as well as further changes along incubation time. It is worth noting that the synthesis pH is close to the isoelectric point of alginate and thus the contribution of H-alginate to the consolidation of the alginate network cannot be neglected. Therefore, at low free Ca^{2+} concentrations, an increase in pH would lead to an increase in alginate polymer repulsion with a concomitant reduction of the compactness due to the loss of the H-alginate contribution to the structure. This can also explain the reduction in the rod size, considering that some of the alginate chains can be released from the junction zones. The presence of gums seems to reduce alginate-alginate repulsion which suggests that they are located in within the rods, particularly between associated polymer chains forming dimers. This hypothesis was deeply analyzed by considering the evolution of α^3 and R^2, the nanostructure parameters describing the size and compactness of these dimers, basic units of construction of the rods (as shown in Figure 3 a and b, respectively). The presence of gums modulates the nanostructure of the dimers generating an increase in their size and a decrease in their compactness, compatible with the hypothesis of gums being intercalated within the dimers. Furthermore, the addition of gums once again induced a higher stability toward an increase in pH. However and regardless of the presence of different excipients, the nanostructure of dimers shows similar characteristics and remains stable during the operation conditions at pH 4.5.

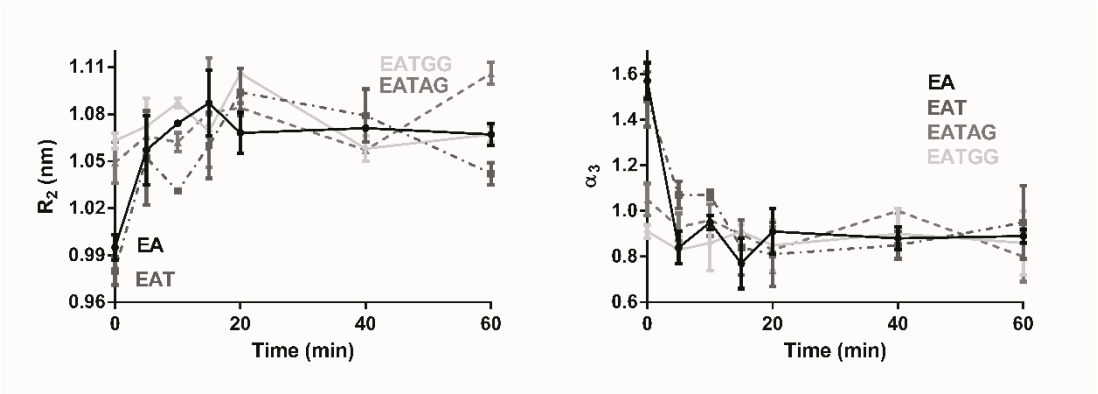

Figure 3. Microstructure parameters of Ca(II)-alginate beads synthesized at pH 3.8 vs. time of incubation in 0.1 M acetate buffer pH 4.5. a. Characteristic size of the Ca(II)-alginate dimers (R_2) deduced from the minima obtained on Kratky plots. b. Fractal dimension at distances lower than R_2 or parameter α_3 of the microstructure derived from log-log SAXS profiles. Standard deviations values are included. E, enzyme; A, alginate; T, trehalose; AG, arabic gum; GG, guar gum.

In order to go a step further in the analysis of the microstructure of the hydrogels during the operation conditions, the evolution of α_1 parameter for each bead composition was analyzed (Figure 4). The parameter $\alpha 1$ is related with the degree of interconnection of the rods composing the structure. Values of α_1 around 1 correspond to randomly oriented rods, while a α_1 close to 2 is indicative of a network composed of well interconnected.[9] All the systems under study showed initial values of α_1 around 1.5 (i. e. for the hydrogel obtained at pH 3.8), characteristic of a consolidated network. The formulations lacking gums additives showed an increase in α_1 when exposed to the operation pH 4.5, reaching values of around 1.8 (for the system with trehalose, EAT, after 20 minutes of incubation). Once established the degree of interconnectivity of rods in aged systems, the α_1 parameter is expected to remain constant in time. One plausible explanation for α_1 fluctuations relies on the increased availability of alginate polymer chains resulting from the partial dissolution of rods, as previously discussed regarding parameter α_3 and R_2. Thus, the presence of free alginate chains could induce the formation of new connections in the network establishing a new equilibrium. In line with this, the presence of gums induces stabilization in the microstructure, resulting in no significant variations in α_1 parameter both with the initial increase in pH and throughout the operation time at pH 4.5.

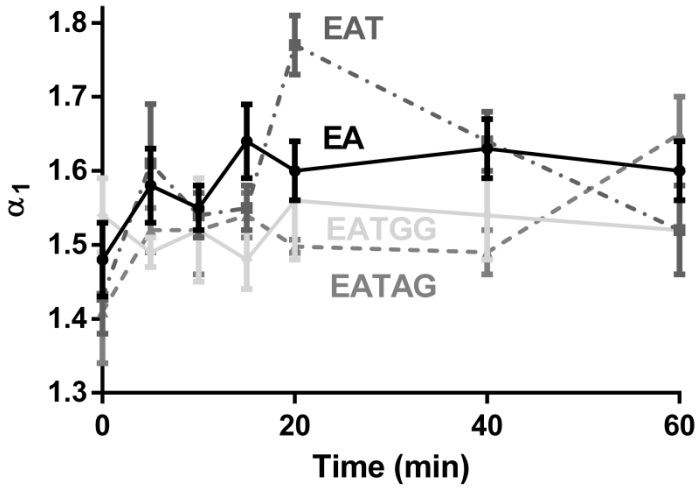

Figure 4. Fractal dimension at distances higher than R or parameter α_1 of the microstructure derived from log-log SAXS profiles. Standard deviation values are included. E, enzyme; A, alginate; T, trehalose; AG, arabic gum; GG, guar gum.

Water self-diffusion coefficient (D_w) determined by LF-NMR for Ca(II)-alginate beads gives valuable information of the overall decrease on the mobility of protons (especially those from water), modulated by the exchange between them and the protons of the biopolymers.[9,22] The magnitude of this decrease depends on reduced flexibility of the biopolymer chains with respect to water and the aggregation state. As expected, all alginate systems gelled at pH 3.8 showed reduced D_w values in comparison with water, $(2.30 \pm 0.01) \times 10^{-9}$ m2 s^{-1},[23] as shown in Table 1. The presence of trehalose in the hydrogels further reduced D_w values. However, the concomitant addition of gums induced a slight increase of D_w with respect to the EAT system. These changes are in well agreement with the water activity and content previously reported.[14] Besides, the measure of D_w can give an idea of the water transport through the aqueous macropores, which can be also related with the diffusion of other water soluble species. The dramatic drop in D_w can be explained from the evolution of parameters α_2 and R_1, which show a significantly higher rod size and compactness for the hydrogel in the absence of additives (EA). This is consistent with highly packed rods which in turn enclose more alginate dimers, reducing the tortuosity through the aqueous macropores.

Table 1. Diffusion coefficients of water (D_w) in beads containing lactase determined by LF-NMR at 25 °C.

System	D_w (10^{-9} m^2/s)
EA	2.1 ± 0.03[a]
EAT	1.492 ± 0.011[c]
EATAG	1.6 ± 0.02[b]
EATGG	1.613 ± 0.013[b]

[a-c] E, enzyme; A, alginate; T, trehalose; AG, arabic gum; GG, guar gum. Standard deviation values are included. Different letters on the columns indicate significant differences between means ($p < 0.05$).

Then, bearing in mind that the modulation of the enzyme activity will be given by the entrance of substrate through the macropores as well as by the overall microstructure of the Ca(II)-alginate gel, the addition of excipients would be expected to modulate lactase activity. Figure 5 shows the effect of the composition of the beads on β-galactosidase stability by measuring the ONP concentration (colored compound) spectrophotometrically. It can be observed that the EAT shows the lowest ratio of enzymatic activity; however the addition of gums as second excipients reverts this detriment caused by trehalose, increasing for guar gum containing beads (EATGG) β-galactosidase activity above the standards of bear Ca(II)-alginate hydrogel (EA). EAT beads present the worst possible scenario: low diffusion and poor microstructure stability. The incorporation of gums palliates this by improving the intrinsic transport properties of the initial hydrogel, in one hand, and more importantly by stabilizing its microstructure. The latter seems to be a determining factor in the performance of these systems during operating conditions.

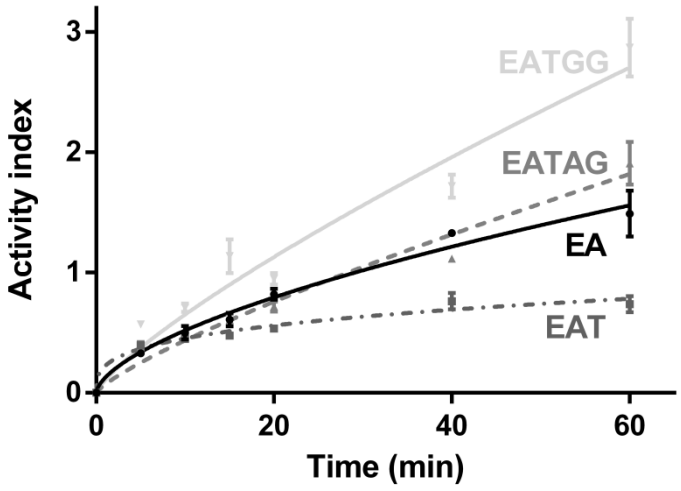

Figure 5. Activity index of lactase in beads vs. time of incubation in 0.1 M acetate buffer pH 4.5. Standard deviations values are included. E, enzyme; A, alginate; T, trehalose; AG, arabic gum; GG, guar gum.

CONCLUSIONS

Though being a key in preserving enzymatic activity toward freezing and dehydration processes, the addition of trehalose as additive in Ca(II)-alginate lactase encapsulation systems prompts important structural changes leading to a loss of enzymatic activity during operation conditions. Trehalose drastically reduces the water self-diffusion coefficient in the starting hydrogel system (synthesized at pH 3.8), concomitant with the reduction in size and compactness of the structure at the scale of alginate rods. The incorporation of gums as second excipients does not revert this last effect, nevertheless induces a significant stabilization in the microstructure not only at the rod scale, but also at smaller and bigger scales. On one hand, gums are shown to induce an important

modulation in the characteristic size and density of alginate dimers (basic units of construction of rods). On the other hand and highly related to this, the variation in the degree of interconnection of rods evidenced in EA and EAT systems (i.e. in the absence of gums) is impeded. It is worth noting that in EA and EAT, this process is facilitated by free alginate polymer chains that become available from partial rod dissolution. Thus, this microstructure stabilization induced by the concomitant addition of guar gum results in an increased lactase activity during operation conditions, improving the performance of the systems with trehalose even above the bear Ca(II)-alginate matrix.

ACKNOWLEDGEMENTS

This work was supported by the Brazilian Synchrotron Light Laboratory (LNLS, Brazil, proposal SAXS1-20160278), Universidad de Buenos Aires (UBACyT 20020130100610BA), Agencia Nacional de Promoción Científica y Tecnológica (ANPCyT PICT 2013 0434 and 2013 1331), CIN-CONICET (PDTS 2015 n° 196), and Consejo Nacional de Investigaciones Científicas y Técnicas. The author María Victoria Traffano-Schiffo wants to thank "Programa para la Formación de Personal Investigador (FPI)" Pre-doctoral Program of the Universitat Politècnica de València (UPV) for support her PhD studies and also her mobility to Argentina.

Supporting Information. Figure S1. log–log SAXS profile plots of representative of Ca(II)-alginate lactase beads for the different systems, incubated in 0.1 M acetate buffer pH 4.5 at different times. E, enzyme; A, alginate; T, trehalose; AG, arabic gum; GG, guar gum. Figure S2. Kratky plots of SAXS data obtained for Ca(II)-alginate beads containing enzyme for the four systems analyzed. The curves at each incubation time were arbitrary shifted up. E, enzyme; A, alginate; T, trehalose; AG, arabic gum; GG, guar gum. Figure S3. Parameter α_1 (a) and α_2 (b) of the microstructure derived from log-log SAXS profiles and R_1 (outer radius of the rods) (c), deduced from the maxima obtained on Kratky plots. Standard deviations values are included. Different letters on the columns (a-e) indicate significant differences between values with $p< 0.05$. E, enzyme; A, alginate; T, trehalose; AG, arabic gum; GG, guar gum.

REFERENCES

(1) Traffano-Schiffo, M. V.; Castro-Giraldez, M.; Fito, P. J.; Santagapita, P. R. *Food Res. Int.* **2017.**

(2) Zhang, Z.; Zhang, R.; Chen, L.; McClements, D. J. *Food Chem.* **2016**, 200, 69-75.

(3) Zhang, Z.; Zhang, R.; McClements, D. J. *Food Hydrocolloid.* **2017**, http://dx.doi.org/10.1016/j.foodhyd.2017.01.005

(4) Estevinho, B. N.; Damas, A. M.; Martins, P.; Rocha, F. *Food Res. Int.* **2014**, 64, 134-140.

(5) Santagapita, P. R.; Mazzobre, M. F.; Buera, M. P. *Food Res. Int.* **2012**, 47, 321-330.

(6) Santagapita, P. R.; Mazzobre, M. F.; Buera, M. P. *Biomacromolecules* **2011**, 12, 3147-3155.

(7) Stokke, B. T.; Draget, K. I.; Smidsrød, O.; Yuguchi, Y.; Urakawa, H.; Kajiwara, K. *Macromolecules* **2000**, 33, 1853-1863.

(8) He, X.; Liu, Y.; Li, H; Li, H. *RSC Adv.* **2016**, 6, 114779-114782.

(9) Sonego, J. M.; Santagapita, P. R.; Perullini, M.; Jobbágy, M. *Dalton Trans.* **2016**, 45, 10050-10057.

(10) Gåserød, T, O.; Paus, D.; Mikkelsen, A.; Skjåk-Bræk, G.; Toffanin, R.; Vittur, F.; Rizzo, R. *Biopolymers* **2000**, 53, 60-71.

(11) Gombotz, W. R.; Wee, S. F. *Adv. Drug Deliver Rev.* **2012**, 64, 194-205.

(12) Waters, D. J.; Engberg, K.; Parke-Houben, R.; Hartmann, L.; Ta, C. N.; Toney, M. F.; Frank, C. W. *Macromolecules* **2010**, 43, 6861-6870.

(13) Agulhon, P.; Robitzer, M.; David, L.; Quignard, F. *Biomacromolecules* **2012**, 13, 215-220.

(14) Traffano-Schiffo, M. V.; Aguirre Calvo, T. R.; Castro-Giraldez, M.; Fito, P. J.; Santagapita, P. R. *Biomacromolecules* **2017**, DOI:10.1021/acs.biomac.7b00202

(15) Dashevsky, A. *Int. J. Pharm.* **1998**, 161, 1-5.

(16) Smidsrød, O.; Larsen, B.; Painter, T.; Haug, A. *Acta Chem. Scand.***1969**, 23, 1573–1580.

(17) Austin, L.; Bower, J. J.; Muldoon, C. *P. Int. Sym. Contr. Release Bioact. Mater.* **1996**, 23, 739-740.

(18) Park, Y. K.; Santi, M. S. S.; Pastore, G. M. *J. Food Sci.* **1979**, 44, 100-103.

(19) Stejskal, E. O.; Tanner, J. E. *J. Chem. Phys.* **1965**, 42, 288-292.

(20) Hester-Reilly, H. J; Shapley, N. C. *J. Magn. Reson.* **2007**, 188, 168-175.

(21) Santagapita, P.; Laghi, L.; Panarese, V.; Tylewicz, U.; Rocculi, P.; Dalla Rosa, M. *Food Bioprocess Technol.* **2013**, 6, 1434-1443.

(22) Aguirre Calvo, T. R; Busch, V. M.; Santagapita, P. R. *LWT-Food Sci. Technol.* **2017**, 77, 406-412.

(23) Holz, M.; Heil, S. R.; Sacco, A. *Phys. Chem. Chem. Phys.*, **2000**, 2, 4740–4742.

SUPPLEMENTARY FILE

Characteristics SAXS profiles and Kratky plots at different times of operation conditions from all the systems analyzed are presented in Figures S1 and S2, respectively).

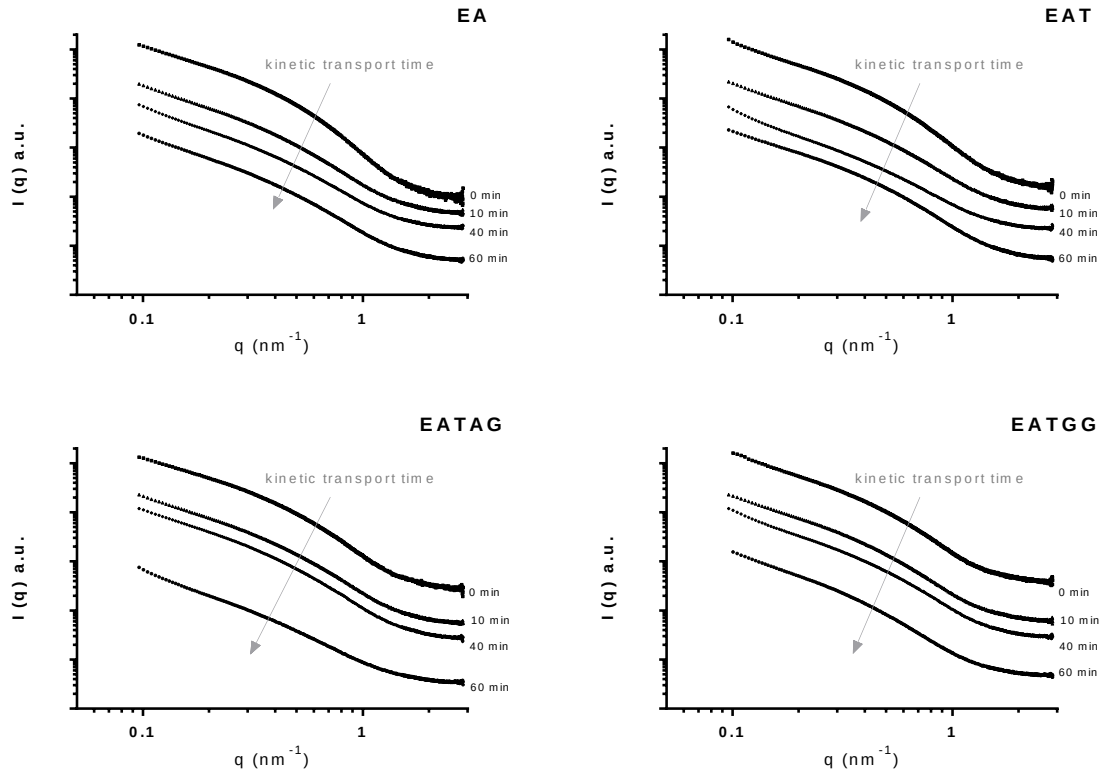

Figure S1. log–log SAXS profile plots of representative of Ca(II)-alginate lactase beads for the different systems, incubated in 0.1 M acetate buffer pH 4.5 at different times. E, enzyme; A, alginate; T, trehalose; AG, arabic gum; GG, guar gum.

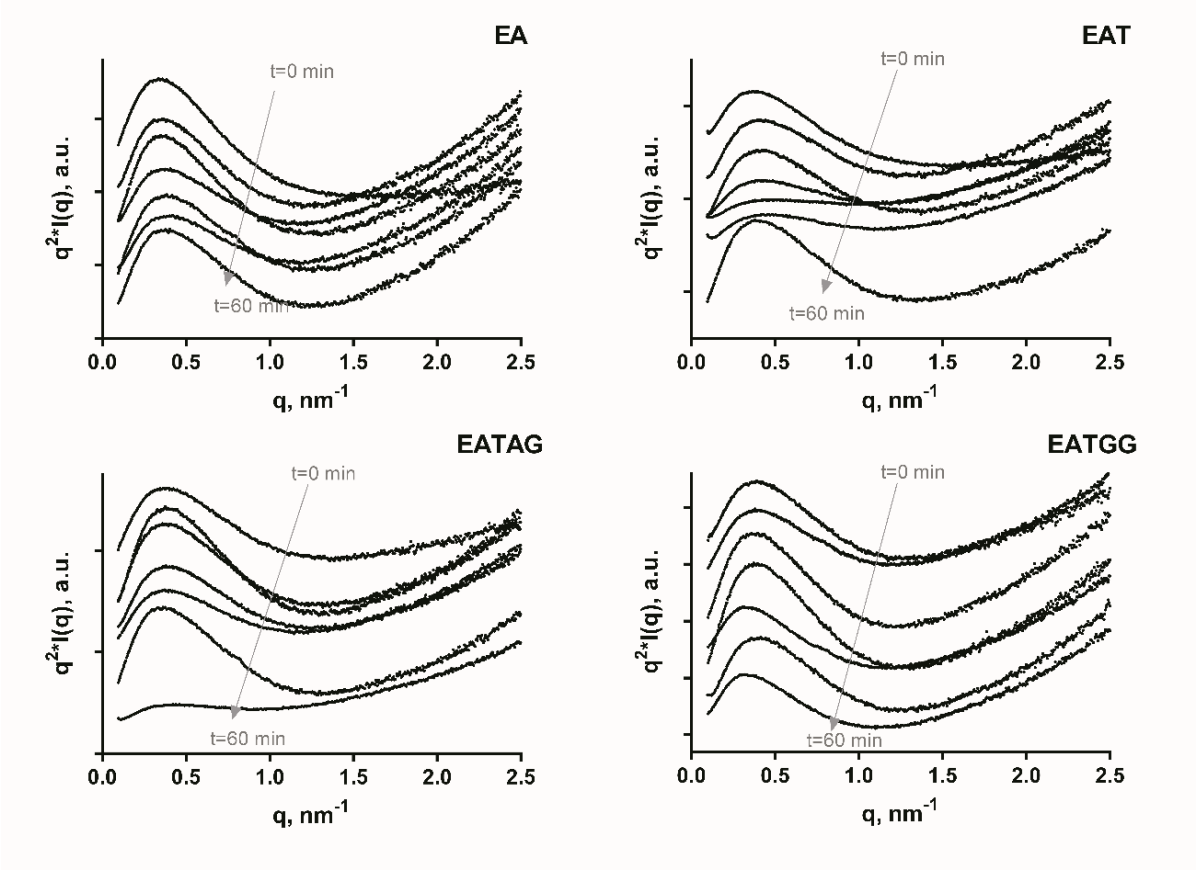

Figure S2. Kratky plots of SAXS data obtained for Ca(II)-alginate beads containing enzyme for the four systems analyzed. The curves at each incubation time were arbitrary shifted up. E, enzyme; A, alginate; T, trehalose; AG, arabic gum; GG, guar gum.

Figure S3 shows the α_1, α_2 and R_1 parameters obtained from the control samples prepared without lactase. Minor changes were observed between the different systems with and without lactase. For instance: the interconnectivity of the rods in the presence of arabic gum was higher in the absence of enzyme. However, neither the rods size nor its compactness was affected by the enzyme in this system. Also, the compactness of the rods in the presence of trehalose was higher in the presence of the enzyme, but the rods size remains unmodified (and showed even lower mean values). If the enzyme is directly involved in the formation of the alginate rods, a change in both size and compactness of the rods is expected, which in turn could affect the interconnection between rods at a larger scale. Then, since slightly changes were observed, we conclude that the microstructure remains the same for all the systems under study in presence or absence of the enzyme.

A complete analysis of the observed changes between the beads containing the different additives can be read in Traffano-Schiffo *et al.*, 2017.

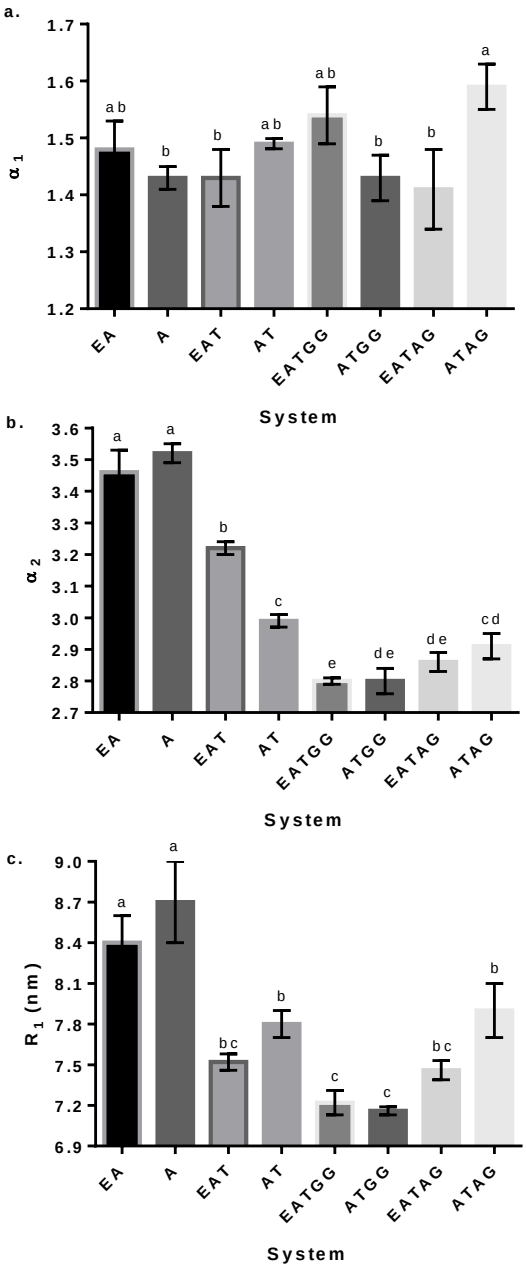

Figure S3. Parameter α_1 (a) and α_2 (b) of the microstructure derived from log-log SAXS profiles and R_1 (outer radius of the rods) (c), deduced from the maxima obtained on Kratky plots. Standard deviations values are included. Different letters on the columns (a-e) indicate significant differences between values with $p< 0.05$. E, enzyme; A, alginate; T, trehalose; AG, arabic gum; GG, guar gum.

5. Difusión y Protección de Resultados

Artículos en Revistas Científicas de Alto Impacto

- **Traffano-Schiffo, M. V.**, Castro-Giraldez, Fito. P. J. (2017). Development of a methodology to categorize chicken meat affected by Deep Pectoral Myopathy. *Meat Science. Artículo enviado.*
- **Traffano-Schiffo, M. V.**, Castro-Giraldez, Colom, R. J., Fito. P. J. (2017). New spectrophotometric system to segregate tissues in mandarin fruit. *Food and Bioprocess Technology. Artículo enviado.*
- **Traffano-Schiffo, M. V.**, Castro-Giraldez, M., Fito, P. J., Perullini, M., & Santagapita P. R. (2017). Gums Induced Microstructure Stability in Ca(II)-alginate Beads Containing Lactase Analyzed by SAXS. *Carbohydrate Polymers. Artículo enviado.*
- **Traffano-Schiffo, M. V.**, Castro-Giraldez, M., Fito, P. J., & Santagapita P. R. (2017). Encapsulation of lactase in alginate-Ca(II) beads: effect of trehalose and gums inclusion and of drying methods. *Food Research International. Artículo enviado.*
- **Traffano-Schiffo, M. V.**, Aguirre Calvo, T. R., Castro-Giraldez, M., Fito, P. J., & Santagapita P. R. (2017). Alginate beads containing lactase: stability and microstructure. *Biomacromolecules,* 18, 1795-1792. DOI: 10.1021/acs.biomac.7b00202
- **Traffano-Schiffo, M. V.**, Castro-Giraldez, Colom, R. J., Fito. P. J. (2017). Innovative spectrophotometric system to determine chicken meat quality. *Innovative Food Science and Emerging Technologies. Artículo enviado.*
- **Traffano-Schiffo, M. V.,** Laghi, L., Castro-Giraldez, M., Tylewicz, U., Romani, S., Ragni, L., Dalla Rosa, M., & Fito, P. J. (2017). Osmotic dehydration of organic kiwifruit pre-treated by pulsed electric fields: Internal transport and transformations analyzed by NMR. *Innovative Food Science & Emerging Technologies*, 41, 259-266. https://doi.org/10.1016/j.ifset.2017.03.012
- **Traffano-Schiffo, M. V.,** Laghi, L., Castro-Giraldez, M., Tylewicz, U., Rocculi, P., Ragni, L., Dalla Rosa, M., & Fito, P. J. (2017). Osmotic dehydration of organic kiwifruit pre-treated by pulsed electric fields and monitored by NMR. *Food Chemistry*, 236, 87-93. http://dx.doi.org/10.1016/j.foodchem.2017.02.046

- ✓ **Traffano-Schiffo, M. V.**, Castro-Giraldez, Colom, R. J., Fito. P. J. (2017). Development of a spectrophotometric system to detect white striping physiopathy in whole chicken carcasses. *Sensors*, 17(5), 1024. doi:10.3390/s17051024
- ✓ **Traffano-Schiffo, M. V.**, Tylewicz, U., Castro-Giraldez, M., Fito, P. J., Ragni, L., & Dalla Rosa, M. (2016). Effect of pulsed electric fields pre-treatment on mass transport during the osmotic dehydration of organic kiwifruit. *Innovative Food Science & Emerging Technologies*, 38, 243-251. https://doi.org/10.1016/j.ifset.2016.10.011
- ✓ **Traffano-Schiffo, M. V.**, Castro-Giráldez, M., Colom, R. J., & Fito, P. J. (2015). Study of the application of dielectric spectroscopy to predict the water activity of meat during drying process. *Journal of Food Engineering*, 166, 285-290. https://doi.org/10.1016/j.jfoodeng.2015.06.030
- ✓ **Traffano-Schiffo, M. V.**, Castro-Giráldez, M.; Fito, P. J., Balaguer, N. (2014). Thermodynamic model of meat drying by infrared thermography. *Journal of Food Engineering*. 128, 103-110. https://doi.org/10.1016/j.jfoodeng.2013.12.024

Capítulo de libro

- ✓ **Traffano-Schiffo, M. V.**, Balaguer, N., Castro-Giráldez, M., Fito, P. J. (2014) *Juice Processing: Quality, Safety and Value-added Opportunities*. Capítulo 11: Thermal emerging technologies in fruit juice processing. Eds: Albert Ibarz, Victor Falguera. Editorial: CRC Press. ISBN: 978-1466577336.

Patentes

- ✓ Fito, P. J., Colom, R. J., Castro-Giraldez, M., Herrero, V., Monzó, J. M., **Traffano-Schiffo, M. V.**, Tébar, A., (2016). *Aparato y método de detección de daño producido por la miopatía del pectoral profundo en aves.* Patente Española Nº P201630062.

- ✓ Castro-Giraldez, M., Colom, R. J., Fito, P. J., Herrero, V., Lidón, J. V., Monzó, J. M., Tébar, A., Traffano-Schiffo, M. V. (2016). *Aparato y método no invasivo de detección de roturas de la cadena de frío en carne congelada.* Patente Española Nº P201630956.

Participaciones en Conferencias y Congresos

- ✓ **Traffano-Schiffo, M. V.**, Aguirre Calvo, T. R., Castro-Giraldez, M., Fito, P. J., & Santagapita P. R. (2017). "Formulation and drying of alginate beads containing lactase: stability, microstructure and controlled release". Tipo de presentación: ***Póster*** en *Food Innova 2017. Cesena, Italia.*
- ✓ **Traffano-Schiffo, M. V.**, Castro-Giráldez, M., Monzó, J., Herrero, V., Colom, R., & Fito P. J. (2017). "Development of a non-destructive detection system of deep pectoral myopathy (DPM) in poultry by dielectric spectroscopy". Tipo de presentación: ***Oral*** en el Food Innova 2017. Cesena, Italia.
- ✓ **Traffano-Schiffo, M. V.**, Laghi, L., Tylewicz, U., Castro-Giraldez, M., Fito, P. J., Ragni, L. and Dalla Rosa, M. (2016). "Study of the water distribution during osmotic dehydration of kiwifruit and the effect of pulsed electric fields as pre-treatment". Tipo de presentación: ***Póster*** en 9th International Conference on Water in Food (EuroFoodWater2016). Leuven, Bélgica.
- ✓ **Traffano-Schiffo, M. V.**, Castro-Giráldez, M. & Fito P. J. (2015). "Study of the viability of the microwave dielectric spectroscopy to monitoring meat drying process". Tipo de presentación: ***Oral*** en el *IX International Workshop on Sensors and Molecular Recognition.* Valencia. España.
- ✓ Hedrera, J., **Traffano-Schiffo, M. V.**, Castro-Giráldez, M. & Fito P. J. (2015). "Study of mandarin tissue microstructure by using dielectric spectroscopy". Tipo de presentación: ***Póster*** en el *II National &I International Student Congress of Food Science & Technology.* Valencia, España.

- **Traffano-Schiffo, M. V.**, Muñoz, M. A., Castro-Giráldez, M. & Fito, P. J. (2014). "Análisis de los espectros dieléctricos como herramienta para el control de la maduración de carne de pollo". Tipo de presnetación: ***Póster*** en el *VIII International Workshop on Sensors and Molecular Recognition*. Valencia, España.

- **Traffano-Schiffo, M. V.**, Muñoz, M. A., Castro-Giráldez, M. & Fito, P. J. (2014). "Análisis de los espectros dieléctricos como herramienta para el control de la maduración de carne de pollo". Tipo de presentación: ***Publicación en el libro de artículos*** (ISBN: 987-84-697-1302-0) en el *VIII International Workshop on Sensors and Molecular Recognition.* Valencia, España.

- **Traffano-Schiffo, M. V.**, Castro-Giráldez, M. & Fito, P. J. (2014). "Dielectric spectrum analysis in Radiofrequency and Microwave range in chicken meat". Tipo de presentación: ***Póster*** en *ISEKI FOOD CONFERENCES 2014*. Atenas, Grecia.

- **Traffano-Schiffo, M. V.**, Castro-Giráldez, M. & Fito, P. J. (2014). "Estudio de la viabilidad de la termografía infrarroja como herramienta de monitorización de la evolución del secado de carne de cerdo". Tipo de presentación: ***Oral*** en el *CIBIA9 Congreso Iberoamericano de Ingeniería de Alimentos*. Valencia, España.

- **Traffano-Schiffo, M. V.**, Castro-Giráldez, M. & Fito, P. J. (2014). "Estudio de la viabilidad de la termografía infrarroja como herramienta de monitorización de la evolución del secado de carne de cerdo". Tipo de presentación: ***Publicación en el libro de artículos*** (ISBN: 978-84-9048-168-4) del *CIBIA9 Congreso Iberoamericano de Ingeniería de Alimentos*. Valencia, España.

- **Traffano-Schiffo, M. V.**, Castro-Giráldez, M. & Fito, P. J. (2013). "Study of ham drying kinetics by Infrared Thermography". Tipo de presentación: ***Póster*** en *INSIDE FOOD SYMPOSYUM*. Leuven, Bélgica.

- **Traffano-Schiffo, M. V.**, Castro-Giráldez, M. & Fito, P. J. (2013). "Study of ham drying kinetics by Infrared Thermography". Tipo de presentación: ***Publicación en el libro de artículos*** del *INSIDE FOOD SYMPOSYUM*. Leuven, Bélgica.

Estancias en el Extranjero

- **UNIVERSITÁ DI BOLOGNA.** Directores: Marco Dalla Rosa y Urszula Tylewicz. Cesena, Italia. 25 de octubre del 2015 – 07 de febrero del 2016. Duración: 3.5 meses.

- **UNIVERSIDAD DE BUENOS AIRES (UBA).** Director: Patricio Santagapita. Buenos Aires. Argentina. 01 de Julio del 2016 – 30 de septiembre del 2016. Duración: 3 meses.

Tesinas de máster dirigidas

- **Chuquizuta Trigoso, Tony Steven** (2014). *DEVELOPMENT OF A NON-DESTRUCTIVE DETECTION SYSTEM OF DEEP PECTORAL MYOPATHY (DPM) IN CHICKEN BY DIELECTRIC SPECTROSCOPY*. Tesina del máster en Ciencia e Ingeniería de los Alimentos, Especialidad en Ingeniería de Procesos y Productos, Instituto de Ingeniería de Alimentos para el Desarrollo, Universidad Politécnica de Valencia (España). **NOTA: 10 (Matrícula de honor).**

- **Évole, Raúl** (2017). DEATH ON ARRIVAL DETECTION IN POULTRY INDUSTRY. Tesina del máster en Ciencia e Ingeniería de los Alimentos, Especialidad en Ingeniería de Procesos y Productos, Instituto de Ingeniería de Alimentos para el Desarrollo, Universidad Politécnica de Valencia (España). ***A presentar.***

Trabajos Fin de Grado dirigidos

- **Hedrera García, Jessica** (2015). *ESTUDIO DE LA DETECCIÓN DE SEMILLAS DE MANDARINAS MEDIANTE EL USO DE LA ESPECTROSCOPIA DIELECTRICA*. Trabajo Fin de

Grado en Ingeniería Agroalimentaria y del Medio Rural, Instituto de Ingeniería de Alimentos para el Desarrollo, Universidad Politécnica de Valencia (España). **NOTA: 10.**

- ✓ **Romero, Sergio** (2015). ANALISIS Y DETECCIÓN DE LAS ESTRIAS BLANCAS EN PECHUGA DE POLLO. Trabajo Fin de Grado en Ingeniería Agroalimentaria y del Medio Rural, Instituto de Ingeniería de Alimentos para el Desarrollo, Universidad Politécnica de Valencia (España). **NOTA: 10.**

Vinculación de la tesis a proyectos

España:

- ✓ Ministerio de Economía Industria y Competitividad, Programa del Plan Nacional. Título del Proyecto: "CONTROL DE CALIDAD Y SEGURIDAD EN CARNE Y PRODUCTOS CARNICOS MEDIANTE ESPECTROSCOPIA DIELETRICA". **Nº AGL2011-30096.**
- ✓ AGENCIA ESTATAL DE INVESTIGACION, Ministerio de Economía, Industria y Competitividad de España, Programa Estatal de I+D+i orientada a los Retos de la Sociedad. Título del Proyecto: "UTILIZACION DE LAS PROPIEDADES DIELECTRICAS EN EL CONTROL DE LA CALIDAD Y DE LA SEGURIDAD DE LA CARNE DE AVE". **Nº AGL2016-80643-R.**

Estancia ***Italia***:

- ✓ FP7 ERA-Net CORE Organic Plus, cofinanciado por la Comisión Europea, Unión Europea "7th Framework Programme under grant agreement Nº 618107".

Estancia ***Argentina***:

- ✓ Agencia Nacional de Promoción Científica y Tecnológica (ANPCyT PICT 2013 0434 and 2013 1331), Argentina. "Relación estructura/función de biopolímeros en cápsulas de polielectrolitos y su influencia en la estabilidad de enzimas de interés farmacéutico y alimentario".

Otros resultados obtenidos durante la tesis

PUBLICACIONES CIENTÍFICAS

- Balaguer, N., Velázquez-Varela, J., **Traffano-Schiffo, M. V.**, Castro-Giráldez, M., & Fito, P. J. (2013). La utilización de sensores basados en la espectroscopia dieléctrica como una buena herramienta para asegurar la calidad y la seguridad alimentaria. *Alimentaria: Revista de tecnología e higiene de los alimentos*, (442), 47-51.

CONGRESOS

- **Traffano-Schiffo, M. V.**, Tylewicz, U., Castro-Giraldez, M., Fito, P. J., Harasym, J., Ragni, L, Laghi, L. & Dalla Rosa M. (2016). "Apple enrichment with β-glucan by vacuum impregnation and PEF treatment". Tipo de presentación: ***Póster*** en *Fruit and Veg Processing, 2nd Euro-Mediterranean Symposium.* Avignon, Francia.
- Tomás Egea, J. A., Fito P. J., Castro-Giráldez, M., & **Traffano-Schiffo, M. V.** (2017). "Sizing burner in drying operations by using alternative energies with environmental sustainability". Tipo de presentación: ***Póster*** en el *III International & IV National Student Congress of Food Science & Technology*. Valencia, España.

6. Conclusiones

Pork meat drying

1. Infrared thermography is a good tool for controlling the meat drying process, which provides information about the heat transfer in biological tissues, being possible to obtain the evolution of the meat emissivity and its clear relationship with the stages proposed for the falling rate period. So, with this technique, it is possible to identify the critical points and the surface temperature of the sample during the treatment.

The model allows us to predict the expansion/compression phenomena suffered by the sample throughout the drying process, predicting also the second order transition in the surface.

2. The loss factor in γ-dispersion presents a direct relationship with the number of water molecules on the sample's surface. It was possible to determine the point of water activity at which the surface temperature reaches the air drying temperature, by using the loss angle at 20 GHz. At this point of water activity, the liquid phase disappears and the internal transport controls the drying process. Finally, it has been possible to develop a useful tool to predict the surface water activity by using the loss angle at 20 GHz.

Chicken meat quality

3. A classification model for quality poultry meat based on a spectrophotometric analysis at radiofrequency and microwave ranges by using the Traffano-Schiffo model has been developed. It has been demonstrated the direct relation between the pH evolution and the dielectric constant at α-dispersion, extending this relation to the generation of lactic acid, at 12 h pmt. It has been demonstrated that the main structural proteins degradation has direct relation with the dielectric constant at β-dispersion, being possible to segregate meat depending on the level of protein degradation.

It has been possible to join the dielectric constants at α and β-dispersions in order to classify poultry meat in PSE, normal and DFD meat qualities. It can be concluded that the spectrophotometry at radiofrequency and microwave ranges represents a good and non-destructive tool able to determine poultry meat quality.

Deep pectoral myopathy in poultry meat

4. By means of a microstructural and physicochemical analysis of *pectoralis minor* and *major*, which includes the analysis of cations, proteins, pH, microstructural changes, or color variations by areas, it has been possible to describe the transformations that occur during an ischemic process with a hemorrhagic or necrotic process, therefore an angina or an infarct. Finally, it has been developed an objective and scientific methodology to categorize the level of the

DPM in poultry. This categorization is able to differentiate three categories: non-damaged, hemorrhagic samples (angina) and necrotic samples (infarct).

White striping physiopathy

5. White striping physiopathy consists of the partial rupture of the pectoral muscle, possibly associated with the overgrowth process of hypertrophic breeds; the organism solves this rupture of the tissue by depositing fat globules in the break area in order to maintain the functionality of contraction-relaxation of the muscular system. The fat content and the relationship between types of fatty acids vary when white striping occurs. The change in fat content is remarkable, rising from 0.5% to 10.1%, exhibiting a higher content of MUFA and SFA fatty acids; thus, WSB cannot be considered to be a healthy food with low saturated fats. Finally, it was possible to detect white striping physiopathy in chicken carcasses with skin using sensors with flat circular surfaces in radiofrequency spectra.

Mandarin fruit

6. It was possible to study deeply all mandarin tissues at macroscopic and microscopic level, to understand and to relate the structure with physicochemical and electric properties. The relaxations parameters (dielectric constant and frequency) of each tissue in α, β and γ-dispersions were obtained. Finally, a tool based on the relaxation dielectric constant in γ-dispersion, able to determine the moisture of the samples in dry basis, has been developed.

Kiwifruit

7. The application of pulsed electric fields as a pre-treatment of the osmotic dehydration in kiwifruit increase the water mass transfer and reduces the final sugar concentration comparing with samples that have not been pre-treated. The water phenomenological coefficient, in osmotic treatment, increases according to the electric fields applied in the pre-treatment. Thus because, the application of electric field prior to the osmotic treatment removes the electrolytes, reducing the activity of Ca^{2+} pump, and leaving alone the aquaporins as a main protein channel of water transmembrane transport and therefore affecting to the regular functionality of cell homeostasis system. However, the sucrose phenomenological coefficient, in osmotic treatment, decrease according to the electric field applied, because the sucrose transmembrane transport is made by the Na^{+} pump, therefore, any reduction of the overall quantity of the electrolytes reduces the sucrose content. PEF pre-treatment opens an amazing opportunity in the design of new products of candying fruits with high dehydration and less sugar content.

8. NMR is a suitable technique for quantifying water molecules according to their situation in the fruit tissue. This technique allows us to obtain the adsorbed water and open the possibility to apply the BET model over the whole range of water activity. It has been demonstrated that the application of electric fields across the plant tissue causes a storage of electrical energy that is converted into free energy to attract and retain water molecules on the surface of membranes and cell walls.

9. It has been proven that the application of an electric field prior to the osmotic dehydration produces a process of plasmolysis proportional to the applied electric field. The induction of the plasmolysis process is caused by the elimination of mobile charges of the medium, such as electrolytes, organic acids, etc.; among them Ca^{+2} is the major culprit because it is not available to fix some of the junctions of the microtubules between the cell wall and the membrane.

In addition, the process of plasmolysis induced by the electric field changes the behavior of kiwifruit tissue during the OD process. In a normal OD, the main transport is the symplastic, whereas if previously treated with PEF, the apoplastic transport is as important as the symplastic, considerably increasing the rate of dehydration.

β-Galactosidase encapsulation in hydrogels of alginate-Ca(II)

10. Alginate-Ca(II) beads containing lactase were successfully produced by the dropping method. Even though the inclusion of secondary excipients negatively influences the enzyme recovery with 20-30% losses, trehalose addition was critical for enzyme conservation during freezing and freeze/thawing treatments. Besides, the presence of guar gum improved the enzyme stability in a better way than in other trehalose containing beads during storage at 4 °C and freeze/thawing. This effect was probably related to a slighter higher molecular mobility on EATGG beads, which could account for a higher degree of rearrangement of the protons excipients inside the beads, allowing a higher degree of interaction with the enzyme.

The establishment of glassy matrix during freezing was critical to assure the maintenance of the lactase activity. The obtained glassy matrices showed similar T_g and Δcp values in all trehalose containing systems, but the inclusion of gums slightly increased the T_m' values, representing a valuable technological improvement.

The microstructure of the alginate-Ca(II) beads showed interesting results: the presence of secondary excipients affected the microstructure, showing rods with smaller cross-sectional radius R and with lower compactness within the rods (α_2) than alginate-Ca(II) beads. However, there were no significant changes in rods interconnection (α_1). This lower compactness of the rods in the presence of trehalose could also explain the higher enzyme activity recovered, having the

enzyme great possibilities of being located within the rods, increasing the possibility of establish more effective interactions.

The addition of both gums resulted in a significant increment of the bead size. However, arabic gum containing beads showed the highest circularity, and the guar gum containing ones the lowest. In this case, the increment in viscosity produced by the addition of guar gum accounts for a higher deformation during dropping. Further analysis should be conducted by changing the guar gum concentration, in order to optimize all the analyzed parameters.

11. Trehalose was critical for β-galactosidase conservation in alginate-Ca(II)beads after drying treatments. Guar gum as a second excipient showed the higher conservation effect for both treatments.

Trehalose was the main responsible of the formation of an amorphous matrix in the beads, showing T_g values close to 40 ºC, assuring very stable systems at ambient temperature. The presence of guar gum produced glassy matrices of high enthalpy values for both types of drying, indicating a key role in the matrix formation and, in turn, in enzyme activity conservation.

According to the size and morphology, VD beads showed smaller size and higher circularity comparing with FD and wet beads. The presence of trehalose significantly incremented the size respect alginate beads for both drying treatments. Besides, gums further increased the size, especially in FD beads. FEG-SEM images have revealed that FD beads had more spongy and voluminous surface, while VD beads showed large cracks (breakable surface). All trehalose-containing beads showed the typical glassy structure, which was supported by the DSC analysis.

For the first time, an isothermal crystallization analysis of alginate-Ca(II) beads containing β-galactosidase was carried out by LF-NMR. It revealed that the ice crystallization inside the beads follows the Avrami kinetics of nucleation and growth. The final ice fraction obtained was in agreement with the freezable water obtained by DSC.

The results of this research open an opportunity in the design and development of new lactose-containing foods able to be consumed by lactose intolerance people.

12. Though being a key in preserving enzymatic activity toward freezing and dehydration processes, the addition of trehalose as additive in Ca(II)-alginate lactase encapsulation systems prompts important structural changes leading to a loss of enzymatic activity during operation conditions. Trehalose drastically reduces the water self-diffusion coefficient in the starting hydrogel system (synthesized at pH 3.8), concomitant with the reduction in size and compactness of the structure at the scale of alginate rods. The incorporation of gums as second excipients does not revert this last effect, nevertheless induces a significant

stabilization in the microstructure not only at the rod scale, but also at smaller and bigger scales. On one hand, gums are shown to induce an important modulation in the characteristic size and density of alginate dimers (basic units of construction of rods). On the other hand and highly related to this, the variation in the degree of interconnection of rods evidenced in EA and EAT systems (i.e. in the absence of gums) is impeded. It is worth noting that in EA and EAT, this process is facilitated by free alginate polymer chains that become available from partial rod dissolution. Thus, this microstructure stabilization induced by the concomitant addition of guar gum results in an increased lactase activity during operation conditions, improving the performance of the systems with trehalose even above the bear Ca(II)-alginate matrix.

7. Bibliografía

Ade-Omowaye, B. I. O., Rastogi, N. K., Angersbach, A., & Knorr, D. (2001). Effects of high hydrostatic pressure or high intensity electrical field pulse pre-treatment on dehydration characteristics of red paprika. *Innovative Food Science & Emerging Technologies*, 2(1), 1-7.

Agre, P., Bonhivers, M., & Borgnia, M. J. (1998). The aquaporins, blueprints for cellular plumbing systems. *Journal of Biological Chemistry*, 273(24), 14659–14662.

Aguirre Calvo, (2013) Encapsulación de licopeno empleando polielectrolitos. Influencia del secado y congelado sobre su estabilidad. Tesis de máster, Facultad de Ciencias Exactas y Naturales, Universidad de Buenos Aires, Buenos Aires, Argentina.

Aguirre Calvo, T. R., Busch, V. M., & Santagapita, P. R. (2017). Stability and release of an encapsulated solvent-free lycopene extract in alginate-based beads. *LWT-Food Science and Technology*, 77, 406-412.

Aguirre Calvo, T., & Santagapita, P. (2016). Physicochemical Characterization of Alginate Beads Containing Sugars and Biopolymers. *Journal of Quality and Reliability Engineering*, 2016.

Allen, C. D., Russell, S. M., & Fletcher, D. L. (1997). The relationship of broiler breast meat color and pH to shelf-life and odor development. *Poultry Science*, 76(7), 1042-1046.

Al-Muhtaseb, A. H., McMinn, W. A. M., & Magee, T. R. A. (2002). Moisture sorption isotherm characteristics of food products: a review. *Food and Bioproducts Processing*, 80(2), 118-128.

Amami, E., Vorobiev, E., & Kechaou, N. (2005). Effect of pulsed electric field on the osmotic dehydration and mass transfer kinetics of apple tissue. *Drying Technology*, 23(3), 581-595.

Amami, E., Vorobiev, E., & Kechaou, N. (2006). Modelling of mass transfer during osmotic dehydration of apple tissue pre-treated by pulsed electric field. *LWT-Food Science and Technology*, 39(9), 1014-1021.

Ammar, J. B., Lanoisellé, J. L., Lebovka, N. I., Van Hecke, E., & Vorobiev, E. (2010). Effect of a pulsed electric field and osmotic treatment on freezing of potato tissue. *Food Biophysics*, 5(3), 247-254.

Andrade P., R. D., Lemus M., R., & Pérez C., C. E. (2011). Models of sorption isotherms for food: uses and limitations. *Vitae*, 18(3), 325-334.

AOAC, 2000. AOAC, Association of official analytical chemist official methods of analysis. Washington, D.C.

Arevalo, P., Ngadi, M. O., Bazhal, M. I., & Raghavan, G. S. V. (2004). Impact of pulsed electric fields on the dehydration and physical properties of apple and potato slices. *Drying technology*, 22(5), 1233-1246.

Austin, L., Bower, J. J., & Muldoon, C. (1996). The controlled release of leukaemia inhibitory factor (LIF) from gels. En Proceedings of the International Symposium on Controlled Release of Bioactive Materials (pp. 739-740).

Azmir, J., Zaidul, I. S. M., Rahman, M. M., Sharif, K. M., Mohamed, A., Sahena, F., Jahurul, M. H. A., Ghafoor, K., Norulaini, N. A. N., & Omar, A. K. M. (2013). Techniques for extraction of bioactive compounds from plant materials: A review. *Journal of Food Engineering*, 117(4), 426-436.

Balaguer, N., Velázquez-Varela, J., Traffano-Schiffo, M. V., Castro-Giráldez, M., & Suñer, P. J. F. (2013). La utilización de sensores basados en la espectroscopia dieléctrica como una buena herramienta para asegurar la calidad y la seguridad alimentaria. *Alimentaria: Revista de tecnología e higiene de los alimentos*, (442), 47-51.

Banaszewska, A., Cruijssen, F. C. A. M., Claassen, G. D. H., & van der Vorst, J. G. A. J. (2014). Effect and key factors of byproducts valorization: The case of dairy industry. *Journal of Dairy Science*, 97(4), 1893-1908.

Barbosa-Cánovas, G. V., A. J. Fontana, S. J. Schmidt, and T. P. Labuza. 2008. Water Activity in Foods: Fundamentals and Applications. John Wiley & Sons.

Barbosa-Cánovas, G. V., Fontana Jr, A. J., Schmidt, S. J., & Labuza, T. P. (2008). *Water activity in foods: fundamentals and applications.* John Wiley & Sons.

Barbut, S., Sosnicki, A. A., Lonergan, S. M., Knapp, T., Ciobanu, D. C., Gatcliffe, L. J., Huff-Lonergan, E., & Wilson, E. W. (2008). Progress in reducing the pale, soft and exudative (PSE) problem in pork and poultry meat. *Meat Science*, 79(1), 46-63.

Barbut, S., Zhang, L., & Marcone, M. (2005). Effects of pale, normal, and dark chicken breast meat on microstructure, extractable proteins, and cooking of marinated fillets. *Poultry Science*, 84(5), 797-802.

Bell, L. N., & Labuza, T. P. (2000). Moisture sorption: practical aspects of isotherm measurement and use. American Association of Cereal Chemists.

Bendall, J. R., & Swatland, H. J. (1988). A review of the relationships of pH with physical aspects of pork quality. *Meat Science*, 24(2), 85-126.

Benedito, J., Carcel, J. A., Rossello, C., & Mulet, A. (2001). Composition assessment of raw meat mixtures using ultrasonics. *Meat Science*, 57(4), 365-370.

Bianchi, M., Capozzi, F., Cremonini, M. A., Laghi, L., Petracci, M., Placucci, G., & Cavani, C. (2004). Influence of the season on the relationships between NMR transverse relaxation data and water-holding capacity of turkey breast meat. *Journal of the Science of Food and Agriculture*, 84(12), 1535-1540.

Bilgili, S. F., & Hess, J. (2008). Green muscle disease. Reducing the incidence in broiler flocks. *Ross Technology*, 8, 48.

Bouzrara, H., & Vorobiev, E. (2003). Solid–liquid expression of cellular materials enhanced by pulsed electric field. *Chemical Engineering and Processing: Process Intensification*, 42(4), 249-257.

Brandebourg, T. (2013). Growth of Muscle from the Myoblast to Whole Muscle. In C. R. Kerth (Ed.), *The Science of Meat Quality* (pp. 1-28). John Wiley & Sons, Inc., Iowa.

Briegel, A., Ortega, D. R., Tocheva, E. I., Wuichet, K., Li, Z., Chen, S., ... & Zhulin, I. B. (2009). Universal architecture of bacterial chemoreceptor arrays. *Proceedings of the National Academy of Sciences*, 106(40), 17181-17186.

Brunauer, S., Emmett, P.H., & Teller, E., 1938. Adsorption of gases in multimolecular layers. *Journal of the American Chemical Society*, 60 (2), 309–319.

Busch, V. M., Pereyra-Gonzalez, A., Šegatin, N., Santagapita, P. R., Ulrih, N. P., & Buera, M. P. (2017). Propolis encapsulation by spray drying: Characterization and stability. *LWT-Food Science and Technology*, 75, 227-235.

Calderón-Miranda, M. L., González, M. F. S. M., Barbosa-Cánovas, G. V., & Swanson, B. G. (1998). Métodos no térmicos para procesamiento de alimentos: Variables e inactivación microbiana. *Brazilian Journal of Food Technology*, 1, 3-11.

Castro Giráldez, M. (2010). Estudio de los espectros dieléctricos para el control de calidad de alimentos. Tesis doctoral, Instituto de Ingeniería de Alimentos para el Desarrollo, Valencia, España.

Castro-Giráldez, M., Aristoy, M., Toldrá, F., & Fito, P. (2010d). Microwave dielectric spectroscopy for the determination of pork meat quality. *Food Research International*, 43(10), 2369-2377.

Castro-Giráldez, M., Balaguer, N., Hinarejos, E., & Fito, P. J. (2014). Thermodynamic approach of meat freezing process. *Innovative Food Science & Emerging Technologies*, 23, 138-145.

Castro-Giráldez, M., Botella, P., Toldrá, F., & Fito, P. (2010c). Low-frequency dielectric spectrum to determine pork meat quality. *Innovative Food Science & Emerging Technologies*, 11(2), 376-386.

Castro-Giraldez, M., Colom, R.J., Fito, P.J., Herrero, V., Lidón, J.V., Monzó, J.M., Tébar, A., Traffano-Schiffo, M.V. (2016). Aparato y método no invasivo de detección de roturas de la cadena de frío en carne congelada. Patente Española Nº P201630956.

Castro-Giráldez, M., Fito, P. J., & Fito, P. (2010a). Application of microwaves dielectric spectroscopy for controlling pork meat (*Longissimus dorsi*) salting process. *Journal of Food Engineering*, 97(4), 484-490.

Castro-Giraldez, M., Fito, P. J., & Fito, P. (2010f). Non-equilibrium thermodynamic approach to analyze the pork meat (*Longissimus dorsi*) salting process. *Journal of Food Engineering*, 99(1), 24-30.

Castro-Giráldez, M., Fito, P. J., Chenoll, C., & Fito, P. (2010b). Development of a dielectric spectroscopy technique for the determination of apple (*Granny Smith*) maturity. *Innovative Food Science & Emerging Technologies*, 11(4), 749-754.

Castro-Giráldez, M., Fito, P. J., Ortolá, M. D., & Balaguer, N. (2013). Study of pomegranate ripening by dielectric spectroscopy. *Postharvest Biology and Technology*, 86, 346-353.

Castro-Giráldez, M., Fito, P. J., Prieto, J. M., Andrés, A., & Fito, P. (2012). Study of the puffing process of amaranth seeds by dielectric spectroscopy. *Journal of Food Engineering*, 110(2), 298-304.

Castro-Giráldez, M., Fito, P. J., Toldrá, F., & Fito, P. (2010e). Physical sensors for quality control during processing. In Fidel Toldrá (Ed.), *Handbook of Meat Processing* (pp.443-456). Wiley-Blackwell Publishing, E.E.U.U.

Castro-Giraldez, M., Fito, P.J., Fito, P., (2011c). Nonlinear thermodynamic approach to analyze long time osmotic dehydration of parenchymatic apple tissue. *Journal of Food Engineering*, 102 (1), 34–42.

Castro-Giráldez, M., Toldrá, F., & Fito, P. (2011a). Low frequency dielectric measurements to assess post-mortem ageing of pork meat. *LWT-Food Science and Technology*, 44(6), 1465-1472.

Castro-Giráldez, M., Tylewicz, U., Fito, P. J., Dalla Rosa, M., & Fito, P. (2011b). Analysis of chemical and structural changes in kiwifruit (*Actinidia deliciosa cv Hayward*) through the osmotic dehydration. *Journal of Food Engineering*, 105(4), 599-608.

Cataldo, A., Piuzzi, E., Cannazza, G., De Benedetto, E., & Tarricone, L. (2010). Quality and anti-adulteration control of vegetable oils through microwave dielectric spectroscopy. *Measurement*, 43(8), 1031-1039.

Chan, J. T., Omana, D. A., & Betti, M. (2011). Effect of ultimate pH and freezing on the biochemical properties of proteins in turkey breast meat. *Food Chemistry*, 127(1), 109-117.

Chico, J. R., & Sánchez, A. R. P. (2012). Competitividad y políticas de seguridad alimentaria de las regiones españolas: el caso de la industria cárnica. *Revista Finanzas y Política Económica*, 4(1), 33-54.

CIE. (1978). International Commission on Illumination, ecommendations on uniform colour spaces, colour, difference equations, psychometric colour terms. CIE publication No. 15 (Suppl.2), (E-1.31) 1971/(TC-1.3). Bureau Central de la CIE, París, Francia.

Ciurczak, E. W., & Igne, B. (2014). Pharmaceutical and medical applications of near-infrared spectroscopy. CRC Press. Taylor & Francis Group, Florida.

Corrales, M., Toepfl, S., Butz, P., Knorr, D., & Tauscher, B. (2008). Extraction of anthocyanins from grape by-products assisted by ultrasonics, high hydrostatic pressure or pulsed electric fields: a comparison. *Innovative Food Science & Emerging Technologies*, 9(1), 85-91.

Damez, J. L., Clerjon, S., Abouelkaram, S., & Lepetit, J. (2008). Beef meat electrical impedance spectroscopy and anisotropy sensing for non-invasive early assessment of meat ageing. *Journal of Food Engineering*, 85(1), 116–122.

Dashevsky, A. (1998). Protein loss by the microencapsulation of an enzyme (lactase) in alginate beads. International Journal of Pharmaceutics, 161(1), 1-5.

Dellarosa, N., Ragni, L., Laghi, L., Tylewicz, U., Rocculi, P., & Dalla Rosa, M. (2016). Time domain nuclear magnetic resonance to monitor mass transfer mechanisms in apple tissue promoted by osmotic dehydration combined with pulsed electric fields. *Innovative Food Science & Emerging Technologies*, *37*, 345-351.

Demirel, Y. (2013). *Nonequilibrium Thermodynamics: Transport and Rate Processes in Physical, Chemical and Biological Systems. Elsevier Science.*

Demirel, Y., & Sandler, S. I. (2001). Linear-nonequilibrium thermodynamics theory for coupled heat and mass transport. *International Journal of Heat and Mass Transfer*, 44(13), 2439-2451.

Dermesonlouoglou, E., Zachariou, I., Andreou, V., & Taoukis, P. S. (2016). Effect of pulsed electric fields on mass transfer and quality of osmotically dehydrated kiwifruit. *Food and Bioproducts Processing*, 100, 535-544.

Dickinson, E. (2003). Hydrocolloids at interfaces and the influence on the properties of dispersed systems. *Food Hydrocolloids*, 17(1), 25-39.

Donsì, F., Ferrari, G., & Pataro, G. (2010). Applications of pulsed electric field treatments for the enhancement of mass transfer from vegetable tissue. *Food Engineering Reviews*, 2(2), 109-130.

Erich, S., Kuschel, B., Schwarz, T., Ewert, J., Böhmer, N., Niehaus, F., ... & Fischer, L. (2015). Novel high-performance metagenome β-galactosidases for lactose hydrolysis in the dairy industry. *Journal of Biotechnology*, 210, 27-37.

Estevinho, B. N., Ramos, I., & Rocha, F. (2015). Effect of the pH in the formation of β-galactosidase microparticles produced by a spray-drying process. *International Journal of Biological Macromolecules*, 78, 238-242.

Estevinho, B. N., Rocha, F., Santos, L., & Alves, A. (2013). Microencapsulation with chitosan by spray drying for industry applications–A review. *Trends in Food Science & Technology*, 31(2), 138-155.

Fagan, C. C., Everard, C., O'Donnell, C. P., Downey, G., & O'Callaghan, D. J. (2005). Prediction of inorganic salt and moisture content of process cheese using dielectric spectroscopy. *International Journal of Food Properties*, 8(3), 543-557.

Fang, Y., Al-Assaf, S., Phillips, G. O., Nishinari, K., Funami, T., Williams, P. A., & Li, L. (2007). Multiple steps and critical behaviors of the binding of calcium to alginate. *The Journal of Physical Chemistry B*, 111(10), 2456-2462.

Fernandes, F. A., Rodrigues, S., Gaspareto, O. C., & Oliveira, E. L. (2006). Optimization of osmotic dehydration of bananas followed by air-drying. *Journal of Food Engineering*, 77(1), 188-193.

Fito, P., Grau, A. M. A., Sorolla, A. M. A., & Baviera, J. M. B. (2001). *Introducción al secado de alimentos por aire caliente* (pp. 43-49). Ed. Universidad Politécnica de Valencia, Valencia. España.

Fito, P., LeMaguer, M., Betoret, N., & Fito, P. J. (2007). Advanced food process engineering to model real foods and processes: The "SAFES" methodology. *Journal of Food Engineering*, 83(2), 173-185.

Fito, P.J., Colom, R.J., Castro-Giraldez, M., Herrero, V., Monzó, J.M., Traffano-Schiffo, M.V., Tébar, A., (2016). Aparato y método de detección de daño producido por la miopatía del pectoral profundo en aves. Patente Española Nº P201630062.

Forrest, J. C., Aberle, E. D., Hedrick, H. B., Jugde, M. D. & Merkel, R. A. (1979). *Fundamentos de ciencia de la carne*. Editorial Acribia, S.A., Zaragoza, España.

Foster, K.R. & Schwan, H.P. (1986). Dielectric properties of tissues-a review. En Charles Polk y Elliot Postow (Eds.), *Handbook of Biological Effects of Electromagnetic Radiation* (pp.27-96). CRC Press, Boca Raton, FL, E.E.U.U.

Giulio, B. D., Orlando, P., Barba, G., Coppola, R., Rosa, M. D., Sada, A., ... & Nazzaro, F. (2005). Use of alginate and cryo-protective sugars to improve the viability of lactic acid bacteria after freezing and freeze-drying. *World Journal of Microbiology and Biotechnology*, 21(5), 739-746.

Gombotz, W. R., & Wee, S. F. (2012). Protein release from alginate matrices. *Advanced Drug Delivery Reviews*, 64, 194-205.

Goula, A. M., & Lazarides, H. N. (2012). Modeling of mass and heat transfer during combined processes of osmotic dehydration and freezing (osmo-dehydro-freezing). *Chemical Engineering Science*, 82, 52-61.

Grahl, T., & Märkl, H. (1996). Killing of microorganisms by pulsed electric fields. *Applied Microbiology and Biotechnology*, 45(1), 148-157.

Greaser, M. L. (1986) Conversion of muscle to meat. In P. J. Bechtel (Ed.), Muscle as Food (pp. 37-87). London: Academic Press.

Grenier, K., Dubuc, D., Chen, T., Artis, F., Chretiennot, T., Poupot, M., & Fournie, J. (2013). Recent advances in microwave-based dielectric spectroscopy at the cellular level for cancer investigations. *IEEE Transactions on Microwave Theory and Techniques*, 61(5), 2023-2030.

Guo, W., Liu, Y., Zhu, X., & Wang, S. (2011a). Dielectric properties of honey adulterated with sucrose syrup. *Journal of Food Engineering*, 107(1), 1-7.

Guo, W., Zhu, X., Liu, Y., & Zhuang, H. (2010). Sugar and water contents of honey with dielectric property sensing. *Journal of Food Engineering*, 97(2), 275-281.

Guo, W., Zhu, X., Nelson, S. O., Yue, R., Liu, H., & Liu, Y. (2011b). Maturity effects on dielectric properties of apples from 10 to 4500 MHz. *LWT-Food Science and Technology*, 44(1), 224-230.

He, X., Liu, Y., Li, H., & Li, H. (2016). Single-stranded structure of alginate and its conformation evolvement after an interaction with calcium ions as revealed by electron microscopy. *RSC Advances*, 6(115), 114779-114782.

Heinz, V., Toepfl, S., & Knorr, D. (2003). Impact of temperature on lethality and energy efficiency of apple juice pasteurization by pulsed electric fields treatment. *Innovative Food Science & Emerging Technologies*, 4(2), 167-175.

Hernández Cázares, A. S. (2010). Control de calidad y seguridad de la carne y productos cárnicos curados mediante el uso de sensores enzimáticos. Tesis doctoral, Instituto de Agroquímica y Tecnología de los Alimentos (IATA), Valencia, España.

Holmes, W. S., Mukhopadhyay, S. C., & Riley, S. G. (2013). Dielectric Properties of Wood for Improved Internal Imaging. In S. C. Mukhopadhyay, K. P. Jayasundera, & A. Fuchs (Eds.), *Advancement in Sensing Technology* (pp. 93-104). Springer Berlin Heidelberg.

Honikel, K. O. (2004). Conversion of muscle to meat. In W. K. Jensen, C. E. Devine, & M. Dikeman (Eds.), *Encyclopedia of meat sciences* (pp. 314-318). Elsevier Academic Press.

Honikel, K. O., & Fischer, C. (1977). A rapid method for the detection of PSE and DFD porcine muscles. *Journal of Food Science*, 42(6), 1633-1636.

Huang, M., Huang, F., Xue, M., Xu, X., & Zhou, G. (2011). The effect of active caspase-3 on degradation of chicken myofibrillar proteins and structure of myofibrils. Food Chemistry, 128(1), 22-27.

Huff Lonergan, E., Zhang, W., & Lonergan, S. M. (2010). Biochemistry of postmortem muscle—Lessons on mechanisms of meat tenderization. *Meat Science*, 86(1), 184-195.

Huff-Lonergan, E. (2010). Chemistry and biochemistry of meat. In F. Toldrá (Ed.), *Handbook of meat processing* (pp. 5-24). Wiley-Blackwell, Iowa, E.E.U.U.

Huff-Lonergan, E., & Lonergan, S. M. (1999). Postmortem mechanisms of meat tenderization: the roles of the structural proteins and the calpain system. In Y. L. Xiong, C. T. Ho, & F. Shahidi, (Eds.), Quality attributes of muscle foods (pp 229-254). New York: Springer Science & Business Media, LLC.

Iglesias, H. A., & Chirife, J. (1995). An alternative to the Guggenheim, Anderson and De Boer model for the mathematical description of moisture sorption isotherms of foods. *Food Research International*, 28(3), 317-321.

ISO 1442:1997 (1997). Methods of test for meat and meat products. Determination of moisture content. BS 4401-3:1997.

Jaitovich, A. A., & Bertorello, A. M. (2006). Na^+, K^+-ATPase: an indispensable ion pumping-*signaling* mechanism across mammalian cell membranes. *Seminars in Nephrology*, 26, 386-392.

Jalté, M., Lanoisellé, J. L., Lebovka, N. I., & Vorobiev, E. (2009). Freezing of potato tissue pre-treated by pulsed electric fields. *LWT-Food Science and Technology*, 42(2), 576-580.

Keeler, J. (2011). Understanding NMR spectroscopy. John Wiley & Sons.

Kent, M., & Anderson, D. (1996). Dielectric studies of added water in poultry meat and scallops. *Journal of Food Engineering*, 28(3), 239-259.

Kent, M., Peymann, A., Gabriel, C., & Knight, A. (2002). Determination of added water in pork products using microwave dielectric spectroscopy. *Food Control*, 13(3), 143-149.

Kijowski, J., Kupińska, E., J. Stangierski, J., Tomaszewska-Gras, J. & Szablewski, T. (2014). Paradigm of deep pectoral myopathy in broiler chickens. *World's Poultry Science Journal*, 70, 125-138.

Knorr, D., & Angersbach, A. (1998). Impact of high-intensity electric field pulses on plant membrane permeabilization. *Trends in Food Science & Technology*, 9(5), 185-191.

Knorr, D., Angersbach, A., Eshtiaghi, M. N., Heinz, V., & Lee, D. U. (2001). Processing concepts based on high intensity electric field pulses. *Trends in Food Science & Technology*, 12(3), 129-135.

Kremer, F. (2002). Dielectric spectroscopy–yesterday, today and tomorrow. *Journal of Non-crystalline Solids*, 305(1), 1-9.

Kuang, W., & Nelson, S. O. (1997). Low-frequency dielectric dispersion from ion permeability of membranes. *Journal of Colloid and Interface Science*, 193(2), 242-249.

Kuttappan, V. A., Brewer, V. B., Apple, J. K., Waldroup, P. W., & Owens, C. M. (2012a). Influence of growth rate on the occurrence of white striping in broiler breast fillets. *Poultry Science*, 91(10), 2677-2685.

Kuttappan, V. A., Lee, Y. S., Erf, G. F., Meullenet, J. F., McKee, S. R., & Owens, C. M. (2012b). Consumer acceptance of visual appearance of broiler breast meat with varying degrees of white striping. *Poultry Science*, 91(5), 1240-1247.

Kuttappan, V. A., Shivaprasad, H. L., Shaw, D. P., Valentine, B. A., Hargis, B. M., Clark, F. D., McKee, S. R., & Owens, C. M. (2013). Pathological changes associated with white striping in broiler breast muscles. *Poultry Science*, 92(2), 331-338.

Laghi, L., Picone, G., & Capozzi, F. (2014). Nuclear magnetic resonance for foodomics beyond food analysis. *TrAC Trends in Analytical Chemistry*, 59, 93-102.

Lametsch, R., Roepstorff, P., & Bendixen, E. (2002). Identification of protein degradation during post-mortem storage of pig meat. Journal of Agricultural and Food Chemistry, 50(20), 5508-5512.

László, P., Vozáry, E., Zana, J., Zsivánovits, G., & Sass, P. (1997). Electrical properties of apple cultivars during ripening and storage. *Acta Horticulture*, 485, 239-247.

Lebovka, N. I., Shynkaryk, N. V., & Vorobiev, E. (2007). Pulsed electric field enhanced drying of potato tissue. *Journal of Food Engineering*, 78(2), 606-613.

Lee, K. Y., & Mooney, D. J. (2012). Alginate: properties and biomedical applications. *Progress in Polymer Science*, 37(1), 106-126.

Leong, S. Y., Richter, L. K., Knorr, D., & Oey, I. (2014). Feasibility of using pulsed electric field processing to inactivate enzymes and reduce the cutting force of carrot (Daucus carota var. Nantes). *Innovative Food Science & Emerging Technologies*, 26, 159-167.

Lesmes, D. P., & Morgan, F. D. (2001). Dielectric spectroscopy of sedimentary rocks. *Journal of Geophysical Research: Solid Earth*, 106, 13329-13346.

Lewicki, P. P. (1997). The applicability of the GAB model to food water sorption isotherms. *International Journal of Food Science & Technology*, 32(6), 553-557.

Li, S., Xu, X., & Zhou, G. (2012). The roles of the actin-myosin interaction and proteolysis in tenderization during the aging of chicken muscle. Poultry Science, 91(1), 150-160.

Li, X. Y., Chen, X. G., Liu, C. S., Peng, H. N., & Cha, D. S. (2008). Effect of trehalose and drying process on the survival of encapsulated Lactobacillus casei ATCC 393. *Drying Technology*, 26(7), 895-901.

Liu, D., Qu, J., Sun, D. W., Pu, H., & Zeng, X. A. (2013). Non-destructive prediction of salt contents and water activity of porcine meat slices by hyperspectral imaging in a salting process. *Innovative Food Science & Emerging Technologies*, 20, 316-323.

Lizhi, H., Toyoda, K., & Ihara, I. (2010). Discrimination of olive oil adulterated with vegetable oils using dielectric spectroscopy. *Journal of Food Engineering*, 96(2), 167-171.

Lomauro, C. J., Bakshi, A. S., & Labuza, T. P. (1985). Evaluation of food moisture sorption isotherm equations. Part I: Fruit, vegetable and meat products. *Lebensmittel-Wissenschaft und-Technologie*, 18(2), 111-117.

López, N., Puértolas, E., Condón, S., Álvarez, I., & Raso, J. (2008). Effects of pulsed electric fields on the extraction of phenolic compounds during the fermentation of must of Tempranillo grapes. *Innovative Food Science & Emerging Technologies*, 9(4), 477-482.

Luengo, E., Álvarez, I., & Raso, J. (2013). Improving the pressing extraction of polyphenols of orange peel by pulsed electric fields. *Innovative Food Science & Emerging Technologies*, 17, 79-84.

Luengo, E., Alvarez, I., & Raso, J. (2015). Phenolic extraction: Pulsed electric fields: A technology for improving phenolic extraction in red wines. *Wine & Viticulture Journal*, *30*(1), 17.

Mahnič-Kalamiza, S., Vorobiev, E., & Miklavčič, D. (2014). Electroporation in food processing and biorefinery. *The Journal of Membrane Biology*, 247(12), 1279-1304.

Maltin, C., Balcerzak, D., Tilley, R., & Delday, M. (2003). Determinants of meat quality: tenderness. *Proceedings of the Nutrition Society*, 62(02), 337-347.

Mandala, I. G., Anagnostaras, E. F., & Oikonomou, C. K. (2005). Influence of osmotic dehydration conditions on apple air-drying kinetics and their quality characteristics. *Journal of Food Engineering*, 69(3), 307-316.

Markx, G. H., & Davey, C. L. (1999). The dielectric properties of biological cells at radiofrequencies: applications in biotechnology. *Enzyme and Microbial Technology*, 25(3), 161-171.

Martinoia, E., Massonneau, A., & Frangne, N. (2000). Transport processes of solutes across the vacuolar membrane of higher plants. *Plant and Cell Physiology*, 41(11), 1175-1186.

Maurel, C., & Chrispeels, M. J. (2001). Aquaporins. A molecular entry into plant water relations. *Plant Physiology*, 125(1), 135-138.

Mazzobre, M. F., Longinotti, M. P., Corti, H. R., & Buera, M. P. (2002). Effect of salts on the properties of aqueous sugar systems, in relation to biomaterial stabilization. 1. Water sorption behavior and ice crystallization/melting. *Cryobiology*, 43(3), 199-210.

McGeehin, B., Sheridan, J. J., & Butler, F. (2001). Factors affecting the pH decline in lamb after slaughter. *Meat Science*, 58(1), 79-84.

McKee, S. (2002). Muscle fiber types and meat quality. *Poultry Digest Online*, 3(10).

Ministerio de Agricultura, Alimentación y Medio Ambiente, (2015). El sector de la carne de aves en cifras.

Moraga, M. J., Moraga, G., Fito, P. J., & Martínez-Navarrete, N. (2009). Effect of vacuum impregnation with calcium lactate on the osmotic dehydration kinetics and quality of osmodehydrated grapefruit. *Journal of Food Engineering*, 90(3), 372–379.

Moreno Pérez, M. (2016). Resonancia Magnética Nuclear aplicada a la síntesis orgánica ya la metabólica. Control de calidad de los alimentos y estudio de los metabolitos celulares. Tesis doctoral. Departamento de Química Inorgánica, Orgánica y Bioquímica. Universidad de Castilla-La Mancha. Ciudad Real, España.

Mudalal, S., Babini, E., Cavani, C., & Petracci, M. (2014). Quantity and functionality of protein fractions in chicken breast fillets affected by white striping. Poultry Science, 93(8), 2108-2116.

Nave, C. R. (2010). Hyperphysics. Department of Physics and Astronomy, Georgia State University, GA.

Nelson, S. O. & Datta, A. K. (2001). Handbook of microwave technology for food application. In A. K. Datta y R. C. Anantheswaran (Eds.). *Dielectric Properties of Food Materials and Electric Field Interactions* (pp. 70) CRC Press, New York, E.E.U.U.

Nelson, S. O. (1999). Dielectric properties measurement techniques and applications. *Transactions of the ASAE-American Society of Agricultural Engineers*, 42(2), 523-530.

Offer, G., & Cousin, T. (1992). The mechanism of drip production-formation of two compartments of extracellular-space in muscle post-mortem. *Journal of the Science of Food and Agricultural*, 58, 107–116.

Ouali, A., Herrera-Mendez, C. H., Coulis, G., Becila, S., Boudjellal, A., Aubry, L., & Sentandreu, M. A. (2006). Revisiting the conversion of muscle into meat and the underlying mechanisms. *Meat Science*, 74(1), 44-58.

Paredi, G., Raboni, S., Bendixen, E., de Almeida, A. M., & Mozzarelli, A. (2012). "Muscle to meat" molecular events and technological transformations: The proteomics insight. *Journal of Proteomics*, 75(14), 4275-4289.

Park, Y. K., Santi, M. S. S., & Pastore, G. M. (1979). Production and characterization of β-galactosidase from *aspergillus oryzae*. *Journal of Food Science*, 44(1), 100-103.

Pethig, R. (1979). Dielectric and Electrical Properties of Biological Materials. J. Wiley & Sons, Chichester.

Pethig, R. (1984). Dielectric properties of biological materials: Biophysical and medical applications. *IEEE Transactions on Electrical Insulation*, (5), 453-474.

Petracci, M., & Cavani, C. (2011). Muscle growth and poultry meat quality issues. *Nutrients*, 4(1), 1-12.

Petracci, M., Mudalal, S., Babini, E., & Cavani, C. (2014). Effect of white striping on chemical composition and nutritional value of chicken breast meat. *Italian Journal of Animal Science*, 13(1).

Petracci, M., Mudalal, S., Bonfiglio, A., & Cavani, C. (2013). Occurrence of white striping under commercial conditions and its impact on breast meat quality in broiler chickens. *Poultry Science*, 92(6), 1670-1675.

Phoon, P. Y., Galindo, F. G., Vicente, A., & Dejmek, P. (2008). Pulsed electric field in combination with vacuum impregnation with trehalose improves the freezing tolerance of spinach leaves. *Journal of Food Engineering*, 88(1), 144-148.

Ponce-Alquicira, E. (2006). Cambios bioquímicos pre y postmortem. In Hui, Y. H., Guerrero, I., Rosmini, M. R. (Eds.), *Ciencia y tecnología de carnes* (pp. 111-135). Limusa, México D.F.

Pötschke, P., Dudkin, S. M., & Alig, I. (2003). Dielectric spectroscopy on melt processed polycarbonate—multiwalled carbon nanotube composites. *Polymer*, 44(17), 5023-5030.

Puértolas, E., Luengo, E., Álvarez, I., & Raso, J. (2012). Improving mass transfer to soften tissues by pulsed electric fields: fundamentals and applications. *Annual Review of Food Science and Technology*, 3, 263-282.

Qin, B. L., Zhang, Q., Barbosa-Canovas, G. V., Swanson, B. G., & Pedrow, P. D. (1994). Inactivation of microorganisms by pulsed electric fields of different voltage waveforms. *IEEE Transactions on Dielectrics and Electrical Insulation*, *1*(6), 1047-1057.

Ramasamy, S., & Moghtaderi, B. (2010). Dielectric properties of typical australian wood-based biomass materials at microwave frequency. *Energy & Fuels*, 24(8), 4534-4548.

Rao, M. A., Rizvi, S. S., Datta, A. K., & Ahmed, J. (Eds.). (2014). *Engineering properties of foods*. CRC Press, Taylor & Francis Group, Boca Raton, FL., E.E.U.U.

Rastogi, N. K., Eshtiaghi, M. N., & Knorr, D. (1999). Accelerated mass transfer during osmotic dehydration of high intensity electrical field pulse pretreated carrots. *Journal of Food Science*, 64(6), 1020-1023.

Rastogi, N. K., Raghavarao, K. S. M. S., Niranjan, K., & Knorr, D. (2002). Recent developments in osmotic dehydration: methods to enhance mass transfer. *Trends in Food Science & Technology*, 13(2), 48-59.

Rosenberg, Z. M. M. (2006). Current trends of β-galactosidase application in food technology. *Journal of Food and Nutrition Research*, 45(2), 47-54.

Sabuncu, A. C., Zhuang, J., Kolb, J. F., & Beskok, A. (2012). Microfluidic impedance spectroscopy as a tool for quantitative biology and biotechnology. *Biomicrofluidics*, 6(3), 034103.

Sadat, A., Mustajab, P., & Khan, I. A. (2006). Determining the adulteration of natural milk with synthetic milk using ac conductance measurement. *Journal of Food Engineering*, 77(3), 472-477.

Santagapita, (2010). Estabilidad de enzimas en medios de distinta movilidad molecular. impacto de interacciones con azúcares y biopolímeros y de la encapsulación. Tesis doctoral, Facultad de Ciencias Exactas y Naturales, Departamento de Industrias. Universidad de Buenos Aires, Buenos Aires, Argentina.

Santagapita, P. R., Mazzobre, M. F., & Buera, M. P. (2011). Formulation and drying of alginate beads for controlled release and stabilization of invertase. *Biomacromolecules*, 12(9), 3147-3155.

Santagapita, P. R., Mazzobre, M. F., & del Pilar Buera, M. (2012). Invertase stability in alginate beads: Effect of trehalose and chitosan inclusion and of drying methods. *Food Research International*, 47(2), 321-330.

Schwan, H. P. (1988). Biological effects of nonionizing radiations: Cellular properties and interactions. *Annals of Biomedical Engineering*, 16, 245–263.

Scotter, C. N. (1997). Non-destructive spectroscopic techniques for the measurement of food quality. *Trends in Food Science & Technology*, 8(9), 285-292.

Sharma, P., Bremer, P., Oey, I., & Everett, D. W. (2014). Bacterial inactivation in whole milk using pulsed electric field processing. *International Dairy Journal*, 35(1), 49-56.

Shaw, D. J., (1992). Introduction to colloid and surface chemistry: Butterworth-Heinemann, Oxford, UK, (pp 1-10).

Shiratake, K., & Martinoia, E. (2007). Transporters in fruit vacuoles. *Plant Biotechnology*, 24(1), 127-133.

Shynkaryk, M. V., Lebovka, N. I., & Vorobiev, E. (2008). Pulsed electric fields and temperature effects on drying and rehydration of red beetroots. *Drying Technology*, 26(6), 695-704.

Siegel, P. H. (2004). Terahertz technology in biology and medicine. *IEEE transactions on microwave theory and techniques*, *52*(10), 2438-2447.

Singh, R. P., & Heldman, D. R. (2001). Introduction to food engineering. Gulf Professional Publishing.

Smith, D. P., Fletcher, D. L., & Papa, C. M. (1992). Post-mortem biochemistry of pekin duckling and broiler chicken pectoralis muscle. *Poultry Science*, 71(10), 1768-1772.

Smith, J., Carr, A., Golding, M., Reid, D., & Zhang, L. (2011). Assessing the use of dielectric spectroscopy to analyse calcium induced compositional and structural changes in a model cheese. *Procedia Food Science*, 1, 1833-1840.

Smulders, F., Hofbauer, P. & Geesink, G. H. (2014). The Conversion of Muscle to Meat. In T. Ninios, J. Lundén, H. Korkeala, & M. Fredriksson-Ahomaa (Eds.), Meat Inspection and Control in the Slaughterhouse (pp. 399-421). Oxford: John Wiley & Sons, Ltd.

Soltani, M., Alimardani, R., & Omid, M. (2011). Evaluating banana ripening status from measuring dielectric properties. *Journal of Food Engineering*, 105(4), 625-631.

Sonego, J. M., Santagapita, P. R., Perullini, M., & Jobbágy, M. (2016). Ca (II) and Ce (III) homogeneous alginate hydrogels from the parent alginic acid precursor: a structural study. *Dalton Transactions*, 45(24), 10050-10057.

Sosa-Morales, M. E., Tiwari, G., Wang, S., Tang, J., Garcia, H. S., & Lopez-Malo, A. (2009). Dielectric heating as a potential post-harvest treatment of disinfesting mangoes, Part I: Relation between dielectric properties and ripening. *Biosystems Engineering*, 103(3), 297-303.

Steudle, E., & Frensch, J. (1996). Water transport in plants: role of the apoplast. *Plant and Soil*, 187(1), 67–79.

Talens, C. (2015). Desarrollo de técnicas combinadas de secado con aire caliente y microondas en la producción de fibra alimentaria a partir de subproductos cítricos. Tesis doctoral, Instituto de Ingeniería de Alimentos para el Desarrollo, Valencia, España.

Talens, C., Castro-Giraldez, M., & Fito, P. J. (2016a). Study of the effect of microwave power coupled with hot air drying on orange peel by dielectric spectroscopy. *LWT-Food Science and Technology*, 66, 622-628.

Talens, C., Castro-Giraldez, M., & Fito, P. J. (2016b). A thermodynamic model for hot air microwave drying of orange peel. *Journal of Food Engineering*, 175, 33-42.

Tedjo, W., Taiwo, K. A., Eshtiaghi, M. N., & Knorr, D. (2002). Comparison of pretreatment methods on water and solid diffusion kinetics of osmotically dehydrated mangos. *Journal of Food Engineering*, 53(2), 133-142.

Timmermann, E. O., Chirife, J., & Iglesias, H. A. (2001). Water sorption isotherms of foods and foodstuffs: BET or GAB parameters?. *Journal of Food Engineering*, 48(1), 19-31.

Toldrá, F., & Reig, M. (2006). Methods for rapid detection of chemical and veterinary drug residues in animal foods. *Trends in Food Science & Technology*, 17(9), 482-489.

Torgovnikov, G. I. (1993). Interaction between the electromagnetic field and wood. main features of dielectric properties of wood. In *Dielectric Properties of Wood and Wood-Based Materials* (pp. 1-19). Springer Berlin Heidelberg.

Torringa, E., Esveld, E., Scheewe, I., van den Berg, R., & Bartels, P. (2001). Osmotic dehydration as a pre-treatment before combined microwave-hot-air drying of mushrooms. *Journal of Food Engineering*, 49(2), 185-191.

Trados, T. (2013). *Encyclopedia of Colloid and Interface Science*. Springer Heidelberg New York Dordrecht London.

Traffano-Schiffo, M. V., Castro-Giráldez, M., Fito, P. J., & Balaguer, N. (2014b). Thermodynamic model of meat drying by infrarred thermography. *Journal of Food Engineering*, 128, 103-110.

Traffano-Schiffo, M. V., Laghi, L., Castro-Giraldez, M., Tylewicz, U., Romani, S., Ragni, L., ... & Fito, P. J. (2017). Osmotic dehydration of organic kiwifruit pre-treated by pulsed electric fields: Internal transport and transformations analyzed by NMR. *Innovative Food Science & Emerging Technologies*, 41, 259-266.

Traffano-Schiffo, M. V., Tylewicz, U., Castro-Giraldez, M., Fito, P. J., Ragni, L., & Dalla Rosa, M. (2016). Effect of pulsed electric fields pre-treatment on mass transport during the osmotic dehydration of organic kiwifruit. *Innovative Food Science & Emerging Technologies*, 38, 243-251.

Traffano-Schiffo, M.V., Balaguer, N., Castro-Giráldez, M. & Fito, P.J. (2014a). Thermal emerging technologies in fruit juice processing. In A. Ibarz, V. Falguera (Eds.). *Juice Processing: Quality, Safety and Value-added Opportunities* (pp. 197-216). CRC Press, Boca Raton, FL., E.E.U.U.

Tsong, T. Y. (1991). Electroporation of cell membranes. *Biophysical Journal*, 60(2), 297.

Tylewicz, U., Fito, P. J., Castro-Giráldez, M., Fito, P., & Dalla Rosa, M. (2011). Analysis of kiwifruit osmodehydration process by systematic approach systems. *Journal of Food Engineering*, 104(3), 438-444.

Tylewicz, U., Tappi, S., Mannozzi, C., Romani, S., Dellarosa, N., Laghi, L., ... & Dalla Rosa, M. (2017). Effect of pulsed electric field (PEF) pre-treatment coupled with osmotic dehydration on physico-chemical characteristics of organic strawberries. *Journal of Food Engineering*. https://doi.org/10.1016/j.jfoodeng.2017.04.028

U.S. Department of Agriculture, A. R. S. 2008. USDA national nutrient database for standard reference, release 21, Nutrient Data Laboratory Home Page. http://www.ars.usda.gov/Services/docs.htm?docid=8964 (Nov. 2009.)

Varlan, A. R., & Sansen, W. (1996). Nondestructive electrical impedance analysis in fruit: normal ripening and injuries characterization. *Electromagnetic Biology and Medicine*, 15(3), 213-227.

Vega-Mercado, H., Gongora-Nieto, M. M., Barbosa-Canovas, G. V., & Swanson, B. G. (2007). Pulsed electric fields in food preservation. In M. S. Rahman (Ed.). *Handbook of Food Preservation* (pp. 783-811). CRC Press, Boca Raton, FL., E.E.U.U.

Velázquez Varela, J. (2014). Estudio de los espectros dieléctricos en alimentos con estructura coloidal. Tesis doctoral, Instituto de Ingeniería de Alimentos para el Desarrollo, Valencia, España.

Velázquez-Varela, J., Fito, P. J., & Castro-Giráldez, M. (2014). Thermodynamic analysis of salting cheese process. *Journal of Food Engineering*, 130, 36-44.

Warris, P.D. (2003). *Ciencia de la carne*. Editorial Acribia, S.A., Zaragoza (España).

Woelfel, R. L., Owens, C. M., Hirschler, E. M., & Sams, A. R. (1998). The incidence and characterization of pale, soft and exudative chicken meat in a commercial plant. *Poultry Science*, 77, 62.

Woelfel, R. L., Owens, C. M., Hirschler, E. M., Martinez-Dawson, R., & Sams, A. R. (2002). The characterization and incidence of pale, soft, and exudative broiler meat in a commercial processing plant. *Poultry Science*, 81(4), 579-584.

Woodward, A. M., Jones, A., Zhang, X. Z., Rowland, J., & Kell, D. B. (1996). Rapid and non-invasive quantification of metabolic substrates in biological cell suspensions using non-linear dielectric spectroscopy with multivariate calibration and artificial neural networks. Principles and applications. *Bioelectrochemistry and Bioenergetics*, 40(2), 99-132.

Wouters, P. C., & Smelt, J. P. (1997). Inactivation of microorganisms with pulsed electric fields: potential for food preservation. *Food Biotechnology*, 11(3), 193-229.

Yang, R. J., Li, S. Q., & Zhang, Q. H. (2004). Effects of pulsed electric fields on the activity of enzymes in aqueous solution. *Journal of Food Science*, 69(4), 241-248.

Yousefi, A., Niakousari, M., & Moradi, M. (2013). Microwave assisted hot air drying of papaya (Carica papaya L.) pretreated in osmotic solution. *African Journal of Agricultural Research*, 8(25), 3229-3235.

Zeeb, B., Saberi, A. H., Weiss, J., & McClements, D. J. (2015). Formation and characterization of filled hydrogel beads based on calcium alginate: factors influencing nanoemulsion retention and release. *Food Hydrocolloids*, 50, 27-36.

Zeuthen, T. (2010). Water-transporting proteins. *Journal of Membrane Biology*, 234(2), 57–73.

Zhang, L. & Barbut, S. (2005a). Rheological characteristics of fresh and frozen PSE, normal and DFD chicken breast meat. British *Poultry Science*, 46, 687-693.

Zhang, L., & Barbut, S. (2005b). Effects of regular and modified starches on cooked pale, soft, and exudative; normal; and dry, firm, and dark breast meat batters. *Poultry Science*, *84*(5), 789-796.

Zhang, Q., Chang, F. J., Barbosa-Cánovas, G. V., & Swanson, B. G. (1994). Inactivation of microorganisms in a semisolid model food using high voltage pulsed electric fields. *LWT-Food Science and Technology*, 27(6), 538-543.

Zhang, Z., Zhang, R., & McClements, D. J. (2017). Lactase (β-galactosidase) encapsulation in hydrogel beads with controlled internal pH microenvironments: Impact of bead characteristics on enzyme activity. *Food Hydrocolloids*, 67, 85-93.

Zhang, Z., Zhang, R., Zou, L., & McClements, D. J. (2016). Protein encapsulation in alginate hydrogel beads: Effect of pH on microgel stability, protein retention and protein release. *Food Hydrocolloid*s, 58, 308-315.

Zhao, J. H., Hu, R., Xiao, H. W., Yang, Y., Liu, F., Gan, Z. L., & Ni, Y. Y. (2014). Osmotic dehydration pretreatment for improving the quality attributes of frozen mango: effects of different osmotic solutes and concentrations on the samples. International *Journal of Food Science & Technology*, 49(4), 960-968.

Zimmermann, U. (1986). Electrical breakdown, electropermeabilization and electrofusion. In *Reviews of Physiology, Biochemistry and Pharmacology* (pp. 175-256). Springer Berlin Heidelberg, New York, E.E.U.U.

Zimmermann, U., Pilwat, G., Beckers, F., & Riemann, F. (1976). Effects of external electrical fields on cell membranes. *Bioelectrochemistry and Bioenergetics*, 3(1), 58-83.

8. Anexos

8.1. Capítulo de Libro

Juice Processing: Quality, Safety and Value-added Opportunities. (2014). *Capítulo 10: Thermal emerging technologies in fruit juice processing.* Eds: Albert Ibarz, Victor Falguera. CRC Press. ISBN 13: 97814665773 - 11.

10 Emerging Technologies in Fruit Juice Processing

María Victoria Traffano-Schiffo, Nuria Balaguer, Marta Castro-Giráldez, and Pedro J. Fito-Suñer

CONTENTS

10.1 INTRODUCTION

Currently, one of the most important aspects concerning the juice industry is the preservation and improvement of the main organoleptic characteristics of its products, in order to cater to the most exigent consumer demands. As a result, optimizing heat treatments during the processing stages is essential for maintaining an equilibrium between food security and retaining the original nutritional quality of the raw material.

The traditional techniques used to apply heat are based on conduction and convection mechanisms. These mechanisms need hot fluids to transmit the energy by gradients of temperature. The main hot fluids are steam (vapor at high pressure), vapor, hot water, and hot air. These fluids are heated by the combustion of fuels or by electricity. Nevertheless, the use of these techniques has been commonly associated with considerable losses of heat on the surfaces of the equipment and installations, the reduction of heat transfer efficiency, and thermal damage by overheating, due to the time required to conduct sufficient heat into the thermal center of foods (Pereira and Vicente, 2010).

In order to address these problems, other techniques have been developed that do not depend on temperature gradients. Radiation technologies in food processing have gained industrial interest and have the potential to replace, at least partially, the traditional, well-established preservation processes (Vicente and Castro, 2007).

The benefits of the emerging heating techniques are mainly a result of internal heat generation. Electric energy exhibits unique properties, such as fast and differential heating, which can be an advantage, and improves the process efficiency and product quality (Ponne and Bartels, 1995). Among these new thermal techniques are ohmic (electric current) and dielectric heating (photon flux).

The aim of this chapter is to provide a general overview of the theoretical basis of new and emerging thermal technologies, emphasizing their potential applications in the juice industry.

8.2. Presentaciones orales en Congresos Internacionales

DEVELOPMENT OF A NON-DESTRUCTIVE DETECTION SYSTEM OF DEEP PECTORAL MYOPATHY (DPM) IN POULTRY BY DIELECTRIC SPECTROSCOPY

María Victoria Traffano-Schiffo[1]; Tony S. Chuquizuta-Trigoso[1]; Marta Castro-Giraldez[1]; Jose M. Monzo[2]; Vicente Herrero[2]; Ricardo J. Colom[2]; Pedro J. Fito[1] (pedfisu@tal.upv.es)

[1]*Instituto de Ingeniería de Alimentos para el Desarrollo, Universitat Politècnica de València, Valencia, España.*
[2]*Instituto de Instrumentación para Imagen Molecular, Universitat Politècnica de València, Valencia, España.*

Keywords. Deep Pectoral Myopathy, chicken meat, DPM categorization, dielectric spectroscopy, radiofrequency.

Introduction. In recent decades, the strong genetic selection has caused positive effects in terms of reproductive parameters and the yields achieved in poultry industries. However, this production intensification has led to an increase in the incidence of internal malformations in chicken and turkey broilers, especially the pectoral muscles, as Deep Pectoral Myopathy (DPM)[1]. DPM disease is characterized by muscle atrophy and necrosis of the deep pectoral that cause hemorrhagic or green colour and rigid texture that make it unsuitable for consumption[2]. Currently, there is no method to detect the DPM, being the visual appearance, the only parameter used. In this context, the use of dielectric spectroscopy in radiofrequency range, complemented by a chemical, biochemical and microstructural study may become feasible for DPM detection, even in whole carcasses with skin. The aim of this research was to develop a scientific methodology to categorise the damage level in chicken breast meat and to determine the feasibility of dielectric spectroscopy technique for identifying the affected breasts with DPM.

Materials and Methods. The experiments were performed using non-damaged and affected (DPM) chicken breasts with 5 hours of post-mortem. Water content, pH, CIE L*a*b* coordinates, differential scanning calorimetry (DSC) and ion content were measured. The microstructure was study by CryoSEM and dielectric properties were measured in radiofrequency range (40 Hz to 1 MHz) by using a flat plate sensor (IuIAD & I3M-UPV) connected to an *Agilent* 4294A impedance analyser.

Results. The DSC and structural analysis shows that after a muscle infarct episode, a high level of collagen degradation (endomysium) is produced, inducing the accumulation of electrolytes in the affected area and generating repulsions between the adjacent collagen covers and a high denaturation level of structural proteins. Based on significant ($p<0.05$) variables such as pH, L* and a* coordinates, DPM damages can be classified into three different categories; 0. Non-damage tissue, 1. Hemorrhagic with haematomas and blood clots and 2. Necrosed tissue.
Regarding to the dielectric properties, the relaxation frequency and the relaxation dielectric constant at α dispersion shows statistically significant differences between the non-damaged tissue and the rest of the samples ($p<0.05$).

Conclusions. A microscopic analysis of the non-damaged tissue and the tissues affected by the DPM were done and it was possible to relate it with the protein degradation. An objective and scientific methodology to categorize the level of the DPM in poultry it has

been developed. It have been demonstrated the feasibility of dielectric spectroscopy as a tool able to detect the breasts affected by DPM in the whole chicken carcasses by the relaxation parameters in α-dispersion range.

References.

1. Kijowski, J., Kupińska, E., J. Stangierski, J., Tomaszewska-Gras, J. & Szablewski, T. (2014). Paradigm of deep pectoral myopathy in broiler chickens. *World's Poultry Science Journal*, 70, 125-138.

2. Petracci, M. & Cavani, C. (2012). Muscle growth and poultry meat quality issues. *Nutrients*, 4, 1-12.

CIBIA9 Congreso Iberoamericano de Ingeniería de Alimentos (2014) Valencia, España. ISBN: 978-84-9048-168-4.

ESTUDIO DE LA VIABILIDAD DE LA TERMOGRAFÍA INFRARROJA COMO HERRAMIENTA DE MONITORIZACIÓN DE LA EVOLUCIÓN DEL SECADO DE CARNE DE CERDO

Traffano-Schiffo, M.V., Castro-Giráldez, M.*; Fito, P.J.

Instituto Universitario de Ingeniería de Alimentos para el Desarrollo, Universidad Politécnica de Valencia, Camino de Vera s/n, 46022 Valencia, España.

*Email: marcasgi@upv.es

RESUMEN

La operación de secado es considerada una de las mejores operaciones unitarias para preservar los productos en el tiempo, aumentando no sólo el período de vida útil sino además el valor del mismo, como es el caso del jamón serrano. Esta operación implica diferentes mecanismos acoplados entre sí, por lo tanto, es necesario analizar y cuantificar cada uno de ellos con el fin de lograr un producto de alta calidad.

En el presente trabajo, se ha utilizado la termografía infrarroja como una técnica capaz de describir el movimiento del agua en el interior de la muestra de carne.

Durante el proceso de secado, se ha registrado de forma continua la masa de la muestra, además de ser monitorizada constantemente mediante una cámara termográfica Optris PI® 160 (Optris GmbH, Berlín, Alemania), en un rango del espectro electromagnético de longitud de onda de 7,5 a 13 µm. La evolución de la emisividad de la carne se obtuvo mediante el uso de un material de referencia (ε = 0,95 - Optris GmbH, Berlín, Alemania) colocada a un lado de la muestra estudiada y registrada también de forma continua.

Se ha demostrado que la temperatura superficial de la muestra disminuye hasta alcanzar temperatura húmeda (24,5 ºC), para luego aumentar hasta alcanzar la temperatura del aire de secado. A excepción de la teoría tradicional del secado, se ha demostrado que existen más etapas involucradas en el proceso. Los resultados con la cámara de infrarrojos han permitido obtener la evolución de la emisividad y su relación con las etapas propuestas para el período de velocidad de secado decreciente. Por lo tanto, es posible mediante esta técnica, identificar los puntos críticos además de la temperatura superficial de la muestra

durante todo el tratamiento, destacando las altas aptitudes de la termografía infrarroja para controlar el proceso de secado.

Palabras claves: Infrarrojos, emisividad, secado, carne.

IX International Workshop on Sensors and Molecular Recognition (2015). Valencia. España. ISBN : 978-84-608-2360-5.

Study of the viability of the microwave dielectric spectroscopy to monitoring meat drying process

M. V. Traffano-Schiffo, M. Castro-Giráldez and P. J. Fito*

Instituto Universitario de Ingeniería de Alimentos para el Desarrollo, Universidad Politécnica de Valencia, Camino de Vera s/n, 46022 Valencia, España. pedfisu@tal.upv.es

Keywords: dielectric properties, microwave, drying meat.

Meat sector is one of the most important in European Union, being ham one of the highest added-value products. It is important to highlight that drying operation is considered the most expensive stage because of the time, control required and the energy consumption.[1]

Currently, food industry is developing modern physical sensors, based in dielectric spectroscopy, in order to improve the quality of its products.[2] In this context, sensors in the microwave range of the electromagnetic spectra play an important role for monitoring meat drying process.

Drying process was performed in two different hot air dryers. One of them, was used to register the mass variation and the second one, to model the desorption isotherm placing in a tray 15 samples in order to measure at different drying times (8, 16, 29, 48 and 115).

Dielectric properties measurements have been performed on raw and dried Longissimus dorsi pork samples by using an *Agilent* 85070E open-ended coaxial probe connected to an *Agilent* E8362B Vector Network Analyser in the frequency range from 500 MHz to 20 GHz. Also, physicochemical determinations were done: mass, volume and water activity.

With this technique it was possible to demonstrate that the dielectric spectroscopy in microwave range is a useful tool able to monitoring meat drying process.

Acknowledgements

The authors acknowledge the financial support from the Spanish Ministerio de Ciencia e Innovación throughout the project AGL2011-30096 and also for the FPI from Universidad Politécnica de Valencia to support Maria Victoria Traffano Schiffo´ s PhD studies. The author Marta Castro-Giráldez wants to thanks to the UPV Postdoctoral Program (PAID-10-14) from Universidad Politécnica de Valencia for their support.

References

1 Traffano-Schiffo, M. V., Castro-Giráldez, M., Fito, P. J., & Balaguer, N. (2014). Thermodynamic model of meat drying by infrarred thermography. *Journal of Food Engineering*, 128, 103-110.

2 Castro-Giráldez, M., Fito, P. J., & Fito, P. (2011). Application of microwaves dielectric spectroscopy for controlling long time osmotic dehydration of parenchymatic apple tissue. Journal of food engineering, 104(2), 227-233.

8.3. Otras publicaciones

Revista Alimentaria (2013). 442, 47-51. España. ISSN: 0300-5755.

La utilización de sensores basados en la espectroscopia dieléctrica como una buena herramienta para asegurar la calidad y la seguridad alimentaria

N. Balaguer, J. Velázquez-Varela, M. V. Traffano-Schiffo, M. Castro-Giráldez, P.J. Fito*

Instituto Universitario de Ingeniería de Alimentos para el Desarrollo
Universidad Politecnica de Valencia
Camino de vera s/n
46022 Valencia, Spain
*pedfidu@tal.upv.es

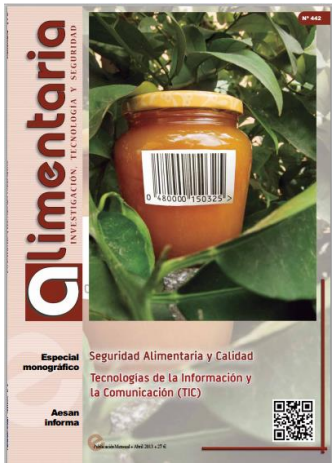

En los últimos años, la industria agroalimentaria ha alcanzado un elevado grado de desarrollo tecnológico adaptándose a los continuos cambios de la sociedad, a las preferencias de los consumidores, a la gran competitividad del mercado y a la globalización de los mismos. De esta forma la innovación tecnológica juega un rol primordial, teniendo como ejes fundamentales: la seguridad y la calidad de los alimentos mediante el control de las materias primas y los procesos. Ante esta situación, surge la necesidad de desarrollar métodos de análisis y control que aseguren la seguridad y la calidad de manera rápida, sencilla y fiable.

A lo largo del tiempo se han utilizado numerosas técnicas destinadas al análisis y control de procesos en la industria agroalimentaria. Tradicionalmente, dichas técnicas se basan en metodologías analíticas complejas y destructivas que obligan a la realización de protocolos tediosos y a la utilización de la estadística para predecir los riesgos del producto en transformación. Dichos métodos, aunque son considerados precisos, requieren de la destrucción de las muestras, una elevada especialización de los operarios y, frente a una alarma en la seguridad alimentaria, presentan tiempos largos de reacción y elevados costes.

A raíz de la creciente demanda de las industrias por obtener un producto de forma rápida, efectiva y acorde con los estándares de seguridad y calidad, ha sido necesario el desarrollo de nuevas tecnologías que permitan optimizar los procesos con el fin de reducir los tiempos de producción y costes operativos. En este contexto, las investigaciones se han centrado en el desarrollo de sensores basados en la interacción de los materiales con la radiación electromagnética. Se trata de sensores capaces de trabajar en las diferentes regiones que componen el espectro magnético: visible, ultravioleta, infrarrojos, microondas, radiofrecuencia y rayos X.

Actualmente, una de las tecnologías en auge para el desarrollo de dichos sensores es la espectroscopia dieléctrica. De hecho, ésta ocupa un lugar importante entre los métodos utilizados para el análisis físico químico tanto de materiales como de tejidos en diversos campos de investigación: medicina (1-4), industria farmacéutica (5), tecnología de alimentos (6), ciencia de los materiales (7-9), (10). Esta técnica determina las propiedades dieléctricas de los alimentos en función de la frecuencia. Las propiedades dieléctricas pueden ser definidas en términos de su permitividad relativa (6). La permitividad relativa (ε_r) es una variable compleja que describe el comportamiento de un sistema frente a la influencia de un campo eléctrico (11-12).Viene definida por la siguiente ecuación:

$$\varepsilon_r = \varepsilon' - j\varepsilon'' \qquad \text{(Ecuación 1)}$$

Publicación en el Congreso Iberoamericano de Ingeniería de Alimentos CIBIA9 (2014).
ISBN: 978-84-9048-168-4

ESTUDIO DE LA VIABILIDAD DE LA TERMOGRAFÍA INFRARROJA COMO HERRAMIENTA DE MONITORIZACIÓN DE LA EVOLUCIÓN DEL SECADO DE CARNE DE CERDO

Traffano-Schiffo, M.V., Castro-Giráldez, M.*; Fito, P.J.

Instituto Universitario de Ingeniería de Alimentos para el Desarrollo, Universidad Politécnica de Valencia, Camino de Vera s/n, 46022 Valencia, España.

*Email: marcasgi@upv.es

RESUMEN

La operación de secado es considerada una de las mejores operaciones unitarias para preservar los productos en el tiempo, aumentando no sólo el período de vida útil sino además el valor del mismo, como es el caso del jamón serrano. Esta operación implica diferentes mecanismos acoplados entre sí, por lo tanto, es necesario analizar y cuantificar cada uno de ellos con el fin de lograr un producto de alta calidad.

En el presente trabajo, se ha utilizado la termografía infrarroja como una técnica capaz de describir el movimiento del agua en el interior de la muestra de carne.

Durante el proceso de secado, se ha registrado de forma continua la masa de la muestra, además de ser monitorizada constantemente mediante una cámara termográfica Optris PI® 160 (Optris GmbH, Berlín, Alemania), en un rango del espectro electromagnético de longitud de onda de 7.5 a 13 µm. La evolución de la emisividad de la carne se obtuvo mediante el uso de un material de referencia ($\varepsilon = 0.95$ - Optris GmbH, Berlín, Alemania) colocada a un lado de la muestra estudiada y registrada también de forma continua.

Se ha demostrado que la temperatura superficial de la muestra disminuye hasta alcanzar temperatura húmeda (24.5º C), para luego aumentar hasta alcanzar la temperatura del aire de secado. A excepción de la teoría tradicional del secado, se ha demostrado que existen más etapas involucradas en el proceso. Los resultados con la cámara de infrarrojos han permitido obtener la evolución de la emisividad y su relación con las etapas propuestas para el período de velocidad de secado decreciente. Por lo tanto, es posible mediante esta técnica, identificar los puntos críticos además de la temperatura superficial de la muestra durante todo el tratamiento, destacando las altas aptitudes de la termografía infrarroja para controlar el proceso de secado.

Palabras claves: Infrarrojos, emisividad, secado, carne.

Introducción

A causa de la fuerte crisis que actualmente atraviesa Europa, la mayoría de las industrias agroalimentarias se han visto afectadas en gran medida. Sin embargo, la industria cárnica Española, ha sufrido un crecimiento en la producción, el consumo y las exportaciones a lo largo de los últimos años. A pesar de este crecimiento, las empresas se han visto obligadas a adaptarse a los continuos cambios que están viviendo en lo que respecta a las demandas y las preferencias de los consumidores, además de adaptarse a las exigencias de exportación (Cruz, 2009).

A causa de lo mencionado anteriormente, las empresas se ven forzadas a optimizar cada una de las etapas de sus procesos productivos. En el caso del jamón serrano, la etapa de secado es considerada como una de las más costosas, tanto desde el punto de vista de costes operativos como de monitorización del proceso, es por ello, que este estudio se centra principalmente en la obtención de sensores en línea, de respuesta rápida y exacta sobre la composición del alimento.

El proceso de secado es promovido por el movimiento del agua, en el cual las transferencias de calor y de masa ocurren de forma simultánea. Es por ello, que es importante desarrollar un modelo que permita optimizar el proceso industrial y así obtener un método de control no destructivo, en línea y rápido.

La Termografía Infrarroja (TI) es una herramienta muy interesante para poder abordar este estudio, la cual proporciona información importante sobre los tejidos biológicos (Workmaster *et al.*, 1999). Esta nueva tecnología, brinda la posibilidad de determinar la cinética de secado de la carne a través de las medidas de la distribución de temperatura en la superficie de las muestras. TI se basa en la medida de la radiación infrarroja que es emitida por la superficie de un cuerpo y así obtener una imagen de su distribución térmica. Esta técnica sin contacto y rápida, permite además obtener un mapa de temperaturas de todo el objeto, diferencia importante con respecto a otros tipos de sensores que brindan información sólo de un punto. Algunas aplicaciones desarrolladas con esta tecnología se realizaron en frutas (Fito *et al.*, 2004; Cuccurullo *et al.*, 2012, Veraverbeke & Verboven, 2005), carne (Gariepy *et al.*, 1989) y calidad y seguridad alimentaria (Gowen *et al.*, 2010), entre otros.

Materiales y Métodos

2.1. Preparación y caracterización de las muestras

El experimental ha sido realizado utilizando muestras frescas de carne de cerdo correspondientes al músculo *Longissimus dorsi* con 1.5 días de post-mortem. Se procedió a la preparación de las muestras (cilindros de 3 cm de diámetro y 1 cm de espesor). Éstos fueron cortados en dirección a las fibras musculares con el fin de asegurar que la difusión de las moléculas de agua se realice en dirección perpendicular con respecto a las mismas.

La masa de las muestras fue determinada utilizando una balanza Mettler Toledo AB304-S con una precisión de ±0,001. Para las medidas de actividad de agua superficial se utilizó un higrómetro de punto de rocío Decagon (Aqualab®, series 3 TE) con una precisión de ± 0.003.

Los análisis de humedad se realizaron siguiendo la norma ISO 1442 (1997) específica para productos cárnicos, en la cual las muestras se deben secar a 110ºC a presión atmosférica durante 48 horas o hasta lograr un peso constante. En el caso de la determinación del volumen, se siguió el método de análisis de imagen utilizando el programa Adobe© Photoshop© CS6 con el objetivo de obtener tanto el diámetro, como el espesor de las muestras. Cabe destacar que la caracterización de las muestras se realizó tanto antes como después del proceso de secado.

2.2. Secado de las muestras

La muestra en estudio fue colocada en el interior de un secadero convectivo, y se le ha registrado la masa de forma continua a lo largo de todo el proceso. Con el fin de determinar la temperatura superficial a lo largo del proceso, se colocó, adyacente a la muestra de estudio, una muestra de referencia con una termocupla situada a una profundidad de 1mm de la superficie. Al otro lado de la muestra se colocó un material de referencia con una emisividad conocida ($\varepsilon = 0.95$ - Optris GmbH, Berlin, Alemania).

Una cámara de infrarrojos Optris PI® 160 (Optris GmbH, Berlín, Alemania) fue instalada frente a la muestra de carne a una distancia inferior a 20 cm., con el objetivo de monitorizar y grabar el proceso de secado. Las temperaturas del material de referencia, de los ambientes, tanto interior como exterior al secadero fueron también registradas por termocuplas tipo K conectadas a un multiplexor Agilent 34901A (Agilent Technologies, Malaysia) y registrado por un sistema de adquisición de datos Agilent 34972A (Agilent Technologies, Malaysia). Dicho Sistema facilitará posteriormente el tratamiento de los datos proporcionados por la cámara de infrarrojos.

La velocidad del aire fue regulada, medida y monitorizada mediante un anemómetro digital de hilo caliente TESTO 425 (precisión ± 0.03 m/s). Considerando estudios previos, la temperatura en el interior del secadero y la velocidad del aire fueron determinadas a 40ºC y 1.5 m/s.

2.3. Medidas de Infrarrojos

Las imágenes en el rango del espectro electromagnético de los infrarrojos fueron obtenidas utilizando una cámara de infrarrojos Optris PI® 160 (Optris GmbH, Berlin, Germany), la cual utiliza un plano focal bidimensional con 160x120 píxeles, en un rango espectral de 7.5 a 13 μm, con una resolución de 0.05 ° C y una precisión de ± 2%. La cámara es capaz de cubrir un rango de temperatura de -20 a 100 º C y posee un campo de visión de 23 º x 17 º con una distancia focal mínima de 0.02 m. La cámara viene acompañada de un software Optris PI Connect (Optris GmbH, Berlín, Alemania).

Resultados y Discusión

3.1. Obtención de la emisividad de la muestra

Con el objetivo de determinar la temperatura superficial de la muestra durante el proceso de secado, ha sido necesario calcular el flujo de energía total de la muestra mediante la ecuación de Planck, la cual fue simplificada por Sthephan-Boltzmann:

$$E_T = \varepsilon_{cam}\sigma T_{cam}^4 \quad (1)$$

Dónde: E_T (W/m^2) representa el flujo de energía total del sistema, el cual es obtenido a partir del flujo de fotones emitido por la muestra durante el tratamiento y es recibido por el sensor piroeléctrico (que se encuentra en el interior de la cámara de infrarrojos). El sensor piroeléctrico es un material que manteniendo su temperatura constante, varía su conductividad, y es capaz de convertir dicha variación en energía recibida. ε_{cam} representa la emisividad que recibe la cámara de infrarrojos (adimensional), σ corresponde a la constante de Stefan-Boltzmann ($5.67 \cdot 10^{-8}$ W/m^{2}K) y T la temperatura (de la muestra o los alrededores en K).

Una vez calculado el flujo de energía total, es necesario estimar la emisividad de la muestra a lo largo del tratamiento, para ello se ha planteado un balance de energía, el cual se puede observar en la Ecuación 2:

$$E_T = \varepsilon_{cam}\sigma T_{cam}^4 = F.\varepsilon_m\sigma T_m^4 + (1 - \varepsilon_{alr})\sigma T_{alr}^4 - (1 - \tau_{aire})F.\varepsilon_m\sigma T_m^4 \quad (2)$$

Dónde: F es el factor geométrico, siendo 1 debido a que la cámara se encuentra en una posición perpendicular con respecto a la muestra, τ corresponde a la transmitividad del aire y los subíndices *m, alr y aire* corresponden a la muestra, alrededores y aire, respectivamente. El primer término representa el flujo de energía que es emitido por la muestra; el segundo, el flujo de energía que es emitido por los alrededores y por último, el tercero, la cantidad de energía que es absorbida por el aire. Cabe destacar que el tercer término es despreciable, ya que como se ha mencionado en el apartado 2.2. la muestra y la cámara se encuentran a una distancia menor a 20 cm.

Como se ha mencionado anteriormente, con el fin de determinar la emisividad de la muestra a lo largo del tratamiento, en primer lugar ha sido necesario obtener el flujo de energía que es emitido por los alrededores. Esto se ha logrado mediante el material de referencia con emisividad conocida (ε = 0.95 - Optris GmbH, Berlin, Germany) que fue colocado de forma adyacente a la muestra en estudio y utilizando la siguiente ecuación (Ecuación 3):

$$E_T^{ref} = 0.95 \,.\sigma\,.\ \mathrm{T}_{\mathrm{ref}}^4 + \mathrm{E}_{\mathrm{alr}} \qquad (3)$$

Dónde, E_T^{ref} corresponde al flujo de energía total del material de referencia (W/m^2) y $\mathrm{T}_{\mathrm{ref}}^4$ es la temperatura del mismo material (K).

Por lo tanto, una vez obtenidos los parámetros mencionados anteriormente, es posible estimar la evolución de la emisividad en función al flujo de energía.

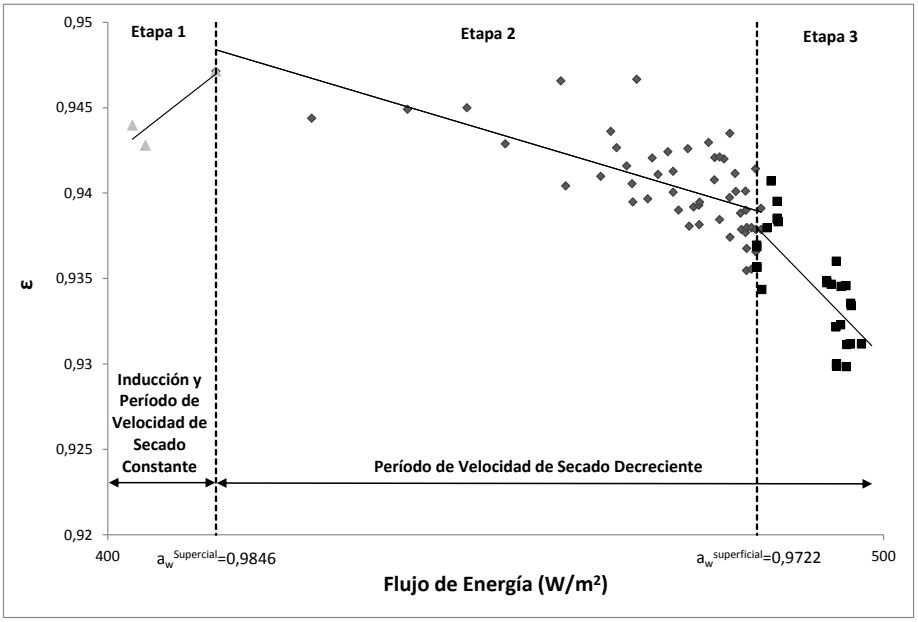

Fig. 2. Evolución de la emisividad de la carne en relación al flujo de energía.

En la Figura 2, es posible observar que existen 3 etapas claramente diferenciadas: la primera a altas humedades y baja temperatura superficial de la muestra, la segunda, en la cual la temperatura aumenta hasta alcanzar la temperatura del aire de secado, y por último, una tercera, en la cual la temperatura se mantiene hasta finalizar el proceso. La teoría tradicional del secado explica el secado en tres etapas: la primera, la cual corresponde al período de inducción, la segunda al período de velocidad de secado constante, mientras que la tercera corresponde al período de velocidad de secado decreciente.

En la Figura 3, se observa el período de inducción y el período de velocidad de secado constante, lo cual corresponde con la etapa 1 propuesta para la Figura 2. A partir de allí, durante el período de velocidad de secado decreciente, se observan dos etapas: una primera etapa, en la cual la temperatura superficial aumenta hasta alcanzar la temperatura del aire de secado, y una segunda etapa en la cual, la temperatura superficial de la muestra se mantiene constante en un valor coincidente con la temperatura del aire de secado.

Cabe destacar que según lo expuesto, la respuesta de la superficie de la muestra a absorber energía radiante (Figura 2) cambia en los mismos puntos críticos que se observan en la Figura 3.

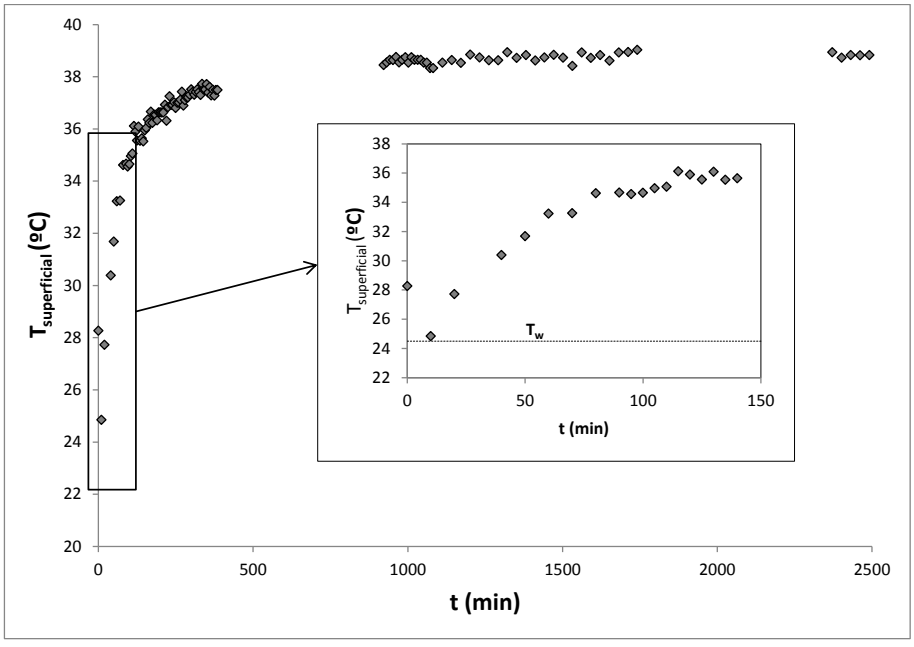

Fig. 3. Temperatura superficial de la muestra a lo largo del proceso de secado.

La Figura 4 muestra la evolución de la actividad de agua superficial con respecto a la temperatura superficial de la muestra. En este caso, tanto la etapa 1 como la etapa 2

corresponden al período de velocidad de secado decreciente. La etapa 1 presenta una gran variación de la temperatura superficial de la muestra y una leve disminución de la actividad de agua superficial, mientras que la etapa 2 presenta una gran variación de la actividad de agua superficial, manteniendo la temperatura de la muestra a la temperatura del aire de secado.

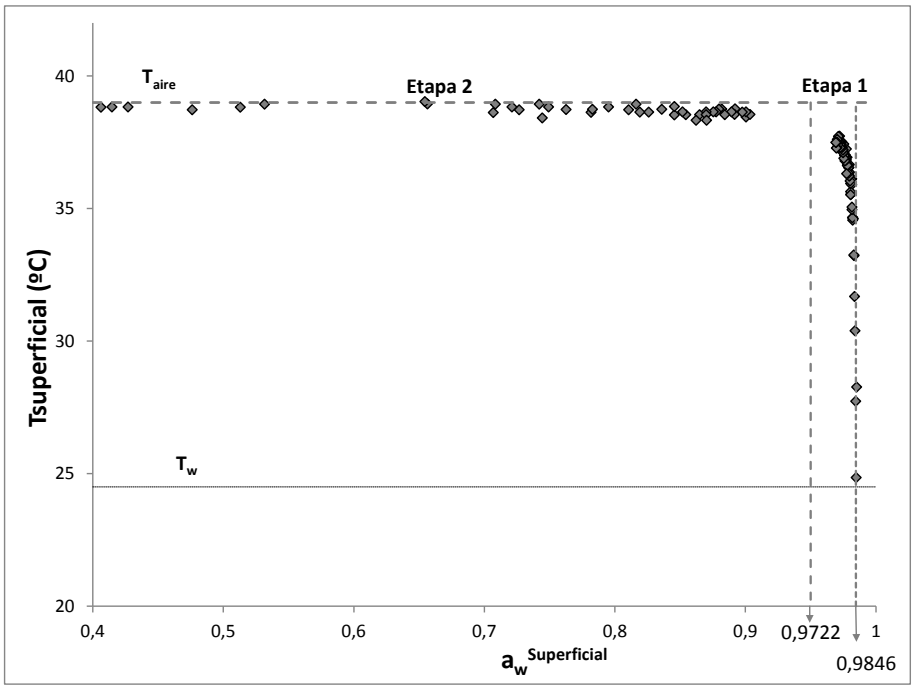

Fig. 4. Actividad de agua superficial de la muestra en relación con su temperatura.

Cabe destacar que a una actividad de agua superficial de 0.9846 se inicia la primera etapa del período de velocidad de secado decreciente, lo cual coincide con el primer cambio en la tendencia de la evolución de la emisividad que se muestra en la Figura 2. La finalización de la primera etapa e inicio de la segunda, se lleva a cabo a una actividad de agua superficial de 0.9722, tal y como se puede observar en la Figura 4, además de en la Figura 2.

Conclusiones

Ha sido posible demostrar que la termografía infrarroja es una buena herramienta para controlar el proceso de secado de carne, ya que provee información sobre la transferencia de calor en tejidos biológicos, haciendo posible obtener la evolución de la emisividad y su clara relación con las etapas propuestas para el período de velocidad de secado decreciente. Por lo tanto, con esta técnica, es posible identificar los puntos críticos y la temperatura superficial de la muestra a lo largo de todo el tratamiento.

Agradecimientos

Los autores agradecen el soporte financiero del Ministerio de Ciencia e Innovación a través del proyecto AGL2011-30096 y además a ERASMUS MUNDUS (Programa Eurotango II) por el financiamiento de los estudios de doctorado de María Victoria Traffano-Schiffo en la Universidad Politécnica de Valencia, España.

La autora Marta Castro-Giráldez agradece al Campus de Excelencia Internacional VLC/CAMPUS por el soporte.

Bibliografía

Cruz, J. (2009). La industria cárnica española sigue creciendo. *Eurocarne,* (175), 1.

Cuccurullo, G., Giordano, L., Albanese, D., Cinquanta, L., Di Matteo M., 2012. Infrared thermography assisted control for apples microwave drying. *Journal of Food Engineering*, 112, 319-325.

Fito, P.J., Ortolá, M. D., De los Reyes, R., Fito, P., De los Reyes, E., 2004. Control of citrus surface drying by image analysis of infrared thermography. *Journal of Food Engineering*, 61, 287-290.

Gariepy, C., Amiot, J., Nadai, S., 1989. Ante-mortem detection of PSE and DFD by infrared thermography of pigs before stunning. *Meat Science*, 25, 37-41.

Gowen, A. A., Tiwari, B. K., Cullen, P. J., McDonnell, K., O´Donnell, C. P., 2010. Applications of thermal imaging in food quality and safety assessment. *Trends in Food Science & Technology*, 21, 190-200.

Veraverbeke, E.A., Verboven, P., Lammertyn, J., Cronje, P., De Baerdemaeker, J., Nicolai, B.M., 2006. Thermographic surface quality evaluation of apple. *Journal of Food Engineering*, 77, 162–168.

Workmaster B. A., Palta, J. P., Wisniewski, M., 1999. Ice nucleation and propagation in cranberry uprights and fruit using infrared video thermography. *Journal of the American Society for Horticultural Science*, USA, 124, 619

Publicación en el VIII International Workshop on Sensors and Molecular Recognition
(2014). Valencia, España. ISBN 978-84-697-1302-0.

Análisis de los espectros dieléctricos como herramienta para el control de la maduración de carne de pollo

Traffano-Schiffo, M.V., Muñoz, M.A., Castro-Giráldez, M. & Fito, P.J.*

Instituto Universitario de Ingeniería de Alimentos para el Desarrollo, Universidad Politécnica de Valencia, Camino de Vera s/n, 46022 Valencia, España. *E-mail: pedfisu@tal.upv.es

RESUMEN

Durante la maduración de la carne, se producen diferentes procesos bioquímicos y fisicoquímicos que determinan la calidad del producto final. Estos procesos, involucran desestructuraciones de las membranas, cambios en el estado de las proteínas, en la movilidad del agua y en la concentración de iones dentro del tejido. El consumidor percibe todos estos cambios a través de las características organolépticas, entre ellas, la terneza, jugosidad, color y el sabor, determinando por lo tanto la aceptabilidad del mismo.
En este contexto, el control de la evolución del proceso de maduración es uno de los elementos claves en la industria de carne que permite obtener un producto de alta calidad. En particular, en la industria de carne de ave, en la que los procesos de maduración se llevan a cabo a una velocidad mucho mayor que en el resto de especies animales, como por ejemplo la carne de cerdo o de ternera; la utilización de sensores no destructivos, de fácil implantación en líneas de producción y de respuesta inmediata, representan una prometedora herramienta para poder hacer frente a este desafío. Entre dichos sensores, destacan los basados en el espectro electromagnético, los cuales permiten detectar los cambios complejos en la estructura muscular mediante las variaciones en las propiedades eléctricas que se producen en el mismo. Es por ello, que un estudio en el rango de las radiofrecuencias (RF) y de las microondas (MW) nos proporciona información valiosa con respecto al estado estructural del sistema, permitiéndonos relacionarla con los cambios post-mortem del tejido muscular.
En el rango de las RF, es posible distinguir dos dispersiones; la dispersión α, la cual representa la orientación de las cargas móviles dentro del sistema biológico en el medio dieléctrico, y la dispersión β la cual está inducida por la orientación de las cargas fijas en la estructura proteica. En el rango de las MW, se encuentra la dispersión γ que está determinada por la orientación de los dipolos de pequeño tamaño molecular (movilidad del agua). Los resultados obtenidos demuestran la viabilidad de la espectroscopia dieléctrica como herramienta para la monitorización de la maduración de la pechuga de pollo (*Pectoralis major*).

Palabras claves: carne de pollo, post-mortem, espectroscopia dieléctrica, microondas, radiofrecuencia, maduración, dispersiones.

INTRODUCCIÓN

Inmediatamente tras el sacrificio del animal, se desarrollan una serie de reacciones químicas y bioquímicas que permiten la transformación del músculo en carne (Ouali *et al*., 2006). Estos cambios afectan de forma positiva al sistema, siendo los responsables de la terneza, jugosidad, aroma y sabor del producto.
Particularmente, la terneza es el resultado de la acción de enzimas proteolíticas endógenas, las catepsinas y calpaínas, las cuales afectan a las proteínas miofibrilares aumentando la terneza de la carne (Castro-Giráldez et al., 2011 & Chéret *et al*., 2007). Sin embargo, algunos autores consideran a un tercer sistema enzimático como responsable de la textura, los proteasomas (Herrera-Mendez *et al*., 2006, Dransfield & Sosnicki, 1999).

Los polipéptidos de tamaño intermedio, que se generan a causa de la acción de las enzimas endógenas, son el sustrato de las enzimas di y tri-peptidil peptidasas, las cuales generan péptidos de pequeño tamaño y aminoácidos libres, que influyen en el sabor y el aroma (Toldrá & Flores, 1998).
Por lo tanto, un estudio del proceso de maduración, especialmente en carne de pollo, en donde los procesos degradativos se producen a una gran velocidad, es de vital importancia. Este estudio nos permitirá determinar el tiempo óptimo de almacenamiento en refrigeración y por lo tanto mejorar los atributos sensoriales y de calidad.
Cabe destacar que el músculo esquelético presenta características eléctricas que cambian con el tiempo post-mortem (Byrne et al., 2000) y, es por ello, que un estudio de las propiedades dieléctricas de la carne en el rango de la radiofrecuencia y las microondas es considerada como una herramienta útil y no destructiva para analizar la evolución de la maduración de la carne de pollo.

MATERIALES Y MÉTODOS

Materia Prima: Los experimentos fueron realizados utilizando pechugas de pollo (*Pectoralis major*) con 4 horas de post-mortem. Los animales fueron proporcionados por el matadero del grupo Sada perteneciente a Nutreco España, S.A., y se mantuvieron a 4 º C hasta su análisis. En la Figura 1 se puede observar el diagrama de flujo del experimental realizado.
Caracterización de la calidad de la carne: Las muestras fueron clasificadas como RFN (Rojas, Firmes y No Exudativas) según la clasificación de Zhang y Barbut (2005).
Análisis Estadísticos: El análisis estadístico de los datos fue llevado a cabo mediante el programa Statgraphics Centurion XVI (Statgraphics, Virgina, U.S.A.). Se realizó una regresión no lineal utilizando la ecuación de Gompertz.

Espectroscopia dieléctrica

Radiofrecuencia: El sistema utilizado para la medición de las propiedades dieléctricas en el rango de la radiofrecuencia (40 Hz a 1 MHz) consiste en un sensor fabricado en colaboración por el Instituto de Ingeniería de Alimentos para el Desarrollo (IuIAD-UPV) y el Instituto de Instrumentación para Imagen Molecular (i3M, UPV), conectado a un analizador de impedancias Agilent 16451B.
Microondas: Para el rango de frecuencias de las microondas (500 MHz a 20 GHz), el sistema utilizado consiste en una sonda coaxial Agilent 85070E conectada a un analizador de redes Agilent E8362B.

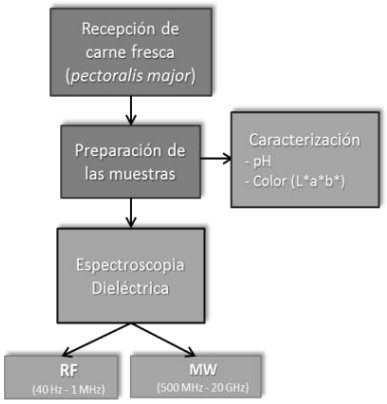

Figura 1. Diagrama de flujo del trabajo de investigación.

RESULTADOS

El presente trabajo se encuentra enmarcado en un macro proyecto en el cual se han analizado cambios bioquímicos y estructurales de la carne durante el tiempo post-mortem, además de los cambios eléctricos mencionados. Dichos análisis comprenden estudios de la microestructura de la carne (análisis de microscopía electrónica de barrido a bajas temperaturas), degradación proteica (Calorimetría Diferencial de Barrido), así como análisis de iones libres (cromatografía de intercambio iónico). Todos estos análisis han servido para la interpretación de los resultados de espectroscopia dieléctrica.

En los tejidos biológicos, se pueden distinguir tres dispersiones características en función de la frecuencia: la dispersión-α, que ocurre desde los Hz hasta los kHz, la cual representa la orientación de las cargas móviles dentro del sistema biológico; un pequeño cambio en el movimiento de iones producirá un aumento de esta dispersión dieléctrica (Kuang & Nelson, 1997). La dispersión-β, desde kHz hasta MHz, la cual está inducida por la orientación de las cargas fijas en la estructura proteica. Por último, la dispersión-γ, la cual es causada principalmente por la orientación y la inducción de las moléculas dipolares, fundamentalmente el agua.

Debemos tener en cuenta que a lo largo del proceso de maduración y a medida que avanza el tiempo post-mortem, se genera un aumento en la señal eléctrica en la dispersión-α que puede ser debida a un aumento en la fuerza iónica causado por los procesos de maduración que generan una bajada del pH de la carne. Sin embargo, en la dispersión-β, la constante dieléctrica disminuye a causa de la desestructuración proteica.

Los cambios que en las propiedades dieléctricas que se llevan a cabo a lo largo del proceso de maduración, pueden ser analizados más fácilmente utilizando frecuencias puntuales. Es por ello que en la figura 2 se ha representado la evolución de la constante dieléctrica a 500 Hz (dispersión-α) y a 1 MHz (dispersión-β) durante el proceso de maduración. Se puede observar que la constante dieléctrica a 500 Hz aumenta significativamente a lo largo del proceso de maduración. Tal y como se ha explicado anteriormente, esto puede ser debido a que durante este proceso se producen procesos fermentativos que provocan una bajada acentuada del pH. Por el contrario, durante la maduración se produce una bajada de la constante dieléctrica a 1 MHz, causada por la degradación de las proteínas estructurales.

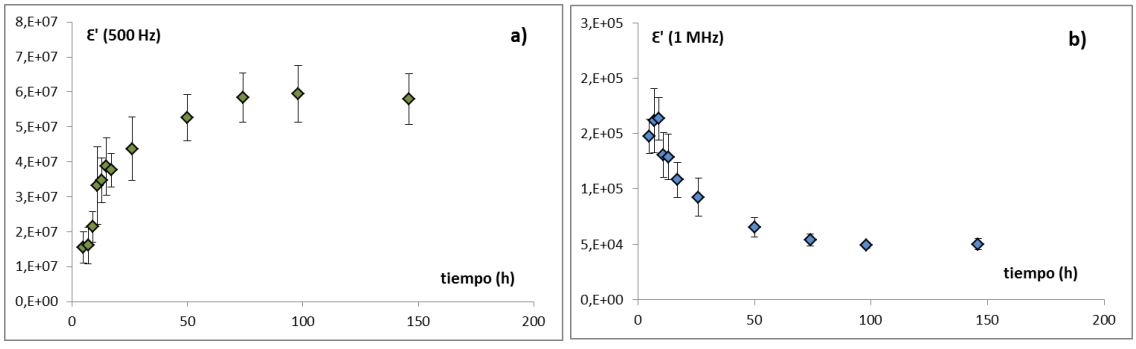

Figura 2. Evolución de la constante dieléctrica. a) a 500 Hz (dispersión-α); b) a 1 MHz (dispersión-β).

Se ha propuesto un modelo matemático basado en tres ecuaciones de Gompertz, simulando el modelo de Debye. Esta ecuación brinda información sobre las dispersiones que se producen en el rango de la radiofrecuencia y de las microondas (frecuencias y constante dieléctrica de la relajación). La siguiente ecuación muestra el acoplamiento de tres ecuaciones de Gompertz con el objetivo de ajustar las tres dispersiones (Ec. 1):

$$l\varepsilon'(\omega) = l\varepsilon'_{\infty} + \sum_{n=1}^{3} \frac{\Delta l\,\varepsilon'_n}{1 + e^{((l\omega^2 - l\omega_n^2)*\alpha_n)}}$$

(1)

Dónde: lε' representa el logaritmo decimal de la constante dieléctrica, **lω** representa el logaritmo decimal de la velocidad angular (obtenido a partir de la frecuencia) y **α** corresponde a las tres pendientes de las dispersiones. Los subíndices ∞ y $\boldsymbol{n}$ representan: el valor mínimo de la constante dieléctrica y la relajación específica (α, β o γ), respectivamente (véase la Figura 3).

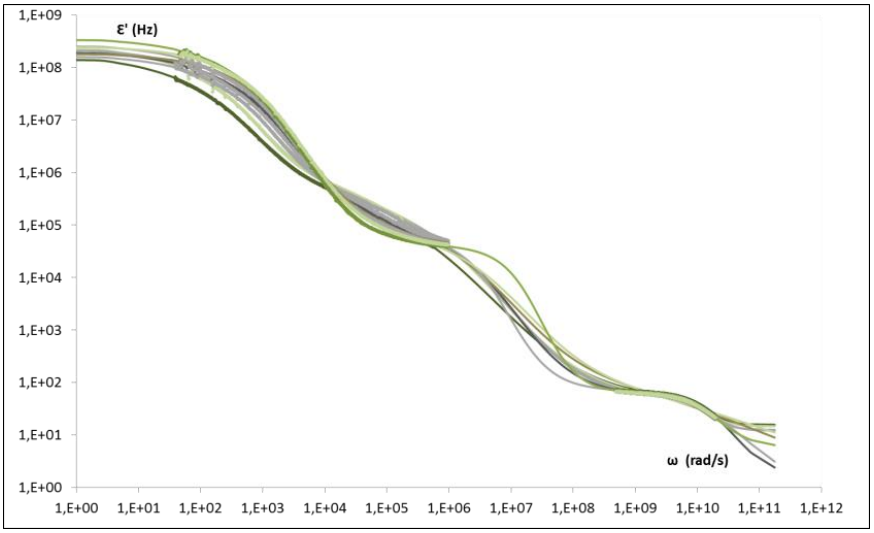

Figura 3. Modelo de Gompertz correspondiente a distintos tiempos post-mortem.

En la figura 3 se muestran los datos experimentales (puntos) junto con el modelo obtenido a través del algoritmo (líneas). Se puede observar que el modelo utilizado se ajusta adecuadamente a los datos experimentales.

CONCLUSIONES

La constante dieléctrica permite determinar el grado de desestructuración y por lo tanto predecir el tiempo de post-mortem de la carne.
Los resultados demuestran que la espectroscopia dieléctrica es una herramienta útil, no invasiva y en línea, que permite controlar el proceso de maduración de la carne de pollo.

Agradecimientos

Los autores quieren agradecer al Ministerio Español de Ciencia e Innovación su apoyo económico mediante el proyecto AGL2011-30096. La autora María Victoria Traffano Schiffo quiere agradecer a ERASMUS MUNDUS (Programa Eurotango II) por el apoyo para realizar sus estudios de doctorado en la Universidad Politécnica de Valencia, España.

REFERENCIAS

Castro-Giráldez, M., Toldrá, F., & Fito, P. (2011). Low frequency dielectric measurements to assess post-mortem ageing of pork meat. *LWT-Food Science and Technology*, 44(6), 1465-1472.

Chéret, R., Delbarre-Ladrat, C., Lamballerie-Anton, M. D., & Verrez-Bagnis, V. (2007). Calpain and cathepsin activities in post mortem fish and meat muscles. *Food Chemistry*, 101(4), 1474-1479.

Dransfield, E., & Sosnicki, A. A. (1999). Relationship between muscle growth and poultry meat quality. *Poultry Science*, 78(5), 743-746.

Herrera-Mendez, C. H., Becila, S., Boudjellal, A., & Ouali, A. (2006). Meat ageing: Reconsideration of the current concept. *Trends in food science & technology*, 17(8), 394-405.

Kuang, W., & Nelson, S. O. (1997). Low-frequency dielectric dispersion of biological tissues: a review with some new insights. *Transactions of the ASAE*, 41, 173-184.

Ouali, A., Herrera-Mendez, C. H., Coulis, G., Becila, S., Boudjellal, A., Aubry, L., & Sentandreu, M. A. (2006). Revisiting the conversion of muscle into meat and the underlying mechanisms. *Meat Science*, 74(1), 44-58.

Toldrá, F., & Flores, M. (1998). The role of muscle proteases and lipases in flavor development during the processing of dry-cured ham. *Critical Reviews in Food Science*, 38(4), 331-352.

Zhang, L., & Barbut, S. (2005). Rheological characteristics of fresh and frozen PSE, normal and DFD chicken breast meat. *British poultry science*, 46(6), 687-693.

8.4. Presentaciones de Póster en Congresos Internacionales

InsideFood SYMPOSIUM 9-12 APRIL 2013 Leuven - Belgium

STUDY OF HAM DRYING KINETICS BY INFRARED THERMOGRAPHY

Traffano-Schiffo, M.V., Castro-Giráldez*, M., Fito, P.J.

Institute of Food Engineering for Development.
Universidad Politécnica de Valencia (Spain).
*marcasgi@doctor.upv.es

ABSTRACT

Drying operation in meat products is one of the best unit operations to preserve the product in time. Drying process involves many behaviors coupled together, and it is necessary to analyze and quantify each behavior in order to reach a high quality product.
In this work, infrared thermography has been used in order to obtain the critical points of the meat drying operation and also a thermodynamic model has been developed to describe the operation.
It has been developed a non-continuous model to obtain the evolution of emissivity and the temperature profiles through drying operation. Temperature profiles have been related with the thermodynamic properties associated with the mass and heat fluxes.
It has been demonstrated that the measure of the emissivity is a good tool to determine the critical points during meat drying. A thermodynamic model, correlating mass and heat fluxes with the changes in the structure has been developed. It has been demonstrated the high possibilities of infrared techniques to control the meat drying process.

INTRODUCTION

In the food industry, meat sector is one of the most important, being ham the product with more value added. During manufacturing process, drying is the more expensive stage because of the time and control requested and the energy consumption.
The drying process is promoted by the movement of water. Latter migrates from the interior of the food to the surface where it evaporates and transports thereof towards the environment. During this operation, some changes happen in the structure of the muscle fibers. Heat and mass transfers occur simultaneously.
Infrared Thermography (IRT) is an interesting option which fulfills these requirements and can provide important information about biological tissues. So, Infrared Thermography is a very important and novel tool to carry out this challenge.

MATERIAL & METHODS

Raw Material. Experiments were done using pork meat. The meat used in the experiment was 1,5 days postmortem.
Drying Process. The sample was dried in a convective dryer, next to another meat reference sample. Mass difference of sample was registered continuously. An infrared camera Optris PI® 160 thermal imager (Optris GmbH, Berlin, Germany) recorded the infrared emission from the sample surface during the process. The dryer air velocity was regulated, measured and controlled by a digital hot wire anemometer TESTO 425. The air velocity values were determinate at 40ºC and 1,5 m/s. A reference material of known emissivity (0,95 - Optris GmbH, Berlin, Germany), was placed next to the sample and record with the infrared camera with the aim to correct the emissivity of the sample. The drying air, meat reference sample and reference material temperature were measured with thermocouples connected to an Agilent multiplexer 34901A (Agilent Technologies, Malaysia) and registered by an Agilent Data Acquisition equipment 34972A (Agilent Technologies, Malaysia).
Measurements.
- **Water Activity.** Hygrometer (DECAGON model Aqualab CX-2, ± 0,003).
- **Moisture.** Drying at 110ºC till constant weigth was reached, ISO 1442 (1997).
- **Volume.** Image Analysis.

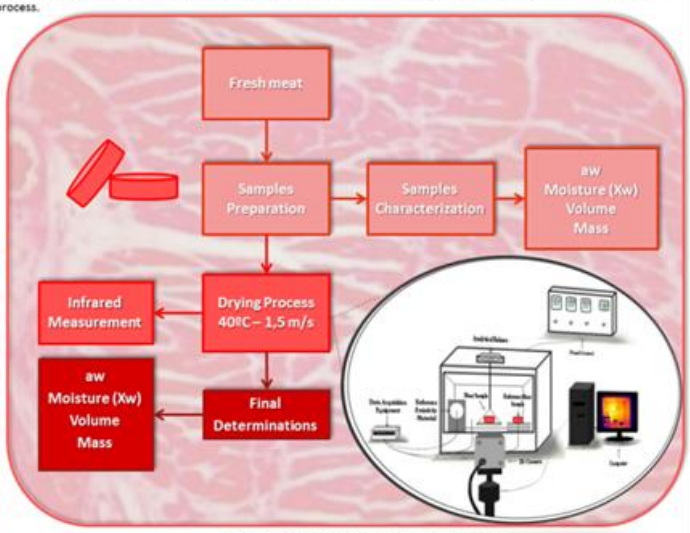

Figure 1. Diagraman of the experimental procedure.

RESULTS

INFRARED TERMOGRAPHY

With the aim of determining the real temperature of the meat surface during drying process, it is necessary to obtain the emissivity of meat, for this purpose it was used the following energy balance equation (Eq. 1).

$$E_T = \varepsilon_{ham}\sigma T_{ham}^4 = F.\varepsilon_{samp}\sigma T_{samp}^4 + (1-\varepsilon_{sur})\sigma T_{sur}^4 - (1-\tau_{air})F.\varepsilon_{samp}\sigma T_{samp}^4 \quad (1)$$

First term represents the energy emitted by the sample (meat), the second one the emitted by the surroundings and the third represents the energy emitted by the sample and absorbed by the air.
To obtain the sample emissivity it was necessary to determine the energy emitted by the surroundings, it was used the equation 2.

$$E_T^{0,95} = 0,95.\sigma.T_{sur}^4 + E_{sur} \quad (2)$$

The evolution of emissivity values with time obtained for the meat sample can be observed in Figure 2.

Fig. 2. Evolution of the meat emissivity during drying process.

The emissivity is a physical property that depends on the chemical variation of the sample surface. In this case, the most important chemical specie that change is the water. Because of that, it is necessary to represent the emissivity values in relation to the water content. Fig. 3 shows the direct relationship that exists between the sample emissivity and its moisture.

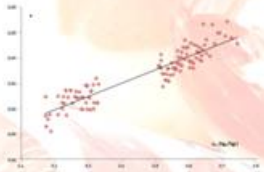

Fig. 3. Evolution of meat emissivity in relation to its moisture content.

KINETICS AND THERMODYNAMICS PROPERTIES

The drying rate was calculated from the moisture sample values obtained previously using the following equation (Eq. 3).

$$Dr = \frac{dx}{dt} \quad (3)$$

In the Figure 4 it can be observed the relationship between the drying rate and the sample moisture.

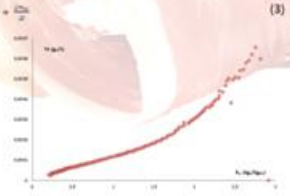

Fig. 4. Drying rate curve with regard to the moisture of the sample.

In figure 5, which represents the sample surface temperature related to its moisture content, can be distinguished the different periods of the drying process. At the beginning of the curve, during the constant velocity period, it can be observed only one point that corresponds with the point in which the sample had its wet surface at 25ºC. After that, as the temperature increases, the falling rate period occurs in two well identifiable different stages.
Stage 1 represents the increase of temperature while the water from the sample is evaporating. At this point, the evaporation energy decreases until the temperature sample surface reaches to the air temperature (approximately equal to 40ºC), while the heating surface energy increases. In the second stage, where the heating surface energy is equal to zero because the temperature is maintained constant, and the energy is needed for increase the inside temperature of the sample while the evaporation energy continues decreasing.

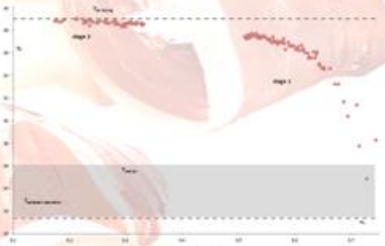

Fig. 5. Sample surface temperature with regard to the moisture of the sample.

CONCLUSIONS

It has been possible to obtain the evolution of the meat emissivity during drying process and it has been demonstrated its clear relationship with its moisture content.

It has been studied the kinetic of the drying process in which it can be distinguished two stages during the falling rate period of the process.

The results showed that the infrared thermography is an important non-contact and non-destructive tool for controlling meat drying process. This technique can be used not only to describe the process, if not also for identifying their critical points, with the aim to obtain a quality product and reduce the operating costs.

Dielectric spectrum analysis in Radiofrequency and Microwave range in chicken meat

Traffano-Schiffo, M.V., Castro-Giráldez, M., Fito, P.J*.

Institute of Food Engineering for Development. Universidad Politécnica de Valencia (Spain).
*pedfito@tal.upv.es

ABSTRACT

Fresh poultry and poultry products industry grows fast in the European market, with different requirements: to increase the production, to reduce the costs, to improve the profits, and to maintain or improve the quality of poultry products. In this sense, it is necessary to apply techniques online, nondestructive, fast and accurate. The dielectric sensors in the range of radiofrequency and microwaves could be an opportunity to the companies in order to improve and grow in the poultry sector.
Nowadays, one of the most important challenges of poultry industry is to determine the meat quality classes (PSE, DFD, RFN) during postmortem period. It should be taken into account that the chicken postmortem period is faster than other species of animals such as pork meat. Dielectric spectroscopy is a suitable and fast tool for the quality determination mentioned above; however, few data in radiofrequency (RF) and microwave (MW) are available in the literature. In the RF range, two different dispersions can be distinguished: α dispersion, which represents the orientation of charges with motion (the chemical species affected are the electrolytes and transport molecules), and β dispersion, which corresponds to the orientation of charges bonded in the solid structure (protein structure). Furthermore, the MW range (γ dispersion) allows describing the mobility of water.
The aim of the present investigation is to analyze the viability of the dielectric properties (in RF and MW range) for determining the quality classes in breast (*Pectoralis major*) chicken.
The results of this work allow us to separate the chicken breasts quality, analyzing the α and β dispersions. It can be concluded that this technique is able to share out chicken breasts as a function of its quality.

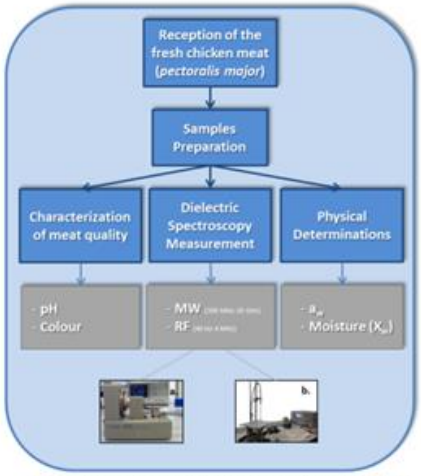

Fig. 1. Diagram of the experimental procedure. **a.** Agilent 16451B parallel plate and **b.** Agilent 85070E open-ended coaxial probe connected to an Agilent E8362B Vector Network Analyzer.

INTRODUCTION

Over the years, the consumption of meat has increased all over the world. Particularly, in Europe the total amount of meat consumed has doubled in the past 50 years, and it still seems to be rising slightly. Thinking about specific types of meats, there are large increases in consumption of especially poultry but also pig meat, whereas the total amount of consumed beef has been relatively stable (Kanerva, 2013). In USA, the consumption of poultry has increased more than double per capita in the last 30 years (Daniel et al., 2010).
However, meat and meat products industries are facing raw material quality issues, because this causes quality and stability problems in the final product. Despite efforts in a rapid and non-destructive detection of the pale, soft and exudative (PSE) and dark, firm and dry (DFD) meats, today this problem remains being one of the major challenges for the food industry. Therefore, sensors based on electromagnetic radiation can provide a huge improvement on the on-line and non-destructive control system.
Dielectric spectroscopy can be a suitable and fast tool for the quality determination mentioned above; however, few data in radiofrequency (RF) and microwave (MW) are available in the literature. There can be distinguished two different dispersions in the RF range: α dispersion – related with the orientation of charges with motion (the chemical species affected are the electrolytes and transport molecules, and β dispersion - corresponding to the orientation of charges bonded in the solid structure (protein structure). The mentioned MW range (γ dispersion) allows describing the mobility of water. The aim of the present investigation is to analyze the viability of the dielectric properties (in RF and MW range) for determining the quality classes in breast (*Pectoralis major*) chicken.

MATERIAL & METHODS

Raw Material: Experiments were done using chicken breast meat with 24 hours of postmortem.
Characterization of Chicken Meat Quality: Chicken breasts were classified based on pH, L* value according to the classification of Zhang & Barbut, 2005. The pH of samples was measured through a punch pH-meter S-20 SevenEasy^{Pro} (Mettler Toledo, Spain). The colour was measured through the surface reflectance spectra in a spectrocolorimeter Minolta CM-3600D (Minolta Co. Ltd., Japan). The colour coordinates CIE L*a*b* (CIE, 1978) were instrumentally calculated based on D65 illuminant and 10° observer.
Dielectric Spectroscopy Measurements: In radiofrequency range, the system used to measure consists of an Agilent 16451B parallel plate fixture connected to an Agilent 16451B impedance analyzer. The frequency range was from 40 Hz to 4 MHz. In the microwave range, the equipment used consists of an Agilent 85070E open-ended coaxial probe connected to an Agilent E8362B Vector Network Analyzer. All determinations were registered from 500 MHz to 20 GHz.
Physical Determinations:
- **Water Activity.** Hygrometer (DECAGON model Aqualab CX-2, ± 0,003).
- **Moisture.** Drying at 110ºC till constant weigth was reached, ISO 1442 (1997).

Statistical analysis: Statistical analysis was carried out with the Statgraphics Centurion XVI Software (Statgraphics, Virgina, U.S.A.). Statistical analysis was a non-linear regression by using three equations of Gompertz.

RESULTS

A mathematical model which consists in three Gompertz equations is proposed, simulating the Debye model. This equation provides the information about the dispersions in radiofrequency and microwave ranges (frequency and dielectric constant of relaxation). The following equation shows the coupling of three Gompertz equations in order to adjust the three dispersions (Eq. 1):

$$\varepsilon'(\omega) = \varepsilon'_{\infty} + \sum_{n=1}^{3} \frac{d1\ \varepsilon'_{1n}}{1 + e^{\gamma(\ln\omega - \ln\omega_n^*) + \alpha_n}} \qquad (1)$$

Where: ε' represents the decimal logarithm of the dielectric constant, $\ln\omega$ represents the decimal logarithm of the angular velocity (obtained from the frequency) and α are the three dispersions slopes. The subscripts ∞ and n represents the minimum value of the dielectric constant and the specific relaxation (α, β or γ), respectively (see **Figure 2**).

The **α-dispersion** is associated to phenomenon of the charge with mobility, soluble or suspended (electrolytes, charges with low molecular weight and high charge) in liquid phase. One little change in ion movement will produce a dielectric dispersion (Kuang and Nelson, 1997).

The **β-dispersion** usually occurs in the frequency region from tens of kHz to tens of MHz. This dispersion covers all the mechanisms involved in the orientation of fixed charges in solid surfaces (proteins, carbohydrates), and it could explain complex conformations of these molecules. These charges may belong to the chemical structure of the food or can be produced by the surface tension of the structure matrix. At the higher frequency range of **β-dispersion** the main interactions are by surface tension charges, this interaction is called Maxwell-Wagner effect.

The **γ-dispersion** is caused mainly by the orientation in the sense of the electric field polarization and the induction of the dipolar molecule (by its spin). In biological systems the most important molecule is water, which is associated to the frequency dependence of the aqueous solution where the particles are suspended (Debye, 1929). When an electric field is applied to the biological system, the dipolar molecules (water) are bound to orientate themselves with the polarity of the force lines of the electric field (Castro-Giráldez *et al.*, 2010).

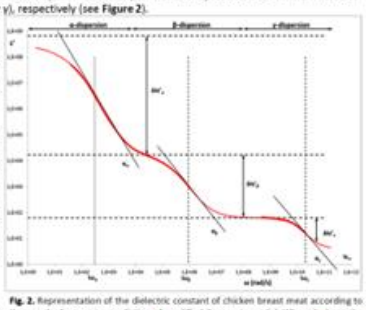

Fig. 2. Representation of the dielectric constant of chicken breast meat according to the angular frequency: prediction of modified Gompertz model. Where (—) are the values of mathematical model and (+) data obtained at 4° C.

Table 1. Gompertz Parameters.

Parameter's	$\varepsilon'_{1\infty}$	$\varepsilon'_{2\infty}$	$\varepsilon'_{3\infty}$
ε'_{∞} (ref.)	0,2 ± 0,2	0,60 ± 0,10	0,2 ± 0,2
$d\varepsilon'_n$	5,7 ± 0,4	6,2 ± 0,5	0,31 ± 0,07
ω_{n_1}	3,71 ± 0,06	3,5 ± 0,5	3,59 ± 0,18
α_n	0,147 ± 0,017	0,23 ± 0,06	0,148 ± 0,008
$d\varepsilon'_{n+1}$	1,5 ± 0,3	0,9 ± 0,8	0,5 ± 0,2
ω_{n_2}	6,7 ± 0,3	6,65 ± 0,22	6,55 ± 0,17
α_n	0,200 ± 0,097	0,148 ± 0,019	0,16 ± 0,08
$d\varepsilon'_{n+2}$	1,66 ± 0,21	1,22 ± 0,10	1,0 ± 0,3
ω_{n_3}	11,28 ± 0,08	11,17 ± 0,21	11,345 ± 0,103
α_n	0,126 ± 0,053	0,1442 ± 0,0096	0,139 ± 0,053

In the **Figure 3 a.** it can be seen the mathematical model proposed and the three characteristics dispersions for the different types of meat qualities. The parameters of Gompertz adjust are shown in **Table 1.**

Comparing the dielectric constant at 40 Hz (alpha dispersion) and at 100 kHz (beta dispersion) a significant difference can be observed between RFN and the rest of the meat qualities (**Figure 3 b.**). Moreover, it is possible to segregate the PSE and DFD meat qualities in the alpha dispersion, because DFD meat quality has a higher pH, therefore the value of the dielectric constant is significantly higher (see **Table 3**). Thus, a sensor measuring at 40 Hz and 100 kHz can segregate the three groups of meat qualities.

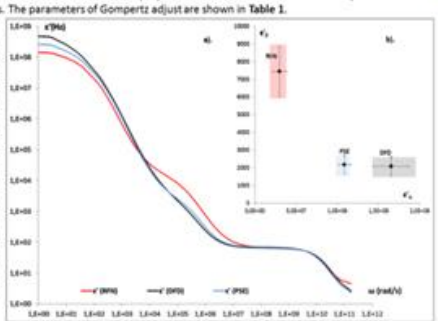

Fig. 3. a). Gompertz model adjusted to the three different chicken meat qualities and **b).** Corresponds to the differences between the chicken meat qualities classes in the frequency ranges of α and β dispersions.

Table 2. Relaxation frequencies at each specific dispersion (α, β or γ) for the samples assayed.

Parameters	$\varepsilon'_{1\infty}$	$\varepsilon'_{2\infty}$	$\varepsilon'_{3\infty}$
ε'_{∞}	1,695 ± 0,0	3,862 ± 1,333	1,303 ± 1,148
$d\varepsilon'_n$	1,0+06 ± 0,0+04	4,0+06 ± 1,0+06	1,0+06 ± 1,0+06
f_{1n}	329,708 ± 133	317,171 ± 187,198	855,431 ± 267,080
$\varepsilon'_{1\beta}$	441,674 ± 101	1616,567 ± 964,518	606,113 ± 111,491
$f_{2\beta}$	6,0+05 ± 0,0+05	7,0+05 ± 2,0+05	6,0+05 ± 2,0+05
$f_{2\beta}$ (MHz)	836,925 ± 478,923	670,772 ± 204,051	582,964 ± 125,430
$\varepsilon'_{2\gamma}$	10,755 ± 2,648	15,595 ± 2,648	10,870 ± 3,364
$f_{2\gamma}$	1,0+10 ± 1,0+09	2,0+10 ± 7,0+09	4,0+10 ± 8,0+09
$f_{2\gamma}$ (MHz)	10,710 ± 5,162	15,403 ± 7,008	10,678 ± 6,351

Table 3. Physical and chemical properties of the samples.

Properties	PSE	RFN	DFD
pH	5,70 ± 0,06	5,94 ± 0,09	6,13 ± 0,07
a_w (a_w/a_{w0})	0,746 ± 0,008	0,798 ± 0,006	0,754 ± 0,005
X_w	0,969 ± 0,003	0,972 ± 0,003	0,969 ± 0,003
L*	58,1 ± 1,5	57 ± 3	55 ± 3
a	-2,4 ± 0,6	-2,0 ± 0,6	-1,2 ± 0,6
b	7,0 ± 0,5	7,5 ± 1,4	8,5 ± 0,4

CONCLUSIONS

- ✓ It has been possible to classify the chicken breasts quality, analyzing the α and β dispersions.
- ✓ The results showed that the dielectric spectroscopy is a good and promising tool, useful to determine the chicken meat quality.

REFERENCES

- Castro-Giráldez, M., Botana, P., Fito, P. J. Plou, P. (2010). Low-frequency dielectric spectrum in assessment meat quality. Innovative Food Science & Emerging Technologies, 11(1), 379-388.
- CIE (1978). International Commission on Illumination. Recommendations on uniform color spaces, color difference equations, psychometric color terms. (Supplement No. 2 of Report 1). (E-1.3.1, 1971/(TC-1-3). Paris, France: Bureau Central de la CIE.
- Daniel, Z. F., Cross, H. J., Koohmaraie, G., & Kerby, R. (2011). Trends in meat consumption in the USA. Public Health Nutrition, 14(04), 575-583.
- Debye, P. (2013). Polar molecules. The Chemical Catalog Co., New York, 1929.
- Gil, 1992; 1997; 1997. Methods of test for meat and meat products. Determination of moisture content. ISO 1442:3-1997.
- Kanerva, M. (2013). Meat consumption in Europe: issues, trends and debates. Anais.
- Kuang, W., & Nelson, S. O. (1997). Low-frequency dielectric dispersion of biological tissues: a review with some new insights. Transactions of the ASAE, 41, 173-184.
- Mehdizadeh, A. E., & Mandavi, R. S. (2005). Industrial microwave heating. IEE Power Engineering series 1. London, UK: Peter Peregrinus LTD.
- Zhang, L., & Barbut, S. (2005). Rheological characteristics of batter and breast PSE, normal and DFD chicken breast meat. British poultry science, 46(6), 647-655.

VIII International Workshop on Sensors and Molecular Recognition (2014).
Valencia, España.

VIII international workshop on sensors and molecular recognition

ANÁLISIS DE LOS ESPECTROS DIELÉCTRICOS COMO HERRAMIENTA PARA EL CONTROL DE LA MADURACIÓN DE CARNE DE POLLO

Traffano-Schiffo, M.V., Muñoz, M.A., Castro-Giráldez, M. & Fito, P.J.*

Instituto de Ingeniería de Alimentos para el Desarrollo.
Universidad Politécnica de Valencia (España).
*pedfito@tal.upv.es

RESUMEN

Durante la maduración de la carne, se producen diferentes procesos bioquímicos y fisicoquímicos que determinan la calidad del producto final. Estos procesos, involucran desestructuraciones de las membranas, cambios en el estado de las proteínas, en la movilidad del agua y en la concentración de iones dentro del tejido. El consumidor percibe todos estos cambios a través de las características organolépticas, entre ellas, la terneza, jugosidad, color y el sabor, determinando por lo tanto la aceptabilidad del mismo.

En este contexto, el control de la evolución del proceso de maduración es uno de los elementos claves en la industria de carne que permite obtener un producto de alta calidad. En particular, en la industria de carne de ave, en la que los procesos de maduración se llevan a cabo a una velocidad mucho mayor que en el resto de especies animales, como por ejemplo la carne de cerdo o de ternera, la utilización de sensores no destructivos, de fácil implantación en líneas de producción y de respuesta inmediata, representan una prometedora herramienta para poder hacer frente a este desafío. Entre dichos sensores, destacan los basados en el espectro electromagnético, los cuales permiten detectar los cambios complejos en la estructura muscular mediante las variaciones en las propiedades eléctricas que se producen en el mismo. Es por ello, que un estudio en el rango de las radiofrecuencias (RF) y de las microondas (MW) nos proporciona información valiosa con respecto al estado estructural del sistema, permitiéndonos relacionarla con los cambios post-mortem del tejido muscular.

En el rango de las RF, es posible distinguir dos dispersiones; la dispersión α, la cual representa la orientación de las cargas móviles en el medio dieléctrico, y la dispersión β la cual está inducida por la orientación de las cargas fijas en la estructura proteica. En el rango de las MW, se encuentra la dispersión γ que está determinada por la orientación de los dipolos de pequeño tamaño molecular (movilidad del agua). Los resultados obtenidos demuestran la viabilidad de la espectroscopia dieléctrica como herramienta para la monitorización de la maduración de la pechuga de pollo (*Pectoralis major*).

INTRODUCCIÓN

Inmediatamente tras el sacrificio del animal, se desarrollan una serie de reacciones químicas y bioquímicas que permiten la transformación del músculo en carne (Ouali *et al.*, 2006). Estos cambios afectan de forma positiva al sistema, siendo los responsables de la terneza, jugosidad, aroma y sabor del producto.

Particularmente, la terneza es el resultado de la acción de enzimas proteolíticas endógenas, las catepsinas y calpaínas, las cuales afectan a las proteínas miofibrilares aumentando la terneza de la carne (Castro-Giráldez et al., 2011 & Chéret *et al.*, 2007). Sin embargo, algunos autores consideran a un tercer sistema enzimático como responsable de la textura, los proteasomas (Herrera-Mendez *et al.*, 2006, Dransfield & Sosnicki, 1999).

Los polipéptidos de tamaño intermedio, que se generan a causa de la acción de las enzimas endógenas, son el sustrato de las enzimas di y tri-peptidil peptidasas, las cuales generan péptidos de pequeño tamaño y aminoácidos libres, que influyen en el sabor y el aroma (Toldrá & Flores, 1998).

Por lo tanto, un estudio del proceso de maduración, especialmente en carne de pollo, en donde los procesos degradativos se producen a una gran velocidad, es de vital importancia. Este estudio nos permitirá determinar el tiempo óptimo de almacenamiento en refrigeración y por lo tanto mejorar los atributos sensoriales y de calidad.

Cabe destacar que el músculo esquelético presenta características eléctricas que cambian con el tiempo post-mortem (Byrne *et al.*, 2000) y, es por ello, que un estudio de las propiedades dieléctricas de la carne en el rango de la radiofrecuencia y las microondas es considerada como una herramienta útil y no destructiva para analizar la evolución de la maduración de la carne de pollo.

MATERIALES & MÉTODOS

Materia Prima: Los experimentos fueron realizados utilizando pechugas de pollo (*Pectoralis major*) de 4 horas de post-mortem. Los animales fueron proporcionados por el matadero del grupo Sada perteneciente a Nutreco España, S.A., y se mantuvieron a 4 ª C hasta su análisis. En la Figura 1 se puede observar el diagrama de flujo del experimental realizado.

Caracterización de la calidad de la carne: Las muestras fueron clasificadas como RFN (Rojas, Firmes y No Exudativas) según la clasificación de Zhang y Barbut (2005).

Análisis Estadísticos: El análisis estadístico de los datos fue llevado a cabo mediante el programa Statgraphics Centurion XVI (Statgraphics, Virgina, U.S.A.). Se realizó una regresión no lineal utilizando la ecuación de Gompertz.

Espectroscopia dieléctrica:

Radiofrecuencia: El sistema utilizado para la medición de las propiedades dieléctricas en el rango de la radiofrecuencia (40 Hz a 1 MHz) consiste en un sensor fabricado en colaboración por el Instituto de Ingeniería de Alimentos para el Desarrollo (IuIAD, UPV) y el Instituto de Instrumentación para Imagen Molecular (i3M, UPV), conectado a un analizador de impedancias Agilent 16451B. **Microondas:** Para el rango de frecuencias de las microondas (500 MHz a 20 GHz), el sistema utilizado consiste en una sonda coaxial Agilent 85070E conectada a un analizador de redes Agilent E8362B.

Figura 1. Diagrama de flujo del trabajo de investigación.

RESULTADOS

El presente trabajo se encuentra enmarcado en un macroproyecto en el cual se han analizado cambios bioquímicos y estructurales de la carne durante el tiempo post-mortem, además de los cambios eléctricos mencionados. Dichos análisis comprenden estudios de la microestructura de la carne (análisis de microscopía electrónica de barrido a bajas temperaturas), degradación proteica (Calorimetría Diferencial de Barrido), así como análisis de iones libres (cromatografía de intercambio iónico). Todos estos análisis han servido para la interpretación de los resultados de espectroscopia dieléctrica.

En los tejidos biológicos, se pueden distinguir tres dispersiones características en función de la frecuencia: la **dispersión-α**, que ocurre desde los Hz hasta los kHz, la cual representa la orientación de las cargas móviles dentro del sistema biológico; un pequeño cambio en el movimiento de iones producirá un aumento de esta dispersión dieléctrica (Kuang & Nelson, 1997). La **dispersión-β**, desde kHz hasta MHz, la cual está inducida por la orientación de las cargas fijas en la estructura proteica. Por último, la **dispersión-γ** es causada principalmente por la orientación y la inducción de las moléculas dipolares, fundamentalmente el agua.

En la Figura 2 es posible observar el comportamiento dieléctrico de las muestras de carne de pollo a lo largo del proceso de maduración en el rango de radiofrecuencia.

Se puede observar como a medida que avanza el tiempo post-mortem, se genera un aumento en la señal eléctrica en la dispersión α que puede ser debida a un aumento en la fuerza iónica causado por los procesos de maduración que generan una bajada del pH de la carne. Sin embargo, en la dispersión β, la constante dieléctrica disminuye a causa de la desestructuración proteica.

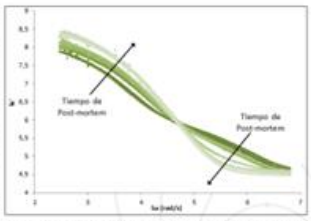

Figura 2. Evolución de la constante dieléctrica durante la maduración (5, 7, 9, 11, 13, 15, 17, 26, 50, 74, 98 y 146 horas de post-mortem)

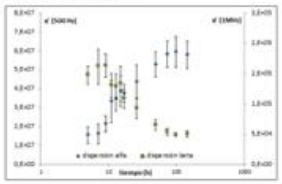

Figura 3. Evolución de la constante dieléctrica a 500 Hz y a 1 MHz.

Todos los cambios observados en la figura 2, pueden ser analizados más fácilmente utilizando frecuencias puntuales. Es por ello que en la figura 3 se ha representado la evolución de la constante dieléctrica a 500 Hz (dispersión α) y a 1 MHz (dispersión β) durante el proceso de maduración. Se puede observar que la constante dieléctrica a 500 Hz aumenta significativamente a lo largo del proceso de maduración. Tal y como se ha explicado anteriormente, esto puede ser debido a que durante este proceso se producen procesos fermentativos que provocan una bajada acentuada del pH. Por el contrario, durante la maduración se produce una bajada de la constante dieléctrica a 1 MHz, causada por la degradación de las proteínas estructurales.

Se ha propuesto un modelo matemático basado en tres ecuaciones de Gompertz, simulando el modelo de Debye. Esta ecuación brinda información sobre las dispersiones que se producen en el rango de la radiofrecuencia y de las microondas (frecuencias y constante dieléctrica de la relajación). La siguiente ecuación muestra el acoplamiento de tres ecuaciones de Gompertz con el objetivo de ajustar las tres dispersiones (Ec. 1):

$$\lg \varepsilon'(\omega) = \lg \varepsilon'_{\infty} + \sum_{\substack{i=\alpha,\beta,\gamma \\ n=1,2,3}}^{3} \frac{\Delta \lg \varepsilon'_{n}}{1 + e^{\left(\frac{\lg \omega - \lg \omega_{n}}{b_{n}}\right)}} \quad (1)$$

Donde: $\lg \varepsilon'$ representa el logaritmo decimal de la constante dieléctrica, $\lg \omega$ representa el logaritmo decimal de la velocidad angular (obtenido a partir de la frecuencia) y **α** corresponde a las tres pendientes de las dispersiones. Los subíndices ∞ y **n** representan: el valor mínimo de la constante dieléctrica y la relajación específica (α, β o γ), respectivamente (véase la **Figura 4**).

En la figura 4 se muestran los datos experimentales (puntos) junto con el modelo obtenido a través del algoritmo (líneas). Se puede observar que el modelo utilizado se ajusta adecuadamente a los datos experimentales.

El algoritmo utilizado para sacar las propiedades eléctricas a frecuencias de relajación (Figura 5), muestra que las relajaciones estudiadas, α y β, siguen la tendencia asociada a cambios químicos y estructurales producidos por el metabolismo de maduración de la carne.

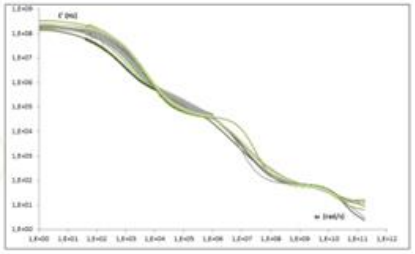

Figura 4. Modelo de Gompertz correspondientes a distintos tiempos post-mortem.

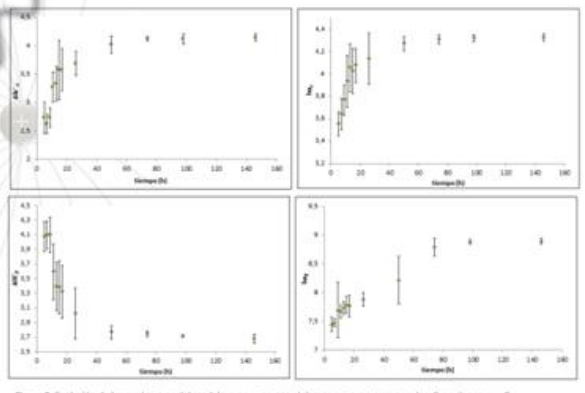

Figura 5. Evolución de los parámetros del modelo propuesto con el tiempo post-mortem para las dispersiones α y β.

CONCLUSIONES

- La constante dieléctrica permite determinar el grado de desestructuración y por lo tanto predecir el tiempo de post-mortem de la carne.
- Los resultados demuestran que la espectroscopia dieléctrica es una herramienta útil, no invasiva y en línea, que permite controlar el proceso de maduración de la carne de pollo.

REFERENCIAS

Con la colaboración de nutreco

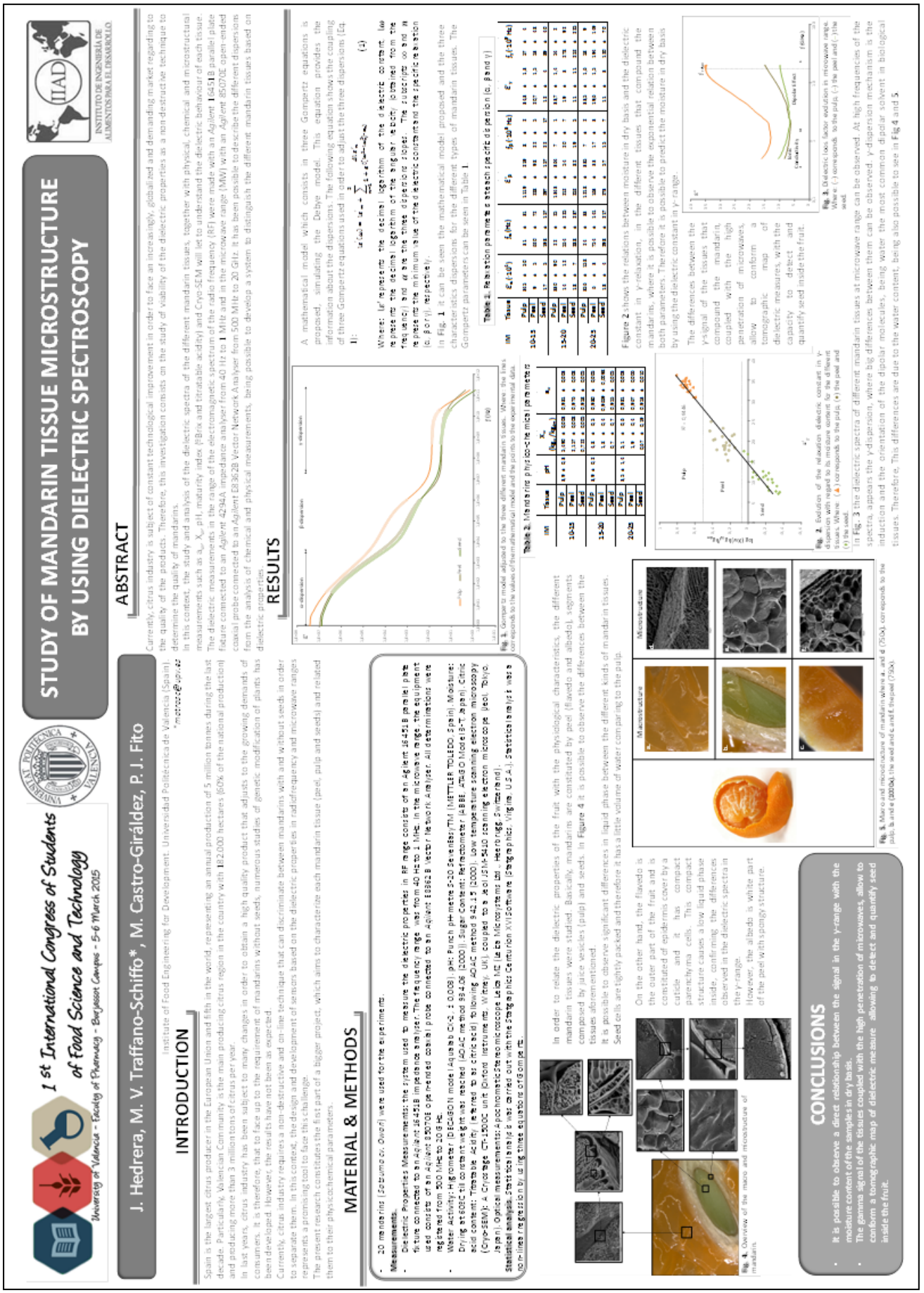
1st International Congress of Students of Food Science and Technology
University of Valencia - Faculty of Pharmacy - Burjassot Campus - 5-6 March 2015
STUDY OF MANDARIN TISSUE MICROSTRUCTURE BY USING DIELECTRIC SPECTROSCOPY
J. Hedrera, M. V. Traffano-Schiffo*, M. Castro-Giráldez, P. J. Fito
Institute of Food Engineering for Development. Universidad Politécnica de Valencia (Spain).
INTRODUCTION
MATERIAL & METHODS
ABSTRACT
RESULTS
CONCLUSIONS

Study of the water distribution during osmotic dehydration of kiwifruit and the effect of pulsed electric fields as pre-treatment

Traffano-Schiffo, M. V.[1], Laghi, L.[2,3], Tylewicz, U.[2*], Castro-Giraldez, M.[1], Fito, P. J.[1], Ragni, L[2,3] and Dalla Rosa, M.[2,3]

[1]Instituto Universitario de Ingeniería de Alimentos para el Desarrollo, Universidad Politécnica de Valencia. Spain.
[2]Department of Agricultural and Food Science, University of Bologna, Cesena, Italy.
[3]Interdepartmental Centre for Agri-Food Industrial Research, University of Bologna, Cesena, Italy.
* urszula.tylewicz@unibo.it

EURO FOOD WATER

INTRODUCTION

Osmotic dehydration (OD) is a conservation technique used to increase the commercial life of fruits. However, OD treatment removes the water from materials (fruits and vegetables) only partially. Therefore, the combined use of OD treatment with other techniques such as Pulsed Electric Fields (PEF) represents a promising tool to improve mass transfer, increasing yields and reducing processing time.
PEF is a non-thermal technology which consist in applying electric pulses through a material placed between two electrodes for very short periods of time (micro- to milli-seconds), which causes structural changes in the cell membrane, such as permeabilization and polarization, and as a consequence the creation of pores.
The coupled treatment (OD/PEF) cause an uncontrolled breakdown of the membranes, about which information can be obtained by registering transverse relaxation time (T_2) weighted signals by means of Time Domain nuclear magnetic resonance (TD-NMR).
Panarese et al. (2012) was able to separately observe, in the pericarp of kiwifruit, water located in extracellular spaces and cytoplasm, water located in vacuole and protons ascribable to water tightly bound to the most rigid biopolymers.

AIM OF THE STUDY

The aim of this work was to analyze the effect of Pulsed Electric Fields (PEF) in mass transfer as a pre-treatment for the OD of kiwifruit (*Actinidia deliciosa cv Hayward*). For this purpose, PEF pre-treatments were done by applying three different voltages (100, 250 and 400 V/cm) and a train of 60 pulses. The OD of the kiwi was carried out by immersing the samples in 61.5% sucrose solution at 25ºC, maintaining a relationship 1:4 (w/w) between the fruit and the OD solution for a contact period of 0, 10, 20, 30, 60 and 120 min. Mass transport phenomena and water distribution into the cellular tissue was studied by time domain nuclear magnetic resonance (TD-NMR).

MATERIAL & METHODS

Raw Material - Organic kiwifruits (*Actinidia deliciosa* cv ''Hayward''). Cylinders of 8 mm diameter and 10 mm length were obtain with a cork borer.
Pulsed electric fields (PEF) treatment - was carried out by applying three different voltages (100, 250 and 400 V/cm) with near-rectangular shape, a train of 60 pulses, a fixed pulse width of 100 ± 2 ms and a repetition time of 10.0 ± 0.1 ms to kiwifruit cylinders placed in a 20 x 20 x 30 mm chamber and filled up with tap water at 25ºC.
Osmotic Dehydration - 61.5% sucrose at 25ºC (relationship 1:4 (w/w)) with contacts periods of 0, 10, 20, 30, 60 and 120 min.
Time domain nuclear magnetic resonance (TD-NMR) - The intensity of the signal and the Proton transverse relaxation time (T_2) was measured by using a Bruker 'The Minispec' spectrometer (Bruker Corporation, Germany) operating at 20 MHz.
Analytical methods – **Mass:** Kern balance ABS 320-4N (±0.0001) (KERN & SOHN GmbH, Germany); **Water Activity:** Hygrometer (DECAGON model Aqualab CX-2, ± 0,003); **Moisture:** Drying the samples at 70 °C until a constant weight was achieved; **Soluble solids:** The soluble solids content was determined at 20°C by measuring the refractive index with a digital refractometer (Krüss Optronic, Germany).

RESULTS

Weight loss %: Immediate observation

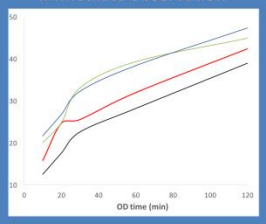

Diff. % of weight loss: After 24h - Immediate observation

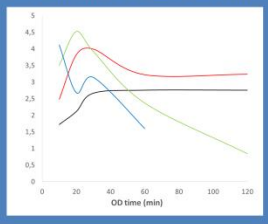

PEF and osmosis act synergistically in the water removal process. The almost perfect superimposition of the 250 and 400 V/cm trends reinforces the observations that the limit between reversible and irreversible process is localizable in a range of 100 and 250 V/cm. Water loss can be considered in any case as a dynamic process, as the observations at 24 hours post-treatment allow to deduce.

Relative intensity and T_2 of the vacuole, as observed by TD-NMR

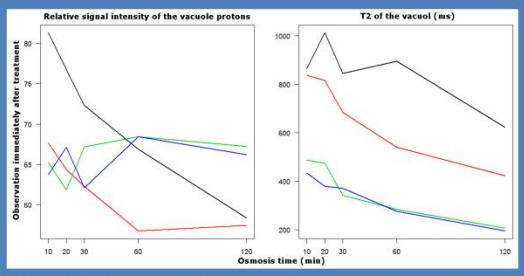

T_2 is mainly dominated by the chemical exchange between water and exchangeable sites of the byopolimers of the structures. Shortening of the T_2 is therefore very sensitive to vacuole water loss, and sugar entrance, stimulated by osmosis. The PEF treatments effects can be divided in two groups, as already noticed in apple by Dellarosa et al (Dellarosa 2016). The application of 100 V/cm (red line) has therefore probably reversible consequences.

Brix value increase %: Immediate observation

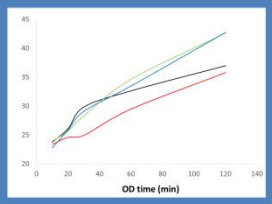

PEF treatment with trains of 100 V/cm pulses led to the lowest brix value increase, compensated by the lowest total mass decrease.

Legend

- No treatment
- 100 V/cm
- 250 V/cm
- 400 V/cm

CONCLUSION

PEF pretreatment at 100 V/cm represented the best compromise between water redistribution/loss and sugar content increase. At higher voltages (250 and 400 V/cm), it was limitedly possible to segregate the signals from some of the compartments of the tissue, suggesting cellular membranes irreversible and diffuse damage. The intensity of 100 V/cm was therefore as an optimal compromise between efficacy for mass transfers during OD and the need to preserve the fruit micro-structure.

BIBLIOGRAPHY

Panarese, V., Laghi, L., Pisi, A., Tylewicz, U., Dalla Rosa, M., & Rocculi, P. (2012). Effect of osmotic dehydration on Actinidia deliciosa kiwifruit: A combined NMR and ultrastructural study. *Food chemistry*, *132*(4), 1706-1712.

Dellarosa, N., Ragni, L., Laghi, L., Tylewicz, U., Rocculi, P., & Dalla Rosa, M. (2016). Time domain nuclear magnetic resonance to monitor mass transfer mechanisms in apple tissue promoted by osmotic dehydration combined with pulsed electric fields. *Innovative Food Science & Emerging Technologies*.

Financial support for this project is provided by funding bodies within the FP7 ERA-Net CORE Organic Plus, and with cofunds from the European Commission

International Conference on Food Innovation foodInnova 2017 — 31st January - 3rd February, 2017 — Cesena - Emilia-Romagna - Italy

FORMULATION AND DRYING OF ALGINATE BEADS CONTAINING LACTASE: STABILITY AND MICROSTRUCTURE

Traffano-Schiffo, M. V.[1]; Aguirre Calvo, T. R.[2]; Castro-Giráldez, M.[1]; Fito, P. J.[1]; Santagapita, P. R.[2*]

[1]InstitutoUniversitario de Ingeniería de Alimentos para el Desarrollo, Universidad Politécnica de Valencia, Camino de Vera s/n, 46022 Valencia, Spain.
[2]Universidad de Buenos Aires, Facultad de Ciencias Exactas y Naturales, Departamento de Industrias y Departamento de Química Orgánica, & CONICET, Buenos Aires, Argentina.
*prs@di.fcen.uba.ar

INTRODUCTION

Several applications of β-galactosidase (lactase) have been reported in recent years, such as the valorization of cheese whey, the improvement of ice creams creaminess, and the production of lactose-free fresh dairy products for lactose intolerance people. However, enzyme stability upon treatment and dosification can be improved. In this context, β-galactosidase encapsulation in hydrogels represents a promising tool. Nevertheless, typical alginate-Ca(II) shows some technological disadvantages such as low resistance to thermal processes and its uncontrolled release, but the combined use of alginate with sugars and/or other biopolymers can be used to overcome these. The aim of this research was to improve the stability of lactase subjected to different thermal treatments by using different formulations.

MATERIALS & METHODS

Beads Generation

Alginate-Ca(II) beads with β-galactosidase (*Aspergillus oryzae*, 0.775 mg/mL) by dropping method

Systems

EA / EAT / EATAG / EATGG
A: Alginate; T: Trehalose, AG: Arabic Gum; GG: Guar Gum

After generation

Characterization

- Feret´s diameter and circularity
- Water content and water activity
- Microstructure by small angle X-ray scattering (SAXS)

Measurements

- β-Galactosidase activity
- Spin–spin relaxation times (T_2) and spin-lattice (T_1) by ^{1}H-LF-NMR

Drying Treatments

- **Vacuum-drying (VD):** at 25 ºC and a pressure of 113 mbar during 24 h.
- **Freeze-drying (FD):** frozen at -18 ºC during 24 h, and lyophilized during 24 h.

Dried Beads → Remaining β-Galactosidase activity

RESULTS

Beads Characterization

EATGG and EATAG beads showed a significant increment of the size due to the increase in viscosity and the interfacial properties, respectively.

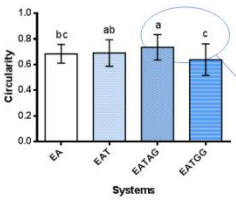

Figure 2. Circularity of the beads.

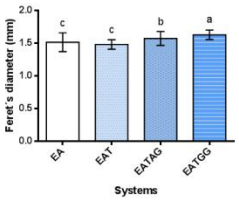

Figure 1. Feret´s diameter of the beads.

EATAG beads showed the highest circularity and EATGG, the lowest. Guar gum viscosity affects the size of the bead, having a drop-like form and arabic gum reduce the deformation due to its interfacial properties.

Beads containing trehalose (polyol) showed significantly lower values of moisture with regard to alginate beads, due to its ability to make multiple hydrogen bonds, replacing water molecules.

Table 1. Water activity and moisture content (kg_w/kg_T).

Systems	a_w	x_w (kg_w/kg_T)
EA	0.939 ± 0.006[a]	0.9683 ± 0.0088[a]
EAT	0.944 ± 0.008[a]	0.852 ± 0.005[c]
EATAG	0.949 ± 0.003[a]	0.871 ± 0.002[b]
EATGG	0.949 ± 0.001[a]	0.872 ± 0.003[b]

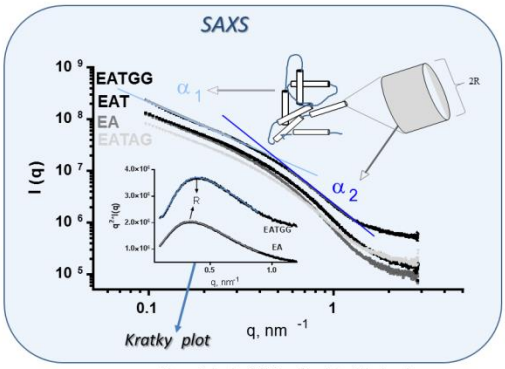

Figure 3. log-log SAXS profile plots of the beads.

Lactase Stability

EA → highest activity index

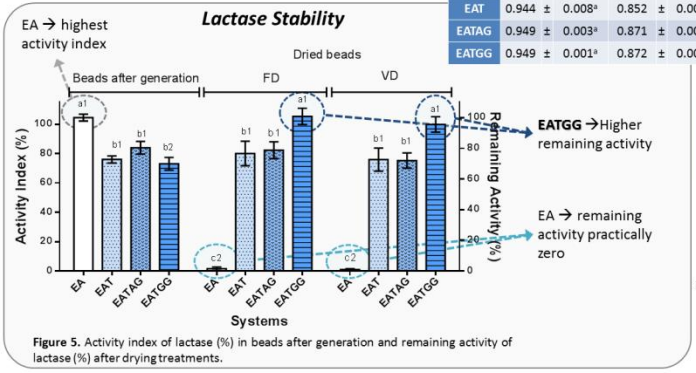

Figure 5. Activity index of lactase (%) in beads after generation and remaining activity of lactase (%) after drying treatments.

The addition of any excipients did not affect the interconnection of the structure (α_1)

Trehalose containing beads showed the smaller cross-sectional radius of the rods (R)

Gums containing beads showed the smaller compactness degree of the rods (α_2) due to the steric hindrance along alginate chains.

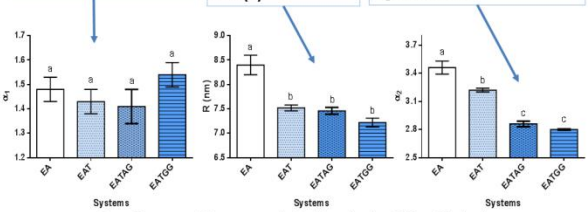

Figure 4. α_1, α_2 and R parameters derived from log-log SAXS and Kratky plots.

LF-NMR Analysis

Table 2. Longitudinal (T_1), transversal (T_{21} and T_{22}) relaxation times and their correspondent amplitudes of beads containing lactase after generation.

Systems	$Amplitude_1$ (%)	T_1 (ms)	$Amplitude_{21}$ (%)	T_{21} (ms)	$Amplitude_{22}$ (%)	T_{22} (ms)
EA	-181 ± 1[a]	1550 ± 10[a]	85.5 ± 0.3[a]	53.9 ± 0.3[c]	14.5 ± 0.3[a]	710 ± 20[a]
EAT	-182 ± 9[a]	1292 ± 12[d]	87.1 ± 0.2[a]	57 ± 1[bc]	12.9 ± 0.2[b]	403 ± 47[b]
EATAG	-193 ± 1[a]	1338 ± 6[c]	86.6 ± 0.9[a]	58.1 ± 0.3[b]	13.3 ± 0.9[ab]	379 ± 62[b]
EATGG	-194 ± 2[a]	1395 ± 15[b]	86 ± 1[a]	66 ± 1[a]	14 ± 1[ab]	495 ± 69[ab]

Trehalose reduced T_1 → lower correlation time with respect to alginate. Gums increases T_1.

T_2 → 2 populations

- T_{21} → H^+ with low mobility → hindrance layers and adsorbed water → > 85% of H^+
- T_{22} → H^+ with high mobility → less associated H^+

EA beads → High T_{22} and low for T_{21}

EATGG
- Increases significantly T_{21} with respect to trehalose-containing beads.
- High T_{22} → slightly higher mobility → higher degree of rearrangement of the H^+ → higher degree of interaction with the enzyme.

CONCLUSIONS

- Alginate-Ca(II) beads containing lactase were successfully produced by the dropping method.
- Trehalose was critical for enzyme conservation after drying treatments.
- Guar gum shows the highest enzyme stability in dried beads, related to its higher mobility (T_{22}) and its capacity of rearrangement, allowing a higher degree of interaction with the enzyme.
- Excipients (T/AG/GG) affected the microstructure, showing rods with smaller cross-sectional radius R and with lower compactness within the rods (α_2) than EA beads.

The authors acknowledge LNLS (Campinas, Brazil), CONICET, CIN-CONICET, ANPCyT and also UBA.

UNIVERSITAT POLITÈCNICA DE VALÈNCIA